TÉCNICO LISBOA

UNIVERSIDADE DE LISBOA

INSTITUTO SUPERIOR TÉCNICO

Stem cell-mediated bone formation on biomimetic 3-D matrices

Marta Monteiro Silva Carvalho

Supervisor: Doctor Deepak Vashishth

Co-Supervisor: Doctor Cláudia Alexandra Martins Lobato da Silva

Thesis approved in public session to obtain the PhD Degree in

Bioengineering

Jury final classification: Pass with Distinction

2018

UNIVERSIDADE DE LISBOA

INSTITUTO SUPERIOR TÉCNICO

Stem cell-mediated bone formation on biomimetic 3-D matrices

Marta Monteiro Silva Carvalho

Supervisor: Doctor Deepak Vashishth

Co-Supervisor: Doctor Cláudia Alexandra Martins Lobato da Silva

Thesis approved in public session to obtain the PhD Degree in Bioengineering

Jury final classification: Pass with Distinction

Jury

Chairperson: Doctor Joaquim Manuel Sampaio Cabral, Instituto Superior Técnico, Universidade de Lisboa

Members of the Committee:

Doctor Deepak Vashishth, School of Engineering, Rensselaer Polytechnic Institute, USA

Doctor Joaquim Manuel Sampaio Cabral, Instituto Superior Técnico, Universidade de Lisboa

Doctor Maria Manuela Estima Gomes, I3B's - Instituto de Investigação em Biomateriais, Biodegradáveis e Biomiméticos, Universidade do Minho

Doctor José Paulo Sequeira Farinha, Instituto Superior Técnico, Universidade de Lisboa

Doctor Cristina Maria Santos Alves de Carvalho Barrias, Instituto Nacional de Engenharia Biomédica

Funding Institutions

FCT - Fundação para a Ciência e Tecnologia

CBIS - Center for Biotechnology & Interdisciplinary Studies, Rensselaer Polytechnic Institute

2018

ABSTRACT

Bone tissue engineering aims to generate functional bone tissue, fabricating biocompatible and biodegradable scaffolds, and developing new approaches to enhance the functionality and bioactivity of the scaffolds, such as the use of growth factors, bioactive peptides or extracellular matrix (ECM) components. Numerous pre-clinical trials with different animal models have generated optimistic results, however, the difficulty to translate it into a clinical setting suggests that some limitations and concerns remain and need to be further addressed to design enhanced bone grafts for bone fracture repair treatment.

By looking deep into nature, we observe that each tissue has its own ECM, with different composition regarding its specificity. It is known that most of the outstanding properties of the bone are related to its matrix constitution. More specifically bone extracellular matrix is composed by an organic and inorganic part, composed by collagen, non-collagenous proteins and hydroxyapatite. Although in smaller amounts, non-collagenous bone proteins can be found in the bone matrix and they have been reported to play important roles in bone mineralization and cellular activities, in particular osteocalcin (OC) and osteopontin (OPN). We evaluated the role of OC and OPN at the cellular level by investigating osteogenic differentiation of mesenchymal stem/stromal cells (MSC) derived from $OC^{-/-}$ $OPN^{-/-}$ mice. We observed that osteogenic differentiation is impaired and, using spectroscopic analysis, we confirmed that mineralization is delayed and the mineral formed by these cells is not mature enough after 21 days of osteogenic differentiation. Therefore, we concluded that OC and OPN are important regulators of bone mineralization at a cellular level, providing new insights into forming high quality bone, relevant for treatment of fracture healing in older and osteoporotic bone. By understanding the fundamental roles of OC and OPN, we applied the synergistic effect of these proteins and developed biomimetic scaffolds for bone tissue engineering that enhance and accelerate the process of bone repair.

Throughout this thesis, we highlighted the crucial role that ECM can play on cell activity, such as on MSC proliferation and osteogenic differentiation, as well as on their angiogenic capacity. New techniques should be focused on designing biomimetic matrices that recapitulate the architecture, composition and structure of native ECM. With this in mind, we explored the use of cell-derived ECM as a biomaterial. We observed that decellularized ECM derived from co-culture of MSC and human umbilical vein endothelial cells (HUVEC) enhances osteogenic differentiation of MSC, up-regulating osteogenic gene expression, and increases the angiogenic potential of these cells. Moreover, we applied these decellularized ECM into electrospun scaffolds and developed cell-derived ECM electrospun polycaprolactone (PCL) scaffolds to be further used in bone tissue engineering applications.

Keywords: Extracellular matrix (ECM), Mesenchymal stem/stromal cells (MSC), Osteocalcin (OC), Osteogenesis, Osteopontin (OPN).

RESUMO

Engenharia do tecido ósseo tem como objectivo criar tecido ósseo funcional, produzindo materiais biocompatíveis e biodegradáveis e desenvolvendo novas abordagens para melhorar a funcionalidade e bioactividade desses mesmos materiais, como a incorporação de factores de crescimento, péptidos bioactivos ou componentes da matriz extracelular (ECM).

Vários ensaios pré-clínicos usando diferentes modelos animais geraram resultados promissores, contudo a dificuldade de traduzir esses resultados num contexto clínico sugere que ainda restam algumas preocupações e limitações que necessitam de ser abordadas para desenvolver melhores implantes ósseos para o tratamento de fractura óssea.

Através da observação da natureza, constatamos que cada tecido tem a sua própria matriz extracelular, com diferentes composições dependendo da sua especificidade. As propriedades excepcionais do osso estão relacionadas com a constituição da sua matriz. Especificamente, a matriz extracelular óssea é composta por uma parte orgânica e inorgânica, composta por colagénio, proteínas não colagenosas e minerais de hidroxiapatite.

Apesar de existirem em pequenas quantidades na matriz óssea, as proteínas não colagenosas, especificamente a osteocalcina (OC) e a osteopontina (OPN), têm sido associadas a funções importantes na mineralização óssea e em actividades celulares. Deste modo, investigámos a função da OC e OPN ao nível celular através do estudo da diferenciação osteogénica de células estaminais mesenquimais (MSC) derivadas de $OC^{-/-}$ $OPN^{-/-}$ ratos. Observámos que a diferenciação osteogénica é afectada e, usando análises espectroscópicas, confirmámos que a mineralização é atrasada e que o mineral formado por estas células não é suficientemente maduro ao fim de 21 dias de diferenciação osteogénica. Deste modo, concluímos que OC e OPN são importantes reguladores de mineralização óssea ao nível celular, fornecendo novas informações sobre a formação de osso de elevada qualidade, um parâmetro relevante para o tratamento de fractura óssea em pacientes idosos e osteoporóticos. Através do conhecimento dos papéis fundamentais da OC e OPN, aplicámos o efeito sinergético destas duas proteínas e desenvolvemos materiais biomiméticos para engenharia do tecido ósseo que possibilitem a aceleração do processo de reparação óssea.

Ao longo desta tese, realçámos o papel fundamental da matriz extracelular na actividade celular, como na proliferação de células estaminais mesenquimais e diferenciação osteogénica, bem como na sua capacidade angiogénica. Novas técnicas deverão focar-se no desenvolvimento de matrizes biomiméticas que recapitulem a arquitectura, composição e estrutura da matriz extracelular natural. Deste modo, explorámos o uso de matriz extracelular descelularizada produzida por células como um possível biomaterial. Constatámos que a matriz extracelular descelularizada derivada de uma co-cultura de células estaminais mesenquimais e células endoteliais da veia umbilical humana (HUVEC) melhora a diferenciação osteogénica das MSC, sobre–expressando marcadores osteogénicos e aumentando o potencial angiogénico dessas células. Além disso, aplicámos essas matrizes em materiais produzidos por electrospinning e desenvolvemos fibras de policaprolactona (PCL) constituídas por matriz extracelular derivada de células para serem usadas em aplicações de engenharia de tecido ósseo.

Palavras-chave: Matriz extracelular (ECM), Células estaminais mesenquimais (MSC), Osteocalcina (OC), Osteogénese, Osteopontina (OPN).

ACKNOWLEDGEMENTS

During this PhD journey I had a lot of important people that helped me and shared with me this adventure. Therefore, I really want to highlight here how valuable you were during this journey.

I would like to start thanking Professor Joaquim Cabral for all the effort in developing the Stem Cell Bioengineering Laboratory and Regenerative Medicine (SCBL-RM) and, in particular, for stimulating new PhD programs and collaborations, putting different people working together in this field. I would like to thank specially for the opportunity that I had to be able to do my PhD in two different universities (IST and RPI).

Many thanks to my supervisors, Professor Deepak and Professor Cláudia for being always so supportive and enthusiastic and approving all my ideas, giving me the independence that I needed to develop this PhD. I truly appreciated working and learning with both of you. Specially, thank you both for complementing each other in my co-supervision.

Professor Deepak, I am very thankful to had the opportunity to join your lab and to learn more about the bone tissue. I am grateful for all the opportunities that you gave me and for valuing my thoughts and ideas. I really learnt a lot and you always made me believe that things could be done, leading me to try different approaches for my research questions and encouraging me to learn new techniques. Moreover, I want to thank you also for making me feel so comfortable at RPI, showing me some beautiful places in the area.

Professor Cláudia, I always appreciated your enthusiasm for Science and your support throughout these years. Thanks for sharing your knowledge and for giving me the freedom to pursue the topics that I was most interested in. I am grateful to be able to translate the work that I started developing at RPI to SCBL-RM and to be always motivated by you. Thank you also for being able to help me to coordinate my PhD project between RPI and IST.

I would like to thank all my SCBL-RM lab colleagues for the companionship, generosity and cooperative spirit.

A special thanks to all Vashishth's lab members. I would like to thank Dr. Atharva Poundarik for all the scientific discussions, but most for all the random talks that we had about science and life in general. Thanks also to Dr. Gyna Sroga for all the shares that we had during these years. I am really happy to be able to share the office with you and to listen all your stories and experiences. Thank you all for the good mood and kindness.

Thanks to Dr. Brigitte Arduine, Dr. Sergey Pryshchep and Dr. Joel Morgan for all the help in this project, allowing me to learn different techniques and being genuinely interested to help me.

A special thanks to João Silva and André Nascimento. I am really happy that I was able to live with you in Troy and shared with you my personal and scientific life. I truly believe that you made Troy a better place to live. André, thank you for all your good mood. You really helped me to forget some scientific “frustrations”. João, I really appreciate having the opportunity to share with you also my research and to be able to develop some “crazy” ideas with you. I truly know that some parts of this project were only possible to be done because of your help and your collaborative spirit. Thank you both!

I also would like to acknowledge Fundação para a Ciência e a Tecnologia (FCT), Portugal, for granting my PhD scholarship (SFRH/BD/52478/2014) and also to Center for Biotechnology and Interdisciplinary Studies (CBIS) funds.

To João, thanks for being so genuine, supportive and for letting me learn with you how life can be so simple. Thank you for your laughs and for always being there for me during these years.

To my family, my mother, my father and my sister. I know how important you have been during these years and I am sure that all your support and love helped me to complete my PhD. Thank you for always being there for me and for all the moments and memories that make my life so good.

TABLE OF CONTENTS

ABSTRACT ……i
RESUMO……iii
ACKNOWLEDGMENTS……v
TABLE OF CONTENTS……vii
LIST OF FIGURES……xv
LIST OF TABLES……xxvii
ABBREVIATIONS……xxix
THESIS MOTIVATION……xxxiii
Aim of studies and research questions……xxxiv
Research strategy……xxxvi
Thesis outline……xxxviii
References……xl

CHAPTER I – INTRODUCTION……1
I.1. Hierarchical structure of bone……1
I.1.1. Macroscopic level……1
I.1.2. Microstructure of bone……5
I.1.3. Nanostructure of bone: mineralized collagen fibril……5
I.2. Biomineralization……9
I.2.1. Evaluation of the quality of minerals formed in cell culture……10
I.2.1.1. X-ray diffraction……10
I.2.1.2. SEM and TEM and related techniques……10
I.2.1.3. Atomic force microscopy……11
I.2.1.4. Light microscopy……11
I.2.1.5. Vibrational spectroscopy and vibrational spectroscopic imaging……11
I.2.1.6. Radiographic and related methods……14
I.2.1.7 Chemical analysis……14
I.3. Bone cells……15
I.3.1. Osteoblasts……15
I.3.2. Osteocytes……16
I.3.3. Osteoclasts……17

I.4. Bone formation, development and repair……17
I.4.1. Intramembranous ossification……18
I.4.2. Endochondral ossification……19
I.4.3. Bone Remodeling……20
I.4.4. Bone Repair……22
I.5. Angiogenesis and osteogenesis……23

I.5.1. Interaction of endothelium and bone……23
I.5.2. Angiogenesis in bone repair……24
I.5.3. VEGF in endochondral and intramembranous ossification during bone repair……..26
I.5.4. VEGF effects on osteogenic differentiation of mesenchymal progenitor and bone regeneration.....27
I.5.5. VEGF effects on recruitment of osteoclasts and immune cells……..……..29
I.5.6. Vascularization in bone tissue engineering……..30
I.6. Bone extracellular matrix……...31
I.6.1. Extracellular matrix……...31
I.6.2. Bone extracellular matrix: characterization, quality and properties……..31
I.6.3. Non-collagenous bone matrix proteins……..33
I.6.3.1. Proteoglycans……..……34
I.6.3.1.1. Aggrecan and versican……34
I.6.3.1.2. Decorin and biglycan……...35
I.6.3.2. Glycoproteins……...35
I.6.3.2.1. Alkaline phosphatase……..……36
I.6.3.2.2. Osteonectin……..……36
I.6.3.2.3. Tetranectin……..……36
I.6.3.2.4. RGD-containing glycoproteins……...…37
I.6.3.2.4.1. Thrombospondin, fibronectin and vitronectin……..…37
I.6.3.2.4.2. Small Integrin-Binding Ligand, N-Lynked Glycoproteins……...38
I.6.3.2.4.2.1. Osteopontin……..……..38
I.6.3.2.4.2.2. Bone Sialoprotein……..……...40
I.6.3.2.4.2.3. Dentin matrix protein 1 and dentin sialophosphoprotein……..……40
I.6.3.3. Gla-Containing Proteins……..……..……41
I.6.3.3.1. Osteocalcin……..……41
I.6.3.3.2. Matrix Gla Protein……..……42
I.6.3.4. Serum Proteins……..……43
I.7. Bone tissue engineering…..……..……47
I.7.1. Clinical need for bone regeneration……..……..……47
I.7.2. Bone grafting……..……..……49
I.7.3. Biomaterials for bone repair……..……..……50
I.7.3.1. Bioactive inorganic materials……..……..50
I.7.3.2. Polymers……..……..……..51
I.7.3.3. Composite materials……..……51
I.7.4. Developing scaffolds in bone tissue engineering……..……..……52
I.7.4.1. Biocompatibility and biodegradation……..……..52

I.7.4.2. Mechanical properties……52
I.7.4.3. Surface properties……53
I.7.4.4. Porosity and pore size……53
I.7.5. Enhancing the functionality of the scaffolds……54
I.7.5.1. Cellular approaches……55
I.7.5.2. BMP and other growth factors……56
I.7.5.3. Bioactive peptides……57
I.7.5.4. Non-collagenous bone proteins in bone tissue engineering……57
I.7.5.4.1. Proteoglycans from bone matrix in bone tissue engineering……58
I.7.5.4.2. Glycoproteins from bone matrix in bone tissue engineering……59
I.7.5.4.2.1. Alkaline phosphatase……59
I.7.5.4.2.2. Osteonectin……59
I.7.5.4.2.3. Fibronectin and vitronectin……59
I.7.5.4.2.4. Osteopontin……60
I.7.5.4.2.5. Bone sialoprotein……61
I.7.5.4.2.6. DMP-1……62
I.7.5.4.3. Gla-containing proteins from bone matrix in bone tissue engineering……63
I.7.5.4.3.1. Osteocalcin……63
I.7.6. Mimicking the *in vivo* microenvironment of the ECM……64
I.7.6.1. ECM as a biomaterial source……64
I.7.6.2. Decellularized native tissue-derived ECM……65
I.7.6.3. Decellularized cell-derived ECM……65
I.7.6.4. Cell-derived matrices fabrication……66
I.7.6.4.1. Cell source……66
I.7.6.4.2. Cell culture methods……67
I.7.6.4.3. Decellularization techniques……68
I.7.6.5. Cell-derived ECM in bone tissue engineering……69
I.7.6.5.1. 3-D scaffolds using cell-derived ECEM for bone tissue engineering……70
I.7.6.5.2. Electrospun fibers using cell-derived ECM for bone tissue engineering……71

I.8. Animal models for bone tissue engineering……78
I.8.1. Rabbits……78
I.8.2. Rodents……80
I.9. Translating bone tissue engineering……81
I.10.References……83

CHAPTER II – The importance of osteocalcin (OC) and osteopontin (OPN) on mesenchymal stem/stromal cells (MSC): Their effects on cell proliferation, differentiation, osteogenic maturation and angiogenesis……....115

II.1. Introduction……116

II.2. Materials & Methods……...118

II.2.1. Bone marrow-derived MSC isolation……..……..……..……..……..……...……..……..…….118

II.2.2. Cell culture……..……..……..……..……..……..……..……..……..……..……..……118

II.2.3. Flow cytometry analysis……...118

II.2.4. Cell morphology……..119

II.2.5. Proliferation assays……...119

II.2.6. Multilineage differentiation assays……..……119

II.2.7. Immunofluorescent staining..……..……120

II.2.8. Calcium quantification assay……..……..120

II.2.9. Alkaline phosphatase activity……..121

II.2.10. qRT-PCR analysis……..……..121

II.2.11. *In vitro* endothelial cell tube formation assay……..…122

II.2.12. Cell migration assay……..……122

II.2.13. Raman and FTIR Spectroscopy……..……..123

II.2.14. Scanning electron microscope evaluation……..……123

II.2.15. GAG disaccharide sample preparation: isolation, digestion and AMAC-labeling……123

II.2.16. Compositional analysis of GAG disaccharides by LC-MS/MS……124

II.2.17. Statistical analysis……....……..……124

II.3 Results……125

II.3.1. Bone marrow-derived MSC isolation and characterization……..…..125

II.3.2. GAG disaccharide composition of $OC^{-/-}$ $OPN^{-/-}$ MSC……...126

II.3.3. Effects of OC and OPN on MSC proliferation ……..…128

II.3.4. Effects of OC and OPN on MSC multilineage differentiation……..……130

II.3.5. Maturation level of mineral species produced by $OC^{-/-}OPN^{-/-}$ MSC……..135

II.3.6. $OC^{-/-}$ $OPN^{-/-}$ MSC proliferation and osteogenic potential are recovered by OC/OPN supplemented extracellularly……..……138

II.3.7. Angiogenic potential of $OC^{-/-}$ $OPN^{-/-}$ MSC……..……140

II.4. Discussion……..…144

II.5. References……..……..149

CHAPTER III – Synergistic effect of extracellularly supplemented OPN and OC on stem cell proliferation, osteogenic differentiation and angiogenic properties……153

III.1. Introduction……154

III.2. Materials & Methods……..…156

III.2.1. Cell culture……156
III.2.2. BM MSC characterization ……156
III.2.2.1. Immunophenotypic analysis……156
III.2.2.2. Multilineage differentiation ability ……156
III.2.3. BM MSC proliferation……157
III.2.4. Osteogenic differentiation of BM MSC ……157
III.2.5. Calcium quantification assay……158
III.2.6. Alkaline phosphatase activity……158
III.2.7. qRT-PCR analysis……158
III.2.8. *In vitro* endothelial cell tube formation assay……159
III.2.9. Preparation of OC/OPN-enhanced scaffolds ……160
III.2.10. *In vivo* bone regeneration in a critical sized-defect rabbit long-bone model……160
III.2.11. Statistical analysis……161

III.3. Results……161
III.3.1. Exogenous effect of OPN and OC supplementation on BM MSC proliferation……161
III.3.2. Exogenous effect of OPN and OC supplementation on BM MSC osteogenic differentiation..163
III.3.3. Exogenous effect of OPN and OC supplementation on angiogenic properties of cells……165
III.3.4. Effects of OPN and OC on local inflammatory response in a critical sized-defect rabbit long-bone model ……167

III.4. Discussion……168
III.5. References……172

CHAPTER IV - Biomimetic matrices for rapidly forming mineralized bone tissue based on stem cell-mediated osteogenesis……177
IV.1. Introduction……178
IV.2. Materials & Methods……180
IV.2.1.Preparation of OC/OPN-enhanced type I collagen matrices ……180
IV.2.2. Cell culture……181
IV.2.3. *In vitro* osteogenesis on OC/OPN-enhanced collagen gels……181
IV.2.4. Cell proliferation and cell morphology ……182
IV.2.5. qRT-PCR analysis……182
IV.2.6 .Calcium quantification assay……183
IV.2.7. Alkaline phosphatase activity……183
IV.2.8. Cell migration assay……184
IV.2.9. *In vitro* endothelial cell tube formation assay……184
IV.2.10. *In vivo* bone regeneration in a critical sized-defect rabbit long-bone model……184

IV.2.11. Scanning electron microscope evaluation ……..…185
IV.2.12. Micro-computed tomography (μ-CT) evaluation……..…185
IV.2.13. Statistical analysis……...185

IV.3. Results……..…186
IV.3.1 .Effects of OC/OPN-enhanced collagen gels on MSC adhesion and proliferation……...186
IV.3.2. Effects of OC/OPN-enhanced collagen gels on osteogenic differentiation ……..189
IV.3.3..Effects of OC/OPN-enhanced collagen gels on angiogenic properties……..……191
IV.3.4. Effects of OC/OPN-enhanced collagen gels on mineralization and mineral quality ……193
IV.3.5. Effects of OC/OPN-enhanced mineralized collagen scaffolds on bone regeneration in a critical sized-defect rabbit long-bone model……...195
IV.3.6. Effects of OC/OPN-enhanced collagen gels on human MSC from different tissue sources……..198

IV.4. Discussion……...199
IV.5. References……..205

CHAPTER V – Cultured cell-derived extracelular matrices to enhance osteogenic differentiation and angiogenic properties of mesenchymal stem/stromal cells……..……..…209
V.1. Introduction……..210
V.2. Materials & Methods……..212
V.2.1. Cell culture……212
V.2.2. Decellularized cultured cell-derived ECM preparation……212
V.2.3. Immunofluorescent staining of cultured cell-derived ECM…….……213
V.2.4. Cell proliferation and osteogenic differentiation assays……..213
V.2.5. Cell morphology assay……...……..214
V.2.6. qRT-PCR analysis……....214
V.2.7. *In vitro* endothelial cell tube formation assay…….....215
V.2.8. Scanning electron microscope evaluation ……...……..215
V.2.9. Statistical analysis…….……...216

V.3. Results……..216
V.3.1. Characterization of decellularized extracellular matrix produced from MSC, HUVEC and co-culture of MSC:HUVEC……..…216
V.3.2. Decellularized cultured cell-derived extracellular matrix promotes the proliferation of BM MSC *in vitro*…….……..……221
V.3.3. Decellularized cultured cell-derived extracellular matrix promotes the osteogenic differentiation of BM MSC *in vitro*……...221
V.3.4. Decellularized cultured cell-derived extracellular matrix enhances angiogenic properties……..……..……..……...223

V.4. Discussion……...225
V.5. References……..….229

CHAPTER VI – Cell-derived extracellular electrospun fibers for bone tissue engineering applications……..……233
VI.1. Introduction……..……234
VI.2. Materials & Methods……...236
VI.2.1. Cell culture……...236
VI.2.2. Decellularized cell-derived ECM preparation……236
VI.2.3. Fabrication of cell-derived ECM electrospun PCL fibers ……..……..……236
VI.2.4.Characterization of cell-derived ECM electrospun scaffolds ……237
VI.2.4.1. Scanning electron microscopy analysis……237
VI.2.4.2. Picro-sirius red staining……..……...…237
VI.2.4.3. FTIR analysis……..……238
VI.2.4.4. Differential scanning calorimetry analysis……..……238
VI.2.4.5. Mechanical tensile testing……..……..……238
VI.2.5. Cell culture on cell-derived ECM electrospun scaffolds 238
VI.2.6. Assessment of MSC osteogenic differentiation on cell-derived ECM electrospun scaffolds…….. 239
VI.2.6.1. ALP activity assay.....239
VI.2.6.2. Calcium assay.....239
VI.2.6.3. Osteogenic staining.....239
VI.2.6.4. Energy dispersive X-ray (EDX) analysis.....240
VI.2.6.5. Quantitative real-time PCR analysis.....240
VI.2.7. Statistical analysis……...241

VI.3. Results……...242
VI.3.1. Lyophilized cell-derived ECM structural characterization……...242
VI.3.2. Cell-derived ECM electrospun scaffold characterization……243
VI.3.3. Effects of cell-derived ECM electrospun PCL fibers on cell proliferation……..……247
VI.3.4. Influence of cell-derived ECM electrospun PCL fibers on osteogenic differentiation……249
VI.3.5. Gene expression analysis……...251

VI.4. Discussion……...252
VI.5. References……256

VII. FINAL REMARKS AND FUTURE DIRECTIONS……259

LIST OF FIGURES

Figure I.1. Complex hierarchy in cortical bone, from the collagen fibril to compact bone (Rho et al. 1998). …1

Figure I.2. Bone hierarchical levels illustrated for long bones: **a)** whole bone, **b)** zoom into epiphysis structure, **c)** zoom into diaphysis structure (Mosby 2004). ……3

Figure I.3. Schematics of periosteum and endosteum. The periosteum forms the outer surface of bone, whereas the endosteum covers the medullary cavity. ……..3

Figure I.4. Cortical and trabecular bone. **a)** Human femoral head structure showing trabecular and cortical bone, **b)** Scanning electron micrograph of a section of femoral head. Adapted from (Mescher *et al.* 2010, McCloskey *et al.* 2006) ……4

Figure I.5. Mineralized fibril structure composed by collagen molecules and mineral nanocrystals. Gap and overlap regions present in the collagen molecules are responsible for the 67nm collagen banding periodicity. Mineral crystals located within the gap zones are oriented with the c-axis parallel to the collagen fibrils (Hulmes 2008). ……6

Figure I.6. Structure of the collagen triple helix: **a)** First high resolution crystal structure of a collagen triple helix, formed from $(ProHypGly)_4$-(ProHypAla)-$(ProHypGly)_5$ (Bella *et al.* 1994), **b)** Ball-and-stick image of a segment of collagen triple helix (Bella *et al.* 1994, Shoulders & Raines 2009). ……...6

Figure I.7. Collagen fibrils observed by TEM seen in the longitudinal section (Facca *et al.* 2010). Scale bar, 1.5 µm. ……7

Figure I.8. Concept of "collagen fiber" structural level. Nano and sub-nanostructure of bone hierarchy by Rho *et al.* 1998. ……..8

Figure I.9. Comparison of XRD diagram for hydroxyapatite and bovine bone. Bone diagram shows broaden of peaks (Boskey *et al.* 2003). ……..9

Figure I.10. Raman spectrum of mouse cortical bone. The regions of major bone mineral and matrix collagen can be found (Mandair *et al.* 2015). ……..12

Figure I.11. Representative Raman and FTIR spectra of bone. **a)** Raman spectrum of bone showing the PO_4^{3-} (945 cm^{-1} and 959 cm^{-1}), CO_3^{2-} (1077-1070 cm^{-1}) bands in hydroxyapatite and the amide I (1720-1616 cm^{-1} and amide III (1250 cm^{-1}) bands in collagen. **b)** FTIR spectrum of bone. The PO_4^{3-} (1200-950 cm^{-1}) and CO_3^{2-} (950-850 cm^{-1}) bands in hydroxyapatite and the amide I (1750-1600 cm^{-1}) and amide II (1600-1520 cm^{-1}) bands in collagen are indicated (Kimura-Suda *et al.* 2013). ……13

Figure I.12. Temporal gene expression during osteoblasts proliferation, differentiation, maturation and mineralization (Stein *et al.* 1990). ……..16

Figure I.13. Schematics of intramembranous ossification. Four steps are represented: **a)** Mesenchymal cells group into clusters, forming osteoblasts and ossification centers. **b)** Secreted osteoid traps osteoblasts into the matrix, differentiating into osteocytes. **c)** Trabecular matrix and periosteum form. **d)** Blood vessels condense into red marrow (Gilbert *et al.* 2000). ……18

Figure I.14. Schematic diagram of endochondral ossification. **a)** Mesenchymal stem cells differentiate into chondrocytes. **b)** Cartilage template forms. **c)** Capillaries penetrate cartilage. Primary ossification center develops. **d)** Cartilage and chondrocytes continue to grow at ends of the bone. **e)** Secondary ossification centers develop. f**)** Cartilage remains at epiphyseal plate and at joint surface as articular cartilage (Bone formation and development, Rice University). ……20

Figure I.15. Schematic diagram of bone remodeling process. Phase 1: osteoclast precursors assemble at the surface of bone and group to form osteoclasts. Phase 2: mature osteoclasts start resorption, forming a cavity. Some factors responsible for osteoblast recruitment are released by the osteoclasts. Mesenchymal stem/stromal cells migrate to the resorption site and differentiate into osteoblasts. Phase 3: osteoblasts lay down unmineralized osteoid. Phase 4: mature osteoblasts are entrapped in the mineralized matrix and form osteocytes. Abnormal remodeling due to defective cell function may result in reduced bone mass and rigidity (Feng et al. 2011). ……21

Figure I.16. Schematics of fracture healing process. **a)** Hematoma is formed in the injury site. **b)** Internal and external calli form. **c)** Cartilage of the callus is replaced by trabecular bone. **d)** Remodeling occurs. ……..23

Figure I.17. Angiogenic response during normal fracture healing. Hypoxia due to the rupture of blood vessels stimulates the production of proangiogenic factors that will recruit inflammatory cells, which contribute to the fracture healing process and produce proangiogenic cytokines. Progenitor cells then migrate to the fracture site and differentiate into cartilage and bone (Stregen *et al.* 2015). ……..25

Figure I.18. VEGF effects in endochondral ossification during bone repair. VEGF may regulate the differentiation of skeletal progenitor cells into chondrocytes or osteoblasts. In endochondral ossification, chondrocytes stop proliferating and become hypertrophic, expressing Osx that is able to induce VEGF expression. High levels of VEGF are produced and stimulate vessel invasion, facilitating the replacement of the cartilaginous template by bony callus. Moreover, osteoblast precursors expressing Osterix also produce high amounts of VEGF that stimulates their differentiation, enhancing bone formation (Hu and Olsen 2016b)……27

Figure I.19.The effects of VEGF in intramembranous ossification during bone repair. Osteoblasts release factors, such as VEGF, stimulated by hypoxia. VEGF can act through its receptors on endothelial cells, inducing angiogenesis, leading to an increase in oxygen and nutrients supply. Increased vascularization may also enhance the migration of stem cells and preosteoblasts and increase the levels of osteogenic growth factors, such as BMP produced by endothelial cells. In turn, osteoblasts also produce angiogenic factors (Hu and Olsen 2016b). ……28

Figure I.20. Synergy of angiogenesis and osteogenesis during intramembranous ossification. **a)** Effects of alterations in the VEGF levels. Physiological levels of VEGF maintain bone homeostasis. However, too little VEGF affects osteoblast differentiation and too much VEGF enhances bone resorption due to osteoclast recruitment. **b)** Osteoblasts produce VEGF that promotes migration and proliferation of endothelial cells. In turn, endothelial cells generate osteogenic growth factors, such as BMP-2 and BMP-4, important for osteogenic differentiation (Adapted from Grosso *et al.* 2017). ……29

Figure I.21. Different strategies to improve vascularization of bone grafts: delivery of angiogenic growth factors, use of endothelial cells to create a vascular network and engineering scaffold properties (Stegen *et al.* 2015). ……30

Figure I.22. Organic components of the bone extracellular matrix. ……32

Figure I.23. Schematic diagram representing the organization of collagen molecules reinforced with calcium phosphate nanocrystals, proteins and growth factors arranged in a semi-regular pattern. ……33

Figure I.24. Proportion of the world population aged 60 years or more. With advances in medicine helping to increase life expectancy, the number of people over the age of 60 is expected to double by 2050 (UNDESA Population Division, World population prospects: the 2015 revision, DVD Edition, 2015). ……..48

Figure I.25. Bone autograft. ……48

Figure I.26. Different bone graft materials used in bone tissue engineering. β-TCP ceramics, hydroxyapatite-based materials and bioactive glasses (Adapted from Stevens *et al.* 2008). ……50

Figure I.27. Hierarchical organization of bone over different length scales. Collagen molecules and hydroxyapatite crystals are organized at the nanoscale level (Stevens and George 2005). ……...51

Figure I.28. Functionalization of 3-D scaffolds for bone regeneration. Different strategies rely on morphological properties, control delivery of bioactive factors and tailoring of the degradation rate (Fernandez-Yague *et al.* 2015). ……...54

Figure I.29. Schematics of different types of scaffolds and strategies that can be applied in bone tissue engineering applications (Fernandez-Yague *et al.*2015). ……..55

Figure I.30. Composition of extracellular matrix (Punjabia et al. 2014). ……64

Figure I.31. Common culture methods used to produce decellularized cell-derived ECM. Cells can be cultured in monolayers and deposit a layer of matrix . To obtain thicker cell-derived ECM, cells can be embedded in a degradable carrier material. Therefore, over time, the degradable material will be replaced by the ECM deposited by the cells (3-D ECM construct after decellularization). Cells can be cultured as aggregates also producing a 3-D ECM. Cells can be cultured on the surface of scaffolds, allowing the matrix to be deposited and decellularization process will remove the cellular components, improving the bioactivity of the scaffold (Fitzpatrick *et al.* 2015). ……...68

Figure I.32. Application of nanofiber-based scaffolds fabricated by electrospinning in the human bod (Liu *et al.* 2012). ……73

Figure I.33. Schematic of electrospinning technique (Wang *et al.* 2013c). ……74

Figure I.34. The electrospinning process. Photograph showing the nozzle where the polymer solution is pumped through. A droplet forms on the nozzle tip, which adopts a conical shape due to the electrical field. Therefore, the fiber forms and is deposited into the collector (Hinderer *et al.* 2016). ……...74

Figure I.35. Bone defect models. a) Calvarial defect, b) Segmental defect, c) Burr hole defect (McGovern *et al*. 2018). ……78

Figure I.36. Surgical protocol for the implantation of a PLGA/TCP/icaritin substitute biomaterial in a rabbit model. **a)** The surgical site is exposed. **b)** A tunnel is drilled through the distal femora. **c,d)**The biomaterial is implanted into the bone tunnel. **e-g)** Microcomputed tomography of the bone defect site. **h)** X-ray image of the bone defect site (Wang *et al.* 2013b). ……...79

Figure I.37. Advances in bone tissue engineering field. **a)** Published articles on bone tissue engineering since mid-1980s in PubMed. **b)** Bone tissue engineering research has focused on different areas, such as biomolecules, cells, matrices and other, including vascularization approaches or bioreactors. Division of the articles published in 2011 according to bone engineering focus (Amini et al. 2012). ……...81

Figure I.38. The Valley of Death for tissue engineering applications. The Valley is created due to the lack of funds to develop scalable/GMP design and manufacturing process and to do large clinical studies to evaluate the safety and efficacy of the product, making it difficult to translate tissue engineering technologies into tissue-engineered products (Adapted from Hollister 2009). ……..……...82

Figure II.1. Bone marrow-derived MSC isolation and characterization. **a)** Schematics of BM-MSC isolation from femur and tibia of $OC^{-/-}$ $OPN^{-/-}$ and WT mice. **b)** Cell morphology after 24h and 4 days of culture. Red: phalloidin, blue: DAPI. Scale bars, 100 µm. **c)** Percentage of cell expression of CD29, CD105, Sca-1 and CD45. **c)** Relative expression levels of *OPN* and *OC* genes in $OC^{-/-}$ $OPN^{-/-}$ MSC compared to WT MSC. ……..……125

Figure II.2. GAG composition of WT MSC and $OC^{-/-}OPN^{-/-}$ MSC. Total GAG **(a)** and HS, CS, HA total amounts **(b)**. Results are presented as mean ± SD of three biological replicates (n=3).……..……...126

Figure II.3. Average relative percentage GAG composition of WT and $OC^{-/-}OPN^{-/-}$ MSC before and after osteogenic differentiation. Results are presented as mean ± SD of three biological replicates (n=3)……..127

Figure II.4. Average relative percentage HS **(a)** and CS **(b)** composition of the different cell types: WT and $OC^{-/-}$ $OPN^{-/-}$ MSC before and after osteogic differentiation. Results are presented as mean ± SD of three biological replicates (n=3).……128

Figure II.5. Proliferation studies of $OC^{-/-}OPN^{-/-}$ and WT MSC. **a,b)** Fold increase **(a)** and cumulative population doublings **(b)** when cells were seeded at 3000 cells/cm^2. **c,d)** Fold increase **(c)** and cumulative population **(d)** when cells were seeded at 10000 cells/cm^2. **e)** Kinetic study during 15 days of cell culture. Data are expressed as mean ± SD; **p<0.01; *p<0.05. ……..……...129

Figure II.6. Multilineage differentiation of $OC^{-/-}OPN^{-/-}$ and WT MSC evaluated by immunohistochemistry. **a)** Adipogenic differentiation after 7 and 15 days (FABP4). **b)** Chondrogenic differentiation after 15 and 21 days (Col II). **c)** Osteogenic differentiation after 7, 15 and 21 days (OPN). Scale bars, 100 µm. ……..131

Figure II.7. OC/OPN-deficiency impairs MSC osteogenic differentiation. **a)** WT and $OC^{-/-}OPN^{-/-}$ MSC were cultured in adipogenic (7 days), osteogenic and chondrogenic differentiation medium (21 days) and stained with Oil Red O to reveal lipid droplets, ALP and Von Kossa stainings to detect mineralization and Alcian Blue to detect glycosaminoglycans. **b)** ALP activity was evaluated after 7, 15 and 21 days of osteogenic differentiation. **c)** Calcium deposits were quantified after 7, 15 and 21 days of osteogenic differentiation. **d,e)** MSC from WT **(d)** and $OC^{-/-}OPN^{-/-}$ **(e)** were cultured in osteogenic differentiation medium for the indicated number of days and calcium deposits were revealed by Xylenol Orange stain (red) (blue:DAPI). Scale bars, 100 µm. Values are means ± SD. **p<0.01 (n=3). ……..……132

Figure II.8. Osteogenic differentiation of $OC^{-/-}OPN^{-/-}$ MSC and WT MSC. **a)** SEM micrographs showing morphology and mineralization of $OC^{-/-}OPN^{-/-}$ and WT MSC after 15, 21 and 30 days of osteogenic differentiation. Scale bars, 4 µm. **b)** EDX microanalysis of mineral nodules from $OC^{-/-}OPN^{-/-}$ MSC after 21 days of osteogenic differentiation. Scale bar, 1 µm. **c)** EDX microanalysis of mineral nodules from WT MSC after 21 days of osteogenic differentiation. Scale bar, 1 µm. ……..……..133

Figure II.9. Gene expression analysis of $OC^{-/-}OPN^{-/-}$ MSC after osteogenic differentiation. WT and $OC^{-/-}OPN^{-/-}$ MSC cultured in osteogenic differentiation medium for the indicated times were analyzed for **a)** Runx2, **b)** Col I, **c)** ALP, **d)** OPN and **e)** OC by qRT- PCR. **p<0.01; *p<0.05 (n=3) . ……134

Figure II.10. Spectroscopy analysis of WT MSC and $OC^{-/-}OPN^{-/-}$ MSC after 21 days of osteogenic differentiation. **a)** FTIR spectra of the WT MSC and $OC^{-/-}OPN^{-/-}$ (KO) MSC without differentiation (no osteo) and after 21 days of differentiation (osteo). The characteristic peaks of amide I (1645cm^{-1}) and amide II (1550 cm^{-1}), carbohydrates, amino acids and lipids can be found. **b)** Raman spectra of WT and $OC^{-/-}OPN^{-/-}$ MSC (KO) after differentiation. Peaks related to cellular components are marked in grey and the region of mineral species was marked in yellow (apatite). KO MSC did not present the apatite peak. ……..135

Figure II.11. Raman spectra of mineral species produced by WT and $OC^{-/-}OPN^{-/-}$ MSC after 15, 21 and 30 days of osteogenic differentiation. **a,c,e)** complete view from 600 to 1500 cm^{-1}, **b,d,f**) the region of mineral species from 900 to 1000 cm^{-1}. ……137

Figure II.12. Effects of OC/OPN supplemented extracellularly on $OC^{-/-}OPN^{-/-}$ MSC proliferation and osteogenic potential. **a)** Proliferation of $OC^{-/-}OPN^{-/-}$ MSC exogenously supplemented with OC and/or OPN (1µg/ml). **b)** Calcium quantification of $OC^{-/-}OPN^{-/-}$ MSC differentiated during 21 days with osteogenic medium

supplemented with OC/OPN (1µg/ml). **c)** Calcium deposits from $OC^{-/-}OPN^{-/-}$ MSC supplemented with OC/OPN were visualized using Xylenol Orange (red) (blue:DAPI). **d)** Comparison of Raman spectrum of WT, $OC^{-/-}OPN^{-/-}$ and $OC^{-/-}OPN^{-/-}$ MSC extracellularly supplemented with OC/OPN. Scale bars, 100 µm. Values are means ± SD. **p<0.01.*p<0.05, compared to $OC^{-/-}OPN^{-/-}$ (n=3) ……..……139

Figure II.13. OC/OPN-deficiency impairs angiogenic properties of MSC. **a)** Tube formation assay evaluating the HUVEC's response to conditioned medium (CM) from $OC^{-/-}OPN^{-/-}$ MSC after 8h post-seeding. **b)** Number of tubular-like structures formed by HUVEC in the tube formation assay. **c)** Migration assay evaluating the HUVEC's migratory response to CM from $OC^{-/-}OPN^{-/-}$ after 4, 8, 10 and 12h. **d)** Quantification of the HUVEC's percentage of migration after different timepoints when exposed to different conditioned medium from WT and $OC^{-/-}OPN^{-/-}$ MSC. DMEM+10% FBS and endothelial growth medium-2 (EGM-2) were used as a positive control and DMEM basal as a negative control. Scale bars, 100 µm. Values are mean ± SD. **p<0.01; *p<0.05 compared with EGM-2 (positive control) (n=3). ……..……..141

Figure II.14. Angiogenic properties of $OC^{-/-}OPN^{-/-}$ MSC. **a)** $OC^{-/-}OPN^{-/-}$ MSC were not able to form a tubular structure in matrigel, compared with WT MSC. **b**) Co-culture of $OC^{-/-}OPN^{-/-}$ MSC with HUVEC were not able to support tubular structure formed by HUVEC. **c)** Co-culture of $OC^{-/-}OPN^{-/-}$ MSC with HUVEC supplemented with OC and/or OPN and VEGF. Scale bars, 100 µm. **d)** Quantification of number of tubular-like structures formed by HUVEC co-cultured with $OC^{-/-}OPN^{-/-}$ (KO) MSC supplemented with OC and/or OPN and VEGF. Values are expressed as mean ± SD. **p<0.01; *p<0.05, compared to HUVEC (n=3) ……..……143

Figure III.1. Human BM MSC characterization. **a)** BM MSC ability to differentiate into osteoblasts, adipocytes and chondrocytes was evaluated. **b)** BM MSC were tested for expression of cell surface markers indicative of MSC (i.e., $CD73^+$, $CD90^+$, $CD105^+$, $HLA\text{-}DR^-$, $CD34^-$, $CD45^-$). **c)** Population doublings of BM MSC expanded at P3, P4 and P5. ……..……..……161

Figure III.2. Exogenous effect of OPN and OC supplementation on BM MSC proliferation. **a)** Effect of OPN on BM MSC proliferation. OPN dose dependently increased BM MSC proliferation activity, with a peak at concentration of 1 µg/ml OPN. **b)** Effect of OC on BM MSC proliferation. OC did not affect BM MSC proliferation activity. No significant differences in proliferation were observed between control and BM MSC treated with OC. **c)** Synergistic effect of OC and OPN on BM MSC proliferation. Cells were seeded at 3000 cells/cm^2. **d)** Fold Increase and Population Doublings of BM MSC pre-treated with OC and/or OPN (1 µg/ml OC and/or 1 µg/ml OPN) for 10 days. Data are presented as mean ± SD. n=3. *p<0.05;**p<0.01, compared with the control (0 µg/ml). ……162

Figure III.3. Exogenous effect of OPN and OC supplementation on BM MSC osteogenic differentiation. **a)** Following treatment with OPN, OC and OC+OPN (1 µg/ml OC and/or 1 µg/ml OPN), osteogenic differentiation of BM MSC was analyzed. Xylenol (red) orange stained calcium minerals in cell culture treated with OC/OPN (blue: DAPI). Osteogenic differentiation and mineralization were detected after 21 days of differentiation. **b)** ALP activity and calcium quantification were enhanced when cells were treated with OC and OC+OPN. **c)** In addition, the mRNA levels of the osteogenic markers Coll, Runx2, OPN and OC were also analyzed by qRT-PCR. **d)** ALP and Von Kossa staining confirmed the osteogenic differentiation after 21 days**.** OC triggered the

mineralization and osteogenic differentiation of BM MSC, since the treatment with OC and OC+OPN increased ALP activity, calcium deposits and mRNA levels of some osteogenic genes **(b, c)**. Data are presented as mean ± SD. n=3. **p<0.01;*p<0.05. Scale bars, 100 μm. ……164

Figure III.4. Exogenous effect of OPN and OC supplementation on angiogenic properties of HUVEC in a dose-dependent study. Tube formation assays were performed **(c)** with the indicated doses of OPN and OC and the number of tubes formed was quantified **(a, c). (a,c)** OPN stimulated the *in vitro* formation of tubular-like structures by HUVEC treated with dose equal or higher than 0.5 μg/ml. **(b,c)** OC did not affect angiogenic properties of HUVEC *in vitro*. Data are presented as mean ± SD. **p<0.01;*p<0.05. Scale bars, 100 μm....165

Figure III.5. Effect of OPN and OC on cell angiogenic properties. **a)** Tube formation assay with conditioned medium from BM MSC and from BM MSC treated with OPN, OC or both OC+OPN. Positive control is HUVEC in endothelial growth medium and negative control is the basal medium (no angiogenic factors). **(b,c)** Quantification of number of tubular-like strcutures **(b)** and branch points **(c)** formed. OPN elicited a pro-angiogenic activity. **d)** VEGF expression levels of BM MSC treated with OC, OPN and OC+OPN for 72h. BM MSC treated with OPN and OC+OPN demonstrated a statistically significant increase in VEGF gene expression. Data are presented as mean ± SD. n=3. **p<0.01; *p<0.05. Scale bars, 100μm. ……166

Figure III.6. Effect of OPN/OC-enhanced scaffold on local inflammatory response and bone formation in vivo. **a)** Representative histological images of the rabbit critical sized-defect at 6 weeks postimplantation. Hematoxylin and Eosin (H&E), Goldner's Trichrome (GT), Von Kossa (VK), Toluidine Blue (TB). Black squares represent the area of new bone formed. **b)** Goldner's Trichrome straining demonstrated new bone formed surrounding the scaffold with connective tissue between the scaffold and new bone. **c)**Tartrate-resistant acid phosphatase (TRAP) staining indicated the presence of osteoclasts between the scaffold region, representing bone remodeling. NB – new bone; CT – connective tissue; S – scaffold. Scale bars, 100 μm. ……..168

Figure IV.1. Design of the biomimetic OC/OPN-enhanced collagen matrices. **a)** Schematic of OC/OPN-enhanced collagen gels. **b)** Schematic of fabrication of OC/OPN-enhanced mineralized collagen scaffolds. **c)** Different concentrations of OC and OPN incorporated into type I collagen gels at 3 mg/ml to create biomimetic matrices, based on the average of OC recovered from human bone (Cairns and Price 1994). Cell proliferation, osteogenic differentiation, mineralization and angiogenesis were the different variables evaluated after cell culture on OC/OPN-enhanced collagen gels. **d)** Left: Representation of the OC/OPN-enhanced mineralized collagen scaffold implanted into a rabbit tibia after 6 weeks of surgery. Right: OC/OPN-enhanced mineralized collagen scaffolds prior to implantation into a rabbit model. ……...186

Figure IV.2. SDS-PAGE protein gel of collagen gel, OC-collagen gel, OPN-collagen gel and OC/OPN-collagen gel confirms the presence of OC/OPN in the matrices. ……...187

Figure IV.3. *In vitro* OC and OPN release from OC/OPN-enhanced collagen gels. OC and OPN levels in PBS were determined by ELISA measurements after 24h and 21 days. Results demonstrated that the biomimetic gels did not release OC and OPN proteins, being able to maintain the proteins on the gel. ……187

Figure IV.4. Effects of OC/OPN-enhanced collagen gels on cell proliferation and osteogenic differentiation of BM MSC. **a)** Fluorescence microscopy images of DAPI (blue) and Phalloidin (red) of BM MSC seeded on top of different substrates 24h and 15 days after cell seeding (OC/OPN #1) under DMEM+10%FBS. Scale bar, 100 μm. **b,c)** Proliferation of BM MSC cultured on OC/OPN-enhanced collagen gels for 15 days under **(b)** DMEM+10%FBS and **(c)** osteogenic differentiation medium. **d)** Percentage of maximum gene expression (collagen I [ColI], runx2, osteopontin [OPN], osteocalcin [OC] and alkaline phosphatase [ALP]) by BM MSC upon culture for 7, 15 and 21 days on control collagen gels and OC/OPN-enhanced collagen gels. Data are expressed as mean ± SD, **p<0.01; *p<0.05. ……..188

Figure IV.5. Relative gene expression (collagen I [Col I], runt-related transcription factor 2 [Runx2], osteopontin [OPN], osteocalcin [OC] and alkaline phosphatase [ALP]) by BM MSC upon culture for 7, 15 and 21 days on control collagen gels, OPN-enhanced collagen gels, OC-enhanced collagen gels and OC/OPN-enhanced collagen gels. Data are expressed as mean ± SD, **P<0.01; *P<0.05, relative to day 21 (Col I, Runx2, OPN, OC) and day 7 (ALP). ……...190

Figure IV.6. Effects of OC/OPN- enhanced collagen gels on BM MSC *in vitro* angiogenic properties assessed by multiple assays. **a)** Cell migration assay. Scratch at t=0h, t=8h and t=24h when HUVEC were treated with EGM-2 (positive control), conditioned medium from BM MSC cultured on control collagen gels and conditioned medium from BM MSC cultured on OC/OPN-enhanced collagen gels. Borders of the scratch at t=0 are indicated with solid lines, borders after migration at t=8 and t=24 hours with dashed lines. **b)** Percentage of migration distance quantification of HUVEC treated with conditioned medium from BM MSC cultured on control collagen gels, OC-collagen gels, OPN-collagen gels and OC/OPN-collagen gels. **c)** VEGF relative expression of BM MSC cultured on OC/OPN-enhanced collagen gels, OC-enhanced collagen gels, OPN-enhanced collagen gels and control collagen gels after 21 days of culture under osteogenic differentiation, normalized to VEGF relative expression of undifferentiated BM MSC. **d-f)** Endothelial cell tube formation assay: **(d)** Tube formation of HUVEC on a Matrigel substrate incubated with EGM-2 (positive control), EBM-2 (negative control) and conditioned medium from BM MSC cultured on collagen gels, OC-collagen gels, OPN-collagen gels and OC/OPN-collagen gels. **e-f)** Number of tubes/field **(e)** and number of branch points/field **(f).** Scale bars, 100μm. Data are expressed as mean ± SD, **p<0.01; *p<0.05**. …….**192

Figure IV.7. Micrographs of BM MSC before and after osteogenic differentiation on OC/OPN-enhanced collagen gels (OC/OPN #1) and control collagen gels. Scale bars, 100 μm. ……..193

Figure IV.8. Effects of OC/OPN-enhanced collagen gels on BM MSC mineralization and ALP activity. **a)** Calcium content quantification of BM MSC on OC/OPN-enhanced collagen gels cultured for 21 days. **b)** Mineralized nodules of MSC after 21 days of culturing in osteogenic differentiation medium on OC/OPN-enhanced collagen gels and control collagen gels without OC/OPN incorporation. The nodules were visualized by Xylenol orange staining. Scale bars, 100 μm. **c-e)** SEM images of BM MSC cultured on OC/OPN-enhanced collagen gels. **c)** OC/OPN-enhanced collagen gels before cell culture, **d,e)** BM MSC mineralization of OC/OPN-enhanced collagen gels after 21 days of osteogenic differentiation. **f)** EDS

spectrum of mineral deposition of BM MSC cultured on OC/OPN-enhanced collagen gels. **g)** ALP activity of BM MSC cultured on OC/OPN-enhanced collagen gels for 15 days and 21 days of differentiation. Data are expressed as mean ± SD, **p<0.01; *p<0.05. ……..……..194

Figure IV.9. Microcomputed tomography images of OC/OPN-enhanced mineralized collagen scaffolds. Scale bars, 1 mm. Reddish areas demonstrate the mineral distribution throughout the scaffold ..……195

Figure IV.10. OC/OPN-enhanced mineralized collagen scaffolds before being implanted into a rabbit model.……195

Figure IV.11. Bone regeneration in a critical sized-defect rabbit long-bone model using OC/OPN-enhanced mineralized collagen scaffolds**. a)** Representative histological images of the rabbit critical sized-defect at 6 weeks postimplantation. Hematoxylin and Eosin (H&E), Goldner's Trichrome (GT), Von Kossa (VK), Toluidine Blue (TB) and Tartrate-resistant acid phosphatase (TRAP) stainings. Panels on the first row are at 100x magnification. Black squares represent the area of new bone formed. Dashed squares represent the area of the implanted scaffold. Scale bars, 100 μm. Panels on the second row are at 200x magnification and represent the area of new bone formation (black squares). Scale bars, 50 μm. Panels on the third row are at 200x magnification and represent the area nearby the implanted scaffold (dashed squares). Black arrows outline the osteoblasts covering the new bone formed. Black arrowheads represent the osteoclasts by TRAP staining, indicating a possible remodeling of bone. White circle represents new vessels formed. Scale bars, 50 μm. **b)** Representative microcomputed tomography images of bone regeneration in the rabbit model at 6 weeks postimplantation. Top row represents a tibial defect, bottom row represents a femoral defect. Scale bars, 1 mm. **c)** Goldner's trichrome staining – detailed investigation. Detailed description of new bone formation within the OC/OPN-enhanced mineralized collagen scaffolds. NB – new bone; CT – connective tissue; S – scaffold. Scale bars, 100 μm. ……...197

Figure IV.12. Proliferation and mineralization of human MSC from different tissue sources cultured on OC/OPN-enhanced collagen gels. **a)** Proliferation of MSC from BM, AT and UCM on OC/OPN-collagen gels after 15 days of culture. **p<0.01; *p<0.05 relative to the control group for each cell source **b)** Calcium quantification of MSC from BM, AT and UCM cultured on OC/OPN-enhanced collagen gels after 21 days of osteogenic differentiation. Data are expressed as mean ± SD, **p<0.01; *p<0.05 relative to the control group for each cell source **c)** Summary of statistically significant differences between each different composition of OC/OPN and control collagen gels, OC-collagen gels and OPN-collagen gels for each cell source (BM, AT, UCM), regarding cell number and calcium quantification after 15 days of culture. **p<0.01, *p<0.05 relative to control collagen gel; ++p<0.01, +p<0.05 relative to OC-collagen gel; ##p<0.01, #p<0.05 relative to OPN-collagen gel; n.s. – not significant. ……..198

Figure V.1. Schematics of decellularization of cultured cell-derived ECM (dECM) derived from BM MSC and HUVEC cultures and co-cultures of BM MSC:HUVEC at different ratios (1:1; 3:1; 1:3). After decellularization, BM MSC were reseeded onto the various dECM and cell proliferation, osteogenic differentiation and angiogenic properties were evaluated…….216

Figure V.2. Characterization of dECM derived from BM MSC and HUVEC cultures and co-cultures of BM MSC:HUVEC at different ratios (1:1;3:1;1:3). Phase contrast microscopy images and DAPI/phalloidin stainings taken before and after decellularization with 20mM NH_4OH + 0.5% Triton solution confirmed the decellularization process. Red: Alexa Fluor® 594 phalloidin; Blue: DAPI. Scale bars, 100 μm. …….....218

Figure V.3. Comparison of dECM derived from MSC, HUVEC, MSC:HUVEC 1:1, MSC:HUVEC 3:1 and MSC:HUVEC 1:3. Immunofluorescent staining images of collagen I, collagen IV, laminin, fibronectin and osteocalcin showed different distribution of the ECM proteins after decellularization. Red: NothernLights™ 557 donkey anti-sheep antibody; Blue: DAPI. Scale bar, 100 μm. ……..…219

Figure V.4. Morphology and cell distrivution of HUVEC when co-cultured with BM MSC at different ratios, before decellularization protocol. When HUVEC were co-cultured with MSC at ratio 1:3 (MSC:HUVEC 1:3), HUVEC rearranged as a capillary-like structure. Scale bars, 200 μm. ……..……219

Figure V.5. Scanning electron microscopy (SEM) images of dECM derived from BM MSC and HUVEC cultures and co-cultures of BM MSC: HUVEC at different ratios (1:1; 3:1; 1:3) after the decellularization protocol. Scale bars, 1 μm. ……..……...220

Figure V.6. *In vitro* proliferation and morphology of BM MSC cultured on different substrates produced by cell-derived ECM. **a)** Numbers of BM MSC cultured on dECM obtained from different cell types and on TCP (No ECM-control). **b)** Representative photomicrographs showing the morphology of BM MSC seeded on dECM and on TCP on day 7. Red: Phalloidin; blue: DAPI. Scale bars, 100 μm. Data are expressed as mean ± SD, **p<0.01; *p<0.05 (n=3). ……..……221

Figure V.7. Osteogenic differentiation of BM MSC on the different dECM substrates obtained. **a)** Representative images of BM MSC stained with alkaline phosphatase (ALP) and Von Kossa (VK) dyes after 21 days of osteogenic induction. **b)** ALP activity of BM MSC differentiated on dECM and TCP (No ECM) after 21 days of osteogenic differentiation. **c)** Calcium quantification of BM MSC differentiated after 21 days on dECM and TCP. **d)** qRT-PCR analysis for determination of the expression of osteogenic genes after 21 days of culture under osteogenic conditions. **e)** Cell morphology of BM MSC differentiated under osteogenic culture medium on different dECM and TCP after 21 days of differentiation. Red: Phalloidin; blue: DAPI. Scale bars, 100 μm. Data are expressed as mean ± SD, **p<0.01; *p<0.05 (n=3). ……..……..222

Figure V.8. The angiogenic promoting effects of the different dECM were investigate by evaluating HUVEC response to conditioned medium from BM MSC cultured on the different substrates: MSC ECM, HUVEC ECM, MSC:HUVEC (1:1) ECM, MSC:HUVEC (3:1) ECM, MSC:HUVEC (1:3) ECM. **a)** Tube formation assay of HUVEC cultured on Matrigel with conditioned medium produced from BM MSC seeded on different dECM and TCP (No ECM, control) after 8h. HUVEC were cultured with VEGF supplemented EGM on Matrigel as a positive control. **b)** Quantification of number of tubes formed by HUVEC on Matrigel cultured with conditioned medium derived from BM MSC cultured on different dECM and TCP after 8h. Scale bars, 100 μm. Data are expressed as mean ± SD, *p<0.05. ……..…224

Figure VI.1. The schemata of the experimental procedure for the fabrication of cell-derived ECM microfibrous scaffolds. ……...237

Figure VI.2. SEM images **(a)** and FTIR spectra **(b)** of the different cell-derived ECM powders. Asterisks and pound symbols are used to indicate the unique peaks in the MSC and HUVEC spectra respectively. All four of these unique peaks can also be seen in the IR spectrum of MSC-HUVEC ECM mixture. Scale bars, 10 μm. ……242

Figure VI.3. Characterization of cell-derived ECM PCL electrospun scaffolds. **a)** SEM images show the presence of ECM on PCL scaffolds. Scale bars, 5 μm. **b)** Fiber diameter distribution of cell-derived ECM PCL electrospun scaffolds. **c)** Pricosirius red staining confirms the presence of collagens in the cell-derived ECM PCL scaffolds, validating the presence of ECM. Scale bars, 50 μm. ……244

Figure VI.4. Mechanical properties of cell-derived ECM PCL scaffolds, obtained after tensile testing. **a)** Representative stress-strain curves. **b)** Elastic modules (MPa). **c)** Ultimate tensile strength (UTS) (MPa). **d)** Elongation. Five different samples (n=5) were used in the analysis. Values are mean ± SD. ……..……245

Figure VI.5. FTIR spectra of the different cell-derived ECM PCL electrospun scaffolds and PCL control scaffolds…….. ……...246

Figure VI.6. DSC thermograms respective to the heating cycle **(a)** and cooling cycle **(b)** of the different cell derived-ECM electrospun scaffolds. Obtained melting **(a)** and crystallization temperatures **(b)** for the different cell derived-ECM electrospun scaffolds are indicated in the respective thermograms. ……..246

Figure VI.7. Effects of cell-derived ECM PCL scaffolds on MSC proliferation. Cell proliferation assay **(a)** and cell morphology assessment by DAPI/Phalloidin staining at day 21 **(b)**. Values are expressed as mean ± SD; **p<0.01. Scale bars, 100 μm ……..……..248

Figure VI.8. SEM morphological analysis of MSC cultured under osteogenic differentiation induction in the different cell-derived ECM electrospun scaffolds at days 7, 14 and 21. Scale bars, 50 μm. ……248

Figure VI.9. Osteogenic differentiation of MSC cultured on cell-derived ECM electrospun fibers. **a)** ALP activity of MSC cultured on cell-derived ECM PCL scaffolds after 14 and 21 days of osteogenic differentiation. **b)** Calcium deposition quantification of MSC seeded on cell-derived ECM PCL scaffolds after 14 and 21 days of osteogenic differentiation. **c)** Alizarin red, ALP and Von Kossa stainings of MSC differentiated on cell-derived ECM scaffolds after 21 days. Alizarin red and Von Kossa confirmed the presence of calcium deposits (reddish and darker areas, respectively). ALP staining demonstrated ALP activity of MSC cultured on all PCL scaffolds. Scale bars, 200 μm. Values are expressed as mean ± SD, **p<0.01; *p<0.05. ……..……250

Figure VI.10. Xylenol orange staining demonstrated calcium deposits after 21 days of osteogenic differentiation. Xylenol orange (red) and DAPI (blue). Scale bars, 100 μm……..…250

Figure VI.11. Morphology and elemental composition analysis of MSC cultured on cell-derived ECM PCL electrospun fibers and PCL electrospun fibers after 21 days of osteogenic differentiation. **a)** SEM images and respective magnification (blank square). **b)** EDS spectrogram for the different cell-derived ECM electrospun scaffolds. Scale bars, 10 μm. ……..…….……251

Figure VI.12. Effects of cell-derived ECM-PCL microfibrous scaffolds on the gene expression of ALP, Runx2, OPN and VEGF of MSC. *p<0.05, **p<0.01 relative to PCL scaffold expression. ……252

LIST OF TABLES

Table I.1. Comparison between different structural and mechanical properties of cortical and trabecular bone. (Adapted from Weiner & Traub 1992, Rho et al. 1998). ……..…4

Table I.2. Angiogenesis-stimulating growth factors. (Adapted from Stregen *et al.* 2015). ……..24

Table I. 3. Proteoglycans in Bone Matrix: protein functions and *in vivo* studies. ……..44

Table I.4. Glycoproteins in Bone Matrix: protein functions and *in vivo* studies. ……..…45

Table I.5. γ Carboxy Glutamic Acid-Containing Proteins in Bone Matrix: protein functions and *in vivo* studies. ……..46

Table I.6. Methods for decellularization of cell-derived bone ECM (Adapted from Cheng *et al.* 2015). ……...69

Table I.7. Summary of decellularized ECM electrospun scaffolds for cartilage and bone tissue engineering applications (Adapted from Elmashhady et al. 2017). ……77

Table I.8. Examples of rabbit bone defect models for testing bone substitute grafts. ……..79

Table I.9. Summary of some examples of rodent bone defect models for testing new substitute biomaterials……80

Table II.1. Sequences of primers used for qRT-PCR analysis. ……121

Table III.1. Sequences of primers used for qRT-PCR analysis. ……159

Table IV.1. Sequences of primers used for qRT-PCR analysis ……183

Table V.1. Sequences of primers used for qRT-PCR analysis ……..215

Table VI.1. Sequences of primers used for qRT-PCR analysis ……241

Table VI.2. Summary of elastic modulus, ultimate tensile strength (%) and ultimate elongation values obtained for the different cell-derived ECM electrospun scaffolds after mechanical tensile testing. Values are expressed as mean ± SD of five independent samples analyzed. ……247

ABBREVIATIONS

#

2-D – Two-Dimensional
3-D – Three – Dimensional
β-TCP - β- Tricalcium Phosphate
µCT – Micro-Computed Tomography

A
A/A – Antibiotic/Antimycotic
ACP – Amorphous Cacium Phosphate
AFM – Atomic Force Microscopy
ALP – Alkaline Phosphatase
Ang-1 – Angiopoeitin-1
AR – Alizarin Red
AT – Adipose Tissue
ATR-FTIR – Attenuated total reflectance - Fourier transform infrared
Au - Gold

B
bFGF – basic Fibroblast Growth Factor
BGLAP – Bone Gama Carboxyglutamic acid-Containing Protein
BM – Bone Marrow
BMP – Bone Morphogenetic Proteins
BMU – Bone Multicellular Unit
BSA – Bovine Serum Albumin
BSP – Bone sialoprotein

C
Ca – Calcium
$CaCl_2$ – Calcium chloride
$Ca_{10}(PO_4)_6(OH)_2$ – Hydroxyapatite
CBFA1 – Core-Binding Factor Alpha-1
CM – Conditioned Media
CO_2 – Carbon Dioxide
Col I – Collagen type I
Col II – Collagen type II
CS – Chondroitin Sulfate
CT – Connective Tissue
Cx43 – Connexin 43

D
DAPI – 4, 6- diamidino-2-phenylindole
DBM – Demineralized Bone Matrix
DCPD – Dicalcium Phosphate Dehydrate
dECM – decellularized Extracellular Matrix
DMEM – Dubecco's Modified Eagle Medium
DMP – Dentin Matrix Protein
DNA – Deoxyribonucleic Acid
DS – Dermatan Sulfate
DSC – Differential Scanning Calorimetry
DSPP – Dentin Sialophosphoprotein

E
EC – Endothelial Cells
ECM – Extracellular Matrix
EDX – Energy Dispersive X-Ray
EGM-2 – Endothelial Growth Medium-2
ESC – Embryonic Stem Cell

F
FABP4 – Fatty Acid Binding Protein 4
FACS – Fluorescent Activated Cell Sorting
FBS – Fetal Bovine Serum
FDA – Food and Drug Administration
FGF - Fibroblast Growth Factor
FI – Fold Increase
FN - Fibronectin
FTIR – Fourier-Transform Infrared

G
GAG – Glycosaminoglycan
GAPDH – Glyceraldehyde 3- Phosphate Dehydrogenase
Gly – Glycine
GT – Goldner's Trichrome

H
HA – Hyaluronan
HAP - Hydroxyapatite
HCL – Hydrochloric Acid
H&E – Hematoxylin &Eosin
HFIP – 1,1,1,3,3,3-hexafluoro-2-propanol
HGF – Hepatocyte Growth Factor
HIF-1α – Hypoxia Inducible Factor -1 α
HS – Heparin Sulfate
HSC – Hematopoietic Stem Cells
HUVEC – Human Umbilical Vein Endothelial Cell

I
IACUC – Institutional Animal Care and Use Committee
IGF – Insulin Growth Factor
IL – Interleukin
iPSC – Induced Pluripotent Stem Cell
IR – Infrared
IRE – Internal Reflection Element

K
KO – Knockout
KS – Keratan Sulfate

L
LC-MS/MS – Liquid Chromatography-Tandem Mass Spectrometry

M
MCP – Monocyte Chemotactic Protein-1
M-CSF – Macrophage Colony-Stimulating Factor
MGP – Matrix Gla Protein
Micro-CT – Micro Computed Tomography
MMP – Matrix MetalloProteinase
mRNA – messenged Ribonucleic Acid
MSC – Mesenchymal Stem/Stromal Cells
MRM – Multiple Reaction Monitoring

N
NaCl – Sodium Chloride
Na_2HPO_4 – Sodium Phosphate dibasic
NB – New Bone
nBG – nanoBioactive Glass
N-CAM – Neural Cell Adhesion Molecule
NCP – Non-Collagenous Proteins
NH_4OH – Ammonium Hydroxide
NMR – Nuclear Magnetic Resonance

O
O_2 – Oxygen
OC – Osteocalcin
OCP – Octacalcium Phosphate

OPG - Osteoprotegerin
OPN – Osteopontin
Osx – Osterix

P
P – Phosphate
Pax1 – Paired box protein
PBS – Phosphate Buffered Saline
PCL – Poly(ε-caprolactone)
PCR – Polymerase Chain Reaction
Pd - Palladium
PDGF – Platelet-Derived Growth Factor
PFA – Paraformaldehyde
PGA – Polyglycolic Acid
PLA – Polylactic Acid
PLECM – Pig Lung Extracellular Matrix
PLGA – Poly(lactic-co-glycolic Acid)
PlGF – Placental Growth Factor

R
RANKL – Receptor Activator of Nuclear Factor Kappa-B Ligand
RGD – Arg-Gly-Asp sequence
RFP – Red Fluorescent Protein
RNA – Ribonucleic Acid
RT – Room Temperature
Runx2 – Runt-related transcription factor 2

S
SAXS – Small-angle X-ray Scattering
SD – Standard Deviation
SDF – Stromal Cell-derived Factor
SDS – Sodium Dodecyl Sulfate
SEM – Standard Error of Mean
SEM – Scanning Electron Microscopy
SIBLING – Small Integrin-Binding Ligand, N-linked Glycoproteins
SPP – Secreted Phosphoprotein
STED – Stimulated Emission Depletion

T
TB – Toluidine Blue
TCP – Tissue Culture Polystyrene
TEM – Transmission Electron Microscopy
TGF-β - Transforming Growth Factor-β
TNF-α – Tumor Necrosis Factor – α
TRAP – Tartrate-Resistant Acid Phosphatase
TSP - Thrombospondin

U
UC – Umbilical cord
UCM – Umbilical Cord Matrix
UTS – Ultimate Tensile Strength

V
VCAM – Vascular Cell Adhesion Molecule 1
VEGF – Vascular Endothelial Growth Factor
VEGFR – Vascular Endothelial Growth Factor Receptor
VK – Von Kossa

X
XO – Xylenol Orange
XRD – X-Ray Diffraction

W
WT - Wildtype

THESIS MOTIVATION

Bone is a dynamic and highly vascularized tissue that has the ability to regenerate and continues to remodel throughout the lifetime of an individual. Nevertheless, large bone defects can be caused by trauma, disease or tumor resections, leading to severe nonunion fractures that can not heal spontaneously, requiring the use of bone grafts. In the United States, annually, more than half a million patients need bone defect repair, with a cost greater than $2.5 billion. Surprisingly, this phenomenon is expected to double by 2050 globally, due to the increased life expectancy (Baroli 2009). Therefore, different strategies to provide efficacious bone grafts are being exploited.

Bone tissue engineering aims to generate functional bone tissue, developing biocompatible and biodegradable scaffolds and developing new approaches to enhance the functionality and bioactivity of the scaffolds, such as the use of growth factors or their combination with cellular approaches. Numerous pre-clinical trials with different animal models have generated optimistic results (Cancedda *et al.* 2007). However, the difficulty to translate it into a clinical setting suggests that some limitations and concerns remain and need to be further addressed to design and develop enhanced bone grafts for bone fracture repair treatment.

By looking deep into nature, we observe that each tissue has its own extracellular matrix (ECM), with different composition regarding its specificity.

Throughout this thesis, we will focus on the development of biomimetic strategies to enhance stem cell-mediated bone formation, in particular we aim to explore the advantages of ECM components. Moreover, we will develop biomimetic scaffolds for bone tissue engineering, in particular by incorporating non-collagenous bone matrix proteins in three dimensional (3-D) matrices or by developing scaffolds incorporated with decellularized cell-derived ECM derived from different cell sources, targeting osteogenic and angiogenic properties. We believe that we will develop different technologies to design biomimetic matrices that will recapitulate in a more reliable way the architecture, composition and structure of native ECM.

Getting inspiration from nature, we want to study bone ECM and its components, more specifically to evaluate the effect of non-collagenous bone ECM proteins, such as osteocalcin (OC) and osteopontin (OPN), in different cellular processes, such as proliferation, osteogenic differentiation, mineralization and angiogenesis. This approach was motivated by some findings in our group on new structural roles of OC and OPN (Poundarik *et al*. 2012, Poundarik *et al.* 2018, Nikel *et al.* 2013) and from our datasets that show these proteins to be present in much higher amounts in newly formed osteonal than older interstitial bone (Sroga *et al.* 2011). Based on how these proteins influence bone morphology (Bailey *el al*. 2017), herein, we will investigate the roles of these two proteins at the cellular level by using bone marrow mesenchymal stem/stromal cells isolated from wildtype (WT) and $OC^{-/-}$ $OPN^{-/-}$ mice and by evaluating supplementation of these proteins extracellularly to the cell culture medium. We believe that by understanding the effect of these proteins at a cellular level, we can develop new matrices for bone tissue engineering applications with selected OC/OPN compositions that can be further applied in other systems in which the production of OC and OPN might be compromised, due to medical conditions or to the age of the patient. In fact, variation of non-collagenous bone protein concentrations in diseased human bones have already been reported (Grynpas *et al.* 1994). Findings to date are that OC and OPN levels are reduced in osteoporotic bone (Boskey 2013) and in older bone tissue (Sroga *et al.* 2011). Moreover, it was reported that older people may have a 10-fold

increased 10-year fracture risk compared with younger people with the same bone mineral density (Kanis 2002). Therefore, with aging there is an increased susceptibility to fractures due to the increase in skeletal fragility. We believe that, since these proteins are important for fracture resistance (Sroga & Vashishth 2012), the development of OC/OPN-enhanced collagen matrices might help to sustain bone formation when patients are not or less able to produce naturally these proteins, producing high quality functional bone to improve bone regeneration.

One of the main challenges that bone tissue engineering faces is to guarantee the bioactivity and functionality of the scaffolds. In fact, isolated ECM proteins have been incorporated into different biomaterials, however most of them fail and can not achieve the functional properties of bone, not being able to mimic the complex and highly organized assemble of macromolecules of the ECM. Therefore, herein, we will assess the properties of decellularized ECM derived from different cell types, such as mesenchymal stem/stromal cells (MSC), human umbilical vein endothelial cells (HUVEC) and co-culture of MSC:HUVEC. By incorporating decellularized cell-derived ECM derived from different cell types we want to evaluate the cell proliferation and osteogenic differentiation responses, designing scaffolds with better functionality and easier to be translated to a clinical context.

Upon implantation *in vivo*, one of the major challenges for clinical-size bone substitutes is the maintenance of cell viability in the graft, which depends on blood vessel supply of oxygen, nutrients and waste removal. Vascularization plays an important role in bone tissue engineering, enabling the reestablishment of an adequate blood flow (Stegen *et al.* 2015). Furthermore, we will also investigate angiogenic properties of cells cultured on different cell-derived ECM matrices and scaffolds, aiming the development of a cell-derived ECM scaffold that will, simultaneously, enhance osteogenesis and angiogenesis.

Aim of studies

Although a lot of research and innovations have been made in bone tissue engineering, the translation of these discoveries into clinical applications on a large scale has still not been done. Indeed, there is a huge gap between all the tissue engineering research and development and the resulting number of commercialized products. New approaches have been developed in order to enhance the functionality of the scaffolds, in particular to create matrices that recapitulate what happens *in vivo*, in the native tissue.

Knowing this, we aim to develop different biomimetic matrices that will enhance stem cell-mediated bone formation. Specifically, this thesis aims to answer to the following research questions:

1. Can we develop **biomimetic matrices** that more **closely recapitulate the *in vivo* microenvironment of bone**? Can we develop these matrices to **enhance simultaneously osteogenesis and angiogenesis**?

2. What are the main roles of non-collagenous bone proteins, **OC and OPN,** at the **cellular level**? Are they important during the **early differentiation** of MSC into osteoblasts? Are they required for **bone mineral maturation**? Can these proteins have also any effect in **angiogenesis**?

3. Is the **synergy** between **OC and OPN** beneficial for stem cell-mediated bone formation? Can we apply it into tissue engineering applications?

We propose that isolation of $OC^{-/-}$ $OPN^{-/-}$ MSC from murine bone marrow (BM) will contribute to address these three questions, evaluating their proliferative potential, angiogenic properties, osteogenic differentiation and mineral maturation, using different spectroscopic techniques.

We hypothesize that $OC^{-/-}$ $OPN^{-/-}$ MSC might have a suppression of proliferative and osteogenic potential, due to the lack of these proteins, since OC and OPN have been reported to play an important role in mineralization and cell proliferation (Boskey 1989).

Moreover, we also hypothesize that OC and OPN act in a synergistic way and their effect should be mimicked in *in vitro* matrices developed to enhance and accelerate bone formation in fracture bone defects.

In fact, bone ECM has not been well exploited to enhance functionality of the scaffolds in bone tissue engineering. In that sense, the following additional research questions will be addressed in this thesis:

1. How can we take **advantage of natural ECM** to enhance **osteogenic and angiogenic** properties of MSC? Could the use of **decellularized ECM derived from different cell types or from co-cultures** contribute to enhance these cellular processes?

2. Can we design *in vitro* a scaffold that **mimics the architecture, composition and structure** of **native ECM** in a more reliable and functional way? Could the **electrospun of cell-derived ECM** contribute to this purpose?

These two last research questions derived from the will to learn and get inspiration from nature. Adding to the need to enhance the functionality and bioactivity of scaffolds, equally important it would be to mimic the native ECM, without having a cellular therapy that is known to have some drawbacks. Ideally, we would like to develop decellularized ECM-scaffolds derived from different cell sources, having the same architecture and composition of native ECM. Moreover, these scaffolds could be commercialized as an “off-the-shelf”, acellular product, being widely available and avoiding any inflammatory or immune reaction, having incorporated the required signals and factors to enhance and accelerate bone regeneration.

Research strategies:

Cell type

Focusing on the ECM components, we evaluated the effects of stem cells when exposed to different ECM components, such as non-collagenous bone matrix proteins and decellularized ECM derived from different cell types. In particular, we used MSC obtained with donor consent. MSC can be isolated from different adult and perinatal sources, such as BM, umbilical cord (UC) and adipose tissue (AT). In all studies, we chose MSC from BM to evaluate the importance of ECM components on modulating the activity of stem cells. Bone tissue harbors the bone marrow, containing stem cells that can differentiate into different lineages and provides a microenvironment that influences the function and differentiation of stem cells. MSC isolated from BM are present in bone tissue and will recapitulate the bone marrow microenvironment .

Isolation of BM MSC from different donors is associated with batch-to batch cellular heterogeneity, therefore we used several MSC donors.

$OC^{-/-}$ $OPN^{-/-}$ *knockout* (KO) as a model to study the synergistic effects of OC/OPN at a cellular level

Based on how these proteins influence bone morphology (Bailey *et al.* 2017), herein, we used a $OC^{-/-}$ $OPN^{-/-}$ KO model to evaluate the roles of these two proteins at the cellular level. Therefore, we isolated MSC from BM derived from WT and $OC^{-/-}$ $OPN^{-/-}$ mice. We further characterized these cells and evaluated how OC/OPN affect the main cellular activities, such as proliferation, multilineage differentiation (adipogenesis, osteogenesis and chondrogenesis), mineralization and angiogenesis. Moreover, we used this model as an approach to evaluate the cellular responses to ECM components extracellularly added do the system, assessing if the $OC^{-/-}$ $OPN^{-/-}$ MSC have the ability to recover their normal phenotype and functionality when OC and OPN are extracellularly supplemented to the cell culture.

Mimicking the bone microenvironment

In this thesis, two different approaches to mimic the bone microenvironment were explored, namely the use of non-collagenous bone ECM proteins and the development of decellularized cell-derived ECM matrices.

<u>OC/OPN-enhanced collagen type I matrices</u>

Bone extracellular matrix is composed by an inorganic part, mainly hydroxyapatite crystals, and an organic part, constituted by collagen and non-collagenous proteins (NCP) *(*Boskey 2007, Young 2003). The non-collagenous proteins, isolated from bone, have been found to be biologically active. Thus, by understanding the properties and functions of these proteins, new strategies mimicking the bone ECM can be designed for bone tissue engineering applications (Mouw *et al.* 2014). However, the function of NCP in bone

regeneration is not yet completely understood. It has been speculated that NCP might have an important role in cell attachment, cell differentiation and regulation of the deposition of hydroxyapatite minerals (Boskey 1989). Furthermore, some of these proteins could be multifunctional, playing different roles in the bone and, therefore, can have a synergistic effect on the cellular behavior and mechanical properties of bone. OPN and OC are some of the most common NCP present in bone matrix. These proteins are involved in bone matrix organization and deposition. Several studies from our group have reported that OC and OPN influence bone morphology and mechanical properties (Poundarik *et al.* 2012, Morgan *et al.* 2015, Bailey *et al.* 2017, Poundarik *et al.* 2018). Due to the specific roles that OC/OPN might have in bone mineralization, we selected them to develop a biomimetic matrix, evaluating the synergistic effect of both proteins on cellular activities and bone regeneration.

Cell-derived ECM from different cell sources

Cultured cell-derived ECM has been studied as a scaffold for tissue engineering, creating a biomimetic microenvironment, providing physical, chemical and mechanical cues for cells and supporting cell adhesion, proliferation, migration and differentiation. Moreover, in this thesis, we investigated the effect of different compositions of decellularized cultured cell-derived ECM produced from different cell types, such as MSC, HUVEC and co-culture of MSC:HUVEC on cell proliferation, osteogenic differentiation and angiogenic properties of human BM MSC.

Different types of scaffolds

In this thesis, we explored different types of scaffolds, such as hydrogels, mineralized scaffolds and electrospun fibers.

Collagen scaffolds

Several biomaterials have been used as carriers in bone tissue engineering approaches, including 3-D collagen-based biomimetic scaffolds (Helary *et al.* 2010, Abou *et al.* 2013). These hydrogel scaffolds are biocompatible, biodegradable with low antigenicity, enabling the support of cell attachment, migration, proliferation and differentiation (Abou *et al.* 2013, Mravic *et al.* 2014). Therefore, we developed OC/OPN-enhanced collagen scaffolds as a strategy to recapitulate *in vitro* the organic part of bone ECM. We designed OC/OPN-enhanced collagen gels and OC/OPN-enhanced mineralized collagen scaffolds to evaluate the synergistic effects, bioactivity and local inflammatory response of OC/OPN on osteogenic potential of MSC.

Electrospun fibers

Electrospinning has been used to fabricate fibrous and porous scaffolds from a variety of materials (Li *et al.* 2002, Sill & von Recum 2008, Yoshimoto *et al.* 2003) with a high surface area for tissue engineering applications. Electrospinning has rapidly gained relevance in the tissue-engineering field due to its

advantages over conventional scaffold fabrication methods (Barnes *et al.* 2007) and its ability to generate fibers similar to the fibrillar structure of native ECM (Li *et al.* 2002, Bhardwaj & Kundy 2010, Li *et al.* 2013). If needed, the nanofibers can be functionalized by incorporating bioactive factors to enhance and control cell proliferation and differentiation (Bhattarai *et al.* 2004, Pant *et al.* 2011). Thus, we fabricated cell-derived 3-D scaffolds with high porosity structure, mimicking the architecture and composition of the natural ECM by electrospinning the cell-derived ECM particles in combination with polycaprolactone (PCL) solution.

Spectroscopic analysis as a technique to evaluate bone mineral quality

Chemical analysis of the calcium and phosphate content of cultures are frequently used to describe mineralization of cell cultures. However, different techniques should be used to evaluate the quality of the mineral produced by cells, since the demonstration of the increase of calcium or phosphate contents with time is not sufficient and does not characterize the quality of the mineral generated.

Several investigators have been using Infrared and Raman spectroscopies to analyze the mineral phase formed in cell cultures (Bohic *et al.* 1998, Nauman *et al.* 2002, Rey *et al.* 1995). Moreover, by using vibrational spectroscopic techniques, researchers have been able to describe the evolution of mineralization during bone maturation, by detecting different phases of mineral formed (Paschalis *et al.* 1996, Verdelis *et al.* 2003, Boskey *et al.* 2003, Tarnowski *et al.* 2002).

Thus, we used Fourier-transform infrared (FTIR) and Raman spectroscopy as two different strategies to assess the quality and maturation level of mineral species produced by MSC. In particular, we were interested on studying the maturation level of mineral species produced by $OC^{-/-}$ $OPN^{-/-}$ MSC to evaluate if the mineral formed was comparable to that in the native bone tissue.

Thesis outline:

In **Chapter I**, we review the bone biology, specifically the hierarchical structure of bone, as well as all the mechanisms related to bone development, formation and repair. We also review some of the research studies performed to date in the bone tissue engineering field, focusing on different approaches to enhance the functionality of the scaffolds, namely the incorporation of bioactive peptides, non-collagenous proteins present in the bone ECM and the use of cell-derived ECM as a biomaterial source.

All the experimental work developed during this PhD is presented in Chapters II to VI.

In **Chapter II**, we isolate and characterize $OC^{-/-}$ $OPN^{-/-}$ mouse bone marrow MSC, exploring their proliferative capability and differentiation potential. We further provide evidence that osteogenic differentiation of $OC^{-/-}$ $OPN^{-/-}$ MSC is impaired, in particular that the mineralization activity of these cells is delayed. FTIR and Raman spectroscopy revealed that the maturation level of the minerals produced by $OC^{-/-}$ $OPN^{-/-}$ MSC is delayed compared to the WT MSC. This work provides important information that confirms that OC and OPN are important regulators of bone mineralization and angiogenesis at a cellular level, providing new insights into forming high quality bone, relevant for treatment of fracture healing in older and osteoporotic bone.

In **Chapter III**, we assess OC and OPN functions as osteoinductive factors, enhancing osteogenesis and angiogenic potential, when added extracellularly to cell culture medium. Furthermore, we evaluate how the synergistic effect of OC and OPN can be applied as an attractive strategy for bone regeneration therapeutics by targeting different vital cellular processes.

In **Chapter IV**, we develop collagen matrices enhanced with two selected key matrix proteins, OC and OPN, as a strategy to mimic the organic part of bone matrix to enhance and accelerate bone regeneration. We demonstrate a new biomimetic strategy to rapidly form mineralized bone tissue and secure a sustained bone formation response by MSC from multiple sources, thus facilitating faster patient recovery and treatment of non-union fractures in aging and diseased population. These OC/OPN-enhanced collagen matrices can be further applied in bone tissue engineering applications.

In **Chapter V**, we explore the effect of different compositions of decellularized cell-derived ECM produced from different cell types, such as MSC, HUVEC and co-culture of MSC:HUVEC, on cell proliferation, osteogenic differentiation and angiogenesis and their potential to be used as a new biomaterial. This work develops important strategies to fabricate cell-derived ECM, in particular from a co-culture system, targeting osteogenesis and angiogenesis, simultaneously.

In **Chapter VI**, we further develop a cell-derived ECM electrospun PCL scaffold as an application for bone tissue engineering. Therefore, we electrospun a mixture of lyophilized decellularized ECM derived from MSC, HUVEC and MSC:HUVEC in PCL solution and investigate the feasibility and functionality of these scaffolds to promote osteogenesis an their capability to enhance cell proliferation.

Finally, in **Chapter VII**, we summarize the main results of this thesis, highlighting their relevance in the bone tissue engineering field, focusing on the acceleration of bone healing treatment. Limitations found in this work are also referred, as well as future research that can be further done.

References

Abou Neel E.A., Bozec L., Knowles J.C., Syed O., Mudera V., Day R., Hyrun J.K. Collagen-emerging collagen based therapies hit the patient. *Adv. Drug Deliv. Rev.,* **65**, 429-456 (2013).

Bailey S. Karsenty G., Gundberg C., Vashishth D. Osteocalcin and osteopontin influence bone morphology and mechanical properties. *Ann. N.Y. Acad. Sci.,* 1-6 (2017).

Barnes C.P., Sell S.A., Boland E.D., Simpson D.G., Bowlin G.L. Nanofiber technology: designing the next generation of tissue engineering scaffolds. *Adv. Drug Deliv. Rev.,* **59**, 1413-1433 (2007).

Baroli B. From natural bone grafts to tissue engineering therapeutics: brainstorming on pharmaceutical formulative requirements and challenges. *J Pham. Sci*., **98**, 1317-1375 (2009).

Bhardwaj N., Kundu S.C. Electrospinning: a fascinating fiber fabrication technique. *Biotechnol. Adv.,* **28**, 325-347 (2010).

Bhattarai S.R., Bhattarai N., Yi H.K., Hwang P.H., Cha D.I., Kim H.Y. Novel biodegradable electrospun membrane: scaffold for tissue engineering. *Biomaterials,* **25**, 2595-2602 (2004).

Bohic S., Pilet P., Heymann D. Effects of leukemia inhibitory factor and oncostatin M on bone mineral formed in *in vitro* rat bone-marrow stromal cell culture: physicochemical aspects. *Biochem. Biophys. Res. Commun.,* **253**, 506-513 (1998).

Boskey A. Mineralization of bones and teeth. *Elements Mag.* **3**, 385-392 (2007).

Boskey A.L. Bone composition: relationship to bone fragility and antiosteoporotic drug effects. *Bonekey Reports,* **2**, 447 (2013).

Boskey A.L., Moore D.J., Amling M., Canalis E., Delany A.M. Infrared analysis of the mineral and matrix in bones of osteonectin-null mice and their wildtype controls. *J. Bone Miner. Res.* **18**, 1005-1011 (2003).

Boskey A.L., Noncollagenous matrix proteins and their role in mineralization. *Bone and Mineral* **6,** 111–123 (1989).

Cancedda R., Giannoni P., Mastrogiacomo M. A tissue engineering approach to bone repair in large animal models and in clinical practice. *Biomaterials*, **28**, 4240-4250 (2007).

Grynpas M.D, Tupy J.H., Sodek J.The distribution of soluble, mineral-bound, and matrix-bound proteins in osteoporotic and normal bones. *Bone* **15**, 505-513 (1994).

Helary, C., Bataille I., Abed A., Illoul C., Anglo A., Louedec L., Letourneur D., Meddahi-Pellé A., Giraud-Guille M.M. Concentrated collagen hydrogels as dermal substitutes. *Biomaterials,* **31**, 481–490 (2010).

Kanis J.A. Diagnosis of osteoporosis and assessment of fracture risk. *Lancet,* **359**, 1929-1936 (2002).

Li H., Wong Y.S., Wen F., Ng K.W., Ng G.K., Venkatraman S.S., Boey F.Y., Tan L.P. Human mesenchymal stem-cell behavior on direct laser micropatterned electrospun scaffolds with hierarchical structures. *Macromol. Biosci.,* **13**, 299-310 (2013).

Li W.J., Laurencin C.T., Caterson E.J., Tuan R.S., Ko F.K. Electrospun nanofibrous structure: a novel scaffold for tissue engineering. *J. Biomed. Mater. Res.,* **60**, 613-621 (2002).

Morgan S., Poundarik A.A., Vashishth D., Do non-collagenous proteins affect skeletal mechanical properties? *Calcif. Tissue Int.,* **97**, 281-291 (2015).

Mouw J.K., Ou G., Weaver V.M. Extracellular matrix assembly: a multiscale deconstruction. *Nat. Rev. Mol. Cell Biol.,* **15**, 771-785 (2014).

Mravic M., Peault B., James A. W. Current trends in bone tissue engineering. *Biomed. Res. Int.,* **2014**, 865270 (2014).

Nauman E.A., Ebenstein D.M., Hughes K.F., Pruitt L., Halloran B.P., Bikle D.D., Keaveny T.M. Mechanical and chemical characteristics of mineral produced by basic fibroblast growth factor-treated bone marrow stromal cells in vitro. *Tissue Eng.*, **8**, 931-939 (2002).

Nikel O. Laurencin D., McCallum S.A., Gundberg C.M., Vashishth D. NMR investigation of the role of osteocalcin and osteopontin at the organic-inorganic interface in bone. *Langmuir* **29**, 13873-13882 (2013).

Pant H.R., Neupan M.P., Pant B., Panthi G., Oh H.J., Lee M.H., Kim H.Y. Fabrication of highly porous poly(ε-caprolactone) fibers for novel tissue scaffold via water-bath electrospinning. *Colloids Surf. B Biointerfaces*, **88**, 587-582 (2011).

Paschalis E.P., DiCarlo E., Betts F., Sherman P., Mendelsohn R., Boskey A.L. FTIR microspectroscopic analysis of human osteonal bone. *Calcif. Tissue Int.,***59**, 480-487 (1996).

Poundarik A.A., Boskey A., Gundberg C., Vashishth D., Biomolecular regulation, composition and nanoarchitecture of bone mineral. *Sci. Rep.,* **8**, 1191 (2018).

Poundarik A.A., Diab T., Sroga G.E., Ural A., Boskey A.L., Gundberg C.M., Vashishth D. Dilatational band formation in bone, *Proc. Natl Acad. Sci. U.S.A.*, **109**, 19178-19183 (2012).

Rey C., Kim H.M., Gerstenfeld L., Glimcher M.J. Structural and chemical characteristics and maturation of the calcium-phosphate crystals formed during the calcification of the organic matrix synthesized by chicken osteoblasts in cell culture. *J. Bone Miner. Res.,* **10**, 1577-1588 (1995).

Sill T.J., von Recum H.A. Electrospinning: applications in drug delivery and tissue engineering. *Biomaterials*, **29**, 1989-2006 (2008).

Sroga G.E., Karim L., Colón W., Vashishth D. Biochemical characterization of major bone-matrix proteins using nanoscale-size bone samples and proteomics methodology. *Mol. Cell. Proteomics*, **10**, M110.006718 (2011).

Sroga G.E., Vashishth D. Effects of bone matrix proteins on fracture and fragility in osteoporosis. *Curr. Osteopor. Rep.* **10**, 141-150 (2012).

Stegen S., van Gastel N., Carmeliet G.Bringing new life to damaged bone:the importance of angiogenesis in bone repair and regeneration. *Bone,* **70**, 19-27 (2015).

Tarnowski C.P., Ignelzi M.A. Jr., Morris M.D. Mineralization of developing mouse calvaria as revealed by Raman microspectroscopy. *J. Bone Miner. Res.*, **17**, 1118-1126 (2002).

Verdelis K., Crenshaw M.A., Paschalis E.P., Doty S., Atti E., Boskey A.L. Spectroscopic imaging of mineral maturation in bovinde dentin. *J. Dent. Res.***, 82**, 697-702 (2003).

Yoshimoto H., Shin Y.M., Terai H., Vacanti J.P. A biodegradable nanofiber scaffold by electrospinning and its potential for bone tissue engineering. *Biomaterials,* **24**, 2077-2082 (2003)

Young M.F. Bone matrix proteins: their function, regulation, and relationship to osteoporosis. *Osteoporos. Int.,* **14**, S35-S42 (2003).

CHAPTER I - INTRODUCTION

I.1 Hierarchical structure of bone

I.1.1. Macroscopic level

Bone is a rigid organ that constitutes part of the vertebral skeleton and provides structural support for the rest of the body. Bone has several vital functions in the body, such as locomotion, by assisting in movement, support and protection of vital internal organs and soft tissues and storage of minerals important for cellular activities, such as calcium and phosphorous, growth factors and cytokines (McLean 1958). Bone also harbors the bone marrow, being responsible for blood cell production (Taichman 2005). Due to these important roles, bone tissue must be mechanically and structurally competent. Thus, from the structural point of view, bone tissue is organized as a hierarchical biocomposite material, built from collagen molecules and mineral nanocrystals.

Bone is a material consisting of an organic and inorganic phase. The organic phase is around 30% of the bone tissue and contains mostly type I collagen molecules (~90% by weight), but also includes non-collagenous proteins (~7%), lipids (~1%) and cells (~2%). The inorganic phase (~70%) is composed by nanocrystals of apatite similar to hydroxyapatite, $Ca_{10}(PO_4)_6(OH)_2$ (Benno *et al.* 2000, Gong *et al.* 1964, Einhorn *et al.* 1994). Mineral crystals incorporate the organic matrix and provide elasticity to the matrix with high elastic modulus.

Interestingly, the amount of bone components varies with age, site, gender, ethnicity, disease and treatment (Boskey & Coleman. 2010, Donnelly *et al.* 2012, Gregson *et al.* 2013, Leslie 2012, Boskey *et al.* 2005, Sroga *et al.* 2011)

Different mechanical forces are constantly being applied to bone tissue, leading to possible microdamages. Therefore, bone adapts to its environment by undergoing modeling and remodeling to remove bone that is damaged and replace it with new bone that is mechanically stronger, preventing bone strength to fail.

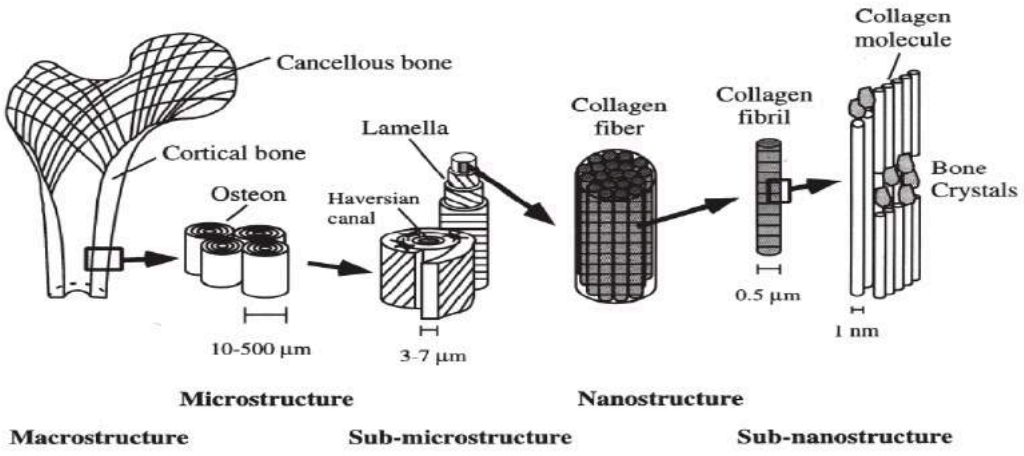

Figure I.1. Complex hierarchy in cortical bone, from the collagen fibril to compact bone (Rho *et al.* 1998).

Bone tissue can be described as a complex hierarchical composite material with six orders of magnitude in dimension. Figure I.1 describes these different levels. Regarding macrostructure (>1 mm), bone tissue can be either cortical or cancellous. The microstructure level is composed by the Haversian system, osteons and trabeculae (10-500 μm). The sub-micron or lamellar level ranges 1-10 μm and the nanostructure level (<1 μm) is composed by an arrangement of fibrillary collagen, minerals and non-collagenous proteins (Weiner & Traub 1992).

Based on its macroscopic morphology, there are five different categories of bones: long bones, short bones, flat bones, irregular bones and sesamoid bones. Long bones include the clavicles, humeri radii, ulnae, metacarpals, femurs, tibiae, fibulae, metatarsals, and phalanges. Long bones are longer than wider and support the weight of the body, facilitating the movement. Short bones include the carpal and tarsal bones, being located in the wrist and ankle joints. Short bones provide stability and some movement. Flat bones include the skull (occipital, parietal, frontal, nasal, lacrimal and vomer), the thoracic cage (sternum and ribs) and the pelvis (ilium, ischium, and pubis). Moreover, flat bones protect internal organs, such as brain, heart and pelvic organs and can provide areas where muscles can attach. Irregular bones include the vertebrae, sacrum, coccyx, and hyoid bone. These bones have an irregular and complex shape to protect internal organs. Sesamoid bones are small and round bones embedded in tendons and they protect tendons from stress and wear. One example of a sesamoid bone is the patella (Clarke 2008, Mosby 2004).

Long bones are composed by diaphysis, metaphysis and epiphysis. Figure I.2 shows these different components of long bones, such as femur or tibia.

The diaphysis is the middle part of a long bone located between the proximal and distal ends of the bone and is composed primarily of dense and hard cortical bone. It forms a cylinder-like hollow shape that contains the medullary cavity filled with marrow and adipose tissue. On the other hand, epiphyses are extreme parts of long bones, at the positions of its joint with adjacent bones, composed of trabecular bone. Proximal epiphysis is the closest to the center of the body, whereas distal epiphysis is the furthest. Between the epiphyses and the diaphysis lies the metaphysis, including the epiphyseal plate (growth plate), the area where bones grow in length composed by a layer of hyaline cartilage. At the joint, the epiphysis is covered with articular cartilage. Interestingly, when the bone stops growing in early adulthood, the cartilage is replaced by osseous tissue and the epiphyseal plate becomes an epiphyseal line. Two types of membranes are present in the medullary cavity of bone: periosteum and endosteum (Figure I.3) The periosteum is the fibrous membrane that covers the outer surface of bones, except where the epiphyses meet other bones to form joints, in which bone is lined by articular cartilage. It contains blood vessels, nerves, lymphatic vessels and is the place where tendons and ligaments attach to bones. The endosteum covers the inner surface of all bones and is where bone growth, repair and remodeling occur (Clarke 2008).

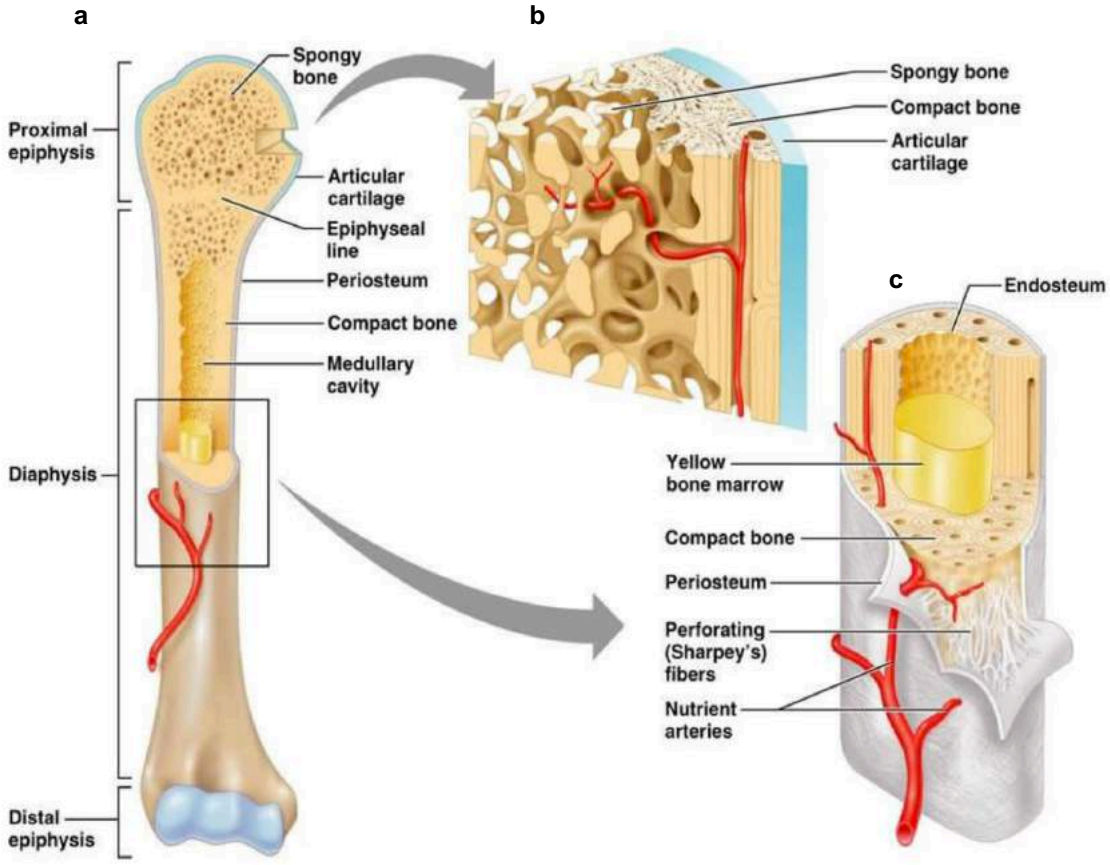

Figure I.2. Bone hierarchical levels illustrated for long bones: **a)** whole bone, **b)** zoom into epiphysis structure, **c)** zoom into diaphysis structure (Mosby 2004).

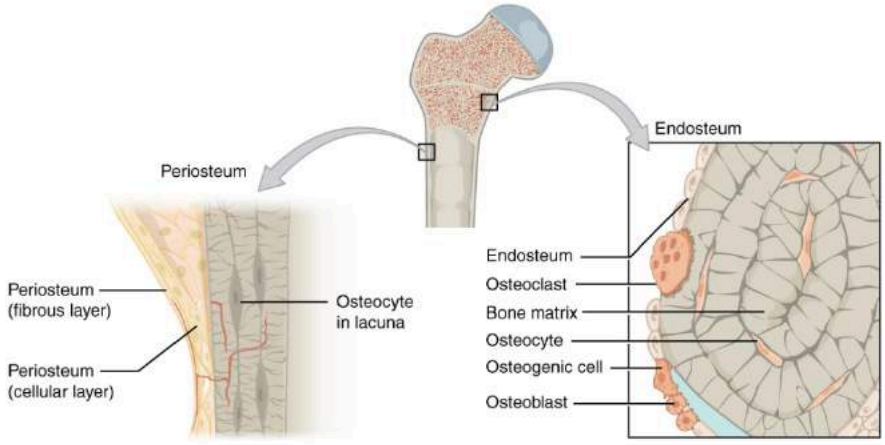

Figure I.3. Schematics of periosteum and endosteum. The periosteum forms the outer surface of bone, whereas the endosteum covers the medullary cavity.

Bone tissue can be described as cortical (or compact) and trabecular (or cancellous, spongy), depending on its structure and different properties (Figure I.4).

The adult human skeleton is composed of 50-80% cortical bone and 20-50% trabecular bone (Eriksen *et al.* 1994, Clarke 2008). Cancellous and compact bone are composed by similar basic material, however the degree of porosity, as well as the tissue organization differ. Thus, the porosity of cortical bone ranges from 5% to 10%, whereas cancellous bone presents higher porosity, ranging from 50% to 90% (Cruess 1982, Weiner & Traub 1992).

Cortical bone is a strong and dense tissue and covers the marrow space. On the other hand, trabecular bone is a porous and more flexible tissue, being the place where hematopoiesis occurs. Some structural and mechanical properties of cortical and trabecular bone are compared in Table I.1. Cortical and trabecular bone not only present a different structure, but the remodeling process of bone differs in both types of bones. Thus, cancellous bone is metabolically more active due to the greater surface area that is accessible to osteoclasts and osteoblasts, the bone cells responsible for the remodeling process in bone (Zysset *et al.* 1999).

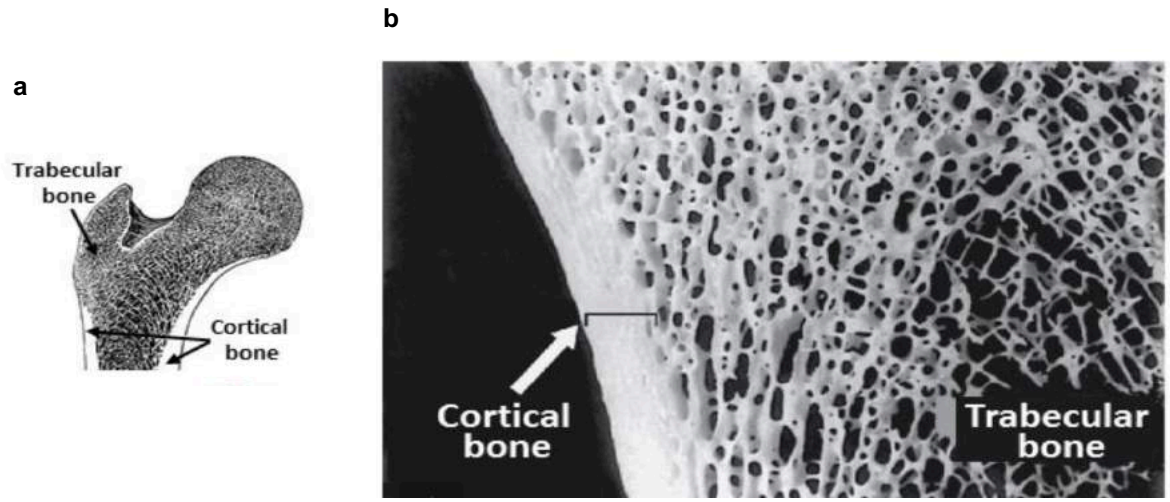

Figure I.4. Cortical and trabecular bone. **a)** Human femoral head structure showing trabecular and cortical bone, **b)** Scanning electron micrograph of a section of femoral head. Adapted from (Mescher *et al.* 2010, McCloskey *et al.* 2006).

Table I.1. Comparison between different structural and mechanical properties of cortical and trabecular bone. (Adapted from Weiner & Traub 1992, Rho et al. 1998).

Tissue properties	Cortical Bone	Trabecular Bone
Volume fraction (mm^3/mm^3)	0.85-0.95	0.05-0.60
Surface fraction (mm^2/mm^3)	2.5	20
Porosity (%)	5-10	50-90
Density (g/cm^3)	1.6-2.0	0.03-0.12
Total skeletal mass (%)	80	20
Young's modulus (GPa)	7-30	0.7-20
Strength (MPa)	100-230	1.0-7.0

I.1.2. Microstructure of bone

The microstructure of cortical bone ranges from the mineralized collagen fibril to the osteon (Figure I.1).

At the microstructure level, cortical bone is arranged in repeating structural units that are called osteons or Harversian system. Harversian systems are cylindrical in shape and their diameters can range from 200-500 μm depending on species and anatomical location (Eriksen *et al.* 1994), having a central canal (Harversian canal), where blood vessels and nerve fibers cross. Harversian canals are surrounded by the concentrically arranged lamellae (~2-7 μm thick), in which osteocytes (mature bone cells) are located (lacunae). A lamella is composed by a layer of mineralized collagen fibril bundles that are arranged together in a circular manner. Lacunae are connected to each other by channels called canaliculi (~100-500 nm in diameter), allowing cell nutrition and communication (lacuna-canaliculi network) (Eriksen *et al.* 1994).

In contrast to cortical bone, trabecular bone is composed of irregular units of thin bone columns that can be partly flattened, called trabeculae (~ 50 μm in diameter) that form an interconnected network that aids cortical bone in distributing load. Overall trabeculae are aligned towards the principal directions of mechanical loading that a bone experiences. Trabecular bone is porous with pore size of the order of 1 mm, being filled with bone marrow, fat and bone cells. Trabecula is composed of concentric lamella with osteocytes lying in lacunae with canaliculi network similar to the one of cortical tissue (Cruess 1982).

Both cortical and trabecular bone are normally formed in a lamellar pattern, in which osteoblasts lay down collagen fibrils in alternating orientation, giving bone higher strength, while osteoclasts are removing old bone (lamellar bone). Moreover, as bone matures, different states of bone can be found. Therefore, woven bone is produced during formation of primary bone or during repair of fracture, consisting of strongly disorganized collagen fibers. It is known that this type of bone is present specially in tissues that form under fast dynamics, such as fetuses, newborns, near a fracture site and in some diseases. Interestingly, lamellar bone replaces woven bone during remodeling process. Bone remodeling occurs during the whole life time in humans and allows the replacement of “old” bone to new bone synthesized by the coordinated and balanced activity of osteoclasts and osteoblasts. This process is responsible for bone adaptation to changes in stresses and forces and microdamage repair (Clarke 2008).

I.1.3. Nanostructure of bone: mineralized collagen fibril

At the nanostructural level of organization, bone tissue consists of collagen molecules and mineral nanocrystals. As mentioned before, the organic phase of bone is mostly composed by type I collagen. Type I collagen fibrils are composed of tropocollagen molecules. Collagen molecules are around 300 nm long and 1.5 nm thick. They are composed of three polypeptide chains that form a triple-helical structure: two α1 (I) chains and one α2 (I) (Hulmes 2008, Lodish *et al.* 2000) (Figure I.5). The triple-helical structure of collagen is built by the Gly-X-Y repeating motif, with glycine (Gly) being present at every third position and X, Y are mainly proline and hydroxyproline (Brodsky & Ramshaw 1997). Figure I.6 shows the first high resolution crystal structure of solution of collagen triple helix. The three polypeptide chains combine to form an alpha helical strand of tropocollagen. Tropocollagen molecules further combine to form collagen fibrils. Their arrangement gives rise to the staggered 67 nm D-periodicity that is observed in type I collagen (Shoulder & Raines 2009). Within these fibrils, gaps and overlap zones can be observed, due to the space between the

ends of the tropocollagen molecules and an offset from row to row. The gap and overlap zones are the source of the characteristic repeat pattern 67nm banding (D-periodicity). This periodicity (repetition of gap and overlap zones) produces a characteristic interference pattern that is observed as bands in transmission electron microscopy (Figure I.7).

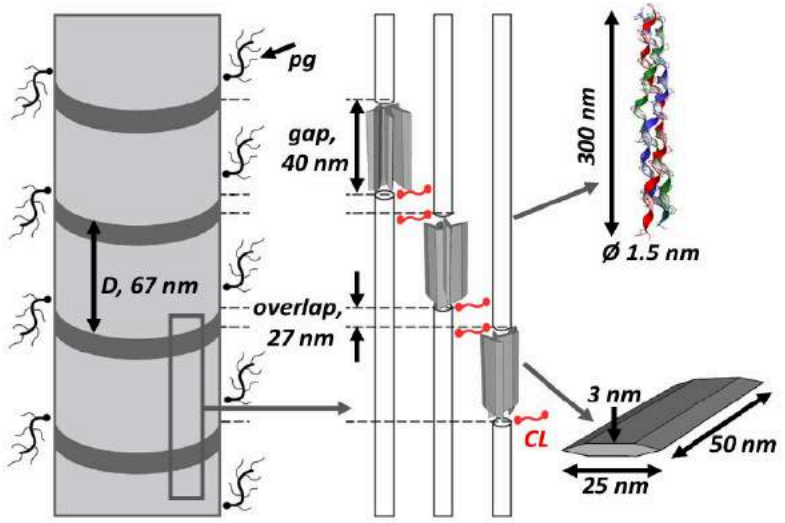

Figure I.5. Mineralized fibril structure composed by collagen molecules and mineral nanocrystals. Gap and overlap regions present in the collagen molecules are responsible for the 67nm collagen banding periodicity. Mineral crystals located within the gap zones are oriented with the c-axis parallel to the collagen fibrils (Hulmes 2008).

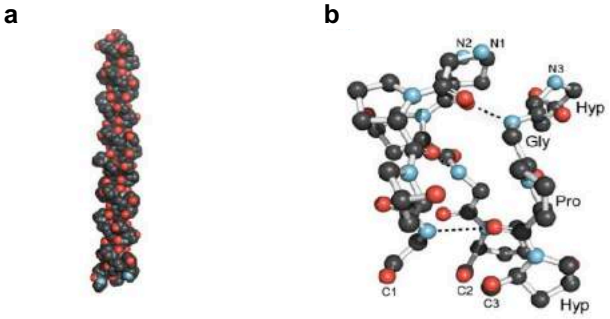

Figure I.6. Structure of the collagen triple helix: **a)** First high resolution crystal structure of a collagen triple helix, formed from $(ProHypGly)_4$-(ProHypAla)-$(ProHypGly)_5$ (Bella *et al.* 1994), **b)** Ball-and-stick image of a segment of collagen triple helix (Bella *et al.* 1994, Shoulders & Raines 2009).

Collagen has mechanical and structural functions. Besides providing a framework for the deposition of mineral crystals and other organic components, collagen provides ductility to bone (Viguet-Carrin *et al.* 2005).

During the post-yield deformation of bone, collagen deformation dissipates energy in bone. Through this deformation, collagen fibrils absorb energy and avoid catastrophic crack propagation to failure in bone (Gutsmann *et al.* 2004). Therefore, the organic matrix of bone plays a major role in providing toughness to bone.

Mineral nanocrystals are platelet-shaped apatite crystals of the size of about 3 x 25 x 50 nm^3 (Ziv *et al.* 1994). Nanocrystals can be located within the gap regions of collagen molecules, oriented with their c-axis (long axis) parallel to the collagen fibrils (Kuhn-Spearing *et al.* 1996, Cui *et al.* 2007) (Figure I.5). Mineral crystals can also grow outside the collagen matrix, called extrafibrillar minerals (Nikolov & Raabe 2008). Crystals may initially form within the gap region of the collagen fibrils, and then proceed into the overlap region, and occasionally grow in to the extrafibrillar space (Chen *et al.* 2011). Interestingly, since the periodicity of the collagen inhibits spatial growth of mineral crystals, the larger size crystals (mineral aggregates) probably are distributed outside the organic matrix and surrounding the mineralized collagen (Cui *et al.* 2007, Rey *et al.* 2009). Various non-collagenous proteins have also been implicated in the nucleation and growth of crystals (Gericke *et al.* 2005).

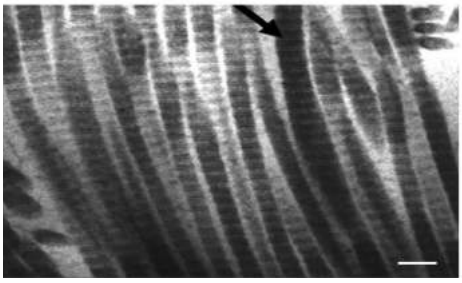

Figure I.7. Collagen fibrils observed by TEM seen in the longitudinal section (Facca *et al.* 2010). Scale bar, 1.5 μm.

Inorganic phase of bone matrix is important to give some rigidity to bone for its mechanical function, enabling bone to withstand different loadings, supporting and protecting the whole organism. Furthermore, inorganic phase of bone matrix can act as a reservoir for storage of calcium and phosphate, helping to maintain the ionic balance in extracellular fluid (Cui *et al.* 2007).

The concept of “collagen fiber” structural level was proposed by J.Y. Rho (Rho *et al.* 1998) and it is represented in Figure I.8. Collagen fibers are composed by a set of collagen fibrils being surrounded with mineral that can also incorporate into the collagen molecules. Therefore, the mineralized collagen fibrils are the basis of bone tissue. These fibrils have a cylindrical shape composed by a set of collagen molecules and mineral nanocrystals.

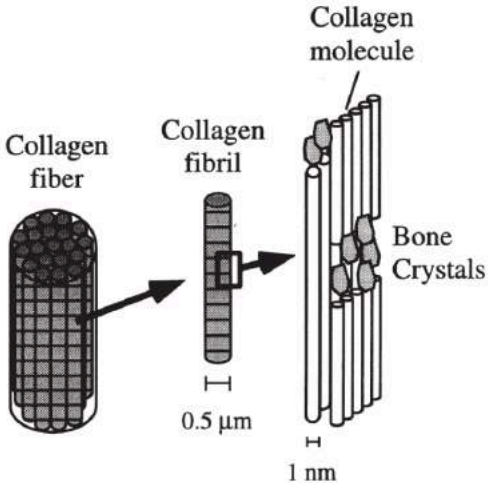

Figure I.8. Concept of "collagen fiber" structural level. Nano and sub-nanostructure of bone hierarchy by Rho *et al.* 1998.

Mineral crystals have been investigated through a wide variety of techniques ranging from X-ray diffraction (XRD) and electron microscopy to Fourier transform infrared (FTIR) microscopy and atomic force microscopy (AFM) (Boskey *et al.* 2003).

Due to the small size of the mineral nanocrystals and their extended surface area of 100-200 m^2/g, bone crystals are metabolically active, interacting with extracellular fluids. Moreover, these small crystals are oriented within collagen molecules and can provide high strength and rigidity of the tissue. Interestingly, the origin of mineral nanocrystal size is still in discussion, whether it is defined by the collagen molecules that act as a template for mineralization of by the specified cellular activity.

Regarding chemical and structural composition, bone mineral crystallographic structure is similar to hydroxyapatite. In fact, bone mineral structure was defined as "an apatite similar to geological hydroxyapatite" by chemical analysis and X-ray diffraction (De Jong 1926, Roseberry *et al.* 1931).

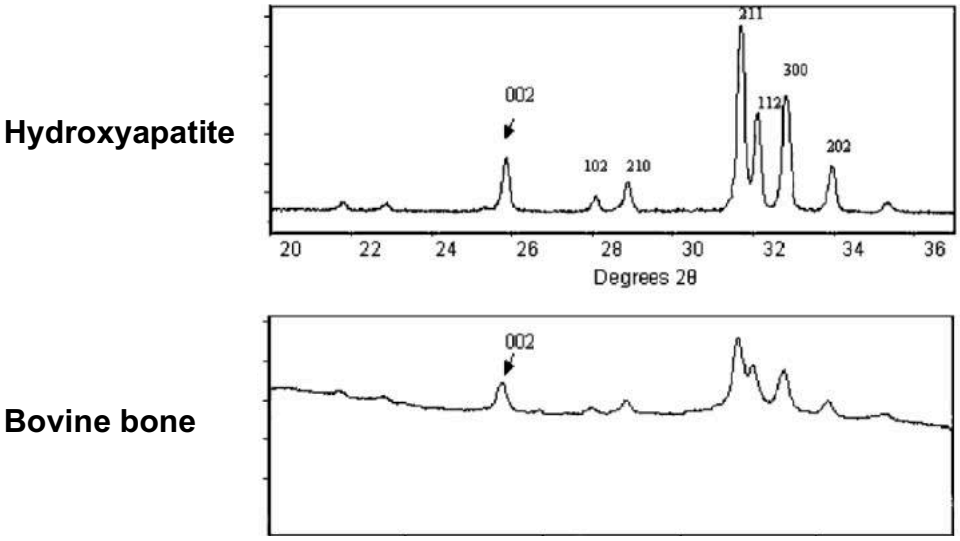

Figure I.9. Comparison of XRD diagram for hydroxyapatite and bovine bone. Bone diagram shows broaden of peaks (Boskey *et al.* 2003).

Although their similarities, there are significant structural and compositional differences between hydroxyapatite and bone mineral. Figure I.9 shows XRD spectrum from bone and hydroxyapatite. It is possible to be observed that bone presents peaks at exact position of hydroxyapatite, but they are largely broadened (Boskey *et al.* 2003), probably due to the nanosize of the crystals, presence of strain, degree of crystallinity and chemical substitutions.

I.2. Biomineralization

In bone, mineralization starts from an heterogeneous solution containing calcium and phosphate ions. The mineral phase that is found in bone is mainly composed by hydroxyapatite (HAP) (Boskey & Pleshko Camacho 2007) and it is located between extracellular matrices of collagen fibers as well as embedded in non-collagenous proteins. Collagen, a fibrillar protein, is the major component of the organic matrix, however other non-collagenous proteins are crucial for the maintenance of the cell-matrix interactions, cell-signaling, regulation of cell metabolism, and control of the mineralization process (Wiesmann *et al.* 2005, Margolis *et al.* 2006).

Physiologic mineral deposition is regulated by cells. The cells produce the extracellular matrix (ECM) that supports the deposition of the mineral (Rey *et al.* 1996). Osteoblasts produce the ECM and initiate and control tissue mineralization (Mackie *et al.* 2008). As osteoblasts become entrapped in mineral, they extend long processes to connect to one another and become osteocytes (Klein-Nulend *et al.* 2003) being connected by this long canalicular network. Osteocytes have a different phenotype than osteoblasts expressing different amounts of phenotypic markers (Morinobu *et al.* 2003, Yang *et al.* 2005, Zhang *et al.* 2006).

Previous studies have shown that hydroxyapatite distribution increases with maturation of bone tissue. Moreover, other mineral species besides hydroxyapatite can be found in bone, such as amorphous calcium phosphate (ACP), octacalcium phosphate (OCP), β-tricalcium phosphate (β-TCP), and dicalcium phosphate dehydrate (DCPD) (Boskey *et al.* 1992).

I.2.1. Evaluation of the quality of minerals formed in cell culture

Currently, most of the published studies about mineralization and osteogenic differentiation only demonstrate the presence of calcium and phosphate ions in cell culture, without showing information whether the mineral formed is similar to hydroxyapatite or if the mineral is deposited with the correct organization on the appropriate matrix (i.e. aligned with collagen). Therefore, in order to characterize the mineral formed in cell culture and to evaluate its similarity to the mineral present in native tissue, different methods have been described to characterize cell culture mineral crystals. Although few studies have been applying these techniques, future research will need this data and information in order to evaluate the quality of the bone formed, specifically for bone tissue engineering applications, in which assuring the quality of newly formed bone is a requisite.

I.2.1.1. X-ray diffraction

X-ray diffraction (XRD) is the most common technique to identify the mineral phase present in a specific material (Wilson 1970). This technique can also be used to measure and calculate the average crystal size and orientation of the mineral crystals. However, to analyze the mineral produced by cell cultures, it is, sometimes, necessary to pool material from multiple cultures, since the mineral yield in cell cultures is often small.

I.2.1.2. SEM, TEM and related techniques

Scanning electron microscopy (SEM) and transmission electron microscopy (TEM) are widely used to demonstrate that the mineral crystals are aligned with respect to the collagen axis, as it can be observed *in situ* calcification. Using TEM, the orientation of the mineral on the collagen substrates can readily be demonstrated (Saruwatari *et al.* 2005, Potter *et al.* 2002, Hao *et al.* 1997, Wen *et al.* 1999) and size of mineral aggregated can be measured. Evaluation of the individual crystals formed in cell cultures can be done using selected area diffraction technique, performed under the TEM. However, to perform these analysis, samples have to be processed and they can be damaged, causing dissolution of the mineral crystals. Therefore, the resulting crystals might differ in size or composition from those initially present in the culture. Due to that reason, very few studies have used electron diffraction technique to identify the presence of hydroxyapatite in cell culture (Hunter *et al.* 1993, Nakagawa *et al.* 1993).

Moreover, energy dispersive X-ray (EDX) technique coupled with an electron microscope can also be used to provide information about the size distribution of the crystals and the chemical composition of the mineral deposited in culture (Bohic *et al.* 1998, Janssen *et al.* 2006, Rohde & Mayer 2007).

I.2.1.3. Atomic force microscopy

Atomic force microscopy (AFM) has been used to visualize living cells and protein surfaces, as well as to evaluate the properties of the crystals formed on the matrix produced by these cells. However, some considerations must be taken while using this technique since the force needed to be applied on the cells must be limited to prevent compression of the cell or, even, cell death. AFM has been used to characterize the growth of hydroxyapatite crystals into enamels prisms in the absence of cells (Chen *et al.* 2005, Habelitz *et al.* 2005). Regarding bone tissue engineering, precultured human bone marrow stromal cells were implanted in a mouse calvaria and AFM was used to characterize the mineral mechanical properties (Mankani *et al.* 2006). In a different study, AFM was applied to characterize the spherical bodies with which mineral is associated in the MLO-A5 late osteoblast/early osteocyte cell line (Barragan-Adjemian *et al.* 2006).

I.2.1.4. Light microscopy

Chemical stains can be applied to observe mineralization of cell cultures under the microscope, however it usually requires fixation. Indeed, at the light microscopic level, the stains used to identify the hydroxyapatite mineral in culture are alizarin red (AR) (which chelates calcium) and Von Kossa (VK) (which is a silver stain that causes silver phosphate to precipitate; the silver is then oxidized, leaving a black precipitate). The AR stain can also be solubilized and quantified spectrophotometrically.

Some fluorescent dyes such as xylenol orange or calcein blue can also be used to observe how calcium minerals distribute in the matrix (Wang *et al.* 2006).

I.2.1.5. Vibrational spectroscopy and vibrational spectroscopic imaging

Several investigators have been using Infrared (IR) and Raman spectroscopies to analyze the mineral phase formed in cell cultures (Bohic *et al.* 1998, Nauman *et al.* 2002, Phillips *et al.* 2006). Infrared and Raman spectroscopies give information on the local environment of ions with asymmetric and symmetric vibrations, respectively (Carden *et al.* 2000). Raman spectroscopy uses the inelastic scattering of light to acquire a vibrational spectrum that represents the chemical constituents of the sample (Tsao *et al.* 2017). Raman imaging is an attractive analytical tool because of its high specificity (fingerprint chemical information), low sensitivity to water and minimal sample preparation. Raman spectroscopy can be used in live cells, since it can be performed with long wavelength light that exhibits low phototoxicity (Schulze *et al.* 2010, Petry *et al.* 2003, Kendall *et al.* 2003, Tarnowski *et al.* 2002). In fact, these techniques have been used an *in situ* single cell detector for different applications, such as detection of cell cycle, cell death and identification of cell

components (Puppels *et al.* 1990, Notingher *et al.* 2004). In fact, Raman spectroscopy has become an attractive technique to evaluate bone quality, since it can be used with cells without fixation or treatment and, in some cases, can be used for non-invasive measurements on live animals (Mandair *et al.* 2015). However, compared with IR spectroscopy, like Fourier transform infrared (FTIR) spectroscopy, Raman spectroscopy has a lower signal/noise ratio. Moreover, IR spectroscopic imaging requires thinner sections, and there is interference from water, therefore, the culture usually is removed from the dish and treated or air-dried, lyophilized or embedded and sectioned. Raman spectroscopy has been used in non-invasive identification of the osteogenic differentiation of human mesenchymal stem/stromal cells (MSC) (Chiang *et al.* 2009, Hung *et al.* 2013), by the detection of hydroxyapatite, and mapping of bone tissue sections (Kazanci *et al.* 2007). On the other hand, Raman imaging has also been explored to monitor the osteogenic differentiation of MSC on 3-D scaffolds (Gao *et al.* 2016).

Figure I.10 shows a typical Raman spectrum of bone tissue. Bone matrix bands consists mostly of collagen type I. Although relative intensities of bands presented in Raman and FTIR spectra may be different, most matrix bands in the Raman spectra are the same as in the FTIR spectra. Only some exceptions occur such as the phenylalanine band present in the Raman spectrum (1003 cm^{-1}) that is weak or absent in the FTIR spectra and the amide II band in FTIR spectra (1540-1580 cm^{-1}) that is absent in the Raman spectra (Morris & Finney 2004).

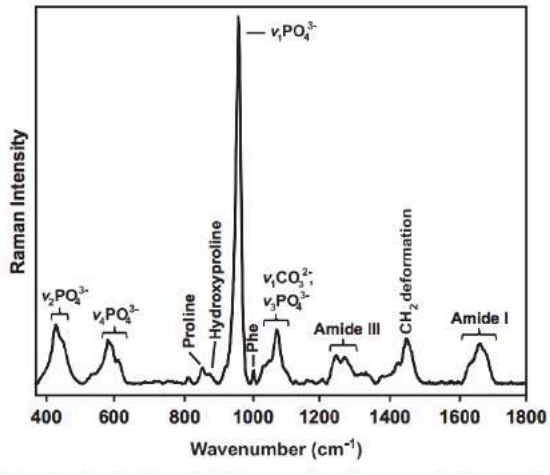

Figure I.10. Raman spectrum of mouse cortical bone. The regions of major bone mineral and matrix collagen can be found (Mandair *et al.* 2015).

Of note, mineral bands that are intense in Raman spectra will be weak in FTIR spectra and vice versa. It is also important to note that there is some variability in the positions of major bands. This variability can be due to differences among human or animal subjects used, such as differences in age and health status. Moreover, there may also be small systematic errors (1-2 cm^{-1}) from instrument drift or miscalibration.

Beyond matrix bands, mineral bands can also be detected by Raman spectroscopy. The most widely used mineral band is a phosphate band at ~960 cm^{-1} ($\nu_1PO_4^{3-}$), which is characteristic of carbonated apatites. The most intense β-type carbonate band at 1070 cm^{-1} ($\nu_1CO_3^{2-}$) for bone mineral lies close to a component of a phosphate band at 1076 cm^{-1} ($\nu_3PO_4^{3-}$), and accurate measurement requires careful band fitting (Awonusi *et al.* 2007).

Fourier transform infrared spectroscopic imaging has been used to characterize changes in the mineral or collagen phase of human bone during various conditions (Faibish *et al.* 2005, Paschalis *et al.* 2003, Boskey & Mendelsohn 2005). This technique has some advantages such as the fact that it enables visualization and measurement of the spatial composition of the tissue. With this technique, it is possible to identify samples, characterize unknown materials and determine the quality of a sample. Furthermore, in standardized conditions, the size of the peaks in the spectrum directly relates to the amount of the material. FTIR may provide a tool for diagnosing some metabolic bone diseases that alter tissue composition (Faibish *et al.* 2005, Boskey and Mendelsohn 2005). FTIR spectra of bone is represented in Figure I.11. The inorganic part of bone is mostly composed of crystalline mineral in the form of hydroxyapatite. Peaks of phosphate (900 to 1200 cm^{-1}), as well as carbonate (850 to 890 cm^{-1}) were described. Amide I peak (1584 to 1720 cm^{-1}) can be also observed and is referred to the organic part of bone, type I collagen.

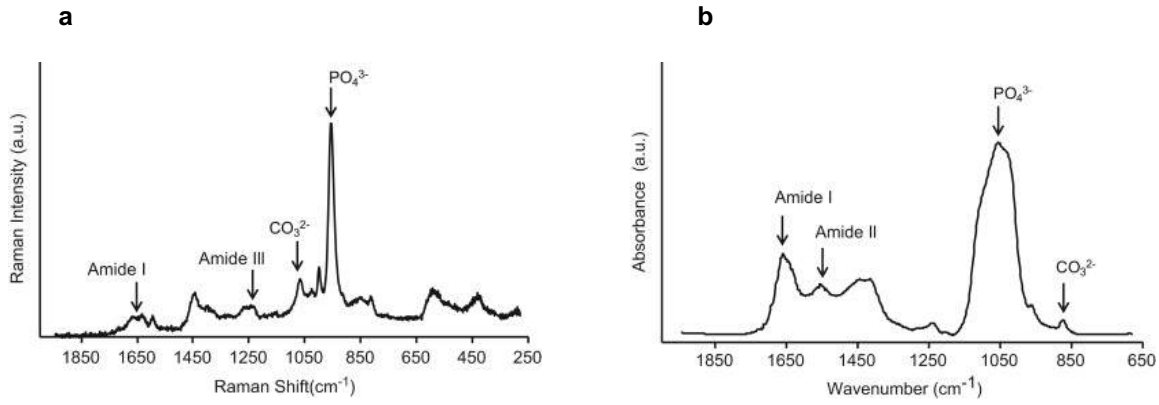

Figure I.11. Representative Raman and FTIR spectra of bone. **a)** Raman spectrum of bone showing the PO_4^{3-} (960 cm^{-1}), CO_3^{2-} (1077-1070 cm^{-1}) bands in hydroxyapatite and the amide I (1720-1616 cm^{-1} and amide III (1250 cm^{-1}) bands in collagen. **b)** FTIR spectrum of bone. The PO_4^{3-} (1200-950 cm^{-1}) and CO_3^{2-} (950-850 cm^{-1}) bands in hydroxyapatite and the amide I (1750-1600 cm^{-1}) and amide II (1600-1520 cm^{-1}) bands in collagen are indicated (Kimura-Suda *et al.* 2013).

By using vibrational spectroscopy techniques, researchers have been able to describe the evolution of mineralization during bone maturation by detecting different phases of mineral formed (Paschalis *et al.* 2003, Boskey *et al.* 2003, Tarnowski *et al.* 2002).

For example, IR spectroscopy of cell cultures can provide information on the characteristics of the mineral present in the culture (Motta *et al.* 2004, Luppen *et al.* 2003, Bonewald *et al.* 2003), whereas IR imaging allows visualization of the distribution of the mineral within the culture (Boskey *et al.* 2000, Boskey *et al.* 1996, Boskey *et al.* 1992b). Thus, temporal and spatial variations within mineralized cultures can be studied. The effects of cell genetic modifications and chemical modulation of the cells can also be evaluated as the culture

progresses using Raman spectroscopy, for example, evaluating mineralization by characterizing the mineral formed at different timepoints. Tsao and colleagues have used Raman spectroscopy to evaluate if the maturation of mineral species was affected by osteocalcin expression level. They found that when osteocalcin gene expression level was suppressed, the mineral species maturation was delayed due to the fact that HAP peak (carbonated apatite) was detected in a later timepoint compared with the control (Tsao *et al* 2017). A different study also used Raman spectroscopy to evaluate the maturation level during osteogenic differentiation of mesenchymal stem/stromal cells in live cells, by detecting different mineral phases involved in osteogenesis such as OCP, β-TCP and HAP (Hung *et al.* 2013).

I.2.1.6. Radiographic and related methods

Radiographic methods are used to detect changes in scattering elements and, thus, can distinguish the presence of calcium, usually as an increase in density. X-ray microcomputed tomography (μCT) can also be used for the study of mineralization in cultures, providing information about porosity and mineral deposition. μCT has been used to monitor scaffolds cultured *in vitro* and implanted *in vivo* (Cartmell *et al.* 2004). μCT provides a three-dimensional information of the culture, in contrast with other techniques. However, this technique does not provide information about the nature of the mineral present. Other techniques are related to nuclear magnetic resonance (NMR). This technique can show the difference in the environments of elements with spin dipoles (^{1}H, ^{31}P), thereby giving information about the changes in the phosphate distribution. In fact, this technique has been used to monitor and quantify bone formation on scaffolds (Potter *et al.* 2002), monitoring relaxation times to obtain maps of mineral deposition (Chesnick *et al.* 2007). Magnetic resonance microscopy has also been used to monitor the mineralization of tissue engineered constructs *in vitro* (Xu *et al.* 2006). This technique provides new information about mineral and matrix without having to dehydrate the tissue, however this equipment is not always available in most of the laboratories, limiting its broad applicability.

I.2.1.7. Chemical analysis

Chemical analysis of the calcium (Ca) and phosphate (P) content of cultures are frequently used to describe mineralization of cell cultures. However, these assays should be done to complement other techniques, since just showing an increase of calcium or phosphate contents with time is not sufficient and does not characterize the produced mineral.

Therefore, measurement of Ca/P ratios for mineral identification requires other techniques to verify that the mineral that was formed is comparable to that in the tissue whose composition is being mimicked.

I.3. Bone cells

Three major bone cell types are typically found in bone tissue and associated with bone homeostasis: osteoblasts, osteocytes and osteoclasts. These cell types are derived from two separate stem cell lineages – the mesenchymal lineage and the hematopoietic lineage.

I.3.1. Osteoblasts

Osteoblasts are cuboidal cells that are located along the bone surface being responsible for form new bone (Capulli *et al.* 2014, Florencio-Silva *et al.* 2015). Osteoblasts are derived from mesenchymal stem/stromal cells (MSC). During the commitment of MSC towards an osteogenic lineage, some specific genes are expressed, such as Runt-related transcription factors 2 (Runx2) and osterix (Osx) (Capulli *et al.* 2014, Florencio-Silva *et al.* 2015, Ducy *et al.* 1997). Runx2 upregulates osteoblast-related genes such as type I collagen (Col I), alkaline phosphatase (ALP), bone sialoprotein (BSP) and osteocalcin (OC) (Fakhry *et al.* 2013).

During osteogenic differentiation, after progenitor cells start to express Runx2 and Col I, there is a proliferation phase, in which ALP activity is present (Capulli *et al.* 2014). Mature osteoblasts are characterized by an increase in the expression of Osx and in the secretion of bone matrix proteins, such as osteocalcin and bone sialoproteins (Glass *et al.* 2005). Osteoblasts undergo morphological changes, becoming large and cuboidal cells. By becoming more mature, osteoblasts start to synthesize bone matrix in two steps: deposition of organic matrix and its mineralization. During deposition of matrix, osteoblasts secrete collagen proteins, mainly type I collagen, but also non-collagenous proteins, such as osteocalcin, osteonectin, bone sialoproteins, osteopontin and proteoglycans, including decorin and biglycans. All these components form the organic bone matrix and create a template for mineralization and production of the mature bone. During mineralization, osteoblasts release matrix vesicles from the apical membrane domain into the newly formed bone matrix. These vesicles can bind the organic components and sulphated proteoglycans can immobilize calcium ions that are stored with the matrix vesicles, due to its negative charge (Florencio-Silva *et al.* 2015, Yoshiko *et al.* 2007, Arana-Chavez *et al.* 1995). Then, osteoblasts secrete enzymes that can degrade the proteoglycans and, therefore, the calcium ions are released. On the other hand, ALP secreted by osteoblasts can also degrade phosphate-containing compounds and allow the release of phosphate ions inside the matrix vesicles. The phosphate and calcium ions inside the vesicles nucleate, forming the hydroxyapatite crystals (Glimcher *et al.* 1998). After that, supersaturation of calcium and phosphate ions occurs inside the matrix vesicles leading to the rupture of these structures and the hydroxyapatite crystals spread to the surrounding matrix (Boivin *et al.* 2002, Boivin *et al.* 2008).

Figure I.12 shows the temporal expression of various genes during the life cycle of the osteoblast phenotype *in vitro* (Stein *et al.* 1990).

At the end of their life cycle, osteoblasts either transform to osteocytes, getting embedded into the mineralized matrix, or die via apoptosis.

In addition to bone formation, osteoblasts can also secrete factors that recruit and promote the differentiation of monocytic lineage cells into osteoclasts, assisting in the initiation of bone resorption.

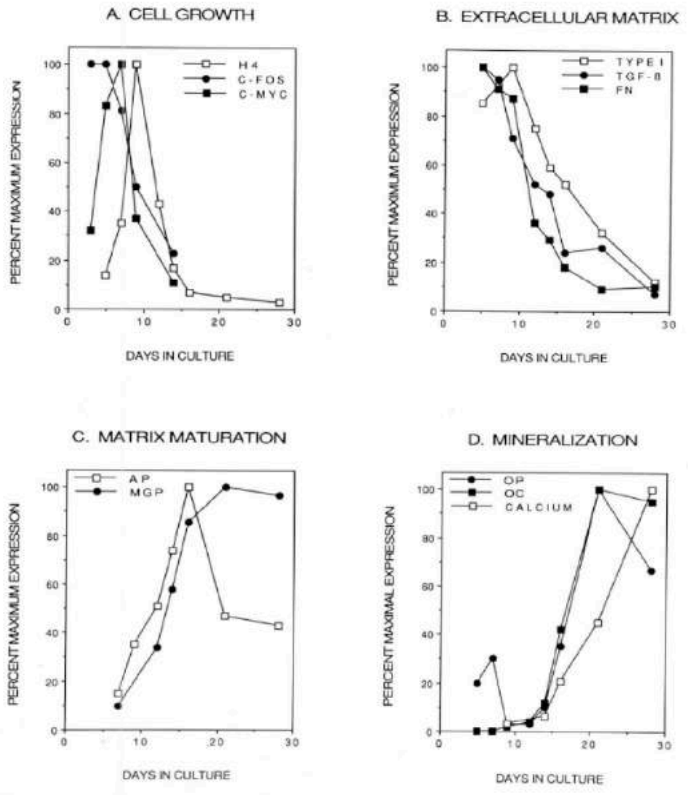

Figure I.12. Temporal gene expression during osteoblasts proliferation, differentiation, maturation and mineralization (Stein *et al.* 1990).

I.3.2. Osteocytes

Osteocytes are located within lacunae surrounded by mineralized bone matrix. Through the canaliculi, the osteocytes form a network and connect to other osteocytes. Osteocytes are derived from MSC lineage through osteogenic differentiation. At the end of bone formation cycle, a subpopulation of osteoblasts becomes osteocytes entrapped into the mineralized bone matrix and some osteoblast markers, such as OC, BSP, Col I and ALP, are downregulated (Mikuni-Takagaki *et al.* 1995). Some studies have demonstrated the role of osteocytic apoptosis in initiating bone resorption (Verbogt *et al.* 2000, Cardoso *et al.* 2009) and the role of osteocytes in mechanotransduction, therefore, osteocytes can regulate bone remodeling process, more specifically bone formation and resorption based on the levels of strain that the bone experiences (Han *et al.* 2004). Osteocytes create an interconnected network in bone responsible for intercellular communication between neighboring osteocytes and osteoblasts, allowing the transmission of mechanical and chemical signals across the network (Knothe Tate *et al.* 2004). Thus, bone can adapt to the external mechanical and chemical inputs that regulate bone homeostasis.

I.3.3. Osteoclasts

Osteoclasts are multinucleated cells, which are derived from mononuclear cells of the hematopoietic cell lineage (Quinn *et al.* 2005, Zaidi *et al.* 2003) under the influence of several factors, such as macrophage colony-stimulating factor (M-CSF), secreted by mesenchymal stem/stromal cells and osteoblasts (Boyce *et al.* 1999), and receptor activator of nuclear factor kappa-B ligand (RANKL), secreted by osteoblasts, osteocytes and stromal cells (Crockett *et al.* 2011). These factors allow the activation of transcription factors and gene expression in osteoclasts (Yavroupoulou *et al.* 2008).

Osteoclastogenesis can be induced when RANKL binds to its receptor RANK (Sodek *et al.* 2000). Osteoprotegerin (OPG) can be produced by different cells, such as osteoblasts and stromal cells (Boyce *et al.* 2008) and it can also bind to RANKL, preventing the interaction of RANK/RANKL and, consequently, inhibiting the osteoclastogenesis (Boyce *et al.* 2008). Therefore, the combination of RANKL/RANK/OPG system is essential to mediate the process of osteoclastogenesis (Phan *et al.* 2004).

Osteoclasts are bone resorbing cells responsible for the resorption of old or damaged bone matrix. When osteoclasts are active, they can form cavities on bone surface called resorption pits. Osteoclasts present a ruffled border, a region next to bone that has extensive membrane folding responsible for resorption. These ruffled border zone is surrounded by the clear zone – a region containing filamentous actin (Väänänen & Horton 1995). In order to remove bone, osteoclasts become polarized, form a ruffled membrane and adhere tightly to the bone matrix via an $\alpha_v\beta_3$ integrin mediated binding to the bone surface to form the "sealing zone". The osteoclast then secretes acid via H^+-ATPase for hydroxyapatite dissolution and proteases for matrix protein digestion, removing the underlying bone.

Osteoclasts express tartrate resistant acid phosphatase (TRAP), an important enzyme important for osteoclast attachment (Hayman *et al.* 2008).

Some bone diseases, such as osteoporosis, are known to have an abnormal increase in osteoclast formation, in which resorption activity exceeds formation of bone, causing decreased bone density that can enhance bone fractures (Feng & McDonald 2011). Osteopetrosis, on the other hand, is a bone genetic disease that affects the formation of osteoclasts and its resorption activity, leading to decreased bone resorption and, consequently, higher accumulation of bone mass (Sobacchi *et al.* 2013). Therefore, in order to maintain bone homeostasis, it is extremely important to have a normal bone remodeling process, without impairment of osteoclast activity.

Although not well explored yet, osteoclasts have also been reported to show other functions, such as being a source of cytokines that influence the activity of other cells. Osteoclasts can produce factors that control osteoblasts during the bone remodeling cycle and may also regulate the hematopoietic stem cell niche (Charles & Aliprantis 2014).

I.4. Bone development, formation and repair

During osteogenesis, there are two different processes of bone formation, intramembranous and endochondral ossification, and both involve the transformation of a preexisting mesenchymal tissue into bone tissue. Intramembranous ossification allows the formation of new bone tissue through the direct conversion of mesenchymal tissue into bone, occurring mostly in the bones of the skull. On the other hand, endochondral

ossification occurs through the differentiation of mesenchymal cells into cartilage, as an intermediate template, that is later replaced by bones.

I.4.1. Intramembranous ossification

During intramembranous ossification, bone is directly synthesized by mesenchymal stem/stromal cells from fibrous connective tissue. This is the process that forms and repairs the flat bones of the skull, clavicles and other irregularly shaped bones. This process of forming new bone is characterized by different phases (Figure I.13). First, new blood vessels are formed in the area, increasing vascularization. At the same time, MSC travel throughout the blood vessels to the site of new bone formation. In this site, MSC can differentiate into osteoblasts, forming the ossification centers. Osteoblasts, then, deposit osteoid (the unmineralized bone extracellular matrix, composed by collagen fibers and non-collagenous proteins) and are then trapped in the matrix, differentiating into osteocytes. Inorganic salts travel through the blood vessels and mineralize the bone matrix, forming hydroxyapatite crystals within the osteoid (Gilbert *et al.* 2000). On the interior of the tissue, small clusters of bone begin to connect with other clusters to form trabeculae around the blood vessels. Osteoblasts near the surface of bone deposit matrix in organized lamellae and form a thin outer layer of compact bone, the periosteum. The periosteum creates a protective layer of compact bone superficial to the trabecular bone. The trabecular bone crowds nearby blood vessels, which eventually condense into red marrow (Figure I.13).

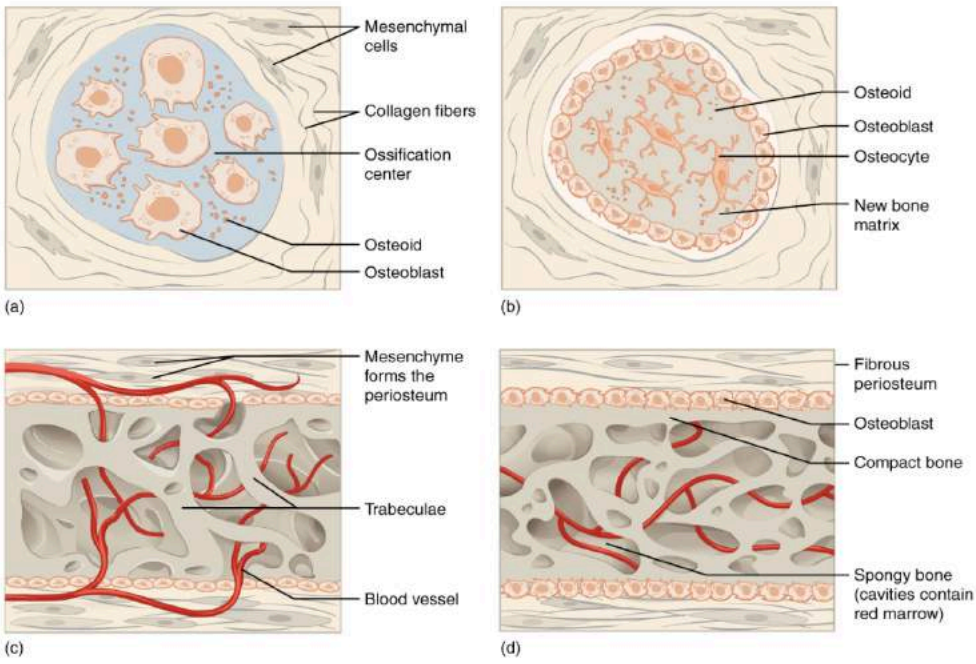

Figure I.13. Schematics of intramembranous ossification. Four steps are represented: **a)** Mesenchymal cells group into clusters, forming osteoblasts and ossification centers. **b)** Secreted osteoid traps osteoblasts into the matrix, differentiating into osteocytes. **c)** Trabecular matrix and periosteum form. **d)** Blood vessels condense into red marrow (Gilbert *et al.* 2000).

Bone morphogenetic proteins (BMP) and transcription factor core-binding factor alpha-1 (CBFA1) are involved in intramembranous ossification process. BMP can activate the CBFA1 gene in the mesenchymal stem cells, activating some osteogenic genes, such as OC and OPN, and other bone-specific extracellular matrix proteins, allowing them to differentiate into osteoblasts (Gilbert *et al.* 2000).

I.4.2. Endochondral ossification

During endochondral ossification, new bone is formed by replacing hyaline cartilage, that serves as a template, with new bone. Endochondral ossification is responsible for the formation of the bones at the base of the skull and long bones. Endochondral ossification involves the formation of cartilage tissue from aggregated mesenchymal stem cells, and the subsequent replacement of cartilage tissue by bone (Horton 1990). This process involves the following steps: formation of a cartilage template, growth of the template, differentiation, vascularization, calcification and bone formation (Figure I.14). First, paracrine factors induce the nearby mesodermal cells to express two transcription factors, *Pax1* and *Scleraxis* that can activate cartilage-specific genes (Cserjesi *et al.* 1995, Sosic *et al.* 1997), leading mesenchymal stem cells to be committed to a chondrogenic lineage. After that, mesenchymal stem cells condense into compact nodules, through the action of N-cadherin and neural cell adhesion molecule (N-CAM) (Oberlender & Tuan 1994, Hall & Miyake 1995) and differentiate into chondrocytes. During the third phase of endochondral ossification, the chondrocytes proliferate very fast and develop the template for the bone, secreting a cartilage-specific extracellular matrix. After proliferating, the chondrocytes stop dividing and increase their volume dramatically, becoming hypertrophic chondrocytes. Moreover, the matrix produced by hypertrophic chondrocytes is changed by enhancing collagen X and fibronectin production to enable it to become mineralized. Furthermore, the hypertrophic chondrocytes die by apoptosis, as the matrix calcifies and nutrients can no longer reach the chondrocytes. The last phase of endochondral ossification involves the invasion of the cartilage template by blood vessels, transporting osteogenic cells with them that will differentiate into osteoblasts. These enlarging spaces eventually combine to become the medullary cavity.

As the cartilage grows, capillaries penetrate it and osteoblasts create the primary ossification center, beginning to form bone matrix on the partially degraded cartilage (Bruder & Caplan 1989, Hatori *et al.* 1995). Moreover, chondrocytes continue to grow at the ends of the bone, increasing the length of the bone at the same time that bone is replacing cartilage in the diaphysis. Thus, after completely skeletal development, cartilage only remains at the joint surface as articular cartilage and between the diaphysis and epiphysis as the epiphyseal plate. Moreover, after birth, the same events occur (matrix mineralization, death of chondrocytes, blood vessel penetration transporting osteogenic cells that differentiate into osteoblasts) in the epiphyseal regions forming the secondary ossification centers.

In normal conditions, the cartilage should be replaced by bone, acting only as a model for the bone that follows.

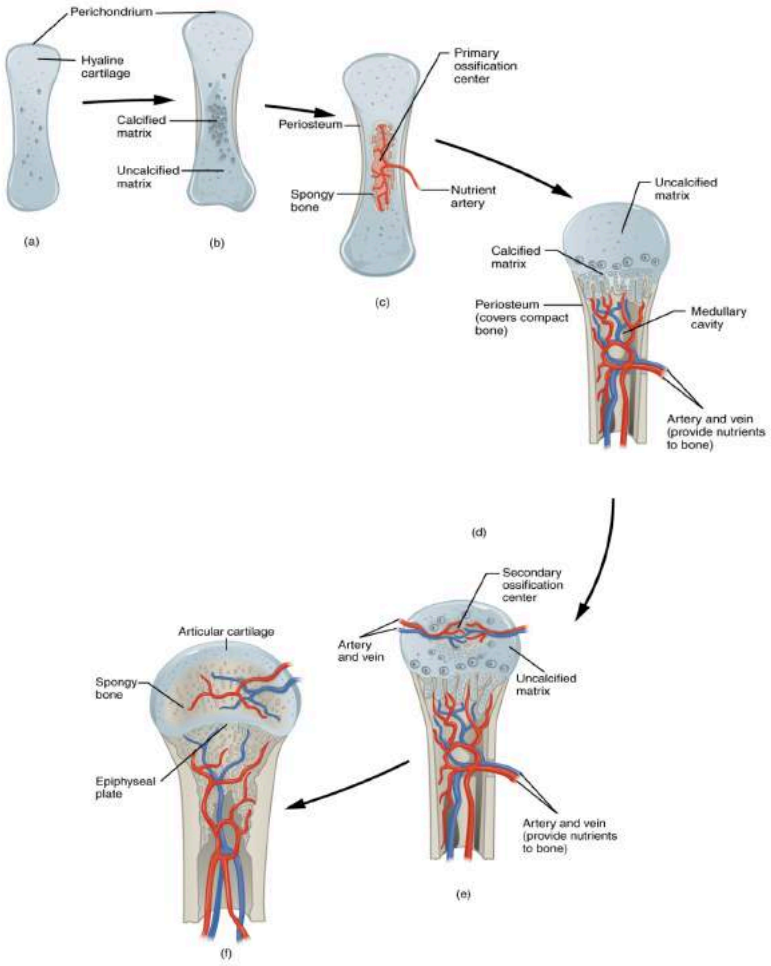

Figure I.14. Schematic diagram of endochondral ossification. **a)** Mesenchymal stem cells differentiate into chondrocytes. **b)** Cartilage template forms. **c)** Capillaries penetrate cartilage. Primary ossification center develops. **d)** Cartilage and chondrocytes continue to grow at ends of the bone. **e)** Secondary ossification centers develop. f**)** Cartilage remains at epiphyseal plate and at joint surface as articular cartilage (Bone formation and development, Rice University).

I.4.3. Bone Remodeling

The process of bone modeling refers to bone formation and bone matrix resorption at different sites of bone tissue, leading to bone changes in size and shape. During adult life, bone undergoes remodeling, a highly complex process, in which old or damaged bone is resorbed and new bone is deposited by osteoblasts (Bilezikian *et al.* 2008). Remodeling process occurs throughout adult life, in both cortical and trabecular bone, and it is influenced by the coordinated action of bone cells, such as osteoblasts and osteoclasts. Together with the replaced bone, these cells form the bone remodeling unit or bone multicellular unit (BMU) (Frost 1973, Andersen *et al.* 2009). The BMU begins with the activation of progenitor cells that differentiate into osteoclasts. The osteoclasts resorb old bone by moving along the long axis of bone to create a cavity. Then, a cement line is laid over the cavity surface and osteoblasts deposit osteoid which then mineralizes to form new bone.

Normal bone remodeling is necessary for fracture repair and skeleton adaptation to mechanical use (Dallas *et al.* 2013). Under normal conditions, the remodeling process results in no net change in bone mass. If an abnormal bone remodeling occurs, with an imbalance of bone resorption and formation, several bone diseases can be developed. Osteoporosis is an example in which excessive resorption by osteoclasts occurs, with an imbalance bone formation by osteoblasts, contributing to bone loss (Khosla *et al.* 2012), whereas, if more new bone is being formed, without a coordinated action of osteoclasts, osteopetrosis can occur (Sobacchi *et al.* 2013). Thus, the equilibrium between bone formation and resorption is necessary and depends on the action of several local and systemic factors including hormones, cytokines, chemokines, and biomechanical stimulation (Phan *et al.* 2004, Crockett *et al.* 2011).

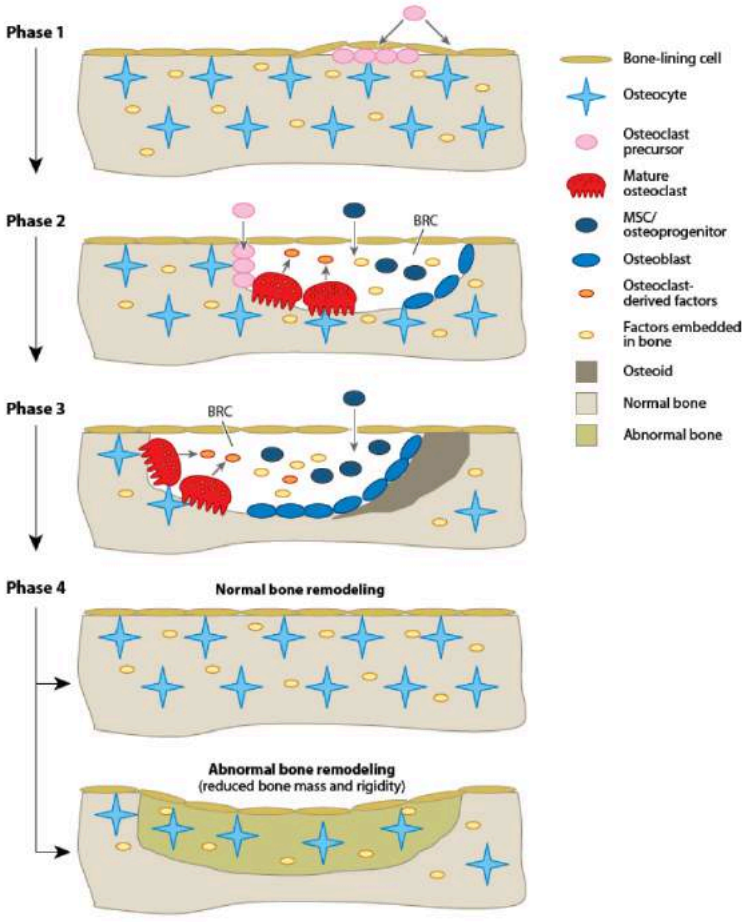

Figure I.15. Schematic diagram of bone remodeling process. Phase 1: osteoclast precursors assemble at the surface of bone and group to form osteoclasts. Phase 2: mature osteoclasts start resorption, forming a cavity. Some factors responsible for osteoblast recruitment are released by the osteoclasts. Mesenchymal stem/stromal cells migrate to the resorption site and differentiate into osteoblasts. Phase 3: osteoblasts lay down unmineralized osteoid. Phase 4: mature osteoblasts are entrapped in the mineralized matrix and form osteocytes. Abnormal remodeling due to defective cell function may result in reduced bone mass and rigidity (Feng et al. 2011).

I.4.4. Bone Repair

Bone tissue has the ability to heal without forming a fibrous scar. Therefore, fracture healing process recapitulates bone development. Nevertheless, bone healing process can fail, leading to delay healing or even to the development of non-union fractures (Marsell & Einhorn 2010, Marsell & Einhorn 2011).

Immediately following the trauma, a hematoma can be observed, consisting of cells from peripheral blood and bone marrow cells. To regenerate bone tissue, different natural processes occur in response to the acute inflammation produced in the fracture site and causes the hematoma to coagulate forming a template for callus formation (Gerstenfeld *et al.* 2003). During this time, proinflammatory molecules are secreted, such as tumor necrosis factor-α (TNF-α), interleukin-1 (IL-1), IL-6, IL-11 and IL-18 (Gerstenfeld *et al.* 2003). These factors recruit inflammatory cells, promote angiogenesis (Sfeir *et al.* 2005) and some of them induce osteogenic differentiation, such as TNF-α (Cho *et al.* 2006). Therefore, MSC can be recruited to the injured site, where they can proliferate and differentiate into osteogenic cells. The molecular mechanism responsible for the recruitment of these cells is still under investigation. It has been suggested that BMP-2 and BMP-7 have an important role in this recruitment (Tsuji *et al.* 2006, Bais *et al.* 2009), specially for bone repair.

During natural fracture healing, both intramembranous and endochondral ossification occurs. However, endochondral ossification is the most common mechanism observed during bone repair. Following the formation of the hematoma, a fibrin-rich granulation tissue forms (Rahn 2002). Chondrocytes from the endosteum create an internal callus by secreting a fibrocartilaginous matrix between the two ends of the broken bone, while the periosteal chondrocytes and osteoblasts create an external callus of hyaline cartilage and bone, respectively, around the outside of the break. Within this tissue, endochondral formation occurs in between the fracture ends, and external to periosteal sites. At the same time, an intramembranous ossification response occurs subperiostally directly adjacent to the distal and proximal ends of the fracture, generating a hard callus.

Moreover, revascularization of the injury site is crucial for successful bone repair (Keramaris *et al.* 2008). Vascularization is mainly regulated by two molecular pathways, an angiopoietin (Ang)-dependent pathway, and a vascular endothelial growth factor (VEGF)-dependent pathway (Tsiridis *et al.* 2007). Therefore, angiopoietins have been shown to enable an initial vascular growth from pre-existing blood vessels in the periosteum (Lehmann *et al.* 2005). On the other hand, the VEGF pathway is the key regulator of vascular regeneration (Keramaris *e al.* 2008), promoting both the formation of new vessels from the aggregation and proliferation of endothelial cells into a vascular plexus (vasculogenesis) and the formation of new vessels from pre-existing ones (angiogenesis) (Kanczler & Oreffo 2008). It was reported that the blocking of VEGF-receptors inhibits vascular in-growth and delays or disrupts the regenerative process (Keramaris *et al.* 2008, Ai-Aql *et al.* 2008).

Moreover, chondrocytes in the primary cartilaginous callus become hypertrophic and the extracellular matrix becomes calcified, starting the replacement of this mineralized cartilage by a hard bony callus. Nevertheless, a second resorptive phase is needed to remodel the hard callus into a lamellar bone structure (Gerstenfeld *et al.* 2003), giving the biomechanical properties of bone.

Due to its complexity, this remodeling process may take years to be completed, in order to achieve a fully regenerated bone structure.

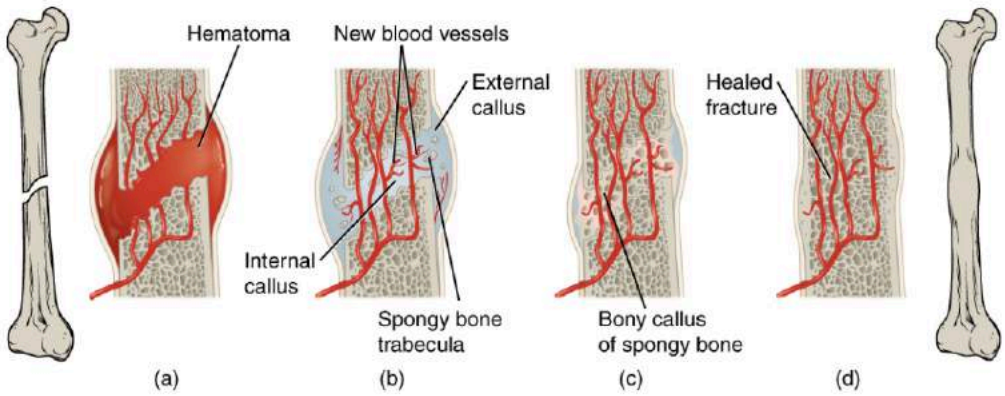

Figure I.16. Schematics of fracture healing process. **a)** Hematoma is formed in the injury site. **b)** Internal and external calli form. **c)** Cartilage of the callus is replaced by trabecular bone. **d)** Remodeling occurs.

I.5. Angiogenesis and osteogenesis

Bone is a highly vascularized tissue that can regenerate itself without the formation of fibrous scar tissue and has the ability to maintain its physiological and mechanical characteristics. Normal fracture healing in adults occurs through intramembranous or endochondral bone formation, closely mimicking skeletal development in the embryo (Stegen *et al.* 2015) and both processes occur in close proximity to vascular ingrowth. Bone regeneration is a complex process that requires highly orchestrated interactions between different cells and signals, such as blood vessels and bone cells (Kanczler & Oreffo 2008). Thus, angiogenesis plays a crucial role in skeletal development and bone fracture repair.

Angiogenesis is the process by which new blood vessels are formed from pre-existing ones. Recent studies have highlighted the fundamental aspects of vessel formation, including vasculogenic assembly, vessel sprouting, lumen formation and vascular remodeling (Adams & Alitalo 2007, Jain 2003).

Bone health depends on vascularization, since blood vessels can provide oxygen, nutrients, minerals and soluble factors, regulating bone homeostasis (Grosso *et al.* 2017, Hankenson et al. 2011). In the bone marrow, the vasculature also provides a microenvironment for hematopoietic stem cells (HSC), regulating their quiescence and mobilization (Kunisaki et al. 2013). Notably, endothelial cells residing in the blood vessels also provide paracrine signals that are responsible for growth, differentiation and regeneration of bone tissue, promoting osteogenesis (Ramasamy et al. 2014).

I.5.1. Interaction of endothelium and bone

The microvascular endothelium is an important part of skeletal tissue, where the interactions between endothelium and bone cells occur, playing a critical role in the homeostasis of bone integrity. In fact, some *in vitro* studies have shown that human umbilical vein endothelial cells (HUVEC) conditioned medium enhanced

the proliferation of human bone marrow (BM) stromal cells. Moreover, Villars and colleagues demonstrated that direct contact between BM MSC and HUVEC *in vitro* enhanced the expression and activity of ALP, an early osteoblastic marker (Villars *et al.* 2000). Both BM MSC and the endothelial network express connexin 43 (Cx43) a specific gap junction protein, being able to communicate via a gap junctional channel constituted at least by Cx43 (Villars *et al.* 2002).

Interestingly, the intercellular signaling pathways of endothelial cells have also been shown to have some effects in the functions of osteoclasts. In fact, osteoclast precursors have been shown to adhere and migrate through the endothelium to bone resorption areas (Imhof and Dunon 1997). Thus, it has been hypothesized that the endothelium may direct osteoclast precursor to specific areas of bone, playing an important role in resorptive process (Parfitt 2000). Therefore, deficient microvascular supply network will also affect the resorption activity resulting in decrease bone formation, regeneration and repair (Glowacki 1998).

I.5.2. Angiogenesis in bone repair

However, despite the remarkable regenerative capacity of bone tissue, fracture healing fails in about 10% of the cases leading to delayed union or non-union fractures (Gowacki 1998). In most of the cases, inappropriate vascularization of the tissue is the major cause of delayed union or non-union during fracture healing (Gowacki 1998). Therefore, adequate blood supply has been shown to be extremely important for successful bone healing.

Table I.2. Angiogenesis-stimulating growth factors. (Adapted from Stregen *et al.* 2015).

	Osteoblastic[1]	***Angiogenic***[2]	***Induction of VEGF***[3]
Angiopoietin	+	+	ND
Fibroblast growth factors	+	+	+
Bone morphogenetic proteins	+	+	+
Insulin-like growth factor family	+	+	+
Platelet-derived growth factor	+	+	+
Transforming growth factor beta family	+	+	+
Vascular endothelial growth factor	+	+	NA

NA- not applicable; ND-not yet determined.

[1] Direct effect on preosteoblasts or osteoblast.

[2] Stimulation of blood vessel formation *in vivo*, direct or indirect.

[3] Induction of VEGF *in vitro* or *in vivo*.

During bone development and normal fracture healing, different factors stimulate angiogenesis directly, such as vascular endothelial growth factor (VEGF), placental growth factor (PlGF), fibroblast growth factor (FGF), various members of the transforming growth factor beta family (TGF-β). Others have angiogenic properties and mainly regulate the production of angiogenic molecules, such as BMP, angiopoietins (Ang-1), Platelet derived growth factor (PDGF) and insulin-like growth factor family members (IGF-1, IGF-2) (Table I.2) (Kanczler & Oreffo 2008, Madeddu *et al.* 2005). Recent developments using *in vitro* and *in vivo* models of osteogenesis and fracture repair have provided a better understanding of the recruitment nature of the vasculature in skeletal development and repair (Brandi *et al.* 2006).

During bone repair process, after fracture, a hematoma is formed at the injury sited due to disruption of blood vessels and fracture site becomes hypoxic. Activation of the hypoxia signaling pathway stimulates the production of VEGF and PlGF by different cell types at the fracture site. Moreover, early blood vessel formation supports the invasion of inflammatory cells, such as neutrophils and macrophages. Neutrophils are recruited to the injury site and can phagocytose tissue debris and microorganisms (Claes *et al.* 2012, Hu and Olsen 2016). Then, macrophages are recruited to remove the dead neutrophils, promote angiogenic response and initiate the repair cascade (Wu *et al.* 2013).

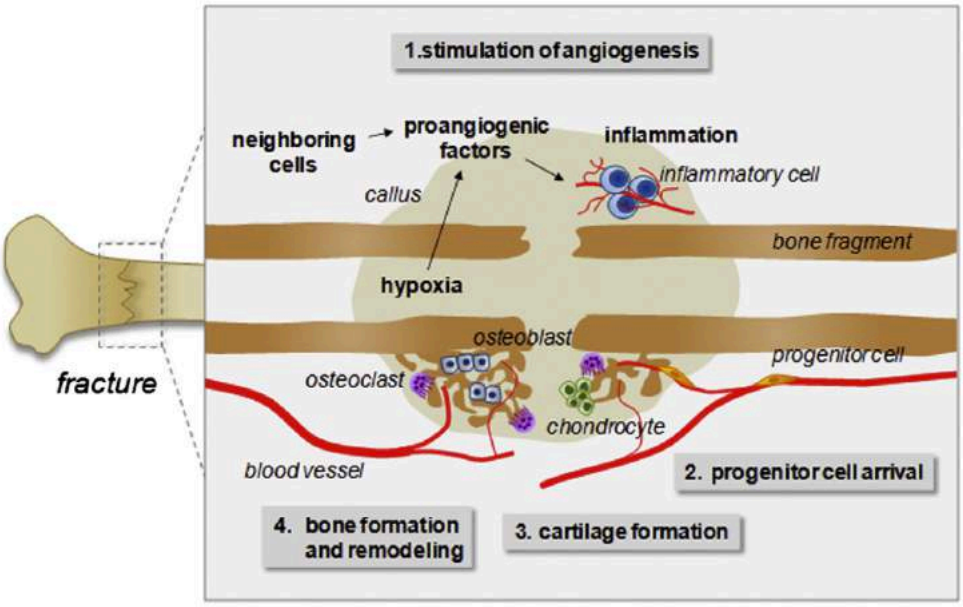

Figure I.17. Angiogenic response during normal fracture healing. Hypoxia due to the rupture of blood vessels stimulates the production of proangiogenic factors that will recruit inflammatory cells, which contribute to the fracture healing process and produce proangiogenic cytokines. Progenitor cells then migrate to the fracture site and differentiate into cartilage and bone (Stregen *et al.* 2015).

Furthermore, the vascular system allows the migration of MSC to the injury site where they proliferate and differentiate into osteoblasts or chondrocytes, promoting bone regeneration by supplying oxygen, nutrients and ions necessary for mineralization.

I.5.3. VEGF in endochondral and intramembranous ossification during bone repair

VEGF belongs to a family of homodimeric proteins consisting of at least 6 members: VEGF-A (VEGF), VEGF-B, VEGF-C, VEGF-D, VEGF-E and PlGF (Ferrara *et al.* 2003, Hu & Olsen 2016b).

Vascular endothelial growth factor-A (VEGF) is one of the most important regulators of angiogenesis, playing important roles in proliferation, migration and activation of endothelial cells as well in permeability of blood vessels (Ferrara *et al.* 2003), being critical for both bone development and regeneration. In these processes, VEGF has a dual role, acting both on endothelial cells to promote their migration and proliferation, and stimulating osteogenesis through the regulation of osteogenic growth factors (Grosso *et al.* 2017, Schipani *et al.* 2009). During endochondral ossification, VEGF is required to promote vessel invasion and recruitment of chondrocytes, allowing the substitution of the cartilaginous template by bony callus (Grosso *et al.* 2017, Gerber *et al.* 1999, Carlevaro *et al.* 2000, Hu and Olsen 2016b). VEGF may regulate the differentiation of skeletal stem cells from bone marrow, periosteum and surrounding muscles into either chondrocytes or osteoblasts. In the later stage of endochondral ossification, chondrocytes in the cartilaginous template stop proliferating and become hypertrophic chondrocytes. These hypertrophic chondrocytes express Osx (Tang *et al.* 2012), a strong inducer of VEGF expression, producing high levels of VEGF (Carlevaro *et al.* 2000, Zelzer *et al.* 2001). The high levels of VEGF will stimulate vessel invasion and facilitate the substitution of the cartilaginous templates by bony callus. Moreover, Osx-expressing osteoblast precursors produce high amounts of VEGF that allows its differentiation into osteoblasts (Figure I.18). On the other hand, VEGF has also been reported to be necessary during intramembranous ossification (Street *et al.* 2002, Carvalho *et al.* 2004, Wan *et al.* 2008, Percival *et al.* 2013). When exposed to hypoxia during inflammation, osteoblasts release factors, such as VEGF, via the hypoxia-inducible factor-1 alpha (HIF-1α) pathway. This activates endothelial cells, and promotes vessel permeability (Wan *et al.* 2008). Vascularization will allow the migration of bone progenitor cells and will enhance the transfer of oxygen, nutrients and minerals required for mineralization. In addition, cells in blood vessels secret also osteogenic factors, such as BMP-2, promoting mineralization and bone formation (Matsubara *et al.* 2012). Moreover, these osteoblasts will then release angiogenic factors, such as PDGF and VEGF, to further support angiogenesis (Figure I.19). Angiogenesis and osteogenesis are, therefore, intimately connected and they must be tightly coupled for physiological bone function. During bone repair, the levels of VEGF are crucial to define the bone healing outcome, since too little VEGF may interrupt communication between blood vessels and bone cells and too much VEGF levels can also compromise bone repair response (Figure I.20). In fact, alteration in vascular growth can compromise physiological bone healing, leading to bone tissue death, osteoporosis and non-union fractures (Dickson *et al.* 1994, Martinez 2002, Feng *et al.* 2010, Fassbender *et al.* 2011, Zhao *et al.* 2012). Moreover, VEGF overexpression may also cause bone resorption due to excessive osteoclast recruitment (Helmrich *et al.* 2013). Therefore, different doses of VEGF can have opposite effects on bone, however the underlying mechanisms through which VEGF regulates bone homeostasis are not yet fully understood and need further investigation.

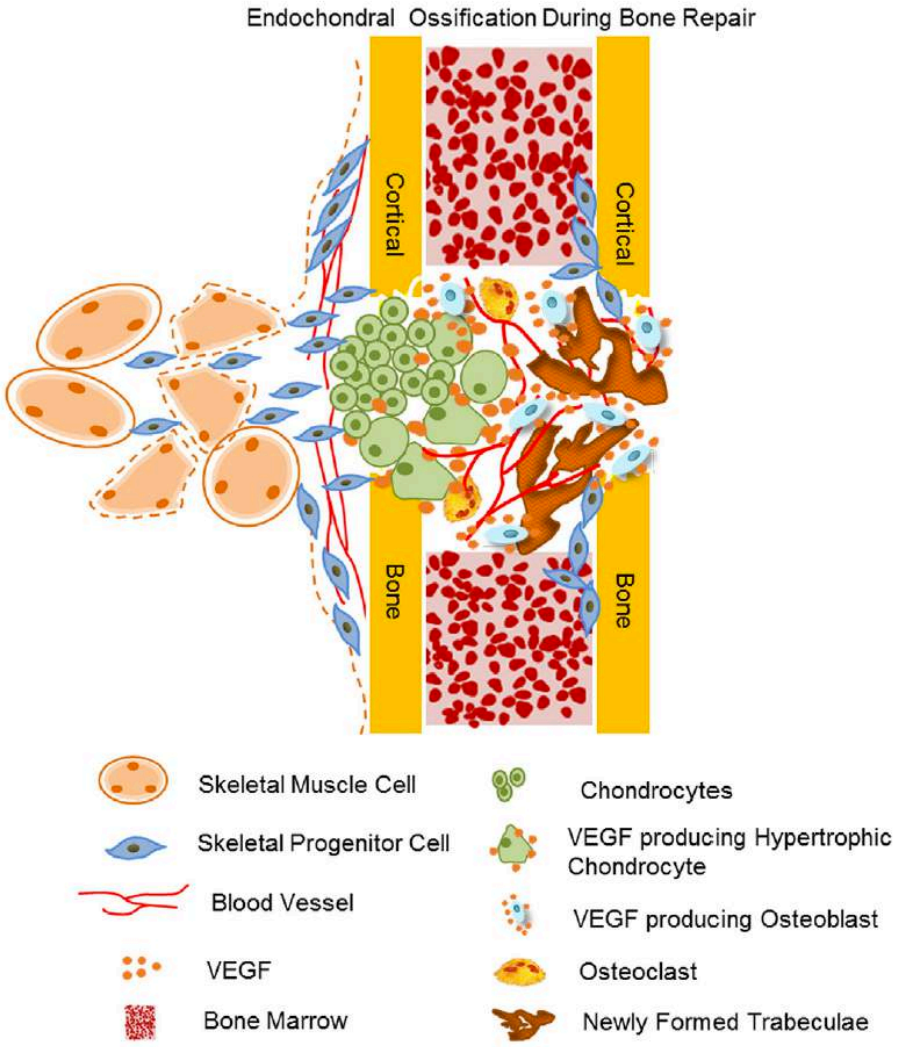

Figure I.18. VEGF effects in endochondral ossification during bone repair. VEGF may regulate the differentiation of skeletal progenitor cells into chondrocytes or osteoblasts. In endochondral ossification, chondrocytes stop proliferating and become hypertrophic, expressing Osx that is able to induce VEGF expression. High levels of VEGF are produced and stimulate vessel invasion, facilitating the replacement of the cartilaginous template by bony callus. Moreover, osteoblast precursors expressing Osterix also produce high amounts of VEGF that stimulates their differentiation, enhancing bone formation (Hu and Olsen 2016b).

I.5.4. VEGF effects on osteogenic differentiation of mesenchymal progenitor and bone regeneration

Osteoprogenitor cells and osteoclasts also express VEGF receptors (Hu and Olsen 2016). Several studies have reported that VEGF can directly affect osteogenic differentiation into osteoblasts. Mayer and colleagues showed that VEGF overexpression in human MSC increased the deposition of mineralized extracellular matrix, while overexpression of a blocker of VEGF (sFLT-1) reduced mineralization (Mayer *et al.* 2005). Moreover, using mice with deletion of VEGF receptors Vegfr1 or Vegfr2 in osteoblasts, Liu and co-workers demonstrated that these mice presented lower bone density and reduced number of osteoprogenitor

cells in the bone marrow, indicating that both receptors in osteoblasts are important for bone formation (Liu *et al.* 2012). A different study from Hu and Olsen confirmed that VEGF is released by osteogenic cells at the injury sites of a cortical bone defect and that VEGF deletion in osteoblasts affects the synergy between angiogenesis and osteogenesis, delaying the bone healing process (Hu and Olsen 2016) (Figure I.20a,b). Besides the important functions of VEGF secreted, intracellular VEGF has been described to control transcriptional regulation and cell survival (Liu et al. 2012).

VEGF can also regulate other molecules, such as bone morphogenic proteins in osteoblasts and endothelial cells (Figure I.20b) (Maes *et al.* 2010, Yang *et al.* 2013). Interestingly, osteoblasts produce BMP-2 that acts in an autocrine manner and stimulates differentiation of osteogenic cells and production of VEGF (Figure I.19). Moreover, due to the production of high levels of VEGF, BMP-2 protein expression is also enhanced (Yang *et al.* 2013). On the other hand, VEGF can up-regulate BMP expression also in endothelial cells (Figure I.20b), inducing osteogenic differentiation and matrix mineralization.

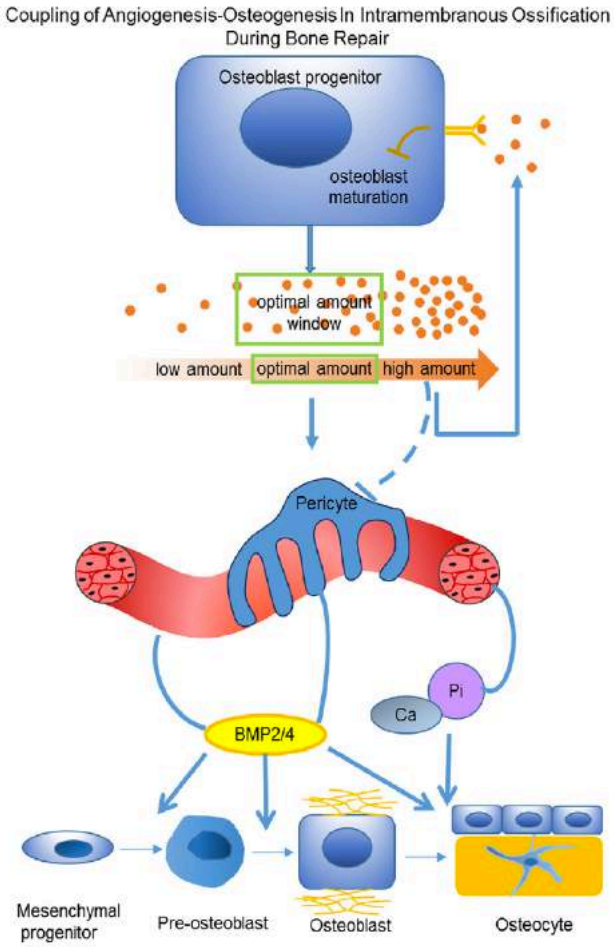

Figure I.19.The effects of VEGF in intramembranous ossification during bone repair. Osteoblasts release factors, such as VEGF, stimulated by hypoxia. VEGF can act through its receptors on endothelial cells, inducing angiogenesis, leading to an increase in oxygen and nutrients supply. Increased vascularization may also enhance the migration of stem cells and preosteoblasts and increase the levels of osteogenic growth factors, such as BMP produced by endothelial cells. In turn, osteoblasts also produce angiogenic factors (Hu and Olsen 2016b).

I.5.5. VEGF effects on recruitment of osteoclasts and immune cells

VEGF has direct and indirect effects on bone development by affecting other cell types involved in bone formation and repair processes. Rather than MSC, osteoprogenitors and osteoblasts, osteoclasts also express both VEGF and VEGF receptors. Moreover, VEGF signaling affects osteoclasts and induces their recruitment, differentiation and activity (Dirckx *et al.* 2013). In the inflammatory phase of bone repair, VEGF expression is induced by hypoxia in osteogenic cells (Street *et al.* 2002), leading to the recruitment of immune cells. In addition, monocytes and macrophages also respond to VEGF signaling, migrating to the injury site (Barleon *et al.* 1996).

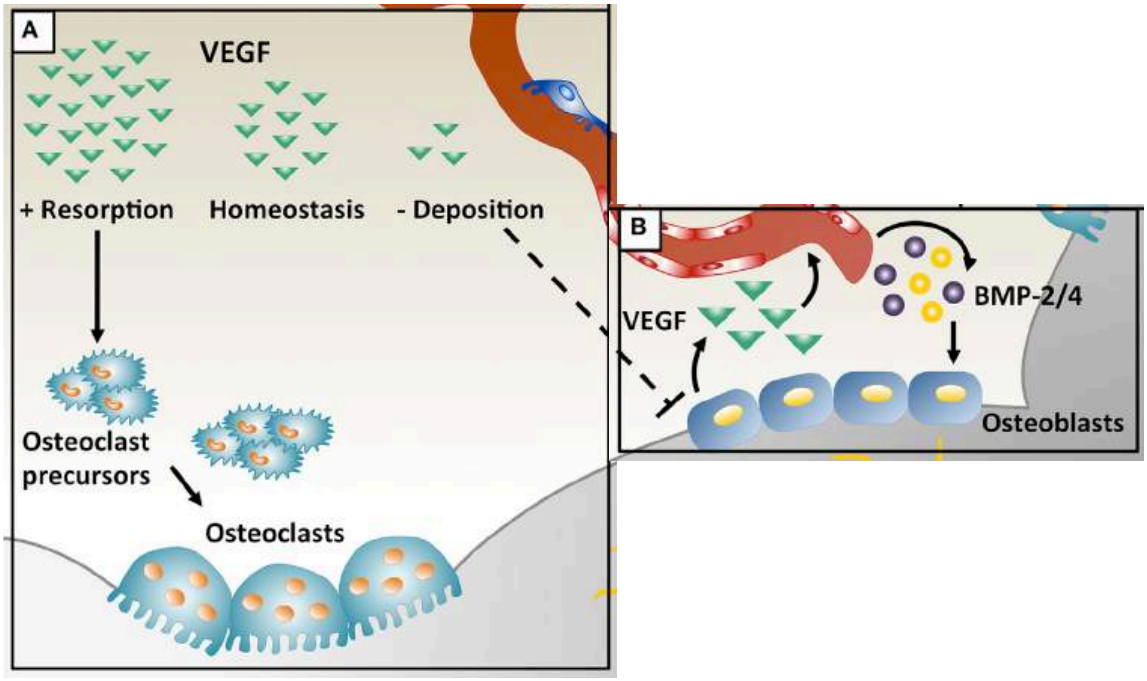

Figure I.20. Synergy of angiogenesis and osteogenesis during intramembranous ossification. **a)** Effects of alterations in the VEGF levels. Physiological levels of VEGF maintain bone homeostasis. However, too little VEGF affects osteoblast differentiation and too much VEGF enhances bone resorption due to osteoclast recruitment. **b)** Osteoblasts produce VEGF that promotes migration and proliferation of endothelial cells. In turn, endothelial cells generate osteogenic growth factors, such as BMP-2 and BMP-4, important for osteogenic differentiation (Adapted from Grosso *et al.* 2017).

I.5.6. Vascularization in bone tissue engineering

Bone tissue engineering has been focusing on developing bone substitutes to replace large bone tissue defects, which can be caused by trauma, surgery or disease. Reconstruction of damaged tissue relies on the combination of a scaffold, osteogenic cells and osteogenic or/and angiogenic growth factors. Vascularization also plays a crucial role in bone tissue engineering, since the reestablishment of an adequate blood flow is a major requirement for the success of bone healing. In fact, upon implantation *in vivo*, a major challenge for clinical-size bone substitutes is the maintenance of cell viability in the graft, which depends on blood vessel supply of oxygen, nutrients and waste removal. After implantation of the scaffold, an angiogenic response is elicited by inflammatory cytokines as part of the normal healing process (Hu and Olsen 2016). Finally, blood vessels deriving from the host vasculature should invade the scaffold, promoting neovascularization. Besides that, during the early stages of bone regeneration, vascularization of the scaffold will also allow the recruitment of different cell types, such as osteoprogenitors, hematopoietic stem cells and immune cells that play crucial roles in tissue remodeling and bone tissue formation (Hu and Olsen 2016). Different strategies to improve vascularization of bone grafts are currently being investigated with limited success. Several approaches have been proposed to improve the vascularization of bone constructs, such as the delivery of angiogenic growth factors, the application of endothelial cells to create a vascular network or the optimization of scaffold properties (Stegen *et al.* 2015) (Figure I.21).

Although progresses have been made in understanding the importance of angiogenesis during bone repair, challenges remain in the design of strategies to improve efficient vascularization and bone formation, thus elucidation of the molecular cross-talk between angiogenesis and osteogenesis is required to exploit the therapeutic potential of VEGF.

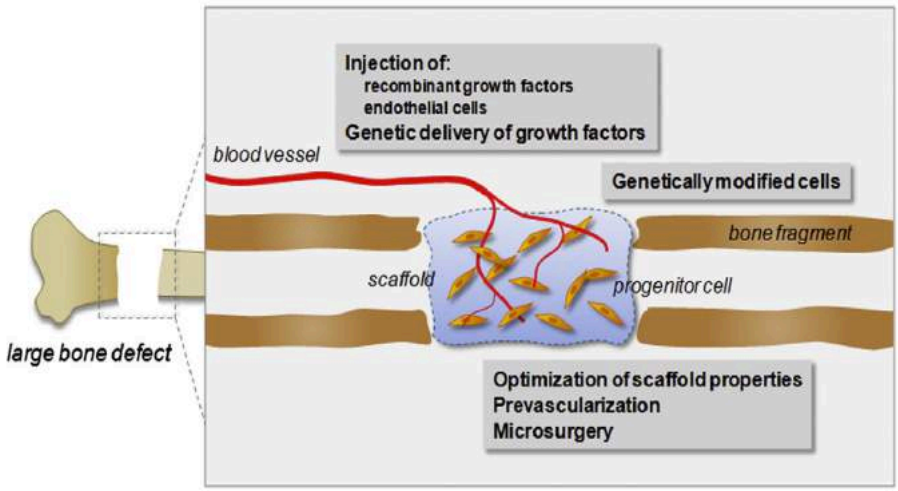

Figure I.21. Different strategies to improve vascularization of bone grafts: delivery of angiogenic growth factors, use of endothelial cells to create a vascular network and engineering scaffold properties (Stegen *et al.* 2015).

I.6. Bone extracelular matrix

I.6.1. Extracellular matrix

Extracellular matrix is present in all tissues and organs and consists of a large variety of macromolecules that can differ in composition and structure from tissue to tissue. However, the major components of ECM are fibrous proteins, such as collagens, elastin, fibronectin, laminins, glycoproteins, proteoglycans and glycosaminoglycans.

Extracellular matrix provides support to cells but also regulates many cellular processes, such as growth, migration, differentiation, survival, homeostasis and morphogenesis (Kleinman *et al.* 1987, Reilly *et al.* 2010, Giancotti *et al.* 1999). Due to its functions, researchers have tried to develop materials that recapitulate the native ECM by coupling or coating some ECM molecules or peptides to synthetic polymers, developing gels or scaffolds from native ECM, such as collagen, or even by collecting tissue or cell-derived ECM and evaluate their efficacy for tissue engineering applications.

Regarding bone tissue, the ECM present in bone plays different roles. Bone matrix can direct bone remodeling through the activity of osteoblasts and osteoclasts. Bone ECM also serves as a scaffold, mainly type I collagen, for mineral deposition. Moreover, bone ECM confers to the tissue structural flexibility. ECM influences osteogenic differentiation of MSC by both direct interactions between cells and ECM, as well as by modulating growth factor activity. Similarly, via cell-ECM interactions, the ECM can influence the differentiation of osteoclasts from undifferentiated macrophage precursor cells (Alford *et al.* 2015).

I.6.2. Bone extracellular matrix: characterization, quality and properties

Most of the outstanding properties of the bone are related to its matrix constitution. Bone extracellular matrix has two components: a mineral part comprising hydroxyapatite (70-90%) and an organic part (10-30%) of primarily collagen (approx. 90% of organic matrix) with the rest being non-collagenous proteins (~10%) (Sroga *et al.* 2011, Vashishth 2007). The organic matrix of bone is mainly composed of collagens, however, Herring and co-workers identified the presence of other non-collagenous proteins (Herring *et al.* 1974) (Figure I.22). Type I collagen is the most prevalent protein in the body and it can be found not only in mineralized but also in non-mineralized tissues, playing a critical role in the structure and function of bone tissue (Vashishth 2007). In bone, it is known that type I collagen is not the only protein responsible for mineralization. Improved technologies have led to the isolation of a large number of non-collagenous matrix proteins. It is known that some matrix proteins bind to collagen, forming fibrils and it is probable that collagen serves as a scaffold upon which nucleators of hydroxyapatite, such as non-collagenous proteins, are oriented (Figure I.23) (Vashishth 2007, Herring *et al.* 1974, Roach 1994). Although some studies have already described the potential roles of these proteins, their contribution into bone tissue engineering applications remains to be well investigated.

Bone matrix quality may be determined by the nature of collagen type I, bone mineral and non-collagenous proteins (Viguet-Carrin *et al.* 2005*,* Fantner *et al.* 2005). Using different characterization techniques and diseased mice models, it has been demonstrated that the nanostructural organization of bone influences the bone properties. Several diseases related with deregulation of type I collagen and mineralization showed impairment of bone quality and some bone properties, such as bone fragility and

strength. For example, mice with osteogenesis imperfecta, a condition derived from mutation in type I collagen, presented bone fragility and reduction in strength (Fratzl *et al.* 1996). Regarding mineralization, osteopetrosis, a condition responsible to hypermineralization of bone, increases bone fragility since it affects interactions between collagen and mineral component that modifies the nature of organization in bone at the nanometer scale (Sobacchi *et al.* 2013). On the other hand, non-collagenous proteins have also been suggested to influence the mechanical quality of bone matrix. Studies on osteopontin (OPN) showed that it behaves like 'glue' in bone (Fantner *et al.* 2007). In the presence of calcium ions, OPN is capable of sacrificial bonding, a nanoscale mechanism that dissipates energy and inhibits crack growth. Osteocalcin (OC), the most abundant bone specific non-collagenous protein, complexes with OPN (Ritter *et al.* 1992) and regulates bone mineralization through its strong affinity toward hydroxyapatite. Previous work from our group found that fracture in bone initiates as dilatational bands that form as a result of OC-OPN interaction. In the absence of either protein, the complex is disrupted, resulting in a dramatic loss of toughness (Poundarik *et al.* 2012).

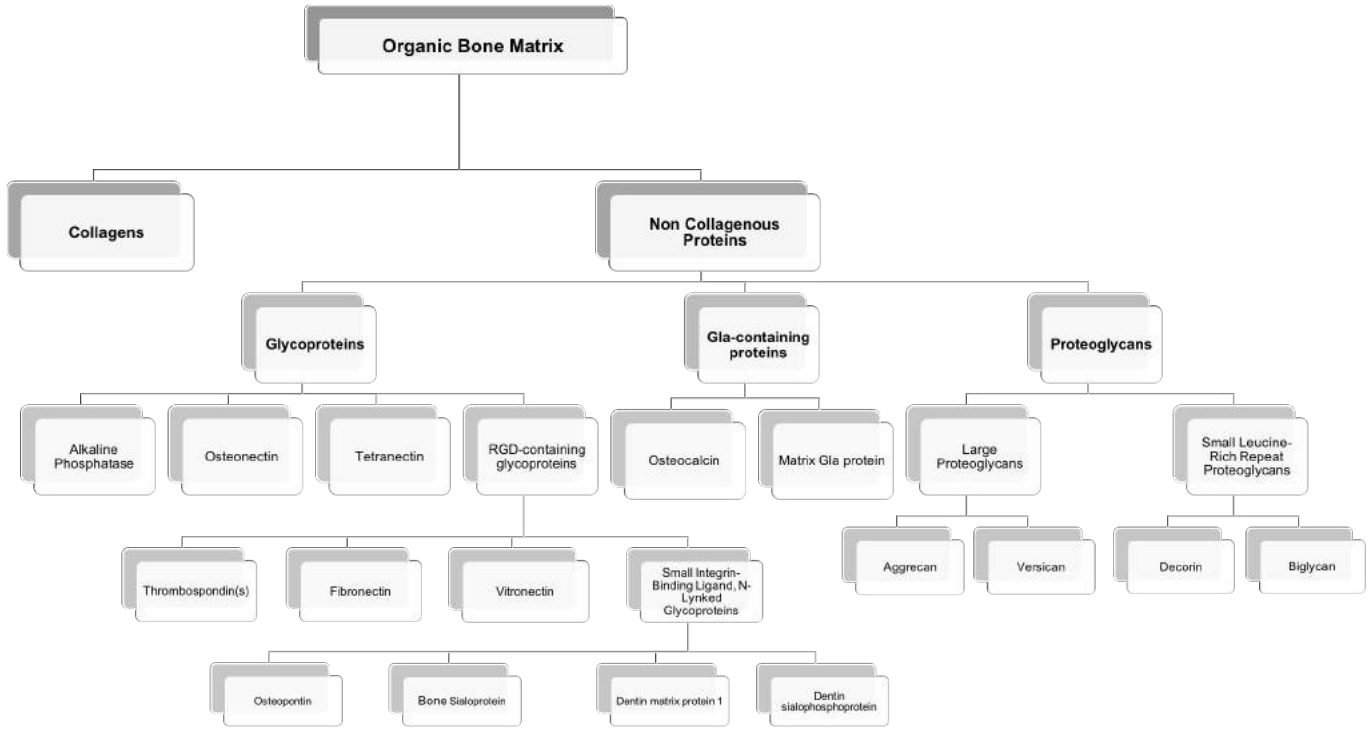

Figure I.22. Organic components of the bone extracellular matrix.

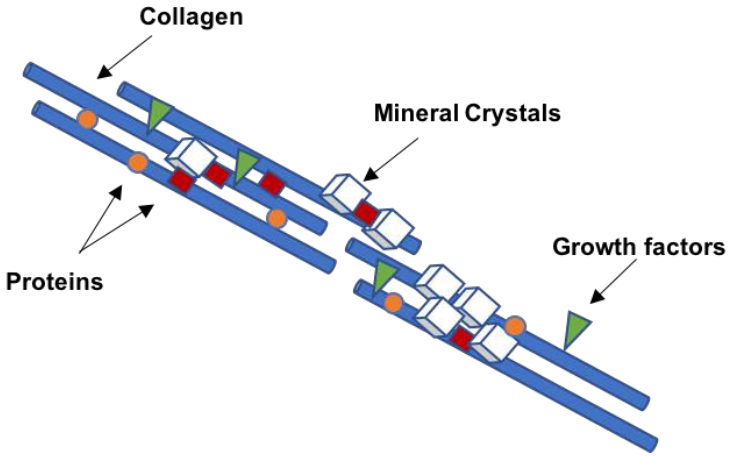

Figure I.23. Schematic diagram representing the organization of collagen molecules reinforced with calcium phosphate nanocrystals, proteins and growth factors arranged in a semi-regular pattern.

I.6.3. Non-collagenous bone matrix proteins

Non-collagenous proteins have been isolated from bone and have been found to be biologically active, even though their function is not yet completely understood. Based on their localization patterns each of these proteins may perform different functions. Therefore, it is extremely important to understand better the properties and functions of these proteins to design strategies for bone tissue engineering applications (Mouw *et al.* 2014). It has been speculated that non-collagenous proteins might have an important role in cell attachment, cell differentiation and regulation of the deposition of hydroxyapatite minerals (Boskey *et al.* 1989). Some of these proteins may be multifunctional, playing different roles in the bone, thus defining a single function may not be sufficient. Also, some of these proteins might work together, having a synergistic effect on cellular behavior and mechanical properties of bone or they can compensate some effects resulting from deregulation of the levels of other non-collagenous proteins present in bone matrix.

Not all types of bones contain the same amounts of the non-collagenous proteins (Roach *et al.* 1994). In humans, for example, cortical bone contains 30x more osteocalcin than trabecular bone, but trabecular bone contains 21x more osteonectin (Ninomiya *et al.* 1990). Moreover, it is possible to find non-collagenous proteins in some other tissues besides bone, specifically OPN presents a general tissue distribution. BSP and OC are also found in other mineralized tissues, such as dentin. Therefore, their importance in bone physiology can not be underestimated. Some studies have reported that mutations in some of these proteins may result in abnormal bone.

The multifunctional properties of these non-collagenous proteins make them attractive agents to be incorporated within an appropriate scaffold for bone tissue engineering applications. These proteins can be used successfully as signaling molecules to direct stem cell recruitment, attachment and differentiation into new bone tissue, creating a mature and mineralized extracellular matrix.

In bone, non-collagenous proteins are mainly composed of two major types: glycoproteins and gamma-carboxyglutamic acid (Gla)-containing proteins, however some proteoglycans can also be found in smaller content (Marcus *et al.* 2013, Bilezikian *et al.* 2008) The most relevant and abundant glycoproteins are represented by alkaline phosphatase, osteonectin, and the cell attachment proteins, which include, but are not limited to, osteopontin and sialoproteins. Of the Gla-containing proteins, osteocalcin is the major component.

I.6.3.1. Proteoglycans

This class of molecules is characterized by the covalent attachment of long chain polysaccharides (glycosaminoglycans, GAG) to core protein molecules. GAG are composed of repeating carbohydrate units that are sulfated to varying degrees and include chondroitin sulfate (CS), dermatan sulfate (DS), keratan sulfate (KS), heparin sulfate (HS) and hyaluronan (HA, unsulfated) (Marcus *et al.* 2013).

These molecules can be more easily found in cartilage matrix, however, endochondral bone formation is mediated by a cartilage template (intermediate cartilage matrix), therefore cartilage molecules can be incorporated into the initial bone tissue (Bilezikian *et al.* 2008).

Proteoglycans have been suggested to be responsible for matrix maintenance, organization (Heinegar and Oldber 1989) and regulation of cartilage calcification (Hunter 1991) through interactions with the GAG chain of type IX collagen and the type II collagen fibrils (Nishimura *et al.* 1989).

Proteoglycans and their component GAG can inhibit hydroxyapatite formation and growth (Chen *et al.* 1984) and they can also chelate calcium (Boskey *et al.* 1989b, Hunter 1987). However, it is not clear yet whether this chelation is involved in the inhibition of mineralization (Chen & Boskey 1985).

A number of proteoglycans have been identified in cartilage matrix and bone matrix, such as the large proteoglycans, aggrecan and versican, and small leucine-rich repeat proteoglycans, such as decorin and biglycan (Fedarko 1994, Yanagishita 1993) (Table I.3).

I.6.3.1.1. Aggrecan and versican

Aggrecan and versican are two large chondroitin sulfate proteoglycans that can be found in bone matrix and can bind to hyaluronan, forming large aggregates.

Aggrecan has been suggested to play an important role in skeletal development, having a molecular weight of approximately 205 kDa. First studies revealed that mice with a mutation of aggecan gene presented cartilage matrix deficiency and are characterized by perinatal lethal dwarfism and craniofacial abnormalities (Watanabe & Yamada 2002). Since the amount of aggrecan present in bone is much lower than in cartilage, it is not completely understood if its presence in bone represents only residual calcified cartilage. Although aggrecan has been reported to have an important role in preventing cartilage calcification, its function in bone is still unknown.

Versican is another CS proteoglycan that can be found at relatively lower levels than aggrecan in cartilage and bone, having a molecular weight of approximately 360 kDa. Versican was reported to be expressed during osteogenesis, in rat bone development (Nakamyra *et al.* 2005). Although versican stimulates chondrocyte proliferation (Zhang *et al.* 1999), its function in cartilage and bone is still unknown. Potentially, it

may serve as a bridge between the extracellular environment and the cell binding to hyaluronan (Kjellän & Lindahl 1991).

I.6.3.1.2. Decorin and Biglycan

Small leucine-rich repeat proteoglycans are another family of proteoglycans that present a protein core with a smaller sizer and a leucine-rich repeat sequence. In cartilage and bone, there are several members of this family, such as decorin and biglycan, exhibiting different patterns of expression and tissue localization, which might be an indicative of different functions.

Decorin has an apparent molecular weight of approximately 130 kDa (Fisher *et al.* 1987) and it has been shown to bind to and regulate the fibrillogenesis of type I, II and VI collagens and collagen-matrix interactions (Vogel & Trotter 1987). In bone, the proposed functions of decorin are the regulation of collagen fibril diameter and fibril orientation, and possibly the prevention of premature osteoid calcification, however it has low affinity for calcium (Boskey *et al.* 1997), in contrast to a high affinity to type I collagen in solution. Studies indicate a role of decorin in matrix mineralization since proteoglycans with low molecular weight are present in type I collagen fibrils but then disappear when mineralization occurs (Fleischmajer *et al.* 1991).

Studies with decorin knockout mice showed skin laxity and fragility and their bones did not demonstrate any visible bone phenotype, however their teeth sowed alteration in matrix properties, presenting an hypomineralized dentin (Goldberg *et al.* 2005).

Biglycan is another small proteoglycan present in both cartilage and bone with a molecular weight of approximately 45 kDa. Although its functions remain to be investigated, in solution, biglycan demonstrated different effects depending on concentration. Low concentrations promoted apatite formation, whereas at higher concentration it inhibited the growth and proliferation of mineral crystals (Boskey *et al.* 1997). These effects appear to be due to the highly specific high-affinity binding of biglycan for apatite.

The biglycan knockout mice presented reduced skeletal growth, having shorter femora, and decreased bone mass (Ameye & Young 2002). Moreover, the decorin and biglycan double knockout mice have additive deficiency in dermis and synergistic effects in bone, and ultrastructural analysis of these mice reveal a complete loss of the basic fibril geometry (Corsi *et al.* 2002). The mineral within these bones has increased crystal size relative to wildtypecontrols (Xu *et al.* 1998). However, the low amount of biglycan present in bone matrix relative to other mineral nucleators and its absence from bone collagen fibrils suggest that its primary function may not be directly related to mineral deposition of bone.

I.6.3.2. Glycoproteins

This class of proteins is characterized by the covalent linkage of sugar moieties attached via asparaginyl or serinyl residues (Bilezikian *et al.* 2008). These glycoproteins may also be further modified by post-translational sulfation and phosphorylation (Table I.4).

I.6.3.2.1. Alkaline phosphatase

Although alkaline phosphatase is not typically reported as a matrix protein, many studies demonstrated that alkaline phosphatase can be released from the surface of osteogenic cells or in a membrane-bound form (matrix vesicles) (Roach 1999, Kirsch *et al.* 1997, Fedarko *et al.* 1990).

in vivo and *in vitro* studies have suggested an important role of alkaline phosphatase in mineralization, since its expression precedes mineralization and it is maintained during early stages of hydroxyapatite deposition (Collin *et al.* 1992). Moreover, hypophosphatasia disease is characterized by having mutations in alkaline phosphatase gene, resulting in improper mineral deposition. Indeed, mice with null mutations for the tissue-nonspecific alkaline phosphatase showed increased osteoid and defective growth plate development, reinforcing the importance of alkaline phosphatase in mineralization (Fedde *et al.* 1999). Furthermore, it was observed that cells that normally do not mineralize will form a mineralized matrix when transfected with the alkaline phosphatase gene (Yoon *et al.* 1989).

I.6.3.2.2. Osteonectin

Osteonectin, also named SPARC (secreted phosphoprotein acidic and rich in cysteine), was the first matrix protein to be isolated from bone, representing 15% of the total non-collagenous matrix protein content in bone. The molecular weight of osteonectin is approximately in the range of 35-45kDa (Bilezikian *et al.* 2008).

Osteonectin is expressed in several tissues during development and, although it is synthesized by osteoblasts, it can also be synthesized by fibroblasts from skin tendon, sclera, and periodontal ligaments. However, most of osteonectin found in the circulation is derived from platelets (Stenner *et al.* 1986, Mundy 1995).

Osteonectin binds to type I collagen (Tyree 1989), types III and V collagens (Kelm *et al.* 1991), thrombospondin (Clezardin *et al.* 1988) and to hydroxyapatite, through high-affinity calcium-binding sites (George &Veins 2008, Termine *et al.* 1981). Its affinity for calcium and phosphate ions suggests that it may promote mineral deposition. However, osteonectin accumulates only within mineralized matrix, suggesting that it is not involved in the initiation of mineralization (Roach *et al.* 1994), but may have an important function in a later phase of mineralization, by regulating growth and proliferation of mineral crystals.

Osteonectin deficient mice showed a poor bone condition, developing osteopenia with a significant loss of trabecular bone associated with a decreased rate in bone formation (Delany *et al.* 2000, Boskey *et al.* 2003), reinforcing the fact that osteonectin might support bone remodeling and maintenance of bone mass (Delany *et al.* 2000). Numerous *in vitro* studies using both intact molecule and peptides derived from different regions of osteonectin reported that osteonectin has been implicated in regulating cell-matrix interactions (Yan *et al.* 1999). However, many of these activities have not been found or tested using osteoblasts (Termine *et al.* 1981)

I.6.3.2.3. Tetranectin

Tetranectin has an approximately molecular weight of 21 kDa (Clemmensen *et al.* 1986). This glycoprotein is expressed by osteoblasts undergoing matrix mineralization, being identified in bone and in

tumors undergoing mineralization (Wewer *et al.* 1994). To date, it is not known the function of tetranectin in bone metabolism, however this protein might be related with matrix mineralization. Overexpression of tetranectin by tumor cells caused an increase in matrix mineralization upon implantation into nude mice (Wewer *et al.* 1994) Tetranectin-deficient mice have shown a delayed fracture healing, indicating that tetranectin could have a role at the early stage of the fracture healing process (Iba *et al.* 2013). On the other hand, tetranectin knockout mice presented a phenotype with severe spinal deformities (Iba *et al.* 2001)

I.6.3.2.4. RGD-containing glycoproteins

Bone extracellular matrix contains some glycoproteins that also have the aminoacid sequence Arginine-Glycine-Aspartic (RGD). These RGD sequences can be recognized by cell surface receptors and promote the attachment between extracellular matrix to cells (Takagi *et al.* 2004). The receptors on the cell surface are integrins formed by one α subunit and one β subunit. Each subunit has a cytoplasmic extension that associates with intracellular signaling pathways, a transmembrane domain, and an extracellular domain (Hynes 2004). The extracellular domains of the α and β subunits configure a binding pocket that recognizes the RGD sequences in the extracellular matrix proteins and mediates the cell-matrix interactions (Takagi *et al.* 2004, Hynes 2004).

In bone matrix, some RGD-containing proteins include thrombospondin, fibronectin, vitronectin and a family of small integrin-binding ligand, N-linked glycoproteins (SIBLING). The SIBLING have been identified by a cluster of genes including osteopontin (OPN), bone sialoprotein (BSP), dentin matrix protein-1 (DMP-1) and dentin sialophosphoprotein (DSPP) (Fisher & Fedarko 2003).

I.6.3.2.4.1. Thrombospondin, fibronectin and vitronectin

Thrombospondin is a glycoprotein with a molecular weight of approximately 450 kDa (Adams & Lawler 2004). Unlike other glycoproteins present in the bone matrix, thrombospondin is less abundant in mineralized bone matrix, but it can be found in several connective tissues. Although its role in bone is still undetermined, thrombospondin has been suggested to be important in bone development and remodeling, especially in collagen fibrillogenesis and its matrix organization (Hankenson *et al.* 2000, Carron *et al.* 1995, Bornstein *et al.* 2000). Thrombospondin can bind to a large number of matrix proteins and cell surface proteins.

Studies with mice that lack thrombospondin (TSP-2 null) presented disordered collagen in their soft tissues, increased cortical bone thickness and density (Hankenson *et al.* 2000), and altered fibroblast cell attachment (Kyriakides *et al.* 1998).

Fibronectin (FN) is one of the most abundant extracellular matrix proteins in bone with a molecular weight of ~400kDa. Moreover, this protein can be found in all extracellular matrices from the body, since it is produced by all connective tissue cells. Some evidences suggest that FN plays an important role during bone development, since it is accumulated in mineralized matrix at an early stage of bone formation (Grzesik *et al.* 1994) and it is highly upregulated in the osteoblastic cell layer. On the other hand, *in vivo* studies showed that FN is a component essential for development of these tissues, since the elimination of the FN gene in transgenic animals is lethal *in utero* and connective tissues do not form (George *et al.* 1993).

Interestingly, the attachment of bone cells to FN *in vitro* uses an RGD-independent mechanism (Grzesik *et al.* 1994). Cell-matrix interactions mediated by FN $\alpha_4\beta_1$ binding may play a role in the maturation sequence of cells in the osteogenic lineage (Bilezikian *et al.* 2008).

Vitronectin has a molecular weight of ~70kDa and it is generally found in matrices containing the fibrillary collagens. *In vitro*, vitronectin has been observed to be produced by osteoblasts (Kumagai *et al.* 1998). This protein has been purposed to function in the attachment of all cell types. In particular, osteogenic cells attach very strongly to vitronectin (Grzesik *et al.* 1994, Rodan & Rodan 1997), mainly via the receptor integrin, $\alpha_v\beta_3$ (Grzesik *et al.* 1994). Another interesting observation was that vitronectin increased in concentration in the unmineralized osteoid prior to mineral deposition (Kumagai *et al.* 1998). This evidence indicates that vitronectin may have an important role in preparing the matrix for mineral deposition (Kumagai *et al.* 1998). However, further studies are needed to understand the role of this protein in bone tissue.

In vivo studies demonstrated that mice that lack vitronectin gene presented a thrombolytic phenotype, however skeletal defects were not observed in these mice (Koschnick *et al.* 2005).

I.6.3.2.4.2. Small Integrin-Binding Ligand, N-Lynked Glycoproteins (SIBLING)

SIBLING are a family of five integrin-binding glycophosphoproteins comprising OPN, BSP, DMP-1, DSP and matrix extracellular phosphoglycoprotein. The genes coding for members of the SIBLING protein family are similarly organized. SIBLING interact with cell surface receptors, such as integrins, mainly through an RGD sequence, and function as modulators of cell adhesion as well as autocrine and paracrine soluble factors (Fisher *et al.* 2001, Staines *et al.* 2012).

All SIBLING proteins undergo similar post-translational modifications such as phosphorylation and glycosylation, very important processes in determining their function.

I.6.3.2.4.2.1. Osteopontin

Osteopontin, also called secreted phosphoprotein (SPP) (Denhardt & Guo 1993, Denhardt & Noda 1998), is an acidic glycoprotein that consists of about 300 aminoacids, with a molecular weight of 34 kDa (Denhardt & Guo 1993). OPN was first identified in bone matrix extracts as the bridge between the cells and hydroxyapatite in the ECM of bone (Sodek *et al.* 2000b), however it can be detected in other tissues and plasma, such as dentin, cartilage, kidney, and vascular tissues (Fratzl *et al.* 1996). In these tissues, this molecule could mediate communication between cells, suggesting that OPN could act both as a structural molecule and as a cytokine (Nanci 1999, Rittling & Denhardt 1999, Denhardt *et al.* 2001).

In bone, it is produced by osteoblasts during the pre-mineralization at late stages of osteoblastic maturation (Denhardt & Guo 1993).

OPN binds to $\alpha_v\beta_1$, $\alpha_v\beta_3$, $\alpha_v\beta_5$, $\alpha_4\beta_1$, $\alpha_5\beta_1$ and $\alpha_9\beta_1$ integrins (Denhardt & Noda 1998, Barry *et al.* 2000), through their RGD domain. The $\alpha_v\beta_3$ integrin is considered to be responsible for major signals in response to the binding of OPN (Miyauchi *et al.* 1991). Additionally, OPN can also present an RGD-independent

mechanism, in which OPN may engage CD44 (Denhardt & Guo 1993, Denhardt & Noda 1998, Katagiri *et al.* 1999). However, details of the interaction of CD44 with OPN remain to be studied. The presence of additional cell receptors, the various isoforms of CD44, and variable post-translational modifications (phosphorylation and glycosylation) of OPN are factors that interefere in this interaction.

OPN has been proposed to regulate many physiological processes such as collagen organization, cell adhesion, cell viability, cell migration, angiogenesis and calcification (Denhardt & Guo 1993, Rodriguez *et al.* 2014).

OPN interacts with several molecules constituting bone matrix. OPN is known to bind covalently to fibronectin via transglutamination, and, consequently, transglutamination of OPN increases its binding to collagen (Kaartinen *et al.* 1999, Kaartinen *et al.* 1997). Ritter and colleagues demonstrated that OPN specifically associates with osteocalcin, forming stable complexes between OPN and OC (Ritter *et al.* 1992). In fact, the mechanisms responsible for bone formation and remodeling likely involve the association of bone matrix proteins into specific complexes that helps the organization of the matrix (Ritter *et al.* 1992).

Moreover, the phosphorylation of OPN has shown significant effect on crystal growth (Gericke *et al.* 2010), regulating bone crystal size. OPN has a high affinity to calcium, therefore it has been suggested to modulate the nucleation of calcium phosphate during mineralization (Boskey *et al.* 1995, Contri *et al.* 1996). Besides its RGD sequence, OPN also contains aspartic acid residues, a high negative charge motif that might be responsible for the binding of OPN to bone mineral, however, initial studies on the OPN-deficient mouse failed to indicate the presence of any major defect in mineralization (Rittling *et al.* 1998). Possibly, the role of OPN in bone mineralization is compensated by other regulatory systems for mineralization or by other non-collagenous proteins.

Studies of genetically OPN knockout mice showed that these mice presented larger crystal size and an increased mineral content (Boskey *et al.* 2002), suggesting the inhibitory role of OPN in hydroxyapatite formation and growth (Boskey *et al.* 2002, Boskey *et al.* 2012). Analysis of the $OPN^{-/-}$ mice has also demonstrated that OPN is important in the function and activity of osteoclasts, specifically in osteoclast attachment, participating in bone resorption (Rittling *et al.* 1998, Asou *et al.* 2001). Studies of ectopic bone implantation demonstrated that bone from OPN-deficient mice implanted into OPN-deficient mice exhibited significantly less resorption and lower number of osteoclasts attached to the surface of the bone compared with wildtype bone implanted intramuscularly in the back of the wildtype mice (5% *vs* 25%, respectively) (Asou *et al.* 2001). However, it is not known whether OPN promotes bone resorption by stimulating angiogenesis or by stimulating bone resorption via signaling through the bone matrix. Asou and colleagues demonstrated a relationship between OPN and bone resorption associated with vascularization (Asou *et al.* 2001), since the number of $CD34^{+}$ vessels in the vicinity of bones implanted in OPN-deficient mice was reduced compared to the number of vessels in wildtype bones. Therefore, it suggests that OPN deficiency may lead to a reduction in neovascularization of the ectopically implanted bones, and, consequently, a reduction in the number of osteoclasts and bone resorption efficiency. It is also possible that OPN may promote the survival of endothelial cells on the bone matrix, facilitating the vascularization of bone tissue.

However, further investigations are required to elucidate the molecular mechanisms of OPN action in mediating responses to inflammation, angiogenesis, osteogenesis and accelerated bone resorption.

I.6.3.2.4.2.2. Bone Sialoprotein

In addition to osteopontin, bone sialoprotein is another major non-collagenous SIBLING that accumulates in bone tissue, in particular in spaces between mineralized collagen fibrils (Franzen & Heinegard 1985). BSP has an apparent molecular weight of, approximately, 75 kDa and its expression is exclusively located to the mineralized tissues, such as bone, dentin, cementum and certain regions of hypertrophic chondrocytes (Fisher *et al.* 1987, Franzen & Heinegard 1985, Bianco *et al.* 1991). In bone, BSP is expressed in abundance by osteoblasts, as well as by osteoclasts, osteocytes and chondrocytes (Gordon *et al.* 2007).

BSP may be multifunctional in osteoblastic metabolism, playing a role in matrix mineralization as supported by the fact that BSP expression appears at a late stage of osteoblastic differentiation, as an early stage of matrix mineralization, and by the fact that BSP has a very high affinity for calcium (Staines *et al.* 2012). *In vitro*, BSP might act as an hydroxyapatite nucleator (Hunter and Goldberg 1993). It has been shown that a concentration of BSP as little as 9 nM is required to nucleate hydroxyapatite. The overexpression of BSP in osteoblasts has been shown to enhance mineralization (Gordon *et al.* 2007) Similarly, osteoblast cultures grown in the presence of an anti-BSP antibody exhibit reduced mineralization (Mizuno *et al.* 2000). Interestingly, when BSP is linked to collagen, a cooperative relationship between both proteins is observed with an increased nucleation potency (Baht *et al.* 2008).

Another important role confirmed with *in vitro* assays is that BSP can mediate cell attachment, most likely through interaction with the $\alpha_v\beta_3$ receptor and it facilitates the *in vitro* attachment of fibroblasts, osteoblasts and osteoclasts (Staines *et al.* 2012).

BSP increases the development of osteoclasts and, therefore, bone resorption, making it crucial for bone remodeling processes (Malaval *et al.* 2008).

First *in vivo* studies demonstrated that BSP-deficient mouse does not exhibit an altered skeletal phenotype, possibly due to compensation of BSP function by other SIBLING proteins, revealing no differences in mineral crystal relative to controls (Aubin *et al.* 1996). However, more recent studies with BSP null mouse showed that it displays shorter, hypomineralized bones with associated higher trabecular bone mass with lower bone turnover (Malaval *et al.* 2008).

I.6.3.2.4.2.3. Dentin matrix protein 1 and dentin sialophosphoprotein

Dentin matrix proteins (DMP) are a group of non-collagenous proteins found in different quantities in the ECM of dentin and bone. Currently, this group consists of four different proteins, namely: dentin matrix protein 1 (DMP-1), dentin phosphophoryn (DPP) or dentin matrix protein 2 (DMP-2), dentin sialoprotein (DSP) and dentin matrix protein 4 (DMP-4) (Qin *et al.* 2007). Over the years, these DMP have been shown to play multiple roles that control important functions ranging from attachment, proliferation and differentiation of stem cells and preosteoblasts to matrix mineralization.

DMP-1 was first isolated from dentin, however it can also be found in bone (George *et al.* 1993b, Sun *et al.* 2011). In bone, DMP-1 is expressed specifically in mineralized tissues by hypertrophic chondrocytes,

osteoblasts, and osteocytes (Feng *et al.* 2003). The RGD domain in DMP-1 binds to $\alpha_5\beta_1$ integrin on the cell surface and stimulates osteogenic differentiation of MSC(Chandrasekaran *et al.* 2013).

DMP-1 is a highly phosphorylated protein with a strong affinity for calcium. DMP-1 has been reported to influence mineralization, facilitating nucleation of hydroxyapatite crystals (Bhatia *et al.* 2012). MC3T3 cells that overexpress DMP-1 promote ECM mineralization (Narayanan *et al.* 2001). Moreover, when phosphorylated, full-length DMP-1 has been shown to inhibit the formation and growth of hydroxyapatite, however, its dephosphorylated form is a nucleator of hydroxyapatite formation (Gericke *et al.* 2010). Additionally, DMP-1 can bind specifically to the N-telopeptide region of type I collagen. Interestingly, nucleation of hydroxyapatite was exclusively found in regions where DMP-1 bound to type I collagen (He *et al.* 2004). Moreover, DMP-1 has been postulated to play a specific role in angiogenesis (Pirotte *et al.* 2011).

The generation of a DMP1-null mouse has further confirmed the potential role of DMP-1 in bone mineralization, since DMP1- knockout mice have significantly lower mineral content when compared with the wildtype control mice (Ling *et al.* 2005, Feng *et al.* 2006)

Dentin sialophosphoprotein (DSPP) is expressed in dentin, bone, cementum and non-mineralizing tissues including the lung and kidney (Verdelis *et al.* 2008). As a single gene, an intact protein has not been isolated. However, two DSPP products, dentin sialoprotein (DSP) and dentin phosphophoryn (DPP), are coexpressed by odontoblasts and pre-ameloblasts at a time when predentin is being secreted. Only DPP has been reported to regulate type I collagen fibrillogenesis (Traub *et al.* 1992) and serve as an effective nucleator for hydroxyapatite formation at lower concentrations and an inhibitor at higher concentrations (Boskey *et al.* 1990), whereas DSP was not an effective modulator of *in vitro* mineralization (Boskey *et al.* 2000)

In vivo data have shown that DSPP knockout mice presented decreased mineral content in both their dentin and their bones (Sreenath *et al.* 2003, Verdelis *et al.* 2008). In humans, a mutation in the DSPP gene results in *dentinogenesis imperfecta*, characterized by dentin hypomineralization and significant tooth decay (Kim *et al.* 2005). Some studies suggest that DSPP has roles not only in the initial mineralization of bone but also in the remodeling of the skeleton and, therefore, on bone turnover (Verdelis *et al.* 2008).

I.6.3.3. Gla-Containing Proteins

Bone contains several proteins that are post-translationally modified by vitamin K-dependent enzymes to form the aminoacid, Gla (Bilezikian *et al.* 2008). Osteocalcin is the major Gla-containing protein, playing an important role in mineralization of bone, whereas matrix Gla protein is known to be more involved in regulating the calcification of cartilage (Table I.5)

I.6.3.3.1. Osteocalcin

Osteocalcin, also known as bone gama carboxyglutamic acid-containing protein (BGLAP), is an approximately 5.8 kDa protein consisting of a single chain of 49-50 amino acids, being the most abundant non-collagenous protein in bone, comprising about 20% of the non-collagenous matrix proteins (Hauschka *et*

al. 1989). OC is secreted by osteoblasts and it is present in dentine and calcified matrix. This protein has three glutamic acid residues at positions 17, 21, and 24 (Poser *et al.* 1980) that bind calcium, and it is vitamin K-dependent. Before being released into the bone extracellular matrix, osteocalcin is carboxylated on their three glutamine acid residues within the osteoblasts, however, both the carboxylated and uncarboxylated forms of OC can be found in the circulation (Poser *et al.* 1980, Wei *et al.* 2015). Its concentration in serum is closely linked to bone metabolism and it is used clinically as a marker of osteoblast activity for the clinical assessment of bone disease (Calvo *et al.* 1996). During bone development, OC production is very low and does not reach maximal levels until late stages of mineralization (Gundberg 2000).

Although its precise mechanism of action is unclear, OC is presumed to influence bone mineralization (Hauschka *et al.* 1978) in part through its ability to bind with high affinity to the mineral component of bone and due to its acidic character (Poser *et al.* 1979). It is thought that by binding hydroxyapatite, OC accelerates the nucleation of hydroxyapatite, playing an active role in the early stages of bone healing (Rammelt *et al.* 2005). Besides that, OC functions in cell signaling and in the recruitment of osteoclasts (Chenu *et al.* 1994) and osteoblasts (Bodine *et al.* 1999), which has active roles in bone resorption and formation, respectively. Subcutaneous implantation of bone particles that were 99% deficient in OC have been shown to be poorly resorbed, suggesting that OC might function as a matrix signal in the recruitment and differentiation of osteoclasts (Glowacki & Lian 1987).

In vivo data showed that OC deficient mice presented an increase in bone formation without impairing bone resorption (Ducy *et al.* 1996) Although the exact mechanism is still unknown, new studies have shown that the uncarboxylated form of OC may act also as an hormone, regulating insulin secretion and glucose homeostasis (Ferron *et al.* 2008). However, its physiological role in mineralization remains uncertain.

I.6.3.3.2. Matrix Gla Protein

Matrix Gla protein (MGP) is the other major Gla-containing protein in the skeleton which was first isolated from bone (Price & Williamson 1985) but has also found to be expressed in a variety of soft tissues (Murshed *et al.* 2004), having a molecular weight of approximately 15 kDa. MGP is known to be more abundant in cartilage than in bone (Price & Williamson 1985). In the skeleton, MGP expression appears early and remains at the same level at all subsequent stages of development (Murshed *et al.* 2004). There is evidence that MGP is an *in vivo* inhibitor of mineralization of cartilage. *In vivo* data showed that mice in which the MGP gene was absented died prematurely because of massive calcification of their tracheal cartilage and blood vessels (Luo *et al.* 1997).

I.6.3.4. Serum Proteins

Several proteins that are not synthesized in bone can also be found in bone matrix. These proteins (immunoglobulins, cytokines, chemokines, growth factors) are brought to bone matrix region through the circulation, being mostly synthesized in the liver and the hematopoietic tissue. It was suggested that hydroxyapatite facilitates the adsorption of these proteins, helping to retain them in the bone matrix (Delmas *et al.* 1984). Although these serum proteins are not produced locally, they may have an important role on bone metabolism. One example of a serum protein that can be found in bone matrix is albumin that is synthesized by the liver. *In* vitro studies showed that albumin inhibits hydroxyapatite growth, influencing hydroxyapatite formation (Garnett *et al.* 1990).

Table I.3. Proteoglycans in Bone Matrix: protein functions and *in vivo* studies.

	***In vivo* studies**	**Function**
Aggrecan	Aggrecan deficient mice presented cartilage matrix deficiency and are characterized by perinatal lethal dwarfism and craniofacial abnormalities.	May have an important role in preventing cartilage calcification.
Versican	Versican deficient mice presented an early lethality.	Potentially, it may serve as a bridge between the extracellular environment and the cell binding to hydroxyapatite. In addition, versican stimulates chondrocyte proliferation.
Decorin	Decorin knockout mice showed skin laxity and fragility and their bones did not demonstrate any visible bone phenotype. However, their teeth showed alteration in matrix properties, presenting an hypomineralized dentin.	Binds to collagen and may regulate fibril diameter and orientation. May prevent premature osteoid calcification, and regulate the collagen-matrix interactions.
Biglycan	The biglycan knockout mice presented reduced skeletal growth, having shorter femora, and decreased bone mass.	May bind to collagen. May be involved in the process of matrix mineralization

Table I.4. Glycoproteins in Bone Matrix: protein functions and *in vivo* studies.

	***In vivo* studies**	**Function**
Alkaline Phosphatase	Tissue-nonspecific alkaline phosphatase deficient mice showed increased osteoid and defective growth plate development.	Possible role in mineralization. Potential calcium ions carrier.
Osteonectin	Osteonectin deficient mice have presented a poor bone status, developing osteopenia.	May promote mineral deposition and regulate growth and proliferation of mineral crystals, supporting bone remodeling. May influence cell cycle, binding to growth factors and through cell-matrix interactions.
Tetranectin	Tetranectin deficient mice have presented a delayed fracture healing.	May regulate matrix mineralization, playing a role in tissue growth and remodeling
Thrombospondin	Thrombospondin deficient mice presented disordered collagen in their soft tissues, increased cortical bone thickness and density and altered fibroblast attachment.	Role in cell attachment. It binds to several matrix proteins and cell surface proteins. Role in bone development and remodeling, collagen fibrillogenesis and its matrix organization.
Fibronectin	Elimination of fibronectin gene in transgenic animals is lethal *in utero*, since connective tissues do not form.	Role in cell attachment. It binds to many matrix proteins and cell surface proteins, like collagen.
Vitronectin	Vitronectin deficient mice have been shown to have a thrombolytic phenotype, but there is no report on whether skeletal defects were apparent in these mice.	Role in cell attachment. It binds to collagen.
Osteopontin	Osteopontin deficient mice presented larger crystal size and an increased mineral content.	Role in cell attachment. It binds with other molecules constituting bone matrix. May regulate mineralization, being an agent for the nucleation of mineral crystals. May regulate bone resorption through osteoclasts attachment and recruitment. May have a specific role in angiogenesis.

Bone Sialoprotein	Bone sialoprotein deficient mice present shorter, hypomineralized bones with higher trabecular bone mass with very low bone formation rate.	Role in cell attachment. May initiate matrix mineralization. It has high affinity for calcium, being an hydroxyapatite nucleator. May increase osteoclastogenesis and bone resorption.
Dentin Matrix Protein 1	Dentin matrix protein-1 deficient mice have significantly lower mineral content when compared with their controls.	Role in cell attachment. It binds to collagen. If phosphorylated, may inhibit the formation and growth of hydroxyapatite, if dephosphorylated it facilitates nucleation of hydroxyapatite crystals, initiating mineralization. May play a role in angiogenesis.
Dentin sialophosphoprotein	Dentin sialophosphoprotein deficient mice have shown decreased mineral content.	May regulate type I collagen fibrillogenesis; Nucleator of hydroxyapatite formation at lower concentrations and inhibitor at higher concentrations.

Table I.5. γ-Carboxy Glutamic Acid-Containing Proteins in Bone Matrix: protein functions and *in vivo* studies.

	***In vivo* studies**	**Function**
Osteocalcin	Osteocalcin deficient mice present an increase in bone formation without impairing bone resorption.	May influence bone mineralization. It has high affinity to calcium, accelerating nucleation of hydroxyapatite and playing an active role in the early stages of bone healing. May regulate activity of osteoclasts and bone resorption.
Matrix Gla Protein	Matrix Gla Protein deficient mice died prematurely due to massive calcification of their tracheal cartilage and blood vessels, indicating a specific role in preventing mineralization.	May function in cartilage metabolism inhibiting mineralization.

I.7. Bone Tissue Engineering

I.7.1. Clinical need for bone regeneration

Bone is a dynamic and highly vascularized tissue that has the ability to regenerate and continues to remodel throughout the lifetime of an individual. Nevertheless, large bone defects can be caused by trauma, disease or tumor resections, leading to severe nonunion fractures that can not heal spontaneously, requiring the use of bone grafts. In the United States, annually, more than half a million patients need bone defect repair, with a cost greater than $2.5 billion. Surprisingly, this phenomenon is expected to double by 2050, globally, due to the increased life expectancy, as seen in Figure I.24 (Baroli *et al.* 2009).

Current clinical treatments for bone repair and regeneration include autologous and allogeneic transplantations using autografts and allografts (Amini *et al.* 2012, Baroli *et al.* 2009, Dimitriou *et al.* 2011, Yaszemski *et al.* 1996). Autografts are the gold standard treatment, which involves the harvest of donor bone from a non-load-bearing and easily accessible site in the patient and transplantation into the defect site (Bauer & Muschler 2000) (Figure I.25). Autografts have the best clinical outcome since these grafts can integrate with host bone and they lack immunogenic reactions (Amini *et al.* 2012). Autografts have osteoinductive components, such as BMP and other growth factors, osteogenic cells and their 3-D porous matrix confers osteoconductivity to the material. Nevertheless, autografts have some limitations such as their short availability and the possible risk of site morbidity associated with the harvest procedure (Silber *et al.* 2003, Lord *et al.* 1988*)*. Moreover, possible complications may occur, such as pain, infection, scarring and patients will eventually experience fractures (Yaszemski *et al.* 1996, Stock & Vacanti 2001).

Allografts are the second most common technique used for bone grafting. In this case, bone tissue from a different donor, often from a cadaver, is transplanted into the defect site. Allogeneic bone is available in different forms, such as demineralized bone matrix (DBM), morcellised and cancellous chips, cancellous and cortical grafts and osteochondral and whole bone segments, depending on the defect site requirements (Amini *et al.* 2012). Allografts have also limitations, namely the higher risk of immunologic rejection, besides infection (Stock & Vacanti 2011). Moreover, allografts have reduced osteoinductive properties and no cellular component, since these grafts are devitalized via irradiation or freeze-drying procedures (Delloye *et al.* 2007, Lord *et al.* 1988).

Consequently, alternative strategies to provide efficacious bone grafts are being exploited. Bone tissue engineering aims to generate functional bone tissue, developing biocompatible and biodegradable scaffolds. New approaches to enhance the functionality of the scaffolds are being developed, such as the use of growth factors or their combination with cellular approaches. Numerous pre-clinical trials with different animal models have generated optimistic results (Cancedda *et al.* 2007). However, the difficulty to translate it into a clinical setting suggests that some limitations and concerns remain and need to be further address to design and develop enhanced bone grafts for bone fracture repair treatment.

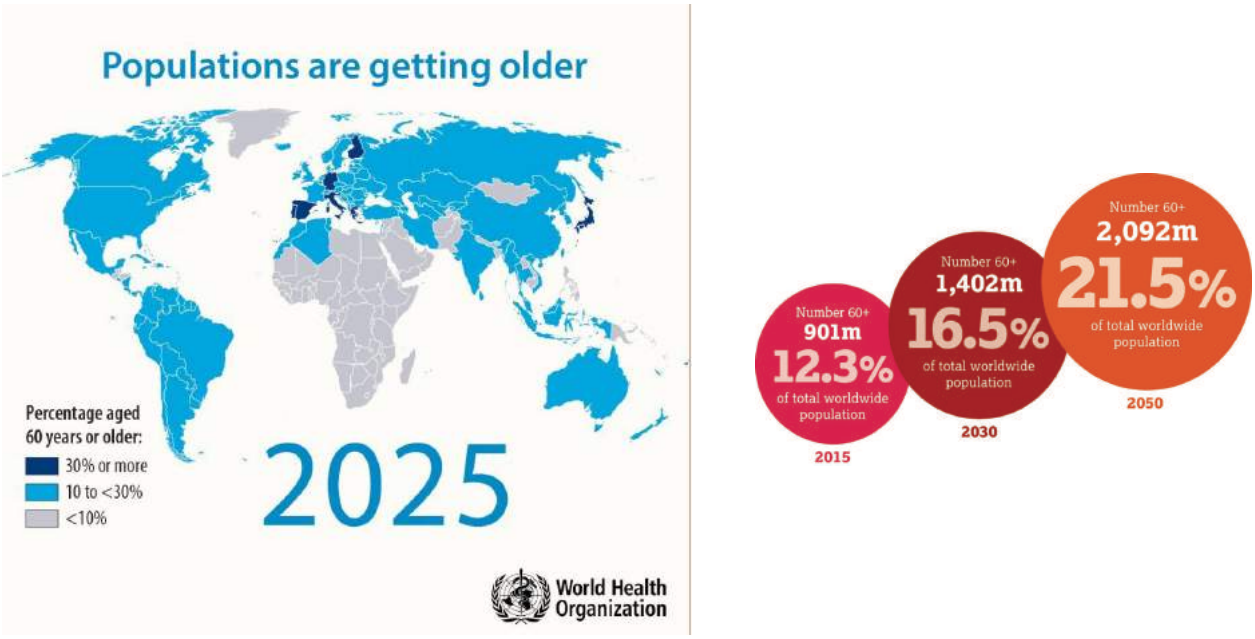

Figure I.24. Proportion of the world population aged 60 years or more. With advances in medicine helping to increase life expectancy, the number of people over the age of 60 is expected to double by 2050 (UNDESA Population Division, World population prospects: the 2015 revision, DVD Edition, 2015).

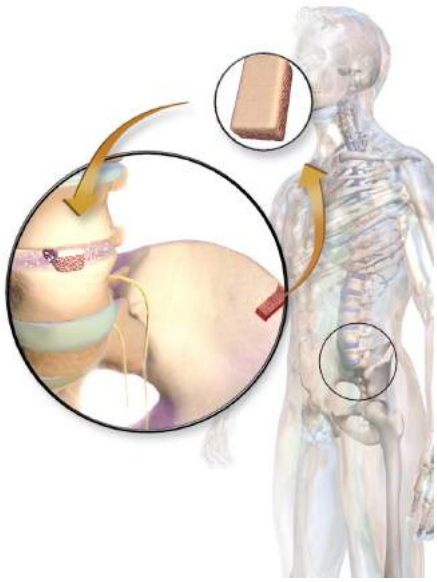

Figure I.25. Bone autograft.

I.7.2. Bone grafting

Interestingly, humans have been trying to find the most efficient way to substitute bone loss and to develop the best bone replacement material for thousands of years. In fact, archeologists have discovered a lot of bones covered with some materials, such as gold and silver. For example, they found a skull of a tribal chief from 2000 BC, in which a bone defect had been covered with a plate of hammered gold (Henkel *et al.* 2013, Sanan & Haines 1997). Ancient Egyptians have been shown to have strong knowledge of orthopaedic and traumatological procedures, having implanted iron prostheses for knee joint replacement as early as 600 BC (Henkel *et al.* 2013, Donati *et al.* 2007).

However, the first modern era report of a bone xenograft procedure is believed to be in 1668, in which a skull defect was successfully treated with a bone xenograft taken from the calvaria of a deceased dog, that was fully incorporated into the skull of the patient (Haeseker 1988). Only in 1820, the first clinical use of a bone autograft to reconstruct skull defects was described (von Walter 1821). In 1881, the first allogenic bone grafting procedure was reported to reconstruct an infected humerus by using tibial bone wedges from three donors that had undergone surgery for skeletal deformity correction (MacEwen 1881).

Major contributions have been made to the development of bone grafting procedures. In the late 1800s, Ollier and Barth described the term 'bone graft' for the first time (Ollier 1867) and presented results of various bone grafting procedures involving the skull and long bones of dogs and rabbits (Barth 1895). Today, Ollier's and Barth's studies are considered to be extremely important in the development of bone grafting procedures.

The first bone bank for allogenic bone grafts was opened in New York in 1945 (Bush 1947), trying to fulfill the increased demand due to the development of new bone grafting techniques. However, as a main limitation of allogenic bone materials, immunological reactions may occur. Currently, antigen structures are well removed from bone substitute materials, however due to the harsh treatment, most of these grafts do not contain osteoinductive factors, such as growth factors, as opposite to autologous bone grafts. As early as 1932, autologous bone grafts have been shown to be a reliable material to be transplanted in a bone defect (Matti 1932).

Nowadays, bone is the second most transplanted material, after blood. Notably, each year, worldwide, more than 3.5 million bone grafts, including autografts and allografts, are performed (Dinopoulos *et al*. 2012).

Currently, material science technology has advanced and enables the development of new bone grafting materials to target bone loss, without compromising the structural and functional properties of bone, as well as promoting accelerated healing and integration into the defect site. Moreover, our society is facing a problem of population aging. In fact, elderly population is more prone to bone fractures and bone diseases, leading to an increase of the number of procedures requiring bone substitutes. In addition, due to the sedentary lifestyle that is taking part in most countries, specially in the high-income countries, the number of bone replacement procedures is expected to grow. As a consequence of that, the current bone grafting market globally is estimated to be in excess of $2.5 billion each year and it is expected to increase at a compound annual growth rate of 7-8% (Dinopoulos *et al.* 2012).

Although new promising solutions for bone reconstruction have been developed, to date most common procedures for bone regeneration still rely on bone grafts, both autologous and allogeneic bone grafts (Yaszemski *et al.* 1996, De Long *et al.* 2007).

I.7.3. Biomaterials for bone repair

Aiming to develop and design new materials for bone tissue engineering to replace the need for autologous and allogeneic bone, scientists have now focused on designing bioactive materials that incorporate biological molecules or cells that can trigger some cellular response, such as cell attachment, proliferation or differentiation (Langer & Vacanti 1993, Hench & Polak 2002). More specifically, these materials should be osteoinductive, promoting the differentiation of progenitor cells into an osteogenic lineage, and osteoconductive by supporting bone growth. Moreover, biomaterials should be able to integrate into the surrounding tissue (osseointegration). Mainly, these materials can be bioactive ceramics, bioactive glasses, biological or synthetic polymers and composites of these (Hench & Polak *et al.* 2002, Kretlow & Mikos 2007, Liu *et al.* 2007).

I.7.3.1. Bioactive inorganic materials

Different inorganic materials with a composition similar to the mineral phase of bone have been used in bone clinical context, such as tricalcium phosphate, hydroxyapatite, bioactive glasses and their combinations (Hench & Polak *et al.* 2002, Kretlow *et al.* 2007, Liu & Czernuszka 2007) (Figure I.26). Interestingly, the resorption rate of bioactive glasses and bioceramics can be tailored, however hydroxyapatite persists for years in the body following implantation. On the other hand, other calcium phosphates have a greater resorption rate but less capability for sustaining load. Due to the fact that these materials are similar to the mineral phase of bone, bioactive inorganic materials are very brittle and their fracture toughness can not match that of bone, so that these materials will not support load, not being an ideal material for load-bearing applications.

Figure I.26. Different bone graft materials used in bone tissue engineering. β-TCP ceramics, hydroxyapatite-based materials and bioactive glasses (Adapted from Stevens *et al.* 2008).

I.7.3.2. Polymers

Biological polymers and synthetic polymers have been used in bone tissue engineering applications. Biological polymers, such as collagen, provide innate biological cues to the cells, favoring cell attachment and recruitment of the cells. However, these polymers have some limitations, such as the potential risk of disease transmission, sourcing and weak mechanical properties. On the other hand, synthetic polymers, such as polylactic acid (PLA), polyglycolic acid (PGA) and polycaprolactone (PCL), can be synthesized to have better mechanical properties and they can be processed using different techniques such as gas foaming (Ma *et al.* 2001), phase separation (Ma *et al.* 2001), electrospinning (Vacanti & Robert 1998) and 3-D printing (Sherwood *et al*. 2002). Using these techniques, it is possible to produce scaffolds with the desired characteristics, such as porosity and surface properties.

These polymers can also be used to generate hydrogels that can be delivered in a minimally invasive manner and gelled *in situ* (e.g. photocrosslinked or ionically), providing a 3-D microenvironment support with high water content. Some hydrogels have already been applied for bone regeneration (Cushing & Anseth 2007, Stevens *et al.* 2004, Lutolf *et al.* 2003, Lutolf *et al.* 2003b), being able to be functionalized with bioactive factors and, moreover, cells can be easily encapsulated (Bhatia *et al.* 2012).

I.7.3.3. Composite materials

Composite materials mimic the organic-inorganic composition of bone, combining the toughness of a polymer with the compressive strength of an inorganic phase. Therefore, these materials have better mechanical properties.

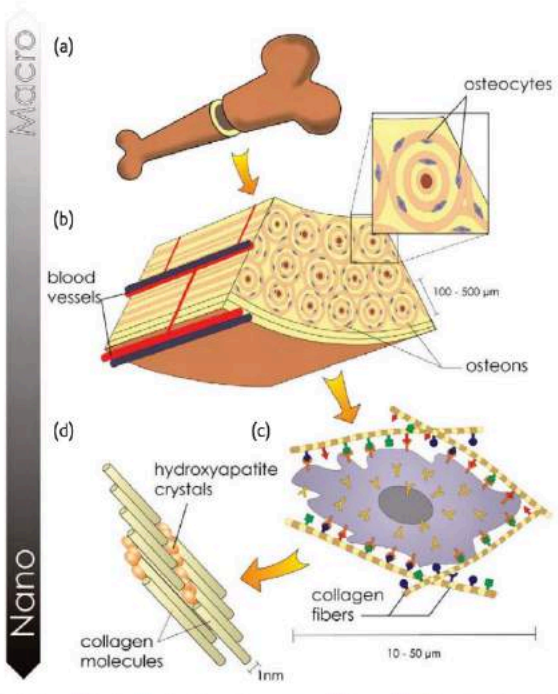

Figure I.27. Hierarchical organization of bone over different length scales. Collagen molecules and hydroxyapatite crystals are organized at the nanoscale level (Stevens and George 2005).

In addition, inorganic components at the nanoscale have shown to be more bioactive compared with microscale, such as hydroxyapatite-collagen nanocomposite systems (Liao *et al.* 2004). Ideally, the material should recreate the nanoscale organization of the mineral and organic components of bone tissue (Figure I.27).

I.7.4. Developing scaffolds in bone tissue engineering

3-D scaffolds materials have been used in bone tissue engineering to guide cell migration, proliferation and differentiation, acting also as temporary mechanical support structure. However, scaffolds should be well designed and developed to meet specific requisites. Therefore, an ideal scaffold should be (i) three-dimensional and highly porous with an interconnected pore network to allow cell growth and transport of nutrients and metabolic waste; (ii) should have surface properties to enhance cell attachment, migration, proliferation and differentiation; (iii) must be biocompatible and biodegradable, not causing an immune reaction and with a controllable degradation rate to allow tissue maturation; (iv) should have mechanical properties similar to the tissue and (v) the scaffold should be easily customized and reproducible (Hutmacher 2000).

I.7.4.1. Biocompatibility and biodegradation

Biocompatibility is an important property that biomaterials should have, not eliciting any immune reaction. At the same time as new tissue is being formed *in vivo*, the scaffold may undergo degradation, due to the release of by-products that should be also biocompatible. Therefore, scaffolds can be eliminated from the body, gradually, through natural mechanisms, by filtration of by-products or after their metabolization, such as bioresorbable scaffolds (Hutmacher 2000).

I.7.4.2. Mechanical properties

Another important parameter to be considered while designing scaffolds for tissue engineering is their mechanical properties, as well as their degradation kinetic. The mechanical properties of the scaffolds should match the structural properties of the tissue (Hollinger & Chaudhari 1992). The scaffold will act as a structural support and will promote cell attachment, migration, proliferation and differentiation, therefore, guiding new bone formation. However, at the same time as new tissue is being formed, the scaffold should be undergoing degradation to allow the total replacement of the scaffold with new tissue engineered bone. It is essential that the rate of degradation is controlled, enabling a balanced bone formation. Since bone is always being subjected with different loads, the scaffold will also give mechanical support and stability at the defect site until new bone is completely formed. In bone tissue engineering, the degradation and resorption kinetics of the scaffold have to be controlled and well tailored, since the scaffold should retain their physical properties for at least 6 months to enable tissue remodeling to achieve stable biomechanical conditions and vascularization at

the defect site (Hutmacher 2000). However, the type of tissue, i.e., cancellous or cortical bone, that is aimed to be engineered also influences the degree of remodeling. In cancellous bone the remodeling process takes 3-6 months, while cortical bone will take approximately 6-12 months to remodel (Hutmacher & Cool 2007). Therefore, it is crucial to select the material to be used for a specific application considering all these parameters, tailoring the mechanical properties and degradation rate according to the specific purpose of the tissue engineered scaffold, not being able to have an ideal material for all bone tissue engineering applications.

I.7.4.3. Surface properties

The surface area of the scaffold is important for the interactions between the biomaterial and the host tissue. When cells adhere to the scaffold, they can sense different cues, such as roughness, topography and surface chemistry, and then transduce these signals via the cytoskeleton to the nucleus resulting in expression of specific proteins that contribute to the cell phenotype (Boyan *et al.* 1996).

Nowadays, technology has evolved in a way that we can manipulate materials at different scale levels, atomic, molecular and supramolecular level and material surfaces can be designed at a similar dimension to the nanoscale of components of bone (Webster & Ahn 2007). For example, hydroxyapatite plates are approximately between 25 nm in width and 35 nm in length while collagen type I is a triple helix 300 nm in length, 0.5 nm in width and with a periodicity of 67 nm (Kaplan *et al.* 1994). Nanomaterials appear as a promising strategy to be used in bone tissue engineering applications due to the close proximity of the scale of native bone. In fact, surfaces with nanometer topography have been shown to promote the availability of aminoacids and proteins for cell adhesion. Indeed, by decreasing the grain size on the scaffold surface bellow 100 nm, the adsorption of some proteins such as fibronectin can be increased (Webster *et al.* 2001).

In vitro studies have shown that osteoblast adhesion, proliferation and differentiation, as well as mineralization, is enhanced on nanomaterials with grain sizes less than 100 nm (Webster *et al.* 2001, Webster *et al.* 1999). For example, a study from Puckett and colleagues showed that the adherence of osteoblasts increased when the surface is covered with nanophase titanium particles (Puckett *et al.* 2008).

I.7.4.4. Porosity and pore size

Porosity is defined as the percentage of void space in the scaffold. Adequate porosity and pore size are extremely important for bone tissue engineering scaffolds since it allows vascularization of the scaffold and migration and proliferation of cells throughout the whole construct. Therefore, porosity is essential to allow vasculature to penetrate into the central regions of the scaffold, allowing the transport of oxygen and nutrients. In fact, increase of porosity and pore size has been shown to influence, positively, bone formation *in vivo*. For example, pores smaller than 100 μm were found to negatively affect vascularization (Hutmacher 2000). Interestingly, these results correlate with the diameter of the physiological Haversian systems in bone tissue (>100 μm).

In vivo studies have also shown that larger pore sizes and higher porosity lead to greater amounts of new bone formation and a faster rate of vascularization. In contrast, small pores favored hypoxic conditions and induced osteochondral formation before osteogenesis occurs (Hutmacher & Cool 2007).

Nevertheless, increased porosity and higher pore size can also compromise the structural integrity of the scaffold, affecting its mechanical properties (Hutmacher *et al.* 2007b). It is extremely important to consider all these different factors when designing and developing scaffolds for bone tissue engineering applications.

I.7.5. Enhancing the functionality of the scaffolds

Recently, the development of biomaterials has been focused on the design of biomimetic materials that can interact with surrounding tissues by biomolecular recognitions (Lutolf *et al.* 2003, Yang *et al.* 2004). The effort to functionalize synthetic scaffolds with biological cues, such as growth factors and ECM peptides, aims the formation of new tissue by eliciting specific cellular responses that may not be present in the native tissue (Figure I.28). Therefore, the properties of the biomaterial can be enhanced, in particular osteogenic differentiation of MSC by inducing expression of osteogenic genes in MSC (Kesireddy & Kasper 2016). Among the several signaling molecules used to induce bone regeneration, bone morphogenetic proteins (BMP) have been used clinically. However, some limitations of the use of BMP have been reported, such as the high doses required and some side-effects. Therefore, another common strategy is the incorporation of cell-binding peptides into biomaterials, mimicking naturally occurring processes such as cell-extracellular matrix signaling, cell proliferation and differentiation (Lee *et al.* 2011).

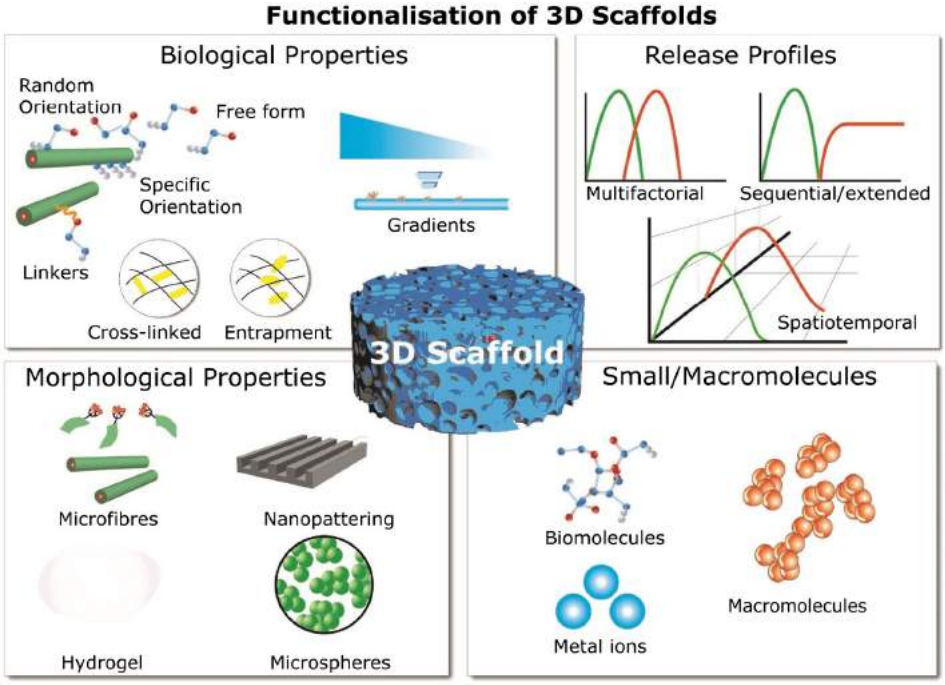

Figure I.28. Functionalization of 3-D scaffolds for bone regeneration. Different strategies rely on morphological properties, control delivery of bioactive factors and tailoring of the degradation rate (Fernandez-Yague *et al.* 2015).

Incorporation of appropriate osteoinductive and osteogenic cues into scaffolds is a promising approach to enhance the functionality of the scaffolds. Moreover, these signals can more efficiently attract the patient's own stem cells and may create a biomimetic microenvironment. Different approaches have been used, such as cellular approaches, incorporation of bioactive peptide motifs, incorporation of BMP or other growth factors, drug delivery and the use of ECM proteins, such as decellularized cell-derived ECM, among others.

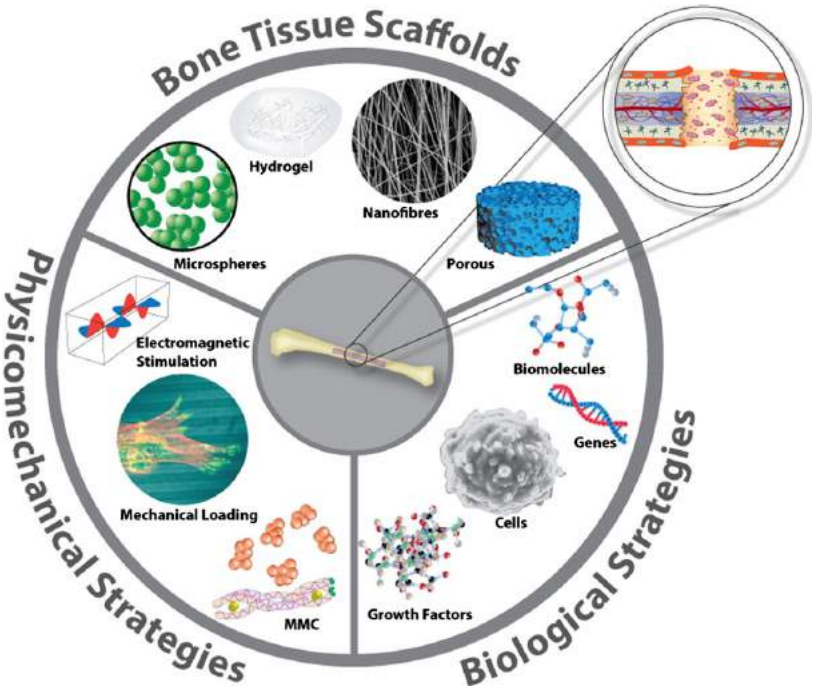

Figure I.29. Schematics of different types of scaffolds and strategies that can be applied in bone tissue engineering applications (Fernandez-Yague *et al.*2015).

I.7.5.1. Cellular approaches

Cellular-based approaches in bone tissue engineering are very effective, specially, during the early stages of bone repair in the recruitment of progenitor cells. Different mechanisms of action have been proposed to explain the enhancement of bone regeneration with cellular-based approaches. Thus, the early release of osteogenic and vasculogenic molecules and growth factors, the induction of recruitment of host osteogenic cells and the actively formation of bone matrix and vascularization of the construct are associated to cellular-based approaches to enhance bone regeneration (Amini *et al.* 2012).

Different cell types have been investigated for bone regeneration such as: mesenchymal stem/stromal cells, embryonic stem cells, induced pluripotent stem cells and stem cells from human exfoliated deciduous teeth (Amini *et al.* 2012).

In fact, MSC can differentiate into bone tissue during the natural bone development process, therefore they have been widely exploited for bone tissue engineering applications. MSC can also be differentiated into adipocytes and chondrocytes. MSC have been defined through the expression of various CD markers (i.e.,

negative for CD34, CD45, CD14, CD11a, CD19, and HLA-DR and positive for STRO-1, CD29, CD73, CD90, CD105, CD106, CD166, CD146, and CD44) (Arvidson *et al.* 2011). MSC can be isolated from different adult sources, such as bone marrow (Bianco *et al.* 2001), peripheral blood (Kuznetsov *et al.* 2001), umbilical cord blood (Rosada *et al.* 2003), synovial membrane (De Bari *et al.* 2001), deciduous teeth (Miura *et al.* 2003), dental pulp (Shi & Gronthos 2003), amniotic fluid (In't Anker *et al.* 2004), adipose tissue (Zuk *et al.* 2002), brain, skin, hear, kidneys and liver (Crisan *et al.* 2008). MSC isolation relies on their ability to adhere to plastic in tissue culture (Caplan 1991). Moreover, these cells can also be derived from embryonic stem cells and induced pluripotent stem cells (Yu *et al.* 2007).

MSC have been incorporated into biomaterials for bone tissue engineering applications as a strategy for accelerated bone formation and healing during bone defect regeneration. Since MSC can differentiate into osteoblasts, these cells have the potential to enhance bone regeneration. In addition, MSC can release osteogenic growth factors, enhancing osteoinductivity of the biomaterial, and stimulate the migration of host progenitor cells and their differentiation.

Pre-clinical trials with scaffolds seeded with MSC have shown accelerated bone repair, in different bone defects, such as critical-size femoral and cranio-maxillofacial defects (Mauney *et al.* 2005). However, some concerns have been raised about the use of MSC as a cellular approach for enhanced bone regeneration. First, several studies have shown that MSC have a maximum limit of population doublings that can be reached. Another limitation is the donor age, since osteogenic differentiation *in vitro* and osteogenesis *in vivo* decreases with donor age (Kagami *et al.* 2011). Moreover, before patient treatment with MSC, approximately 4-6 weeks are required for cell expansion and long-term culture may increase the possibility of abnormal karyotype development and malignant cell transformation. Lastly, fetal bovine serum (FBS) is widely used during in vitro expansion and it is known to be able to trigger an immune response by the xenogenic proteins. Therefore, new reagents that do not contain components from animal origin have been developed and are now being used for MSC expansion to be finally incorporated in clinical applications.

I.7.5.2. BMP and other growth factors

Different key molecules have been reported to regulate fracture healing and have been used in clinical context to enhance bone repair and accelerate normal bone healing to reduce the time of fracture treatment. Their clinical use combined with bone grafts has increased in the last years. However, there are still several concerns about their use, including safety, specially regarding the high concentrations of growth factors required to obtain the desired effect, the high cost of treatment and the potential for ectopic bone formation (Argintar *et al.* 2010).

BMP have been the most extensively proteins investigated, since they have been reported as potent osteoinductive factors. BMP can induce the mitogenesis of MSC and their differentiation into an osteogenic lineage. Several clinical trials have been going on to evaluate the safety and efficacy of the use of BMP as osteoinductive bone-graft substitute for bone regeneration. In fact, BMP-2 and BMP-7 have been approved for clinical use in a variety of clinical conditions including non-union, open fractures, joint fusion and critical bone defects (Giannoudis and Einhorn 2009).

Besides BMP, other growth factors have been shown to enhance bone regeneration, acting in different cellular processes such as proliferation, chemotaxis, osteogenesis and angiogenesis (Nauth *et al.* 2010,

Simpson *et al.* 2006), including PDGF, TGF- β, IGF-1, VEGF and FGF, among others (Dimitriou *et al.* 2005). Therefore, different *in vitro* and *in vivo* studies have evaluated these factors alone or in combination, presenting controversial results (Nauth *et al.* 2010, Simpson *et al.* 2006).

I.7.5.3. Bioactive peptides

The most commonly used peptide for surface modification is Arg-Gly-Asp (RGD) (Koivunen *et al.* 1995, Shin *et al.* 2002, Massia *et al.* 1991), the signaling domain derived from fibronectin and laminin and also found in collagen. These peptides can be chemically attached to polymers to facilitate cellular interactions at an injury site. Specifically, RGD peptides have been shown to enhance differentiation, proliferation and mineralization when attached to the surface of various biodegradable materials (Yang *et al.* 2001, Schaffner & Dard 2003). Biomimetic polylactic acid (PLA) scaffolds modified with RGD peptides have been prepared and shown to promote the attachment and growth of osteoblasts (Shin *et al.* 2002). It has been reported that by controlling the distribution of RGD on hydrogels by nanopatterning, it is possible to maximize its beneficial effects on adhesion, survival, and differentiation of MSC (Wang *et al.* 2013, Wang *et al.* 2013b)

Additionally, other peptide sequences have been immobilized on different scaffolds, such as Tyr-Ile-Gly-Ser-Arg (YIGSR) and Ile-Lys-Val-Ala-Val (IKVAV) in laminin (Vukicevic *et al.* 1990) Arg-Glu-Asp-Val (REDV) and leucine-aspartic-acid-valine (LDV) in fibronectin (Aota *et al.* 1991).

Short peptide fragments from collagen have been used for surface modification in numerous studies (Shin *et al.* 2003). For example, Bhatnagar and colleagues identified a cell-binding domain P15 (GTPGPQGIAGQRGVV) from type I collagen that supported ECM synthesis (Bhatnagar *et al.* 1999). Similarly, another type I collagen peptide - GFOGER was used to functionalize surfaces and showed to support the expression of osteogenic genes, including osteocalcin and bone sialoprotein, and to induce matrix mineralization in a manner similar to type I collagen (Reyes & García 2004, Reyes *et al.* 2007).

I.7.5.4. Non-collagenous bone proteins in bone tissue engineering

Collagen has already been described to be extremely important as a template to create bone tissue, however the question that remains to answer is which of the other components from bone matrix besides collagen are essential to engineer new bone tissue.

Recently, investigators have been focusing on using the native non-collagenous proteins from bone matrix to enhance the properties of the scaffolds, such as cell recruitment, proliferation and differentiation into an osteogenic lineage, regarding bone tissue applications. Although great improvements on incorporating peptides on biomimetic materials have already been achieved, the influence of the non-collagenous bone matrix proteins on osteogenic differentiation remains to be evaluated, even though these proteins have been identified some decades ago. Thus, *in vitro* and *in vivo* studies must be conducted to understand better the functions of the bone matrix constituents and how these proteins can be applied in bone tissue engineering strategies.

Few works have been using components of the organic bone matrix other than collagen to create bone substitutes. Johnson and colleagues used a composite alloimplant of human bone morphogenetic protein and autolysed allogeneic bone containing a mixture of extracellular matrix proteins. In a clinical trial, they were possible to achieve body union in 24 of 25 cases of resistant nonunions. However, the addition of BMP as osteoinductive factors did not allow any conclusion on the performance of the non-collagenous bone matrix proteins alone (Johnson & Urist 2000).

Sun and co-workers integrated non-collagenous proteins from bone extracellular matrix into gelatin scaffolds to form an artificial matrix, mimicking natural ECM, enhancing osteogenesis and mineralization (Sun *et al.* 2013).

Depending on the end use, various combinations of the functional domains of non-collagenous bone extracellular matrix proteins can be incorporated into scaffolds to elicit responses for bone tissue regeneration. Indeed, an additive and synergistic effect has been reported when combining more than one ECM protein/peptide.

Most of the peptides incorporated into the scaffolds have integrin-binding RGD sequences to enhance cell binding to scaffolds, however the addition of other ECM proteins, like BSP, OPN or OC, have shown to enhance mineralization, to accelerate bone healing and to induce angiogenesis (Kruger *et al.* 2013, He *et al.* 2012, Rammelt *et al.* 2005). Thus, a combination of non-collagenous bone matrix might be an impressive strategy to improve the properties of the scaffold, giving the “ideal” cues to accelerate the process of bone healing.

I.7.5.4.1. Proteoglycans from bone matrix in bone tissue engineering

Proteoglycans are known to be important to support the growth and development of cells through their signaling and structural properties.

For tissue engineering purposes, synthetic peptido-glycosaminoglycans (peptido-GAG) have been synthesized since they have shown promising results for biomedical applications (Wyers & Linhardt 2013). These peptido-GAG could replicate many of biological functions of decorin, specifically they could modulate fibril formation and the stiffness of the new tissue and promote cellular adhesion (Paderi & Panitch 2008, Sistiabudi *et al.* 2009). Also, aggrecan peptido-GAG have been used to enhance the properties of some scaffolds in cartilage (Stuart *et al.* 2011).

For bone tissue engineering applications, few works have been incorporated collagen and GAG into a scaffold to provide a suitable 3-D environment to induce osteogenic differentiation of mesenchymal stem/stromal cells (Farrell *et al.* 2006). Aiming to mimic the natural structure and composition of bone tissue, novel scaffolds comprising collagen, GAG and calcium phosphate crystals have been fabricated (Harley *et al.* 2010).

The glycosaminoglycan chondroitin-sulfate has been used for bone tissue engineering applications, since chondroitin sulfate was reported to support osteogenic differentiation of MSC, increasing the regeneration ability of injured bone. A chondroitin sulfate bioglass composite encapsulating bone marrow cells was reported to induce bone regeneration *in vivo* in cooperation with BMP (Yang *et al.* 2015). Also, a chondroitin

sulfate collagen scaffold was generated as a BMP delivery system and showed high biocompatibility and osteogenic stimulation (Keskin *et al.* 2005).

Hyaluronic acid has been utilized in recent years in several medical fields. This glycosaminoglycan is an optimal biomaterial for tissue engineering, being used as a carrier for regenerative growth factors (Fujioka-Kobayashi *et al.* 2016).

I.7.5.4.2. Glycoproteins from bone matrix in bone tissue engineering

There have been several reports of the use of glycoproteins derived from bone matrix to enhance cell binding in association with a variety of different scaffolds in tissue engineering applications, such as alkaline phosphatase, osteonectin, fibronectin, vitronectin, osteopontin, bone sialoprotein and DMP-1.

I.7.5.4.2.1. Alkaline phosphatase

For bone tissue engineering applications, ALP has been immobilized on microporous nanofibrous fibrin scaffolds to enhance the mineralization ability of these scaffolds and osteogenic differentiation *in vitro* and *in vivo* (Osathanon *et al.* 2009). These scaffolds are non-toxic, biodegradable, and support cell proliferation and differentiation *in vitro*. Furthermore, the immobilized ALP fibrin scaffolds supported bone formation in a mouse calvarial defect model (Osathanon *et al.* 2009).

I.7.5.4.2.2. Osteonectin

In native bone, osteonectin may bind selectively to both collagen and hydroxyapatite. Some studies have been incorporating osteonectin into composites to regulate the mineralization process. A nano-hydroxyapatite/collagen/osteonectin complex was developed to mimic the hierarchical structure of natural bone from nanoscale to microscale, which surpasses the limitation of mineralized pure collagen synthesized *in vitro* (Liao *et al.* 2009). In fact the formation of the mineralized collagen nanofibers was influenced by the presence of osteonectin (Sarvestani *et al.* 2008).

I.7.5.4.2.3. Fibronectin and vitronectin

Fibronectin and vitronectin have been used for surface modification by coating these proteins to make biomimetic materials to promote cell adhesion and proliferation (Hidalgo-Bastida & Cartmell 2010). Although the ECM affinity for cell adhesion has been well reported and confirmed, the optimal ECM coating for osteogenic differentiation is still not clear. Further studies are being conducting, focusing in combining more than one different ECM protein in the coating to enhance cell adhesion and differentiation, with the ultimate goal to develop functional constructs for clinical skeletal regeneration. Cacchioli and colleagues reported that the vitronectin peptide conjugated onto titanium surfaces increased cell attachment rate, showing a higher ratio of mineralized surface to bone surface and more extended bone-to-implant contact in a rabbit *in vivo* model (Salasznyk *et al.* 2004, Kundu & Putnam 2006). Fibronectin has been reported as a potent adhesive

ligand that particularly stimulates the anchorage of mesenchymal stem/stromal cells and has been widely used as a coating on bioactive nanocomposite scaffolds, enhancing adhesion and proliferation of cells into scaffolds (Lee *et al.* 2015).

By using a robotic-dispensing technique, it was possible to generate fibronectin-immobilized nanobioactive glass (nBG)/polycaprolactone (PCL) (FN-nBG/PCL) scaffolds with an open pore architecture. With the addition of these cell-adhesive motifs, like fibronectin, into the surface of the scaffold, cellular adhesion and differentiation processes might be accelerated (Won *et al.* 2015).

Recently, strategies for bone tissue engineering involve the combination of materials such as ECM proteins and growth factors with nanohydroxyapatite as a promising application for bone reconstruction (Mohamadyar-Toupkanlou *et al.* 2017). Therefore, Toupkanlou and colleagues incorporated nanohydroxyapatite in electrospun nanofibrous PCL scaffolds coated with fibronectin, demonstrating the synergistic effect of fibronectin and nanohydroxyapatite on enhancing calcium deposition, collagen synthesis, early ALP activity and upregulating osteogenic specific genes both *in vitro* and *in vivo* (Mohamadyar-Toupkanlou *et al.* 2017).

Lee and co-workers construct a novel osteoinductive FN matrix fusion protein (oFN) containing FNIII9 and FNIII10 modules, the key cell-binding domain of fibronectin, and an osteoinductive sequence from BMP-2 and investigated the osteogenic activity of oFN-loaded collagen matrix (Lee *et al.* 2015). The engineered oFN matrix fusion protein resulted in more effective bone regeneration by promoting cellular adhesion and differentiation (Lee *et al.* 2015). Thus, it showed that the design of fusion proteins could represent a highly relevant approach for bone tissue engineering.

I.7.5.4.2.4.Osteopontin

OPN plays an important role in adhesion, remodeling and osseointegration at the biomaterial/tissue interface that is commonly found surrounding mineralized tissues (McKee & Nanci 1996). OPN plays a role in cell attachment to ECM and is responsible for the recruitment of osteoblasts during the early stage of bone formation (Shapses *et al.* 2003). Somerman and co-workers showed that the attachment of osteoblasts to OPN was dose dependent and was mediated by a conservative RGD peptide sequence (Somerman *et al.* 1989).

Some peptides were already derived from OPN and have been reported to bind to collagen and to induce biomineralization (McKee & Nanci 1996). A work by Shin and colleagues showed that oligo(poly(ethylene glycol) fumarate hydrogels modified with OPN-derived peptide influenced osteoblast proliferation and migration (Shin *et al.* 2004). OPN can also interact with multiple cell surface receptors, having an active role in many physiological processes like wound healing, bone turnover, inflammation and angiogenesis (Denhardt & Guo 1993). Although, Shin and colleagues demonstrated that OPN-derived peptide hydrogels enhance cell migration, the effect of OPN on osteogenic differentiation of MSC was not investigated. On the other hand, He and colleagues described an hydrogel that combined OPN, BMP-2 and RGD sequence to provide a favorable microenvironment for osteogenic and vasculogenic differentiation of marrow stromal cells that could be used for bone tissue engineering applications (He *et al.* 2012).

Lee and colleagues showed that a collagen-binding motif (GLRSKSKKFRRPDIQYPDATDEDITSHM) found in OPN could specifically bind collagen without chemical conjugation and demonstrated capacity to form hydroxyapatite *in vitro* and *in vivo* (Lee *et al.* 2007)

OPN has been reported as inducing bone formation by inhibiting osteoclast resorption and more importantly by increasing angiogenesis (Denhardt & Guo 1993). In fact, it has been reported that the peptide SVVYGLR, corresponding to amino acids residues 162-168 of OPN, induces vasculogenic differentiation of the bone marrow cells (Egusa *et al.* 2009). This peptide induces tube formation by progenitor endothelial cells in 3-D collagen gels with as much potency as VEGF (Egusa *et al.* 2009). Hamada and co-workers developed CO_3 apatite-collagen sponges containing the SVVYGLR motif as a scaffold and implemented into a tissue defect created in rat tibia. This scaffold promoted angiogenesis inside the graft, suggesting the incorporation of OPN into biomaterials for bone tissue engineering applications that require angiogenesis (Hamada *et al.* 2007).

I.7.5.4.2.5. Bone sialoprotein

Many groups have been exploring the functions of BSP to be used in a therapeutic device to repair bone defects, enhancing their osteoinductive capacity (Kruger *et al.* 2013). In fact, BSP implants are an attractive candidate for bone applications since BSP plays an important role in osteogenic differentiation, binds type I collagen with high affinity and binds $\alpha_v\beta_3$ and $\alpha_v\beta_5$ integrins, which mediate cell signaling and differentiation (Kruger *et al.* 2013). BSP has been shown to be essential in osteogenic differentiation of bone marrow cells cultured on type I collagen. Moreover, BSP plays an essential role in the formation of calcified nodules. Due to the high affinity with collagen, BSP combined with collagen facilitates cell migration, attachment, proliferation and differentiation through RGD and non-RGD binding of integrins (Kruger *et al.* 2013).

Instead of using the whole protein, some investigators have been exploring the properties of the amino acids sequence 35-62 of rat BSP, corresponding to the collagen-binding peptide derived from BSP (Choi *et al.* 2013). The *in vivo* studies demonstrated that hydroxyapatite implants containing 6 mg of this BSP-derived collagen-binding peptide placed into the rabbit calvarial defects stimulated new bone formation within 2 weeks after implantation as compared to untreated or hydroxyapatite scaffolds alone. Other groups have also shown that the presence of BSP in some collagen implants, *in vivo*, stimulates osteogenic differentiation and bone repair (Xu *et al.* 2007), by upregulating the expression of genes associated with early osteogenic differentiation, as early as 4 days after implantation. Another interesting result observed in this study was that by day 7 after surgery, cell proliferation, matrix mineralization and vascular invasion extended into the central regions of the BSP-collagen implants. Instead, when using only collagen as implants, the central regions of the implant were not affected. In conclusion, defects where BSP-collagen scaffolds were implanted presented new bone formation and remodeling in the whole areas of the defect, whereas defects that were implanted with collagen alone only demonstrated new bone formation in the areas near the host bone (Kruger *et al.* 2013).

Another group has shown that silk-based materials can be used instead of type I collagen. These scaffolds were functionalized with BSP to enhance osteogenesis (Gomes *et al.* 2013). These studies demonstrated that this new BSP-scaffold induced mineralization, enhancing the mineral deposition and

osteogenic differentiation of human mesenchymal stem/stromal cells, when compared with silk scaffold alone (Gomes *et al.* 2013).

Some investigators have been focusing on the BSP-RGD peptide, instead of the entire protein. Therefore, Rezania and colleagues have covalently grafted BSP-RGD peptide from rat/mouse bone sialoprotein on quartz surfaces and showed that this peptide promoted ECM mineralization (Rezania & Healey 2000). Moreover, Drevelle and co-workers used PCL films functionalized with BSP-RGD peptide and demonstrated an enhancement of cell spreading of MC3T3-E1 mouse preosteoblasts and an improvement of their responsiveness to BMP-2 (Drevelle *et al.* 2010). More recently, this BSP-RGD peptide showed increased mineralization of human MSC cultured on hydrogels, enhancing the expression of osteogenic markers (Jha *et al.* 2014).

Similarly, Rapuano has used a fragment from human BSP corresponding to residues 278-293 (hBSP278-293) and showed that BSP-coated plastics have better adhesion capacity, since more MC3T3-E1 cells were found attached to these surfaces (Rapuano *et al.* 2004).

I.7.5.4.2.6. DMP-1

Recently, dentin has been explored as a new material to be used for tissue engineering of tooth structure, since dentin is a calcified tissue. Comparing with enamel, dentin is less mineralized and more elastic and it contains, approximately, 70% hydroxyapatite (Li *et al.* 2011). In the extracellular matrix, the bioactive proteins of human dentin are known to be necessary for dentinogenesis (Chun *et al.* 2011). Many researches have been trying to create scaffolds that mimic the structure of natural dentin to use in dentin regeneration applications (Lluch *et al.* 2009). Indeed, some reports have already demonstrated that treated dentin matrix could induce precursor cell to differentiate into dentin (Li *et al.* 2011), providing a natural and biocompatible scaffold.

Currently, efforts have been made to study the role of these dentin matrix, specifically for tissue regeneration (Yang *et al.* 2012, Guo *et al.* 2012). Since this is a new field in tissue engineering, there are yet few studies using a particular dentin protein or peptide into scaffolds for bone tissue engineering applications, however some reports have already shown that DMP-1 plays multi-functional roles, being very attractive to be used in tissue engineering applications (Ravindran & George 2015). To this end, DMP-1 has been incorporated in biomimetic collagen constructs to regenerate soft tissues such as the dental pulp tissue (Alsanea *et al.* 2011). Alsanea and colleagues demonstrated that dental pulp stem cells incorporated within a collagen scaffold in the presence of DMP-1 can differentiate into odontoblast-like cells, secreting a highly vascularized collagenous matrix.

Although DMP-1 is originally from dentin matrix, it can also be found in bone matrix and can be applied to bone tissue regeneration. Indeed, DMP-1 derived peptides have been shown to induce transformation of amorphous calcium phosphate to crystalline hydroxyapatite, demonstrating that this signaling molecule incorporated with the biomimetic scaffold could enhance nucleation of crystalline hydroxyapatite, generating high quality engineered tissues capable of withstanding the mechanical loading that bones are normally subjected to (Xu *et al.* 2011).

Playing with the most important domains of DMP-1, many peptides have been synthesized to be incorporated into scaffolds designed for tissue engineering applications (Ravindran & George 2015). Besides the nucleating motifs from DMP-1, synthetic peptides that also contain the type I collagen binding domain were generated for repair of carious dentin. The main idea is to enhance the link between DMP-1 and collagen scaffolds and to take advantages of the DMP-1 nucleating domain to facilitate calcium binding and transformation to crystalline hydroxyapatite.

Recently, DMP-1 has been shown to stimulate MSC to differentiate into osteoblasts (Ravindran & George 2015). Thus, DMP-1 could be explored in bone tissue engineering applications to enhance osteogenesis, by incorporating the whole protein or the nucleating domain of DMP-1 to induce osteogenic differentiation. However, further studies are required to incorporate DMP-1 as a signaling molecule for bone tissue engineering applications.

I.7.5.4.3. Gla-containing proteins from bone matrix in bone tissue engineering

I.7.5.4.3.1. Osteocalcin

Osteocalcin is the most abundant non-collagenous protein in bone ECM (Poser *et al.* 1980, Price & Williamson 1985). OC expression is closely related to bone metabolism including bone mineralization and turnover (Ducy *et al.* 1996).

An OC-derived scaffold was described by Rammelt and colleagues (Rammelt *et al.* 2005). They investigated whether the addition of OC into the scaffold enhanced bone healing around hydroxyapatite/collagen composites in a rat tibia model and demonstrated that OC activates both osteoclasts and osteoblasts during early bone formation (Rammelt *et al.* 2005).

Another study used rhOC/$FN_{III9-10}$ fusion protein to functionalize a collagen matrix for bone tissue engineering (Kim *et al.* 2015). They demonstrated that rhOC/$FN_{III9-10}$–functionalized collagen matrices are more effective in the osteogenic differentiation of preosteoblasts than non-treated collagen matrices or even $rhFN_{III9-10}$–functionalized collagen matrices. These scaffolds enhanced cell adhesion, mostly by the fibronectin domain, but also could improve osteogenic differentiation of preosteoblasts, upregulating osteogenic gene markers.

Regarding the effect of osteocalcin on angiogenesis, Cantatore and colleagues showed for the first time in a well-established *in vivo* angiogenic assay that OC exogenously applied to chick embryo chorioallantoic membrane stimulates angiogenesis and that response was similar to that obtained with FGF-2 (Cantatore *et al.* 2005). Therefore, OC might be applied in bone tissue engineering to enhance mineralization and angiogenesis in a defect site, improving the efficiency of bone healing.

I.7.6. Mimicking the *in vivo* microenvironment of the ECM

I.7.6.1. ECM as a biomaterial source

ECM is a highly complex system of organized assembly of macromolecules and signaling factors (Fitzpatrick *et al.* 2015). ECM is responsible to provide tissue structure and mechanical properties of tissue but also acts in different cellular aspects essential in development and tissue repair, being an ideal substrate for cell adhesion, coordinating cell migration, survival, proliferation and differentiation. ECM is mainly composed by fibrillary proteins (e.g. collagens, fibronectin, laminin), glycosaminoglycans (e.g. heparin sulphate, chondroitin sulphate, hyaluronan), proteoglycans (e.g. decorin, versican, aggrecan) and matricellular proteins (e.g. osteopontin, thrombospondin) (Frantz *et al.* 2010). These ECM components may also be involved in the binding, sequestration and stabilization of signaling molecules incorporated within the matrix. Although being composed by the above mentioned components, the composition and distribution of the matrix components will vary with the type of tissue and can be altered during the different stages of tissue development and even due to some pathological conditions.

Therefore, tissue engineering and regenerative medicine focus on designing biomaterials that can recapitulate the different ECM functions and architecture, facilitating cell recruitment, adhesion, proliferation and differentiation (Wang *et al.* 2013). Indeed, some synthetic materials have been developed by using isolated ECM components, such as collagen, fibrin or hyaluronan or a combination of different ECM proteins (Mistry *et al.* 2005). These proteins have been coated into the biomaterials or even incorporated into them through different coupling methods. Although some progresses have been made, these materials fail to achieve the molecular complexity and organization of native tissue, leading researchers to apply the native ECM as a biomaterial source.

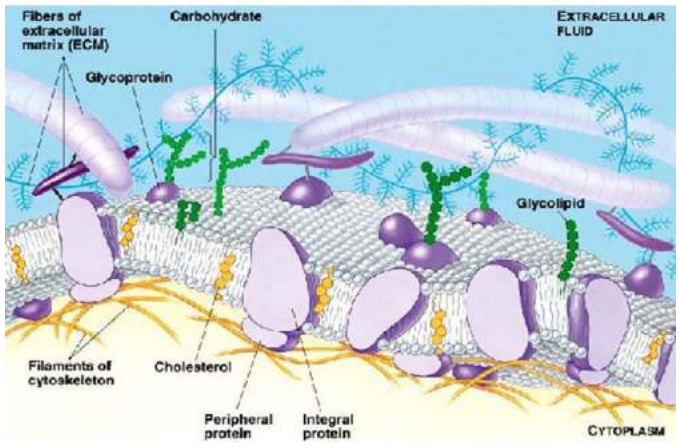

Figure I.30. Composition of extracellular matrix (Punjabia et al. 2014).

I.7.6.2. Decellularized native tissue-derived ECM

Native ECM can be obtained from allogeneic tissues (living donor/cadaver) or xenogenic tissues (animals) after cleaning and decellularization, in order to remove any cellular material. In pre-clinical research and clinical therapies, some tissues have already been decellularized, such as skin, urinary bladder matrix, blood vessels and heart valves. Due to the fact that this graft is obtained from decellularization of whole mature organ, its structure and tissue architecture is preserved (Ott *et al.* 2008, Petersen *et al.* 2010). Moreover, the decellularized tissue is suitable to be used as a graft since it matches the biophysical requirements (Papadimitropoulos *et al.* 2015). Some studies have already shown, in fact, that decellularized native ECM can promote bone repair (Papadimitropoulos *et al.* 2015, Zimmermann *et al.* 2011). However, there are some limitations of using native ECM as a graft. Indeed, to reduce the risk of disease transmission, harsh decellularization treatments are required (Greenwald *et al.* 2001, Laurencin *et al.* 2012, De Long *et al.* 2007), leading to the loss of bioactive components present in the ECM (Zimmermann *et al.* 2011). Another limitation is the uncontrolled tissue variability that occurs due to the age, health, gender of the tissue donor (Fitzpatrick *et al.* 2015).

Regarding bone tissue, bone ECM can be processed by treatment with acid (Urist *et al.* 1967) to generate demineralized bone matrix (DBM). DBM has a gel-like consistency that can be processed as powder or granules and, therefore, can be used as bone filling material, since it does not offer a structural support. Nevertheless, this material contains collagenous proteins and growth factors, such as BMP, FGF, TGF. As mentioned before as a limitation of decellularized native ECM, DBM has also uncontrolled variability, depending not only on the donor (Schwartz *et al.*1998), but also on the sterilization method used (Munting *et al.* 1988). Therefore, it is quite impossible to predict and guarantee the osteoinductive properties of this material.

I.7.6.3. Decellularized cell-derived ECM

ECM derived from cultured cells appears as an alternative to native tissue-derived ECM. Cell-derived ECM is composed by a complex and organized mixture of macromolecules that can mimic the native tissue microenvironment and can be obtained by decellularization of *in vitro* cell cultures. Cell-derived ECM acts as a reservoir of multiple growth factors, such as factors involved in inflammation (*i.e.* MCP-1, M-CSF, IL-8), angiogenesis (*i.e.* VEGF) and remodeling (*i.e.* MMP-13, OPG) (Bourgine *et al.* 2014). Cell-derived ECM has greater ability for customization, in contrast to tissue-derived ECM, since it is possible to select the desired cells to produce the ECM, the culture system (2D *vs* 3D; static *vs* perfusion), the application of some stimuli to modulate ECM production and also the possibility to modify, genetically, the cell sources to enhance the expression or sub-express some specific molecules (Fitzpatrick *et al.* 2015). Cell-derived ECM has been used also as coating, by depositing these molecules on the surface of the biomaterials to enhance their bioactivity and osteoinductive properties. However, cell-derived ECM has also some limitations with respect to tissue-derived matrices, since cell-derived ECM has poorer mechanical properties, not being able to be used in some specific applications.

In order to understand better how cell-derived ECM acts, further research is required to identify the interactions between the ECM signals and the host cells and to understand the different mechanisms of action. Besides that, it is important to identify and quantify, precisely, the composition of the ECM produced by different cell types to understand how the cell-derived ECM will influence cell behavior and to evaluate in which applications the cell-derived ECM generated by different cell types should be used.

In vitro, cell-derived ECM from different cell types has been shown to sustain cell expansion and to enhance MSC osteogenic differentiation (Lai *et al.* 2010, Lin *et al*. 2012, Pham *et al.*2008, Datta *et al.* 2005, Datta *et al.* 2006). *In vivo*, cell-derived ECM presented good vascularization (Pham *et al.* 2008) and was able to promote remodeling onto an immature osteoid tissue (Sadr *et al.* 2012).

I.7.6.4. Cell-derived matrices fabrication

The production of cell-derived ECM depends on three important aspects: cell source, cell culture method and decellularization method.

I.7.6.4.1. Cell source

The cell source is essential to determine the resulting composition of the ECM. Therefore, cells derived from different tissues typically yield matrices that mimic the composition of their natural tissue matrix.

Fibroblasts, a cell type found in connective tissues, have the ability to produce an ECM rich in collagens. MSC have also been used to produce cell-derived ECM due to their common use in tissue engineering applications and their ability to deposit ECM that can mimic different tissues by varying the culture condition methods, such as bone, cartilage and adipose tissue (Fitzpatrick *et al.* 2015). The properties of human umbilical vein endothelial cells (HUVEC) ECM have also been investigated. Enhanced osteogenic differentiation of human bone marrow MSC was observed in a β-TCP scaffold incorporated with HUVEC ECM (Kang *et al.* 2012). Another study from Gong and colleagues demonstrated that HUVEC ECM enhanced adhesion, proliferation and endothelial differentiation of stem cells from exfoliated deciduous teeth (Gong *et al.* 2017*)*.

It is extremely important to identify the ECM components produced by different cell types, so that we can target specific clinical conditions. Lu and colleagues, indeed, compared the composition of matrices derived from fibroblasts, chondrocytes and MSC (Lu *et al.* 2011). Although this study did not quantify the relative amounts of ECM components, it demonstrated the effect of different cell sources on matrix composition. This study showed that all matrices stained positive for type I collagen, type II collagen, fibronectin, vitronectin, laminin and decorin. However, versican was only detected in ECM derived from chondrocytes and aggrecan was not detected in ECM derived from fibroblasts (Lu *et al.* 2011).

To generate cell-derived ECM, primary cells and cell lines can be used. Primary cells can be directly harvested from tissues and do not need to be manipulated and passaged, recapitulating in a more reliable way the native *in vivo* phenotype and microenvironment. However, native ECM is produced by multiple cell types present in its specific niche, whereas primary cells are isolated into a monoculture. Another limitation of

primary cells is the availability of these cells, since it is usually required a high amount of cells for a specific application, being necessary to expand *in vitro* these cells. Indeed, passaging of cells, as well as their *in vitro* manipulation, may alter cell behavior and native phenotype.

On the other hand, immortalized cell lines can be used to generate cell-derived ECM, since they can yield high number of homogenous cells. The main disadvantage of immortalized cell lines is the fact that they are often derived from tumors and can differ from primary cell phenotypes. Moreover, it is important to consider that these cell-derived ECM may not be suitable to use if mimicking a specific tissue microenvironment is important. However, immortalized cell lines have been shown to be an appropriate solution if a specific desired molecular components are needed, such as components that promote angiogenesis (Fitzpatrick *et al.* 2015).

Recently, genetic engineering of cell lines has also been exploited since it will enhance or decrease the expression of desired key molecular elements in the ECM.

Therefore, it is important to think carefully which cell type should be used for a specific application, understanding, first, what is the desired outcome and in which context will the cell-derived ECM be applied, for example as a cell substrate or as a biomaterial coating. New technologies are also emerging and can be used to enhance and tailor the cell-derived ECM to mimic the natural microenvironment, enhancing some properties that could be affected due to some pathological condition. However, it is important to highlight that a proper identification and quantification of these ECM components should be guaranteed, to understand their biological effects.

I.7.6.4.2. Cell culture methods

Cell culture methods will also influence the production of cell-derived ECM. The most common methods to produce cell-derived ECM are to culture cells as adherent monolayers (2-D), as coatings on scaffold surfaces or as multicellular aggregates (3-D) and then, decellularize it. However, some cell culture parameters can also affect and alter the ECM composition, such as hypoxic conditioning (Pei *et al.* 2012). Mechanical preconditioning can also be applied to improve the mechanical properties of the generated ECM (Quint *et al.* 2011, Syedain *et al.* 2011). Therefore, as noted, by altering the cell culture methods, cell-derived ECM composition can mimic better the native microenvironment.

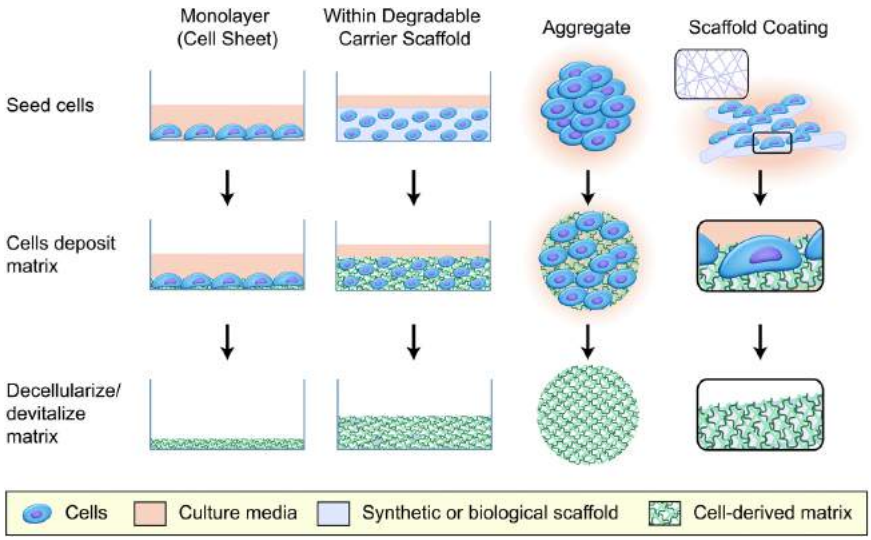

Figure I.31. Common culture methods used to produce decellularized cell-derived ECM. Cells can be cultured in monolayers and deposit a layer of matrix. To obtain thicker cell-derived ECM, cells can be embedded in a degradable carrier material. Therefore, over time, the degradable material will be replaced by the ECM deposited by the cells (3-D ECM construct after decellularization). Cells can be cultured as aggregates also producing a 3-D ECM. Cells can be cultured on the surface of scaffolds, allowing the matrix to be deposited and decellularization process will remove the cellular components, improving the bioactivity of the scaffold (Fitzpatrick *et al.* 2015).

I.7.6.4.3. Decellularization techniques

After culturing the cells in the desired way, the ECM will be produced and deposited. Further, the cellular components need to be removed from the ECM in order to obtain a cell-derived ECM without allogenic or xenogenic cellular antigens and immunogenic components, such as DNA, minimizing the risk of adverse immunological responses (Badylak *et al*. 2009).

Different techniques have been used to disrupt and remove the cellular components from the ECM based on chemical, physical and/or enzymatic processing methods. Indeed, there is no standard method of decellularizing cell-derived ECM and the selection of the decellularization method should be considered by balancing between the preservation of the molecular composition and the structural integrity of the matrix, since some methods are known to affect some of these two major aspects.

Chemical decellularization uses alkaline or acidic reagents, such as ammonium hydroxide, peracetic acid, and/or detergents (Triton X-100, SDS, CHAPS) to solubilize and disrupt the cellular components. As mentioned before, this method is very efficient in removing cellular components, however it can lead to the loss of some ECM components, such as glycosaminoglycans, and can also affect the ECM structure.

On the other hand, physical methods, such as lyophilization and freeze-thaw cycling have shown to fail, sometimes, to remove all cellular components of the ECM. Although it may enable retention of more ECM components, it can also affect the ECM structure. DNase treatment can also be combined with these treatments to degrade the remaining DNA (Gilbert *et al.* 2006), however it can induce sterile inflammatory responses in humans (Zheng *et al.* 2005).

Regarding bone tissue engineering, several groups have applied different decellularization methods to obtain cell-derived ECM incorporated into different scaffolds. Tour and colleagues seeded rat calvarial osteoblasts with hydroxyapatite particles and compared different decellularization techniques, such as three freeze-thaw cycles and the treatment with 0.5% Triton X-100 buffer containing 20mM NH_4OH in PBS for 3 min at 37ºC. Their results showed that Triton X-100 treatment preserved the ECM architecture by maintaining the fibrillar network in contrast with the freeze-thaw treatment which disrupted the fibrillar structure, leading to a disorganized matrix (Tour *et al.* 2011, Cheng *et al.* 2014). However, other groups have already reported successful decellularization by using three cycles of freeze-thaw treatment only (Datta *et al.* 2005, Thibault *et al.* 2010, Cheng *et al.* 2015). It is important to note that, since there is no standard method of decellularization to produce cell-derived ECM, optimization studies should be done to obtain cell-derived ECM with good quality, retaining the bioactive components needed for a specific application.

Different decellularization techniques of cell-derived ECM are summarized in Table I.6.

Table I.6. Methods for decellularization of cell-derived ECM for bone tissue engineering (Adapted from Cheng *et al.* 2015).

Tissue type	Decellularization method	Sterilization	Cell repopulation	References
Rat femoral and tibial bone marrow-derived MSC cultured on titanium fiber mesh scaffolds	Three freeze/thaw cycles	Unspecified	Rat bone marrow-derived MSC	Datta *et al.* 2005 Pham *et al.* 2008
Rat osteoblasts and dermal fibroblasts cultured on synthetic hydroxyapatite microparticles	0.5% Triton X-100 for 3 min at 37 ºC	Unspecified	None	Tour *et al.* 2011
Rat bone marrow-derived MSC cultured on PCL scaffold	Three freeze/thaw cycles Ultrasonication for 10 min	Ethylene oxide	Rat bone marrow-derived MSC	Thibault *et al.* 2010
Mouse bone marrow-derived MSC	0.5% Triton X-100 for 5 min at 37 ºC	Unspecified	Mouse bone marrow-derived MSC	Sun *et al.* 2011b

I.7.6.5. Cell-derived ECM in bone tissue engineering

Several bone substitutes have tried to mimic the ECM specific features to induce and accelerate bone healing (Fitzpatrick *et al.* 2015). Different features should be considered in bone tissue engineering, such as structure, mechanical properties and osteoinductive properties, such as the presence of growth factors, minerals and cytokines.

Both macro-structure (e.g. pore shape, geometry and size distribution) and micro-structural features (e.g. presence of micropores, surface roughness and nanotopography) influence the osteoinductivity of bone substitutes (Decaris *et al.* 2012). The mechanical properties of engineered substrates also play a key role, as the osteogenic phenotype of MSC is induced by stiff substrates with an elasticity ranging from 25 to 40 kPa, corresponding to stiffness in physiological osteoid (Lv *et al.* 2015). On the other hand, biochemical factors

provide signals to control the behavior of osteogenic cells. Therefore, bone ECM acts as reservoir of different and complex cytokines and growth factors that are important for osteogenesis (such as BMP) and angiogenesis (such as VEGF).

Although some progresses in material sciences have been made, most of the developed synthetic substitutes are merely osteoconductive, lacking some osteoinductive properties (Datta *et al.* 2005). Some growth factors and ECM proteins or peptides have been added into these scaffolds to improve their bioactivity (Lau *et al.* 2012), however it is still difficult to recreate the complex structure of native ECM. Therefore, optimization of the combination of proteins required for a specific application, as well as their doses, need further studies.

Cell-derived ECM appears as a nature-inspired approach to be used in orthopedic tissue engineering and as a regenerative strategy to improve the current clinical practices for repairing large bone defects by generating materials with osteoinductive properties. Currently, off-the-shelf materials are commercially attractive. Moreover, cell-free extracellular matrices seem to be easier to implement in a clinical context. Therefore, cell-derived ECM can be applied as a scaffold coating to enhance the biological and osteoinductive capacity of materials. This ECM can also be integrated into synthetic scaffolds and used as cell culture substrates for expanding and differentiating stem cells and osteoblasts to be further used for bone cell therapies.

Another advantage of using cell-derived ECM for bone tissue engineering applications is the potential for the formation of autologous grafts, since it is possible to use autologous cells, patient-specific cells, to create, *in vitro,* the cell-derived ECM.

Different studies have already reported that cell-derived osteogenic ECM can be created *in vitro* using mesenchymal stem/stromal cells (Datta *et al.* 2005, 2006, Decaris *et al.* 2012, Sun *et al.* 2011b, Thibault *et al*. 2010, Zeitouni *et al* .2012), fibroblasts (Tour *et al.* 2011), chondrocytes (Lau *et al.* 2012) or osteoblasts (Tour *et al.* 2011) in the presence of osteogenic media. In the absence of osteogenic growth factors, cell-derived ECM has also been shown to enhance expansion of mesenchymal colony forming units and preserve their stem cell properties (Chen *et al.* 2007).

ECM derived from MSC have been shown to be able to repair mouse calvarial defects. In fact, Zeitouni and co-workers demonstrated the efficiency of decellularized human MSC-derived ECM reseeded with human MSC pretreated with GW9662, a small molecule that directs stem cells towards osteogenesis (Zeitouni *et al.* 2012). In fact, after 3 weeks, decellularized cell-seeded ECM resulted in 80-100% bone healing compared to 30% to 60% healing with decellularized ECM only and MSC only treatment groups, respectively.

Therefore, translational application of cell-derived ECM may involve coating commonly used orthophedic biomaterials for bone repair with cultured cell-derived ECM produced *in vitro* or the use of cell-derived ECM incorporated into scaffolds to enhance osteoinduction and osseointegration.

I.7.6.5.1. 3-D scaffolds using cell-derived ECM for bone tissue engineering

3-D scaffolds have been designed to incorporate cultured cell-derived ECM produced *in vitro*, since it can enhance biological activity of the scaffolds and it may retain biological factors that contribute to the osteogenic

differentiation of cells. Scaffolds using different materials, such as organic and inorganic, have been developed. Thibault and colleagues created rat MSC-derived ECM by seeding rat bone marrow-derived MSC onto electrospun poly (e-caprolactone) (PCL) fiber mesh scaffolds (Thibault *et al.* 2010). Calcium deposition, an important indicator of late stage differentiation of osteoblasts (Bancroft *et al.* 2002), was higher in ECM/PCL scaffolds than PCL scaffolds alone, suggesting that the enhancement of osteogenic differentiation may be due to the retention of osteogenic factors in the cell-derived ECM. Some studies have also report that cell-derived ECM presents a sufficient level of biological activity to induce and sustain the osteogenic differentiation of cells in the absence of exogenous osteogenic supplementation, providing a novel method for the delivery of biological factors for bone tissue engineering (Datta *et al.* 2005, Pham *et al.* 2008).

Titanium has been commonly used to produce orthopedic implants. Therefore, Datta and colleagues developed a decellularized rat MSC-derived ECM incorporated with titanium fiber mesh and seeded rat bone marrow-derived MSC onto it. ALP activity, as well as calcium content were enhanced in cell-ECM/titanium constructs compared with constructs without ECM (Datta *et al.* 2005). Moreover, gene expression studies revealed that the presence of ECM in the titanium constructs upregulated some osteogenic markers such as ALP, osteocalcin, osteomodulin, osteopontin and Runx2 compared to cells seeded on titanium mesh alone (Pham *et al.* 2008).

Hydroxyapatite is an inorganic material also present in bone matrix. Some studies have already reported that hydroxyapatite can enhance cellular processes, such as osteogenic differentiation of MSC. Tour and colleagues have incorporated hydroxyapatite with ECM derived *in vitro* from either rat calvarial osteoblasts or dermal fibroblasts and implanted these scaffolds into rat calvarial defects (Tour *et al.* 2011). The presence of ECM into the hydroxyapatite scaffolds induced new bone formation compared to hydroxyapatite alone, even in the absence of stem cells or growth factors.

A different strategy has also been used in which, instead of culturing cells onto the material to produce decellularized cell-derived matrices, cell-derived ECM can be generated separately, *in vitro*, and then transferred onto the surfaces of the scaffolds without losing their osteogenic potential. Decaris and co-workers have demonstrated that decellularized MSC-derived ECM produced in monolayer on tissue culture plastic can retain their composition and accelerate osteogenesis (Decaris *et al.* 2012). After that, they were able to collect the decellularized cell-derived matrices by scraping the decellularized ECM off plates in the presence of acetic acid and then used it to coat 3-D PLGA scaffolds (Decaris *et al.* 2012b), demonstrating that ECM was able to retain its ability to enhance osteogenic differentiation of MSC.

I.7.6.5.2. Electrospun fibers using cell-derived ECM for bone tissue engineering

Electrospun fibrous scaffolds can be produced from synthetic polymers or natural polymers. Synthetic polymers, such as polylactic acid (PLA), polyglycolic acid (PGA), poly(ε-caprolactone) (PCL) and poly(lactic-co-glycolic) acid (PLGA), are generally biologically inert, lacking functional sites to interact with cells, and due to their low hydrophilicity they lack cell affinity, however their exact composition and chemistry are well characterized and they can provide physical support to the cells (Goyal *et al.* 2017, Guvendiren & Burdick 2013). On the other hand, natural polymers, such as collagen, gelatin, elastin, silk and fibrin, present bioactivity and provide good biocompatibility, however it is difficult to control their degradation properties and

they usually present lower mechanical strength. Therefore, some strategies have been developed to incorporate bioactive signals into synthetic polymers such as chemically tether biochemical cues to the polymer backbone, however it requires the presence of functionalizable pendant chains or end groups in the polymer (Yoo *et al.* 2009).

Cell-derived ECM has been incorporated into electrospun fibers to enhance their bioactivity. One approach is to allow cells to deposit their native ECM onto the scaffold and then decellularize it, generating an ECM-polymer composite scaffold that has bioactive signals (Datta *et al.* 2005, Levorson *et al.* 2014, Rutledge *et al.* 2014). Moreover, a less common approach using cell-derived ECM into electrospun fiber has been investigated. In this case, cell-derived ECM is synthesized *in vitro* and collected. After some treatment and lyophilization, this cell-derived ECM is incorporated into the polymer solution and electrospun together, forming electrospun fibers with ECM incorporated (Thakkar *et al.* 2013).

Electrospinning has been used to fabricate fibrous and porous scaffolds from a variety of materials (Li *et al.* 2002, Sill and von Recum 2008, Yoshimoto *et al.* 2003) with a high surface area for tissue engineering applications. It is known that cellular responses, such as migration, proliferation and differentiation, may differ by varying matrix properties, such as fiber and pore sizes (Hinderer *et al.* 2016, Badami *et al.* 2006). Electrospinning has rapidly gained relevance in the tissue-engineering field due to its advantages over conventional scaffold fabrication methods (Barnes *et al.* 2007) and its ability to generate fibers similar to the fibrous structures of native ECM, being a cost-effective process (Li *et al.* 2002, Bhardwaj & Kundu. 2010). If needed, the nanofibers can be functionalized by incorporating bioactive factors to enhance and control cell proliferation and differentiation (Bhattarai *et al.* 2004). Moreover, some interesting features such as large specific surface area, high porosity and spatial interconnectivity of elecrospun nanofibers make them well suited for nutrient transport, cell communication and efficient cellular responses (Jang *et al.* 2009).

The electrospinning set-up is composed by a syringe connected to a syringe pump, a collector and a high voltage power supply (Figure I.33) (Huang *et al.* 2003, Hinderer *et al.* 2016, Wang *et al.* 2013c). The polymer solution is pumped through the syringe and forms a droplet on the needle tip. By applying high voltage, a charge imbalance is created and the solution is pulled towards the collector through the static electric field. (Figure I.33). As the polymer solution leaves the needle, the solvent evaporates and a solid fibrous network is formed (Barnes *et al.* 2007, Sill and von Recum 2008). While conventional polymer processing techniques generally create fibers 10 μm or larger in diameter, the nanofibers generated from electrospinning can mimic the submicron diameter and geometry typical of native ECM, while maintaining active cell-binding domains. Electrospun scaffolds also possess adjustable porosities of up to more than 90 % (Cui *et al.* 2007). Therefore, electrospun scaffolds have been successfully applied in neural, skin, cardioavascular, heart and bone tissue engineering (Lee *et al.* 2009, Zhou *et al.* 2008, Hsiao *et al.* 2013, Jang *et al.* 2009) (Figure I.32).

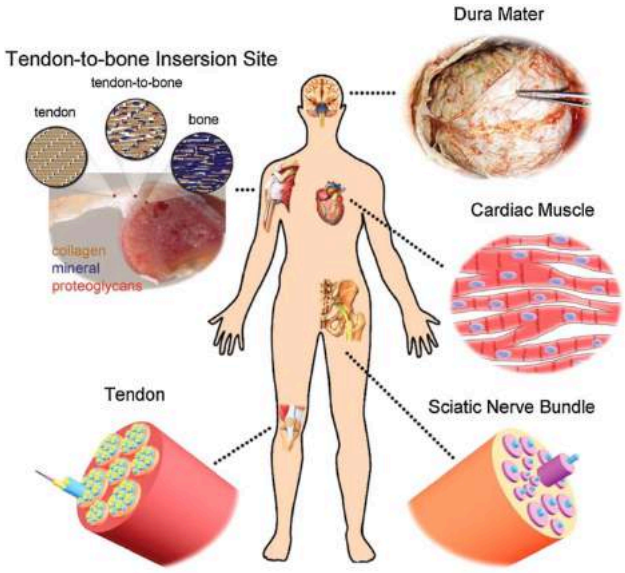

Figure I.32. Application of nanofiber-based scaffolds fabricated by electrospinning in the human body (Liu *et al.* 2012).

Bone tissue has an hierarchical organization over length scales ranging from macro- to nano-structured components. When designing biomimetic scaffolds for bone tissue engineering, some parameters should be considered, such as: (1) to mimic the nanofibrous collagen ECM, (2) be highly porous to allow cellular processes and efficient transport of nutrients, oxygen and waste products, and (3) to be able to withstand mechanical stresses during bone tissue formation (Holzwarth & Ma 2011, Stevens *et al.* 2008).

Regarding bone tissue engineering, electrospinning is an attractive approach to produce nanofibers similar to those of collagen fibers in bones, thus recapitulating in a precise way the native structure of bone tissue (Zhang *et al.* 2008). Notably, nanofibrous materials have also been reported to interact with stem cells and stimulate autocrine/paracrine growth factor signaling pathways (Narayanan *et al.* 2017).

In fact, different studies have already shown that electrospun matrices can enhance bone healing. Laurencin and colleagues showed that delivery of rat MSC along with biomimetic electrospun matrices enhanced ligament repair by showing increased mechanical strength and improved tissue organization (Peach *et al.* 2017). However, the surface properties of most electrospun nanofibers cannot meet the requirement for optimal bone regenerative performance, not being able to direct cellular differentiation towards an osteogenic lineage (Bhattacharyya *et al.* 2009). Therefore, applying a surface modification strategy based in cell-derived ECM onto electrospun nanofiber scaffolds is very attractive for bone tissue engineering applications.

Indeed, one of the first examples of electrospinning ECM proteins was performed by the Chaikof group where they spun a 1 wt% solution of type I collagen with polyethylene oxide to create a collagen mesh (Huang *et al.* 2001). Some decades after, native decellularized ECM has been electrospun (Gibson *et al.* 2014, Garrigues *et al.* 2014, Gao *et al.* 2017).

Although electrospinning is a simple and cost-effective method to generate 3-D fibers, it has some limitations. Due to the need of high electrical fields and harsh solvents, challenges remain to maintain protein functions.

Some studies have already created electrospun hybrid scaffolds that combine synthetic materials with natural proteins to overcome limitations observed with scaffolds alone. These studies showed that the introduction of a protein/polymer hybrid such as gelatin, elastin or collagen with PCL provides favorable mechanical properties and binding sites for cell attachment and proliferation. However, there is still a need to better recapitulate key features of the native ECM including their mechanical and biochemical properties.

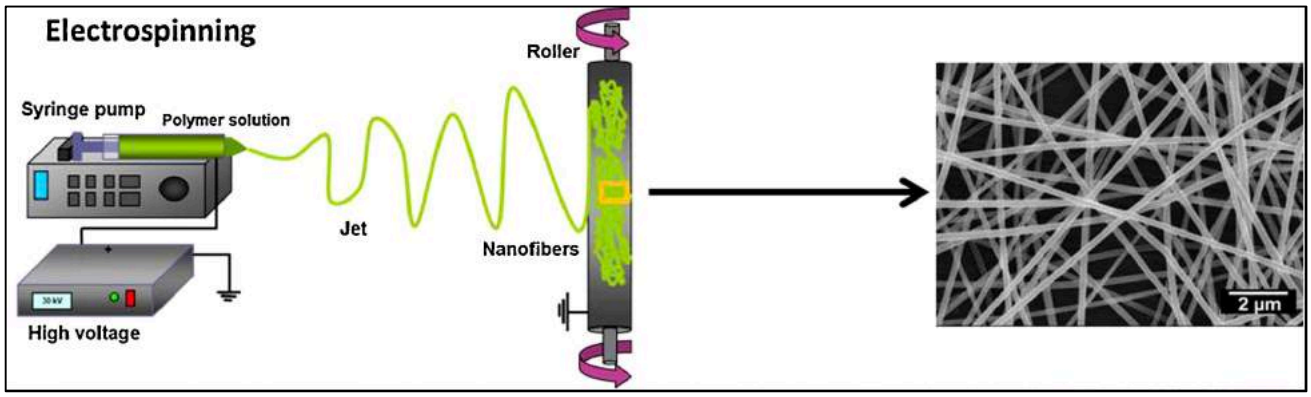

Figure I.33. Schematic of electrospinning technique (Wang *et al.* 2013c).

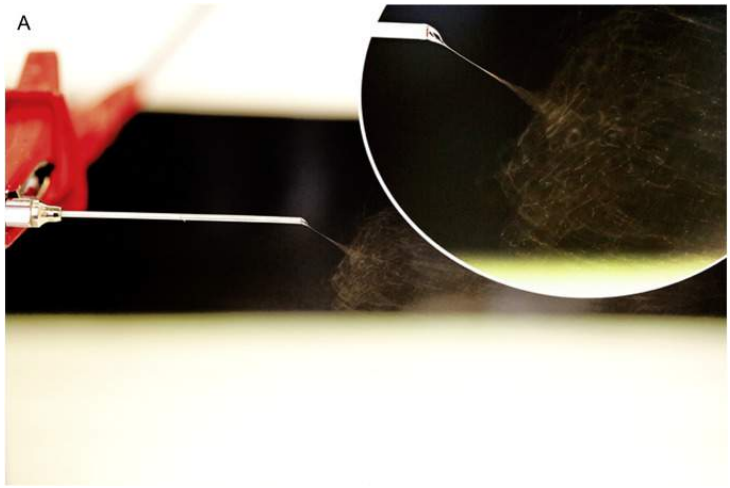

Figure I.34. The electrospinning process. Photograph showing the nozzle where the polymer solution is pumped through. A droplet forms on the nozzle tip, which adopts a conical shape due to the electrical field. Therefore, the fiber forms and is deposited into the collector (Hinderer *et al.* 2016).

Several researchers have created composite scaffolds consisting of decellularized ECM and synthetic polymers using electrospinning. These scaffolds have shown superior mechanical properties and maintenance of bioactivity in various tissue engineering applications (Table I.7). Young and colleagues have designed a copolymer electrospun scaffold consisting of PLA and decellularized pig lung extracellular matrix

(PLECM) as an *in vitro* airway smooth muscle model. They observed that this scaffold promotes growth and attachment of human bronchial smooth muscle cells (Young *et al.* 2017). A different study from Gao and co-workers combined decellularized meniscus extracellular matrix (DMECM) with PCL *via* electrospinning to fabricate random and aligned microfibers. They showed that these fibers had good hydrophilicity which contributed to cell attachment. Moreover, the mechanical properties of the DMECM/PCL fibers were more similar to the human meniscus and meniscus cells seeded on these scaffolds were able to proliferate and upregulate the expression of some genes such as collagen I, aggrecan and Sox 9 (Gao *et al.* 2017).

Baiguera and colleagues developed electrospun gelatin fibers incorporating rat decellularized brain extracellular matrix and demonstrated that these scaffolds provide a suitable microenvironment for MSC adhesion, proliferation and survival. Moreover, they observed that the presence of the brain matrix may induce cell differentiation towards neural precursor cells (Baiguera *et al.* 2014).

Decellularized tissue-derived ECM has also been studied for wound healing applications. Kim and colleagues obtained heart decellularized ECM and produced nanofibrous electrospun scaffolds. They demonstrated that heart decellularized ECM provided pro-angiogenic factors that enhanced angiogenesis, providing a good wound healing response and reducing scarring (Kim *et al.* 2018).

For bone tissue engineering applications, Gibson and co-workers incorporated decellularized ECM nanoparticles from bone into a biosynthetic nanofiber composite scaffold. Porcine bone ECM was isolated from decalcified femoral diaphysis and the resulting nanoparticles were mixed with PCL and electrospun to create nanofibers (Gibson *et al.* 2014). These scaffolds were able to upregulate the gene expression of osteogenic markers such as Runx2, osteocalcin and collagen I in human adipose derived stem cells compared to PCL scaffolds.

Cultured cell-derived ECM has also been used in combination with electrospinning techniques for bone tissue engineering. *In vitro* cultured cell-derived ECM has demonstrated to be capable of tissue repair and remodeling. Moreover, cell-derived matrix can be patient-specific and will overcome the risk of disease transmission and immunological reaction commonly associated with xenogenic and allogenic decellularized ECM scaffolds. More studies to determine the structure and composition of these cell-derived ECM are required, as well as to investigate their efficacy in *in vivo* models.

Furthermore, Shtrichman and colleagues cultured mesenchymal progenitor cells on electrospun PCL and PLGA scaffolds and decellularized it to generate decellularized cell-derived ECM grafts. Then, these electrospun scaffolds with or without cell-derived ECM were implanted subcutaneously in mice to evaluate their biocompatibility. They observed that PCL and PLGA scaffolds, without ECM incorporated, showed high levels of immune response and reduced integration with the host tissue. On the other hand, PCL and PLGA scaffolds containing decellularized ECM demonstrated improved integration, reduced immune response and greater angiogenic capacity (Shtrichman *et al.* 2014).

In another study, pre-osteoblasts were cultured on electrospun PCL scaffolds followed by decellularization process. The PCL-ECM scaffold improved cell proliferation and osteogenic differentiation (Jeon *et al.* 2016). Fu and colleagues have also developed a strategy in which they produce PLA nanofibers with MC3T3-E1 cell-derived ECM for bone tissue engineering. They used the same approach reported in the previous studies, in which cells are seeded, allowed to growth and then decellularized. They demonstrated that ECM was successfully preserved on nanofiber surface while maintaining the nanostructure of electrospun fibers. ECM-

PLA nanofibers enhanced mouse bone marrow stromal cells adhesion, proliferation and promoted early osteogenic differentiation of these cells, suggesting that cell-derived ECM leads to an improvement on their performance for bone tissue engineering (Fu *et al.* 2018).

However, most of the studies reported here, so far, develop strategies to decorate electrospun nanofibers using cell-derived ECM to improve their performance, by seeding cells onto the nanofibers, allowing them to grow and followed by a decellularization technique to obtain the ECM-nanofiber.

Moreover, a more challenging approach has emerged, in which the cultured cell-derived ECM is processed and collected *in vitro* and then added to the polymer solution to be electrospun to generate nanofibers with cell-derived ECM already incorporated. Thakkar and colleagues prepared ECM by decellularizing human MSC cultured in two different media: basic medium and chondrogenic medium. The obtained ECM was then combined with PCL dissolved in 1, 1, 1, 3, 3, 3-hexafluoro-2-propanol (HFIP) and electrospun fibers were produced. After that, chondrocytes were cultured on the scaffolds containing the two different ECM produced *in vitro*. This study demonstrated that the ECM presence resulted in a significant difference in chondrocyte metabolic activity compared to PCL scaffolds alone, showing higher expression of some genes, such as collagen II and aggrecan, demonstrating promising results for cartilage tissue engineering (Thakkar *et al.* 2013).

Table I.7. Summary of decellularized ECM electrospun scaffolds for cartilage and bone tissue engineering applications (Adapted from Elmashhady et al. 2017).

Scaffold composition	Decellularization method	Morphological and mechanical properties	Cell and tissue interactions	References
Cartilage and Bone Tissue Engineering				
Poly hydroxyalkanoate (PHA) scaffolds functionalized with human cartilage particles (5 mg/ml)	2% SDS, nucleases and 0.02% EDTA	ECM particle size ~5.06 µm Fiber diameter ~879.53 µm	Increased chondrogenic marker expression in human adipose derived stem cells and human primary chondrocytes.	Masaeli *et al.* 2017
PCL electrospun with porcine bone, liver, lung, cartilage, fat and spleen ECM (10%)	Triton X-100, EDTA, nucleases, $MgCl_2$	ECM particle size ~ 71-334 nm Fiber diameter ~50-1100 nm	Scaffolds with bone, cartilage and fat ECM supported osteogenic differentiation of human adipose derived stem cells	Gibson *et al.* 2014
PCL electrospun with 20% decellularized meniscus ECM	Pepsin, acetic acid, differential centrifugation	Fiber diameter ~1.41 µm Yield stress ~1.75 MPa Tensile Modulus ~175 MPa Fiber diameter ~0.58 µm Modulus ~40kPa	Scaffolds with decellularized ECM increased cell viability, chondrogenic marker expression as well as collagen and GAG secretion	Gao *et al.* 2017
PCL electrospun with cartilage derived ECM (0.08 g/ml) in single or multi-layered constructs	Frozen, lyophilized, and physically pulverized	Fiber diameter ~0.58 µm Modulus ~40 kPa	Multilayered scaffolds with decellularized ECM promoted increased human adipose derived stem cells infiltration and chondrogenic marker expression	Garrigues *et al.* 2014
O_2 plasma treated PCL/ ECM fibrous mats derived from mouse MC3T3-E1 cells	Freeze/thaw cycles in liquid nitrogen and 37º C water bath	Fiber diameter ~ 1.5 µm Young's Modulus ~9.1 Mpa Surface Roughness ~644.8 nm	Scaffolds supported proliferation of MC3TC-E1 cells *in vitro*, and increased calcium deposition, suggesting osteogenic differentiation	Jeon *et al.*2016
PLA electrospun with cell-derived ECM from MC3T3-E1 cells	1% SDS	Fiber diameter ~600 nm	Scaffolds with decellularized ECM enhanced mouse bone marrow stromal cell adhesion, proliferation and osteogenic differentiation	Fu *et al.* 2018
PCL electrospun with human mesenchymal stem cell-derived ECM (0.0125% wt/v)	20 mM ammonium hydroxide (NH_4OH), nucleases	Fiber diameter ~180-1730 nm	Increased chondrogenic marker expression in chondrocytes	Thakkar *et al.* 2013

I.8. Animal models for bone tissue engineering

Prior to testing in human beings, *in vitro* and *in vivo* studies should be done to evaluate bone scaffolds efficacy and safety. Different bone defects have been applied to evaluate bone substitute biomaterials *in vivo.*

In bone defects, part of the bone is damaged or missing due to trauma or surgery. Most of the bone defects can heal spontaneously under physiological environmental conditions. Nevertheless, in large bone defects, such as critical bone defects, surgical procedures are needed to repair it, since these defects do not heal spontaneously and lead to non-union fractures, if not treated.

The main four types of defects are the calvarial defect, long bone or segmental defect, partial cortical defect and cancellous bone defect models (Bigham-Sadegh *et al.* 2015), being the segmental and calvarial bone defects the most widely used in the literature. Figure I.35 shows the prevalent bone defect models.

Different animal models have been used to evaluate the efficacy and safety of a bone graft, such as rat/mouse (Zwingenberger *et al.* 2013, Zanchetta *et al.* 2012 ,Skaliczki *et al.* 2012, Kumar & Ponnazhagam 2012), rabbit (Zhang *et al.* 2012, Hussain *et al.* 2012, Schneider *et al.* 2010), dog (Yano *et al.* 2012, Lee *et al.* 2009b), sheep (Zhu *et al.* 2011, Reichert *et al.* 2010), goat (Lippens *et al.* 2010, Koeter *et al.* 2009) and pig (Wehrhan *et al.* 2012, Carstens *et al.* 2005).

The chosen animal model should demonstrate both significant physiological and pathophysiological analogies in comparison to humans. It must be manageable to operate and the costs of acquisition and care should also be considered (Pearce *et al.* 2007). The following are the most frequently used animal models for creating bone defects to test biomaterials to be used in bone tissue engineering.

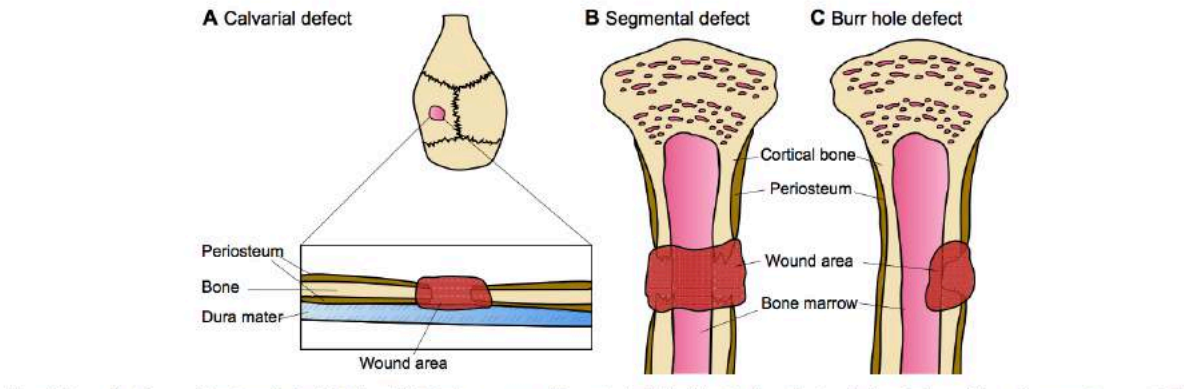

Figure I.35. Bone defect models. a) Calvarial defect, b) Segmental defect, c) Burr hole defect (McGovern *et al*. 2018).

I.8.1. Rabbits

Rabbits are the most used animals for musculoskeletal research (Neyt *et al.* 1998), the first choice to test *in vivo* new bone biomaterials. It was reported that there were similarities in bone mineral density and the fracture toughness of mid-diaphyseal bone between rabbits and humans (Wang *et al.* 1998). Besides, in

comparison with other species, rabbit has faster skeletal change and bone turnover (Castaneda *et al.* 2006). Rabbits are easily available, and easy to house and handle.

Some studies have already reported good results using bone grafts in this animal model (Table I.8). In fact, Walsh and colleagues (Walsh *et al.* 2008) investigated three commercially available and clinically used β-TCP bone graft substitutes with the same chemistry (Vitoss, Osferion, Chronos), but with various macro-and microscopic characteristics, using a bilateral tibial metaphyseal defect model on New Zealand white rabbits. Moreover, Gauthier and co-workers used a cylindrical 7-10 mm critical size bone defect rabbit model to investigate the efficiency of an injectable calcium phosphate bone substitute (Gauthier *et al.* 2005) Table I.8. summarizes some rabbit bone defect models for testing bone substitute biomaterials.

Table I.8. Examples of rabbit bone defect models for testing bone substitute grafts.

Defect site	Defect size	Bone grafts	Ref.
Tibiae	5 mm wide, 5 mm long 6 mm in diameter 5 mm in length	β -TCP bone graft substitutes Hydroxyapatite 60%/ β-TCP 40% β-TCP, collagen I, rhFGF-2	Walsh *et al.* 2008 Calvo-Guirado *et al.* 2012 Komaki *et al.* 2006
Femur	7x10 mm^2 cylinder 3 mm in diameter, 15 mm long 6 mm diameter x 5mm cylinder	Injectable calcium phosphate bone substitutes PLGA/TCP/icaritin Magnesium scaffolds	Gauthier *et al.* 2005 Wang *et al.* 2013d Liu *et al.* 2014
Calvaria	10 mm diameter x 1.2 mm 9 mm diameter	Apatite-coated zirconia Low-molecular-weight silk fibroin	Kim *et al.*2008 Lee *et al.*2010
Ulna	12 mm segment of midshaft ulnar 15 mm segment of midshaft ulnar	PLGA/TCP/icaritin/BMP-2 scaffolds BMP-2/PLGA-coated gelatin sponge	Chen *et al.* 2014 Kokubo *et al.* 2003

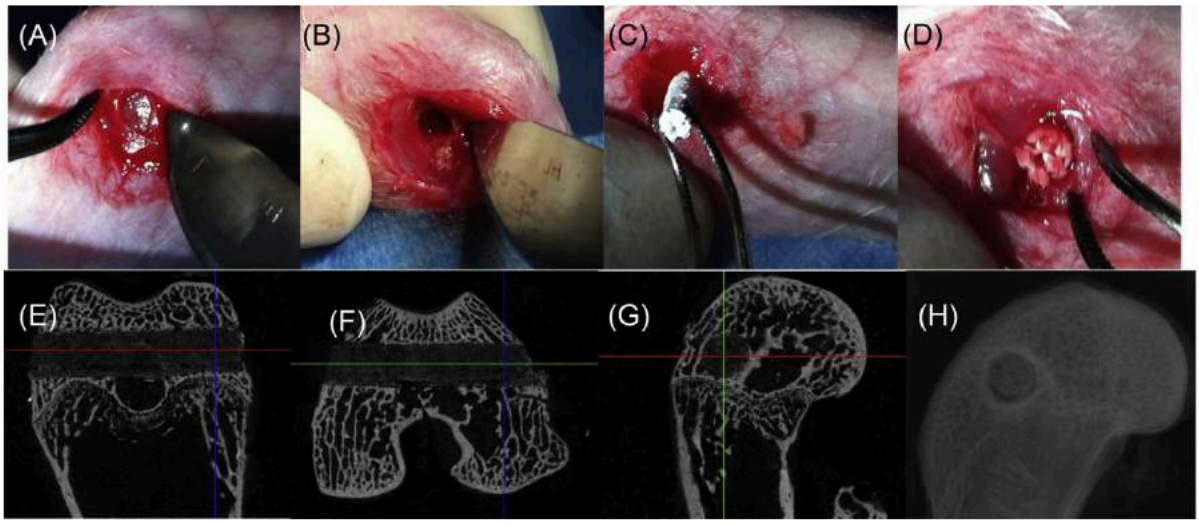

Figure I.36. Surgical protocol for the implantation of a PLGA/TCP/icaritin substitute biomaterial in a rabbit model. **a)** The surgical site is exposed. **b)** A tunnel is drilled through the distal femora. **c,d)**The biomaterial is implanted into the bone tunnel. **e-g)** Microcomputed tomography of the bone defect site. **h)** X-ray image of the bone defect site (Wang *et al.* 2013b).

I.8.2. Rodents

Rodents have also been used in preclinical studies for testing biomaterials, especially due to their small size. However, rodents have small-sized long bones and thin and fragile cortices (An *et al.* 1998). Besides, rodent models do not show Haversian-type remodeling in the cortex, while larger animals do.

Bone grafts, such as calcium phosphate and collagen, have been implanted in rodent models. Table I.9. summarizes some examples of rodent bone defect models for testing new bone grafts. Kondo and colleagues demonstrated the biocompatibily of purified β-TCP scaffolds using a rat femur defect model (Kondo *et al.* 2005). Moreover, Inzana and co-workers implanted a 3-D printed composite calcium phosphate and collagen scaffold into a critical murine femur defect to study the *in vivo* properties of the scaffold (Inzana *et al.* 2014).

Table I.9. Summary of some examples of rodent bone defect models for testing new substitute biomaterials.

Defect site	Defect size	Bone grafts	References
Distal femur	2 mm diameter and depth	β -TCP bone graft substitutes	Kondo *et al.* 2005
	2 mm diameter and 3 mm in length	Polymer containing TGF-β	Tielinen *et al.* 2001
Midfemur	2 mm in length	Composite calcium phosphate and collagen	Inzana *et al.* 2014
	5 mm in length	Marrow cells and porous ceramic	Ohgushi *et al.* 1989
	5 mm in length	BMP-silk composite matrices	Kirker-Head *et al.* 2007
Calvaria	4 mm diameter	iPSCs/silk scaffold	Ye *et al.* 2011
	8 mm diameter	PLGA and adipose-derived stem cells	Yoon *et al.*2007

I.9. Translating bone tissue engineering

The number of published papers on tissue engineering and biomaterials have been increasing exponentially (Figure I.37a). Although a lot of research and innovations have been made in bone tissue engineering field, the translation of these discoveries into clinical applications on a large scale has still not been done. Indeed, there is a huge gap between all the tissue engineering research and development and the resulting number of commercialized products. This gap between research and commercialization is called the "Valley of Death", since most of the companies end up "dying" between the scientific technology development of the product and its commercialization, usually due to the lack of funds (Hollister 2009) (Figure I.38). Most of the reasons for the lack of funds is the cost intensive high-technologies required for the development of the product and the large scale preclinical and clinical studies needed to be able to demonstrate efficacy and safety of the product and to be approved by regulatory bodies (Hollister 2009).

Moreover, all these difficulties need to be overcome so that the "jump" between research and commercialization can be done. Thus, aiming to translate orthopedic bone engineering products from bench to bedside, some points should be addressed, such as the development of good manufacturing processes (GMP), the design of a scalable process and, very important, to assess the clinical demands for specific scaffold characteristics (Dawson & Oreffo 2008, Hollister & Murphy 2011). Ideally, a scaffold should meet some requirements to have any chance to be clinically translated. Therefore, they should: i) meet FDA approval, ii) have a cost-effective manufacturing process, iii) be easily sterilized, iv) allow easy handling without requiring extensive procedures in the operation room, v) be radiographically distinguishable from newly bone formed, so it can be monitored, vi) enable minimally invasive implantation (Kneser *et al.* 2006, Logeart-Avramoglou *et al.* 2005).

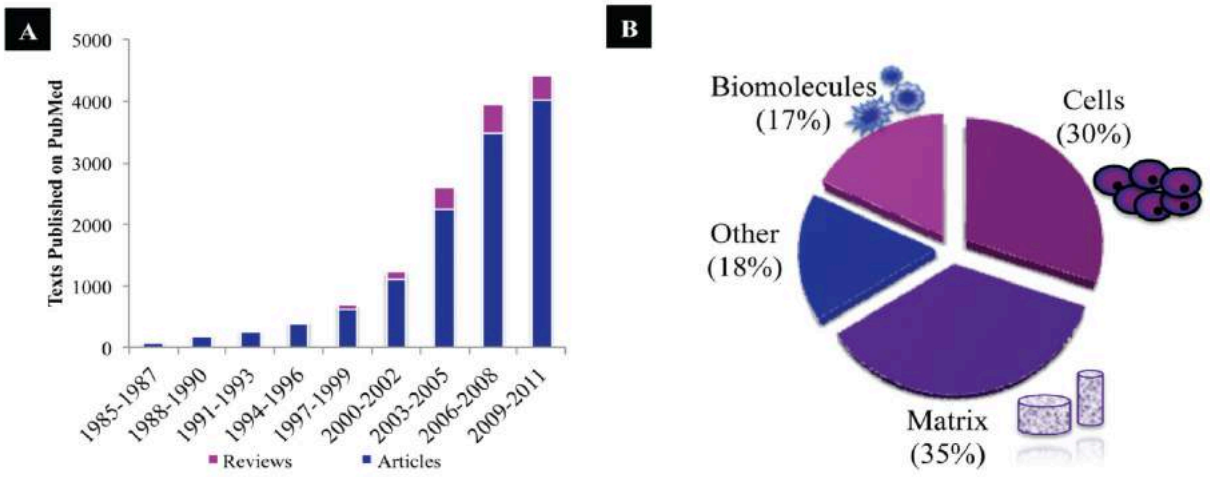

Figure I.37. Advances in bone tissue engineering field. **a)** Published articles on bone tissue engineering since mid-1980s in PubMed. **b)** Division of the articles published in 2011 according to bone engineering focus. Bone tissue engineering research has focused on different areas, such as biomolecules, cells, matrices and others, including vascularization approaches or bioreactors (Amini et al. 2012).

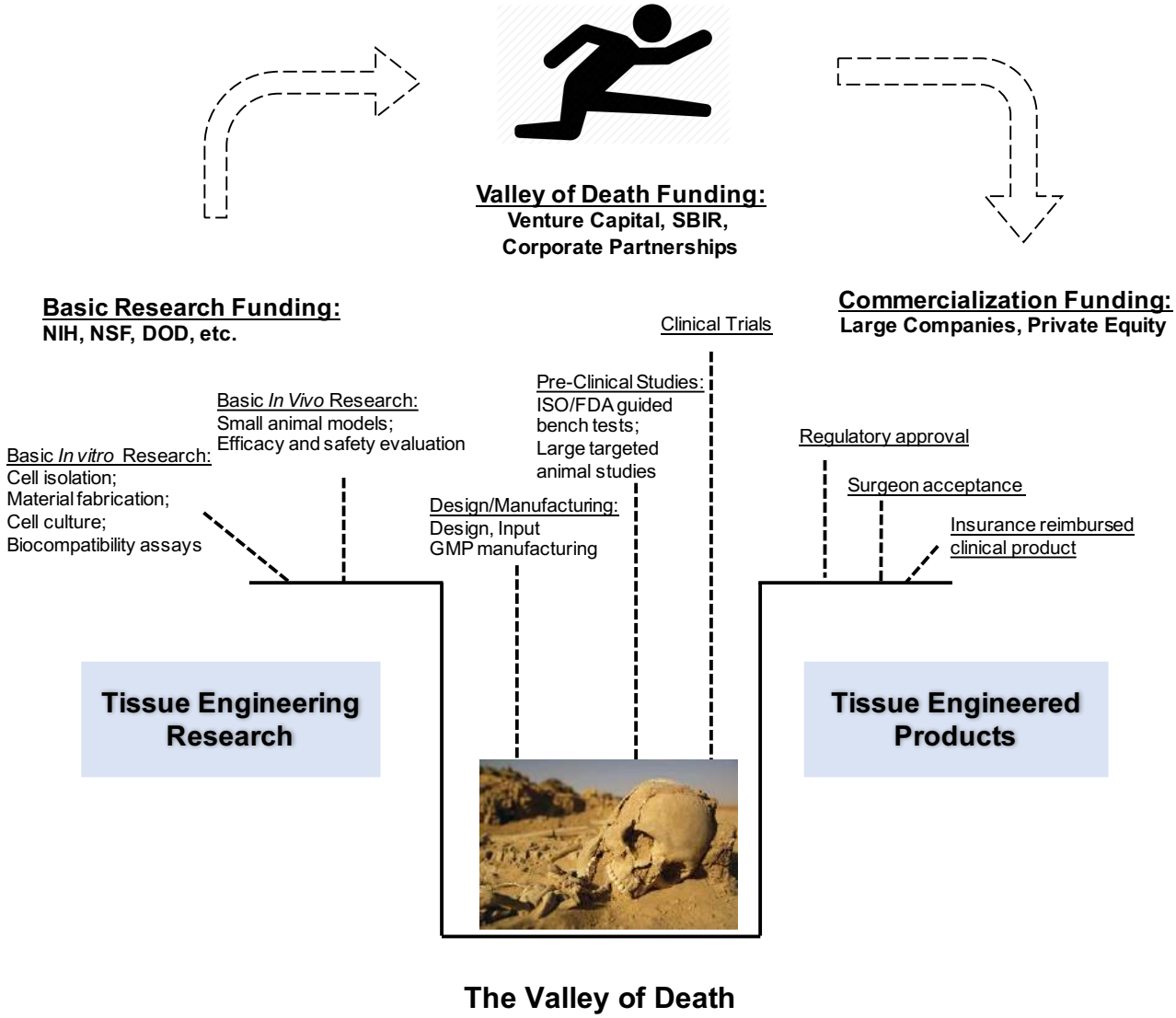

Figure I.38. The Valley of Death for tissue engineering applications. The Valley is created due to the lack of funds to develop scalable/GMP design and manufacturing process and to do large clinical studies to evaluate the safety and efficacy of the product, making it difficult to translate tissue engineering technologies into tissue-engineered products (Adapted from Hollister 2009).

I.10. References

Adams J.C., Lawler J. The thrombospondins. *Int. J. Biochem. Cell. Biol.,* **36**, 961-968 (2004).

Adams R.H., Alitalo K. Molecular regulation of angiogenesis and lymphangiogenesis. *Nat.Rev. Mol. Cell Biol.,* **8**, 464-478 (2007).

Ai-Aql Z.S., Alagl A.S., Graves D.T., Gerstenfeld L.C., Einhorn T.A. Molecular mechanisms controlling bone formation during fracture healing and distraction osteogenesis. *J. Dent. Res.,* **87**, 107-118 (2008).

Alford A.I., Kozloff K.M, Hankenson K.D. Extracellular matrix networks in bone remodeling. *Int.J.Biochem. Cell Biol.* **65**, 20-31 (2015).

Alsanea R., Ravindran S., Fayad M.I., Johnson B.R., Wenckus C.S., Hao J., George A. Biomimetic approach to perforation repair using dental pulp stem cells and dentin matrix protein. *J. Endod.,* **37**, 1092-1097 (2011).

Ameye L., Young M.F., Mice deficient in small leucine-rich proteoglycans: Novel *in vivo* models for osteoporosis, osteoarthritis, Ehlers-Danlos syndrome, muscular dystrophy, and corneal diseases. *Glycobiology,* **12,** 107R-116R (2002).

Amini A.R., Laurencin C.T., Nukavarapu S.P. Bone Tissue Engineering: recent advances and challenges. *Crit. Rev. Biomed. Eng.* **40**, 363-408 (2012).

An Y.H., Freidman R.J.. Animal models in orthopaedic research. *Boca Raton, FL: CRC Press* (1998).

Anatomy and physiology. Chapter 6. Bone tissue and the skeletal system. 6.4 Bone formation and development, Rice University, https://opentextbc.ca/anatomyandphysiology/chapter/6-4-bone-formation-and-development/.

Andersen T.L., Sondergaard T. E., Skorzynska K. E., Dagnaes-Hansen F., Plesner T.L., Hauge E.M., Plesner T., Delaisse J.M. A physical mechanism for coupling bone resorption and formation in adult human bone. *Am. J. Pathol.*,**174**, 239–247 (2009).

Aota S., Nagai T. Yamada K. M. Characterization of regions of fibronectin besides the arginine-glycine-aspartic acid sequence required for adhesive function of the cell-binding domain using site-directed mutagenesis. *J. Biol. Chem*., **266**, 15938-15943 (1991). 1991,266, 15938–15943.

Arana-Chavez V.E., Soares A.M.V., Katchburian E. Junctions between early developing osteoblasts of rat calvaria as revealed by freeze-fracture and ultrathin section electron microscopy. *Arch. Hist. Cyt.*, **58**, 285–292 (1995).

Argintar E., Edwards S., Delahay J. Bone morphogenetic proteins in orthopaedic trauma surgery. *Injury*, **42**, 730-734 (2010).

Arvidson K., Abdallah B.M., Applegate L.A., Baldini N., Cenni E., Gomez-Barrena E., Granchi D., Kassem M., Konttinen Y.T., Mustafa K., Pioletti D.P., Sillat T., Finne-Wistrand A. Bone regeneration and stem cells. *J. Cell. Mol. Med.* **15**, 718-746 (2011)

Asou Y., Rittling S. R., Yoshitake H., Tsuji K., Shinomiya K., Nifuji A., Denhardt D. T., Noda M. OPN facilitates angiogenesis, accumulation of osteoclasts and resorption in ectopic bone. Endocrinology, **142**, 1325–1332 (2001).

Aubin J.E., Gupta A.K., Zirngbl R., Rossant J., Knockout mice lacking bone sialoproteins expression have bone abnormalities. *J Bone Miner Res,* **11S,** S29 (1996).

Awonusi A., Morris M.D., Tecklenburg M.M. Carbonate assignment and calibration in the Raman spectrum of apatite. *Calcif. Tissue Int.,* **81**, 46-52 (2007).

Badami A.S., Kreke M.R., Thompson M.S., Riffle J.S., Goldstein A.S. Effect of fiber diameter on spreading, proliferation, and differentiation of osteoblastic cells on electrospun poly (lactic acid) substrates. *Biomaterials*, **27**, 596-606 (2006).

Badylak S.F., Freytes D.O., Gilbert T.W. Extracellular matrix as a biological scaffold material: structure and function. *Acta Biomater.,* **5**, 1-13 (2009).

Baht G.S., Hunter G.K., Goldberg H.A. Bone sialoprotein–collagen interaction promotes hydroxyapatite nucleation. *Matrix Biology,* **27**, 600–608. (2008).

Baiguera S., Del Gaudio C., Lucatelli E., Kuevda E., Boieri M., Mazzanti B., Bianco A., Macchiarini P. Electrospun gelatin scaffolds incorporating rat decellularized brain extracellular matrix for neural tissue engineering. *Biomaterials*, **35**, 1205-1214 (2014).

Bais M.V., Wigner N., Young M., Toholka R., Graves D.T., Morgan E.F, Gerstenfeld L.C., Einhorn T.A. BMP2 is essential for post natal osteogenesis but not for recruitment of osteogenic stem cells. *Bone*, **45**, 254-266 (2009).

Bancroft G.N., Sikavitsas V.I., van den Dolder J., Sheffield T.L., Ambronse C.G., Jansen J.A., Mikos A.G. Fluid flow increases mineralized matrix deposition in 3D perfusion culture of marrow stromal osteoblasts in a dose-dependent manner. *Proc. Natl. Acad. Sci. U.S.A.*, **99**, 12600 (2002).

Barleon B., Sozzani S., Zhou D., Wich H.A., Mantovani A., Marmé D. Migration of human monocytes in response to VEGF is. mediated via the VEGF receptor flt-1. *Blood*, **87**, 3336-3343 (1996).

Barnes C.P., Sell S.A., Boland E.D., Simpson D.G., Bowlin G.L. Nanofiber technology: Designing the next generation of tissue engineering scaffolds. *Adv. Drug Deliv. Rev.*, **59**, 1413-1433 (2007).

Baroli B. From natural bone grafts to tissue engineering therapeutics: brainstorming on pharmaceutical formulative requirements and challenges. *J Pham. Sci*., **98**, 1317-1375 (2009).

Barragan-Adjemian C., Nicolella D., Dusevich V., Dallas M.R., Eick J.D., Bonewald L-F. Mechanism by which MLO-A5 late osteoblasts/early osteocytes mineralize in culture: similarities with mineralization of lamellar bone. *Calcif. Tissue Int.* **79**, 340-353 (2006).

Barry S. T., Ludbrook S. B., Murrison E., Horgan C. M. Analysis of the alpha4beta1 integrin OPN interaction. *Exp. Cell. Res.* **258**, 342–351 (2000).

Barth A. Histologische Untersuchung über Knochen implantationen. *Beitr Pathol Anat Allg Pathol.* **17**, 65–142 (1895).

Bauer T. W., Muschler G. F. Bone graft materials. An overview of the basic science. *Clin. Orthop. Relat. Res*. **371**, 10-27 (2000).

Bella J., Eaton M., Brodsky B. Berman H.M. Crystal and molecular structure of a collagen-like peptide at 1.9A resolution. Science, **266**, 75-81 (1994).

Benno N., Brian M., Joachim M. Biomechanics and biology of movement. *Champaign, III: Human Kinetics* (2000).

Bhardwaj N., Kundu S.C. Elctrospinning: a fascinating fiber fabrication technique. *Biotechnol. Adv.,* **28**, 325-347 (2010).

Bhatia A., Albazzaz M., Espinoza Orias A.A., Inoue N., Miller L.M., Acerbo A., George A., Sumner D.R. Overexpression of DMP1 accelerates mineralization and alters cortical bone biomechanical properties in vivo. *J Mech. Behav. Biomed. Mater.,* **5**, 1-8 (2012).

Bhatnagar R.S., Qian J. J., Wedrychowska A., Sadeghi M., Wu Y. M., Smith N. Design of biomimetic habitats for tissue engineering with P-15, a synthetic peptide analogue of collagen. *Tissue Eng.,* **5**, 53–65 (1999).

Bhattacharyya S., Kumbar S.G., Khan Y.M., Nair L.S., Singh A., Krogman N.R., Brown P.W., Allcock H.R., Laurencin C.T. Biodegradable polyphosphazene-nanohydroxyapatite composite nanofibers: scaffolds for bone tissue engineering. *J. Biomed. Nanotechnol.*, **5**, 69-75 (2009).

Bhattarai S.R., Bhattarai N., Yi H.K., Hwang P.H., Cha D.I., Kim H.Y. Novel biodegradable electrospun membrane: scaffold for tissue engineering. *Biomaterials*, **25**, 2595-2602 (2004).

Bianco P., Fisher L.W., Young M.F., Termine J.D., Robey P.G., Expression of bone sialoprotein (BSP) in developing human tissues. *Calcif Tissue Int,* **49**, 421-426 (1991).

Bianco P., Riminucci M., Gronthos S., Robey P.G. Bone marrow stromal stem cells: nature, biology, and potential applications. *Stem Cells.* **19**, 180-192 (2001).

Bigham-Sadegh A, Oryan A. Selection of animal models for preclinical strategies in evaluating the fracture healing, bone graft substitutes and bone tissue regeneration and engineering. *Connect. Tissue Res*., **56**, 175-194 (2015).

Bilezikian J.P., Raisz L.G., Martin T.J. Principles of bone biology, 3rd Edition, Academic Press (2008).

Bodine P. V., Komm B. S. Evidence that conditionally immortalized human osteoblasts express an osteocalcin receptor. *Bone,* **25**, 535–543 (1999).

Bohic S., Pillet P., Heymann D. Effects of leukemia inhibitory factor and oncostatin M on bone mineral formed in in vitro rat bone-marrow stromal cell culture: physicochemical aspects. *Biochem. Biophys. Res. Commun.,* **253**, 506-513 (1998).

Boivin G., Bala Y., Doublier A., Farlay D., Ste-Marie L.G., Meunier P.J., Delmas P.D. The role of mineralization and organic matrix in the microhardness of bone tissue from controls and osteoporotic patients. *Bone*, **43**, 532-538 (2008).

Boivin G., Meunier P.J. The degree of mineralization of bone tissue measured by computerized quantitative contact microradiography. *Calcif. Tissue Int.*, **70**. 503–511 (2002).

Bonewald L.F., Harris S.E., Rosser J., Dallas M.R., Dallas S.L., Camacho N.P., Boyan B., Boskey A. von Kossa staining alone is not sufficient to confirm that mineralization in vitro represents bone formation. *Calcif. Tissue Int.,* **72**, 537-547 (2003).

Bornstein P., Kyriakides T.R., Yang Z., Armstrong L.C., Birk D.E., Thrombospondin 2 modulates collagen fibrillogenesis and angiogenesis. *J. Invest. Dermatol. Symp. Proc.,* **5,** 61-66 (2000).

Boskey A.L., Stiner D., Binderman I., Doty S.B. Type I collagen influences cartilage calcification: an immunoblocking study in differentiating chick limb-bud mesenchymal cell cultures. *J. Cell Biochem.,* **79**, 89-102 (2000).

Boskey A.L., Doty S.B., Stiner D., Binderman I. Viable cells are a requirement for in vitro cartilage calcification. *Calcif. Tissue Int.* **58**, 177-185 (1996).

Boskey A. Bone mineral crystal size. *Osteoporos. Int.* **14**, *Suppl 5,* S16-20 (2003).

Boskey A., Mendelsohn R., Infrared analysis of bone in health and disease. *J. Biomed. Opt.,* **10***,* 031102 (2005).

Boskey A.L. Hydroxyaopatite formation in a dynamic gel system: Effects of type I collagen, lipids, and proteoglycans. *J. Phys. Chem.,* **93,** 1628-1633 (1989b)

Boskey A.L. Noncollagenous matrix proteins and their role in mineralization. *Bone Miner.* **6**, 111-123 (1989).

Boskey A.L., Christensen B., Taleb H., Sorensen E.S. Post-translational modification of osteopontin: effects on in vitro hydroxyapatite formation and growth. *Bioch. and Biophy. Res. Comm.*, **419**, 333–338. (2012).

Boskey A.L., Maresca M., Doty S., Sabsay B., Veis A., Concentration-dependent effects of dentin phosphophoryn in the regulation of *in vitro* hydroxyapatite formation and growth. *Bone Miner., **11,*** 55-65 (1990).

Boskey A.L., Moore D.J., Amling M., Canalis E., Delany A.M. Infrared analysis of the mineral and matrix in bones of osteonecin-null mice and their wild-type controls. *J. Bone Miner. Res.,* **18,** 1005-1011 (2003b).

Boskey A.L., Spevak L., Doty S. B., Rosenberg L., Effects of bone CS-proteoglycans, DS-decorin, and DS-biglycan on hydroxyapatite formation in a gelatin gel. *Calcif. Tissue Int.*, **61,** 298-305 (1997).

Boskey A.L., Spevak L., Paschalis E., Doty S.B., McKee M.D. Osteopontin deficiency increases mineral content and mineral crystallinity in mouse bone. *Calcif. Tissue Int.* **71**, 145–154 (2002).

Boskey A.L., Spevak L., Tan M., Doty S.B. ,Butler W.T. Dentin sialoprotein (DSP) has limited effects on *in vitro* apatite formation and growth. *Calcif. Tissue Int.*, **67,** 472-478 (2000).

Boskey A.L., Coleman R. Aging and bone. *J. Dent. Res.*, **89**, 1333-1348 (2010).

Boskey A. L. OPN and related phosphorylated sialoproteins, effects on mineralization. *Ann. N. Y. Acad. Sci.*, **760**, 249–256 (1995).

Boskey A.L., Pleshko Camacho N. FT-IR imaging of native and tissue-engineered bone and cartilage. *Biomaterials*, **28**, 2465-2478 (2007).

Boskey A.L., Stiner D., Doty S.B., Binderman I., Leboy P. Studies of mineralization in tissue culture: optimal conditions for cartilage calcification. *Bone Miner.,* **16**, 11-36 (1992).

Boskey A.L., Camacho N.P., Mendelsohn R., Doty S.B., Binderman I. FT-IR microscopic mappings of early mineralization in chick limb bud mesenchymal cell cultures. *Calcif. Tissue Int,* **51**, 443-448 (1992b).

Bourgine P., Scotti C. , Pigeot S., Tschang L. , Todorov A. Jr., Martin I. Osteoinductivity of engineered cartilaginous templates devitalized by inducible apoptosis. *Proc. Natl. Acad. Sci. U.S.A.,* **111**, 17426-17431 (2014).

Boyan B.D., Hummert T.W., Dean D.D., Schwartz Z. Role of material surfaces in regulating bone and cartilage cell response. *Biomaterials*, **17**, 137-146 (1996).

Boyce B.F., Xing L. Functions of RANKL/RANK/OPG in bone modeling and remodeling. Arch. Biochem Biophys., **473**, 139-146 (2008).

Boyce B.F., D. E. Hughes, K. R. Wright, L. Xing, and A. Dai, “Recent advances in bone biology provide insight into the pathogenesis of bone diseases,” Laboratory Investigation, vol. 79, no. 2, pp. 83–94 (1999).

Brandi M.L., Collin-Osdoby P. Vascular biology and skeleton, *J. Bone Miner. Res.,* **21**,183-192 (2006).

Brodsky B., Ramshaw J.A. The collagen triple-helix structure. *Matrix Biol.*, **15**, 545-554 (1997)**.**

Bruder S.P., Caplan A. I. Cellular and molecular events during embryonic boné development. *Connect. Tissue Res.,* **20**, 65-71 (1989).

Bush L.F. The use of homogenous bone grafts; a preliminary report on the bone bank. *J. Bone Joint Surg. Am.* **29**, 620-628 (1947).

Calvo M. S., Eyre D. R., Caren M. G. Molecular basis and clinical application of biological markers of bone turnover. *Endocr. Rev.,* **17**, 333–368 (1996).

Calvo-Guirado J., Delgado-Ruız R., Ramírez-Fernández M., Maté-Sánchez J., Ortiz-Ruiz A., Marcus A.. Histomorphometric and mineral degradation study of Ossceram: a novel biphasic B-tricalcium phosphate, in critical size defects in rabbits. *Clin. Oral Implants Res.,* **23**, 667-675 (2012).

Cancedda R., Giannoni P., Mastrogiacomo M. A tissue engineering approach to bone repair in large animal models and in clinical practice. *Biomaterials*, **28**, 4240-4250 (2007).

Cantatore F.P., Crivellato E., Nico B., Ribatti D. Osteocalcin is angiogenic in vivo. *Cell Biol. Int.,* **29**, 583-585 (2005).

Caplan A., Mesenchymal stem cells. *J. Orthopaedic Res.* **9,** 641–650 (1991).

Capulli M., Paone R., Rucci N. Osteoblast and osteocyte: games without frontiers. *Arch. Biochem. Biphys.,* **561**, 3-12 (2014).

Carden A., Morris M.D. Application of vibrational spectroscopy to the study of mineralized tissues (review). *J. Biomed. Opt.,* **5**, 259-268 (2000).

Cardoso L, Herman B.C., Verbogt O., Laudier D., Majeska R.J., Schaffler M.B. Osteocyte apoptosis controls activation of intracortical resorption in response to bone fatigue. *J. Bone Miner. Res.,* **24**, 597-605 (2009).

Carlevaro M.F., Cermelli S., Cancedda R., Descalzi Cancedda F. Vascular endothelial growth factors (VEGF) in cartilage neovascularization and chondrocyte differentiation: auto-paracrine role during endochondral bone formation. *J. Cell. Sci.,* **113**, 59-69 (2000).

Carron J.A., Fraser W. C, Gallagher J.A., Thrombospondin promotes resorption by osteoclasts *in vitro*. *Biochem. Biophys. Res. Commun.,* **213**, 1017-1025 (1995).

Carstens M.H., Chin M., Li X.J. In situ osteogenesis: regeneration of 10-cm mandibular defect in porcine model using recombinant human bone morphogenetic protein-2 (rhBMP-2) and Helistat absorbable collagen sponge. *J. Craniofac. Surg.,* **16**, 1033-1042 (2005).

Carvalho R.S., Einhorn T.A., Lehmann W., Edgar C., Al-Yamani A., Apazidis A., Pacicca D., Clemens T.L., Gerstenfeld L.C. The role of angiogenesis in a murine tibial model of distraction osteogenesis. *Bone*, **34**, 849-861 (2004).

Castaneda S., Largo R., Calvo E., Rodriguez-Salvanes F., Marcos M.E., Diaz-Curiel M., et al. Bone mineral measurements of subchondral and trabecular bone in healthy and osteoporotic rabbits. *Skelet. Radiol.*, **35**, 34-41 (2006).

Chan W.D., Goldberg H.A., Hunter G.K., Dixon S.J., Rizkalla A.S. Modification of polymer networks with bone sialoprotein promotes cell attachment and spreading. *J. Biomed. Mater. Res. A.,* **94**, 945-952 (2010).

Chandrasekaran S., Ramachandran A., Eapen A., George A. Stimulation of periodontal ligament stem cells by dentin matrix protein 1 activates mitogen-activated protein kinase and osteoblast differentiation. *J. Periodontol.* **84**, 389-395 (2013).

Charles J.F., Aliprantis A.O., Osteoclasts: more than 'bone eaters', *Trends Mol. Med.*, **20,** 449-459 (2014).

Chen C. C., Boskey A.L., Mechanisms of proteoglycan inhibition of hydroxyapatite growth. *Calcif. Tissue Int.*, **37,** 395-400 (1985).

Chen C.C., Boskey A.L., Rosenberg L.C., The inhibitory effect of cartilage proteoglycans on hydroxyapatite growth. *Calcif. Tissue Int.,* **36,** 285-290 (1984).

Chen P.Y., Toroian D., Price P.A., McKittrick J. Minerals form a continuum phase in mature cancellous bone. *Calcif. Tissue Int.*, **88**, 351-361 (2011).

Chen S.H., Zheng L.Z., Xie X.H., Wang X.L., Lai Y.X., Chen S.K., Zhang M., Wang Y., Griffith J.F., Qin L. Comparative study of poly (lactic-co-glycolic acid)/-tricalcium phosphate scaffolds incorporated or coated with osteogenic growth factors for enhancement of bone regeneration. *J. Orthop. Transl.* **2**, 91-104 (2014).

Chen H., Clarkson B.H., Sun K., Mansfield J.F. Self-assembly of synthetic hydroxyapatite nanorods into an enamel prism-like structure. *J. Colloid Interface Sci.,* **288**, 97-103 (2005).

Cheng C.W., Solorio L.D., Alsberg E. Decellularized tissue and cell-derived extracellular matrices as scaffolds for orthopaedic tissue engineering. *Biotechnol. Adv.,* **32**, 462-484 (2014).

Chen X.D., Dusevich V., Feng J.Q., Manolagas S.C., Jilka R.L. Extracellular matrix made by bone marrow cells facilitates expansion of marrow-derived mesenchymal progenitor cells and prevents their differentiation into osteoblasts. *J. Bone Miner Res.* **22**, 1943 (2007).

Chesnick I.E., Avallone F.A., Leapman R.D., Landis W.J., Eidelman N. Potter K. Evaluation of bioreactor-cultivated bone by magnetic resonance microscopy and FTIR microspectroscopy. *Bone*, **40**, 904-912 (2006).

Chenu C, Colucci S., Grano M., Zigrino P., Barattolo R., Zambonin G., Baldini N., Vergnaud P., Delmas P.D., Zallone A.Z. Osteocalcin induces chemotaxis, secretion of matrix proteins, and calcium-mediated intracellular signaling in human osteoclast-like cells. *J. Biol. Chem.* **127**, 1149–1158 (1994).

Chiang H.K., Peng F.Y., Hung S.C., Feng Y.C. In situ Raman spectroscopic monitoring of hydroxyapatite as human mesenchymal stem cells differentiate into osteoblasts. *J. Raman Spect.*, **40**, 546-549 (2009).

Cho H.H., Kyoung K.M., Seo M.J., Kim Y.J., Bae Y.C., Jung J.S. Overexpression of CXCR4 increases migration and proliferation of human adipose tissue stromal cells. *Stem Cells Dev.*, **15**, 853-864 (2006).

Choi Y. J., Lee J. Y., Chung C.P. Park Y.J. Enhanced osteogenesis by collagen-binding peptide from bone sialoprotein in vitro and in vivo," *J. Biomed. Mater. Res.A,* **101**, 547-554 (2013).

Chun S.Y., Lee H.J., Choi Y.A., Kim K.M., Baek S.H., Park H.S., Kim J.Y., Ahn J.M., Cho J.Y., Cho D.W., Shin H.I., Park E.K., et al. Analysis of the soluble human tooth proteome and its ability to induce dentin/tooth regeneration. *Tissue Eng. Part A*, **17**, 181-191 (2011).

Claes L., Recknagel S., Ignatius A. Fracture healing under healthy and inflammatory conditions. *Nat. Rev. Rheumatol.,* **8**, 133-143 (2012).

Clarke B. Normal bone anatomy and physiology. *Clin. J. Am. Soc. Nephrol.*, **3**, S131-139 (2008).

Clemmensen I., Petersen L.C., Kluft C. Purification and characterization of a novel, oligomeric, plasminogen kringle 4 binding protein from human plasma: Tetranectin. *Eur. J. Biochem.,* **156,** 327-333 (1986).

Clezardin P., Malavel L., Ehrensperger A.-S., Delmas P., Dechavanne M., McGregor J.L. Complex formation of human thrombospondin with osteonectin. *Eur. J .Biochem.*, **175,** 275-284 (1988).

Collin P., Nefussi J.R., Wetterwald A., Nikolas V., Boy-Lefever M.L., Fleisch H., Forest N., Expression of collagen, osteocalcin and bone alkaline phosphatase in a mineralizing rat osteoblastic cell culture. *Calcif. Tissue Int.,* **50,** 175-183 (1992).

Contri M. B., Boraldi F., Taparelli F., De Paepe A., Ronchetti, I. P. Matrix proteins with high affinity for calcium ions are associated with mineralization within the elastic fibers of pseudoxanthoma elasticum dermis. *Am. J. Pathol.,* **148**, 569–577 (1996).

Corsi A., Xu T., Chen X.D., Boyde A., Liang J., Mankani M., Sommer B., Iozzo R.V., Eichstetter I., Robey P.G., Bianco P., Young M.F. Phenotypic effects of biglycan deficiency are linked to collagen fibril abnormalities, are synergized by decorin deficiency, and mimic Ehlers-Danlos-like changes in bone and other connective tissues. *J. Bone Miner. Res.,* **17,** 1180-1189 (2002).

Crisan M., Yap S., Casteilla L., Chen C.W., Corselli M., Park T.S., Andriolo G., Sun B., Zheng B., Zhang L., Norotte C., Teng P.N., Traas J., Schugar R., Deasy B.M., Badylak S., Buhring H.J. Giacobino J.P., Lazzari L., Huard J., Péault B. A perivascular origin for mesenchymal stem cells in multiple human organs. *Cell Stem Cell.* **3**, 301-313 (2008).

Crockett J. C., Mellis D. J., Scott D. I., Helfrich M. H., New knowledge on critical osteoclast formation and activation pathways from study of rare genetic diseases of osteoclasts: focus on the RANK/RANKL axis. *Osteoporos. Int.*, **22**, 1-20 (2011).

Cruess, R.L. Physiology of Bone Formation, Function, and Destruction. Chapter 9 in The Musculoskeletal System: Embryology, Biochemistry, and Physiology. Edited by Cruess, R.L. Churchill Livingstone, New York (1982).

Cserjesi P., Brown D., Ligon K.L., Lyons G.E. Copeland N.G., Gilbert D.J., Jenkins N.A., Olson E.N. Scleraxis :a basic helix-loop-helix protein that prefigures skeletal formation during mousse embryogenesis. *Development,* **121**, 1099-1110 (1995)**.**

Cui F. Z., Li, Y & Ge, J. Self-assembly of mineralized collagen composites. *Mat. Sci. Eng. R: Reports* **57**, 1-27 (2007).

Cushing M. C., Anseth K. S. Materials science. Hydrogel cell cultures. *Science*, **316**, 1133-1134 (2007).

Dallas S. L., Prideaux M., Bonewald L.F. The osteocyte: an endocrine cell ... and more. *Endocr. Rev.*, 34, 658-690 (2013).

Datta N., Holtorf H.L., Sikavitsas V.I., Jansen J.A., Mikos A.G. Effect of bone extracellular matrix synthesized in vitro on the osteoblastic differentiation of marrow stromal cells. *Biomaterials*, **26**, 971-977 (2005).

Datta N., Pham Q.P., Sharma U., Sikavitsas V.I., Jansen J.A., Mikos A.G. In vitro generated extracellular matrix and fluid shear stress synergistically enhance 3D osteoblastic differentiation. *Proc. Natl. Acad. Sci. U.S.A*, **103**, 2488-2493 (2006).

Dawson J.I., Oreffo R.O. Bridging the regeneration gap: stem cells, biomaterials and clinical translation in bone tissue engineering. *Arch. Biochem. Biophys.* **473**, 124-131 (2008).

De Bari C., Dell'Accio F., Tylzanowski P., Luyten F.P. Multipotent mesenchymal stem cells from adult human synovial membrane. *Arthritis. Rheum*., **44**, 1929-1942 (2001).

Decaris M.L., Mojadedi A., Bhat A., Leach J.K. Transferable cell-secreted extracellular matrices enhance osteogenic differentiation. *Acta Biomater.*, **8**, 744-752 (2012).

Decaris M.L., Binder B.Y., Soicher M.A., Bhat A., Leach J.K. Cell-derived matrix coatings for polymeric scaffolds. *Tissue Eng. Part A.,* **18**, 2148-2157 (2012b).

De Jong, W.F. Le substance minerale dans le os. *Recl. des. Trav. Chim. des Pays-Bas*, 445-450 (1926).

De Long W.G. Jr., Einhorn T.A., Koval K., McKee M., Smith W., Sanders R., Watson T.. Bone grafts and bone graft substitutes in orthopaedic trauma surgery. A critical analysis. *J Bone Joint Surg Am*. **89**, 649–658 (2007).

Delany A.M., Amling M., Priemel M., Howe C., Baron R., Canalis E., Osteopenia and decreased bone formation in osteonectin-deficient mice. *J Clin. Invest*, **105,** 915-923 (2000).

Delloye C., Cornu O., Druez V., Barbier O. Bone allografts: what they can offer and what they cannot. J. Bone Join Surg. Br., **89**, 574-579 (2007).

Delmas P. D., Tracy R. P., Riggs B. L., Mann, K. G. Identification of the noncollagenous proteins of bovine bone by two-dimensional gel electrophoresis. *Calcif. Tissue Int.* **36**, 308–316 (1984).

Denhardt D.T., Guo X. Osteopontin: a protein with diverse functions. *FASEB J*. **7,** 1475–1482 (1993).

Denhardt, D. T., Noda, M. OPN expression and function: Role in bone remodeling. *J. Cell. Biochem.* **30**, 92–102 (1998).

Denhardt, D. T., Noda, M., O'Regan, A. W., Pavlliln, D., and Berman, J. S.(2001). Opn as a means to cope with environmental insults: Regulation of inflammation, tissue remodeling, and cell survival. J. Clin. Invest. **107,** 1055-1061(2001).

Dickson K., Katzman S., Delgado E., Contreras D. Delayed unions and nonunion of open tibial fractures. Correlation with arteriography results. *Clin. Orthop. Relat. Res*., **302**, 189-193 (1994).

Dimitriou R., Jones E., McGonagle D., Giannoudis P.V. Bone regeneration: current concepts and future directions. *BMC Med.* **9**, 66 (2011).

Dimitriou R., Tsiridis E., Giannoudis P.V. Current concepts of molecular aspects of bone healing. *Injury.,* **36**, 1392-1404 (2005).

Dinopoulos H., Dimitriou R., Giannoudis P.V. Bone graft substitutes: What are the options? *Surgeon*. **10**, 230-239 (2012).

Dirckx N., Van Hul M., Maes C. Osteoblast recruitment to sites of bone formation in skeletal development, homeostasis and regeneration. *Birth Defects Res. C Embryo Today,* **99**, 170-191 (2013).

Donati D., Zolezzi C., Tomba P., Viganò A. Bone grafting: historical and conceptual review, starting with an old manuscript by Vittorio Putti. *Acta Orthop.,* **78,** 19–25 (2007).

Donnelly E., Meredith D.S., Nguyen J.T., Boskey A.L. Bone tissue composition varies across anatomic sites. *J. Orthop. Res.,* **30,** *700-706* (2012).

Drevelle O., Bergeron E., Senta H., Lauzon M.A., Roux S., Grenier G-, Faucheux N. Effect of functionalized polycaprolactone on the behaviour of murine preosteoblasts*. Biomaterials*, **31**, 6468-6476 (2010).

Ducy P., Desbois C., Boyce B., Pinero G., Story B., Dunstan C., Smith E., Bonadio J., Goldstein S., Gundberg C., Bradley A., Karsenty G., Increased bone formation in osteocalcin-deficient mice. *Nature* **382,** 448-452 (1996).

Ducy P., Zhang R., Geoffroy V., Ridall A.L., Karsenty G. Osf2/Cbfa1: a transcriptional activator of osteoblast differentiation. *Cell,* **89**, 747-754 (1997).

Egusa H., Kaneda Y., Akashi Y., Hamada Y., Matsumoto T., Saeki M., Thakor D.K., Tabata Y., Matsuura N., Yatani H., Enhanced bone regeneration via multimodal actions of synthetic peptide SVVYGLR on osteoprogenitors and osteoclasts. *Biomaterials* **30,** 4676–4686 (2009).

Einhorn T.A. Bone metabolism and metabolic bone disease. *In Ortohopaedic Knowledge Update 4 Home Study Syllabus* (J.W. Frymoyer, ed) Am. Acad. Orhop. Surg., Rosemont, 69-88 (1994).

Eriksen E.F., Axelrod D.W., Melsen F. Bone Histomorphometry. *New York Raven Press,* pp1-12 (1994).

Facca S., Cortez C., Mendoza-Palomares C., Messadeg N., Dierich A., Johnston A.P., Mainard D., Voegel J.C., Caruso F., Benkirane-Jessel N. Active multilayered capsules for in vivo bone formation. *Proc. Natl. Acad. Sci. U.S.A.,* **107**, 3406-3411 (2010).

Faibish D., Gomes A., Boivin G., Binderman I., Boskey A. Infrared imaging of calcified tissue in bone biopsies from adults with osteomalacia. *Bone*, **36**, 6-12 (2005).

Fakhry M., Hamade E., Badran B., Buchet R., Magne D. "Molecular mechanisms of mesenchymal stem cell differentiation towards osteoblasts. *World J. Stem Cells*, **5**, 136–148 (2013).

Fantner G. E., Adams J., Turner P., Thurner P. J., Fisher L. W., Hansma P. K. Nanoscale ion mediated networks in bone: osteopontin can repeatedly dissipate large amounts of energy. *Nano Letters*, **7**, 2491-2498 (2007).

Fantner G. E., Hassenkam T., Kindt J. H., Weaver J. C., Birkedal H., Pechenik, L., Cutroni J.A., Cidade G.A., Stucky G.D., Morse D.E., Hansma P.K. Sacrificial bonds and hidden length dissipate energy as mineralized fibrils separate during bone fracture. *Nat. Mater.*, **4**, 612-616 (2005).

Farrell E., O'Brien F.J., Doyle P., Fischer J., Yannas I., Harley B.A., O'Connell B., Prendergast P.J., Campbell V.A. A collagen-glycosaminoglycan scaffold supports adult rat mesenchymal stem cell differentiation along osteogenic and chondrogenic routes. *Tissue Eng.* **12**, 459-468 (2006).

Fassbender M., Strobel C., Rauhe J.S., Bergmann C., Schmidmaier G., Wildemann B. Local inhibition of angiogenesis results in an atrophic non-union in a rat osteotomy model. *Eur. Cell. Mater.,* **22**, 1-11 (2011).

Fedarko N.S., Bianco P., Vetter U.K., Robey P.G., Human bone cell enzyme expression and cellular heterogenecity: Correlation of alkaline phosphatase enzyme activity with cell cycle. *J. Cell. Physiol.,* **144,** 115-121 (1990).

Fedarko N.S., Isolation and purification of proteoglycans. *EXS,* **70**, 9-35 (1994).

Fedde K.N., Blair L., Silverstein J., Coburn S.P., Ryan L.M., Weinstein R.S., Waymire K., Narisawa S., Millan J. L., MacGregor G. R., Whyte G.M., Alkaline phosphatase knockout mice recapitulate the metabolic and skeletal defects of infantile hypophosphatasia. *J. Bone Miner. Res.,* **14,** 2015-2026 (1999).

Feng J.Q., Huang H., Lu Y., Ye L., Xie Y., Tsutsui T.W., Kunieda T., Castranio T, Scott G., Bonewald L.B. The dentin matrix protein 1 (Dmp1) is specifically expressed in mineralized, but not soft, tissues during development. *J. Dent. Res.,* **82,** 776–780. (2003).

Feng J.Q., Ward L.M., Liu S., Lu Y., Xie Y., Yuan B., Yu X., Rauch F., Davis S.I., Zhang S., Rios H., Drezner M.K., Quarles L.D., Bonewald L.F., White K.E. Loss of DMP1 causes rickets and osteomalacia and identifies a role for osteocytes in mineral metabolism. *Nat. Genet.* **38**, 1310-1315 (2006).

Feng X., McDonald J.M. Disorders of bone remodeling. *Annu. Rev. of Pathol.*,**6**, 121-145 (2011).

Feng Y., Yang S.H., Xiao B.J., Xu W.H., Ye S.N., Xia T., Zheng D., Liu X.Z., Liao Y.F. Decreased in the number and function of circulation endothelial progenitor cells in patients with avascular necrosis of the femoral head. *Bone*, **46**, 32-40 (2010).

Fernandez-Yague M.A., Abbah S.A., McNamara L., Zeugolis D.I., Pandit A., Biggs M.J. Biomimetic approaches in bone tissue engineering: integrating biological and physicomechanical strategies. *Adv. Drug Deliv. Rev.,* **84**, 1-29 (2015).

Ferrara N., Gerber H.P., LeCouter J. The biology of VEGF and its receptors, *Nat Med.,* **9**, 669-676 (2003).

Ferron M., Hinoi E., Karsenty G., Ducy P. Osteocalcin differentially regulates beta cell and adipocyte gene expression and affects the development of metabolic diseases in wild-type mice. *Proc. Nat.I Acad. Sci. U. S. A.,* **105**, 5266.5270 (2008).

Fisher L. W., Torchia D. A., Fohr B., Young M. F., Fedarko N. S. Flexible structures of SIBLING proteins, bone sialoprotein and osteopontin. *Biochem. Biophys. Res. Commun.* **280**, 460–465 (2001).

Fisher L.W., Fedarko N.S., Six genes expressed in bones and teeth encode the current members of the SIBLING family of proteins. *Connect. Tissue Res.,* **44,**33-40 (2003).

Fisher L.W., Hawkins G. R., Tuross N. Termine J.D., Purification and partial characterization of small proteoglycans I and II, bone sialoproteins I and II, and osteonectin from the mineral compartment of developing human bone. *J. Biol. Chem*., **262,** 9702-9708 (1987).

Fitzpatrick L. E., McDevitt T.C. Cell-derived matrices for tissue engineering and regenerative medicine application. *Biomater. Sci.*, **3**, 12-24 (2015).

Fleischmajer R.A., Fisher L.W., MacDonald E.D., Jacobs Jr. L., Perlish J.S, Termine J.D.Decorin interacts with fibrillary collagen of embryonic and adult human skin. *J. Struct. Biol.,* **106,** 82-90 (1991).

Florencio-Silva R., Sasso G.R., Sasso-Cerri E., Simões M.J., Cerri P.S. Biology of bone tissue: structure, function, and factors that influence bone cells. *Biomed. Res. Int.,* **2015**, 421746 (2015).

Frantz C., Stewart K.M., Weaver V.M. The extracellular matrix at a glance. *J. Cell. Sci.* **123**, 4195-4200 (2010).

Franzen A. Heinegard D., Isolation and characterization of two sialoproteins present only in bone calcified matrix. *Biochem J.*, **232**, 715-724 (1985).

Fratzl P., Paris O., Klaushofer K., LandisW. J. Bone mineralization in an osteogenesis imperfecta mouse model studied by small-angle x-ray scattering. *J. Clin. Invest.* ,**97**, 396-402 (1996).

Frost, H.M. Bone remodeling and its relationship to metabolic boné diseases (Orthopaedic Lectures Vol. III) Bone modeling and skeletal modeling errors. Orthopaedic Lectures Vol. IV. Charles C. Thomas Inc., Springfield, Illinois (1973).

Fujioka-Kobayashi M., Schaller B., Kobayashi E., Hernandez M., Zhang Y., Miron R.J. Hyaluronic acid gel-based scaffolds as potential carrier for growth factors: an in vitro bioassay on its osteogenic potential. *J. Clin. Med.,* **5**, 112 (2016).

Fu Y., Liu L., Cheng R., Cui W. ECM decorated electrospun nanofiber for improving bone tissue regeneration. *Polymers*, **10**, 272 (2018).

Gao Y., Xu C. Wang L. Non-invasive monitoring of the osteogenic differentiation of human mesenchymal stem cells on a polycaprolactone scaffold using Raman imaging. *RCS Adv.,* **6**, 61771-61776 (2016).

Gao S., Chen M., Wang P., Li Y., Yuan Z., Guo W., Zhang Z., Zhang X., Jing X., Li X., Liu S., Sui X., Xi T., Guo Q. An electrospun fiber reinforced scaffold promotes total meniscus regeneration in rabbit meniscectomy model. *Acta Biomater.,* **73**, 127-140 (2018).

Garnett J., Dieppe P. The effects of serum and human albumin on calcium hydroxyapatite crystal growth. *Biochem. J.,* **266,** 863–868 (1990).

Gauthier O., Mu¨ller R., von Stechow D., Lamy B., Weiss P., Bouler J.-M., et al. In vivo bone regeneration with injectable calcium phosphate biomaterial: a three-dimensional microcomputed tomographic, biomechanical and SEM study. *Biomaterials,* **26**, 5444-5453 (2005).

George A, Veis A. Phosphorylated proteins and control over apatite nucleation, crystal growth, and inhibition. *Chem. Rev.,*108:4670-4693 (2008).

George A., Sabsay B., Simonian P.A., Veis A. Characterization of a novel dentin matrix acidic phosphoprotein, Implications for induction of biomineralization. *J.Biol. Chem.,* **268**, 12624–12630 (1993b).

George E.L., Georges-Labouesse E.N., Patel-King R.S., Rayburn H., Hynes R.O. Defects in mesoderm, neural tube and vascular development in mouse embryos lacking fibronectin. *Development,* **119,** 1079-1091 (1993).

Gerber H.P., Vu T.H., Ryan A.M., Kowalski J., Werb Z., Ferrara N. VEGF couples hypertrophic cartilage remodeling, ossification and angiogenesis during endochondral bone formation. *Nat. Med.,* **5**, 623-628 (1999).

Gericke A., Qin C., Spevak L., Fujimoto Y., Butler W.T., Sorensen E.S., Boskey A.L. Importance of phosphorylation for osteopontin regulation of biomineralization. *Calcif. Tissue Int.,* **77**, 45-54 (2005).

Gericke A., Qin C., Sun Y., Redfern R., Redfern D., Fujimoto Y., Taleb H., Butler W.T. Boskey A.L. Different forms of DMP1 play distinct roles in mineralization. *J. Dent. Res.* **89**, 355–359 (2010).

Gerstenfeld L.C., Cullinane D.M., Barnes G.L., Graves D.T., Einhorn T.A. Fracture healing as a post-natal developmental process: molecular, spatial, and temporal aspects of its regulation. *J. Cell. Biochem.*, **88**, 873-884 (2003).

Giancotti F.G., Ruoslahti E. Integrin signaling. *Science,* **285**, 1028-1032 (1999).

Giannoudis P.V., Einhorn T.A. Bone morphogenetic proteins in musculoskeletal medicine. *Injury*, **40**, S1-3 (2009).

Gibson M., Beachley V., Coburn J. Blandinelli P.A., Mao H.Q., Elisseeff J. Tissue extracellular matrix nanoparticle presentation in eletrospun nanofibers. *Biomed. Res. Int.,* **2014**, 469120 (2014).

Gilbert S.F., Sunderland M.A. Osteogenesis: the development of bones. Developmental biology 6th edition, Sinauer Associates, (2000).

Gilbert T.W., Sellaro T.L., Badylak S.F. Decellularization of tissues and organs. *Biomaterials*, **27**, 3675-3683 (2006).

Glass D.A.II, Bialek P., Ahn J.D. Starbuck M, Patel M.S., Clevers H, Taketo M.M, Long F., McMahon A.P., Lang R.A., Karsenty G. Canonical Wnt signaling in differentiated osteoblasts controls osteoclast differentiation. *Dev. Cell.,* **8**, 751–764 (2005).

Glimcher M. J. The nature of the mineral phase in bone. In: *Metabolic Bone Disease*, M. J. Glimcher, Ed., pp. 23–50, Academic Press, San Diego, CA, USA (1998).

Glowacki J. Angiogenesis in fracture repair. *Clin Orthop Relat Res*., **87**, 57-66 (1998).

Glowacki J., Lian J.B. Impaired recruitment and differentiation of osteoclast progenitors by osteocalcin-deplete bone implants. *Cell Differ.,* **21**, 247-254 (1987).

Goldberg M., Septier D., Rapoport O., Iozzo R.V., Young M. F., Ameye, L.G. Targeted disruption of two small-leucine-rich proteoglycans, biglycan and decorin, excerpts divergent effects on enamel and dentin formation. *Calcif. Tissue Int.,* **77,** 297-310 (2005).

Gomes S., Leonor I.B., Mano J.F., Reis R.L., Kaplan D.L. Spider silk-bone sialoprotein fusion proteins for bone tissue engineering. *Soft Matter*, **7**, 4964-4973 (2011).

Gong J.K., Arnold J.S., Cohn S.H. Composition of trabecular and cortical bone. *Anat. Rec.* **149**,325-331 (1964).

Gong T., Heng B.C., Xu J., Zhu S., Yuan C., Lo E.C., Zhang C. Decellularized extracellular matrix of human umbilical vein endothelial cells promotes endothelial differentiation of stem cells from exfoliated deciduous teeth. *J. Biomed. Mater. Res. A*., **105**, 1083-1093 (2017).

Goyal R., Guvendiren M., Freeman O., Mao Y., Kohn J. Optimization of polymer-ECM composite scaffolds for tissue engineering: effect of cells and culture conditions on polymeric nanofiber mats. *J. Funct. Biomater.,* **8**, 1 (2007).

Gordon J.A., Tye C.E., Sampaio A.V., Underhill T.M., Hunter G.K., Goldberg H.A. Bone sialoprotein expression enhances osteoblast differentiation and matrix mineralization in vitro. Bone, **41,** 462–473 (2007).

Greenwald A.S. , Boden S.D. , Goldberg V.M. , Khan Y. , Laurencin C.T. , Rosier R.N. Bone-graft substitutes: facts, fictions, and applications. *J. Bone Joint Surg. Am.*, **83**, 98-103 (2001).

Gregson C.L., Paggiosi M.A., Crabtree N., Steel S.A., McCloskey E., Duncan E.L., Fan B., Shepherd J.A., Fraser W.D., Smith G.D., Tobias J.H. Analysis of body composition in individuals with high bone mass reveals a marked increase in fat mass in women but not men. *J. Clin. Endocrinol. Metab.*, **98**, 818-828 (2013).

Grosso A., Burger M.G., Lunger A., Schaefer D.J., Banfi A., Di Maggio N. It takes two to tango: coupling of angiogenesis and osteogenesis for bone regeneration. *Front. Bioeng. Biotechnol.,* **5**, 68 (2017).

Grzesik W.J., Robey P.G. Bone matrix RGD glycoproteins: Immunolocalization and interaction with human primary osteoblastic bone cells *in vitro*. *J. Bone Miner. Res.,* **9,** 487-496 (1994)

Gundberg C.M., Biochemical markers of bone formation. *Clin Lab. Med.,* **20**, 489-501 (2000).

Guo W., Gong K., Shi H., Zhu G., He Y., Ding B., Wen L., Jin Y. Dental follicle cells and treated dentin matrix scaffold for tissue engineering the tooth root. *Biomaterials,* **33**, 1291-1302 (2012).

Gutsmann T., Fantner G.E., Kindt J.H., Venturoni M., Danielsen S., Hansma P.K. Force Spectroscopy of collagen fibers to investigate their mechanical properties and structural organization. *Biophys. J.,* **86**, 3186-3193 (2004).

Guvendiren M., Burdick J.A. Engineering synthetic hydrogel microenvironments to instruct stem cells. *Curr. Opin. Biotechol.,* **24**, 841-846 (2013).

Habelitz S., Denbesten P.K., Marshall S.J., Marshall G.W., Li W. Amelogenin control over apatite crystal growth is affected by the pH and degree of ionic saturation. *Orthod. Craniofac. Res.,* **8**, 232-238 (2005).

Haeseker B. Mr. Job van Meekeren (1611–1666) and surgery of the hand. *Plast. Reconstr. Surg.* **82**, 539–546 (1988).

Hall B.K., Miyake T. Divide, accumulate, differentiate: Cell condensations in skeletal development revisites. *Int. J. Dev. Biol.*, **39**, 881-893 (1995).

Hamada Y., Egusa H., Kaneda Y., Hirata I., Kawaguchi N., Hirao T., Matsumoto T., Yao M., Daito K., Suzuki M., Yatani H., Daito M., Okazaki M., Matsuura N., Synthetic osteopontin-derived peptide SVVYGLR can induce neovascularization in artificial bone marrow scaffold biomaterials. *Dent. Mater. J.,* **26,** 487–492 (2007).

Han Y., Cowin S.C., Schaffle M.B., Weinbaum S. Mechanotransduction and strain amplification in osteocyte cell processes. *Proc. Natl. Acad. Sci. U.S.A.*, **101**, 16689-16694 (2004)

Hankenson K.D., Bain S.D, Kyriakides T.R., Smith E.A., Goldstein S.A., Bornstein P. Increased marrow-derived osteoprogenitor cells and endosteal bone formation in mice lacking thrombospondin 2. *J. Bone Miner. Res.,* **15**, 851-862 (2000).

Hankenson K.D., Dishowitz M., Gray C., Schenker M. Angiogenesis in bone regeneration. *Injury,* **42**, 556-561 (2011).

Hao J., Shi S., Niu Z., Xun Z., Yue L., Xiao M. Mineralized nodule formation by human dental papilla cells in culture. *Eur. J. Oral Sci.,* **105**, 318-324 (1997).

Harley B.A., Lynn A.K., Wissner-Gross Z., Bonfield W., Yannas I.V., Gibson L.J. Design of a multiphase osteochondral scaffold. II. Fabrication of a mineralized collagen–glycosaminoglycan scaffold. *J.Biomed. Mater. Res. A,* **92**, 1066-1077 (2010).

Hatori M., Klatte K.J., Teixeira C.C., Shapiro I.M. End labeling studies of fragmented DNA in avian growth plate: evidence for apoptosis in terminally differentiated chondrocytes. *J.Bone Miner. Res.,* **10**, 1960-1968 (1995).

Hauschka P. V., Lian J. B., Cole D. E. C., Gundberg C. M. Osteocalcin and matrix Gla protein: vitamin K-dependent proteins in bone. *Physiol. Rev.* **69**, 990–1047 (1989).

Hauschka P. V., Reid M. L. Timed appearance of a calcium-binding protein containing g-carboxyglutamic acid in developing chick bone. *Dev. Biol.,* **65**, 431–436 (1978).

Hayman A. R (2008). Tartrate-resistant acid phosphate (TRAP) and the osteoclast/immune cell dichotomy. Autoimmunity, **41**, 218-223 (2008).

He G., George A.. Dentin matrix protein 1 immobilized on type I collagen fibrils facilitates apatite deposition in vitro. *J Biol Chem*. **279**, 11649-11656 (2004)**.**

He X., Yang X., Jabbar E. Combined effect of osteopontin and BMP-2 derived peptides grafted to an adhesive hydrogel on osteogenic and vasculogenic differentiation of marrow stromal cells. *Langmuir*, **28**, 5387–5397 (2012).

Heinegar D., Oldberg A., Structure and biology of cartilage and bone matrix noncollagenous macromolecules. *FASEB J*., **3**, 2042-3053 (1989).

Helmrich U., Di Maggio N., Guven S., Groppa E., Melly L., Largo R.D., Heberer M., Martin I., Scherberich A., Banfi A. Osteogenic graft vascularization and bone resorption by VEGF-expressing human mesenchymal progenitors. *Biomaterials,* **34**, 5025-5035 (2013).

Hench L. L., Polak J. M. Third-generation biomedical materials. *Science,* **295**, 1014-1017 (2002)

Henkel J., Woodruff M.A., Epari D.R., Steck R., Glatt V., Dickinson I.C., Choong P.F., Schuetz M.A., Hutmacher D.W. Bone regeneration based on tissue engineering conceptions — a 21st century perspective. *Bone Res.* **25**, 216-248 (2013).

Herring G.M., Ashton B.A. The isolation of soluble proteins, glycoproteins and proteoglycans from bone. *Prep. Biochem.* **4**, 179-200 (1974).

Hidalgo-Bastida LA., Cartmell S.H. Mesenchymal stem cells, osteoblasts and extracellular matrix proteins: enhancing cell adhesion and differentiation for bone tissue engineering. *Tissue Eng. Part B Rev.* **16**, 405-412 (2010).

Hinderer S., Layland S.L., Schenke-Layland K. ECM and ECM-like materials – Biomaterials for applications in regenerative medicine and cancer therapy. *Adv. Drug Deliv. Rev.,* **97**, 260-269 (2016).

Hollinger J.O., Chaudhari A. Bone regeneration materials for the mandibular and craniofacial complex. *Cells Mater.,* **2**, 143-151 (1992).
Hollister S.J. Scaffold engineering: a bridge to where? *Biofabrication*, **1**, 012001 (2009).

Hollister S.J., Murphy W.L. Scaffold translation: barriers between concept and clinic. *Tissue Eng. Part B Rev*., **17**, 459-474 (2011).

Holzwarth J.M., Ma P.X. Biomimetic nanofibrous scaffolds for bone tissue engineering. *Biomaterials*, **32**, 9622-9629 (2011).

Horton W.A. The biology of bone growth. *Growth Genet. Horm.*, **6**, 1-3 (1990).

Hsiao C.W., Bai M.Y., Chang Y., Chung M.F., Lee T.Y., Wu C.T., Maiti B., Liao Z.X., Li R.K., Sung H.W. Electrical coupling of isolated cardiomyocyte clusters grown on aligned conductive nanofibrous meshes for their synchronized beating. *Biomaterials*, **34**, 1063-1072 (2013).

Hu K., Olsen B.R. Osteoblast-derived VEGF regulates osteoblast differentiation and bone formation during bone repair. *J. Clin. Invest.,* **126**, 509- 526 (2016).

Hu K., Olsen B.R. The roles of VEGF in bone repair and regeneration. *Bone,* **91**, 30-36 (2016b).

Huang Z.M., Zhang Y.Z., Kotaki M., Ramakrishna S. A review on polymer nanofibers by electrospinning and their applications in nanocomposites. *Compos. Sci. Technol.,* **63**, 2223-2253 (2003).

Huang L., Nagapudi K., Apkarian R.P., Chaikof E.L. Engineered collagen-PEO nanofibers and fabrics. *J. Biomater. Sci. Polym. Ed.,* **12**, 979-993 (2001).

Hulmes D.J.S. Collagen diversity, synthesis and assembly. In: *Collagen, Structure and Mechanics*, Springer, New York, Chapter 2, 15-47 (2008).

Hung P.S., Kuo Y.C., Chen H.G., Chiang H.K., Lee O.K. Detection of osteogenic differentiation by differential mineralized matrix production in mesenchymal stromal cells by Raman spectroscopy. *PLoS ONE,* **8**, e65438 (2013).

Hunter G. H. Role of proteoglycan in the provisional calcification of cartilage. *Clin Orthop Rel Res*, **262,** 256-263 (1991).

Hunter G.K. An ion-exchange mechanism of cartilage calcification. *Connect. Tissue Res.,* **16**, 111-120 (1987).

Hunter G.K., Goldberg H.A. Nucleation of hydroxyapatite by bone sialoproteins. *Proc. Natl. Acad. Sci. U.S.A.,* **90**, 8562-8565 (1993).

Hussain I., Moharamzadeh K., Brook I.M. Jose de Oliveira Neto P, Salata L.A. Evaluation of osteoconductive and osteogenic potential of a dentin-based bone substitute using a calvarial defect model. *Int. J. Dent*. 2012, 396316 (2012).

Hutmacher D.W. Scaffolds in tissue engineering bone and cartilage. *Biomaterials.*, **21**, 2529-2543 (2000).

Hutmacher D.W., Cool S. Concepts of scaffold-based tissue engineering—the rationale to use solid free-form fabrication techniques. *J Cell. Mol. Med.,* **11**, 654-669 (2007b).

Hutmacher D.W., Schantz J.T., Lam C.X., Tan K.C., Lim T.C. State of the art and future directions of scaffold-based bone engineering from a biomaterials perspective. *J. Tissue Eng. Regen. Med.* 1, 245-260 (2007).

Hynes R.O. The emergence of integrins: A personal and historical perspective. *Matrix Biol,* **23,** 333-340 (2004).

Iba K., Abe Y., Chikenji T., Kanaya K., Chiba H., Sasaki K., Dohke T., Wada T., Yamashita T. Delayed fracture healing in tetranectin-deficient mice. *J. Bone Miner. Metab.* **31**, 399-408 (2013).

Iba K., Durkin M.E., Johnsen L., Hunziker E., Damgaard-Pedersen K., Zhang H., Engvall E., Albrechtsen R., Wewer U.M. Mice with a targeted deletion of the tetranectin gene exhibit a spinal deformity. *Mol. Cell. Biol.* **21**, 7817-7823 (2001).

Imhof B.A., Dunon D. Basic mechanism of leukocyte migration. *Horm. Metab. Res.,* **29**, 614-621 (1997).

In't Anker P.S., Scherjon S.A., Kleijburg-van der Keur C., de Groot-Swings G.M., Claas F.H., Fibbe WE., Kanhai E.E. Isolation of mesenchymal stem cells of fetal or maternal origin from human placenta. *Stem Cells*., **22**, 1338-1345 (2004).

Inzana J.A., Olvera D., Fuller S.M., Kelly J.P., Graeve O.A., Schwarz E.M., et al. 3D printing of composite calcium phosphate and collagen scaffolds for bone regeneration. *Biomaterials*, **35**, 4026-3034 (2014).

Jain R.K., Molecular regulation of vessel maturation. *Nat. Med.,* **9**, 685-693 (2003).

Jang J.H., Castano O., Kim H.W. Electrospun materials as potential platforms for bone tissue engineering. *Adv. Drug Deliv. Rev*., **6**, 1065-1083 (2009).

Janssen F.W., Oostra J., Oorschot A. van Blitterswijk C.A. A perfusion bioreactor system capable of producing clinically relevant volumes of tissue-engineered bone: in vivo bone formation showing proof of concept. *Biomaterials*, **27**, 315-323 (2006).

Jeon H.J., Lee J.Y., Lee H., Kim G.H. Nanostructured surface of electrospun PCL/dEM fibres treated with oxygen plasma for tissue engineering. *RCS Advances*, **6**, 32887-32896 (2016).

Jha A.K., Jackson W.M., Healy K.E. Controlling osteogenic stem cell differentiation via soft bioinspired hydrogels. *PLoS One,* **9**, e98640 (2014).

Johnson E.E., Urist M.R. Human bone morphogenetic protein allografting for reconstruction of femonral nonunion. *Clin. Orthop. Rel. Res.,* **371**, 61-74 (2000).

Kaartinen M. T., Pirhonen A., Linnala-Kankkunen A., Maenpaa P. H. Cross-linking of OPN by tissue transglutaminase increases its collagen binding properties. *J. Biol. Chem.,* **274**, 1729–1735 (1999).

Kaartinen M. T., Pirhonen A., Linnala-Kankkunen A., Maenpaa P. H. Transglutaminase-catalyzed cross-linking of OPN is inhibited by osteocalcin. *J. Biol. Chem.,* **272,** 22736–22741 (1997).

Kagami H., Agata H., Tojo A. Bone marrow stromal cells (bone marrow-derived multipotent mesenchymal stromal cells) for bone tissue engineering: basic science to clinical translation. *Int. J. Biochem. Cell. Biol.***43**, 286-289 (2011).

Kanczler J.M., Oreffo R.O. Osteogenesis and angiogenesis: the potential for engineering bone. *Eur. Cell. Mater.,* **15**, 100-114 (2008).

Kang Y., Kim S., Bishop J., Khademhosseini A., Yang Y. The osteogenic differentiation of human bone marrow MSCs on HUVEC-derived ECM and β-TCP scaffold. *Biomaterials*, **33**, 6998-7007 (2012).

Kaplan F.S., Hayes W.C., Keaveny T.M., Boskey A., Einhorn T.A., Iannotti J.P. Formation and function of bone. In: *Simon SR, editor. Orthopedic Basic Science. American Academy of Orthopedic Surgeons*; Rosemont, Illinois, 127-184 (1994).

Katagiri Y. U., Sleeman J., Fujii H., Herrlich P., Hotta H., Tanaka K., Chikuma S., Yagita H., Okumura K., Murakami M., Saiki I., Chambers A. F., Uede T. CD44 variants but not CD44s cooperate with beta1-containing integrins to permit cells to bind to OPN independently of arginine-glycine-aspartic acid, thereby stimulating cell motility and chemotaxis. *Cancer Res.,* **59**, 219-226 (1999).

Kazanci M., Wagner H.D., Manjubala N.I., Gupta H.S., Paschalis E., Roschger P., Fratzl P. Raman imaging of two orthogonal planes within cortical bone. *Bone*, **41**, 456-461 (2007).

Kelm Jr. R. J., Mann K.G. The collagen binding specificity of bone and platelet osteonectin is related to differences in glycosylation. *J. Biol. Chem.,* **266**, 9632-9639 (1991).

Kendall C., Stone N., Shepherd N., Geboes K., Warren B., Bennett R., Barr H. Raman spectroscopy, a potential tool for the objective identification and classification of neoplasia in Barrett's oesophagus. *J. Pathol.*, **200**, 602-609 (2003).

Keramaris N.C., Calori G.M., Nikolaou V.S., Schemitsch E.H., Giannoudis P.V. Fracture vascularity and bone healing: a systematic review of the role of VEGF. *Injury*, **39**, S45-47 (2008).

Kesireddy V., Kasper F.K. Approaches for building bioactive elements into synthetic scaffolds for bone tissue engineering. *J. Mater. Chem. B.*, **4**, 6773-6786 (2016).

Keskin D.S., Tezcaner A., Korkusuz P., Korkusuz F., Hasirci V. Collagen-chondroitin sulfate-based PLLA-SAIB-coated rhBMP-2 delivery system for bone repair. *Biomaterials,* **26**, 4023– 4034 (2005).

Khosla S., Oursler M. J., Monroe D. G. Estrogen and the skeleton. *Trends Endocrinol. Metab*., **23**, 576-581 (2012).

Kim H.W., Shin S.Y., Kim H.E., Lee Y.M., Chung C.P., Lee H.H., Rhyu C. Bone formation on the apatite-coated zirconia porous scaffolds within a rabbit calvarial defect. *J. Biomater. Appl.* **22**, 485-504 (2008).

Kim T.H., Jung Y., Kim S.H. Nanofibrous electrospun heart decellularized extracellular matrix-based hybrid scaffold as wound dressing for reducing scarring in wound healing. *Tissue Eng. Part A*, **24**, 830-848 (2018).

Kim J.W., Hu J.C., Lee J.I., Moon S.K., Kim Y.J., Jang K.T., Lee S.H., Kim C.C., Hahn S.H. Simmer J.P. Mutational hot spot in the DSPP gene causing dentinogenesis imperfecta type II. *Hum. Gen.,* **116**, 186–191 (2005).

Kim S.G. Lee D.S., Lee S., Jang J.H. Osteocalcin/fibronectin-functionalized collagen matrices for bone tissue engineering. *J. Biomed. Mater. Res. A.,* **103**, 2133-2140 (2015).

Kimura-Suda H., Kajiwara M., Sakamoto N., Kobayashi S., Ijiro K., Yurimoto H., Yamato H. Studies on bone metabolism by using isotope microscopy, FTIR imaging, and micro-Raman spectroscopy. *J. Oral Biosc.* **2**, 61-65 (2013).

Kirker-Head C., Karageorgiou V., Hofmann S., Fajardo R., Betz O., Merkle H.P., et al. BMP-silk composite matrices heal critically sized femoral defects. *Bone*, **41**, 247-255 (2007).

Kirsch T., Nah H.D., Shapiro I. M., Pacifici M., Regulated production of mineralization-competent matrix vesicles in hypertrophic chondrocytes. *J. Cell. Biol.,* **137,** 1140-1160 (1997).

Kjellän L, Lindahl U., Proteoglycans: structures and interactions. *Annu. Rev. Biochem., **60**,* 443-475 (1991).

Klein-Nulend J., Nijweide P.J., Burger E.H. Osteocyte and bone structure. *Curr. Osteoporos. Rep.,* **1**, 5-10 (2003).

Kleinman H.K., Luckenbill-Edds L., Cannon F.W., Sephel G.C. Use of extracellular matrix components for cell culture. *Anal. Biochem.,* **166**, 1-13 (1987).

Kneser U., Schaefer D.J., Polykandriotis E., Horch R.E. Tissue engineering of bone: the reconstructive surgeon's point of view. *J. Cell. Mol. Med.*, **10**, 7-19 (2006).

Knothe Tate M.L., Adamson Jr, Tami A.E., Bauer T.W. The Osteocyte. *Int. J. Biochem. Cell Biol.,* **36**, 1-8 (2004).

Koeter S., Tigchelaar S.J., Farla P., Driessen L., van Kampen A., Buma P. Coralline hydroxyapatite is a suitable bone graft substitute in an intra-articular goat defect model. *J. Biomed. Mater. Res. B Appl. Biomater.,* **90**, 116-122 (2009).

Koivunen E., Wang B., Dickinson C. D. Ruoslahti E. Peptides in cell adhesion research. *Methods Enzymol.,* **245**, 346-369 (1994).

Kokubo S., Fujimoto R., Yokota S-, Fukushima S., Nozaki K., Takahashi K., et al. Bone regeneration by recombinant human bone morphogenetic protein-2 and a novel biodegradable carrier in a rabbit ulnar defect model. *Biomaterials*, **24**, 1643-1651 (2003).

Komaki H., Tanaka T., Chazono M., Kikuchi T. Repair of segmental bone defects in rabbit tibiae using a complex of b-tricalcium phosphate, type I collagen, and fibroblast growth factor-2. *Biomaterials*, **27**, 5118-5126 (2006).

Kondo N., Ogose A., Tokunaga K., Ito T., Arai K., Kudo N., et al. Bone formation and resorption of highly purified b-tricalcium phosphate in the rat femoral condyle. *Biomaterials*, **26**, 5600-5608 (2005).

Koschnick S., Konstantinides S., Schafer K., Crain K., Loskutoff D.J. Thrombotic phenotype of mice with a combined deficiency in plasminogen activator inhibitor 1 and vitronectin. *J. Thromb. Haemost.,* **3**, 2290- 2295 (2005).

Kretlow J. D., Mikos A. G. Review: mineralization of synthetic polymer scaffolds for bone tissue engineering. *Tissue Eng.* **13**, 927-938 (2007).

Kruger T.E., Miller A.H., Wang J. Collagen scaffolds in bone sialoprotein-mediated bone regeneration. *ScientificWorldJournal*, **2013**, 812718 (2013).

Kuhn-Spearing, L. T., Rey, C., Kim, H. M. & Glimcher, M. J. Carbonated apatite nanocrystals of bone. In: *Synthesis and processing of nanocrystalline powder* (ed. Bourell, D.1) 206 (1996).

Kumagai T., Lee I., Ono Y., Maeno M.,Takagi M., Ultrastuctural localization and biochemical characterization of vitronectin in developing rat bone. *Histochem. J.,* **30**, 111-119 (1998).

Kumar S., Ponnazhagan S. Mobilization of bone marrow mesenchymal stem cells in vivo augments bone healing in a mouse model of segmental bone defect. *Bone*, **50**, 1012-1018 (2012).

Kundu A.K., Putnam A.J. Vitronectin and collagen I differentially regulate osteogenesis in mesenchymal stem cells. *Biochem. Biophys. Res. Commun.*, **347**, 347-357 (2006).

Kunisaki Y., Bruns I., Scheiermann C., Ahmed J., Pinho S., Zhang D., Mizoguchi T., Wei Q., Lucas D., Ito K., Mar J.C., Bergman A., Frenette P.S. Arteriolar niches maintain haematopoietic stem cell quiescence. *Nature,* **502**, 637-643 (2013).

Kuznetsov S.A., Mankani M.H., Gronthos S., Satomura K., Bianco P., Robey P.G. Circulating skeletal stem cells. *J. Cell. Biol.,* **153**, 1133–1140 (2001).

Kyriakides T.R., Zhu Y.H., Smith L.T., Bain S.D., Yang Z., Lin M.T., Danielson K.G., Iozzo R.V., LaMarca M., McKinney C.E., Ginns E. I., Bornstein P. Mice that lack thrombospondin 2 display connective tissue abnormalities that are associated with disordered collagen fibrillogenesis, an increased vascular density, and a bleeding diathesis. *J. Cell. Biol.,* **140**, 419-430 (1998).

Lai Y., Sun Y., Skinner C.M., Son E.L., Lu Z., Tuan R.S., Jilka R.L., Ling J. and Chen X.D. Reconstitution of marrow-derived extracellular matrix ex vivo: a robust culture system for expanding large-scale highly functional human mesenchymal stem cells. *Stem Cells Dev.,* **19**, 1095-1107 (2010).

Langer R., Vacanti, J. P. Tissue engineering. *Science,* **260**, 920-926 (1993).

Lau T.T., Lee L.Q., Vo B.N., Su K., Wang D.A. Inducing ossification in an engineered 3D scaffold-free living cartilage template. *Biomaterials*, **33**, 8406 (2012).

Laurencin C.T., Khan Y. Regenerative engineering. *Sci. Transl. Med.* **4**, 160ed9 (2012).

Lee E.H., Kim J.Y., Kweon H.Y., Jo Y.Y., Min S.K., Park Y.W., Choi J.Y., Kim S.G. A combination graft of low-molecular-weight silk fibroin with Choukroun platelet-rich fibrin for rabbit calvarial defect. *Oral Surg. Oral Med. Oral Pathol. Oral Radiol. Endodontol.,* **109**, 33-38 (2010).

Lee J.Y., Choi Y.S., Lee S.J., Chung C.P., Park Y.J. Bioactive peptide-modified biomaterials for bone regeneration. *Curr. Pharm. Des.* **17**, 2663-2676 (2011).

Lee J., Tran Q., Seeba G., Wikesjo U.M., Susin C. The critical-size supraalveolar peri-implant defect model: reproducibility in histometric data acquisition of alveolar bone formation and osseointegration. *J Clin. Periodontol.*, **36**,1067-1074 (2009b).

Lee S., Lee D.S., Choi I., Pham le B.H., Jang J.H.Design of an osteoinductive extracellular fibronectin matrix protein for bone tissue engineering. *Int. J. Mol. Sci.* **16**, 7672-7681 (2015).

Lee S.H., Shin H. Matrices and scaffolds for delivery of bioactive molecules in bone and cartilage tissue engineering. *Adv. Drug Deliv. Rev.* **59**, 339-359 (2007).

Lee J.Y., Bashur C.A., Goldstein A.S., Schmidt C.E. Polypyrrole-coated electrospun PLGA nanofibers for neural tissue applications. *Biomaterials*, **30**, 4325-4335 (2009).

Lehmann W., Edgar C.M., Wang K., Cho T.J., Barnes G.L., Kakar S., Graves D.T., Rueger J.M., Gerstenfeld L.C., Einhorn T.A. Tumor necrosis factor alpha (TNF-alpha) coordinately regulates the expression of specific matrix metalloproteinases (MMPS) and angiogenic factors during fracture healing. *Bone*, **36**, 300-310 (2005).

Leslie W. Ethnic differences in bone mass –clinical implications. *J. Clin. Endocrinol. Metab.,* **97**, 4329-4340 (2012).

Levorson E.J., Mountziaris P.M., Hu O., Kasper F.K., Mikos A.G. Cell-derived polymer/extracellular matrix composite scaffolds for cartilage regeneration part 1: investigation of cocultures and seeding densites for improved extracellular matrix deposition. *Tissue Eng. Part C Methods*, **20**, 340-357 (2014).

Li R., Guo W., Yang B., Guo L., Sheng L., Cheng G., Li Y., Zuo Q., Xie D., An X., Chen Y., Tian W. Human treated dentin matrix as a natural scaffold for complete human dentin tissue regeneration. *Biomaterials*, **32**, 4525-4538 (2011).

Li W.J., Laurencin C.T., Caterson E.J., Tuan R.S., Ko F.K. Electrospun nanofibrous structure: a novel scaffold for tissue engineering. *J. Biomed. Mater. Res.,* **60**, 613-621 (2002).

Liao S. S., Cui F.Z., Zhu X.D. Osteoblasts adherence and migration through three-dimensional porous mineralized collagen based composite: nHAC/PLA. *J. Bioactive Compat. Polym.* **19**, 117 (2004).

Liao S., Ngiam M., Chan C.K., Ramakrishna S. Fabrication of nano hydroxyapatite/ collagen/ osteonectin composites for bone graft applications. *Biomed. Mater.,* **4,** 025019 (2009).

Lin H., Yang G., Tan J., Tuan R.S., Influence of decellularized matrix derived from human mesenchymal stem cells on their proliferation, migration and multi-lineage differentiation potential. *Biomaterials,* **33**, 4480–4489 (2012).

Ling Y., Rios H.F., Myers E.R., Lu Y., Feng J.Q. Boskey A.L. DMP1 depletion decreases bone mineralization in vivo: an FTIR imaging analysis. *J. Bone Miner. Res.,* **20**, 2169–2177 (2005).

Lippens E., Vertenten G., Girones J., Declercq H., Saunders J., Luyten J., et al. Evaluation of bone regeneration with an injectable, in situ polymerizable Pluronic F127 hydrogel derivative combined with autologous mesenchymal stem cells in a goat tibia defect model. *Tissue Eng. Part A*, **16,** 617-627 (2010).

Liu C. Z., Czernuszka J. T. Development of biodegradable scaffolds for tissue engineering: a perspective on emerging technology. *Mater. Sci. Technol.,* **23**, 379-391 (2007).

Liu Y. Berendsen A.D., Jia S., Lotinun S., Baron R., Ferrara N., Olsen B.R. Intracellular VEGF regulates the balance between osteoblast and adipocyte differentiation. *J. Clin. Invest.,* **122,** 3101-3113 (2012).

Liu Y.J., Yang Z.Y., Tan L.L., Li H., Zhang Y.Z. An animal experimental study of porous magnesium scaffold degradation and osteogenesis. *Braz. J. Med. Biol. Res.* **47**, 715-720 (2014).

Lluch A.V., Fernandez A.C., Ferrer G.G., Pradas M.M. Bioactive scaffolds mimicking natural dentin structure. *J. Biomed. Mater. Res. B Appl. Biomater.,* **90**, 182-194 (2009).

Lodish H., Berk A., Zipursky S.L, Matsudaira P., Baltimore D., Darnell J. Molecular Cell Biology,4th edition, ed. Freeman W.H., New York (2000).

Logeart-Avramoglou D., Anagnostou F., Bizios R., Petite H. Engineering bone: challenges and obstacles. *J. Cell. Mol. Med.,* **9**, 72-84 (2005).

Lord, C. F., Gebhardt M.C., Tomford W.W., Mankin H.J. Infection in bone allografts. Incidence, nature, and treatment. *J. Bone Joint Surg. Am.* **70**, 369-376 (1988).

Lu H., Hoshiba T., Kawazoe N., Kod I., Song M., Chena G. Cultured cell-derived extracellular matrix scaffolds for tissue engineering. Biomaterials, **32**, 9658-9666 (2011).

Luo G., Ducy P., McKee M.D., Pinero G.J., Loyer E., Behringer R.R., Karsenty G., Spontaneous calcification of arteries and cartilage in mice lacking matrix GLA protein. *Nature* **386**, 78-81 (1997).

Luppen C.A., Smith E., Spevak L., Boskey A.L., Frenkel B. Bone morphogenetic protein-2 restores mineralization in glucocorticoid-inhibited MC3T3-E1 osteoblast cultures. *J. Bone Miner. Res.* **18**, 1186-1197 (2003).

Lutolf M.P. Lauer-Fields J.L., Schmoekel H.G., Metters A.T., Weber F.E., Fields G.B., Hubbell J.A. Synthetic matrix metalloproteinase-sensitive hydrogels for the conduction of tissue regeneration: engineering cell-invasion characteristics. *Proc. Natl. Acad. Sci. USA,* **100**, 5413-5418 (2003).

Lutolf M.P., Weber F.E., Schmoekel H.G., Schense J.C., Kohler T., Muller R., Hubbell J.A. Repair of bone defects using synthetic mimetics of collagenous extracellular matrices. *Nat. Biotechnol.* **21**, 513-518 (2003b).

Ma P. X., Choi J. W., Biodegradable polymer scaffolds with well-defined intereconnected spherical pore network. *Tissue Eng.* **7**, 23-33 (2001).

MacEwen W. Observations concerning transplantation of bone illustrated by a case of inter-human osseous transplantation, whereby over two-thirds of the shaft of a humerus was restored. *Proc. Roy. Soc. Lond.* **32,** 232-247 (1881).

Mackie E.J., Ahmed Y.A., Tatarczuch L., Chen K.S., Mirams M. Endochondral ossification: how cartilage is converted into bone in the developing skeleton. *Int. J. Biochem. Cell. Biol.,* **40**, 46-62 (2008).

Madeddu P. Therapeutic angiogenesis and vasculogenesis for tissue regeneration. *Exp Physiol.,* **90**, 315-326 (2005).

Maes C., Gloossens S., Bartunkova S., Drogat B., Coenegrachts L., Stockmans I., Moermans K., Nyabi O., Haigh K, Naessens M., Haenebalcke L., Tuckermann J.P., Tjwa M., Carmeliet P., Mandic V., David J.P., Behrens A., Nagy A., Carmeliet G., Haigh J.J. Increased skeletal VEGF enhances beta-catenin activity and results in excessively ossified bone. *EMBO J.,* **29**, 424-441 (2010).

Malaval L., Wade-Gueye N.M., Boudiffa M., Fei J., Zirngibl R., Chen F., Laroche N., Roux J.P., Burt-Pichat B., Duboeuf F.Bone sialoprotein plays a functional role in bone formation and osteoclastogenesis. *J. Exp. Med.* **205**, 1145–1153 (2008).
Mandair G.S., Morris M.D. Contributions of Raman spectroscopy to the understanding of bone strength. *Bonekey Rep.*, **4**, 620 (2015).

Mankani M.H., Kuznetsov S.A., Wolfe R.M., Marshall G.W., Robey P.G. In vivo bone formation by human bone marrow stromal cells: reconstruction of the mouse calvarium and mandible. *Stem Cells.*, **24**, 2140-2149 (2006).

Marcus R., Feldman D., Dempster D. W., Luckey M., Cauley J.A. Osteoporosis, 4th Edition, Academic Press (2013).

Margolis H.C., Beniash E., Fowler C.E. Role of macromolecular assembly of enamel matrix proteins in enamel formation. *J. Dent. Res.,* **85**, 775-793 (2006).

Marsell R., Einhorn T.A. Emerging bone healing therapies. *J. Orthop. Trauma*., **24**, S4-8 (2010).

Marsell R., Einhorn T.A. The biology of fracture healing. *Injury*, **42**, 551-555 (2011).

Martinez P. Age-related changes in parathyroid-related protein and vascular endothelial growth factor in human osteoblastic cells. *Osteoporos. Int.,* **13**, 874-881 (2002),

Masaeli E., Karamali F., Loghmani S., Eslaminejad M.B., Nasr-Esfahani M.H. Bio-engineered electrospun nanofibrous membranes using cartilage extracellular matrix particles. *J. Mater. Chem. B,* **5**, 765-776 (2017).

Massia S.P., Hubbel J.A. An RGD spacing of 440 nm is sufficient for integrin alpha V beta 3-mediated fibroblast spreading and 140 nm for focal contact and stress fiber formation. *J. Cell. Biol.,* **114**, 1089-1100 (1991).

Matsubara H., Hogan D.E., Morgan E.F., Morlock D.P., Einhorn T.A., Gerstenfeld L.C. Vascular tissues are a primary source of BMP2 expression during bone formation induced by distraction osteogenesisi. *Bone*, **51**, 168-180 (2012).

Matti H. Ueber die freie. Transplantation von Knochenspongiosa*. Langenbecks Arch Clin Chir.* 168-236 (1932).

Mauney J.R., Volloch V., Kaplan D.L. Role of adult mesenchymal stem cells in bone tissue engineering applications: current status and future prospects. *Tissue Eng.*, **11**, 787-802 (2005).

Mayer H., Bertram H., Lindemaier W., Korff T., Weber H., Weich H. Vascular endothelial growth factor (VEGF-A) expression in human mesenchymal stem cells: autocrine and paracrine role on osteoblastic and endothelial differentiation. *J. Cell Biochem.,* **95**, 827-839 (2005).

McCloskey C., Furnival T. Structure of bone and implant materials. Available at http://www.doitpoms.ac.uk/tlplib/bones/index.php.

McGovern J.A., Griffin M., Hutmacher D.W. Animal models for bone tissue engineering and modelling disease. *Dis. Model. Mech.* **11**, dmm033084 (2018).

McKee M.D., Nanci A., Osteopontin at mineralized tissue interfaces in bone, teeth, and osseointegrated implants: ultrastructural distribution and implications for mineralized tissue formation, turnover, and repair. *Microsc Res Tech.* **33,** 141-164 (1996).

McLean F.C. The ultrastucture and function of bone. *Science*, **127**, 451-456 (1958).

Mescher A. Junqueira's Basic Histology Text and Atlas. *McGraw Hill Medical* (2010).

Mikuni-Takagaki Y., Kakai Y., Satoyoshi M., Kawano E., Suzuki Y., Kawase T., Saito S. Matrix mineralization and the differentiation of osteocyte-like cells in culture. *J. Bone Miner. Res.,* **10**, 231-242 (1995).

Miura M., Gronthos S., Zhao M., Lu B., Fisher L.W., Robey P.G, Shi S. SHED: stem cells from human exfoliated deciduous teeth. *Proc. Natl. Acad. Sci. U.S.A*., **100**, 5807-5812 (2003).

Miyauchi A., Alvarez J., Greenfield E. M., Teti A., Grano M., Colucci S., Zambonin-Zallone A., Ross F. P., Teitelbaum S. L., Cheresh D. Recognition of OPN and related peptides by an v3 integrin. *Osteoporos. Int*., **1**, 132-135 (1991).

Mizuno M., Imai T., Fujisawa R., Tani H., Kuboki Y. Bone sialoprotein (BSP) is a crucial factor for the expression of osteoblastic phenotypes of bone marrow cells cultured on type I collagen matrix. *Calcif. Tissue Int.,* **66,** 388–396 (2000).

Mohamadyar-Toupkanlou F., Vasheghani-Farahani E., Hanaee-Ahvaz H., Soleimani M., Dodel M., Havasi P., Ardeshirtlajimi A., Taherzadeh E.S. Osteogenic differentiation of MSCs on fibronectin coated and nHA-modified scaffolds. *ASAIO J.,* **63**, 684-691 (2017).

Morinobu M., Ishijima M., Rittling S.R., Tsuji K., Yamamoto H., Nifuji A., Denhardt D.T., Noda M. *J.Bone Miner.Res.,* **18**, 1706-1715 (2003).

Morris M.D., Finney W.F. Recent developments in Raman and infrared spectroscopy and imaging of bone tissue. *Spectroscopy*, **18**, 155-159 (2004).

Mosby C.V. Gray's Anatomy: The anatomical basis of clinical practice, 39th edition (2004).

Motta A., Migliaresi C., Faccioni F. Torricelli P., Fini M., Giardino R. Fibroin hydrogels for biomedical applications: preparation, characterization and in vitro cell culture studies. *J. Biomater. Sci. Polym. Ed.* **15**, 851-864 (2004).

Mouw J.K., Ou G., Weaver V.M. Extracellular matrix assembly: a multiscale deconstruction. *Nat. Rev. Mol. Cell. Biol.,* **15,** 771-785 (2014).

Mundy G.R. Bone remodeling and its disorders. *Martin Dunitz*, London, 1995.

Munting E., Wilmart J.F., Wijne A., Hennebert P., Delloye C. Effect of sterilization on osteoinduction. Comparison of five methods in demineralized rat bone. *Acta Orthop. Scand,.* **59**, 34-38 (1988).

Murshed M., Schinke T., McKee M.D., Karsenty G. Extracellular matrix mineralization is regulated locally: Different roles of two Gla-containing proteins. *J. Cell. Bio.l,* **165**, 625-630 (2004).

Nakagawa Y., Shimizu K., Hamamoto T., Kotani S., Yamamuro T. Electron microscopy of calcification during high-density suspension culture of chondrocytes. *Calcif. Tissue Int.,* **53**, 127-134 (1993).

Nakamyra M., Sone S., Takahashi I., Mizoguchi I., Echigo S., Sasano Y. Expression of versican and ADAMTS1, 4, and 5 during bone development in the rat mandible and hind limb. *J Histochem. Cytochem.,* **53,** 1553-1562 (2005).

Nanci A. Content and distribution of noncollagenous matrix proteins in bone and cementum: Relationship to speed of formation and collagen packing density. *J. Struct. Biol.,* **126**, 256–269 (1999).

Narayanan K., Srinivas R., Ramachandran A., Hao J., Quinn B., George A. Differentiation of embryonic mesenchymal cells to odontoblast-like cells by overexpression of dentin matrix protein1. *Proc. Natl. Acad. U.S.A.* **98**, 4516-4521 (2001).

Narayanan G., Bhattacharjee M., Nair L.S., Laurencin C.T., Musculoskeletal tissue regeneration: the role of the stem cells. *Regen. Eng. Transl. Med.,* **3**, 133-165 (2017).

Nauman E.A., Ebenstein D.M., Hughes K.F., Pruitt L., Halloran B.P., Bikle D.D., Keaveny T.M. Mechanical and chemical characteristics of mineral produced by basic fibroblast growth factor-treated bone marrow stromal cells in vitro. *Tissue Eng.,* **8**, 931-939 (2002).

Nauth A., Giannoudis P.V., Einhorn T.A., Hankenson K.D., Friedlaender G.E., Li R., Schemitsch E.H. Growth factors: beyond bone morphogenetic proteins. *J. Orthop. Trauma*., **24**, 543-546 (2010).

Neyt J., Buckwalter J.A., Carroll N. Use of animal models in musculoskeletal research. *Iowa Orthop. J*. 18, 118-123 (1998).

Nikolov S., Raabe D. Hierarchical modeling of the elastic properties of bone and submicron scales: the role of extrafibrillar mineralization. *Biophys. J.* **94**, 4220-4232 (2008).

Ninomiya J.T., Tracy R.P., Calore J.D., Gendreau M.A., Kelm R.J., Mann K.G. Heterogeneity of human bone. J. Bone Min. Res. 5: 933-938 (1990).

Nishimura I., Muragaki Y., Olsen B.R. Tissue-specific forms of type IX collagen-proteoglycan arise from the use of two widely separated promoters. *J Biol Chem*, **264,**20033-20041 (1989).

Notingher I., Bisson I., Bishop A.E., Randle W.L., Polak J.M., Hench L.L. In situ spectral monitoring of mRNA translation in embryonic stem cells during differentiation in vitro. *Anal. Chem.,* **76**, 3185-3193 (2004).

Oberlender S.A., Tuan R.S. Expression and functional involvement of N-cadherin in embryonic limb chondrogenesis. *Development,* **120**, 177-187 (1994).

Ohgushi H., Goldberg V.M., Caplan A.I. Repair of bone defects with marrow cells and porous ceramic: experiments in rats. *Acta Orthop.,* **60**, 334-339 (1989).

Ollier L.L. Traite experimental et clinique de la regeneration des os et de la production artificielle du tissu osseux. V. Masson Vol. I and Vol. II. (1867).

Osathanon T., Giachelli C.M., Somerman M.J., Immobilization of alkaline phosphatase on microporous nanofibrous fibrin scaffolds for bone tissue engineering. *Biomaterials*, **30**, 4513-4521 (2009).

Ott H.C., Matthiesen T.S., Goh S.K., Black L.D., Kren S.M., Netoff T.I., Taylor D.A. Perfusion-decellularized matrix: using nature's platform to engineer a bioartificial heart. *Nat Med*., **14**, 213-221 (2008).

Paderi J.E., Panitch A. Design of a synthetic collagen-binding peptidoglycan that modulates collagen fibrillogenesis. *Biomacromolecules*, **9**, 2562-2566 (2008).

Papadimitropoulos A., Scotti C., Bourgine P., Scherberich A., Martin I. Engineered decellularized matrices to instruct bone regeneration processes. *Bone*, **70**, 66-72 (2015).

Parfitt A.M. The mechanism of coupling: a role for the vasculature. *Bone,* **26**, 319-323 (2000).

Paschalis E.P., Burr D.B., Mendelsohn R., Hock J.M., Boskey A.L. Bone mineral and collagen quality in humeri of ovariectomized cynomolgus monkeys given rhPTH (1-34) for 18 months. *J. Bone Miner. Res.,* **18**, 769-775 (2003).

Peach M.S., Ramos D.M., James R., Morozowich N.L., Mazzocca A.D., Doty S.B., Allcock H.R., Kumbar S.G., Laurencin C.T. Engineered stem cell niche matrices for rotator cuff tendon regenerative engineering. *PLoS One*, **12**, e0174789 (2017).

Pearce A.I., Richards R.G., Milz S., Schneider E., Pearce S.G. Animal models for implant biomaterial research in bone: a review. *Eur Cell Mater.,* **13**, 1-10 (2007).

Pei M., Shoukry M., Li J., Daffnere S.D., France J.C., Emery S.E. Modulation of in vitro microenvironment facilitates synovium-derived stem cell-based nucleous pulposus tissue regeneration. *Spine*, **37**, 1538-1547 (2012).

Percival C.J. Richtsmeier J.T. Angiogenesis and intramembranous osteogenesis. *Dev Dyn.,* **242**, 909-922 (2013).

Petersen T.H., Calle E.A., Zhao L., Lee E.J., Gui L., Raredon M.B., Gavrilov K., Yi T., Zhuang Z.W., Breuer C., Herzog E., Niklason L.E. Tissue-engineered lungs for in vivo implantation. *Science*, **329**,538–541(2010).

Petry R., Schmitt M., Popp J. Raman spectroscopy – A prospective tool in the life sciences. *Chem. Phys. Chem.*, **4**, 14-30 (2003).

Pham Q.P., Kasper F.K., Mistry A.S., Sharma U., Yasko A.W., Jansen J.A. Analysis of the osteoinductive capacity and angiogenicity of an in vitro generated extracellular matrix. *J. Biomed. Mater. Res. A.,* **88**, 295-303 (2008).

Phan T.C., Xu J., Zheng M.H., Interaction between osteoblast and osteoclast: impact in bone disease. *Histol. Histopathol.*, **19,** 1325-1344 (2004).

Phillips J.E., Hutmacher D.W., Guldberg R.E., García A.J. Mineralization capacity of Runx2/Cbfa1-genetically engineered fibroblasts is scaffold dependent. *Biomaterials*, **27**, 5535-5545 (2006).

Pirotte S., Lamour V., Lambert V., Alvarez Gonzalez M.L., Ormenese S., Noel A. Dentin matrix protein 1 induces membrane expression of VE-cadherin on endothelial cells and inhibits VEGF-induced angiogenesis by blocking VEGFR-2 phosphorylation. *Blood***, 117**, 2515-2516 (2011).

Poser J.W., Esch F.S., Ling N.C., Price P.A. Isolation and sequence of the vitamin K-dependent protein from human bone. Undercarboxylation of the first glutamic acid residue. *J. Biol. Chem*. **255**, 8686-8691 (1980).

Poser, J. W., Price, P. A. A method for decarboxylation of g-carboxyglutamic acid in proteins. *J. Biol. Chem.* **254**, 431–436 (1979).

Potter K., Leapman R.D., Basser P.J., Landis W.J. Cartilage calcification studied by proton nuclear magnetic resonance microscopy. *J. Bone Miner. Res.,* **17**, 652-660 (2002).

Poundarik A.A., Diab T., Sroga G.E., Ural A., Boskey A.L., Gundberg C.M., Vashishth D. Dilatational band formation in bone, *Proc. Natl Acad. Sci. U.S.A.*, **109**, 19178-19183 (2012).

Price P.A., Williamson M.K. Primary structure of bovine matrix Gla protein, a new vitamin K-dependent bone protein. *J. Biol. Chem.,* **260**, 14791-14975 (1985).

Puckett S., Pareta R., Webster T.J. Nano rough micron patterned titanium for directing osteoblast morphology and adhesion. *Int. J.Nanomedicine*., **3**, 229-241 (2008).

Punjabia P.B., Chauhan N.P.S., Jangid N.P., Junejad P. Biodegradable conducting polymers for tissue engineering applications. In: *Encyclopedia of Biomedical Polymer and Polymeric Biomaterials. Publisher: Taylor and Francis, Editors: Munmaya Mishra* (2014).

Puppels G.J., Demul F.F.M., Otto C., Greve J., Robertnicoud M., Arndtjovin D.J., Jovin T.M., Studying single living cells and chromossomes by confocal Raman microspectroscopy. *Nature*, **347**, 301-303 (1990).

Qin C., D'Souza R., Feng J.Q. Dentin matrix protein 1 (DMP1): new and important roles for biomineralization and phosphate homeostasis. *J. Dent. Res.* **86**, 1134-1141 (2007).

Quinn J.M, Gillespie M.T. Modulation of osteoclast formation. *Biochem. Biophys. Res. Commun.,* **328***,* 739-745 (2005).

Quint C., Kondo Y., Manson R.J., Lawson J.H., Dardik A., Niklason L.E. Decellularized tissue-engineered blood vessel as an arterial conduit. *Proc. Natl. Acad. Sci. U.S.A.,* **108**, 9214-9219 (2011).

Rahn BA. Bone healing: histologic and physiologic concepts. In: Fackelman GE, editor. Bone in clinical orthopedics. Thieme; Stuttgart, NY, pp. 287–326 (2002).

Ramasamy S.K., Kusumbe A.P., Wang L., Adams R.H. Endothelial Notch activity promotes angiogenesis and osteogenesis in bone. *Nature,* **407**, 376-380 (2014).

Rammelt S., Neumann M., Hanisch U., Reinstorf A., Pompe W., Zwipp H., Biewener A., Osteocalcin enhances bone remodeling around hydroxyapatite/collagen composites. *J. Biomed. Mater. Res. A,* **73**, 284-294 (2005).

Rapuano B.E., Wu C., MacDonald D.E. Osteoblast-like cell adhesion to bone sialoprotein peptides. *J. Orthop. Res.* **22**, 353-361 (2004).

Ravindran S., George A., Dentin matrix proteins in bone tissue engineering. *Adv. Exp. Med. Biol.*, **881**, 129-142 (2015).

Reichert J.C., Epari D.R., Wullschleger M.E., Saifzadeh S., Steck R., Lienau J., et al. Establishment of a preclinical ovine model for tibial segmental bone defect repair by applying bone tissue engineering. *Tissue Eng. Part B Rev.,* **16,** 93-104 (2010).

Reilly G.C., Engler A.J. Intrinsic extracellular matrix properties regulate stem cell differentiation. *J. Biomech.,* **43**, 55-62 (2010).

Rey C., Combes C., Drouet C., Glimcher M.J. Bone mineral: update on chemical composition and structure. *Osteoporos. Int.,* **20**, 1013-1021 (2009).

Rey C., Kim H.M., Gerstenfeld L., Glimcher M.J. Characterization of the apatite crystals of bone and their maturation in osteoblast cell culture: comparison with native bone crystals. *Connect. Tissue Res.*, **35**, 343-349 (1996).

Reyes C.D., García A.J. Alpha2beta1 integrin-specific collagen-mimetic surfaces supporting osteoblastix differentiation *J. Biomed. Mater. Res. Part A,* **69**, 591-600 (2004).

Reyes C.D., Petrie T.A., Burns K.L., Scwartz Z., García A.J. Biomolecular surface coating to enhance orthopaedic tissue healing and integration. *Biomaterials*, **28**, 3228-3235 (2007).

Rezania A., Healy K.E. The effect of peptide surface density on mineralization of a matrix deposited by osteogenic cells. *J. Biomed. Mater. Res.* 52, 595-600 (2000).

Rho J.Y., Kuhn-Spearing L., Zioupos P. Mechanical properties and the hierarchical structure of bone. *Med. Engi. Phys.*, **20**, 92-102 (1998).

Ritter N. M., Farach-Carson M. C., Butler,W. T. Evidence for the formation of a complex between osteopontin and osteocalcin. *J. Bone Miner. Res.,* **7**, 877-885 (1992).

Rittling S. R., Denhardt D. T. OPN function in pathology: Lessons from OPN-deficient mice. *Exp. Nephrol.* **7**, 103–113 (1999).

Rittling S. R., Matsumoto,H. N., McKee M. D., Nanci A., An X. R., Novick K. E., Kowalski A. J., Noda M., Denhardt D. T.Mice lacking OPN show normal development and bone structure but display altered osteoclast formation in vitro. *J. Bone Miner. Res.*, **13**, 1101–1111 (1998).

Roach H.I. Why does bone matrix contain non-collagenous proteins. *Cell. Biol. Int.,* **18**, 617-628 (1994).

Roach H.I., Association of matrix acid and alkaline phosphatases with mineralization of cartilage and endochondral bone. *Histochem. J.*, **31,** 53-61 (1999).

Rodan S.B., Rodan G.A., Integrin function in osteoclasts, *J. Endocrinol.,* **154**, S47-S56 (1997).

Rodriguez D.E., Thula-Mata T., Toro E.J., Gower L.B., Multifunctional role of osteopontin in directing intrafibrillar mineralization of collagen and activation of osteoclasts. *Acta Biomaterial.,* **10** 494-507 (2014).

Rohde M., Mayer H. Exocytotic process as a novel model for mineralization by osteoblasts in vitro and in vivo determined by electron microscopic analysis. *Calcif. Tissue Int.,* **80**, 323-336 (2007).

Rosada C., Justesen J., Melsvik D., Ebbesen P., Kassem M. The human umbilical cord blood: a potential source for osteoblast progenitor cells. *Calcif. Tissue Int.,* **72**, 135-142 (2003).

Roseberry H.H., Hasting A.B., Morse J.K. X-ray analysis of bone and teeth. *J. Biol. Chem.*, **90**, 395-407 (1931).

Rutledge K., Cheng Q., Pryzhkova M., Harris G.M., Jabbarzadeh E. Enhanced differentiation of human embryonic stem cells on extracellular matrix-containing osteomimetic scaffolds for bone tissue engineering. *Tissue Eng. Part C Methods*, **20**, 865-874 (2014).

Sadr N., Pippenger B.E., Scherberich A., Wendt D., Mantero S., Martin I. Enhancing the biological performance of synthetic polymeric materials by decoration with engineered, decellularized extracellular matrix. *Biomaterials* **33**, 5085-5093 (2012).

Salasznyk R.M., Williams W.A., Boskey A., Batorsky A., Plopper G.E. Adhesion to vitronectin and collagen I promotes osteogenic differentiation of human mesenchymal stem cells. *J. Biomed. Biotechnol.*, **2004**, 24-34 (2004).

Sanan A., Haines S.J. Repairing holes in the head: a history of cranioplasty. *Neurosurgery*, **40**, 588-603 (1997).

Sarvestani A.S., He X., Jabbari E. Osteonectin-derived peptide increases the modules of a bone-mimetic nanocomposite. *Eur. Biophys. J.,* **37**, 229-234 (2008).

Saruwatari L., Aita H., Butz F., Nakamura H.K., Ouyang J., Yang Y., Chiou W.A., Ogawa T. Osteoblasts generate harder, stiffer, and more delamination-resistant mineralized tissue on titanium than on polystyrene, associated with distinct tissue micro- and ultrastructure. *J. Bone Miner. Res.,* **20**, 2002-2016 (2005).

Schaffner P., Dard M.M. Structure and function of RGD peptides involved in bone biology. *Cell. Mol. Life Sci.,* **60**, 119-132 (2003).

Schipani E., Maes C., Carmeliet G., Semenza G.L. Regulation of osteogenesis-angiogenesis coupling by HIFs and VEGF. *J Bone Miner. Res*., **24**, 1347-1353 (2009).

Schneider G., Blechschmidt K., Linde D., Litschko P., Korbs T., Beleites E. Bone regeneration with glass ceramic implants and calcium phosphate cements in a rabbit cranial defectmodel. *J. Mater. Sci. Mater. Med*. **21**, 2853-2859 (2010).

Schulze H.G., Konorov S.O., Caron N.J., Piret J.M., Blades M.W., Turner R.F.B. Assessing differentiation status of human embryonic stem cells noninvasively using Raman microspectroscopy. *Anal. Chem.,* **82**, 5020-5027 (2010).

Schwartz Z., Somers A., Mellonig J.T. , Carnes D.L. Jr ., Dean D.D. , Cochran D.L., Boyan B.D. Ability of commercial demineralized freeze-dried bone allograft to induce new bone formation is dependent on donor age but not gender. *J. Periodontol.,* **69**, 470-47 (1998).

Sfeir C., Ho L., Doll B.A., Azari K., Hollinger J.O. Fracture repair. In: *Lieberman JR, Friedlaender GE, editors*. Bone regeneration and repair. Humana Press; Totowa, NJ, pp. 21–44 (2005).

Shapses S.A., Cifuentes M., Spevak L., Boskey A.L., Denhardt D.T. Osteopontin facilitates bone resorption, decreasing bone mineral crystallinity and content during calcium deficiency. *Calcif. Tissue Int.,* **73,** 86-92 (2003).

Sherwood J. K. Riley S.L., Palazzolo R., Brown S.C., Monkhouse D.C., Coates M., Griffith L.G., Landeen L.K., Ratcliffe A. A three-dimensional osteochondral composite scaffold for articular cartilage repair. *Biomaterials*, **23**, 4739-4751 (2002).

Shi S., Gronthos S. Perivascular niche of postnatal mesenchymal stem cells in human bone marrow and dental pulp. *J. Bone Miner. Res*., **18**, 696-704 (2003).

Shin H., Jo S., Mikos A.G. Biomimetic materials for tissue engineering. *Biomaterials*, **24**, 4353–4364 (2003).

Shin H., Jo S., Mikos A.G., Modulation of marrow stromal osteoblast adhesion on biomimetic oligo[poly(ethylene glycol) fumarate] hydrogels modified with Arg-Gly-Asp peptides and a poly(ethyleneglycol) spacer. *J. Biomed. Mater Res. A,* **61**, 169-179 (2002).

Shin H., Zygourakis K., Farach-Carson M.C., Yaszemski M.J., Mikos A.G. Attachment, proliferation, and migration of marrow stromal osteoblasts cultured on biomimetic hydrogels modified with an osteopontin-derived peptide. *Biomaterials* **25,** 895-906 (2004).

Shoulders M.D., Raines R.T. Collagen structure and stability. *Annu. Rev. Biochem*., **78**, 929-958 (2009).

Shtrichman R., Zeevi-Levin N., Zaid R., Barak E., Fishman B., Ziskind A., Shulman R., Novak A.., Avrahami R., Livne E., Lowenstein L., Zussman E., Itskovitz-Eldor J. The generation of hybrid electrospun nanofiber layer with extracellular matrix derived from human pluripotent stem cells for regenerative medicine applications. *Tissue Eng. Part A.,* **20**, 2756-2767 (2014).

Silber, J. S., Anderson D.G., Daffner S.D., Brislin B.T., Leland J.M., Hilibrand A.S., Vaccaro A.R., Albert T.J. Donor site morbidity after anterior iliac crest bone harvest for single-level anterior cervical discectomy and fusion. *Spine* **28**, 134-139 (2003).

Sill T.J., von Recum H.A. Electrospinning: applications in drug delivery and tissue engineering. *Biomaterials*, **29**, 1989-2006 (2008).

Simpson A.H., Mills L., Noble B. The role of growth factors and related agents in accelerating fracture healing. *J. Bone Joint Surg. Br.,* **88**, 701-705 (2006).

Sistiabudi R., Paderi J., Panitch A., Ivanisevic A. Modification of native collagen with cell-adhesive peptide to promote RPE cell attachement on Bruch's membrane. *Biotechnol. Bioeng.,* **102**, 1723-1729 (2009).

Skaliczki G., Weszl M., Schandl K., Major T., Kovacs M., Skaliczki J., *et al.* Compromised bone healing following spacer removal in a rat femoral defect model. *Acta Physiol. Hung*, **99**, 223-32 (2012)**.**

Sobacchi C., Schulz A., Coxon F. P., Villa A., Helfrich M.H. Osteopetrosis: genetics, treatment and new insights into osteoclast function. *Nat. Rev. Endocrinol*.,**9**, 522–536 (2013).

Sodek J., McKee M.D. Molecular and cellular biology of alveolar bone. *Periodontol. 2000*, **24**, 99-126 (2000).

Sodek K. L., Tupy J. H., Sodek J., Grynpas M. D. Relationships between bone protein and mineral in developing porcine long bone and calvaria. *Bone,* **26**, 189–198 (2000b).

Somerman M.J., Prince C.W., Butler W.T., Foster R.A., Moehring J.M., Sauk J.J., Cell attachment activity of the 44 kilodalton bone phosphoprotein is not restricted to bone cells. *Matrix* **9,** 49-54 (1989).

Sosic D., Brand-Saberi B., Schmidt C., Christ B., Olson E.N. Regulation of *paraxis* expression and somite formation by ectoderm- and neural tube-derived signals. *Dev. Biol.*, **185**, 229-243 (1997).

Sreenath T., Thyagarajan T., Hall B., Longenecker G., D'Souza R., Hong S., Wright J.T., MacDougall M., Sauk J., Kulkarni A.B. 2003 Dentin sialophosphoprotein knockout mouse teeth display widened predentin zone and develop defective dentin mineralization similar to human dentinogenesis imperfecta type III. *J. Biol. Chem.* **278**, 24874–24880 (2003).

Sroga G.E., Karim L., Colon W., Vashishth D. Biochemical Characterization of Major Bone-Matrix Proteins Using Nanoscale-Size Bone Samples and Proteomics Methodology. *Mol. Cell. Proteomics,* **10**, M110.006718 (2011).

Staines K.A. MacRae V.E., Farquharson C. The importance of the SIBLING family of proteins on skeletal mineralization and bone remodeling. *J. Endocrinol.* **214**, 241-255 (2012).

Stegen S., van Gastel N., Carmeliet G. Bringing new life to damaged bone: the importance of angiogenesis in bone repair and regeneration. *Bone,* **70**, 19-27 (2015).

Stein G.S., Lian J.B., Owen T.A. Relationship of cell growth to the regulation of tissue-specific gene expression during osteoblast differentiation. *FASEB J.*, **4**, 3111-3123 (1990).

Stenner D.D., Tracy R.G., Riggs B.L., Mann K.G. Human platelets contain and secrete osteonectin. *Proc. Nat. Acad. Sci. U.S.A.,* **83**, 6892 (1986).

Stevens M.M. Biomaterials for bone tissue engineering. *Materials today*, **11**, 18-25 (2008).

Stevens M.M., George J.H., Exploring and engineering the cell surface interface. Science, **310**, 1135–1138 (2005).

Stevens, M.M. Qanadilo H.F., Langer R., Prasad Shastri V. A rapid-curing alginate gel system: utility in periosteum-derived cartilage tissue engineering. *Biomaterials*, **25**, 887-894 (2004).

Stock U.A., Vacanti J.P. Tissue Engineering: current state and prospects. *Annu. Rev. Med.* **52**, 443 (2001).

Street J. Bao M., deGuzman L., Bunting S., Peale F.V.Jr., Ferrara N., Steinmetz H., Hoeffel J., Cleland J.L., Daugherty A., van Bruggen N., Redmond H.P., Carano R.A., Filvaroff E.H. Vascular endothelial growth factor stimulates bone repair by promoting angiogenesis and bone turnover. *Proc. Natl. Acad. Sci. U.S.A.* **99**, 9656-9661 (2002).

Stuart K., Paderi J., Snyder P.W., Freeman L., Panitch A. Collagen-binding peptidoglycans inhibit MMP mediated collagen degradation and reduce dermal scarring. *PLoS One*, **6**, e22139 (2011).

Sun Y., Chen L., Ma S., Zhou J., Zhang H., Feng J.Q., Qin C. Roles of DMP1 processing in osteogenesis, dentinogenesis and chondrogenesis. Cells, Tissues, Organs, **194,** 199–204 (2011).

Sun Y., Jiang Y., Liu Q., Gao T., Feng J.Q., Dechow P., D'Souza R.N., Qin C., Liu X. Biomimetic engineering of nanofibrous gelatin scaffolds with noncollagenous proteins for enhanced bone regeneration. *Tissue Eng. Part A.*, **19**, 1754-1763 (2013).

Sun Y., Li W., Lu Z., Chen R., Ling J., Ran Q., Jilka R.L., Chen X.D. Rescuing replication and osteogenesis of aged mesenchymal stem cells by exposure to a young extracellular matrix. *FASEB J.,* **25**, 1474-1485 (2011b).

Syedain Z.H., Meier L.A., Bjork J.W., Lee A., Tranquillo R.T. Implantable arterial grafts from human fibroblasts and fibrin using a multi-gradtpulsed flow-stretch bioreactor with noninvasive strength monitoring. *Biomaterials*, **32**, 714-722 (2011).

Taichman R.S. Blood and bone: two tissues whose fates are intertwined to create the hematopoietic stem cell niche. *Blood*, **105**, 2631 –2639 (2005).

Takagi J. Structural basis for ligand recognition by RGD (Arg-Gly-Asp)- dependent integrins. *Biochem. Soc. Trans.,* **32**, 403-406 (2004).

Tang W.J., Yang F., Li Y., de Crombrugghe B., Jiao H., Xiaoo G., Zhang C. Transcriptional regulation of vascular endothelial growth factor by osteoblast-specific transcription factor OSterix (OSx) in osteoblasts. *J. Biol. Chem.,* **287**, 1671-1678 (2012).

Tarnowski C.P., Ignelzi M.A., Morris M.D. Mineralization of developing mouse calvaria as revealed by Raman microspectroscopy. *J. Bone Miner. Res.,* **17**, 1118-1126 (2002).

Termine J.D., Kleinman H.K., Whitson S.W., Conn K.M, McGarvey M.L., Martin G.R. Osteonectin, a bone-specific protein linking mineral to collagen. *Cell*, 99-105 (1981).

Thakkar S., Ghenes C.A., Ahmed M., Kelder C. van Blitterswijk C., Saris D.B.F., Fernandes H.A.M., Moroni L. Mesenchymal stromal cell-derived extracellular matrix influences gene expression of chondrocytes. *Biofabrication*, **5**, 025003 (2013).

Thibault R.A., Scott Baggett L., Mikos A.G., Kasper F.K. Osteogenic differentiation of mesenchymal stem cells on pregenerated extracellular matrix scaffolds in the absence of osteogenic cell culture supplements. *Tissue Eng. Part A.*, **16**, 431-440 (2010).

Tielinen L., Manninen M., Puolakkainen P., Kellomäki M., Tormälä P., Rich J., et al. Inability of transforming growth factor-b1, combined with a bioabsorbable polymer paste, to promote healing of bone defects in the rat distal femur. *Arch. Orthop. Trauma Surg.,* **121**,191-196 (2001).

Tour G., Wendel M., Tcacencu I. Cell-derived matrix enhances osteogenic properties of hydroxyapatite. *Tissue Eng. Part A.,* **17**, 127-137 (2011).

Traub , A. Jodaikin W., Arad T., Veis A.,Sabsay B., Dentin phosphophoryn binding to collagen fibrils. *Matrix*, **12,** 197-201 (1992).

Tsao Y.T., Huang Y.J., Wu H.H., Liu Y.A., Liu Y.S., Lee O.K. Osteocalcin mediates biomineralization during osteogenic maturation in human mesenchymal stromal cells. *Int. J. Mol. Sci*, **18**, E159 (2017).

Tsiridis E., Upadhyay N., Giannoudis P. Molecular aspects of fracture healing: which are the important molecules? *Injury,* **38**, S11-25 (2007).

Tsuji K., Bandyopadhyay A., Harfe B.D., Cox K., Kakar S., Gerstenfeld L., Einhorn T., Tabin C.J., Rosen V. BMP2 activity, although dispensable for bone formation, is required for the initiation of fracture healing. *Nat. Genet.*, **38**, 1424-1429 (2006).

Tyree B., The partial degradation of osteonectin by a bone-derived metalloprotease enhances binding to type I collagen. *J. Bone Miner. Res.,* **4,** 877-883 (1989).

Urist M.R., Silverman B.F., Buring , K. , Dubuc F.L., Rosenberg J.M**.** The bone induction principle. *Clin. Orthop. Relat. Res.* **53**, 243-283 (1967).

Väänänen H.K., Horton M. The osteoclast clear zone is a specialized cell-extracellular matrix adhesion structure. *J. Cell. Sci.,* **108**, 2729-2732 (1995).

Vacanti J. P., Robert R. S., *US Patent,* 5,770,193, (1998).

Vashishth D. The role of the collagen matrix in skeletal fragility. *Current Osteoporosis Reports,* **5**, 62-66 (2007).

Verbogt O., Gibson G.J., Schaffler M.B. Loss of osteocyte integrity in association with microdamage and bone remodeling after fatigue in vivo. *J. Bone Miner. Res.,* **15**, 60-67 (2000).

Verdelis K., Ling Y., Sreenath T., Haruyama N., MacDougall M., van der Meulen M.C., Lukashova L., Spevak L., Kulkarni A.B., Boskey A.L. DSPP effects on in vivo bone mineralization. *Bone,* **43** ,983–990 (2008).

Viguet-Carrin S., Garnero P. Delmas P.D. The role of collagen in bone strength. *Osteoporos. Int.***17***,* 319-336 (2005).

Villars F., Bordenave L., Bareille R., Amédée J. Effect of human endothelial cells on human bone marrow stromal cell phenotype: role of VEGF? *J. Cell Biochem.,* **79**, 672-685 (2000).

Villars F., Guillotin B., Amédée T., Dutoya S., Bordenave L., Bareille R., Amédée J. Effect of HUVEC on human osteoprogenitor cell differentiation needs heterotypic gap junction communication. *Am. J. Physiol. Cell Physiol.* **282**, C775-785 (2002).

Vogel K.G., Trotter J.A. The effect of proteoglycans on the morphology of collagen fibrils formed *in vitro*. *Collagen Rel. Res.*, **7,** 105-114 (1987).

Von Walter P. J Chir und Augen-Heilkunde, **2**,571 (1821).

Vukicevic S., Luyten F. P., Kleinman H. K., Reddi A.H. Differentiation of canalicular cell processes in bone cells by basement membrane matrix components: regulation by discrete domains of laminin. *Cell*, **63**, 437-445 (1990).

Walsh W.R., Vizesi F., Michael D., Auld J., Langdown A., Oliver R., et al. Beta-TCP bone graft substitutes in a bilateral rabbit tibial defect model. *Biomaterials, **29**,* 266.271 (2008).

Wan C., Gilbert S.R., Wang Y., Cao X., Shen X., Ramaswamy G., Jacobsen K.A., Alaql Z.S., Eberhardt A.W., Gerstenfeld L.C., Einhorn T.A., Deng L., Clemens T.L. Activation of the hypoxia- inducible factor-1 alpha pathway accelerates bone regeneration. *Proc. Natl. Acad. Sci. U.S.A.*, **15**, 686-691 (2008).

Wang X, Mabrey J.D., Agrawal C.M.. An interspecies comparison of bone fracture properties. *Biomed. Mater. Eng.,* **8**, 1-9 (1998).

Wang X., Yan C., Ye K., He Y., Li Z., Ding J. Effect of RGD nanospacing on differentiation of stem cells. *Biomaterials*, **34**, 2865-2874 (2013).

Wang X., Ye K., Li Z., Yan C., Ding J. Adhesion, proliferation, and differentiation of mesenchymal stromal cells on RGD nanopatterns of varied nanospacings. *Organogenesis,* **9**, 280-286 (2013b).

Wang X., Ding B., Li B. Biomimetic electrospun nanofibrous structures for tissue engineering. *Mater. Today*, **16**, 229-241 (2013c).

Wang X.L., Xie X.H., Zhang G., Chen S.H., Yao D., He K., et al. Exogenous phytoestrogenic molecule icaritin incorporated into a porous scaffold for enhancing bone defect repair. *J.Orthop. Res.,* **31**, 164-172 (2013d).

Wang Y.H., Liu Y., Maye P., Rowe D.W. Examination of mineralized nodule formation in living osteoblastic cultures using fluorescent dyes. *Biotechnol. Prog.,* **22**, 1697-1701 (2006).

Watanabe H., Yamada Y. Chondrodysplasia of gene knockout mice for aggrecan and link protein. *Glycoconjugate J.*, **19**, 269-273 (2002).

Webster T.J., Ahn E.S. Nanostructured biomaterials for tissue engineering bone. *Adv Biochem Eng Biotechnol.* **103**, 275-308 (2007).

Webster T.J., Schadler L.S., Siegel R.W., Bizios R. Mechanisms of enhanced osteoblast adhesion on nanophase alumina involve vitronectin. *Tissue Eng.*, **7**, 291-301 (2001).

Webster T.J., Siegel R.W., Bizios R. Osteoblast adhesion on nano-phase ceramics. *Biomaterials,* **20**, 1221-1227 (1999).

Wehrhan F., Amann K., Molenberg A., Lutz R., Neukam F.W., Schlegel K.A.. PEG matrix enables cell-mediated local BMP-2 gene delivery and increased bone formation in a porcine critical size defect model of craniofacial bone regeneration. *Clin. Oral Implants Res.,* **23**, 805-813 (2012).

Wei J., Karsenty G. An overview of the metabolic functions of osteocalcin. *Curr. Osteoporos. Rep.* **13**, 180-185 (2015).

Weiner S.,Traub W. Bone structure: from angstroms to microns. *FASEB J*., **6**, 879-885 (1992).

Wen H.B., Moradian-Oldak J., Fincham A.G. Modulation of apatite crystal growth on bioglass by recombinant amelogenin. *Biomaterials*, **20**, 1717-1725 (1999).

Wewer U.M., Ibaraki K., Schjorring P., Durkin M.E., Young M.F., and Albrechtsen R., A potential role for tetranectin in mineralization during osteogenesis. *J. Cel.l Biol.,* **127,** 1767-1775 (1994).

Wiesmann H.P., Meyer U., Plate U., Höhling H.J. Aspects of collagen mineralization in hard tissue formation. *Int. Rev. Cytol.* **242**, 121-156 (2005).

Wilson A. Elements of X-Ray Chrystallography. Addison Wesley; Reading, MA (1970).

Won J.E., Mateos-Timoneda M.A., Castano O., Planell J.A., Seo S.J., Lee E.J., Han C.M., Kim H.W. Fibronectin immobilization on to robotic-dispensed nanobioactive glass/polycaprolactone scaffolds for bone tissue engineering. *Biotechnol. Lett.,* **37**, 935-942 (2015).

Wu A.C., Raggatt L.J., Alexander K.R., Pettit A.R. Unraveling macrophage contributions to bone repair. *Bonekey Rep.,* **2**, 373 (2013).

Wyers A., Linhardt R.J. Neoproteoglycans in tissue engineering. *FEBS J.* **280**, 2511-2522 (2013).

Xu H., Cao B., George A., Mao C. Self-assembly and mineralization of genetically modifiable biological nanofibers driven by beta- structure formation. *Biomacromolecules,* **12**, 2193-2199 (2011).

Xu L., Anderson A. L., Lu Q., Wang J. Role of fibrillary structure of collagenous carrier in bone sialoprotein-mediated matrix mineralization and osteoblast differentiation. *Biomaterials*, **28**, 750-761 (2007).

Xu T., Bianco P., Fisher L.W., Longenecker G., Smith E., Goldstein S., Bonadio J., Boskey A. L., Heegaard A. L., Sommer B., Satomyra K., Dominguez P., Zhao C., Kulkarini A. B., Robey P.G., Young M. F., Targeted disruption of the biglycan gene leads to an osteoporosis-like phenotype in mice. *Nat Genet,* **20,** 78-82 (1998).

Xu H., Othman S.F., Hong L., Peptan I.A., Magin R.L. Magnetic resonance microscopy for monitoring osteogenesis in tissue-engineered construct in vitro. *Phys. Med. Biol.,* **51**, 719-732 (2006).

Yan Q., and Sage E. H. SPARC, a matricellular glycoprotein with important biological functions. *J. Histochem. Cytochem.,* **47**,1495–1506 (1999).

Yanagishita M.Function of proteoglycans in the extracellular matrix. *Acta Pathol. Japonica,* **43,** 283-293 (1993).

Yang B., Chen G., Li J., Zuo Q., Xie D., Chen Y. Wang H., Zheng X., Long J., Tang W., Guo W., Tian W. Tooth root regeneration using dental follicle cell sheets in combination with a dentin matrix-based scaffold. *Biomaterials*, **33,** 2449-2461 (2012).

Yang S., Guo Q., Shores L.S., Aly A., Ramakrishnan M., Kim G.H., Lu Q., Su L., Elisseeff J.H. Use of a chondroitin sulfate bioadhesive to enhance integration of bioglass particles for repairing critical-size bone defects. *J. Biomed. Mater. Res. A,* **103**, 235–242 (2015).

Yang W., Guo D., Harris M.A., Cui Y., Gluhak-Heinrich J., Wu J., Chen X.D. Skinner C., Nyman J.S., Edwards J.R., Mundy G.R., Lichtler A., Kream B.E., Rowe D.W., Kalajzic I., David V., Quarles D.L., Villareal D., Scott G., Ray M., Liu S., Martin J.F., Mishina Y., Harris S.E. Bmp2 in osteoblasts of periosteum and trabecular none links bone formation to vascularization and mesenchymal stem cells. *J. Cell. Sci.,* **126**, 4085-4098 (2013).

Yang X.B., Bhatnagar R.S, Li S., Oreffo R.O.C. Biomimetic collagen scaffolds for human bone cell growth and differentiation. *Tissue Eng.* **10**, 1148-1159 (2004).

Yang X.B., Roach H.I., Clarke N.M., Howdle S.M., Quirk R., Shakesheff K.M., Oreffo R.O. Human osteoprogenitor growth and differentiation on synthetic biodegradable structures after surface modification. *Bone*, ***29,*** 523-531 (2001).

Yang W., Lu Y., Kalajzic I., Guo D., Harris M.A., Gluhak-Heinrich J., Kotha S., Bonewald L.F., Feng J.Q., Rowe D.W., Turner C.H., Robling A.G., Harris S.E. Dentin matrix protein 1 gene cis-regulation: use in osteocytes to characterize local responses to mechanical loading in vitro and in vivo. *J. Biol. Chem.* **280**, 20680-20690 (2005).

Yano K., Namikawa T., Uemura T., Hoshino M., Wakitani S.,Takaoka K., et al. Regenerative repair of bone defects with osteoinductive hydroxyapatite fabricated to match the defect and implanted with combined use of computer-aided design, computer-aided manufacturing, and computerassisted surgery systems: a feasibility study in a canine model. *J. Orthop Sci.*, **17**, 484-489 (2012).

Yaszemski, M.J, Payne R.G., Haynes W.C., Langer R. Evolution of bone transplantation: molecular, cellular and tissue strategies to engineer human bone. *Biomaterials* **17,** 175-185 (1996).

Yavropoulou M.P, Yovo J.G. Osteoclastogenesis-current knowledge and future perspectives*. J. Musculoskelet. Neuronal Interact*., **8**, 204-216 (2008).

Ye J.H., Xu Y.J., Gao J., Yan S.G., Zhao J., Tu Q., Zhang J., Duan X.J., Sommer C.A., Mostoslavsky G., Kaplan D.L., Wu Y.N., Zhang C.P., Wang L., Chen J. Critical size calvarial bone defects healing in a mouse model with silk scaffolds and SATB2-modified iPSCs. *Biomaterials*, **32**, 5065-5076 (2011).

Yoo H.S., Kim T.G., Park T.G. Surface-functionalized electrospun nanofibers for tissue engineering and drug delivery. *Adv. Drug Deliv. Rev.,* **61**, 1033-1042 (2009).

Yoon E., Dhar S., Chun D.E., Gharibjanian N.A., Evans G.R.D. In vivo osteogenic potential of human adipose-derived stem cells/poly lactide-co-glycolic acid constructs for bone regeneration in a rat critical-sized calvarial defect model.*Tissue Eng.,* **13**, 619-627 (2007).

Yoon K., Golub E., Rodan G.A., Alkaline phosphatase transfected cells promote calcium and phosphate deposition. *Connect. Tissue Res.,* **22,** 17-25 (1989).

Yoshiko Y., Candeliere G. A., Maeda N, Aubin J.E. Osteoblast autonomous Pi regulation via Pit1 plays a role in bone mineralization. *Mol. Cell. Biol.*, **27**, 4465–4474 (2007).

Yoshimoto H., Shin Y.M., Terai H., Vacanti J.P. A biodegradable nanofiber scaffold by electrospinning and its potential for bone tissue engineering. *Biomaterials*, **24**, 2077-2082 (2003).

Young B.M., Shankar K., Allen B.P., Pouliot R.A., Schneck M.B., Mikhaiel N.S., Heise R.L. Electrospun decellularized lung matrix scaffold for airway smooth muscle culture. *ACS Biomater. Sci. Eng.*, **3**, 3480-3492 (2017).

Yu J., Vodyanik M.A., Smuga-Otto K., Antosiewicz-Bourget J., Frane J.L., Tian S., Nie J., Jonsdottir G.A., Ruotti V., Stewart R., Slukvin I.I. Thomson J.A. Induced pluripotent stem cell lines derived from human somatic cells. *Science,* **318**, 1917-1920 (2007).

Zaidi M., Blair H.C., Moonga B.S., Abe E., Huang C.L. Osteoclastogenesis, bone resorption and osteoclast-based therapeutics. *J. Bone Miner. Res.,* **18***,* 599-609 (2003).

Zanchetta P., Lagarde N., Uguen A., Marcorelles P. Mixture of hyaluronic acid, chondroitin 6 sulphate and dermatan sulphate used to completely regenerate bone in rat critical size defect model. *J. Craniomaxillofac. Surg.* **40**, 783e7 (2012).

Zeitouni S., Krause U., Clough B.H., Halderman H., Faster A., Blalock D.T., Chaput C.D., Sampson H.W., Gregory C.A. Human mesenchymal stem cell-derived matrices for enhanced osteoregeneration. *Sci. Transl. Med.*, **4**, 132ra55 (2012).

Zelzer E., Glotzer D.J., Hartmann C., Thomas D., Fukai N., Soker S., Olsen B.R. Tissue specific regulation of VEGF expression during bone development requires Cbfa1/Runx2. *Mech. Dev.,* **106**, 97-106 (2001).

Zhang X., Cai Q., Liu H., Heng B.C., Peng H., Song Y., et al. Osteoconductive effectiveness of bone graft derived from antler cancellous bone: an experimental study in the rabbit mandible defect model. *Int. J. Oral Maxillofac. Surg.* **41**, 1330-1337 (2012).

Zhang Y., Cao L., Kiani C., Yang B. L., Hu W., Yang B.B. Promotion of chondrocyte proliferation by versican mediated by G1 domain and EGF-like motifs. *J. Cell. Biochem.*, **73,** 445-457 (1999).

Zhang K., Barragan-Adjemian C., Ye L., Kotha S., Dallas M., Lu Y., Zhao S., Harris M., Harris S.E., Feng J.Q., Bonewald L.F. E11/gp38 selective expression in osteocytes: regulation by mechanical strain and role in dendrite elongation. *Mol. Cell Biol.,* **26**, 4539-4552 (2006).

Zhang Y., Venugopal J.R., El-Turki A., Ramakrishna S., Su B., Lim C.T. Electrospun biomimetic nanocomposite nanofibers of hydroxyapatite/chitosan for bone tissue engineering. *Biomaterials*, **29**, 4314-4322 (2008).

Zhao Q. Shen X., Zhang W., Zhu G., Qi J., Deng L., Mice with increased angiogenesis and osteogenesis due to conditional activation of HIF pathway in osteoblasts are protected from ovariectomy induced bone loss. *Bone,* **50**, 763-770 (2012).

Zheng M.H., Chen J., Kirilak Y., Willers C., Xu J., Wood D. Porcine small intestine submucosa (SIS) is not an acellular collagenous matrix and contains porcine DNA: possible implications in human implantation. *J. Biomed. Mater. Res. B Appl. Biomater.,* **73**, 61-67 (2005).

Zhou Y., Yang D., Chen X., Xu Q., Lu F., Nie J. Electrospun water-soluble carboxyethyl chitosan/poly(vinyl alcohol) nanofibrous membrane as potential wound dressing for skin regeneration. *Biomacromolecules*, **9**, 349-354 (2008).

Zhu X.S., Zhang Z.M., Mao H.Q., Geng D.C., Zou J., Wang G.L., et al. A novel sheep vertebral bone defect model for injectable bioactive vertebral augmentation materials. *J Mater. Sci. Mater. Med.*, **22**, 159-164 (2011).

Zimmermann G., Moghaddam A. Allograft bone matrix versus synthetic bone graft substitutes. *Injury*, **42**, S16-21 (2011).

Ziv V., Weiner S. Bone crystal sizes: a comparison of transmission electron microscopic and X-ray diffraction line width broadening techniques. *Connect. Tissue Res.* **30**, 165-175 (1994).

Zuk P.A., Zhu M., Ashjian P., De Ugarte D.A., Huang J.I., Mizuno H., Alfonso Z.C., Fraser J.K., Benhaim P., Hedrick M.H. Human adipose tissue is a source of multipotent stem cells. *Mol. Biol. Cell.* **13**, 4279-4295 (2002).

Zwingenberger S., Niederlohmann E., Vater C., Rammelt S., Matthys R., Bernhardt R. et al. Establishment of a femoral critical-size bone defect model in immunodeficient mice*. J. Surg. Res.,* **181**, 7-14 (2013).

Zysset P.K, Guo X.E., Hoffler C.E., Moore K.E., Goldstein S.A. Elastic modulus and hardness of cortical and trabecular bone lamellae measured by nanoindentation in the human femur. J. Biomech., **32**, 1005-1012 (1999).

CHAPTER II – The importance of osteocalcin (OC) and osteopontin (OPN) on mesenchymal stem/stromal cells (MSC): their effects on cell proliferation, differentiation, osteogenic maturation and angiogenesis

Outline

Non-collagenous proteins in the bone extracellular matrix (ECM), such as osteocalcin (OC) and osteopontin (OPN), are known to control different aspects of mineralization, however their roles in mesenchymal stem/stromal cells (MSC) differentiation are still unknown. The aim of this study was to investigate the roles of OC and OPN in mineral species production during osteogenesis induced by differentiating MSC into osteoblasts.

MSC were derived from bone marrow aspirates of tibia and femur of $OC^{-/-}$ $OPN^{-/-}$ mice and Wildtype (WT) control mice. We found that proliferation of $OC^{-/-}$ $OPN^{-/-}$ MSC was affected and their capacity to differentiate into osteoblasts was decreased, although $OC^{-/-}$ $OPN^{-/-}$ MSC were able to differentiate into adipogenic and chondrogenic lineages. After 21 days of osteogenic differentiation, calcium deposition levels of $OC^{-/-}$ $OPN^{-/-}$ MSC demonstrated a significant reduction compared with WT MSC. These results were confirmed using histochemical stainings (Von Kossa and ALP stainings), Xylenol orange staining, as well as immunofluorescence stainings. After osteogenic differentiation, mRNA levels of osteogenic markers (Col I, Runx2, OPN, OC) were downregulated in $OC^{-/-}$ $OPN^{-/-}$ MSC, confirming the impairment of osteogenesis.

Using Raman spectroscopy and Fourier-transform infrared spectroscopy (FTIR), we found that the maturation of mineral species was affected by the suppression of OC and OPN levels. The mineral species maturation from $OC^{-/-}$ $OPN^{-/-}$ MSC was delayed compared with the control group. After 21 days of osteogenic differentiation, minerals produced by WT MSC presented the peak of hydroxyapatite (HAP) at 960 cm^{-1}, however this peak was not observed in minerals produced by $OC^{-/-}$ $OPN^{-/-}$ MSC. On the other hand, minerals produced by $OC^{-/-}$ $OPN^{-/-}$ MSC presented a Raman signal of β-TCP at 970 cm^{-1}, an HAP precursor, after 21 days of osteogenic differentiation. Interestingly, only after 30 days of osteogenic differentiation, the HAP peak was detected in mineral species produced by $OC^{-/-}$ $OPN^{-/-}$ MSC, indicating that when OC and OPN were insufficiently expressed the maturation of mineralization was delayed.

Moreover, the angiogenic potential of $OC^{-/-}$ $OPN^{-/-}$ MSC was impaired and the role of extracellular OC and OPN in MSC angiogenesis and osteogenic differentiation was further demonstrated. When $OC^{-/-}$ $OPN^{-/-}$ MSC were supplemented with extracellular OC and OPN, MSC were able to regain their proliferative potential and their osteogenic differentiation capacity. Notably, when OPN was added extracellularly, the angiogenic potential of $OC^{-/-}$ $OPN^{-/-}$ MSC was reestablished, indicating that OPN is an important key mediator of angiogenesis.

These results confirmed, at a cellular level, that OC and OPN are important regulators of bone mineralization and provide new insights into forming high quality bone, relevant for treatment of fracture healing in older and osteoporotic bone.

II.1. Introduction

Skeletal tissue remodeling is a fundamental process that undergoes throughout life. Bone remodeling is characterized by the degradation of mineralized tissue as a result of osteoclast resorption, followed by the recruitment of osteoprogenitor cells that differentiate into mature osteoblasts. These cells can produce new mineralized bone extracellular matrix (ECM) composed of different proteins that are responsible to support mineralization (Hadjidakis & Androulakis 2006). Several ECM molecules have been shown to contribute to regulation of osteoblast survival and differentiation, including fibronectin (Globus *et al.* 1998), collagen (Carvalho *et al.* 2003, Suzawa *et al.* 2002), osteopontin (Huang *et al.* 2004, Kojima *et al.* 2004), vitronectin (Salasznyk *et al.* 2004) and bone sialoproteins (Gordon *et al.* 2007).

Bone extracellular matrix has two components: a mineral part comprising hydroxyapatite (70-90%) and an organic part (10-30%) of primarily collagen (approx. 90% of organic matrix) with the rest being non-collagenous proteins (~10%) (Sroga *et al.* 2011, Vashishth 2007), including glycoproteins and proteoglycans. Although non-collagenous proteins correspond to a small amount of the total protein mass of the bone ECM, they have been found to be biologically active and to modulate different functions in bone such as cell adhesion (Harris *et al.* 2000, Horton *et al.* 1995, Roche *et al.* 1999), cell differentiation (Ravindran & George 2014), mineralization (Harris *et al.* 2000, Boskey 1989) and bone resorption/remodeling (Razzouk *et al.* 2002, Ek-Rylander *et al.* 1994). Of these non-collagenous proteins, osteopontin (OPN) and osteocalcin (OC) are two of the most abundant, representing 10-20% of the non-collagenous proteins in bone tissue (Sroga *et al.* 2011).

Moreover, abnormal expression of proteoglycans in bone pathologic conditions has also been suggested to modulate bone mineralization (Theocharis *et al.* 2006). Proteoglycans consist of a core protein onto which glycosaminoglycan (GAG) side-chains are attached (Mania *et al.* 2009). Therefore, changes in GAG composition of bone matrix may help to understand mineralization process.

OPN is an arginine-glycine-aspartate (RGD)-containing adhesive glycoprotein (Denhardt & Guo 1993) and, through their RGD domain, it can bind to $\alpha_v\beta_3$ integrins. Additionally, OPN can also present an RGD-independent mechanism by engaging CD44 (Weber *et al.* 1996), a cell surface adhesion molecule, involved in cell-cell and cell-matrix interactions. The precise function of OPN is still unknown, however its ability to bind several components suggests that OPN may have a multifaceted role in the regulation of several physiological processes such as collagen organization, cell adhesion, cell viability, cell migration, angiogenesis and mineralization (Sroga *et al.* 2011, Denhardt & Guo 1993, Rodriguez *et al.* 2014). In contrast, OC is the most abundant bone specific non-collagenous protein in bone ECM and it plays a crucial role in matrix mineralization, having affinity for calcium, through its gama-carboxyglutamic acids (Ducy *et al.* 1996). OC also acts in cell signalling and bone resorption and deposition, by recruiting osteoclasts and osteoblasts, respectively (DeFranco *et al.* 1991).

Previous studies conducted by our group and others have demonstrated the role of OPN and/or OC as structural molecules in bone matrix (Sroga *et al.* 2011, Nikel *et al.* 2013, Morgan *et al.* 2015, Bailey *et al.* 2017), linking the organic and inorganic matrices by forming a tether between collagen fibrils and mineral crystals (Poundarik *et al.* 2012). Moreover, loss and modification of OC and/or OPN from bone matrix, known to occur with tissue age (Sroga *et al.* 2011) and with aging in humans (Boskey & Coleman 2010, Plantalech *et*

al. 1991, Ingram *et al.* 1994, Grynpas *et al.* 1994), lead to loss of structural integrity (Poundarik *et al.* 2012) and altered mineralization (Boskey *et al.* 1989b, Rodriguez *et al.* 2014).

At the cellular level, several studies have suggested that alterations in the levels of OPN and OC, by genetic ablation or antibody neutralization, in stem cell cultures may have a negative effect on mineralization possibly due to impaired osteogenic differentiation of mesenchymal stem/stromal cells (MSC) (Chen *et al.* 2014). *In vivo* studies have also reported the retarded bone formation capacity of $OPN^{-/-}$ MSC. Moreover, some studies have demonstrated that OC modulates the mineral species maturation during osteogenic differentiation of MSC (Tsao *et al.* 2017).

Therefore, in this study we hypothesized that reduced expression of both OPN and OC has a negative impact on cell proliferation, osteogenic differentiation, mineralization and angiogenesis *in vitro*.

Biomineralization occurs from a heterogeneous solution composed by calcium and phosphate ions. Hydroxyapatite (HAP), $Ca_{10}(PO_4)_6(OH)_2$, is the major mineral component of bone tissue and can be found between extracellular matrices of collagen fibers, as well as embedded in non-collagenous proteins. Previous studies have shown that HAP distribution increased with maturation of bone tissue and it can be used as a biomarker during osteogenic differentiation of MSC. Moreover, different mineral species can be found in bone besides HAP, such as amorphous calcium phosphate (ACP), octacalcium phosphate (OCP), β-tricalcium phosphate (β -TCP) and dicalcium phosphate dihydrate (DCPD) (Boskey 1992, Johnsson & Nancollas 1992).

Different techniques have been applied to detect these mineral species during mineralization, such as Raman and Fourier-transform infrared (FTIR) spectroscopy (Hung *et al.* 2013, Egusa *et al.* 2014, Stewart *et al.* 2002). Raman spectra of MSC-derived osteoblasts indicated that these mineral species are produced at different stages of osteogenic differentiation (Hung *et al.* 2013). Thus, we have also developed a protocol using Raman spectroscopy to evaluate the maturation of $OC^{-/-}$ $OPN^{-/-}$ MSC-derived osteoblasts by monitoring the production of different mineral matrices, including HAP, OCP and β-TCP. However, the mechanism of different mineral species production is still unclear.

In this study, we isolated bone marrow-derived MSC from WT and $OC^{-/-}$ $OPN^{-/-}$ mice and examined the role of both OPN and OC together in the regulation of cell proliferation, trilineage differentiation ability (adipogenic, chondrogenic and osteogenic) and angiogenic properties. Moreover, using spectroscopic analysis, we assessed the maturation level of mineral species produced by $OC^{-/-}$ $OPN^{-/-}$ MSC.

Furthermore, the angiogenic potential of $OC^{-/-}$ $OPN^{-/-}$ MSC was investigated, since these non-collagenous proteins have been reported to have important roles in angiogenesis (Chakraborty *et al.* 2008, Tang *et al.* 2007, Takahashi *et al.* 2002, Cantatore *et al.* 2005). We further evaluated the effects of extracellular OPN and OC by applying exogenous OC/OPN during MSC osteogenic differentiation.

We confirmed that OC and OPN are involved in regulation of proliferation, osteogenic differentiation, mineralization and angiogenesis of MSC. OC and OPN deficiency impaired the differentiation of MSC by significant reduction of mineralization. Osteogenic gene expression markers, such as Runx2, Col I, OC and OPN were downregulated in the *OC/OPN*-deficient MSC, resulting in a significant delay of osteogenesis and mineralization.

This study presented evidences of close association between OC/OPN and MSC proliferation, mineralization and angiogenesis, providing new insights about how these proteins can act at the cellular level.

II.2. Materials & Methods

II.2.1. Bone marrow-derived MSC isolation

$OC^{-/-}$ $OPN^{-/-}$ mutant C57BL6 mice were obtained from Prof. Caren Gundberg (Dept. of Orthopedics and Rehabilitation, Yale). Wildtype control mice (C57BL6) were purchased from the Jackson Laboratory (Bar Harbor, ME, USA). All procedures were approved by the Institutional Animal Care and Use Committee (IACUC) of Rensselaer Polytechnic Institute.

Mice aged eight months were sacrificed and femur and tibia were collected. MSC were isolated from tibia and femur bone marrow (BM) according to previous protocols (Nadri *et al.* 2007). Briefly, bone marrow aspirate was flushed into a tube and the solution was triturated extensively. Then, the solution was carefully added onto Ficoll (GE Healthcare, Chicago, IL) and centrifuged at 400 rcf for 40 min. After that, the top layer was discarded and the second layer was collected. After some washes, low-glucose Dulbecco's Modified Eagle Medium (DMEM: Gibco, Grand Island, NY) supplemented with 15% fetal bovine serum (FBS: Gibco) and 1% antibiotic-antimycotic (Gibco) (DMEM+15% FBS) was added to the cell pellet and transferred to a T-75 flask and kept at 37ºC, 5% O_2, 5%CO_2 in an humidified atmosphere. Non-adherent cells were removed after 72 hours. Medium was changed every 3-4 days. After confluence, cells were cryopreserved in liquid nitrogen.

II.2.2. Cell culture

BM MSC from WT and $OC^{-/-}$ $OPN^{-/-}$ mice were thawed and plated on T-75 flasks using DMEM+15%FBS (Gibco) and kept at 37ºC, 5%O_2 and 5%CO_2 in an humidified atmosphere. Medium renewal was performed every 3-4 days. Cells between passages 2 and 9 were used. Human umbilical vein endothelial cells (HUVEC) were purchased from Lonza (Basel, Switzerland) and maintained in commercial Endothelial Growth Medium-2 (EGM-2: Lonza) at 37ºC, 21% O_2 and 5%CO_2.

II.2.3. Flow cytometry analysis

Cells were harvested and washed with the staining buffer. The cells were suspended in staining buffer at a concentration of 1 $x10^7$ cells/ml. 100 µl of cell suspension was incubated for 45 min at room temperature in the dark with each antibody (CD29, CD105, Sca-1, CD45) or with the corresponding isotype control antibody (R&D Systems, Minneapolis, MN). Following the incubation, excess antibody was removed by washing the cells with the staining buffer. Flow cytometric analysis was performed using LSR II flow cytometer (BD Biosciences, San Jose, CA). BD FACSDiva™ software was used for data analysis.

II.2.4. Cell morphology

$OC^{-/-}$ $OPN^{-/-}$ and WT MSC were seeded on 24-well plates (5000 cells/cm^2, DMEM+15% FBS) and cell morphology was assessed after 24 h and 4 days of culture. Cells were washed twice with phosphate-buffered saline (PBS: Gibco) fixed with 4% paraformaldehyde (PFA: Santa Cruz Biotechnology, Dallas, TX) for 20 min and then permeabilized with 0.1% Triton X-100 (Sigma-Aldrich, St. Louis, MO) for 10 min. After permeabilization, cells were incubated with phalloidin (Invitrogen, Carlsbad, CA) (dilution 1:250, 2 µg/ml) for 45 min in the dark. Then, cells were washed twice with PBS and counterstained with DAPI (Invitrogen) (1.5 µg/ml) for 5 min and then washed with PBS. The fluorescent staining was imaged by fluorescence microscope (Olympus IX51 Inverted Microscope: Olympus America Inc., Melville, NY) and recorded by an attached digital camera.

II.2.5. Proliferation assays

$OC^{-/-}$ $OPN^{-/-}$ and WT MSC were expanded during 9 consecutive passages. Cells were plated into a 12 well-plate at two different cell seeding densities: 3000 cells/cm^2 and 10000 cells/cm^2 using DMEM+15% FBS as growth medium. After reaching 80% confluency, cells were harvested using TrypLE™ solution (Gibco) and plated into a different well, using the same cell densities. Fold increase and cumulative population doublings were calculated for each cell type and for both cell densities.

A kinetic study was also performed in a 12-well plate at a density of 5000 cells/cm^2 per well in triplicate. After day 1, 4, 7,12 and 15, cells from $OC^{-/-}$ $OPN^{-/-}$ and WT were harvested and counted to calculate cell growth curves.

II.2.6. Multilineage differentiation assays

To verify multipotency of mouse MSC, an *in vitro* differentiation assay kit from R&D Systems was used. MSC were grown in 24-well plate with medium changes every 3-4 days. For adipogenic differentiation, MSC were cultured in DMEM+10%FBS (Gibco) with adipogenic supplement containing hydrocortisone, isobutylmethylxanthine, and indomethacin (adipogenic differentiation medium, R&D Systems). The presence of adipocytes was verified by staining for triglycerides with Oil Red O (Sigma-Aldrich), an indicator of intracellular lipids accumulation. For osteogenic differentiation, MSC were cultured in DMEM+10%FBS (Gibco) with osteogenic supplement containing dexamethasone, ascorbic acid and β-glycerophosphate (osteogenic differentiation medium, R&D Systems). These cultures were then stained with alkaline phosphatase (ALP) and Von Kossa stainings to identify ALP activity and calcium deposition, respectively, indicating active osteoblasts. For chondrogenic differentiation, MSC were transferred to a conical tube and chondrogenic differentiation medium was added, containing dexamethasone, ascorbate-phosphate, proline, pyruvate, recombinant human TGF-β3 and ITS supplement (insulin, transferrin, selenious acid, bovine serum albumin, and linoleic acid, R&D Systems). These cultures were stained with Alcian Blue (Sigma-Aldrich).

For histological stainings cells were fixed with 4% of PFA for 20 min. Then, cells were rinsed in miliQ water during 15 min and then incubated with the different reagents, such as Oil Red O for adipogenic

differentiation and Alcian Blue for chondrogenic diffentiation. For osteogenic differentiation, cells were incubated with a Fast Violet solution (Sigma-Aldrich) and Naphthol AS-MX Phosphate Alkaline solution (Sigma-Aldrich) in a final concentration of 4% (v/v) for 45 min, at room temperature in the dark. Cells were, then, washed three times with miliQ water and once with PBS. Then, Von Kossa staining was performed by incubating the cells with a 2.5% silver nitrate solution (Sigma-Aldrich) during 30 min at room temperature in the dark. Cells were washed three times with miliQ water and visualized using an inverted microscope (Olympus IX51 Inverted Microscope) at a magnification of 10x, and recorded by an attached digital camera.

To visualize the mineral deposits formed in the cell culture after osteogenic differentiation, a 20 mM Xylenol orange (XO) solution (Sigma-Aldrich) was added to the previously fixed cells and incubated for 1 h at room temperature in the dark. After that, cells were washed with miliQ water and the cell nuclei were counterstained with DAPI (Invitrogen) (1.5 µg/ml) for 5 min and then washed with PBS. The fluorescent staining of the produced minerals was imaged by fluorescence microscope (Olympus IX51 Inverted Microscope) and recorded by an attached digital camera.

II.2.7. Immunofluorescent staining

MSC were plated in 24-well plate and adipogenic, chondrogenic and osteogenic differentiation were induced. After different timepoints of differentiation, cells were washed with PBS and fixed with 4% PFA for 20 min at room temperature. Then, cells were washed three times with 1% bovine serum albumin (BSA) in PBS for 5 min. Cells were permeabilized and blocked with a solution of 0.3%Triton X-100, 1% BSA and 10% donkey serum in PBS at room temperature for 45 min. Primary antibodies including goat anti-mouse FABP4, sheep anti-mouse collagen II and goat anti-mouse osteopontin (10 µg/ml in 0.3%Trinton X-100, 1%BSA, 10% donkey serum) (R&D Systems) were added into the samples followed by incubation overnight at 4ºC. After washing with 1%BSA in PBS, a NorthernLights^{TM} 557-conjugated anti-goat IgG secondary antibody and anti-sheep IgG secondary antibody(dilution 1:200 in 1%BSA PBS) (R&D Systems) was added into the samples and incubated in the dark for 1 h at room temperature. Finally, the cell nuclei were counterstained with DAPI (Invitrogen) (1.5 µg/ml) for 5 min and then washed with PBS. The fluorescent staining was imaged by fluorescence microscope (Olympus IX51 Inverted Microscope) and recorded by an attached digital camera.

II.2.8. Calcium quantification assay

For determination of total calcium content, samples (n=3) were washed twice with PBS (Gibco) and extracted in 0.5M HCl solution (Sigma-Aldrich). Accumulated calcium was removed from the cellular component by shaking overnight at 4ºC. The consequent supernatant was utilized for calcium determination according to the manufacturer's instructions contained in the calcium colorimetric assay kit (Stanbio Laboratory, Boerne, TX). Absorbance at 550 nm was measured for each condition and normalized to the total number of cells, after 7, 15 and 21 days of osteogenic differentiation.

II.2.9. Alkaline phosphatase activity

ALP activity was detected using a colorimetric ALP kit (BioAssays Systems, Hayward, CA) according to the manufacturer's protocol. Samples (n=3) were washed with PBS (Gibco) and were incubated in the lysis buffer (0.1% Triton X-100 in PBS) by shaking for 30 min at room temperature. The lysate was added to p-nitrophenyl phosphate solution (10 mM) provided with the ALP kit. The absorbance was measured at 405 nm and normalized to the total number of cells in each sample, after 7, 15 and 21 days of osteogenic differentiation.

II.2.10. qRT-PCR analysis

Total RNA was extracted with a RNeasy Mini Kit (QIAGEN, Hilden, Germany). cDNA was synthesized from 20 ng of total RNA using iScript^{TM} Reverse Transcription Supermix (Bio-Rad, Hercules, CA). Reaction mixtures (20μl) were incubated in a thermal cycler for 5 min at 25ºC, 30 min at 42ºC and 5 min at 85ºC and then were maintained at 4ºC. The sequences of the specific primer sets used are given in Table II.1.

The quantitative reverse transcription-polymerase chain reaction (qRT-PCR) was performed using PowerUp SYBR Green Master Mix (Applied Biosystems, Foster City, CA) and StepOnePlus real-time PCR system (Applied Biosystems). All reactions were carried out at 95ºC for 10 min, followed by 40 cycles of 95ºC for 15 sec and 60ºC for 1 min and all were performed in triplicate. β-actin was used as internal control. A threshold cycle (Ct) was observed in the exponential phase of amplification, and quantification of relative expression levels was performed with the use of standard curves for target genes and endogenous control. Geometric means were used to calculate the ΔΔCt values and are expressed as $2^{-\Delta\Delta Ct}$. The mean values from triplicate analysis were compared. The value of undifferentiated WT MSC samples (control) was set as 1 and was used to calculate the fold difference in the target gene.

Table II.1. Sequences of primers used for qRT-PCR analysis

Genes	Sequences
***β*-actin**	For: 5' TTC CAG CCT TCC TTC TTG GG Rev: 5' TGT TGG CAT AGA GGT CTT TTA CGG
Col I	For:5' GCT CCT CTT AGG GGC CAC T Rev: 5' CCA CGT CTC ACC ATT GGG G
Runx2	For: 5' CCA CGG CCC TCC CTG AAC TCT Rev: 5' ACT GGC GGG GTG TAG GTA AAG GTG
ALP	For: 5' CCA ACT CTT TTG TGC CAG AGA Rev: 5' GGC TAC ATT GGT GTT GAG CTT TT
OPN	For: 5' AGC AAG AAA CTC TTC CAA GCA A Rev: 5' GTG AGA TTC GTC AGA TTC ATC CG
OC	For: 5' GCC CTG AGT CTG ACA AAG GTA Rev: 5' GGT GAT GGC CAA GAC TAA GG

II.2.11. *In vitro* endothelial cell tube formation assay

In order to study the role of OC and OPN on angiogenesis a tube formation assay was performed. Red fluorescent protein (RFP)-tagged human umbilical vein endothelial cells (HUVEC) ($2x10^4$ cells) were cultured on a Matrigel substrate (50 μl/well) (Corning, Corning, NY) in a 96-well plate (37ºC, 21% O_2, 5%CO_2), incubated with conditioned medium (CM) from WT and $OC^{-/-}$ $OPN^{-/-}$ MSC. This conditioned medium was collected after 72 h in DMEM basal (without FBS) (37ºC, 5%O_2, 5% CO_2). HUVEC were also incubated with DMEM+10%FBS and endothelial growth medium (EGM-2: Lonza), as positive controls, whereas DMEM basal was used as a negative control. After incubation for 8h at 37ºC, three photomicrographs per well were imaged by fluorescence microscope (Olympus IX51 Inverted Microscope) and the number of tubes formed were counted with the use of ImageJ (NIH) software.

To evaluate the angiogenic properties of $OC^{-/-}$ $OPN^{-/-}$ MSC, these MSC were also cultured on a Matrigel substrate with DMEM+10% FBS for 8h at 37ºC. Photomicrographs were taken to evaluate the ability of MSC to form a capillary structure.

In a different assay, $OC^{-/-}$ $OPN^{-/-}$ and WT MSC were co-cultured with RFP-tagged HUVEC (1:1, $2x10^4$ cells) and cultured on a Matrigel substrate using EGM-2 to evaluate HUVEC distribution. Moreover, to evaluate the extracellular effect of OC and OPN, the co-cultures of HUVEC and $OC^{-/-}$ $OPN^{-/-}$ MSC were cultured on a Matrigel substrate with EGM-2 supplemented with OC fragment 1-49 human (Sigma-Aldrich) and/or recombinant human OPN (R&D Systems) (1 μg/ml) or with recombinant human VEGF (R&D Systems) (50 ng/ml). Therefore, after 8h of incubation at 37ºC, micrographs were taken under fluorescence microscope (Olympus IX51 Inverted Microscope) and the number of tubes formed were counted with the use of ImageJ (NIH) software, to analyze if HUVEC were able to recover their tube formation capability.

II.2.12. Cell migration assay

24-well tissue culture plates were collagen-coated by incubation in 0.2 mg/ml of collagen type I solution (Sigma-Aldrich) for 2h at 37ºC before rinsing with PBS (Gibco). Each well was seeded with HUVEC at 10000cells/cm^2 and maintained at 37ºC, 21% O_2, 5% CO_2 conditions for 48h to allow cell adhesion and the formation of a confluent monolayer. These confluent monolayers were then scratched with a sterile pipette tip, creating a scratch (wound) of approximately 0.25-0.3mm in width. After creating the scratch, culture medium was then removed and replaced with conditioned medium which had been generated from WT and $OC^{-/-}OPN^{-/-}$ MSC cultured for 72h using growth medium DMEM without FBS (37ºC, 5% O_2, 5%CO_2).

Migration of HUVEC was monitored by collecting images at various time intervals (0h, 4h, 8h 10h and 12h) after the scratch was performed. The migration distance was quantified with the use of ImageJ (NIH) software, measuring the width of the scratch at previously defined points along its length (top, middle and bottom of the field of view). Data has been presented as extent of the cell migration, i.e. the percentage by which HUVEC migrate for each given time point compared with the original scratch width.

II.2.13. Raman and FTIR Spectroscopy

For sample preparation, MSC were harvested at different timepoints and were washed twice with dH_2O. After that, cells were kept at -80ºC and were then freeze-dried. Lyophilized samples were used for Raman and FTIR analysis.

Raman microscope (Senterra Raman microscope: Bruker, Billerica, MA) was used as the setup of Raman spectroscopy. A 100mW laser operating at 785 nm was used to provide the Raman excitation light source. The objective lens used was 20x. Raman signals were collected from the spectrum between 600 and 1800 cm^{-1} with an integration time of 20 s. Raman spectra were obtained from at least 3 locations selected from each sample. Three independent samples were performed. Multipoint baseline correction by OPUS software (Bruker) was used.

Attenuated total reflectance-Fourier transform infrared (ATR-FTIR) spectra of lyophilized minerals from cell cultures were collected with a Varian 660-IR FTIR spectrophotometer (Varian Inc. USA).

II.2.14. Scanning electron microscope evaluation

The morphological and structural characterization of MSC was performed using a field emission scanning electron microscope (FE-SEM, FEI-Versa 3D Dual Beam, Hillsboro, OR). Elemental analysis of MSC after osteogenic differentiation was performed using a scanning electron microscope attached with an energy dispersive electron probe X-ray analyzer (SEM-EDS: Carl Zeiss ultra 1540 dual beam FIB/SEM system). Prior to imaging, samples were dehydrated using a graded series of ethanol and dried in a critical CO_2 freeze dryer. Then, samples were mounted on a holder and sputter-coated with a thin layer of 60% gold-40% palladium (Au-Pd). Samples were imaged at several magnifications using an accelerating voltage of 2-3 kV.

II.2.15. GAG disaccharide sample preparation: isolation, digestion and AMAC-labeling

Cells (WT and $OC^{-/-}$ $OPN^{-/-}$ MSC) were treated with the BugBuster 10X Protein Extraction Reagent (Millipore Sigma, MA USA) and sonicated for 1 hour. Then, samples were desalted by passing through a 3 KDa molecular weight cut off (MWCO) spin column (Millipore, MA USA), and washed three times with distilled water. The casing tubes were replaced and 300 µl of digestion buffer (50 mM ammonium acetate containing 2 mM calcium chloride adjusted to pH 7.0) was added to the filter unit. Afterwards, recombinant heparin lyases I, II, III (pH optima 7.0−7.5) and recombinant chondroitin lyase ABC (10 mU each, pH optimum 7.4) were added to each sample, mixed well by pipetting. Samples GAG enzymatic digestion was conducted by incubation overnight at 37°C. The enzymatic reaction was terminated by centrifugation to remove the enzymes and the filter unit was washed twice with 200 µl of distilled water. The final filtrates containing the disaccharide products were lyophilized and kept at -20°C until labelling.

Dried cell samples were 2-Aminoacridone (AMAC)-labelled by adding 10 µl of 0.1M AMAC in dimethylsulfoxide (DMSO)/acetic acid (17/3, V/V) solution by incubating at room temperature for 10 min, followed by addition of 10 µl of 1M aqueous $NaCNBH_4$ solution and incubation for 1 hour at 45°C. A mixture containing all 17 chondroitin sulfate (CS), heparin sulfate (HS) and hyaluronic acid (HA) disaccharide

standards prepared at a concentration of 0.5 ng/µl was similarly AMAC-labeled and used for each run as an external standard. After the AMAC-labeling reaction, the samples were centrifuged and respective supernatants were recovered.

II.2.16. Compositional analysis of GAG disaccharides by LC-MS/MS

The disaccharide analysis was performed according to a previously reported method (Sun *et al.* 2015). LC was performed on an Agilent 1200 LC system at 45 °C using an Agilent Poroshell 120 ECC18 (2.7 µm, 3.0 × 50 mm) column. Mobile phase A (MPA) was 50 mM ammonium acetate aqueous solution, and the mobile phase B (MPB) was methanol. The mobile phase passed through the column at a flow rate of 300 µl/min. The gradient used was the following: 0-10 min, 5-45% B; 10-10.2min, 45-100%B; 10.2-14min, 100%B; 14-22min, 100-5%B. The injection volume used for all the samples was 5 µl.

A triple quadrupole mass spectrometry system equipped with an ESI source (Thermo Fisher Scientific, San Jose CA, USA) was used a detector. The online MS analysis was performed at the Multiple Reaction Monitoring (MRM) mode with the MS parameters: negative ionization mode with a spray voltage of 3000 V, a vaporizer temperature of 300 °C, and a capillary temperature of 270 °C.

Data analysis was performed using Thermo Xcalibur™ software (Thermo Fisher Scientific, San Jose CA, USA). The disaccharides in different cell samples were quantified via comparison of the sample peak area to that of an external standard.

II.2.17. Statistical analysis

Each experiment was conducted in triplicate. Statistical analysis of the data was performed using Student's t-test, comparing each condition with the WT control groups at the same timepoint, using GraphPad Prism version 7. The statistical significance of results is reported at 95% confidence intervals ($P<0.05$).

II.3. Results

II.3.1. Bone marrow-derived MSC isolation and characterization

MSC cell lines were isolated from bone marrow (BM) of $OC^{-/-}OPN^{-/-}$ and WT adult mice (Figure II.1a). Cell morphology was evaluated by staining the cells with DAPI and phalloidin after 24 hours and 4 days of cell culture. The morphology of MSC from WT and OC/OPN double knockout (KO) mice was similar, however we could observe that after 4 days of cell culture, WT MSC proliferated much more than $OC^{-/-}OPN^{-/-}$ MSC, since higher number of WT MSC were observed compared with $OC^{-/-}OPN^{-/-}$ MSC (Figure II.1b).

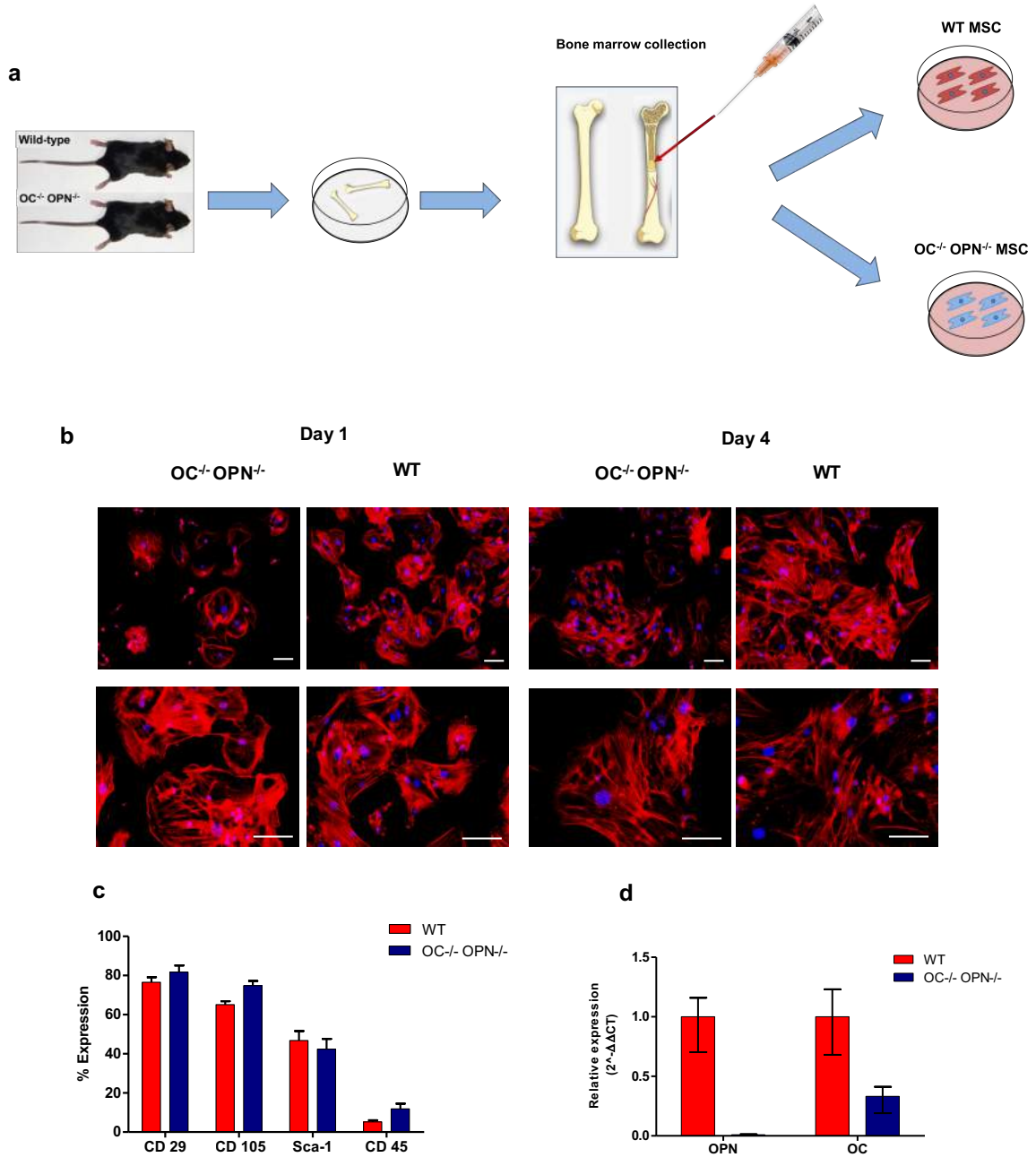

Figure II.1. Bone marrow-derived MSC isolation and characterization. **a)** Schematics of BM-MSC isolation from femur and tibia of $OC^{-/-}$ $OPN^{-/-}$ and WT mice. **b)** Cell morphology after 24h and 4 days of culture. Red: phalloidin, blue: DAPI. Scale bars, 100 µm. **c)** Percentage of cell expression of CD29, CD105, Sca-1 and CD45. **d)** Relative expression levels of *OPN* and *OC* genes in $OC^{-/-}$ $OPN^{-/-}$ MSC compared to WT MSC.

The expression of surface markers such as CD105, CD29 and Sca-1 was confirmed by flow cytometry, as well as the absence of expression of the surface marker CD45 for MSC isolated from both WT and $OC^{-/-}OPN^{-/-}$ mice, confirming the successful isolation of MSC from both groups. The downregulation of OC and OPN osteogenic genes was also confirmed by qRT-PCR for $OC^{-/-}$ $OPN^{-/-}$ MSC.

II.3.2. GAG disaccharide composition of $OC^{-/-}$ $OPN^{-/-}$ MSC

The total amount of GAG (Figure II.2a), as well as the respective heparin sulfate (HS), chondroitin sulfate (CS) and hyaluronic acid (HA) GAG amounts (Figure II.2b) for WT and $OC^{-/-}$ $OPN^{-/-}$ MSC were obtained after liquid chromatography-tandem mass spectrometry (LC-MS/MS) analysis and normalized to the same total cell numbers ($1x10^5$ cells per sample). As it is possible to observe in Figure II.2, $OC^{-/-}OPN^{-/-}$ MSC presented higher GAG content than WT MSC. Regarding HS, CS and HA total composition, there were evident differences in the GAG compositions of the different cell types (Figure II.2b). $OC^{-/-}$ $OPN^{-/-}$ MSC were composed mainly by CS (153.27 ng/ml), followed by lower average amounts of HS (31.11 ng/ml) and HA (20.93 ng/mg). WT MSC were composed by CS (5.67 ng/ml), HS (3.83 ng/ml) and lower amounts of HA (0.22 ng/ml). Interestingly, the total amount of GAG decreased when cells were differentiated under osteogenic differentiation medium after 21 days for both cell types (WT and $OC^{-/-}$ $OPN^{-/-}$). WT MSC differentiated into an osteogenic lineage were composed by a very low amount of GAG, compared with $OC^{-/-}$ $OPN^{-/-}$ MSC differentiated into osteoblasts.

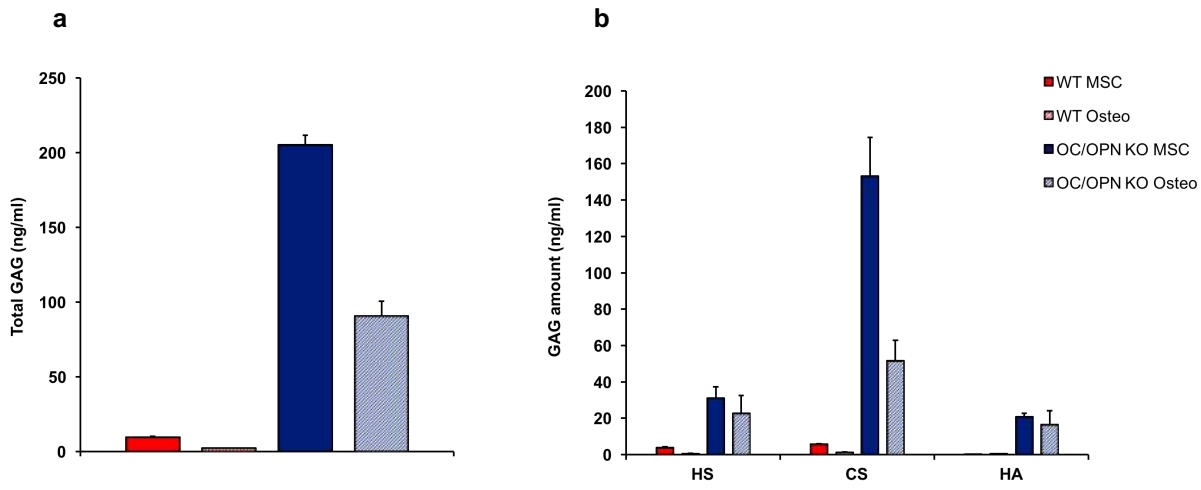

Figure II.2. GAG composition of WT MSC and $OC^{-/-}$ $OPN^{-/-}$ MSC. **a)**Total GAG amount (ng/ml). **b)** HS, CS, HA total amounts (ng/ml). Results are presented as mean ± SD of three biological replicates (n=3).

The average GAG disaccharide percentage compositions of $OC^{-/-}$ $OPN^{-/-}$ MSC were determined and compared with WT MSC (Figure II.3). Both undifferentiated cells (WT and $OC^{-/-}$ $OPN^{-/-}$ MSC) presented significantly different HS, CS and HA percentage compositions, however when both cell types were differentiated into osteoblasts, they presented similar GAG disaccharide percentage composition. In terms of GAG relative percentages, WT MSC were mainly composed by CS (59%), followed closely by HS (39%) and HA (2%). Moreover, $OC^{-/-}$ $OPN^{-/-}$ MSC presented a higher relative average percentage of CS (75%), HA (11%) and lower relative average percentages of HS (14%) when compared to WT MSC. After 21 days of osteogenic differentiation treatment, both MSC types were mainly composed by CS (WT: 55%, $OC^{-/-}$ $OPN^{-/-}$: 58%) with lower amounts of HS (WT: 28%, $OC^{-/-}$ $OPN^{-/-}$: 25%) and HA (WT: 18%, $OC^{-/-}$ $OPN^{-/-}$: 18%).

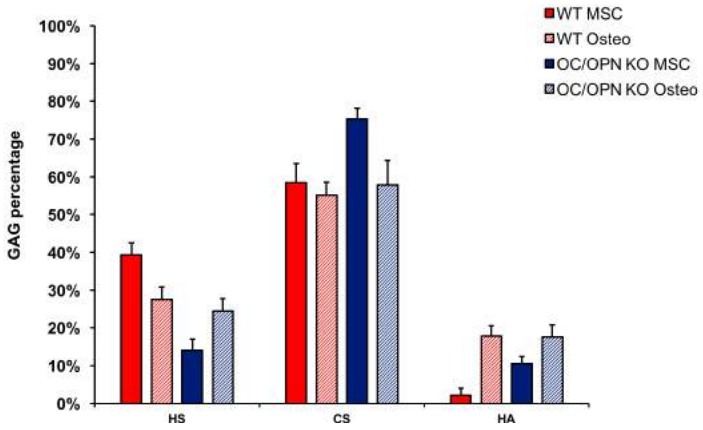

Figure II.3. Average relative percentage GAG composition of WT and $OC^{-/-}$ $OPN^{-/-}$ MSC before and after osteogenic differentiation. Results are presented as mean ± SD of three biological replicates (n=3).

The compositional analysis of the GAG disaccharides of WT and $OC^{-/-}$ $OPN^{-/-}$ MSC was performed after enzymatic digestion of isolated GAG samples with heparin lyase I, II, III and chondroitin lyase ABC. The disaccharides were then AMAC-labelled by reductive amination and analyzed by LC-MS/MS. The HS and CS disaccharide relative composition percentage for the different cell types is presented in Figure II.4. For all the cells, HS was comprised primarily of 0S, followed by NS and N2S (Fig. II.4a). However, some differences were noticed in the HS disaccharide percentage composition present in the different types of cells. $OC^{-/-}OPN^{-/-}$ MSC presented a higher relative percentage of 0S when compared to WT MSC. On the other hand, WT MSC presented higher relative percentage of NS2S and NS than $OC^{-/-}OPN^{-/-}$ MSC. When cells were differentiated into osteoblasts, the HS relative percentage did not change dramatically. In terms of CS disaccharides, all the cells were primarily composed by 4S, 6S and 0S (Figure II.4b). The relative percentage of 4S and 0S were quite similar between both cells (WT and $OC^{-/-}OPN^{-/-}$ MSC). However, $OC^{-/-}$ $OPN^{-/-}$ MSC presented significantly higher relative percentage of 6S when compared to WT MSC. Notably, when WT MSC were differentiated into osteoblasts, the CS relative percentage was similar to cells undifferentiated. However, some differences were observed when $OC^{-/-}$ $OPN^{-/-}$ MSC were differentiated compared to undifferentiated cells. Of

note, the relative percentage of 2S6S and 4S6S increased when $OC^{-/-}$ $OPN^{-/-}$ MSC were differentiated into osteoblasts. In addition, the relative percentage of 6S and 0S dramatically decreased when cells were differentiated.

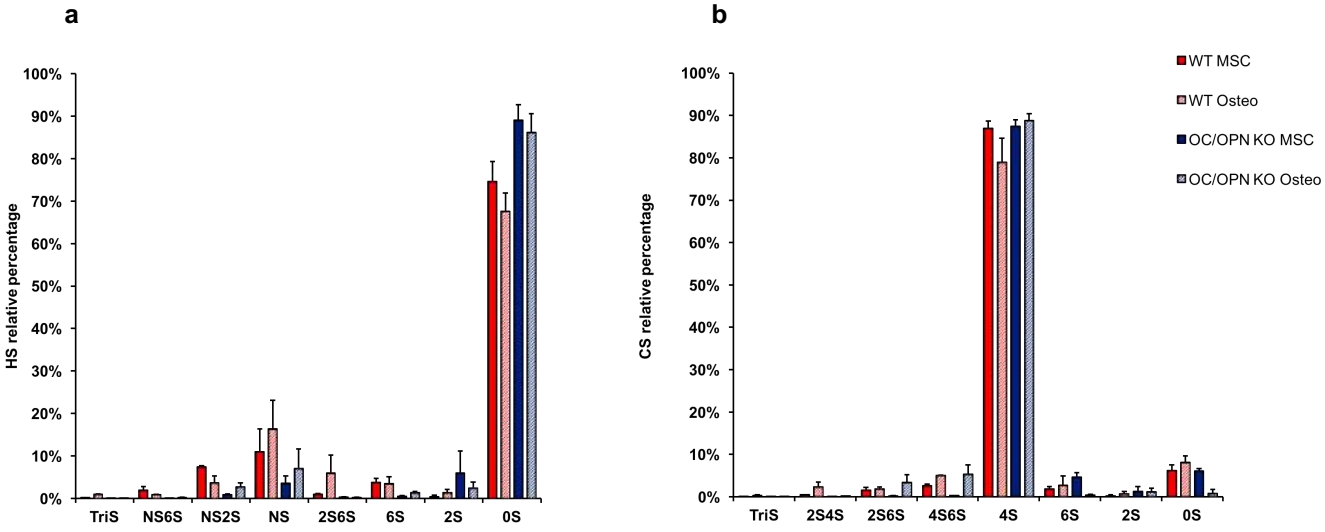

Figure II.4. Average relative percentage HS **(a)** and CS **(b)** composition of the different cell types: WT and $OC^{-/-}$ $OPN^{-/-}$ MSC before and after osteogenic differentiation. Results are presented as mean ± SD of three biological replicates (n=3).

II.3.3. Effects of OC and OPN on MSC proliferation

Aiming to understand how the lack of OC and OPN ($OC^{-/-}$ $OPN^{-/-}$) would influence the proliferative capacity of MSC, cells were cultured for nine passages and cumulative population doublings and fold increases were plotted for each passage (Figure II.5). Thus, different cell seeding densities were studied, 3000 cells/cm^2 and 10000cells/cm^2, representing low and high density, respectively.

$OC^{-/-}$ $OPN^{-/-}$ MSC cultured at 3000 cells/cm^2 (low density) took 71 days to complete nine passages, while WT MSC took only 48 days. When cultured at a higher density (10000 cells/cm^2), $OC^{-/-}$ $OPN^{-/-}$ MSC reached nine passages after 49 days, while WT MSC only took 34 days. At the end of the ninth passage, cumulative population doublings of 9.96 ± 0.78 and 16.18 ± 0.52 were obtained for WT MSC cultured at 10000 cells/cm^2 and 3000 cells/cm^2, respectively. On the other hand, at the end of the ninth passage, $OC^{-/-}$ $OPN^{-/-}$ MSC only achieved cumulative population doublings of 6.17 ± 0.14 and 7.57 ± 0.1, when cultured at 10000 cells/cm^2 and 3000 cells/cm^2, respectively.

Passaging density affected MSC proliferation potential. Interestingly, the proliferative potential of $OC^{-/-}$ $OPN^{-/-}$ MSC was always affected, even when two different seeding densities were investigated, reaching cumulative population doublings lower than WT MSC for both cell seeding densities.

We characterized $OC^{-/-}OPN^{-/-}$ and WT MSC growth curves measuring cell numbers at different timepoints during 15 days. MSC were plated at 5000 cells/cm^2 in a 12 well-plate and a kinetic study was performed. $OC^{-/-}$ $OPN^{-/-}$ MSC presented a slower growth rate than WT MSC. Interestingly, only after 7 days in culture,

$OC^{-/-}OPN^{-/-}$ MSC started to proliferate faster, reaching higher cell numbers. After 15 days in culture, WT MSC reached a cell number of $5.42x10^4$ ±0.47, whereas $OC^{-/-}$ $OPN^{-/-}$ MSC achieved 4.39 $x10^4$± 0.38 cells.

Therefore, the lack of OC and OPN retarded the proliferation of MSC. The proliferation rate was higher in WT MSC than in the $OC^{-/-}$ $OPN^{-/-}$ MSC.

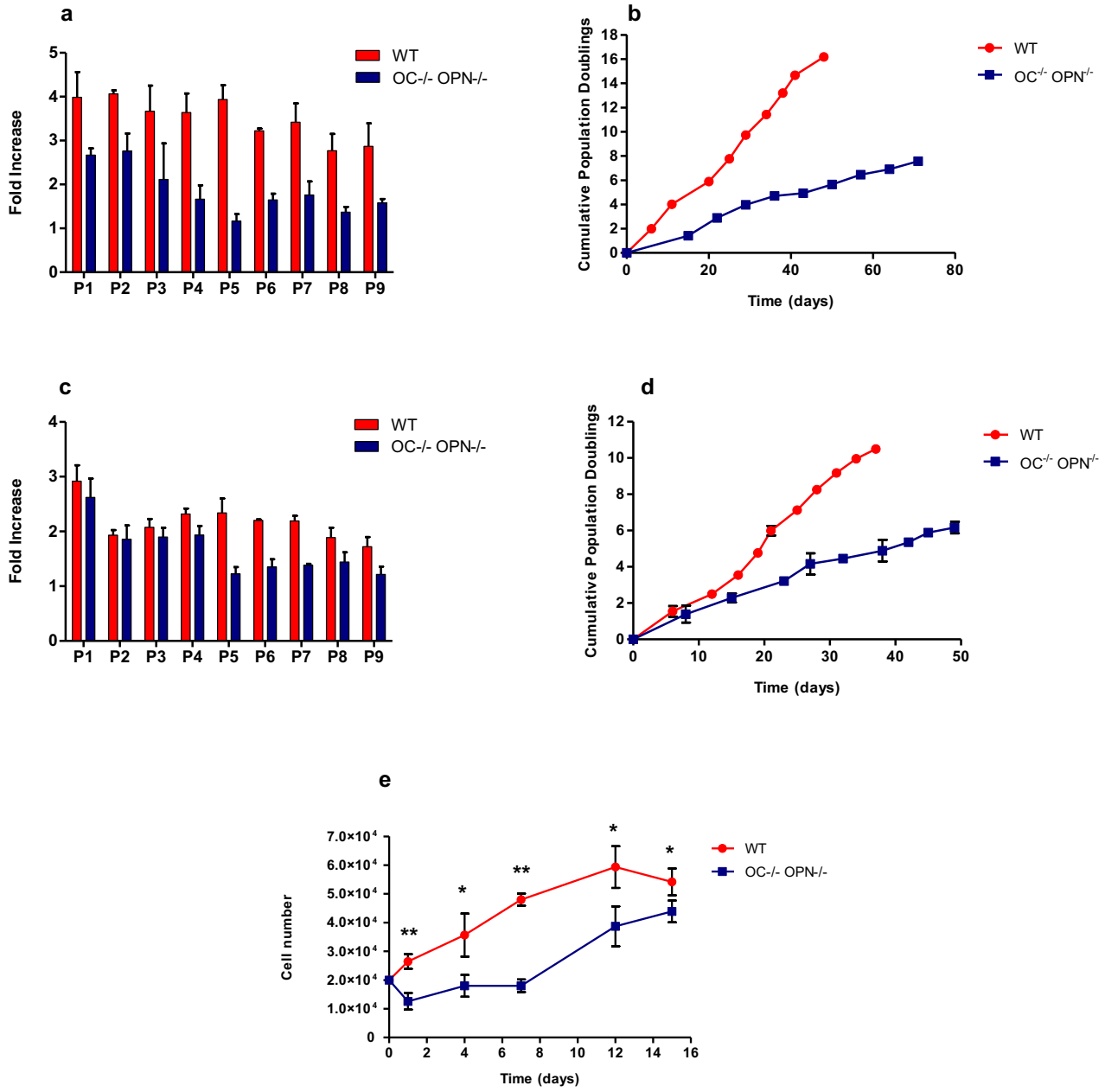

Figure II.5. Proliferation studies of $OC^{-/-}OPN^{-/-}$ and WT MSC. **a,b)** Fold increase **(a)** and cumulative population doublings **(b)** when cells were seeded at 3000 cells/cm^2. **c,d)** Fold increase **(c)** and cumulative population **(d)** when cells were seeded at 10000 cells/cm^2. **e)** Kinetic study during 15 days of cell culture (5000 cells/cm^2). Data are expressed as mean ± SD; **p<0.01; *p<0.05 (n=3).

II.3.4. Effects of OC and OPN on MSC multilineage differentiation

Moreover, aiming to understand the effects of the absence of OC and OPN on MSC differentiation, WT MSC and $OC^{-/-}$ $OPN^{-/-}$ MSC were cultured in adipogenic, chondrogenic and osteogenic medium.

Following treatment with adipogenic differentiation medium, the $OC^{-/-}$ $OPN^{-/-}$ MSC changed to express Oil Red O-stained vesicles, showing that KO cells differentiated into adipocytes, like WT MSC (Figure II.7a). The expression of FABP4 was also confirmed by immunocytochemistry (Figure II.6a). Furthermore, after chondrogenic induction, the cells changed to show deposition of extracellular matrix in the pellet culture, stained with Alcian blue (Figure II.7a). Collagen type II, a biomarker of chondrocytes, was also detected for both cells, WT and $OC^{-/-}$ $OPN^{-/-}$ MSC (Figure II.6b). Regarding osteogenic differentiation, $OC^{-/-}$ $OPN^{-/-}$ MSC demonstrated less extension of mineralization compared with WT MSC at the same conditions. Although $OC^{-/-}$ $OPN^{-/-}$ MSC stained for ALP, fewer extension of calcium deposits in the matrix produced by $OC^{-/-}OPN^{-/-}$ MSC after 21 days of osteogenic differentiation was observed by Von Kossa and Xylenol orange stainings (Figure II.7a,d,e). Immunocytochemistry also confirmed that $OC^{-/-}OPN^{-/-}$ MSC did not express OPN (Figure II.6c).

Calcium levels quantification demonstrated that the kinetics of osteogenic differentiation by $OC^{-/-}$ $OPN^{-/-}$ MSC was significantly retarded compared to WT MSC (Figure II.7c), as we observed that after 15 days of differentiation, an increase of calcium levels was observed only on WT MSC. Additionally, calcium quantification demonstrated that $OC^{-/-}$ $OPN^{-/-}$ MSC produced smaller amount of mineral content after 21 days of differentiation, compared to WT MSC. These results were further confirmed with Xylenol Orange staining, indicating a smaller extent of mineralization for $OC^{-/-}OPN^{-/-}$ MSC (Figure II.7d,e).

SEM micrographs demonstrated higher amounts of nodules produced in the WT MSC after 15 and 21 days of osteogenic differentiation (Figure II.8a), compared with $OC^{-/-}$ $OPN^{-/-}$ MSC. Interestingly, after 30 days of osteogenic differentiation, WT MSC and $OC^{-/-}$ $OPN^{-/-}$ MSC showed the same morphology presenting both mineralized nodules. Moreover, elemental analysis of both cell types after 21 days of osteogenic differentiation demonstrated the presence of the same components, presenting Ca and P in their composition (Figure II.8b,c).

Gene expression analysis at different timepoints, showed that $OC^{-/-}$ $OPN^{-/-}$ MSC downregulated some osteogenic genes compared with WT MSC (Figure II.9). *Runx2* gene expression was impaired by the lack of OC and OPN during the 21 days of osteogenic differentiation. In addition, although a slight increase was observed in Col I expression after 21 days of differentiation for both cell types, the relative expression of Col I from $OC^{-/-}$ $OPN^{-/-}$ MSC was statistically significantly lower than WT MSC. As expected, WT MSC upregulated the expression of OPN and OC genes during osteogenic differentiation, however $OC^{-/-}$ $OPN^{-/-}$ MSC did not demonstrate expression of these genes. In contrast, ALP gene expression level was enhanced in $OC^{-/-}$ $OPN^{-/-}$ MSC compared to WT MSC. Interestingly, the expression of ALP was enhanced after 7 and 15 days of differentiation but it decreased after 21 days for both cell types, reaching its peak after 15 days of osteogenic differentiation. Additionally, only ALP gene expression levels were not affected by the lack of *OC* and *OPN* genes (Figure II.9c). Notably, ALP activity of $OC^{-/-}$ $OPN^{-/-}$ MSC was also not affected (Figure II.7b).

Taken together, these results show that $OC^{-/-}$ $OPN^{-/-}$ MSC were able to differentiate into adipogenic and chondrogenic lineage, indicating that these cells display multipotency, however the absence of OC and OPN impaired the osteogenic differentiation of MSC, analyzed by different methods.

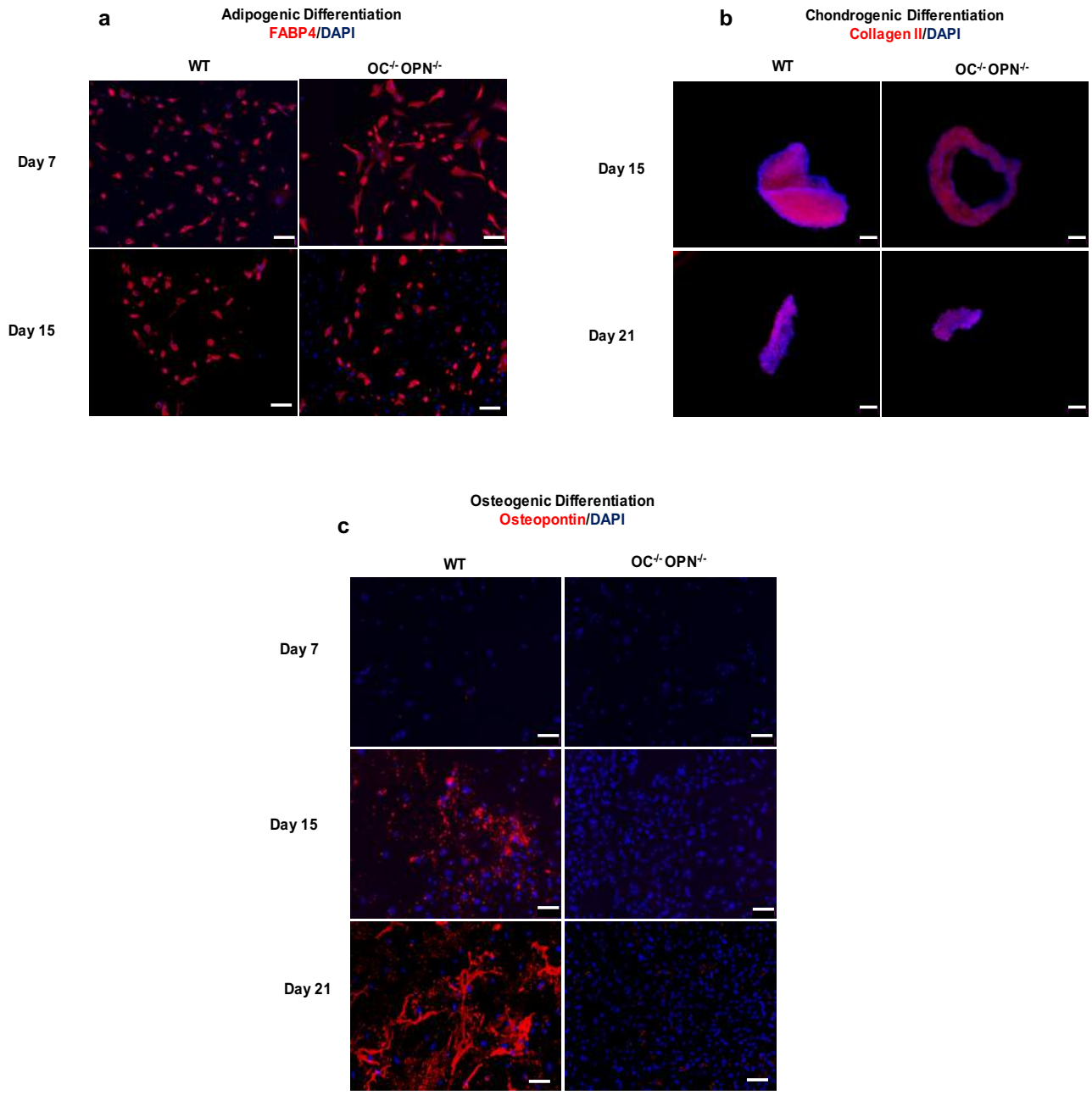

Figure II.6. Multilineage differentiation of $OC^{-/-}$ $OPN^{-/-}$ and WT MSC evaluated by immunocytochemistry. **a)** Adipogenic differentiation after 7 and 15 days (FABP4). **b)** Chondrogenic differentiation after 15 and 21 days (Col II). **c)** Osteogenic differentiation after 7, 15 and 21 days (OPN). Scale bars, 100 µm.

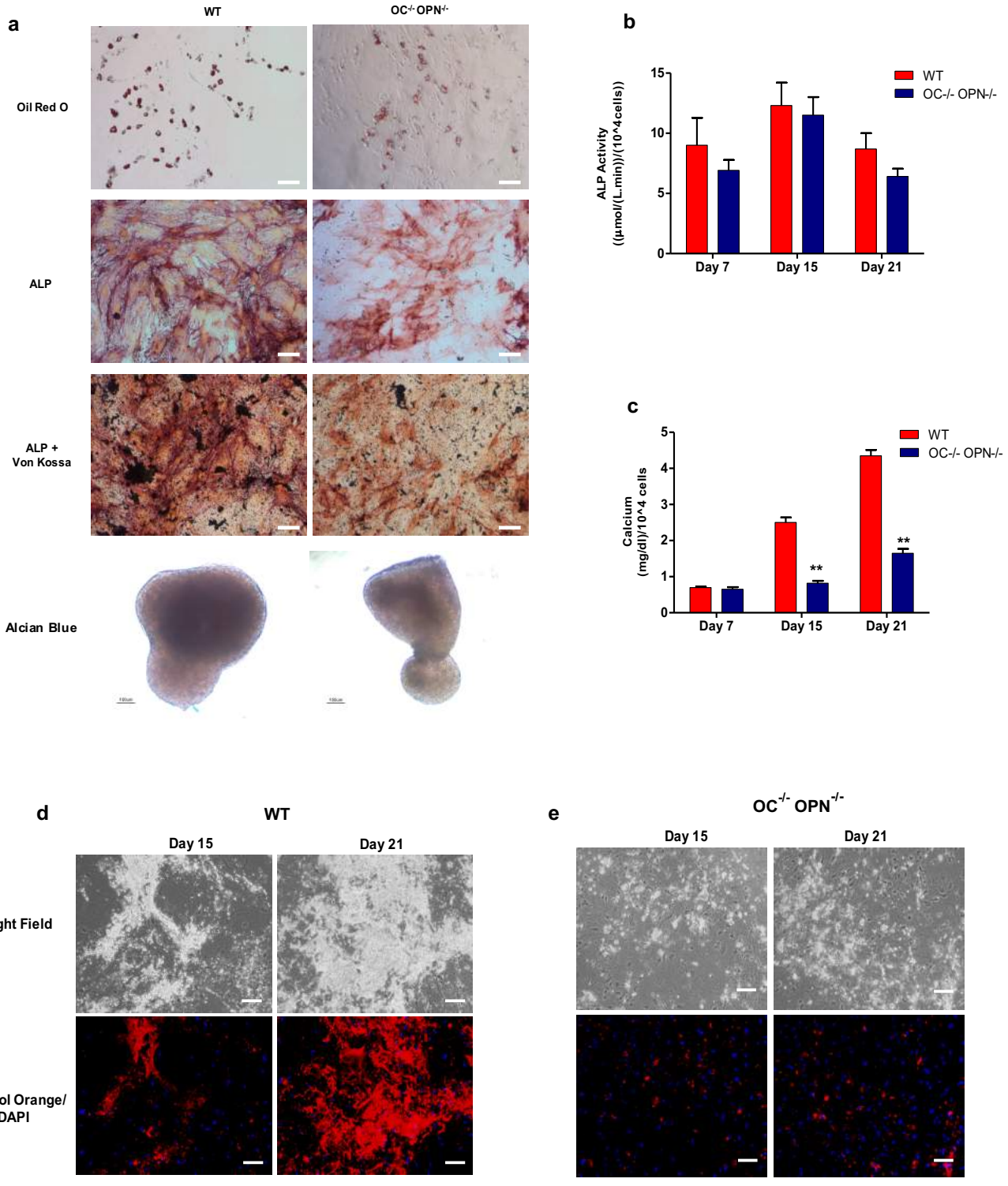

Figure II.7. OC/OPN-deficiency impairs MSC osteogenic differentiation. **a)** WT and $OC^{-/-}OPN^{-/-}$ MSC were cultured in adipogenic (7 days), osteogenic and chondrogenic differentiation medium (21 days) and stained with Oil Red O to reveal lipid droplets, ALP and Von Kossa stainings to detect mineralization and Alcian Blue to detect glycosaminoglycans. **b)** ALP activity was evaluated after 7, 15 and 21 days of osteogenic differentiation. **c)** Calcium levels were quantified after 7, 15 and 21 days of osteogenic differentiation. **d,e)** MSC from WT **(d)** and $OC^{-/-}OPN^{-/-}$ **(e)** were cultured in osteogenic differentiation medium for the indicated number of days and calcium deposits were revealed by Xylenol Orange stain (red) (blue:DAPI). Scale bars, 100 µm. Values are means ± SD. **p<0.01 (n=3).

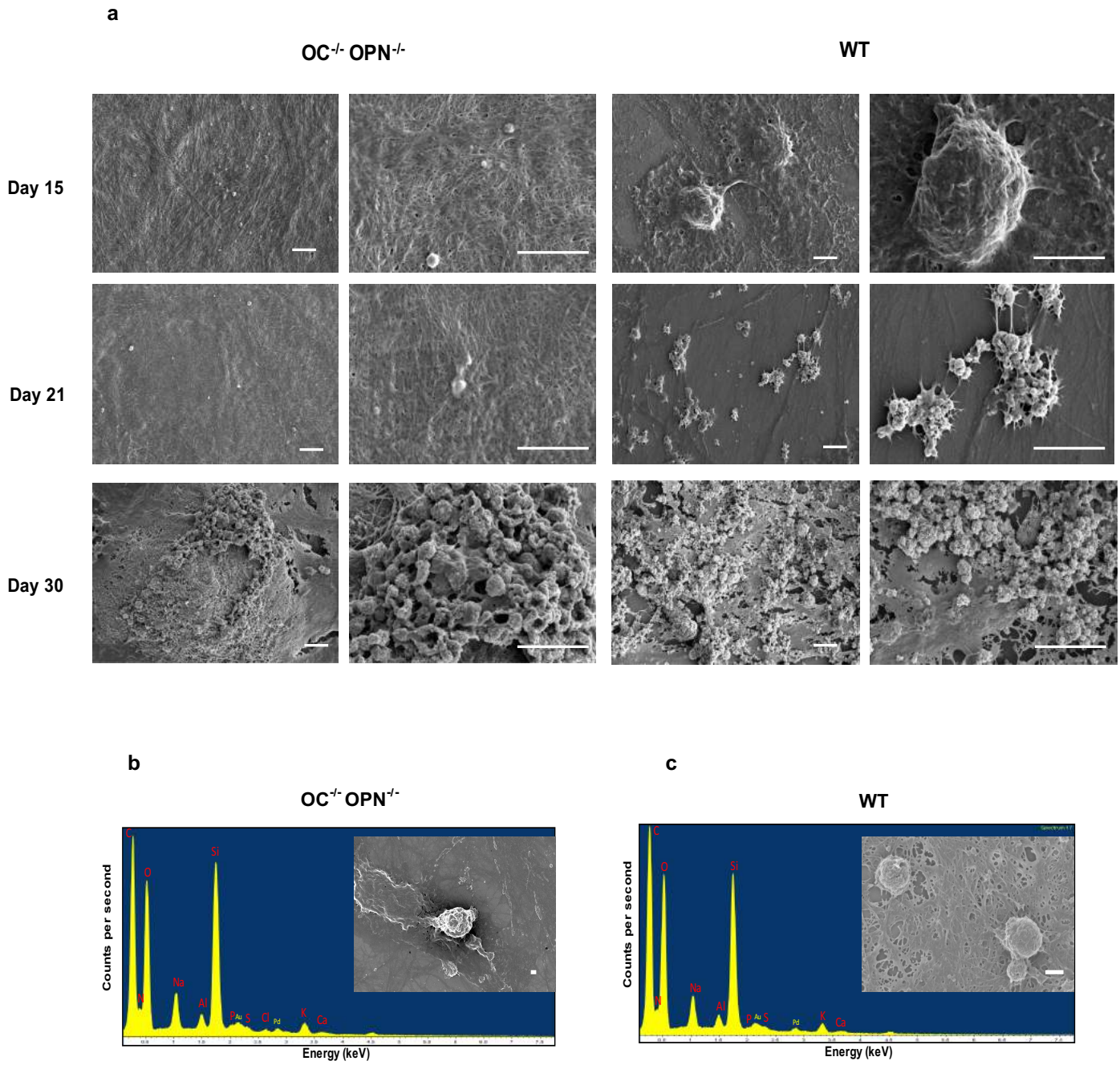

Figure II.8. Osteogenic differentiation of $OC^{-/-}$ $OPN^{-/-}$ MSC and WT MSC. **a)** SEM micrographs showing morphology and mineralization of $OC^{-/-}$ $OPN^{-/-}$ and WT MSC after 15, 21 and 30 days of osteogenic differentiation. Scale bars, 4 µm. **b)** EDX microanalysis of mineral nodules from $OC^{-/-}$ $OPN^{-/-}$ MSC after 21 days of osteogenic differentiation. Scale bar, 1 µm. **c)** EDX microanalysis of mineral nodules from WT MSC after 21 days of osteogenic differentiation. Scale bar, 1 µm.

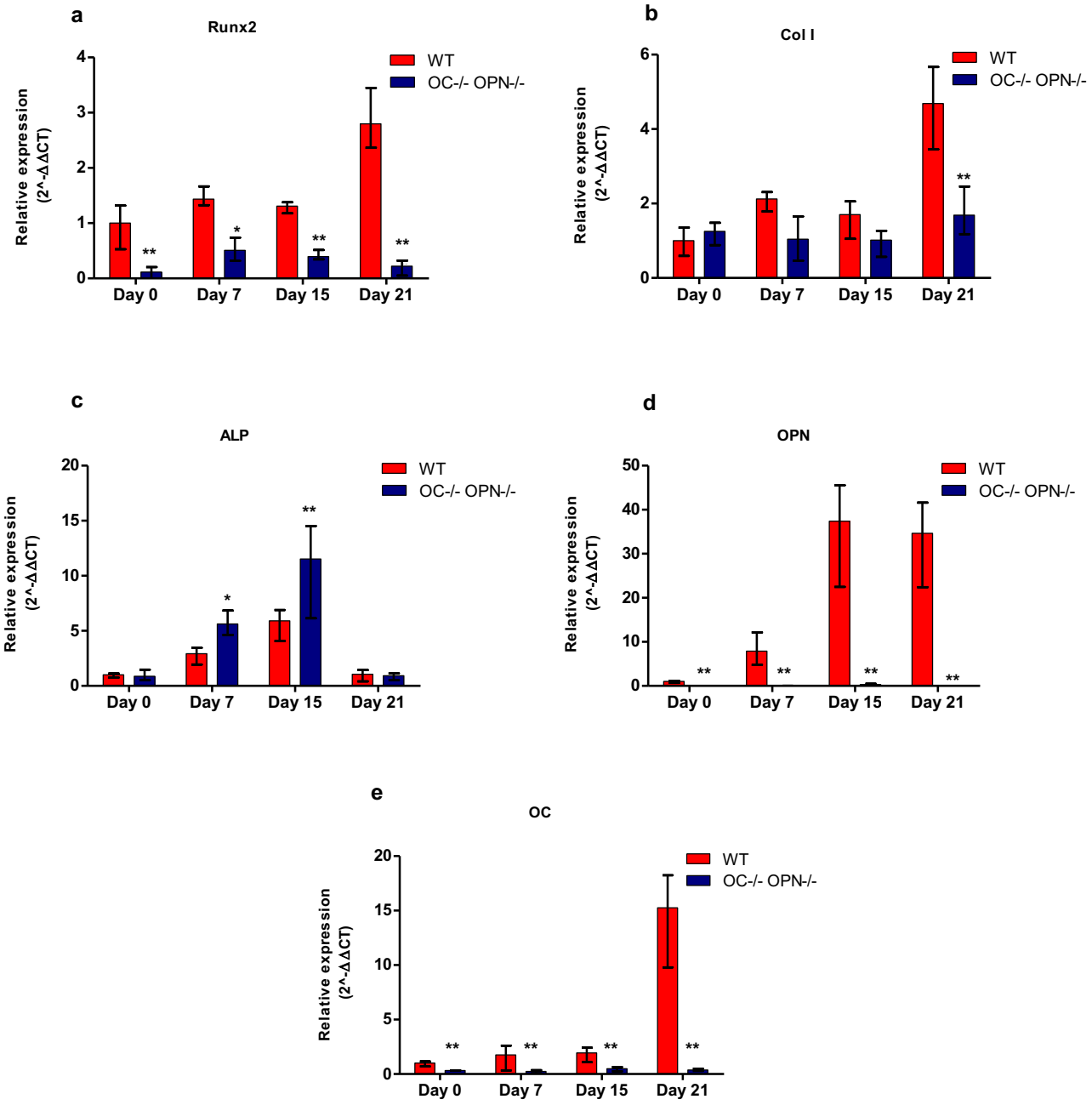

Figure II.9. Gene expression analysis of $OC^{-/-}$ $OPN^{-/-}$ MSC after osteogenic differentiation. WT and $OC^{-/-}$ $OPN^{-/-}$ MSC cultured in osteogenic differentiation medium for the indicated times were analyzed for **a)** Runx2, **b)** Col I, **c)** ALP, **d)** OPN and **e)** OC by qRT-PCR. **p<0.01; *p<0.05 (n=3).

II.3.5. Maturation level of mineral species produced by $OC^{-/-}$ $OPN^{-/-}$ MSC

To further understand how osteogenic differentiation was being impaired due to the absence of OC and OPN, we evaluated the roles of OC and OPN in mineral species production during osteogenic differentiation of MSC, more specifically we were interested on studying the maturation level of mineral species produced by $OC^{-/-}$ $OPN^{-/-}$ MSC, using spectroscopic analysis, such as FTIR and Raman spectroscopy.

After 21 days of osteogenic differentiation, FTIR spectra of the sample produced by WT MSC became similar to the typical infrared vibrations of phosphate, carbonate and amide I and II. The presence of crystalline apatite was verified by a split phosphate band (500 to 635 cm^{-1}) (Figure II.10a).

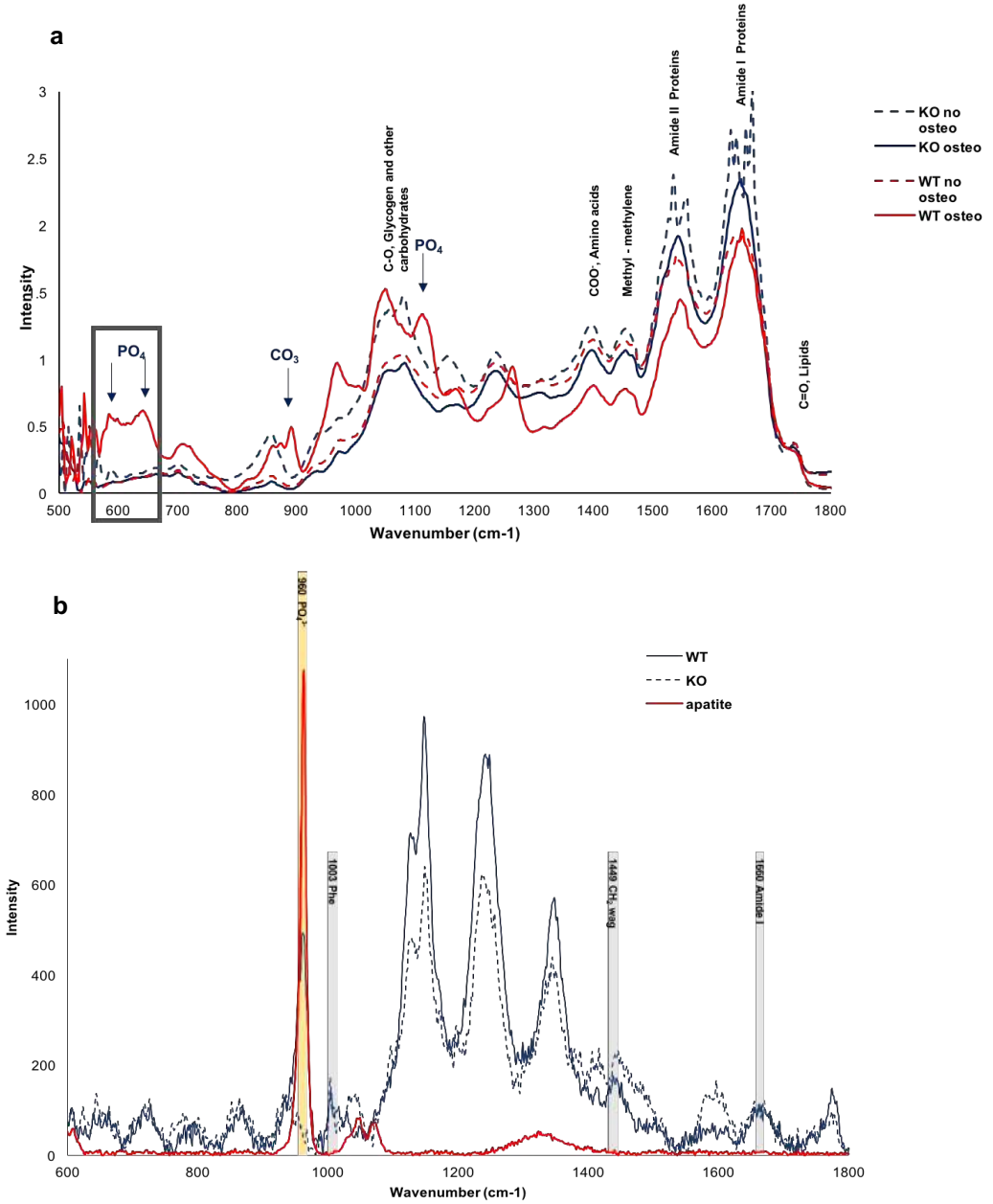

Figure II.10. Spectroscopy analysis of WT MSC and $OC^{-/-}$ $OPN^{-/-}$ MSC after 21 days of osteogenic differentiation. **a)** FTIR spectra of the WT MSC and $OC^{-/-}$ $OPN^{-/-}$ (KO) MSC without differentiation (no osteo) and after 21 days of differentiation (osteo). The characteristic peaks of amide I (1645cm^{-1}) and amide II (1550 cm^{-1}), carbohydrates, amino acids and lipids can be found. **b)** Raman spectra of WT and $OC^{-/-}$ $OPN^{-/-}$ MSC (KO) after 21 days of osteogenic differentiation. Peaks related to cellular components are marked in grey and the region of mineral species is marked in yellow (apatite). KO MSC did not present the apatite peak.

In contrast, the sample produced by $OC^{-/-}$ $OPN^{-/-}$ MSC did not demonstrate the absorption peaks associated with major bone-related molecular species. Moreover, the spectrum generated by $OC^{-/-}$ $OPN^{-/-}$ MSC after 21 days of osteogenic differentiation was similar to the spectra of WT and $OC^{-/-}$ $OPN^{-/-}$ MSC before differentiation (no osteo) (Figure II.10a). This FTIR result confirmed that the absence of OC and OPN impairs mineralization of MSC.

In order to elucidate the differential production of mineralized matrix during osteogenic differentiation of MSC, Raman spectra were recorded on day 0, 15, 21 and 30 of osteogenic differentiation. The region of Raman spectra of cellular components was marked in grey and the region of mineral species was marked in yellow (Figure II.10b). Peaks related to cellular components, such as phenylalanine (1003 cm^{-1}), CH_2 wag (1449 cm^{-1}) and amide I (1660 cm^{-1}), were present in Raman spectra from both $OC^{-/-}$ $OPN^{-/-}$ and WT MSC. Figure II.11. demonstrates Raman spectra of both cell types after 15, 21 and 30 days of osteogenic differentiation. Raman spectra were dissected in detail as depicted in the region from 900 to 1000 cm^{-1}. Previous studies have demonstrated that OCP is the precursor of mineralized matrix at the early stage mineralization and it also participates in HAP synthesis during bone formation (Anada *et al.* 2008, Alt 2002). The Raman signal of OCP at 957 cm^{-1} was detected in WT MSC at day 15 of osteogenic differentiation, however no detectable peak was observed for $OC^{-/-}$ $OPN^{-/-}$ MSC (Figure II.11a,b). At day 21 of osteogenic differentiation, the OCP signal could not be detected anymore and, further, WT MSC presented the HAP peak at 960 cm^{-1} (Figure II.11c,d). On the other hand, $OC^{-/-}$ $OPN^{-/-}$ MSC did not present the HAP peak, however a small signal of β-TCP at 970 cm^{-1}, a HAP precursor, was found after 21 days of differentiation. β-TCP is known to contribute to HAP synthesis which can be used as an early stage marker of MSC-osteoblast differentiation.

These data show that OCP at 957 cm^{-1} was only observed after 15 days of differentiation for minerals produced by WT MSC and that after 21 days of differentiation, hydroxyapatite minerals were produced by WT MSC, since the HAP peak at 960 cm^{-1} was found. Interestingly, after 21 days of differentiation $OC^{-/-}$ $OPN^{-/-}$ MSC did not produce HAP minerals, since this peak was not detectable. In contrast, a small peak of β-TCP was found, indicating that, after 21 days of differentiation, the mineral produced by $OC^{-/-}$ $OPN^{-/-}$ MSC was not mature enough. After only 7 days of osteogenic differentiation, no detectable peak related with mineral species was found.

Using spectroscopic analysis, we confirmed that mineralization was impaired after 21 days of osteogenic differentiation. Raman spectroscopy analysis confirmed that not only after 21 days of differentiation $OC^{-/-}$ $OPN^{-/-}$ MSC produced less mineral, but also the mineral produced was not sufficiently mature, since the HAP peak was not detected (Figure II.11c,d)

Furthermore, we increased the osteogenic differentiation culture time and, after 30 days of differentiation, the Raman spectrum of the mineral produced by $OC^{-/-}OPN^{-/-}$ presented the HAP peak, demonstrating that by increasing the time of differentiation, the minerals produced were composed mostly of hydroxyapatite (Figure II.11e,f). Therefore, we concluded that when OC and OPN were insufficiently expressed the maturation of mineralization was delayed.

These results confirmed that OC and OPN are important in regulating mineralization process during osteogenic differentiation of MSC and demonstrated that Raman spectroscopy is a powerful tool to measure the maturation level of MSC-osteoblast differentiation by detecting the intensity changes of mineral components in MSC.

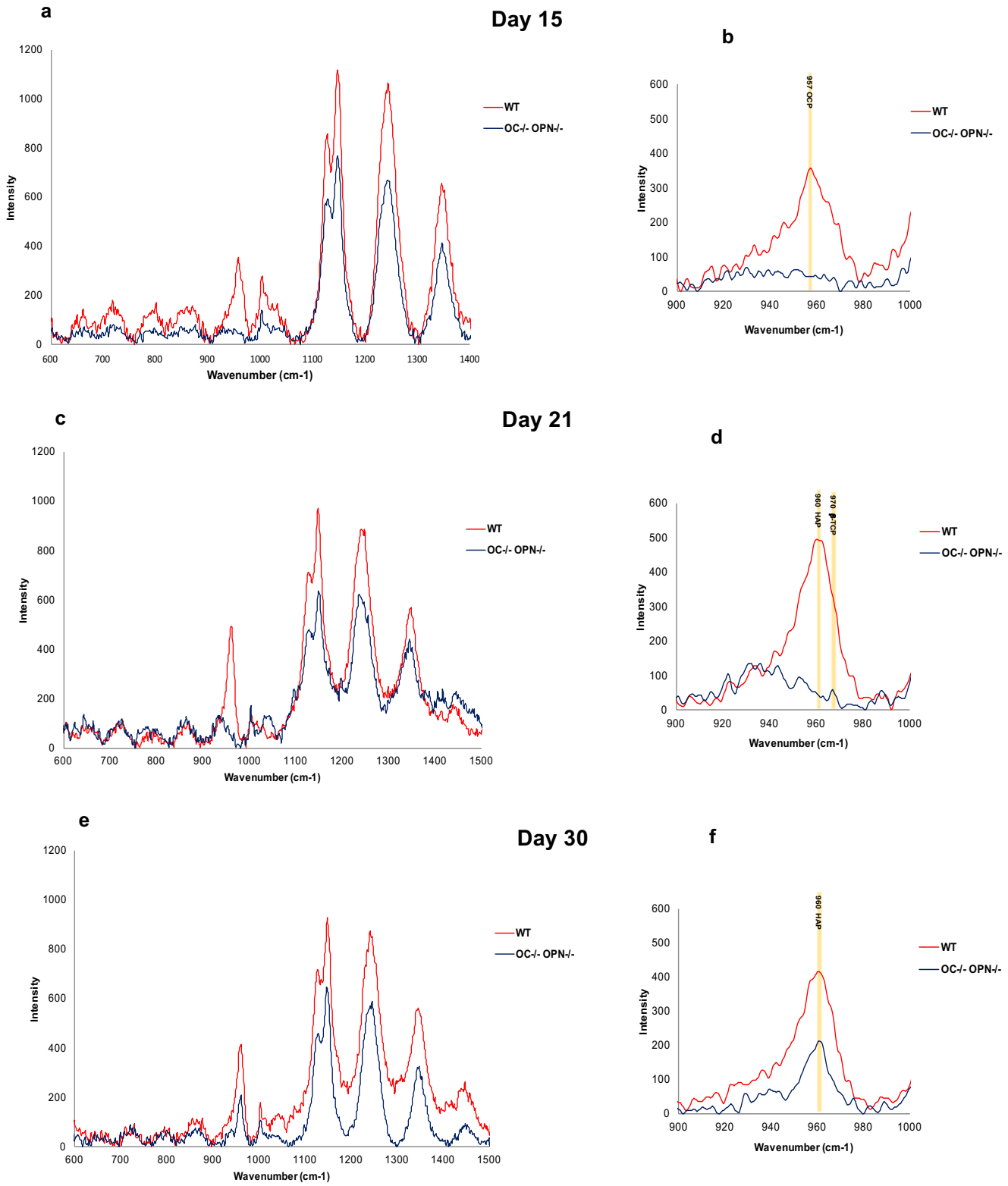

Figure II.11. Raman spectra of mineral species produced by WT and $OC^{-/-}$ $OPN^{-/-}$ MSC after 15, 21 and 30 days of osteogenic differentiation. **a,c,e)** complete view from 600 to 1500 cm^{-1}, **b,d,f**) the region of mineral species from 900 to 1000 cm^{-1}.

II.3.6. $OC^{-/-}$ $OPN^{-/-}$ MSC proliferative and osteogenic potential are recovered by OC/OPN supplemented extracellularly

To understand whether the loss of proliferative capacity by $OC^{-/-}$ $OPN^{-/-}$ MSC is associated with the lack of OC and/or OPN, these proteins were added extracellularly to the cell culture (1 µg/ml each protein) and a kinetic study was performed during 15 days. After OC treatment, no significant increase in proliferation was observed. However, after OPN, as well as OC/OPN treatment, MSC seem to recover their proliferative potential, increasing cell number after 4 days of culture. Indeed, $OC^{-/-}$ $OPN^{-/-}$ MSC supplemented with both OC and OPN or with only OPN presented similar growth rate as WT MSC, reaching the same cell number after 15 days of proliferation (Figure II.12a). This result suggests that OPN might act on proliferative capacity of MSC, however OC failed to induce proliferation. $OC^{-/-}$ $OPN^{-/-}$ MSC were able to recover their proliferative potential by adding extracellularly proteins, such as OPN.

To further investigate the effects of extracellular OC and OPN in MSC osteogenic differentiation, we applied exogenously OC and OPN (OC/OPN) during osteogenic differentiation. Notably, extracellular supplementation of OC/OPN in the osteogenic differentiation medium enabled the MSC to regain their capacity for osteogenic differentiation, shown by the significant increase in calcium levels quantification and visualized using Xylenol orange stain (Figure II.12b,c). Although mineralization was enhanced, the results obtained by $OC^{-/-}$ $OPN^{-/-}$ MSC supplemented with OC/OPN did not completely achieve the results obtained with WT MSC. Interestingly, after 21 days of osteogenic differentiation, Raman spectroscopy demonstrated that the mineral formed by $OC^{-/-}$ $OPN^{-/-}$ MSC supplemented exogenously with OC/OPN was composed by HAP, as observed for mineral species produced by WT MSC. On the other hand, as it was previously demonstrated, minerals generated by $OC^{-/-}$ $OPN^{-/-}$ MSC (without extracellular supplementation) did not present the HAP peak, suggesting a more immature mineral production.

These data suggest that OC and OPN exert their regulatory role in MSC differentiation mainly in an extracellular manner.

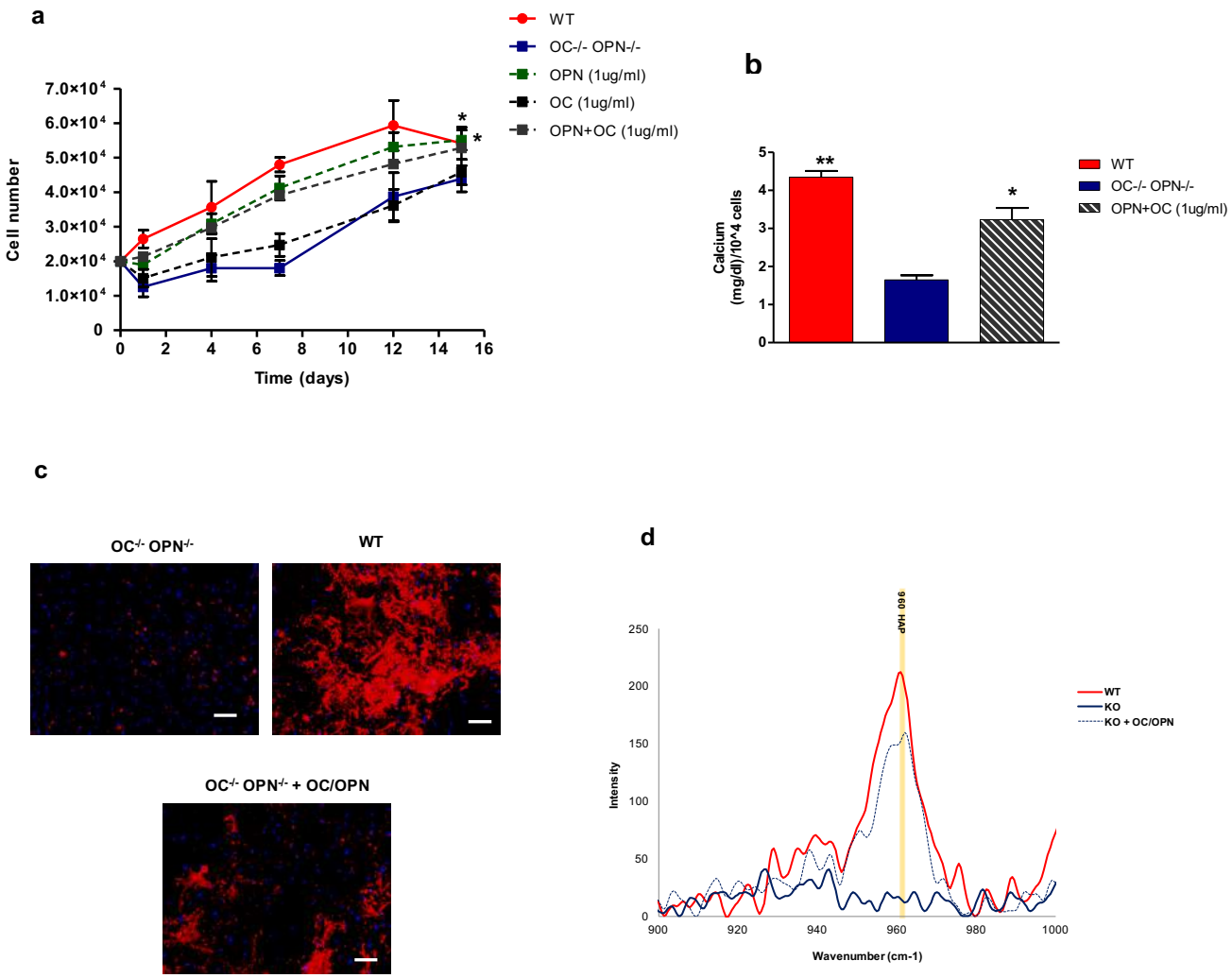

Figure II.12. Effects of OC/OPN supplemented extracellularly on $OC^{-/-}$ $OPN^{-/-}$ MSC proliferation and osteogenic potential. **a)** Proliferation of $OC^{-/-}$ $OPN^{-/-}$ MSC exogenously supplemented with OC and/or OPN (1µg/ml). **b)** Calcium quantification of $OC^{-/-}$ $OPN^{-/-}$ MSC differentiated during 21 days with osteogenic medium supplemented with OC/OPN (1µg/ml). **c)** Calcium deposits from $OC^{-/-}$ $OPN^{-/-}$ MSC supplemented with OC/OPN were visualized using Xylenol Orange (red) (blue:DAPI). **d)** Comparison of Raman spectrum of WT, $OC^{-/-}$ $OPN^{-/-}$ and $OC^{-/-}$ $OPN^{-/-}$ MSC extracellularly supplemented with OC/OPN after 21 days. Scale bars, 100 µm. Values are means ± SD. **p<0.01.*p<0.05, compared to $OC^{-/-}$ $OPN^{-/-}$ (n=3).

II.3.7. Angiogenic potential of $OC^{-/-}$ $OPN^{-/-}$ MSC

OPN is a potent angiogenic factor, which promotes proliferation, migration and capillary formation of endothelial cells (Dai *et al.* 2009). OC has also been reported to stimulate angiogenesis *in vivo* (Cantatore *et al.* 2005). Therefore, angiogenic potential was assessed *in vitro* by performing functional tube formation assays and a migration assay. Conditioned medium was collected from WT and $OC^{-/-}$ $OPN^{-/-}$ MSC cultured for 72 hours with DMEM basal medium (without FBS supplementation).

Therefore, CM from both cell types were collected and incubated with HUVEC seeded on the top of a matrigel gel for 8h. As shown in Figure II.13a, HUVEC cultured with CM from $OC^{-/-}$ $OPN^{-/-}$ MSC ($OC^{-/-}$ $OPN^{-/-}$ CM) were not able to form a capillary-like network. Moreover, conditioned medium from WT MSC (WT CM) started to form a network with some branches interconnected, after 8h post seeding. HUVEC incubated with DMEM+10%FBS and EGM-2 were used as positive controls, since both media have angiogenic factors and FBS that will enable HUVEC to form tubular structures when seeded in a matrigel substrate. DMEM basal was used as a negative control, since this medium does not contain any important factor for angiogenesis. Our results demonstrated that WT CM did not improve angiogenic properties of HUVEC, since the number of tubes did not increase compared with DMEM basal (medium without angiogenic factors), presenting the same weak tubular structures as DMEM basal. Notably, the absence of tubular structures formed by HUVEC was observed when $OC^{-/-}$ $OPN^{-/-}$ CM was added to HUVEC culture, leading us to conclude that the absence of these two proteins impairs angiogenesis *in vitro*.

In a different assay, we evaluated if the conditioned medium collected from $OC^{-/-}$ $OPN^{-/-}$ MSC would have any effect on the migratory ability of HUVEC. Studying the migration of cells in a 2-D confluent monolayer in highly controlled *in vitro* conditions allows to investigate if the lack of OC and OPN would impair the migratory capability of HUVEC. Therefore, a scratch was performed in a confluent monolayer of HUVEC cultured with CM from WT MSC and $OC^{-/-}$ $OPN^{-/-}$ MSC and cell migration was investigated at different timepoints. EGM-2 added to the cell culture was used as a positive control. Interestingly, when HUVEC were incubated with CM from WT MSC, after 8h, the “wound” size decreased, due to the migration of HUVEC towards the site (Figure II.13c). The same effect was observed for the positive control, EGM-2, due to the angiogenic factors present in these media. However, when HUVEC were seeded with $OC^{-/-}$ $OPN^{-/-}$ CM, the scratch diameter slightly changed, indicating that HUVEC’s migration capability was impaired due to the lack of OC and OPN. Notably, after 12h, the wound site was almost closed when HUVEC were seeded with WT CM, presenting a percentage of migration of 77%. This phenomenon could be explained due to the presence of secreted factors from MSC in the conditioned medium that are known to enhance the migration of cells. After 12h, conditioned medium from $OC^{-/-}$ $OPN^{-/-}$ MSC only allowed a percentage of migration of 26% (Figure II.13c,d).

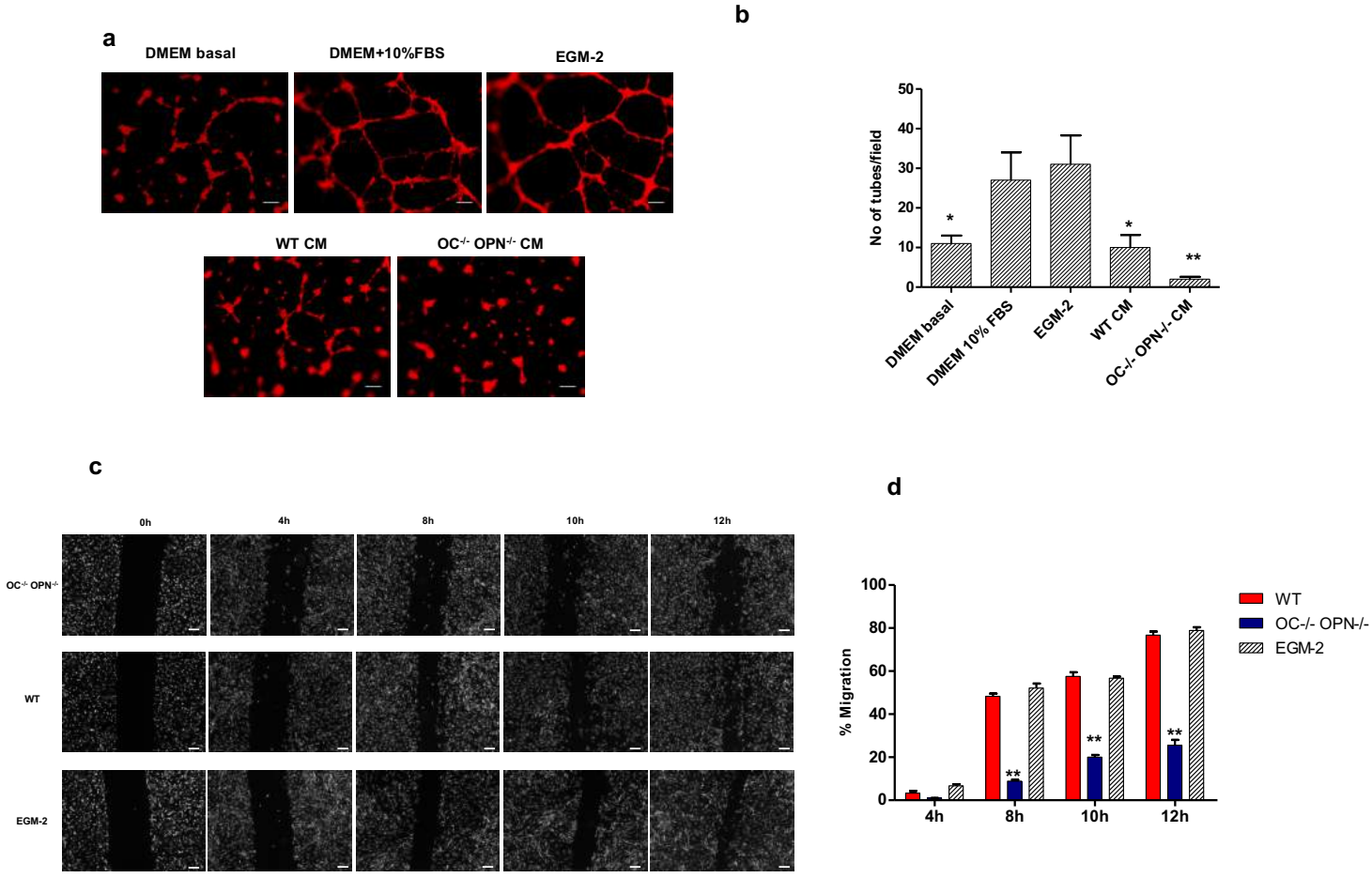

Figure II.13. OC/OPN-deficiency impairs angiogenic properties. **a)** Tube formation assay evaluating the HUVEC's response to conditioned medium (CM) from $OC^{-/-}$ $OPN^{-/-}$ MSC and WT MSC after 8h post-seeding. **b)** Number of tubular-like structures formed by HUVEC in the tube formation assay. **c)** Migration assay evaluating the HUVEC's migratory response to CM from $OC^{-/-}$ $OPN^{-/-}$ and WT MSC after 4, 8, 10 and 12h. **d)** Quantification of the HUVEC's percentage of migration after different timepoints when exposed to different conditioned medium from WT and $OC^{-/-}$ $OPN^{-/-}$ MSC. DMEM+10% FBS and endothelial growth medium-2 (EGM-2) were used as a positive control and DMEM basal as a negative control. Scale bars, 100 µm. Values are mean ± SD. **p<0.01; *p<0.05 compared with EGM-2 (positive control) (n=3.)

Furthermore, the angiogenic potential of these cells, WT MSC and $OC^{-/-}OPN^{-/-}$ MSC, was also evaluated by performing a tube formation functional assay using a co-culture of MSC and HUVEC. Firstly, the results demonstrated that WT MSC alone seeded on matrigel gel were able to form a tubular structure, even without being co-cultured with HUVEC (Figure II.14a). On the other hand, $OC^{-/-}OPN^{-/-}$ MSC were not able to form a tubular network, presenting only long branches not interconnected. These results already showed that the double knockout of OC/OPN affects the angiogenic capacity of MSC, evaluated by this functional assay (Figure II.14a).

After that, WT MSC and $OC^{-/-}$ $OPN^{-/-}$ MSC were co-cultured with HUVEC and seeded onto a matrigel gel, to evaluate the cooperation between HUVEC and MSC. HUVEC were RFP-tagged and, after 2h, 4h, 8h and 24h post seeding, HUVEC distribution and morphology were observed. As expected, HUVEC alone were able to form a capillary structure after 2h, since HUVEC were seeded with EGM-2 medium, containing angiogenic factors. 4h after seeding, the network structure became more robust with interconnected branches. After 24h, tube's length increased, however the capillary structure was maintained (Figure II.14b).

Co-culture between WT MSC and HUVEC also demonstrated the same pattern as HUVEC alone, allowing HUVEC to form a well-defined capillary structure (Figure II.14b). Indeed, it has been reported that co-culture of endothelial cells and MSC enhance their proliferation and angiogenic properties (Liang *et al.* 2017), since MSC can support angiogenesis.

Notably, when $OC^{-/-}$ $OPN^{-/-}$ MSC were co-cultured with HUVEC, HUVEC started to form tubes after 2h, however, after 8h the tubular structures were not able to be maintained and were disrupted, as observed in Figure II.14b. After 24h, the tubes were completely destroyed. Therefore, we confirmed that the absence of OC and OPN would impair angiogenesis, since the co-culture of $OC^{-/-}OPN^{-/-}$ MSC with HUVEC was not able to maintain and support the tubular structure formed by HUVEC after only 8h. On contrary, WT MSC co-cultured with HUVEC were able to sustain their tubular morphology.

Aiming to understand which protein was responsible for the impairment of the angiogenic capacity of HUVEC, we co-cultured $OC^{-/-}$ $OPN^{-/-}$ MSC with HUVEC and supplemented the medium with OC or/and OPN. Tube formation was evaluated after 8h post seeding. We observed that, when OC and OPN were added to the system, as well as just OPN, HUVEC that were co-cultured with $OC^{-/-}$ $OPN^{-/-}$ MSC were able to form tubes, however when only OC was supplemented to the cell culture, HUVEC did not form the same capillary structure. Figure II.14d showed that the number of tubes formed by HUVEC co-cultured with $OC^{-/-}$ $OPN^{-/-}$ MSC with OPN and OPN/OC exogenously supplemented in the medium increased, compared with HUVEC co-cultured with $OC^{-/-}$ $OPN^{-/-}$ MSC without supplementation. Therefore, we confirmed that the absence of OPN is the responsible factor that affects angiogenesis. Even though HUVEC were able to recover their tubular structure when OPN was added to the culture medium, HUVEC co-cultured with WT MSC demonstrated a more robust tubular morphology with more interconnected tubes, leading us to conclude that, although it helps, extracellularly supplementation of OPN as a compensatory strategy did not present the same enhanced results as WT MSC. HUVEC co-cultured with WT MSC showed significant tube formation on matrigel, whereas only few tubes were formed by HUVEC co-cultured with $OC^{-/-}$ $OPN^{-/-}$ MSC (Figure II.14c).

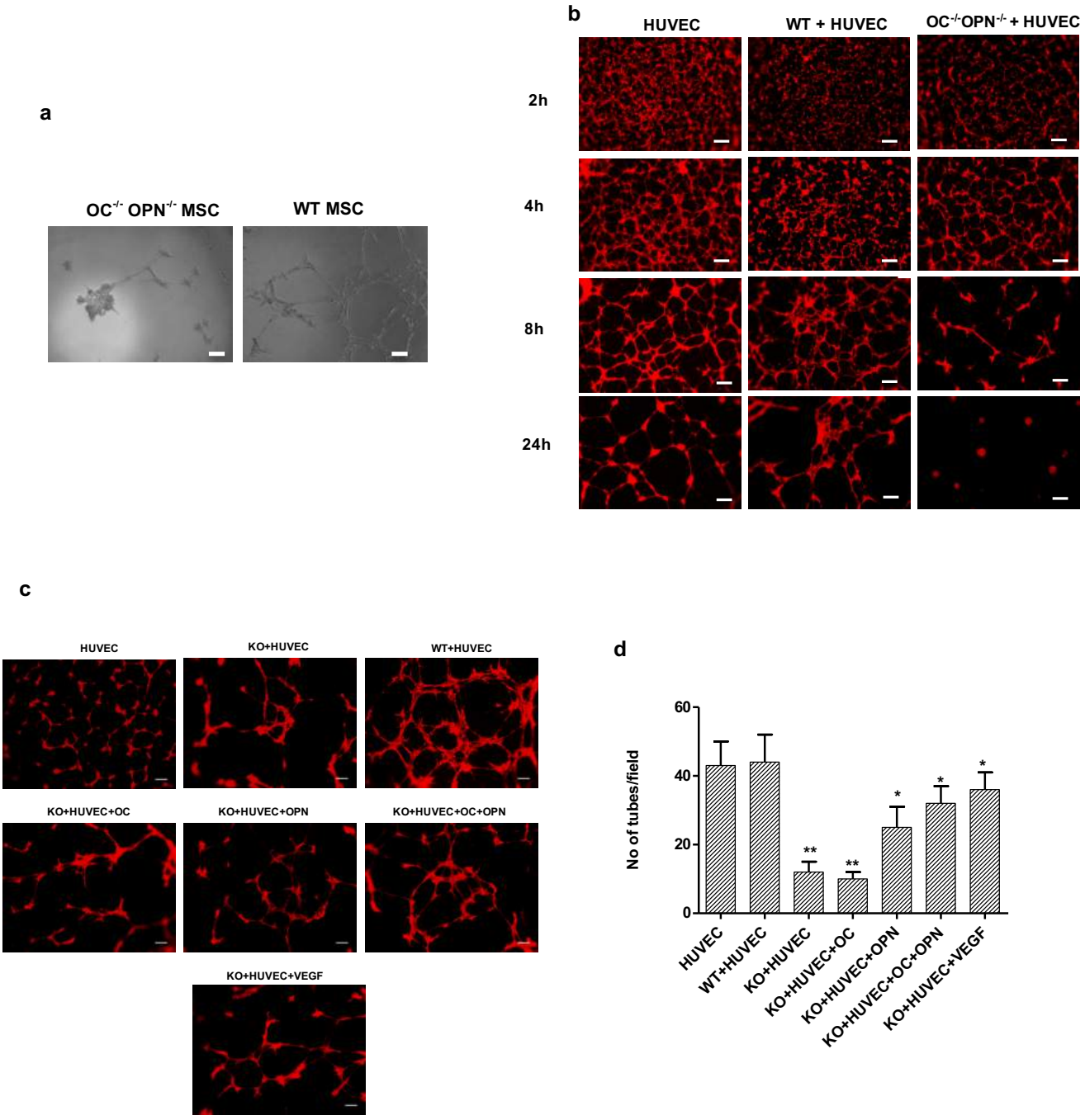

Figure II.14. Angiogenic properties of $OC^{-/-}$ $OPN^{-/-}$ MSC. **a)** $OC^{-/-}$ $OPN^{-/-}$ MSC were not able to form a tubular structure in matrigel, compared with WT MSC. **b**) Co-culture of $OC^{-/-}$ $OPN^{-/-}$ MSC with HUVEC were not able to support tubular structure formed by HUVEC. **c)** Co-culture of $OC^{-/-}OPN^{-/-}$ MSC with HUVEC supplemented with OC and/or OPN and VEGF. Scale bars, 100 µm. **d)** Quantification of number of tubular-like structures formed by HUVEC co-cultured with $OC^{-/-}$ $OPN^{-/-}$ (KO) MSC supplemented with OC and/or OPN and VEGF. Values are expressed as mean ± SD. **p<0.01; *p<0.05, compared to HUVEC (n=3).

II.4. Discussion

Several studies from our group have reported that OC and OPN influence bone morphology and mechanical properties (Poundarik *et al.* 2012, Morgan *et al.* 2015, Bailey *et al.* 2017, Poundarik *et al.* 2018). In fact, despite our group has already seen that bone morphology of either $OC^{-/-}$ or $OPN^{-/-}$ single knockout mice was not different from each other or from WT mice, bones from mice lacking both OC and OPN ($OC^{-/-}$ $OPN^{-/-}$) were shorter, with thicker cortices and larger cortical areas compared with WT and single knockout $OC^{-/-}$ and $OPN^{-/-}$ groups, suggesting a synergistic role of OC/OPN regarding bone morphology (Bailey *et al.* 2017). In particular, we observed that the removal of both proteins induced morphological adaptations at the structural level to maintain bone strength. Our next goal was to investigate the synergistic effect of these two proteins at the cellular level. We decided to evaluate MSC derived from $OC^{-/-}$ $OPN^{-/-}$ mice because single knockout mice models (for example $OPN^{-/-}$ or $OC^{-/-}$) alone fail to elucidate the specific roles of non-collagenous proteins in the different cellular processes, since the loss of one protein may be compensated by the other. Therefore, we isolated MSC from the bone marrow of $OC^{-/-}OPN^{-/-}$ mice and characterized these cells, investigating the roles of OC and OPN on cell proliferation, differentiation ability and angiogenic capacity. Successful isolation and expansion of the primary MSC from the bone marrow of WT and double knockout mice ($OC^{-/-}$ $OPN^{-/-}$) enabled us to carry out the subsequent investigation.

$OC^{-/-}$ $OPN^{-/-}$ MSC demonstrated the same phenotype as WT MSC, expressing CD29, CD105, Sca-1 and having lower levels of CD45 (Shen *et al.* 2011) (Figure II.1c). However, we observed that the proliferative potential of $OC^{-/-}$ $OPN^{-/-}$ MSC was impaired by the lack of OC and OPN, compared with WT MSC. Indeed, a kinetic study performed with these cells demonstrated a slower growth rate than WT MSC, reaching lower cell numbers (Figure II.5e).

Having $OC^{-/-}$ $OPN^{-/-}$ MSC a slower growth rate that WT MSC but presenting similar surface markers, further characterization of these cells in respect to ECM was attempted in order to find some clues for the differences observed between $OC^{-/-}$ $OPN^{-/-}$ MSC and WT MSC.

GAG are the major constituents of proteoglycans and can be found in multiple tissues being important components of the ECM. GAG are known to participate in different physiological processes by modulating signaling pathways that regulate several cellular processes. Moreover, GAG are important for controlling hydration and swelling pressure due to their negatively charges, maintaining their biomechanical properties. In addition, the sulfation patterns in the GAG chains allow the interaction with growth factors, cell surface receptors, enzymes, cytokines, chemokines and proteins that are associated with several biological processes, such as development, cell growth and differentiation (Papy-Garcia *et al.* 2017, Wang *et al.* 2017, Gasimli *et al.* 2014, Kjellén *et al.* 2018). Concordantly, we believe that the characterization of the GAG content, composition and sulfation patterns on $OC^{-/-}$ $OPN^{-/-}$ MSC is critical for a better understanding of ECM role in directing cellular responses, in particular in regulating mineralization.

In this work, we used a previously developed method of liquid chromatography-tandem mass spectrometry (LC-MS/MS) with multiple reaction monitoring (MRM) (Sun *et al.* 2015) to characterize $OC^{-/-}$ $OPN^{-/-}$ MSC and WT MSC in terms of their GAG content, composition and sulfation pattern. $OC^{-/-}$ $OPN^{-/-}$ MSC were mainly composed by CS and presented higher amounts and relative percentages of this GAG than WT MSC (Figure II.2b, Figure II.3). Interestingly, the amount of GAG produced by $OC^{-/-}$ $OPN^{-/-}$ MSC increased dramatically when compared with WT MSC. As OC and OPN are the most abundant non-collagenous bone

proteins present in bone matrix, it is predicted that the lack of these proteins will induce the production of other important non-collagenous bone matrix proteins to compensate the lack of OC/OPN. Therefore, we hypothesize that bone ECM increases its GAG content as a compensatory mechanism, synthesizing a matrix richer in GAG. Each cell type secretes unique and specific ECM to fulfil the biological requirements of its native tissue. Here, we observed that although the amount of GAG produced by WT and $OC^{-/-}$ $OPN^{-/-}$ MSC after osteogenic differentiation was different, their relative percentage (CS, HS, HA) was quite similar. Engfeldt and Hjerpe demonstrated that the total amount of GAG in bone tissue, mainly CS, seems to decrease while the degree of mineralization increases (Engfeldt and Hjerpe 1976). Therefore, we hypothesize that the decrease of GAG content observed when MSC were osteogenically differentiated for both cell types (WT and $OC^{-/-}OPN^{-/-}$) was due to the deposition of a more mature mineralized matrix, indicating a late phase of bone mineralization due to the induction of osteogenic differentiation. Our results indicate that, in terms of CS disaccharides, all cell types, undifferentiated and after osteogenic differentiation, were mainly composed by 4S. Indeed, different works have already shown that 4S CS disaccharide was the major GAG present in bone tissue (Engfeldt and Hjerpe 1976, Waddington *et al.* 1989).

Several reports have shown that OPN exerts an important effect on different types of cells, increasing the proliferation of tumor cells (Luo *et al.* 2011, Pazolli *et al.* 2009*,* Saleh *et al.* 2016*)*, neural stem cells (Rabenstein *et al. 2015)*, vascular smooth muscle cells (Lee *et al*. 2016*)* and hepatic progenitor cells (Liu *et al*. 2015). We, therefore, hypothesize that the lack of secreted OPN was the main responsible of the impairment of proliferation observed by $OC^{-/-}$ $OPN^{-/-}$ MSC. Furthermore, we supplemented the culture medium with OC and/or OPN extracellularly and observed that $OC^{-/-}$ $OPN^{-/-}$ MSC were able to recover their proliferative potential when supplemented with 1 µg/ml of OPN and 1 µg/ml of OPN and OC (Figure II.12a). We confirmed that the lack of OPN is the responsible for the impairment of proliferation capacity observed by $OC^{-/-}$ $OPN^{-/-}$ MSC, since when only OC was added to the culture medium $OC^{-/-}$ $OPN^{-/-}$ MSC did not enhance proliferation.

We also focused on the effects of OC and OPN in regulating MSC differentiation and we observed that, although adipogenic and chondrogenic differentiation did not present any significant differences, osteogenic differentiation of $OC^{-/-}$ $OPN^{-/-}$ MSC seemed to be retarded when compared to WT MSC. In fact, the lower amount of calcium levels, as well as, micrographs of the mineral produced by $OC^{-/-}$ $OPN^{-/-}$ MSC demonstrated an impairment of mineral production by these double knockout cells. Interestingly, SEM micrographs showed that $OC^{-/-}$ $OPN^{-/-}$ MSC presented lower amount of mineral nodules after 15 and 21 days of osteogenic differentiation, compared with WT MSC (Figure II.8a). Moreover, gene expression levels of osteogenic markers demonstrated that $OC^{-/-}$ $OPN^{-/-}$ MSC downregulated most of the osteogenic genes, such as *Runx2*, *Col I*, *OC* and *OPN*. Interestingly, ALP expression levels were enhanced in $OC^{-/-}$ $OPN^{-/-}$ MSC compared to WT MSC. Aiming to better understand the quality of the mineral produced by these cells, we analyzed these minerals using FTIR and Raman spectroscopy. Results showed that after 21 days of osteogenic differentiation, FTIR spectra of minerals produced by $OC^{-/-}$ $OPN^{-/-}$ MSC did not present the absorption peaks associated with major bone-related molecular species, such as phosphate and carbonate, in contrast with WT MSC. FTIR spectra of WT and $OC^{-/-}$ $OPN^{-/-}$ MSC demonstrated absorption peaks associated with cellular components, such as amide groups, carbohydrates, and amino acids before and after osteogenic differentiation. Raman spectroscopy was used to characterize the differentiation process of stem cells over time. Using Raman spectroscopy, we were able to characterize the maturation level of minerals produced by

$OC^{-/-}$ $OPN^{-/-}$ MSC. The results showed that after 15 days of osteogenic differentiation, WT MSC were able to produce OCP (957 cm^{-1}), a hydroxyapatite precursor, whereas the minerals produced by $OC^{-/-}$ $OPN^{-/-}$ MSC did not present the OCP peak. Indeed, after 21 days of osteogenic differentiation, HAP was detected in the minerals produced by WT cells, indicating a late stage of the differentiation. However, $OC^{-/-}$ $OPN^{-/-}$ MSC did not present HAP peak (960 cm^{-1}), instead a β-TCP peak was detected (970 cm^{-1}), also a hydroxyapatite precursor. Notably, the hydroxyapatite peak was only detected in the minerals produced by $OC^{-/-}$ $OPN^{-/-}$ MSC after 30 days of osteogenic differentiation. We observed that the maturation of mineral species was delayed compared to the control group. These results suggest an impairment and delay of osteogenic differentiation of stem cells lacking OC and OPN. This phenomenon confirms, at a cellular level, that OC and OPN are important regulators of bone mineralization during osteogenic differentiation of MSC.

In fact, during the crystal growing of biomineralization process, OC has been reported to accelerate nucleation of hydroxyapatite and inhibit hydroxyapatite precipitation (Ducy *et al.* 1996). Previous studies have already reported that both OC and OPN have specific roles in the biomolecular regulation of mineral in bone and together they are major determinants of the quality of bone mineral (Poundarik *et al.* 2018). Poundarik and colleagues have shown that OC and OPN regulate bone mineral crystal size and organization in a codependent manner (Poundarik *et al.* 2018). Our data showed that the inhibition of osteogenesis was due to the downregulation of some osteogenic gene markers involved in osteogenesis, such as *Runx2*, *Col I*, *OC* and *OPN* (Figure II.9). The mechanism responsible for the osteogenic downregulation requires further investigation.

Our studies also demonstrated that $OC^{-/-}$ $OPN^{-/-}$ MSC proliferation and osteogenic potential were recovered when OC/OPN were extracellularly supplemented. In fact, $OC^{-/-}$ $OPN^{-/-}$ MSC produced more calcium deposits after 21 days of osteogenic differentiation when OC/OPN were exogenously applied. Moreover, Raman spectroscopy demonstrated that after 21 days of osteogenic differentiation, when OC/OPN were exogenously added to the culture medium, minerals produced by $OC^{-/-}$ $OPN^{-/-}$ cells were mainly composed by HAP (960 cm^{-1}) as the minerals produced by WT MSC. Moreover, when OC/OPN were not present in the culture medium, HAP peak was not detected by Raman spectroscopy, demonstrating that the mineral produced by these cells was not sufficiently mature. However, although an increase of calcium accumulation was observed when both OC/OPN proteins were added to the medium, $OC^{-/-}$ $OPN^{-/-}$ MSC continued to produce lower amount of calcium levels compared with WT MSC. These data suggest that OC and OPN exert their regulatory role in MSC differentiation mainly in an extracellular manner.

Regarding angiogenesis, MSC derived from murine or human bone marrow cells have the ability to regulate new blood vessel formation, stability and function (Zhou *et al.* 2012, Kachgal *et al.* 2011). Thus, we assess the effects of OC and OPN on the angiogenic potential.

Cell migration plays an important role in the process of angiogenesis. Many cytokines can enhance the migration of MSC, such as monocyte chemoattractant protein-1 (MCP-1) and stromal cell-derived factor-1 (SDF-1) (Grudzinska *et al.* 2013, Ryu *et al.* 2010), therefore we hypothesize that the lack of OPN and OC in MSC could impair the migration of MSC, since some non-collagenous proteins, such as OPN, have been reported to participate in the recruitment and migration of cells (Rabenstein *et al.* 2015, Poggio *et al.* 2011, Tuck *et al.* 2003). In this study, a wound scratch assay demonstrated that conditioned medium from $OC^{-/-}$ $OPN^{-/-}$ MSC did not promote the migration of HUVEC after 12 h, unlike the conditioned medium from WT

MSC. Indeed, it is known that MSC secrete angiogenic factors that could enhance the migratory effects of cells. We, therefore, concluded that the fact that OC and OPN are not being secreted by MSC influence negatively the migration of HUVEC. Using the same approach in a tube formation assay, we observed that angiogenic capacities of HUVEC are diminished when conditioned medium from $OC^{-/-}$ $OPN^{-/-}$ was used, demonstrated by the reduction of number of tubes formed. However, the mechanism of action related with the reduction of angiogenic potential should be further studied. We hypothesize that the lack of OC and OPN would decrease the angiogenic potential of these cells directly, since OPN has been reported as a pro-angiogenic factor (Dai *et al.* 2009), but we believe that, indirectly, these proteins might also compromise the amount and composition of other cytokines and soluble factors present in the conditioned medium of $OC^{-/-}$ $OPN^{-/-}$ MSC. For example, OPN is known to induce VEGF expression (Ramchandani *et al.* 2015) thus, we hypothesize that the lack of OPN in the culture medium, could also downregulate the amount of VEGF or other angiogenic factors, and, therefore, diminish the angiogenic potential. Further studies, should focus on analyzing the different cytokines and growth factors secreted by $OC^{-/-}$ $OPN^{-/-}$ MSC to understand the real mechanism of action.

Furthermore, we observed that WT MSC were able to form tubes on a matrigel substrate by itself, whereas $OC^{-/-}$ $OPN^{-/-}$ MSC lack their ability to form capillary-like structures in a tube formation assay (Figure II.14a).

We also studied the effect of $OC^{-/-}$ $OPN^{-/-}$ MSC on HUVEC ability to form tubes, when co-culturing both cells. It has been previously demonstrated that co-culture of HUVEC and MSC can form a vascular tissue-like network *in vitro* through the stimulation of VEGF production (Grellier *et al.* 2009). These cell-cell co-culture may activate different signaling pathways to enhance the biological effects of MSC.

We observed that when HUVEC were co-cultured with WT MSC and $OC^{-/-}$ $OPN^{-/-}$ MSC, HUVEC started to form tubular structures after 4h. However, after 8h, HUVEC co-cultured with $OC^{-/-}$ $OPN^{-/-}$ MSC were not able to sustain and support their interconnected network and after 24h the tubes were completely destroyed and only sparse agglomerates of HUVEC were possible to be observed (Figure II.14b). In fact, OPN secreted by cancer cells was reported to act as a potent angiogenic factor contributing to tumor growth in several cancer types (Chakraborty *et al.* 2008, Tang *et al.* 2007, Takahashi *et al.* 2002). OPN has been shown to promote vascular formation in murine neuroblastoma (Takahashi et al. 2002) and inhibition of OPN levels induces a suppression of angiogenesis in gastric cancer (Tang *et al.* 2007). Therefore, we believe that the lack of OPN is also the responsible for the loss of HUVEC tubular structure after 8h in a matrigel substrate. To confirm our hypothesis, we supplemented the co-culture of HUVEC and $OC^{-/-}$ $OPN^{-/-}$ MSC with OC and/or OPN. When HUVEC were co-cultured with WT MSC a more robust and interconnected capillary structure was created, however results showed that when HUVEC were co-cultured with $OC^{-/-}OPN^{-/-}$ MSC and supplemented extracellularly with OPN, their tubular structure was able to be sustained after 8h. The number of tubes formed after 8h when OPN and OPN/OC added extracellularly were significantly higher compared with the control (HUVEC + $OC^{-/-}OPN^{-/-}$) and, interestingly, similar to the results obtained when HUVEC and $OC^{-/-}$ $OPN^{-/-}$ MSC co-cultures were supplemented with VEGF. Therefore, we believe that OPN is important for angiogenesis, acting directly or indirectly, through the stimulation of other angiogenic factors. Further assays need to be done to understand better the mechanism of action of this protein.

We showed that OC/OPN deficiency impaired the proliferation, osteogenic differentiation, mineralization and angiogenic potential of MSC. These results demonstrated the importance of OC/OPN for the normal function of MSC, specifically for osteogenesis and angiogenesis, two important mechanisms for bone repair.

Moreover, most used techniques to confirm osteogenic differentiation rely on using osteogenic gene expression and histological staining techniques, such as the Von Kossa and Alizarin Red methods, being difficult to determine the quality of bone-like calcium phosphate mineral produced by the cells. Therefore, new techniques have been emerging to verify the presence and quality of the mineral formed, such as FTIR and Raman spectroscopy. We believe that these techniques will allow a better understanding about the similarities of the mineral produced *in vitro* with the native osteoblasts, generating quantitative and precise outputs that can be used as quality control to establish a well-defined protocol for osteogenic differentiation of cells. Herein, we developed and applied a protocol to evaluate the maturation level of the minerals produced by MSC at different timepoints of osteogenic differentiation, providing new insights in the quality and composition of the mineral produced *in vitro*.

Taken together, these results confirmed, at a cellular level, that OC and OPN are important regulators of bone mineralization and angiogenesis and provide new insights into forming high quality bone, relevant for treatment of fracture healing in older and osteoporotic bone.

II.5. References

Alt K.W. Principles of bone biology. *Homo-Journal of Comparative Human Biology*, 2nd edition, **53**, 191–192 (2002).

Anada T., Kumagai T., Honda Y., Masuda T., Kamijo R. Kamakura S., Yoshihara N., Kuriyagawa T., Shimauchi H., Suzuki O.Dose-dependent osteogenic effect of octacalcium phosphate on mouse bone marrow stromal cells. *Tissue Eng. Part A,* **14**, 965–978 (2008).

Bailey S. Karsenty G., Gundberg C., Vashishth D. Osteocalcin and osteopontin influence bone morphology and mechanical properties. *Ann. N.Y. Acad. Sci.,***1409**, 74-84 (2017).

Boskey A., Maresca M., Appel J. The effects of noncollagenous matrix proteins on hydroxyapatite formation and proliferation in a collagen gel system. *Connect. Tissue Res.*, **21**, 171-176 (1989b).

Boskey A.L. Noncollagenous matrix proteins and their role in mineralization. *Bone and Mineral* **6,** 111–123 (1989).

Boskey A.L.,Coleman R. Aging and bone. *J. Dent. Res.* **89**, 1333-1348 (2010).

Boskey, A.L. Mineral-matrix interactions in bone and cartilage. *Clin. Orthop. Relat. Res.,* **281**, 244-274 (1992).

Cantatore F.P., Crivellato E., Nico B., Ribatti D. Osteocalcin is angiogenic in vivo. *Cell Biol. Int.,* **29**, 583-585 (2005).

Carvalho R.S., Kostenuik P.J., Salih E., Bumann A., Gerstenfeld L.C. Selective adhesion of osteoblastic cells to different integrin ligands induces osteopontin gene expression. *Matrix Biol.,* **22**, 241-249 (2003).

Chakraborty G., Jain S., Kundu G.C. Osteopontin promotes vascular endothelial growth factor-dependent breast tumor growth and angiogenesis via autocrine and paracrine mechanisms. *Cancer Res.,* **68**, 152-161 (2008).

Chen Q., Shou P. Zhang L., Xu C., Zheng C., Han Y., Li W., Huang Y., Zhang X., Shao C., Roberts Al., Rabson A.B., Ren G., Zhang Y., Wang Y., Denhardt D.T., Shi Y. An osteopontin-integrin interaction plays a critical role in directing adipogenesis and osteogenesis by mesenchymal stem cells. *Stem Cells.,* **32**, 327-337 (2014).

Dai J., Peng L., Fan K., Wang H., Wei R., Ji G., Cai J., Lu B., Li B., Zhang D., Kang Y., Tan M., Qian W., Guo Y. Osteopontin induces angiogenesis through activation of PI3K/AKT and ERK1/2 in endothelial cells. *Oncogene,* **28**, 3412 (2009).

DeFranco D.J. Glowacki J. Cox K.A., Lian J.B. Normal bone particles are preferentially resorbed in the presence of osteocalcin-deficient bone particles in vivo. *Calcif. Tissue Int.,* **49,** 43-50 (1991).

Denhardt D.T., Guo X. Osteopontin: a protein with diverse functions. *FASEB J.*, **7,** 1475–1482 (1993).

Ducy P., Desbois C., Boyce B., Pinero G., Story B., Dunstan C., Smith E., Bonadio J., Goldstein S., Gundberg C., Bradley A., Karsenty G. Increased bone formation in osteocalcin-deficient mice. *Nature,* **382,** 448-452 (1996).

Egusa H., Kayashima H., Miura J., Uraguchi S., Wang F., Okawa H., Sasaki J., Saeki M., Matsumoto T., Yatani H. Comparative analysis of mouse-induced pluripotent stem cells and MSC during osteogenic differentiation in vitro. *Stem Cells Dev.,* **23**, 2156-2169 (2014).

Ek-Rylander B., Flores M., Wendel M., Heinegard D., Andersson G. Dephosphorylation of osteopontin and bone sialoprotein by osteoclastic tartrate-resistant acid phosphatase. Modulation of osteoclast adhesion in vitro. *J. Biol. Chem.*, **269**, 14853-14856 (1994).

Engfeldt B., Hjerpe A., Glycosaminoglycans of human bone tissue at different stages of mineralization. *Acta Pathol. Microbiol. Scand. A.*, **84**, 95-106 (1976).

Gasimli L., Hickey A.M., Yang B., Li G., Dela Rosa M., Nairn A. V., Kulik M.J., Dordick J.S., Moremen K.W., Dalton S., Linhardt R.J. Changes in glycosaminoglycan structure on differentiation of human embryonic stem cells towards mesoderm and endoderm lineages. *Biochim. Biophys. Acta - Gen. Subj.*, **1840**, 1993–2003 (2014).

Globus R.K, Doty S.B, Lull J.C., Holmuhamedov E., Humphries M.J. , Damsky C.H. Fibronectin is a survival factor for differentiated osteoblasts. *J. Cell. Sci.*, **111,** 1385-1393 (1998).

Gordon J.A., Tye C.E., Sampaio A.V., Underhill T.M., Hunter G.K., Goldberg H.A. Bone sialoprotein expression enhances osteoblast differentiation and matrix mineralization in vitro. *Bone*, **41**, 462-473 (2007)**.**

Grellier M., Ferreira-Tojais N., Bourget C., Bareille R., Guillemot F., Amédée J. Role of vascular endothelial growth factor in the communication between human osteoprogenitors and endothelial cells. *J. Cell. Biochem.,* **106**, 390–398 (2009).

Grudzinska M.K., Kurzejamska E., Bojakowski K., Soin J., Lehmann M.H., Reinecke H., Murry C.E., Soderberg-Naucler C., Religa P. Monocyte chemoattractant protein 1-mediated migration of mesenchymal stem cells is a source of intimal hyperplasia. *Arterioscler. Thromb. Vasc. Biol.,* **33**, 1271-1279 (2013).

Grynpas M.D, Tupy J.H., Sodek J. The distribution of soluble, mineral-bound, and matrix-bound proteins in osteoporotic and normal bones. *Bone,* **15**, 505-513 (1994).

Hadjidakis D.J., Androulakis I.I. Bone remodeling. *Ann. N.Y. Acad. Sci.,* **1092**, 385-396 (2006).

Harris N.L., Rattray K.R., Tye C.E., Underhill T.M., Somerman M.J., D'Errico J.A., Chambers A.F., Hunter G.K., Goldberg H.A. Functional analysis of bone sialoprotein: identification of the hydroxyapatite-nucleating and cell-binding domains by recombinant peptide expression and site-directed mutagenesis. *Bone*, **27**, 795-802 (2000).

Horton M.A., Nesbit M.A., Helfrich M.H. Interaction of osteopontin with osteoclast integrins. *Ann. N. Y. Acad. Sci.*, **760**, 190-200 (1995).

Huang W., Carlsen B., Rudkin G., Berry M., Ishida K. , Yamaguchi D.T., Miller T.A. .Osteopontin is a negative regulator of proliferation and differentiation in MC3T3-E1 pre-osteoblastic cells. *Bone*, **34**, 799-808 (2004).

Hung P.S., Kuo Y.C., Chen H.G., Chiang H.H., Lee O.K. Detection of osteogenic differentiation by differential mineralized matrix production in mesenchymal stromal cells by Raman spectroscopy PLoS One, **8**, e65438 (2013).

Ingram R.T. Park Y.K., Clarke B.L., Fitzpatrick L.A. Age- and gender- related changes in the distribution of osteocalcin in the extracellular matrix of normal male and female bone. Possible involvement of osteocalcin in bone remodeling. *J. Clin. Invest.,* **93**, 989-997 (1994).

Johnsson, M.S., Nancollas, G.H. The role of brushite and octacalcium phosphate in apatite formation. *Crit. Rev. Oral Biol. Med.,* **3**, 61-82 (1992).

Kachgal S., Putnam A.J. Mesenchymal stem cells from adipose and bone marrow promote angiogenesis via distinct cytokine and protease expression mechanisms. *Angiogenesis,* **14**, 47-59 (2011).

Kjellén L., Lindahl U. Specificity of glycosaminoglycan–protein interactions. *Curr. Opin. Struct. Biol.,* **50**, 101–108 (2018).

Kojima H., Uede T., Uemura T. In vitro and in vivo effects of the overexpression of osteopontin on osteoblast differentiation using a recombinant adenoviral vector. *J. Biochem. (Tokyo)*, **136**, 377-386 (2004).

Lee S.J., Baek S.E., Jang M.A., Kim C.D. Osteopontin plays a key role in vascular smooth muscle cell proliferation *via* EGFR-mediated activation of AP-1 and C/EBP beta pathways. *Pharm.Res.,* **108**, 1-8 (2016).

Liang T., Zhu L., Gao W., Gong M., Ren J., Yao H., Wang K., Shi D., Coculture of endothelial progenitor cells and mesenchymal stem cells enhanced their proliferation and angiogenesis through PDGF and Notch signaling. *FEBS Open Biol.,* **7**, 1722-1736 (2017).

Liu Y., Cao L., Chen R., Zhou X., Fan X., Liang Y., Jia R., Wang H., Liu G., Guo Y., Zhao J. Osteopontin promotes hepatic progenitor cell expansion and tumorigenicity via activation of b-catenin in mice. *Stem Cells,* **33**, 3569-3580 (2015).

Luo X., Ruhland M.K., Pazolli E., Lind A.C., Stewart S.A.Osteopontin stimulates preneoplastic cellular proliferation through activation of the MAPK pathway. *Mol. Cancer Res.,* **9**, 1018-1029 (2011).

Mania V.M., Kallivokas A.G., Malavaki C., Asimakopoulou A.P., Kanakis J., Theocharis A.D., Klironomos G., Gatzounis G., Mouzaki A., Panagiotopoulos E., Karamanos N.K. A comparative biochemical analysis of glycosaminoglycans and proteoglycans in human orthotopic and heterotopic bone. *IUBMB Life*, **61**, 447-452 (2009).

Morgan S. Poundarik A.A., Vashishth D. Do non-collagenous proteins affect skeletal mechanical properties? *Calcif. Tissue Int.,* **97**, 281-291 (2015).

Nadri S., Soleimani M., Hosseni R.H., Massumi M., Atashi A., Izadpanah R. An efficient method for isolation of murine bone marrow mesenchymal stem cells. *Int. J. Dev. Biol.,* **51**, 723-729 (2007).

Nikel O., Laurencin D., McCallum S.A., Gundberg C.M., Vashishth D. NMR investigation of the role of osteocalcin and osteopontin at the organic-inorganic interface in bone. *Langmuir,* **29**, 13873-13882 (2013).

Papy-Garcia D., Albanese P. Heparan sulfate proteoglycans as key regulators of the mesenchymal niche of hematopoietic stem cells. *Glycoconj. J.*, **34**, 377–391 (2017).

Pazolli E., Luo X., Brehm S., Carbery K., Chung J.J., Prior J.L., Doherty J., Demehri S., Salavaggione L., Piwnica-Worms D., Stewart S.A. Senescent stromal-derived osteopontin promotes preneoplastic cell growth. *Cancer Res.,* **69**, 1230-1239 (2009).

Plantalech L. Guillaumont M., Vergnaud P., Leclercq M., Delmas P.D. Impairment of gamma carboxylation of circulating osteocalcin (bone gla protein) in elderly women. *J. Bone Miner. Res.,***6,** 1211-1216 (1991).

Poggio P. Grau J.B., Field B.C., Sainger R., Seefried W.F., Rizzolio F., Ferrari G. Osteopontin controls endothelial cell migration in vitro and in excised human valvular tissue from patients with calcific aortic stenosis and controls*. J. Cell. Physiol.,* **226**, 2139-2149 (2011).

Poundarik A.A., Boskey A., Gundberg C., Vashishth D. Biomolecular regulation, composition and nanoarchitecture of bone mineral. *Sci. Rep.,* **8**, 1191 (2018).

Poundarik A.A., Diab T., Sroga G.E., Ural A., Boskey A.L., Gundberg C.M., Vashishth D. Dilatational band formation in bone. *Proc. Natl. Acad. Sci. U.S.A.,* **109,** 19178–19183 (2012).

Rabenstein M., Hucklenbroich J., Willuweit A., Ladwig A., Fink G.R., Schroeter M., Langen K.J., Rueger M.A. Osteopontin mediates survival, proliferation and migration of neural stem cells through the chemokine receptor CXCR4. *Stem Cell. Res. Ther.,* **6**, 99 (2015).

Ramchandani D., Weber G.F.Interactions between osteopontin and vascular endothelial growth factor: Implications for cancer. *Biochem. Biophys. Acta,* **1855,** 202-222 (2015).

Ravindran S., George A. Multifunctional ECM proteins in bone and teeth. Exp. Cell Res., **325**, 148-154 (2014).

Razzouk S., Brunn J.C., Qin C., Tye C.E., Goldberg H.A., Butler W.T. Osteopontin posttranslational modifications, possibly phosphorylation, are required for in vitro bone resorption but not osteoclast adhesion. *Bone*, **30**, 40-47 (2002).

Roche P., Goldberg H.A., Delmas P.D., Malaval L. Selective attachment of osteoprogenitors to laminin. *Bone,* **24**, 329-336 (1999).

Rodriguez D.E., Thula-Mata T., Toro E.J., Yeh Y.W., Holt C., Holliday L.S. Gower L.B. Multifunctional role of osteopontin in directing intrafibrillar mineralization of collagen and activation of osteoclasts. *Acta Biomater.,* **10,** 494-507 (2014).

Ryu C.H., Park S.A., Kim S.M., Lim J.Y., Jeong C.H., Jun J.A., Oh J.H., Park S.H., Oh W.I., Jeun S.S. Migration of human umbilical cord blood mesenchymal stem cells mediated by stromal cell-derived factor-1/CXCR4 axis via Akt, ERK, and p38 signal transduction pathways. *Biochem, Biophys. Res. Commun.,* **398**, 105-110 (2010).

Salasznyk R.M., Williams W.A., Boskey A., Batorsky A., Plopper G.E. Adhesion to vitronectin and collagen I promotes osteogenic differentiation of human mesenchymal stem cells. *J. Biomed. Biotechnol.*, **2004**, 24-34 (2004).

Saleh S., Thompson D.E., McConkey J., Murray P., Moorehead R.A. Osteopontin regulates proliferation, apoptosis, and migration of murine claudin-low mammary tumor cells. *BMC cancer,* **16**, 359 (2016).

Shen J., Tsai Y.T., Dimarco N.M., Long M.A., Sun X., Tang L. Transplantation of mesenchymal stem cells from young donors delays aging in mice. *Sci. Rep.*, **1**, 67 (2011).

Sroga G.E., Karim L., Colón W., Vashishth D. Biochemical characterization of major bone-matrix proteins using nanoscale-size bone samples and proteomics methodology. *Mol. Cell. Proteomics* **10,** M110.006718 (2011).

Stewart, S., Shea, D.A., Tarnowski, C.P., Morris, M.D., Wang, D., Franceschi, R., Lin, D.L., Keller, E. Trends in early mineralization of murine calvarial osteoblastic cultures: A Raman microscopic study. *J. Raman Spectrosc.*, **33**, 536–543 (2002).

Sun X., Li L., Overdier K.H., Ammons L.A., Douglas I.S., Burlew C.C., Zhang F., Schmidt E.P., Chi L., Linhardt R.J. Analysis of total human urinary glycosaminoglycan disaccharides by liquid chromatography-tandem mass spectrometry. *Anal. Chem.,* **87**, 6220–6227 (2015).

Suzawa M., Tamura Y., Fukumoto S., Miyazono K., Fujita T., Kato S. Takeuchi Y. Stimulation of Smad1 transcriptional activity by Ras-extracellular signal-regulated kinase pathway: a possible mechanism for collagen-dependent osteoblastic differentiation. *J. Bone Miner. Res.*, **17**, 240-248 (2002).

Takahashi F., Akutagawa S., Fukumoto H., Tsukiyama S., Ohe Y., Takahashi K., Fukuchi Y., Saijo N., Nishio K. Osteopontin induces angiogenesis of murine neuroblastoma cells in mice. *Int. J. Cancer,* **98**, 707-712 (2002).

Tang H. Wang J. Bai F., Hong L., Liang J., Zhai H., Lan M., Zhang F., Wu K., Fan D.Inhibition of osteopontin would suppress angiogenesis in gastric cancer. *Biochem. Cell. Biol*., **85**, 103-110 (2007).

Theocharis A.D., Seidel C., Borset M., Dobra K., Baykov V., Labropoulou V., Kanakis I., Dalas E., Karamanos N.K., Sundan A., Hjerpe A. Serglycin constitutively secreted by myeloma plasma cells is a potent inhibitor of bone mineralization in vitro. *J.Biol. Chem.*, **281**, 35116-35128 (2006).

Tsao Y.T., Huang Y.J., Wu H.H., Liu Y.A., Liu Y.S., Lee O.K. Osteocalcin mediates biomineralization during osteogenic maturation in human mesenchymal stromal cells. 2017 *Int. J. Mol. Sci.,* **18**, E159 (2017).

Tuck A.B., Hota C., Wilson S.M., Chambers A.F. Osteopontin-induced migration of human mammary epithelial cells involves activation of EGF receptor and multiple signal transduction pathways. *Oncogene*, **22**, 1198-1205 (2003).

Vashishth D. The role of the collagen matrix in skeletal fragility. *Curr. Osteoporos. Rep.* **5,** 62–66 (2007).

Waddington R.J., Embery G., Last, K.S. Glycosaminoglycans of human alveolar bone. *Arch. Oral Biol.*, **34**, 587–589 (1989).

Wang M., Liu X., Lyu Z., Gu H., Li D., Chen H. Glycosaminoglycans (GAGs) and GAG mimetics regulate the behavior of stem cell differentiation. *Colloids Surfaces B Biointerfaces*., **150**, 175–182 (2017).

Weber G.F. Ashkar S., Glimcher M.J., Cantor H. Receptor-ligand interaction between CD44 and osteopontin (Eta-1). *Science,* **271,** 509–512 (1996).

Zhou B., Tsaknakis G., Coldwell K.E., Khoo C.P., Roubelakis M.G., Chang C.H., Pepperell E., Watt S.M. A novel function for the haemopoietic supportive murine bone marrow MS-5 mesenchymal stromal cell line in promoting human vasculogenesis and angiogenesis. *Br. J. Haematol*., **3**, 299-311 (2012).

CHAPTER III – Synergistic effect of extracellularly supplemented OPN and OC on stem cell proliferation, osteogenic differentiation and angiogenic properties

Outline

A high demand for functional bone grafts is being observed worldwide, especially due to the increased life expectancy. Osteoinductive components should be incorporated into functional bone grafts, accelerating cell recruitment, cell proliferation, angiogenesis and new bone formation at a defect site. Non-collagenous bone matrix proteins, especially osteopontin (OPN) and osteocalcin (OC), have been reported to regulate some physiological process, such as cell migration and bone mineralization. However, the effects of OPN and OC on cell proliferation, osteogenic differentiation, mineralization and angiogenesis are still undefined. Therefore, we assessed the exogenous effect of OPN and OC supplementation on human bone marrow mesenchymal stem/stromal cells (BM MSC) proliferation and osteogenic differentiation. OPN dose-dependently increased the proliferation of BM MSC, as well as improved the angiogenic properties of human umbilical vein endothelial cells (HUVEC) by increasing the number of tubular-like structures *in vitro*. On the other hand, OC enhanced the differentiation of BM MSC into osteoblasts and demonstrated an increase in extracellular calcium levels and ALP activity, as well as higher mRNA levels of mature osteogenic markers osteopontin and osteocalcin. *In vivo* assessment of OC/OPN-enhanced scaffolds in a critical sized-defect rabbit long-bone model revealed that OC/OPN did not cause any inflammatory response, while bone tissue was being formed with active tissue remodeling. Taken together, these results suggest that OC and OPN stimulate bone regeneration by inducing stem cell proliferation, osteogenesis and enhancing angiogenic properties. The synergistic effect of OC and OPN observed in this study can be applied as an attractive strategy for bone regeneration therapeutics by targeting different vital cellular processes.

III.1. Introduction

The repair of large bone defects is a major clinical orthopedic need with a high demand. In fact, the treatment of bone loss has dramatically increased in the last decades, especially due to the large number of bone-related medical conditions that require clinical interventions and due to the dramatic growth of an aging population. For example, in the United States alone, around 8 million people, each year, break a bone, causing fractures (Holmes 2017). Moreover, for 5-10% of individuals with a broken bone, the fracture will fail to heal under the usual treatment, causing non-union bone fractures (Holmes 2017). To address these needs, treatments and therapies, such as autografts, allografts and bone substitutes are often used, however some side effects and availability have limited their wide-scale application (Chiarello *et al.* 2013). In particular, the scarcity of bone graft donors, as well as the higher risk of immunologic rejection and infection, limit the clinical use of allografts (Stock & Vacanti *et al.* 2011, Campana *et al.* 2014). Autografts have also some limitations, such as their short availability and the possible risk of site morbidity, pain, infection, scarring, associated with the harvest procedure (Stock & Vacanti *et al.* 2001).

Tissue engineering technologies offer advances to regenerate bone including the development of scaffolds that can release growth factors in a controlled manner, such as bone morphogenetic protein-2 (BMP-2) and basic fibroblast growth factor (bFGF) proteins (De Witte *et al.* 2018). These growth factors have great potential for tissue engineering and regenerative medicine. However, they too have associated disadvantages including immunogenicity, relatively high cost, large molecular weight (100-200 a.a.), *in vitro* instability, and difficulty in sterilization (Huang *et al*. 2018). Consequently, recent studies have focused on investigating the interaction between cell membrane receptors and extracellular matrix proteins (Fernandez-Yague *et al.* 2015, Heino *et al.* 2009, Schultz *et al*. 2009) and the result lend support to strategies that employ and mimic the bone extracellular matrix in a more reliable way, such as the use of osteoinductive peptides (Hu *et al.* 2013).

Bone extracellular matrix consists of two different components: an organic matrix, constituted by collagen and non-collagenous proteins (NCP) (Boskey 2007, Young 2003), and an inorganic phase, composed mainly by hydroxyapatite crystals (Boskey 2007, Young 2003). The NCP, isolated from bone, have been found to be biologically active. Thus, by understanding the properties and functions of NCP, new strategies mimicking the bone extracellular matrix could be designed for bone tissue engineering applications (Mouw *et al.* 2014). However, the function of NCP in bone regeneration is not yet completely understood. It has been speculated that NCP might have an important role in cell attachment, cell differentiation and regulation of the deposition of hydroxyapatite minerals (Boskey 1989, Al-Qtaitat *et al.* 2014). Furthermore, some of these proteins could be multifunctional, playing different roles in the bone and, therefore, can have a synergistic effect on the cellular behavior and mechanical properties of bone. Osteopontin (OPN) and osteocalcin (OC) are some of the most common non-collagenous proteins present in bone matrix.

Osteopontin is an acidic glycoprotein that consists of about 300 amino acids, with a molecular weight of 34 kDa (Denhardt & Guo 1993, Icer *et al.* 2018). In bone, OPN is produced by osteoblasts during pre-mineralization at the late stages of osteoblastic maturation (Denhardt & Guo 1993). OPN binds to $\alpha_v\beta_1$, $\alpha_v\beta_3$, $\alpha_v\beta_5$, $\alpha_4\beta_1$, $\alpha_5\beta_1$ and $\alpha_9\beta_1$ integrins (Denhardt & Guo1993, Barry *et al.* 2000) through its arginine-glycine-aspartate (RGD) domain. Additionally, OPN can also present an RGD-independent mechanism, in which OPN may engage CD44 (Denhardt & Guo 1993, Denhardt & Noda 1998, Katagiri *et al.* 1999). Osteopontin has been proposed to regulate many physiological processes such as collagen organization, cell adhesion, cell viability, cell migration,

angiogenesis and calcification (Denhardt & Guo 1993, Rodriguez *et al.* 2014). Besides the RGD sequence, OPN also contains aspartic acid residues, high negative charge motifs, that might be responsible for its high affinity to calcium (Rittling *et al.*1998). Therefore, OPN has been suggested to modulate the nucleation of calcium phosphate during mineralization (Boskey 1995, Contri *et al.* 1996).

Osteocalcin is an approximately 5.8 kDa protein consisting of a single chain of 49-50 amino acids, being the most abundant non-collagenous protein in bone (Hauschka *et al.* 1989). Osteocalcin is secreted by osteoblasts and it is present in dentine and calcified matrix. This protein has three glutamic acid residues at positions 17, 21, and 24 (Poser *et al.* 1980) that bind calcium. During bone development, OC production is very low and does not reach maximal levels until late stages of mineralization (Gundberg 2000). Although its precise mechanism of action is unclear, OC is presumed to influence bone mineralization (Hauschka & Reid 1978, Ducy *et al.* 1996, Zoch *et al.* 2016), in part through its ability to bind with high affinity to the mineral component of bone and due to its acidic character (Poser & Price 1979). Thus, OC accelerates the nucleation of hydroxyapatite, playing an active role in the early stages of bone healing (Rammelt *et al.* 2005). Additionally, OC also plays an important role in the recruitment of osteoclasts (Chenu *et al.* 1994) and osteoblasts (Bodine & Komm 1999), which have active roles in bone resorption and formation, respectively.

Therefore, the multifunctional properties of these NCP make them attractive agents for bone tissue engineering applications. Furthermore, bone regeneration involves the connection between blood vessels and bone cells (Kanczler & Oreffo 2008), in which angiogenesis plays a special role in the repair and regeneration of bone tissue by supplying the critical nutrients and oxygen to enhance bone healing (Cinotti *et al.* 2013, Cui *et al.* 2013). In fact, OPN has been reported as an important angiogenic factor, inducing angiogenesis of endothelial cells, in bone regeneration and tumor growth (Chakraborty *et al.* 2008, Dai *et al.* 2009). Furthermore, OPN has the ability to regulate VEGF secretion and angiogenesis (Chakraboty *et al.* 2006). Similarly, it is presumable that OC induces angiogenesis (Neve *et al.* 2013). Indeed, OC has been reported as angiogenic *in vivo* (Cantatore *et al.* 2005). However, the relationship between OC and angiogenesis is still not well defined and studied. Additionally, although OPN and OC are known to be vital for bone formation, the effect of these non-collagenous bone matrix proteins on stem cell proliferation, osteogenic differentiation and angiogenesis are still undefined. Thus, the goal of this study is to investigate the effect of OPN and OC on human bone marrow mesenchymal stem/stromal cells (BM MSC) proliferation, osteogenic differentiation, mineralization and to evaluate the angiogenic properties on human vein endothelial cells (HUVEC), by analyzing their osteoinductive and pro-angiogenic properties, and the possible synergistic effect of these two proteins.

III.2. Materials & Methods

III.2.1. Cell culture

Human BM MSC used here are part of the cell bank available at the Stem Cell Engineering Research Group (SCERG), iBB-Institute for Bioengineering and Biosciences at Instituto Superior Técnico (IST). Originally, human bone marrow aspirates were obtained from local hospitals under collaboration agreements with iBB-IST. All human samples were obtained from healthy donors after written informed consent according to the Directive 2004/23/EC of the European Parliament and of the Council of 31 March 2004 on setting standards of quality and safety for the donation, procurement, testing, processing, preservation, storage and distribution of human tissues and cells (Portuguese Law 22/2007, June 29), with the approval of the Ethics Committee of the respective clinical institutions. Isolated cells were kept frozen in liquid/vapour nitrogen tanks until further use.

Human BM MSC from three different donors were thawed and plated on T-75 flasks using low-glucose Dulbecco's Modified Eagle Medium (DMEM: Gibco, Grand Island, NY) supplemented with 10% fetal bovine serum (FBS MSC qualified: Gibco) and 1% antibiotic-antimycotic (Gibco) and kept at 37ºC, 5%CO_2 and 21%O_2 in an humidified atmosphere. Medium was changed every 3-4 days. Three independent donors and three biological replicates per each donor (n=3) were used on all experiments. BM MSC between passages 3 and 5 were used. HUVEC were purchased from Lonza (Basel, Switzerland) and maintained in commercial Endothelial Growth Medium-2 (EGM-2: Lonza). HUVEC between passages 3 and 6 were used.

III.2.2. BM MSC characterization

III.2.2.1. Immunophenotypic analysis

BM MSC were tested for expression of cell surface markers indicative of MSC (i.e., $CD73^+$, $CD90^+$, $CD105^+$, $HLA\text{-}DR^-$, $CD34^-$, $CD45^-$), using a panel of mouse anti-human monoclonal antibodies (Biolegend, San Diego, CA). Therefore, cells were incubated with each antibody for 20 min in the dark at room temperature and then washed with phosphate buffer saline (PBS, Gibco) and fixed with 2% of paraformaldehyde (PFA, Santa Cruz Biotechnology, Dallas, TX). Isotype controls were also prepared. Samples were analyzed in a FACScalibur (Becton Dickinson, Franklin Lakes, NJ) flow cytometer and CellQuest™ software (Becton Dickinson) was used for acquisition and analysis.

III.2.2.2. Multilineage differentiation ability

BM MSC ability to differentiate into osteoblasts, adipocytes and chondrocytes was evaluated. BM MSC were cultured at 3000 cells/cm^2 on 12-well plates with DMEM+10%FBS. After reaching 80% confluence, osteogenesis was induced using StemPro® Osteogenesis Differentiation Kit (Gibco) and adipogenesis was induced using StemPro® Adipogenesis Differentiation Kit (Gibco). The medium was changed twice a week for 14 days. Cells were then washed and fixed with 2% of PFA for 20 min. Then, cells were rinsed in miliQ water during 15 min. Regarding osteogenic differentiation, cells were incubated with a Fast Violet solution (Sigma-

Aldrich, St. Louis, MO) and Naphthol AS-MX Phosphate Alkaline solution (Sigma-Aldrich) in a final concentration of 4% (v/v) for 45 min, at room temperature in the dark. Cells were, then, washed three times with miliQ water and once with PBS. Von Kossa staining was performed by incubating the cells with a 2.5% silver nitrate solution (Sigma-Aldrich) during 30 min at room temperature in the dark to evaluate the deposits of calcium.

For adipogenic differentiation, after fixation cells were incubated with Oil-Red-O solution (Sigma-Aldrich) (0.3% in isopropanol) at room temperature for 1h to evaluate the accumulation of lipids.

Cells were washed three times with miliQ water and visualized using a fluorescence microscope at a magnification of 10x, and recorded by an attached digital camera.

In order to differentiate BM MSC into chondrocytes, BM MSC were plated as droplets (10 µl) ($2x10^7$ cells/ml) on ultra-low attachment culture plates. After 1h, StemPro® Chondrogenesis Differentiation Kit (Gibco) was added and the medium was changed twice a week for 14 days. Then, cells were washed with PBS and fixed with 2%PFA for 20 min. After fixation, cells were washed with distilled water and incubated with 1% Alcian Blue solution (Sigma-Aldrich) at room temperature for 1h to detect synthesis of proteoglycans.

III.2.3. BM MSC proliferation

In order to evaluate the effect of different concentrations of OC and OPN on BM MSC proliferation, human BM MSC were seeded at 1000 cells/cm^2 in 96-well plates. Different concentrations of OPN and OC were exogenously applied to the cell culture (0, 0.01, 0.05, 0.1, 0.2, 0.5, 1 µg/ml), based on previous works (Kang *et al.* 2008, Yu *et al.* 2011, Hu *et al.* 2013). Recombinant human OPN protein was purchased from R&D Systems and human OC fragment 1-49 was purchased from Sigma-Aldrich. After exposure to various doses, the effect of OC and OPN on BM MSC proliferation was evaluated using AlamarBlue® cell viability reagent (Molecular Probes, Eugene, OR) (n=3). AlamarBlue® cell viability reagent was added to the cells and incubated at 37ºC in 5% CO_2 chamber for 2.5h. Fluorescence was quantified (560nm – 590nm) and compared to a calibration curve to access number of cells under each condition. Cell viability was measured in triplicates in all groups.

Aiming to assess the synergistic effect of both proteins, BM MSC were seeded at 3000 cells/cm^2 in 24 well-plates. 1 µg/ml of OPN and/or 1 µg/ml of OC were added to the cell culture growth medium (DMEM+10%FBS) and the number of cells was evaluated at different timepoints using AlamarBlue® cell viability reagent, as previously described. Human BM MSC cultured with only DMEM+10%FBS (without OC/OPN supplementation) were used as control.

Fold increase (FI) in total cell number was calculated as the ratio of cells obtained divided by the number of cells plated at day 0. The number of population doublings (PD) was calculated using the equation PD= log(FI)/log(2).

III.2.4. Osteogenic differentiation of BM MSC

Human BM MSC were plated in 24-well plates at 3000 cells/cm^2. After 24h, in order to evaluate the effect of exogenous OPN and OC supplementation on BM MSC osteogenic differentiation, 1 µg/ml OPN or/and 1 µg/ml OC were added to the osteogenic differentiation medium (StemPro® Osteogenesis Differentiation Kit:

Gibco) and added to each well. Medium was changed every 3-4 days. The time at which the osteogenic medium was added is referred to as day 0. After 21 days of osteogenic differentiation, samples were stained with alkaline phosphatase (ALP) and Von Kossa stainings. Cells that were not cultured with osteogenic medium, were also stained and used as controls. The cell culture medium was removed and cells were washed with phosphate-buffered saline (PBS, Gibco). Cells were fixed with 2% of PFA for 20 min. Then, cells were rinsed in miliQ water during 15 min and further incubated with a Fast Violet solution (Sigma-Aldrich) and Naphthol AS-MX Phosphate Alkaline solution (Sigma-Aldrich) in a final concentration of 4% (v/v) for 45 min, at room temperature in the dark. Cells were, then, washed three times with miliQ water and once with PBS. Von Kossa staining was performed by incubating the cells with a 2.5% silver nitrate solution (Sigma-Aldrich) during 30 min at room temperature in the dark. Cells were washed three times with miliQ water and visualized using a fluorescence microscope at a magnification of 10x, and recorded by an attached digital camera.

To visualize the calcium minerals formed in the cell culture after osteogenic differentiation, a 20 mM Xylenol orange (XO) solution (Sigma-Aldrich) was added to the previously fixed cells and incubated for 1 h at room temperature in the dark. After that, cells were washed with miliQ water and the cell nuclei were counterstained with DAPI (Invitrogen) (1.5 µg/ml) for 5 min and then washed with PBS. The fluorescent staining of the produced minerals was imaged by fluorescence microscope (Olympus IX51 Inverted Microscope).

III.2.5. Calcium quantification assay

For determination of total calcium content, samples (n=3) were washed twice with PBS (Gibco) and extracted in 0.5 M HCl solution (Sigma-Aldrich). Accumulated calcium was removed from the cellular component by shaking overnight at 4ºC. The consequent supernatant was utilized for calcium determination according to the manufacturer's instructions contained in the calcium colorimetric assay kit (Sigma-Aldrich). Total calcium was calculated from calcium standard solution prepared in parallel. Absorbance at 575 nm was measured for each condition and normalized to the total number of cells, after 21 days of osteogenic differentiation.

III.2.6. Alkaline phosphatase activity

ALP activity was detected using a colorimetric ALP kit (BioAssays Systems, Hayward, CA) according to the manufacturer's protocol. Samples (n=3) were washed with PBS (Gibco) and were incubated in the lysis buffer (0.1% Triton X-100 in PBS) by shaking for 30 min at room temperature. The lysate was added to p-nitrophenyl phosphate solution (10 mM) provided with the ALP kit. The absorbance was measured at 405 nm and normalized to the total number of cells in each sample, after 21 days of osteogenic differentiation.

III.2.7. qRT-PCR analysis

Total RNA was extracted with a RNeasy Mini Kit (QIAGEN, Hilden, Germany). cDNA was synthesized from 20 ng of total RNA using iScript™ Reverse Transcription Supermix (Bio-Rad, Hercules, CA). Reaction mixtures (20µl) were incubated in a thermal cycler (Veriti 96-well thermal cycler: Applied Biosystems, Foster City, CA) for 5 min at 25ºC, 30 min at 42ºC and 5 min at 85ºC and then were maintained at 4ºC. Gene expression levels

of collagen I, Runx2, osteopontin, osteocalcin and vascular endothelial growth factor (VEGF) were assessed. The sequences of the specific primer sets used are given in Table III.1.

The quantitative reverse transcription-polymerase chain reaction (qRT-PCR) was performed using SYBR® Green PCR Master Mix (Applied Biosystems) and StepOnePlus real-time PCR system (Applied Biosystems). All reactions were carried out at 95ºC for 10 min, followed by 40 cycles of 95ºC for 15 sec and 60ºC for 1 min, according to manufacturer's instructions; all were performed in triplicate. Glyceraldehyde 3-phosphate dehydrogenase was used as internal control to normalize differences in total RNA levels in each sample. A threshold cycle (Ct) was observed in the exponential phase of amplification, and quantification of relative expression levels was performed with the use of standard curves for target genes and endogenous control. Geometric means were used to calculate the $\Delta\Delta$Ct values and are expressed as $2^{-\Delta\Delta Ct}$. The mean values from triplicate analysis were compared. The value of each control sample (undifferentiated cells) was set as 1 and was used to calculate the fold difference in the target gene.

Table III.1. Sequences of primers used for qRT-PCR analysis

Genes	Sequences
GAPDH	For: 5' AAC AGC GAC ACC CAC TCC TC Rev: 5' CAT ACC AGG AAA TGA GCT TGA CAA
Col I	For: 5' CAT CTC CCC TTC GTT TTT GA Rev: 5' CCA AAT CCG ATG TTT CTG CT
Runx2	For: 5' AGA TGA TGA CAC TGC CAC CTC TG Rev: 5' GGG ATG AAA TGC TTG GGA ACT
OPN	For: 5' ATG AGA TTG GCA GTG ATT Rev: 5' TTC AAT CAG AAA CCT GGA A
OC	For: 5' TGT GAG CTC AAT CCG GCA TGT Rev: 5' CCG ATA GGC CTC CTG AAG C
VEGF	For: 5' GGA GGA GGG CAG AAT CAT CAC Rev: 5' GGT CTC GAT TGG ATG GCA GT

III.2.8. *In vitro* endothelial cell tube formation assay

In order to study the effect of exogenous OC and OPN supplementation on angiogenic properties of HUVEC, a three-dimensional capillary-like tube formation assay was performed (n=3). HUVEC ($2x10^4$ cells) were cultured on a Matrigel substrate (50 μl/well) (Corning, Corning, NY) in a 96-well plate. Different concentrations of OC and OPN (0, 0.01, 0.05, 0.1, 0.2, 0.5, 1 μg/ml) were added to each well (4 wells per group) in endothelial basal media (EBM, Lonza). Same concentrations of OC and OPN used in the cell proliferation assay were used. After incubation for 8h at 37ºC, three photomicrographs per well were taken under light microscopy (Leica DM IL LED with EC3 camera system) and the number of tubes formed were counted with the use of ImageJ (NIH) software.

A different approach was used to evaluate the possible effect of OC and OPN on stimulating BM MSC to secrete more angiogenic factors that would enhance the formation of a capillary structure from HUVEC. Therefore, conditioned medium (CM) (without FBS) obtained from BM MSC (control) and from BM MSC treated with OC and/or OPN (1 µg/ml OC and/or 1 µg/ml OPN) after 72 h was added to HUVEC cultured on a Matrigel substrate. As a negative control, HUVEC were incubated with DMEM basal medium (Gibco) and, as a positive control, HUVEC were incubated with EGM-2 (Lonza). After incubation for 8h at 37ºC, cells were labeled by adding calcein AM (Corning) (8 µg/ml) and incubated for 30 min at 37ºC. Three photomicrographs per well were taken under fluorescence microscope and the number of tubular-like structures and branch points formed were counted with the use of ImageJ (NIH) software.

III.2.9. Preparation of OC/OPN-enhanced scaffolds

For the *in vivo* studies, bovine type I collagen fibrous sheets (Advanced Biomatrix, Carlsbad, CA) were mineralized in the presence of OC/OPN, to produce OC/OPN-enhanced mineralized collagen matrices. Therefore, the scaffolds (6x6x5 mm^3) were incubated, first, in a 1M $CaCl_2$ solution in the presence of 150 µg/ml OC, then with150 µg/ml OPN at 37ºC (pH=7.4) for 24 h. The scaffolds were washed twice with PBS and freeze-dried. Next, the scaffolds were incubated with 1M Na_2HPO_4 at 37ºC (pH=7.4) for 24 hours and freeze-dried. The mineralized scaffolds were sterilized using ethylene oxide.

III.2.10. *In vivo* bone regeneration in a critical sized-defect rabbit long-bone model

New Zealand White female rabbits weighting more than 3.25 kg were used to assess the *in vivo* bone forming capacity of OC/OPN-enhanced scaffolds. All methods were carried out in accordance with relevant guidelines and regulations. All animal experimental protocols were approved by Intistitutional Animal Care and Use Committee (IACUC) at Spring Valley Laboratories (IACUC approval number: SVL-315). Bilateral surgery was performed to each rabbit to create a critical sized-defect in the distal femoral condyle. A medial skin incision of approximately 4 cm was made in the rabbit's hind leg. The skin was retracted laterally to allow for a lateral arthrotomy of the stifle joint. Once the femur was exposed, a lateral arthrotomy was performed and the joint opened. A transcondylar defect (approximately 6 mm diameter by 12 mm deep) was created in the femur. After creating the defect, the site received a final rinse with saline to remove any residual particulate and the OC/OPN-enhanced mineralized scaffolds were implanted and the soft tissues and skin were closed using non-absorbable sutures. The animals were sacrificed 6 weeks after implantation. The retrieved specimens were fixed in formalin solution and prepared for histological analysis. The specimens were embedded in methyl methacrylate and sections were cut and subjected to staining for Hematoxylin and Eosin (H&E), Goldner's Trichrome (GT), Von Kossa (VK), Toluidine Blue (TB) and Tartrate-Resistant Acid Phosphatase (TRAP)/TB. Digital images were captured with an Olympus IX51 inverted microscope.

III.2.11. Statistical analysis

Each experiment was conducted in triplicates. Statistical analysis of the cell proliferation data was performed using unpaired Student's t-test for single comparison, comparing each condition with the control at the same timepoint. Statistical analysis of all the remaining data was performed by ANOVA for multiple comparisons, using GraphPad Prism version 7. Tukey's multiple comparisons test was performed to determine statistically significant differences ($p<0.05$).

III.3. Results

III.3.1. Exogenous effect of OPN and OC supplementation on BM MSC proliferation

BM MSC were previously tested for expression of cell surface markers indicative of MSC (i.e., $CD73^+$, $CD90^+$, $CD105^+$, $HLA\text{-}DR^-$, $CD34^-$, $CD45^-$), and their ability to differentiate into osteoblasts, adipocytes, and chondrocytes (Dominici *et al.* 2007) (Figure III.1).

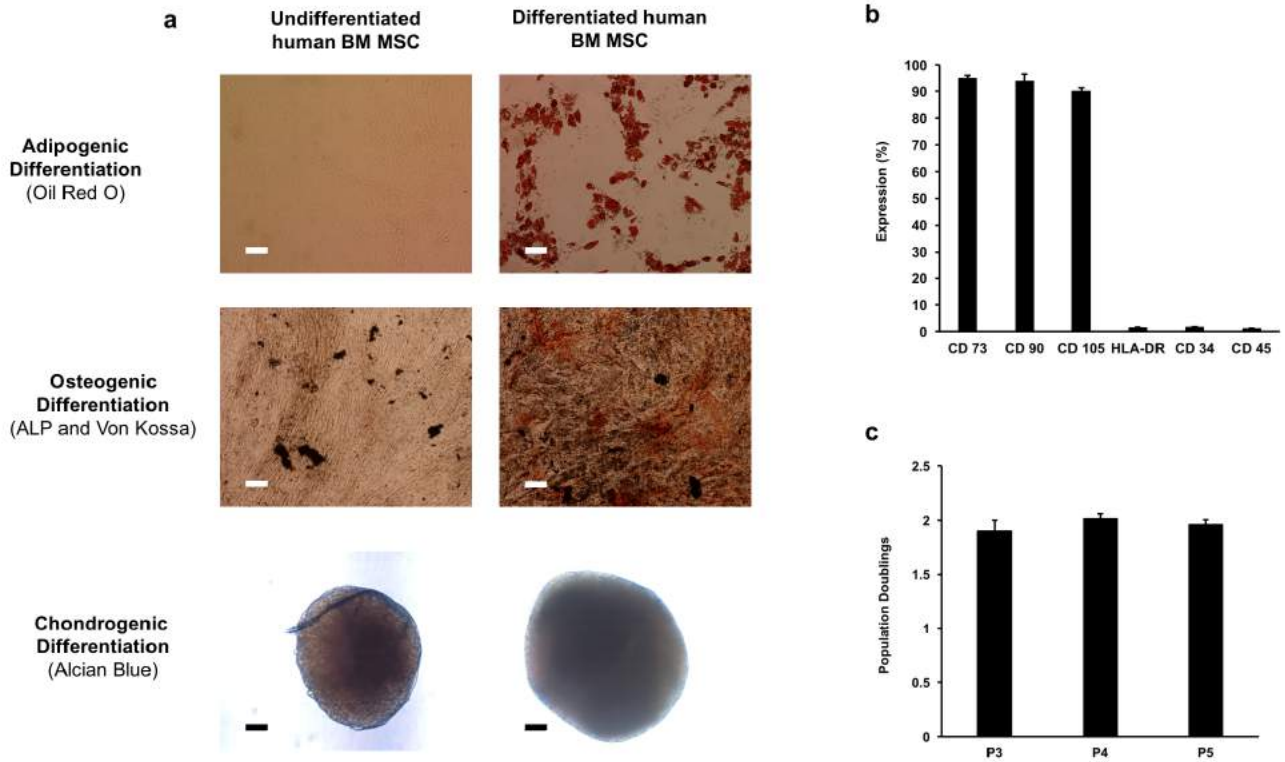

Figure III.1. Human BM MSC characterization. **a)** BM MSC ability to differentiate into osteoblasts, adipocytes and chondrocytes was evaluated. **b)** BM MSC were tested for expression of cell surface markers indicative of human MSC (*i.e.,* $CD73^+$, $CD90^+$, $CD105^+$, $HLA\text{-}DR^-$, $CD34^-$, $CD45^-$). **c)** Population doublings of BM MSC expanded at P3, P4 and P5.

To analyze the effect of exogenous OPN and OC on BM MSC proliferation, different concentrations of OPN and OC were independently applied in the cell growth medium. After exposure to various doses (0, 0.01, 0.05, 0.1, 0.2, 0.5, 1 µg/ml) of recombinant human OPN, we found that OPN treatment affected cell proliferation in a dose-dependent manner (Figure III.2a). These results demonstrated that a direct application of exogenous OPN dose-dependently triggered the proliferation of BM MSC throughout the course of the culture period. In fact, the cell number at day 12 was increased by 0.5-fold when applying exogenously 1 µg/ml of OPN (Figure III.2a). This data showed that when added more than 0.1 µg/ml of OPN to cell culture medium, the number of cells increased significantly after 12 days of culture. On the other hand, OC treatment alone did not affect cell proliferation (Figure III.2b). All the OC doses applied exogenously to the cell culture demonstrated the same cell growth trend, without enhancing the proliferation of BM MSC (Figure III.2b).

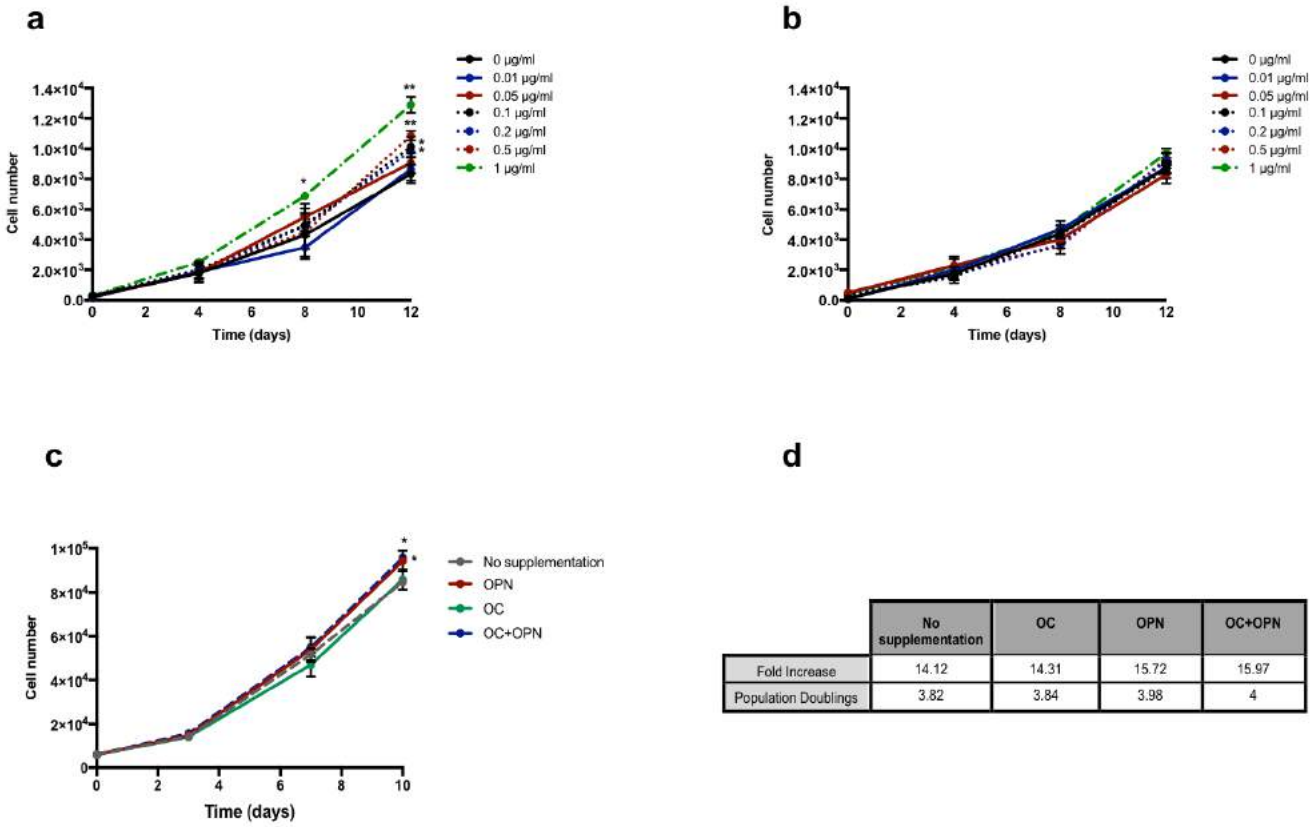

	No supplementation	OC	OPN	OC+OPN
Fold Increase	14.12	14.31	15.72	15.97
Population Doublings	3.82	3.84	3.98	4

Figure III.2. Exogenous effect of OPN and OC supplementation on BM MSC proliferation. **a)** Effect of OPN on BM MSC proliferation. OPN dose dependently increased BM MSC proliferation activity, with a peak at concentration of 1 µg/ml OPN. **b)** Effect of OC on BM MSC proliferation. OC did not affect BM MSC proliferation activity. No significant differences in proliferation were observed between control and BM MSC treated with OC. **c)** Synergistic effect of OC and OPN on BM MSC proliferation. Cells were seeded at 3000 cells/cm^2. **d)** Fold Increase and Population Doublings of BM MSC pre-treated with OC and/or OPN (1 µg/ml OC and/or 1 µg/ml OPN) for 10 days. Data are presented as mean ± SD. n=3, *p<0.05;**p<0.01, compared with the control (0 µg/ml).

After the first protein screening and aiming to assess the synergistic effect of both proteins, OPN and OC, on BM MSC proliferation, we supplemented exogenously the cell growth medium with OPN, OC, and both OC/OPN (1 µg/ml OPN or/and 1 µg/ml OC) (Figure III.2c). As seen previously (Figure III.2b), OC alone did not significantly affect cell proliferation, however, when OPN was used in combination with OC, the cell number was significantly enhanced, after 10 days of culture (Figure III.2c). When OPN alone was added in the cell culture medium, the total number of cells obtained was also higher than the control (no supplementation). These results show that OPN might be the trigger to enhance proliferation of BM MSC and this positive effect is not affected by the addition of OC into the culture (Figure III.2c).

III.3.2. Exogenous effect of OPN and OC supplementation on BM MSC osteogenic differentiation

To analyze the exogenous effect of both proteins (OPN and OC) on BM MSC osteogenic differentiation, we supplemented the osteogenic differentiation medium with OPN, OC, and both OC/OPN (1 µg/ml OPN or/and 1 µg/ml OC) (Figure III. 3). When BM MSC were differentiated for a period of 21 days using osteogenic medium supplemented with OC, an obvious increase in their ALP activity and amount of calcium was shown (Figure III.3b). These results confirm that OC is important for differentiation of MSC into an osteogenic lineage. Indeed, the extracellular addition of OC also increased mRNA levels of OPN and OC, suggesting that exogenous application of OC was sufficient to induce late osteogenic markers expression (Figure III.3c). Interestingly, the same results were observed when OPN and OC were both added to the differentiation culture medium. Osteogenically-induced MSC in the presence of 1 µg/ml of OPN and 1 µg/ml of OC enhanced the levels of calcium and ALP activity, as well as the levels of the late osteogenic marker OPN and OC. However, when OPN alone was exogenously applied, no dramatic differences in osteogenesis was observed. Xylenol orange staining confirmed that more calcium minerals were produced when BM MSC were treated with OC and OC/OPN (Figure III.3a), validating the results obtained with calcium quantification assay (Figure III.3b). ALP and Von Kossa stainings (Figure III.3d) also demonstrated that the presence of both proteins in the cell culture enhanced osteogenic differentiation of BM MSC.

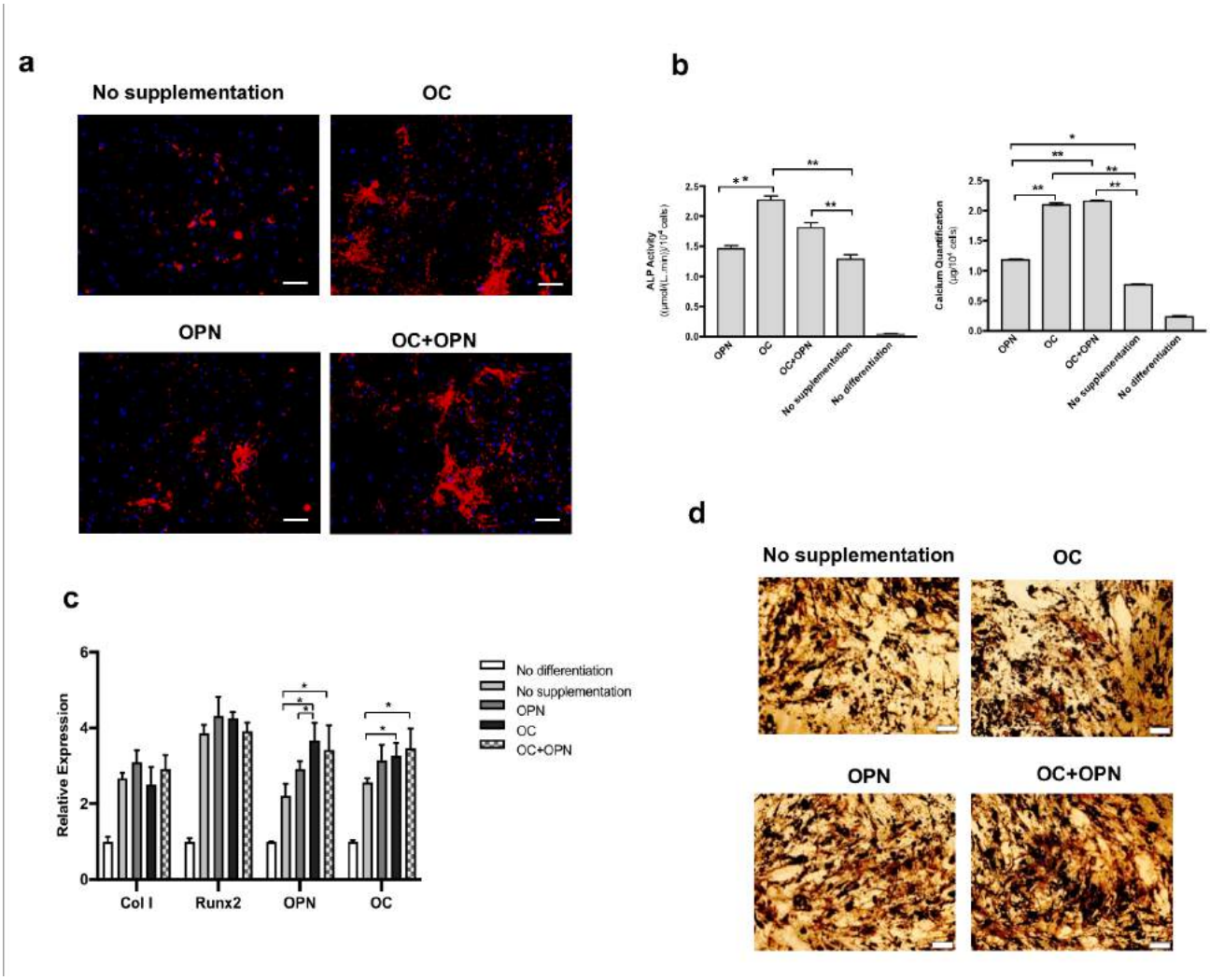

Figure III.3. Exogenous effect of OPN and OC supplementation on BM MSC osteogenic differentiation. **a)** Following treatment with OPN, OC and OC+OPN (1 µg/ml OC and/or 1 µg/ml OPN), osteogenic differentiation of BM MSC was analyzed. Xylenol orange (red) stained calcium minerals in cell culture treated with OC/OPN (blue: DAPI). Osteogenic differentiation and mineralization were detected after 21 days of differentiation. **b)** ALP activity and calcium quantification were enhanced when cells were treated with OC and OC+OPN. **c)** In addition, the mRNA levels of the osteogenic markers Col I, Runx2, OPN and OC were also analyzed by qRT-PCR. **d)** ALP and Von Kossa stainings confirmed the osteogenic differentiation after 21 days**.** OC triggered the mineralization and osteogenic differentiation of BM MSC, since the treatment with OC and OC+OPN increased ALP activity, calcium deposits and mRNA levels of some osteogenic genes **(b, c)**. Data are presented as mean ± SD. n=3. **p<0.01;*p<0.05. Scale bars, 100 µm.

III.3.3. Exogenous effect of OPN and OC supplementation on angiogenic properties of cells

To investigate the role of OPN and OC in stimulating angiogenic properties of cells, a three-dimensional capillary tube formation assay was performed, in which HUVEC were applied on the top of a matrigel gel in the presence of exogenously added OC and OPN. As shown in Figure III.4a,c, OPN dose-dependently stimulated the well-organized, capillary-like networks compared with control groups (without supplementation). The results showed that the number of tubular-like structures formed after OPN treatment increased, however, only when HUVEC were treated with more than 0.5 µg/ml of OPN, a significant increase of number of tubes formed was observed. In contrast, OC supplementation did not demonstrate any increase in the number of tubular-like structures compared with the control group (Figure III.4b,c). Although OC treatment did not enhance angiogenic properties of HUVEC, this protein did not demonstrate an anti-angiogenic effect, indicating that the addition of OC into cell culture does not affect angiogenesis.

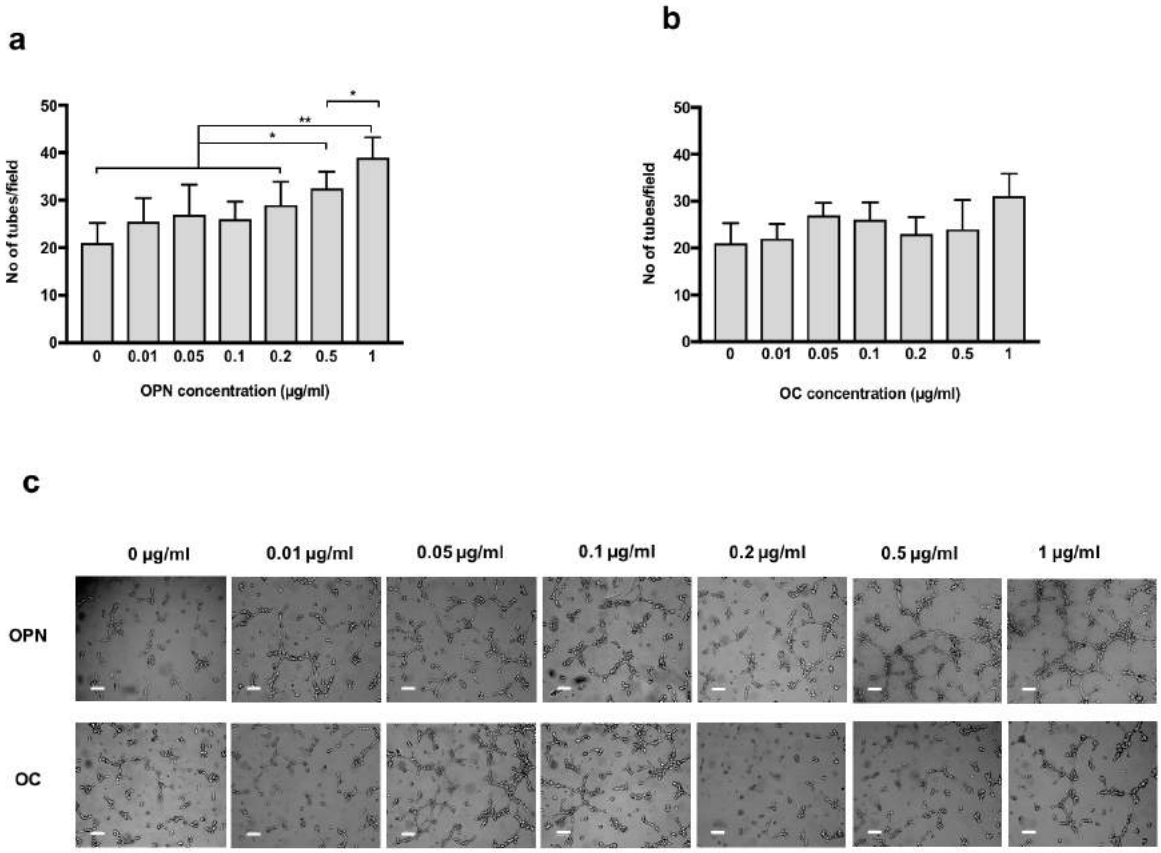

Figure III.4. Exogenous effect of OPN and OC supplementation on angiogenic properties of HUVEC in a dose-dependent study. Tube formation assays were performed **(c)** with the indicated doses of OPN and OC and the number of tubes formed was quantified **(a, c). (a,c)** OPN stimulated the *in vitro* formation of tubular-like structures by HUVEC treated with dose equal or higher than 0.5 µg/ml. **(b,c)** OC did not affect angiogenic properties of HUVEC *in vitro*. Data are presented as mean±SD. **p<0.01;*p<0.05. Scale bars, 100 µm.

To better understand if OPN and OC could enhance cellular angiogenic properties in *vitro*, a different approach was performed using the same tube formation assay. In particular, conditioned medium from BM MSC treated with or without OC/OPN supplementation (1 µg/ml OPN or/and 1 µg/ml OC during 72 h) was added to HUVEC that were seeded on matrigel to form the capillary-like structure. The aim of this experiment was to investigate the possible role of OPN and OC in enhancing the secretion of angiogenic factors from BM MSC evaluated by the formation of endothelial tubular networks.

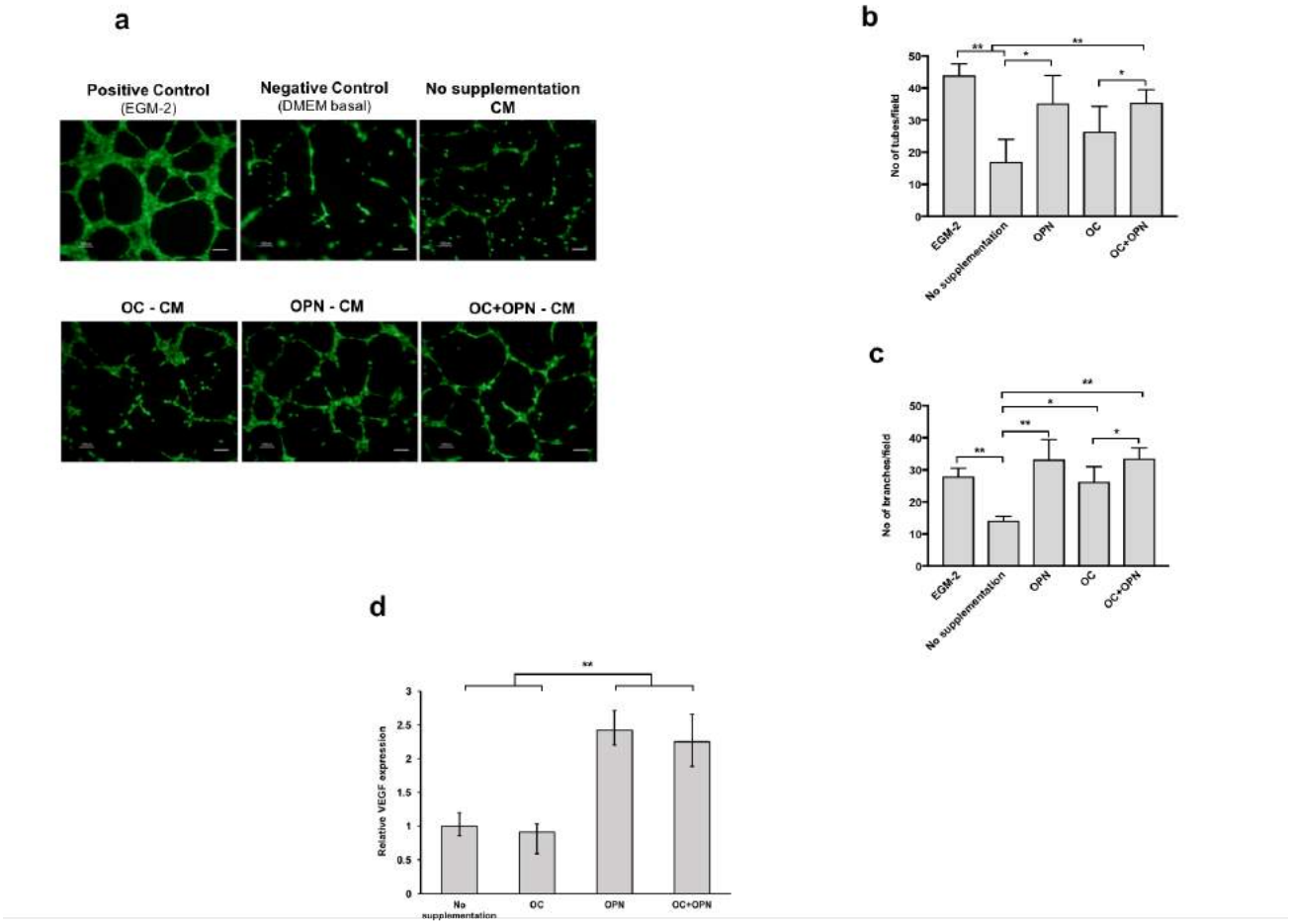

Figure III.5. Effect of OPN and OC on cell angiogenic properties. **a)** Tube formation assay with conditioned medium from BM MSC and from BM MSC treated with OPN, OC or both OC+OPN. Positive control is HUVEC in endothelial growth medium and negative control is the basal medium (no angiogenic factors). **(b,c)** Quantification of number of tubular-like structures **(b)** and branch points **(c)** formed. OPN elicited a pro-angiogenic activity. **d)** VEGF expression levels of BM MSC treated with OC, OPN and OC+OPN for 72h. BM MSC treated with OPN and OC+OPN demonstrated a statistically significant increase in VEGF gene expression. Data are presented as mean±SD. n=3. **p<0.01; *p<0.05. Scale bars, 100 µm.

As shown in Figure III.5, all the conditions that were exposed to conditioned medium from BM MSC could form tubular-like structures due to the secreted factors produced by these cells. Although these tubular structures were formed when conditioned medium from BM MSC (no supplementation) and conditioned medium from BM MSC treated with OC were used, their structure was not well defined. The negative control used was basal medium that was not exposed to cell culture, and therefore did not contain any angiogenic factor that would enhance tube formation. Besides total number of tubular-like structures, total number of branch points were also measured to evaluate interconnectivity between the tubular structure. Therefore, when conditioned medium from BM MSC, cultured with OPN and OPN/OC supplementation, was used, a significant improvement in the number of tubular-like structures formed and in the number of branch points was observed, indicating that the presence of OPN was responsible for the improvement of angiogenic activity of the cells. These results are consistent with the previous experiment in which OPN treatment enhanced angiogenic capacity (Figure III.4a,c).

Interestingly, BM MSC treated with OPN and OC+OPN for 72h demonstrated a statistically significant increase in VEGF gene expression levels, confirming the effects of OPN supplementation on enhancing VEGF gene expression levels.

III.3.4. Effects of OPN and OC on local inflammatory response in a critical sized-defect rabbit long-bone model

We then sought to determine the local inflammatory response of OC/OPN-scaffolds. Therefore, we developed a mineralized collagen scaffolds, supplemented with both OPN and OC. After inducing a long bone critical-sized defect in a rabbit model, OC/OPN-enhanced mineralized collagen scaffolds were introduced in the defect and foreign body reaction was evaluated while new bone was being formed.

Therefore, the surgical incision site was observed for wound healing and signs of infection daily for at least ten days following surgery. No signs of inflammation, discharge or wound dehiscence and abscess were observed. No specimen revealed any evidence of infection or foreign body reaction, and all wounds showed a good healing response.

After 6 weeks, new bone formation was observed surrounding the scaffold (Figure III.6a,b), as seen with Goldner's Trichrome (GT) and Von Kossa (VK) stains. Moreover, connective tissue was found between the new bone formed and the scaffold implanted. Osteoblasts were seen covering the new bone formed (arrows). Osteoclasts were found surrounding the scaffold by Tartrate-resistant acid phosphatase (TRAP) staining (Figure III.6c), indicating an initial stage of bone remodeling.

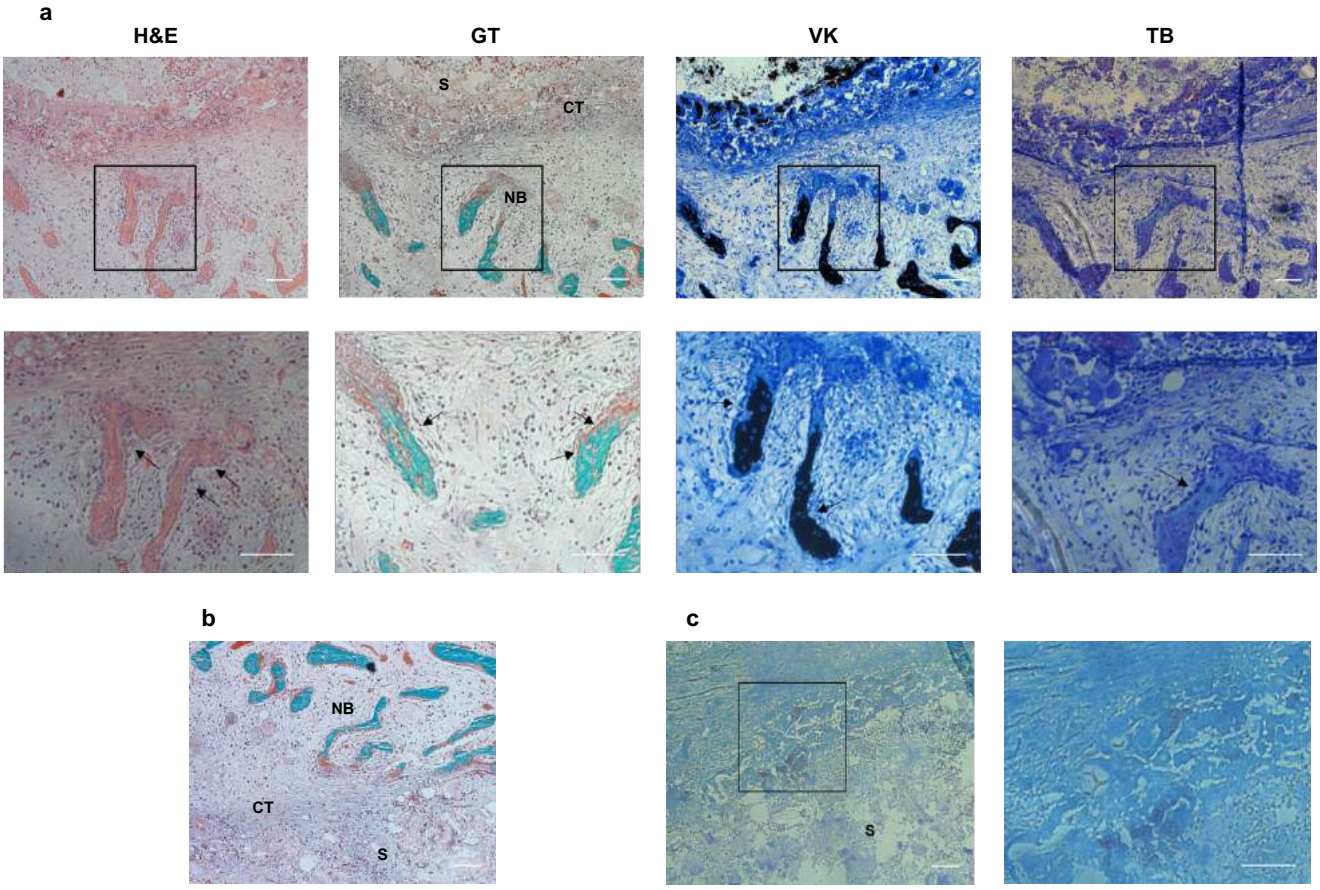

Figure III.6. Effect of OPN/OC-enhanced scaffold on local inflammatory response and bone formation *in vivo*. **a)** Representative histological images of the rabbit critical sized-defect at 6 weeks postimplantation. Hematoxylin and Eosin (H&E), Goldner's Trichrome (GT), Von Kossa (VK), Toluidine Blue (TB). Black squares represent the area of new bone formed. Black arrows represent the osteoblasts covering the new bone. **b)** Goldner's Trichrome straining demonstrated new bone formed surrounding the scaffold with connective tissue between the scaffold and new bone. **c)**Tartrate-resistant acid phosphatase (TRAP) staining indicated the presence of osteoclasts between the scaffold region, representing bone remodeling. NB – new bone; CT – connective tissue; S – scaffold. Scale bars, 100 µm.

III.4. Discussion

Autologous and allogenic bone grafts are still the most common treatments for bone healing. However numerous studies have reported limitations, disadvantages and complications of these current clinical treatments (Roberts *et al.* 2012, Wang & Yeung 2017). To surpass these obstacles, functional bone grafts need to be designed by incorporating osteoinductive components that accelerate cell recruitment, proliferation, vascularization and osteogenic differentiation and result in bone regeneration at the defect site (Khan *et al.* 2012). In fact, allograft treatments lack osteoinductive agents, leading to major limitations of such treatments. To this end, this study evaluated the effect of the non-collagenous bone matrix proteins, OC and OPN, on BM MSC proliferation, osteogenic differentiation and HUVEC capillary-like structure formation by analyzing their osteoinductive and pro-angiogenic properties. Here, for the first time, we demonstrate the synergistic effects of OC and OPN on stem cell proliferation, osteogenic differentiation and angiogenic properties *in vitro* and evaluate their local inflammatory response in an *in vivo* model.

OPN is a non-collagenous bone matrix protein that can be produced by all the bone cells, such as osteocytes, osteoblasts and osteoclasts. Regarding cell proliferation, previous reports have reported controversial effects of OPN. OPN was shown to increase proliferation of various tumor cells (Luo *et al.* 2011, Pazolli *et al*. 2009, Saleh *et al*. 2016), neural stem cells (Rabenstein *et al.* 2015), vascular smooth muscle cells (Lee *et al.* 2016) and hepatic progenitor cells (Liu *et al*. 2015). Furthermore, absence of OPN demonstrated a decreased cell proliferation of tumor cells (Matsuura *et al.* 2011) and erythroblasts (Kang *et al.* 2008). However, a different effect of OPN on cell proliferation was observed for hematopoietic stem cells, suppressing their proliferation through the induction of quiescence (Nilsson *et al.* 2005). Regarding bone marrow MSC, thus far non-conclusive effects of OPN on proliferation have been reported.

Results presented here found that OPN increased the proliferation of BM MSC in a dose-dependent manner. In fact, when added in more than 0.1 µg/ml concentration of OPN in cell culture medium, OPN increased the number of cells significantly (Figure III.2a). These results can be explained by considering that MSC express the OPN receptor CD44 (Raheja *et al.* 2008), a cell-surface glycoprotein involved in cell-cell interactions, cell adhesion and migration. In contrast to OPN, OC when added exogenously to the cell culture did not improve the proliferation of BM MSC and demonstrated the same trend at all doses applied exogenously (Figure III.2b).

In comparison to OPN, OC is a non-collagenous, vitamin K-dependent protein secreted during the late stage of osteogenic differentiation. The presence of the three residues of γ-carboxiglutamatic acid, specific of the active form of OC protein, allows the protein to bind calcium and consequently hydroxyapatite (Neve *et al.* 2013), providing a function that has been well conserved through evolution (Laizé *et al.* 2005). OC has been shown to bind strongly to bone mineral hydroxyapatite (Dowd *et al.* 2003, Hauschka & Carr 1982) and it complexes with and links to collagen through OPN (Ritter *et al.* 1992). Although OC did not improve proliferation, we found that OC, when exogenously applied in the stem cell culture, enhanced ALP activity and increased the amount of calcium levels, while demonstrating increase in the mRNA levels of expression of late osteogenic markers, osteocalcin and osteopontin. Therefore, we believe that the enhancement of osteocalcin and osteopontin gene expression levels observed, when BM MSC were treated with OC, is a possible mechanism for the demonstrated increase in extracellular calcium levels and ALP activity, producing a more mature matrix. Thus, OC could be used as an osteoinductive component, stimulating osteogenic capability of cells (Figure III.3). On the other hand, when OPN was exogenously added to the stem cell culture, no drastic improvement in osteogenic differentiation was observed. In fact, Xylenol orange staining indicated more calcium minerals when cells were supplemented with both OC and OPN, when compared with cells treated with only OPN or without any supplementation (Figure III.3a).

Each protein separately seems to have a different and very specific function on the cell culture. Based on results presented above, we believe that OPN was responsible for the improvement in cell proliferation, while OC triggered the enhancement of osteogenic differentiation. Notably, when OC and OPN were both added to the culture, osteogenic differentiation was enhanced, as well as proliferation, suggesting an association of the effects of both proteins.

The precise role of OC in mineralization remains unclear. Some studies demonstrated that mature OC is secreted into the microenvironment and can bind the calcium ions in hydroxyapatite, enabling formation of hydroxyapatite crystals (Price *et al.* 1976, Zoch *et al.* 2016). However, other studies showed that OC functions

as an inhibitor of bone mineralization (van de Loo *et al.* 1987). Thus, data obtained in literature is controversial. However, the dual role of OC in bone can be presumed as acting as a regulator of bone mineralization and regulating osteoblast and osteoclast activity. Based on our results, we hypothesize that OC and OPN work in a synergistic manner to support mineral-organic interaction and helping mineral crystals nucleation (Poundarik *et al.* 2018).

Angiogenesis is a complex process required for bone development and fracture healing, in which the formation of new blood vessel occurs (Lu *et al.* 2006). Some pro-angiogenic factors secreted during bone healing, including vascular endothelial growth factor (VEGF), platelet derived growth factor (PDGF), transforming growth factor ß (TGF- ß), fibroblast growth factors (FGF) and bone morphogenetic proteins (BMP) and they are known to be involved also in the bone repair cascade (Saran *et al.* 2014). In fact, VEGF production is stimulated by osteoinductive factors. The close association between angiogenesis and osteogenesis, makes pro-angiogenic factors that are implicated in both neovascularization and bone formation, important therapeutic agents for bone regeneration. The ability of pro-angiogenic factors like VEGF, FGF-2, BMP-2 and BMP-7 to accelerate fracture repair when administered exogenously is well documented (Street *et al.* 2002, Deckers *et al.* 2002, Eckardt *et al.* 2005).

In the above context, we assessed the possible function of OPN and OC on angiogenesis, acting as pro-angiogenic factors, when administered exogenously. After treatment with various doses of OPN, a notable increase in the formation of tubular-like structures by HUVEC was observed (Figure III.4a,c). In fact, OPN has the ability to regulate VEGF secretion and angiogenesis (Chakraborty *et al.* 2006*)*. Furthermore, it was reported that OPN secreted by cancer cells acts as a potent angiogenic factor contributing to tumor growth in several cancer types (Chakraborty *et al.* 2008, Tang *et al.* 2007, Takahashi *et al.* 2002, Wang *et al.* 2011). OPN has been shown to promote vascular formation in murine neuroblastoma (Takahashi *et al.* 2002) and inhibition of OPN levels induces a suppression of angiogenesis in gastric cancer (Tang *et al.* 2007). Our results confirmed that OPN enhances the ability of endothelial cells to form capillary-like structures. In fact, tube formation assay demonstrated an increase of number of tubular-like structures formed when more than 0.5 µg/ml of OPN was added to the culture. Future studies should focus on identifying and quantifying the amount of angiogenic factors secreted by cells that were exposed with OPN.

Although OC did not enhance angiogenic properties, adding OC into the culture did not reverse nor decrease the pro-angiogenic effects observed with OPN. Moreover, conditioned medium from BM MSC treated with OPN and from BM MSC treated with OC and OPN also enhanced the number of tubular-like structures formed by HUVEC, creating a more defined capillary-like structure, with more interconnected tubular structures, when compared with conditioned medium from BM MSC without any treatment (Figure III.5). Moreover, BM MSC treated with OPN and treated with both OC and OPN enhanced VEGF gene expression levels. We believe that the increase of VEGF gene expression levels supports the angiogenic activity of HUVEC and stimulates BM MSC to secrete more angiogenic factors (Figure III.5d). However, further studies are required to evaluate the amount and composition of angiogenic factors secreted by these cells. Therefore, to generate vascularized engineered bone tissue constructs, the combination of OPN and OC presents a new approach to, simultaneously, promote osteogenesis and angiogenesis. Our described direct positive effect of OPN and OC on osteogenesis and angiogenesis constitutes a novel aspect in stem-cell mediated regeneration of bone tissue. However, it is important to highlight that further studies should be done to confirm that the angiogenic activity of

OPN is not inducing any tumor formation, since its high proliferative and angiogenic properties are also similar to tumor formation process.

To further confirm that these two proteins do not cause any local inflammatory response, we developed OC/OPN-enhanced mineralized scaffolds that were introduced in a long bone critical-sized defect in a rabbit model. Notably, OC/OPN-enhanced mineralized collagen scaffolds did not promote any adverse reaction, while new bone was being formed. Moreover, after 6 weeks, osteoblasts were found surrounding the new bone formed (Figure III.6).

We believe that these findings will help the development of new scaffolds for bone regeneration, in which the incorporation of both OPN and OC may enhance the cell recruitment and proliferation, promoting cells to sense the osteoinductive signals and enhance their osteogenic differentiation, producing a more mature matrix and allowing the regeneration of the defect site with new bone tissue. Our findings strongly suggest that the synergistic effect of OC and OPN may be used to improve stem cell culture conditions, enhancing proliferation and osteogenic differentiation of stem cells by adding these peptides into the culture medium. However, we believe that the concentrations of each protein should be investigated, carefully, for each cell type and culture medium used.

In conclusion, our results, combined with previously reported studies, confirm that the biological function of OPN on BM MSC is not exclusively related to the biomineralization process. OPN also plays an important role in cellular proliferation and angiogenesis. Moreover, OC is important for mineralization, enhancing osteogenic differentiation of BM MSC and mineralization. We believe that the application of both OPN and OC can be used as an attractive strategy for bone tissue engineering to target and enhance different cellular processes, such as cell adhesion, cell proliferation, osteogenic differentiation and angiogenesis.

III.5. References

Al-Qtaitat A.I., Aldalaen S.M. A review of non-collagenous proteins; their role in bone. *Am. J. Life Sci.,***2***,* 351-355 (2014).

Barry S.T., Ludbrook S.B., Murrison E., Horgan C.M. Analysis of the alpha4beta1 integrin-OPN interaction. *Exp. Cell Res.* **258**, 342-351 (2000).

Bodine P.V., Komm B.S. Evidence that conditionally immortalized human osteoblasts express an osteocalcin receptor. *Bone,* **25**, 535-543 (1999).

Boskey A.L. Mineralization of bones and teeth. *Elements Mag.,* **3**, 385-392 (2007).

Boskey A.L. Noncollagenous matrix proteins and their role in mineralization. *Bone Miner.,* **6**, 111-123 (1989).

Boskey A.L. OPN and related phosphorylated sialoproteins, effects on mineralization. *Ann. N.Y. Acad. Sci.,* **760**, 249-256 (1995).

Campana V., Milano G., Pagano E., Barba M., Cicione C., Salonna G., Lattanzi W., Logroscino G. Bone substitutes in orthopaedic surgery: from basic science to clinical practice. *J. Mater. Sci. Mater. Med.,* **25**, 2445-2461 (2014).

Cantatore F.P., Crivellato E., Nico B., Ribatti D. Osteocalcin is angiogenic in vivo. *Cell Biol. Int.,* **29**, 583-585 (2005).

Chakraborty G. Jain S. Kundu G.C. Osteopontin promotes vascular endothelial growth factor-dependent breast tumor growth and angiogenesis via autocrine and paracrine mechanisms. *Cancer Res.,* **68**, 152-161 (2008).

Chakraborty G., Jain S., Behera R., Ahmed M., Sharma P., Kumar V., Kundu G.C. The multifaceted roles of osteopontin in cell signaling, tumor progression and angiogenesis. *Curr. Mol. Med.,* **6**, 819-830 (2006).

Chenu C., Colucci S., Grano M., Zigrino P., Barattolo R., Zambonin G., Baldini N., Vergnaud P., Delmas P.D., Zallone A.Z. Osteocalcin induces chemotaxis, secretion of matrix proteins, and calcium-mediated intracellular signaling in humam osteoclast-like cells. *J. Biol. Chemm.,* **127**, 1149-1158 (1994).

Chiarello E., Cadossi M., Tedesco G., Capra P., Calamelli C., Shehu A., Giannini S. Autograft, allograft and bone substitutes in reconstructive orthopedic surgery. *Aging Clin. Exp. Res.,* **25**, S101-103 (2013).

Cinotti G., Corsi A., Sacchetti B., Riminucci M., Bianco P., Giannicola G. Bone ingrowth and vascular supply in experimental spinal fusion with platelet-rich plasma. *Spine,* **38**, 385-391 (2013).

Contri M.B., Boraldi F., Taparelli F., De Paepe A., Ronchetti I.P. Matrix proteins with high affinity for calcium ions are associated with mineralization within the elastic fibers of pseudoxanthoma elasticum dermis. *Am. J. Pathol.,* **148**, 569-577 (1996).

Cui Q., Dighe A.S., Irvine J.N. Jr. Combined angiogenic and osteogenic factor delivery for bone regenerative engineering. *Curr. Pharm. Des.* **19**, 3374-3383 (2013).

Dai J., Peng L., Fan K., Wang H., Wei R., Ji G., Cai J., Lu B., Zhang D., Kang Y., Tan M., Qian W., Guo Y. Osteopontin induces angiogenesis through activation of PI3K/AKT and ERK1/2 in endothelial cells. *Oncogene* **24**, 34112-3422 (2009).

De Witte T.M., Fratila-Apachitei L.E., Zadpoor A.A., Peppas N.A. Bone tissue engineering via growth factor delivery: from scaffolds to complex matrices. *Regen. Biomater*., **5**, 197-211 (2018).

Deckers M.M., van Bezooijen R.L., van der Horst G., Hoogendam J., van Der Bent C., Papapoulos S.E., Löwik C.W. Bone morphogenetic proteins stimulate angiogenesis through osteoblast-derived vascular endothelial growth factor A. *Endocrinology* **143**, 1545-1553 (2002).

Denhardt D.T., Noda M. OPN expression and function: role in bone remodeling. *J. Cell. Biochem.* **30**, 92-102 (1998).

Denhardt D.T., Guo X. OPN, a protein with diverse functions. *FASEB J.* **7**, 1475-1482 (1993).

Dowd T.L., Rosen J.F., Li L., Gundberg C.M. The three-dimensional structure of bovine calcium ion-bound osteocalcin using 1H NMR spectroscopy. *Biochemistry,* **42**, 7769-7779 (2003).

Ducy P., Desbois C., Boyce B., Pinero G., Story B., Dunstan C., Smith E., Bonadio J., Goldstein S., Gundberg C., Bradley A., Karsenty G. Increased bone formation in osteocalcin-deficient mice. *Nature,* **382**, 448-452 (1996).

Eckardt H., Ding M., Lind M., Hansen E.S., Christensen K.S., Hvid I. Recombinant human vascular endothelial growth factor enhances bone healing in an experimental nonunion model. *J. Bone Joint. Surg.* **87-B**, 1434-1438 (2005).

Fernandez-Yague M.A., Abbah S.A., McNamara L., Zeugolis D.I., Pandit A., Biggs M.J. Biomimetic approaches in bone tissue engineering: integrating biological and physicomechanical strategies. *Adv. Drug Deliv. Rev.,* **84**, 1-29 (2015).

Gundberg C.M. Biochemical markers of bone formation. *Clin. Lab. Med.,* **20**, 489-501 (2000).

Hauschka P.V., Reid M.L.Timed appearance of a calcium-binding protein containing g-carboxyglutamic acid in developing chick bone. *Dev. Biol.,* **65**, 431-436 (1978).

Hauschka P.V., Carr S.A. Calcium-dependent α-helical structure in osteocalcin. *Biochemistry,* **21**, 2538-2547 (1982).

Hauschka P.V., Lian J.B., Cole D.E., Gundberg C.M. Osteocalcin and matrix Gla protein: vitamin K-dependent proteins in bone. *Physiol. Rev.,* **69**, 990-1047 (1989).

Heino J., Käpylä J. Cellular receptors of extracellular matrix molecules. *Curr. Pharm. Des.,* **15**, 1309-1317 (2009).

Holmes D. Non-union bone fracture: a quicker fix. *Nature,* **550**, S193 (2017).

Hu X., Zhang P., Xu Z., Chen H., Xie X. GPNMB enhanced bone regeneration by promoting angiogenesis and osteogenesis: potential role for tissue engineering bone. *J.Cell. Biochem.* **114**, 2729-2737 (2013).

Huang K.H., Lin Y.H., Shie M.Y., Lin C.P. Effects of bone morphogenic protein-2 loaded on the 3D-printed MesoCs scaffolds. *J. Formos. Med. Assoc.,* S0929-6646(18)30333-4 (2018).

Icer M.A., Gezmen-Karadag M.The multiple functions and mechanisms of osteopontin. *Clin. Biochem.,* **59***,* 17-24 (2018).

Kanczler J.M., Oreffo R.O. Osteogenesis and angiogenesis: the potential for engineering bone. *Eur. Cell. Mater.* **15**, 100-114 (2008).

Kang J.A., Zhou Y., Weis T.L., Liu H., Ulaszek J., Satgurunathan N., Zhou L., van Besien K., Crispino J., Verma A., Low P.S., Wickrema, A. Osteopontin regulates actin cytoskeleton and contributes to cell proliferation in primary erythroblasts. *Journal of Biological Chemistry,* **283***,* 6997-7006 (2008).

Katagiri Y.U., Sleeman J., Fujii H., Herrlich P., Hotta H., Tanaka K., Chikuma S., Yagita H., Okumura K., Murakami M., Saiki I., Chambers A.F., Uede T. CD44 variants but not CD44s cooperate with beta-1 containing integrins to permit cells to bind to OPN independently of arginine-glycine-aspartic acid, thereby stimulating cell motility and chemotaxis. *Cancer Res.,* **59**, 219-226 (1999).

Khan W.S., Rayan F., Dhinsa B.S., Marsh D. An osteoconductive, osteoinductive, and osteogenic tissue-engineered product for trauma and orthopaedic surgey: how far are we? *Stem Cells Int.* **Vol.2012**, Article ID 236231 (2012).

Laizé V., Martel P., Viegas C.S., Price P.A., Cancela M.L. Evolution of matrix and bone gamma-carboxyglutamic acid proteins in vertebrates. *J. Biol. Chem.,* **280**, 266659-26668 (2005).

Lee J. L. Wang M.J., Sudhir P.R., Chen G.D., Chi C.W. Chen J.Y. Osteopontin promotes integrin activation through outside-in and inside-out mechanism: OPN-CD44V interaction enhances survival in gastrointestinal cancer cells. *Cancer Res.* **67**, 2089-2097 (2007).

Lee S.J., Baek S.E., Jang M.A., Kim C.D. Osteopontin plays a key role in vascular smooth muscle cell proliferation *via* EGFR-mediated activation of AP-1 and C/EBPbeta pathways. *Pharm.Res.,* **108**, 1-8 (2016).

Liu Y., Cao L., Chen R., Zhou X., Fan X., Liang Y., Jia R., Wang H., Liu G., Guo Y., Zhao J. Osteopontin promotes hepatic progenitor cell expansion and tumorigenicity via activation of b-catenin in mice. *Stem Cells,* **33**, 3569-3580 (2015).

Lu C., Marcucio R., Miclau T. Assessing angiogenesis during fracture healing. *Iowa Orthop. J.* **26**, 17-26 (2006).

Luo X., Ruhland M.K., Pazolli E., Lind A.C., Stewart S.A. Osteopontin stimulates preneoplastic cellular proliferation through activation of the MAPK pathway. *Mol. Cancer Res,.* **9**, 1018-1029 (2011).

Matsuura M., Suzuki T., Suzuki M., Tanaka R., Ito E., Saito T. Statin-mediated reduction of osteopontin expression induces apoptosis and cell growth arrest in ovarian clear cell carcinoma. *Oncol. Rep.* **25**, 41-47 (2011).

Mouw J.K., Ou G., Weaver V.M. Extracellular matrix assembly: a multiscale deconstruction. *Nat. Rev. Mol. Cell Biol.* **15**, 771-785 (2014).

Neve A., Corrado A., Cantatore F.P. Osteocalcin: skeletal and extra-skeletal effects. *J. Cell. Physiol.,* **228**, 1149-1153 (2013).

Nilsson S.K., Johnston H.M., Whitty G.A., Williams B., Webb R.J., Denhardt D.T., Bertoncello I., Bendall L.J., Simmons P.J., Haylock D.N. Osteopontin, a key component of the hematopoietic stem cell niche and regulator of primitive hematopoietic progenitor cells. *Blood,* **106**, 1232-1239 (2005).

Pazolli E., Luo X., Brehm S., Carbery K., Chung J.J., Prior J.L., Doherty J., Demehri S., Salavaggione L., Piwnica-Worms D., Stewart S.A. Senescent stromal-derived osteopontin promotes preneoplastic cell growth. *Cancer Res.,* **69**, 1230-1239 (2009).

Poser J.W., Price P.A. A method for decarboxylation of g-carboxyglutamic acid in proteins. *J. Biol. Chem.,* **254**, 431-436 (1979).

Poser J.W., Esch F.S., Ling N.C., Price P.A. Isolation and sequence of the vitamin K-dependent protein from human bone. Undercarboxylation of the first glutamic acid residue. *J. Biol. Chem.* **255**, 8685-8691 (1980).

Poundarik A.A., Boskey A., Gundberg C., Vashishth D. Biomolecular regulation, composition and nanoarchitecture of bone mineral. *Scientific Reports,* **8**, 1191 (2018).

Price P.A., Otsuka A.A., Poser J.W., Kristaponis J., Raman N. Characterization of a gamma-carboxyglutamic acid-containing protein from bone. *Proc. Natl Acad. Sci. U.S.A.,* **73**, 1447-1451 (1976).

Rabenstein M., Hucklenbroich J., Willuweit A., Ladwig A., Fink G.R., Schroeter M. Langen K.J., Rueger M.A. Osteopontin mediates survival, proliferation and migration of neural stem cells through the chemokine receptor CXCR4. *Stem Cell. Res. Ther.,* **6**, 99 (2015).

Raheja L.F., Genetos D.C., Yellowley C.E. Hypoxic osteocytes recruit human MSs through an OPN/CD44-mediated pathway. *Biochem. and Bioph. Res. Comm.,* **366**, 1061-0166 (2008).

Rammelt S., Neumann M., Hanisch U., Reinstorf A., Pompe W., Zwipp H., Biewener A. Osteocalcin enhances bone remodeling around hydroxyapatite/collagen composites. *J. Biomed. Mater. Res. A.,* **73**, 284-294 (2005).

Ritter N.M., Farach-Carson M.C., Butler W.T. Evidence for the formation of a complex between osteopontin and osteocalcin. *J. Bone Miner. Res.,* **7**, 877-885 (1992).

Rittling S.R., Matsumoto H.N., McKee M.D., Nanci A., An X.R., Novick K.E., Kowalski A.J., Noda M., Denhardt D.T. Mice lacking osteopontin show normal development and bone structure but display altered osteoclast formation in vitro. *J.Bone Miner. Res.,* **13**, 1101-1111 (1998).

Roberts T.T., Rosenbaum A.J. Bone grafts, bone substitutes and othobiologics. The bridge between basic science and clinical advancements in fracture healing. *Organogenesis,* **8**, 114-124 (2012).

Rodriguez D.E., Thula-Mata T., Toro E.J., Yeh Y.W., Holt C., Holliday L.S., Gower L.B. Multifunctional role of osteopontin in directing intrafibrillar mineralization of collagen and activation of osteoclasts. *Acta Biomaterialia,* **10**, 494-507 (2014).

Saleh S., Thompson D.E., McConkey J., Murray P., Moorehead R.A. Osteopontin regulates proliferation, apoptosis, and migration of murine claudin-low mammary tumor cells. *BMC cancer,***16**, 359 (2016).

Saran U., Gemini Piperni S., Chatterjee S. Role of angiogenesis in bone repair. *Arch. Biochem. Biophys.* **1**, 109-117 (2014).

Schultz G.S., Wysocki A. Interactions between extracellular matrix and growth factors in wound healing. *Wound Repair Regen.,* **17**, 153-162 (2009).

Stock U.A., Vacanti J.P. Tissue Engineering: current state and prospects. *Annu. Rev. Med.* **52**, 443 (2001).

Street J., Bao M., deGuzman L., Bunting S., Peale F.V. Jr., Ferrara N., Steinmetz H., Hoeffel J., Cleland J.L., Daugherty A., van Bruggen N., Redmond H.P., Carano R.A., Filvaroff E.H. Vascular endothelial growth factor stimulates bone repair by promoting angiogenesis and bone turnover. *Proc. Natl. Acad. Sci. U.S.A.,* **99**, 9656-9661 (2002).

Takahashi F., Akutagawa S., Fukumoto H., Tsukiyama S., Ohe Y., Takahashi K., Fukuchi Y., Saijo N., Nishio K. Osteopontin induces angiogenesis of murine neuroblastoma cells in mice. *Int. J. Cancer* **98**, 707-712 (2002).

Tang H., Wang J., Bai F., Hong L., Liang J., Gao J., Zhai H., Lan M., Zhang F., Wu K., Fan D. Inhibition of osteopontin would suppress angiogenesis in gastric cancer. *Biochem. Cell. Biol*. **85**, 103-110 (2007).

van de Loo P.G., Soute B.A., van Haarlem L.J., Vermeer C. The effect of Gla-containing proteins on the precipitation of insoluble salts. *Biochem. Biophys. Res. Commun.,* **142**, 113-119 (1987).

Wang W., Yeung K.W.K. Bone grafts and biomaterials substitutes for bone defect repair: a review. *Bioactive Materials,* **2**, 224-247 (2017).

Wang Y., Yan W., Lu X., Qian C., Zhang J., Li P., Shi L., Zhao P., Fu Z., Pu P., Kang C., Jiang T., Liu N., You Y. Overexpression of osteopontin induces angiogenesis of endothelial progenitor cells via the avß3/PI3K/AKT/eNOS/NO signaling pathway in glioma cells. *Eur. Jour. Cell Biol.* **90**, 642-648 (2011).

Weber G.F., Ashkar S., Glimcher M.J., Cantor H. Receptor-ligand interaction between CD44 and osteopontin (Eta-1). *Science* **271**, 509-512 (1996).

Young M.F. Bone matrix proteins: their function, regulation, and relationship to osteoporosis. *Osteoporos. Int.* **14**, S35-S42 (2003).

Zoch M.L., Clemens T.L., Riddle R.C. New insights into the biology of osteocalcin. *Bone,* **82**, 42-49 (2016).

CHAPTER IV – Biomimetic matrices for rapidly forming mineralized bone tissue based on stem cell-mediated osteogenesis

Outline

Bone regeneration, following fracture, relies on autologous and allogenic bone grafts. However, majority of fracture population consists of older individuals with poor quality bone associated with loss and/or modification of matrix proteins critical for bone formation and mineralization. Allografts suffer from same limitations and carry the risk of delayed healing, infection, immune rejection and eventual fracture. In this work, we apply a synergistic biomimetic strategy to develop matrices that rapidly form high quality bone - a critical aspect of fracture healing of weight bearing bones. Collagen matrices, enhanced with two selected key matrix proteins, osteocalcin (OC) and osteopontin (OPN), increased the rate and quantity of synthesized bone matrix by increasing mesenchymal stem/stromal cell (MSC) proliferation, accelerating osteogenic differentiation, enhancing angiogenesis and showing a sustained bone formation response from MSC obtained from a variety of human tissue sources (bone marrow, fat and umbilical cord). In vivo assessment of OC/OPN-mineralized scaffolds in a critical sized-defect rabbit long-bone model revealed bone tissue and vessel formation. We demonstrate a new biomimetic strategy to rapidly form mineralized bone tissue and secure a sustained bone formation response by MSC from multiple sources, thus facilitating faster patient recovery and treatment of non-union fractures in aging and diseased population. Acellular biomimetic matrices elicit bone regeneration response from MSC, obtained from multiple tissue sources, and can be used in variety of scaffolds and made widely available.

IV.1. Introduction

New promising solutions for bone reconstruction have been developed due to the increased clinical demand for tissue engineered bone (Yaszemski *et al.* 1996). In fact, each year in United States alone, more than one million non-union fractures are treated (Yaszemski *et al.* 1996, Giannotti *et al.* 2013). To date most common procedures for bone regeneration still rely on bone grafts, both autologous or allogeneic bone grafts (Yaszemski *et al.* 1996). However, these approaches have drawbacks and are not ideal for bone regeneration. In the case of autografts, possible complications may occur, such as pain, infection, scarring and patients will eventually experience fractures (Yaszemski *et al.* 1996, Stock and Vacanti 2001). Allografts have also similar limitations, namely the higher risk of immunologic rejection, besides infection (Stock and Vacanti 2001).

Although bone has a regenerative capacity of healing without forming a fibrous scar, this biological process can fail, leading to delayed healing or development of non-union fractures, significantly impacting the economics and patient's quality of life (Giannotti *et al.* 2013). Acceleration of the fracture healing process would bring some benefits, such as the reduction of medical costs and enhancement of quality of life by decreasing pain and increasing patient's mobility (Giannotti *et al.* 2013). Even though materials science technology has resulted in clear improvements and breakthroughs for bone tissue engineering applications, challenges to achieve functional and mechanically competent bone growth remain (Lutolf *et al.* 2003). In particular, it lacks a carefully crafted strategy, similar to one employed *in vivo*, to address various aspects of forming functional load bearing bone.

Bone formation *in vivo* is the result of different sequential stages that include the recruitment, migration and proliferation of osteoprogenitors cells from surrounding tissues followed by their osteoblastic differentiation, matrix formation and tissue mineralization (Phillips *et al.* 2005). It is known that most of the outstanding properties of the bone are related to its matrix constitution (Sroga *et al.* 2011). By looking deep into nature, we observe that most of the tissues are composed of collagen (Hesse *et al.* 2010). However, only few of these tissues like bone, containing distinct extracellular matrix (ECM) compositions, are mineralized. Therefore, the composition of the bone extracellular matrix defines its unique properties and bone matrix composition is indeed different from the others extracellular matrices in the organism.

Bone extracellular matrix has two components: a mineral part comprising hydroxyapatite (70-90%) and an organic part (10-30%) of primarily collagen (approx. 90% of organic matrix) with the rest being non-collagenous proteins (~10%) (Sroga *et al.* 2011, Vashishth *et al.* 2007). Collagen plays a critical role in the structure and function of bone tissue (Vashishth *et al.* 2007). Within the group of non-collagenous proteins, osteocalcin (OC) and osteopontin (OPN) are the most abundant, representing 10-20% of the non-collagenous proteins (Sroga *et al.* 2011). Together, collagen and the non-collagenous matrix proteins allow for the deposition of hydroxyapatite.

During childhood and adolescence, bone growth process is most active and enables long bones to increase in diameter and to change shape. In adult vertebrates, bones are constantly being remodeled, due to the regulation of bone resorption and formation processes. Interestingly, when investigating protein contents in osteonal *versus* interstitial bone tissue, our group demonstrated that, compared to older bone, OC and OPN are found in higher levels in younger bone, highlighting the potential role and/or regulation of these non-

collagenous proteins in bone formation, remodeling and mineralization (Sroga *et al.* 2011). Although it is well known that the skeletal tissue is controlled by hormonal regulation, bone non-collagenous proteins trapped within bone ECM have been reported to play a critical role in regulating the normal and pathological skeletal growth and remodeling (Sroga *et al.* 2011, Gundberg *et al.* 2003).

OPN is an arginine-glycine-aspartate (RGD)-containing adhesive glycoprotein (Denhardt *et al.* 1993). This protein was first identified in bone matrix, however it can be detected in other tissues, such as dentin, cartilage, kidney, and vascular tissues (Denhardt *et al.* 1993). OPN can bind to $\alpha_v\beta_3$ integrins through their RGD domain. Additionally, OPN can also present an RGD-independent mechanism, in which OPN may engage CD44 (Weber *et al.* 1996), a cell surface adhesion molecule, involved in cell-cell and cell-matrix interactions. OPN has been proposed to regulate many physiological processes such as collagen organization, cell adhesion, cell viability, cell migration, angiogenesis and calcification (Sroga *et al.* 2011, Denhardt *et al.* 1993, Rodriguez *et al.* 2014). OC is the most abundant bone specific non-collagenous protein in bone extracellular matrix that has been conserved in bone through evolution. It has affinity for calcium, playing an important role in matrix mineralization (Ducy *et al.* 1996). OC also functions in cell signalling and the recruitment of osteoclasts and osteoblasts, having important roles in bone resorption and deposition, respectively (DeFranco *et al.* 1991).

Recent studies conducted by our group and others have demonstrated the role of OPN and/or OC as structural molecules in bone matrix linking the organic and inorganic matrices and contributing to structural integrity of bone (Sroga *et al.* 2011, Nikel *et al.* 2013, Moragan *et al.* 2015, Bailey *et al.* 2017). Moreover, loss and modification of OC and/or OPN from bone matrix, known to occur with tissue age (Sroga *et al.* 2011) and with aging in humans (Boskey and Coleman 2010, Plantalech *et al.* 1991, Ingram *et al.* 1994, Grynpas *et al.* 1994), lead to loss of structural integrity (Poundarik *et al.* 2012) and altered mineralization (Boskey 1989, Rodriguez *et al.* 2014). Thus, autografts as well as allografts, typically obtained from older donors or patients that were subjected to total hip arthroplasty procedures (Passias and Bono 2006), are likely to contain bone tissue that is structurally compromised and not fully functional to promote mineralization.

Bone marrow mesenchymal stem/stromal cells (BM MSC) have been suggested for cell-based tissue engineering therapies, due to their potent immunomodulatory properties, capacity for self-renewal and ability to differentiate into different cell lineages, such as bone, cartilage and fat (Caplan 1991, Dominici *et al.* 2006). Under defined conditions *in vitro (*e.g., dexamethasone, ascorbic acid, β-glycerophosphate), it is possible to direct MSC along an osteogenic lineage. During this phase, alterations in cellular morphology, proliferation and gene expression lead to secretion of an organized extracellular matrix on which calcium phosphate is deposited as hydroxyapatite crystals (Bruder *et al.* 1997).

We posited that non-collagenous proteins from bone ECM, specifically OC and OPN, may be combined to design a novel biomimetic collagen matrix that accelerates bone healing response. To this end, we assess the synergistic effect of OC/OPN on different aspects of bone regeneration including MSC proliferation, osteogenic differentiation, mineralization and angiogenic properties (Figure IV.1). We evaluated 5 different concentrations of OC/OPN combinations, above and below bone matrix physiological levels, and identified biomimetic OC/OPN-enhanced collagen matrices that enhance early osteogenic differentiation of MSC and sustain bone formation response (Figure IV.1). The presence of these proteins on the matrix was confirmed

by a SDS-PAGE protein gel (Figure IV.2) and by measuring the amount of OC and OPN released from the collagen gels after 24h and 21 days (Figure IV.3).

Effects of OC/OPN-enhanced collagen matrices were also evaluated on human MSC from different sources to address the broad application of this approach for bone regeneration. This study aims to develop a new strategy for rapidly forming and sustaining functional bone formation by utilizing OC and OPN and determining the mechanism for their synergistic effect on bone regeneration. To confirm the synergistic effect of these two bone ECM proteins, OC-enhanced collagen matrices and OPN-enhanced collagen matrices were also investigated.

IV.2. Materials & Methods

IV.2.1. Preparation of OC/OPN-enhanced type I collagen matrices

To design the biomimetic OC/OPN-enhanced collagen gels, we used type I collagen at 3 mg/ml and we based on the physiological levels that Cairns and Price reported in bone, 1mg OC per 1 g of collagen (Cairns and Price 1994) (3 µg/ml of OC). Physiologically, the content of OPN is known to be lower than OC. To optimize our results, different concentrations of OC and OPN were tested, by varying the amount of OC and OPN incorporated into the type I collagen gels, above and below bone matrix physiological levels (Figure IV.1c).

Recombinant human OPN protein was purchased from R&D Systems and human OC fragment 1-49 was purchased from Sigma-Aldrich. Different concentrations of OC and OPN (Figure IV.1c) were combined to 100 µl of chilled purified bovine type I collagen solution (PureCol: Advanced BioMatrix, San Diego, CA) at a final concentration of 3 mg/ml with gentle swirling. pH of mixture was adjusted to 7.2-7.6 using sterile 0.1 M NaOH (Sigma-Aldrich, St. Louis, MO). To prevent gelation, the temperature of mixture was maintained at 2–10ºC. 100 µl of OC/OPN-enhanced collagen solution was added to each well from a 96-well plate. To form gel, the plate was incubated at 37ºC for 2h. After incubation, the OC/OPN-enhanced collagen gels were hydrated in culture medium 1h at 37ºC, prior to cell culture.

To evaluate the amount of proteins released from the collagen matrices, phosphate buffer saline (PBS: Gibco, Grand Island, NY) was added to the OC/OPN-enhanced collagen gels (all the combinations) and to the OC and OPN-collagen gels for 24h and 21 days. After that, the PBS in contact with the matrices was collected and the concentrations of OC and OPN were measured by enzyme-linked immunosorbent assays (ELISA: R&D Systems, Minneapolis, MN), according to the manufacturer's instructions contained in the human OPN or OC quantikine ELISA kit (R&D Systems).

For the *in vivo* studies, bovine type I collagen fibrous sheets (Advanced BioMatrix) were mineralized in the presence of OC/OPN, to produce OC/OPN-enhanced mineralized collagen matrices. Therefore, the scaffolds (6x6x5 mm^3) were incubated, first, in a 1 M $CaCl_2$ solution in the presence of 60 µg/ml OC, then with 12 µg/ml OPN at 37ºC (pH=7.4) for 24h. The scaffolds were washed twice with phosphate buffer saline (Gibco) and freeze-dried. Next, the scaffolds were incubated with 1 M Na_2HPO_4 at 37ºC (pH=7.4) for 24h and freeze-dried. The mineralized scaffolds were sterilized using ethylene oxide (Figure IV.1b).

IV.2.2. Cell culture

Human MSC used are part of the cell bank available at the Stem Cell Engineering Research Group (SCERG), Institute for Bioengineering and Biosciences (iBB) at Instituto Superior Técnico (IST). MSC were previously isolated/expanded according to protocols previously established at iBB-IST (Simões *et al.* 2013, Gimble *et al.* 2007, dos Santos *et al.* 2010). Originally, human tissue samples were obtained from local hospitals under collaboration agreements with iBB-IST (bone marrow: Instituto Português de Oncologia Francisco Gentil, Lisboa; adipose tissue: Clínica de Todos-os-Santos, Lisboa; umbilical cord: Hospital São Francisco Xavier, Lisboa, Centro Hospitalar Lisboa Ocidental, Lisboa). All human samples were obtained from healthy donors after written informed consent according to the Directive 2004/23/EC of the European Parliament and of the Council of 31 March 2004 on setting standards of quality and safety for the donation, procurement, testing, processing, preservation, storage and distribution of human tissues and cells (Portuguese Law 22/2007, June 29), with the approval of the Ethics Committee of the respective clinical institution. Isolated cells were kept frozen in liquid/vapour nitrogen tanks until further use.

Human MSC from different sources were thawed and plated on T-75 flasks using low-glucose Dulbecco's Modified Eagle Medium (DMEM: Gibco, Grand Island, NY) supplemented with 10% fetal bovine serum (FBS MSC qualified: Gibco) and 1% antibiotic-antimycotic (Gibco) and kept at 37ºC, 5% CO_2 and 21% O_2 in an humidified atmosphere. Medium renewal was performed every 3-4 days. Cells between passages 3 and 6 were used. Three independent donors from each tissue source were used on all experiments. The cells were tested for expression of cell surface markers indicative of MSC (i.e., $CD73^+$, $CD90^+$, $CD105^+$, HLA-DR^-, $CD34^-$, $CD45^-$), and their ability to differentiate into osteoblasts, adipocytes, and chondrocytes. Human umbilical vein endothelial cells (HUVEC) were purchased from Lonza (Basel, Switzerland) and maintained in commercial Endothelial Growth Medium-2 (EGM-2: Lonza).

Three different MSC cell donors were used for each experiment. Each experiment was performed in triplicates.

IV.2.3. *In vitro* osteogenesis on OC/OPN-enhanced collagen gels

Human MSC were enzymatically lifted from their plates using TrypLE™ solution (Gibco) and re-suspended at 10000 cells/cm^2. Then, 100µl of the cell suspension was seeded onto the confined area of the collagen gel and the cells were allowed to attach to the collagen gel for 24h. After 24h, the medium was removed and the non-adherent cells were washed twice with PBS. DMEM+10%FBS was added to the cell culture on OC/OPN-enhanced collagen gels to allow cell expansion. After 5 days, osteogenic differentiation medium (StemPro® Osteogenesis Differentiation Kit: Gibco) was added to each collagen gel to induce osteogenic differentiation. Medium was changed every 3-4 days. The time at which the osteogenic medium was added is referred to as day 0 and cell culture was maintained for more 21 days after adding the osteogenic medium. The area covered by cells was visualized using a fluorescence microscope (Olympus IX51 Inverted Microscope: Olympus America Inc., Melville, NY) and recorded by an attached digital camera. After 21 days of osteogenic differentiation, samples were stained with 20 mM Xylenol orange (Sigma-Aldrich) for calcium phosphate mineral deposits and images were acquired.

IV.2.4. Cell proliferation and morphology

The effect of OC/OPN-enhanced collagen gels on MSC proliferation was evaluated using AlamarBlue® cell viability reagent (Molecular Probes, Eugene, OR) (n=3). AlamarBlue® cell viability reagent was added to the cells and incubated at 37ºC in 5% CO_2 chamber for 2.5h. Fluorescence was quantified (560 nm – 590 nm) and compared to a calibration curve to access the metabolic activity of viable cells under each condition. Cell proliferation was measured in triplicates in all groups. The capacity of OC/OPN-enhanced collagen gels to promote BM MSC proliferation was assessed after 5, 10 and 15 days of culture using DMEM+10%FBS and also osteogenic differentiation medium as culture medium.

To assess cell morphology, after 24h and 15 days of proliferation, cells were washed twice with PBS, fixed with 4% paraformaldehyde (PFA: Santa Cruz Biotechnology, Dallas, TX) for 20 min and then permeabilized with 0.1% Triton X-100 (Sigma-Aldrich) for 10 min. After permeabilization, cells were incubated with phalloidin (Invitrogen, Carlsbad, CA) (dilution 1:250, 2 µg/ml) for 45 min in the dark. Then, cells were washed twice with PBS and counterstained with DAPI (Invitrogen) (1.5 µg/ml) for 5 min and then washed with PBS. The fluorescent staining was imaged by fluorescence microscope (Olympus IX51 Inverted Microscope: Olympus America Inc., Melville, NY) and recorded by an attached digital camera.

IV.2.5. qRT-PCR analysis

Total RNA was extracted with a RNeasy Mini Kit (QIAGEN, Hilden, Germany). cDNA was synthesized from 20 ng of total RNA using iScript™ Reverse Transcription Supermix (Bio-Rad, Hercules, CA). Reaction mixtures (20 µl) were incubated in a thermal cycler (Veriti 96-well thermal cycler: Applied Biosystems, Foster City, CA) for 5 min at 25ºC, 30 min at 42ºC and 5 min at 85ºC and then were maintained at 4ºC. The sequences of the specific primer sets used are given in Table IV.1.

The quantitative reverse transcription-polymerase chain reaction (qRT-PCR) was performed using SYBR® Green PCR Master Mix (Applied Biosystems) and StepOnePlus real-time PCR system (Applied Biosystems). All reactions were carried out at 95ºC for 10 min, followed by 40 cycles of 95ºC for 15 sec and 60ºC for 1 min; all were performed in triplicate. Glyceraldehyde 3-phosphate dehydrogenase was used as internal control to normalize differences in total RNA levels in each sample. A threshold cycle (Ct) was observed in the exponential phase of amplification, and quantification of relative expression levels was performed with the use of standard curves for target genes and endogenous control. Geometric means were used to calculate the $\Delta\Delta$Ct values and are expressed as $2^{-\Delta\Delta Ct}$. The mean values from triplicate analysis were compared. The value of each control sample (undifferentiated cells) was set as 1 and was used to calculate the fold difference in the target gene.

Table IV.1. Sequences of primers used for qRT-PCR analysis.

Genes	Sequences
GAPDH	For: 5' AAC AGC GAC ACC CAC TCC TC Rev: 5' CAT ACC AGG AAA TGA GCT TGA CAA
Col I	For: 5' CAT CTC CCC TTC GTT TTT GA Rev: 5' CCA AAT CCG ATG TTT CTG CT
Runx2	For: 5' AGA TGA TGA CAC TGC CAC CTC TG Rev: 5' GGG ATG AAA TGC TTG GGA ACT
ALP	For: 5' ACC ATT CCC ACG TCT TCA CAT TT Rev: 5' AGA CAT TCT CTC GTT CAC CGC C
OPN	For: 5' ATG AGA TTG GCA GTG ATT Rev: 5' TTC AAT CAG AAA CCT GGA A
OC	For: 5' TGT GAG CTC AAT CCG GCA TGT Rev: 5' CCG ATA GGC CTC CTG AAG C
VEGF	For: 5' GGA GGA GGG CAG AAT CAT CAC Rev: 5' GGT CTC GAT TGG ATG GCA GT

IV.2.6. Calcium quantification assay

For determination of total calcium content, samples (n=3) were washed twice with PBS (Gibco) and extracted off a well of a 96-well plate in 0.5M HCl solution (Sigma-Aldrich). Accumulated calcium was removed from the cellular component by shaking overnight at 4ºC. The consequent supernatant was utilized for calcium determination according to the manufacturer's instructions contained in the calcium colorimetric assay kit (Sigma-Aldrich). Total calcium was calculated from calcium standard solution prepared in parallel. Absorbance at 575 nm was measured for each condition and normalized to the total number of cells, after 21 days of osteogenic differentiation.

IV.2.7. Alkaline phosphatase activity

Alkaline phosphatase (ALP) activity was detected using a colorimetric ALP kit (BioAssays Systems, Hayward, CA) according to the manufacturer's protocol. Samples (n=3) were washed with PBS (Gibco) and were incubated in the lysis buffer (0.1% Triton X-100 in PBS) by shaking for 30 min at room temperature. The lysate was added to p-nitrophenyl phosphate solution (10 mM) provided with the ALP kit. The absorbance was measured at 405 nm and normalized to the total number of cells in each sample. ALP activity assay was performed after 15 and 21 days of osteogenic differentiation.

IV.2.8. Cell migration assay

24-well tissue culture plates were collagen-coated by incubation in 0.2 mg/ml of collagen type I solution (Sigma) for 2h at 37ºC before rinsing with PBS (Gibco). Each well was seeded with HUVEC at 10000cells/cm^2 and maintained at 37ºC and 5% CO_2 for 48h to allow cell adhesion and the formation of a confluent monolayer. These confluent monolayers were then scratched with a sterile pipette tip, creating a scratch (wound) of approximately 0.25-0.3 mm in width. After creating the scratch, culture medium was then removed and replaced with conditioned medium which had been generated from BM MSC cultured for 4 days at 10000 cells/cm^2 using growth medium DMEM+10%FBS on (i) control collagen gels without OC and OPN incorporation, (ii) OC-enhanced collagen gels, (iii) OPN-enhanced collagen gels and (iv) OC/OPN-enhanced collagen gels (OC/OPN#1). All scratch assays were performed in triplicate.

Migration of HUVEC was monitored by collecting images at various time intervals (0h, 4h, 8h and 24h) after the scratch was performed (Leica DM IL LED with EC3 camera system). The migration distance was quantified with the use of ImageJ (NIH) software, measuring the width of the scratch at previously defined points along its length (top, middle and bottom of the field of view). Data has been presented as extent of the cell migration, i.e. the percentage by which HUVEC migrate for each given time point compared with the original scratch width.

IV.2.9. *In vitro* endothelial cell tube formation assay

To evaluate the angiogenic potential of the OC/OPN-enhanced collagen gels, conditioned medium obtained from BM MSC cultures on biomimetic collagen gels was collected and used to test the tube formation assay by culturing HUVEC on a Matrigel substrate (50μl/well) (Corning, Corning, NY). HUVEC ($2x10^4$ cells) were cultured in a 96-well plate with 100 μl/well (4 wells per group) of conditioned medium from BM MSC cultures on (i) control collagen gels without OC and OPN incorporation, (ii) OC-enhanced collagen gels, (iii) OPN-enhanced collagen gels and (iv) OC/OPN-enhanced collagen gels (OC/OPN#1). As a negative control, HUVEC were incubated with endothelial basal medium (EBM-2: Lonza) and, as a positive control, HUVEC were incubated with endothelial growth medium (EGM-2: Lonza). After incubation for 8h at 37ºC, three photomicrographs per well were taken under light microscopy (Leica DM IL LED with EC3 camera system). The number of branch points and tubes formed were counted with the use of ImageJ (NIH) software.

IV.2.10. *In vivo* bone regeneration in a critical sized-defect rabbit long-bone model

New Zealand White female rabbits weighting more than 3.25 kg were used to assess the *in vivo* bone forming capacity of OC/OPN-enhanced collagen matrices and its biocompatibility. The rabbits were anesthetized with a subcutaneous injection of ketamine (35 mg/kg body weight) and acepromazine (0.75 mg/kg body weight). Bilateral surgery was performed to each rabbit (n=3) to create a critical sized-defect in the distal femoral condyle and proximal tibia. A medial skin incision of approximately 4 cm was made in the rabbit's hind leg. The skin was retracted laterally to allow for a lateral arthrotomy of the stifle joint. Once the femur was exposed, a lateral arthrotomy was performed and the joint opened. A transcondylar defect

(approximately 6 mm diameter by 12 mm deep) was created in the femur. The point of drilling was located by finding the midpoint of the lateral condyle from the lateral fabellae to the most anterior portion of the lateral trochlea. A unicortical defect (approximately 5 mm diameter by 10 mm deep) was created in the proximal tibia at the level of the tibial tuberosity. The point of drilling was the medial side, level with the tibial tuberosity. After creating the defect, the site received a final rinse with saline to remove any residual particulate and the OC/OPN-enhanced collagen matrices were implanted in both femur and both tibia and the soft tissues and skin were closed using non-absorbable sutures. The animals were sacrificed 6 weeks after implantation. The retrieved specimens were fixed in formalin solution and prepared for micro-computed tomography and histological analysis. The specimens were embedded in methyl methacrylate and sections were cut and subjected to staining for Hematoxylin and Eosin (H&E), Goldner's Trichrome (GT), Von Kossa (VK), Toluidine Blue (TB) and Tartrate-Resistant Acid Phosphatase (TRAP)/TB. Digital images were captured with an Olympus IX51 inverted microscope associated with a digital camera. All methods were carried out in accordance with relevant guidelines and regulations. All animal experimental protocols were approved by Institutional Animal Care and Use Committee (IACUC) at Spring Valley Laboratories (IACUC approval number: SVL-315).

IV.2.11. Scanning electron microscope evaluation

Scanning electron microscope attached with an energy dispersive electron probe X-ray analyzer (SEM-EDS: Carl Zeiss ultra 1540 dual beam FIB/SEM system) was used to observe collagen gels fibrils and mineral deposition on OC/OPN-enhanced collagen gels after MSC culture. Cell culture samples were rinsed with PBS and then fixed in 2% glutaraldehyde for 5 min, after which they were dehydrated in a graded series of ethanol and dried in a critical CO_2 freeze dryer (Tousimis Autosamdri-815). After sputter-coating with gold, the specimens were examined at an accelerating voltage of 2.5-5 kV.

IV.2.12. Micro-computed tomography (µ-CT) evaluation

Tomograms of cylindrical pins were acquired and three-dimensional reconstruction was performed using an X-ray scanner (*Viva*CT 40, Scanco Medical) with a voxel resolution of ~10 µm. The parameters for the scans were 635 projections, 199 ms exposure time, 70 Kvp and 112 µA current. Images were reconstructed using the SCANCO software.

IV.2.13. Statistical analysis

Each experiment was conducted in triplicate. Statistical analysis of the data was performed using one-way ANOVA at the same timepoint, using GraphPad Prism version 7 software. The statistical significance of results is reported at 95% confidence intervals ($P<0.05$).

IV.3. Results

IV.3.1. Effects of OC/OPN-enhanced collagen gels on MSC adhesion and proliferation

Fluorescence microscopy images of DAPI and Phalloidin of bone marrow (BM) MSC seeded on top of OC/OPN-enhanced collagen gels 24 hours after seeding suggested that the cells attached efficiently onto all substrates. Qualitatively, the cells were randomly distributed and displayed their native spread morphology (Figure IV.4.a). The capacity of the OC/OPN-enhanced collagen gels to promote BM MSC proliferation is shown in Figure IV.4b,c for cells cultured using DMEM+10%FBS (growth medium) and osteogenic medium (differentiation medium). After 15 days, BM MSC were present in higher number when cultured onto OC/OPN-enhanced collagen gels than onto the control collagen gels, suggesting that the combination of OC and OPN has a significant impact in proliferation of BM MSC. This effect was not only observed when cells were cultured using growth medium DMEM+10% FBS, but also when cells were cultured under osteogenic differentiation conditions for 15 days. Figure IV.4a shows fluorescence microscopy images of DAPI and phalloidin of BM MSC cultured after 15 days under DMEM+10%FBS, suggesting that OC/OPN-enhanced collagen gels presented more cells compared with the control.

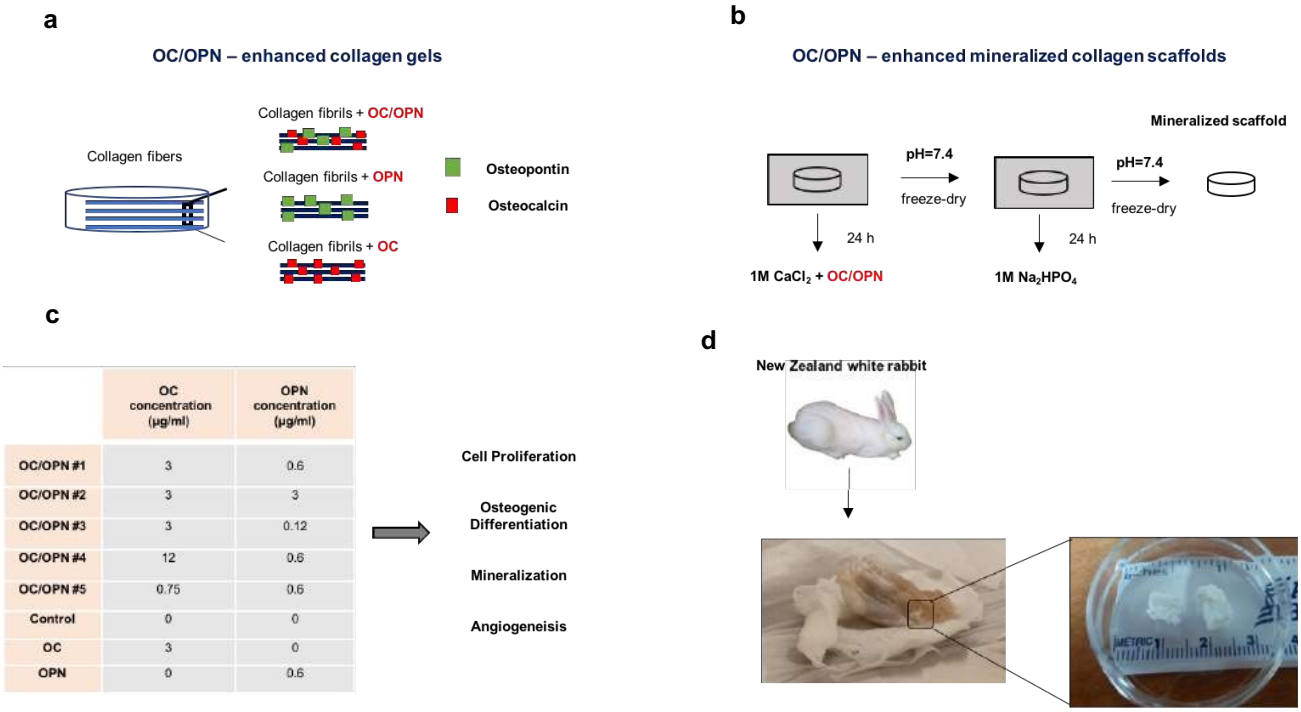

Figure IV.1. Design of the biomimetic OC/OPN-enhanced collagen matrices. **a)** Schematic of OC/OPN-enhanced collagen gels. **b)** Schematic of fabrication of OC/OPN-enhanced mineralized collagen scaffolds. **c)** Different concentrations of OC and OPN incorporated into type I collagen gels at 3 mg/ml to create biomimetic matrices, based on the average of OC recovered from human bone (Cairns and Price 1994). Cell proliferation, osteogenic differentiation, mineralization and angiogenesis were the different variables evaluated after cell culture on OC/OPN-enhanced collagen gels. **d)** Left: Representation of the OC/OPN-enhanced mineralized collagen scaffold implanted into a rabbit tibia after 6 weeks of surgery. Right: OC/OPN-enhanced mineralized collagen scaffolds prior to implantation into a rabbit model.

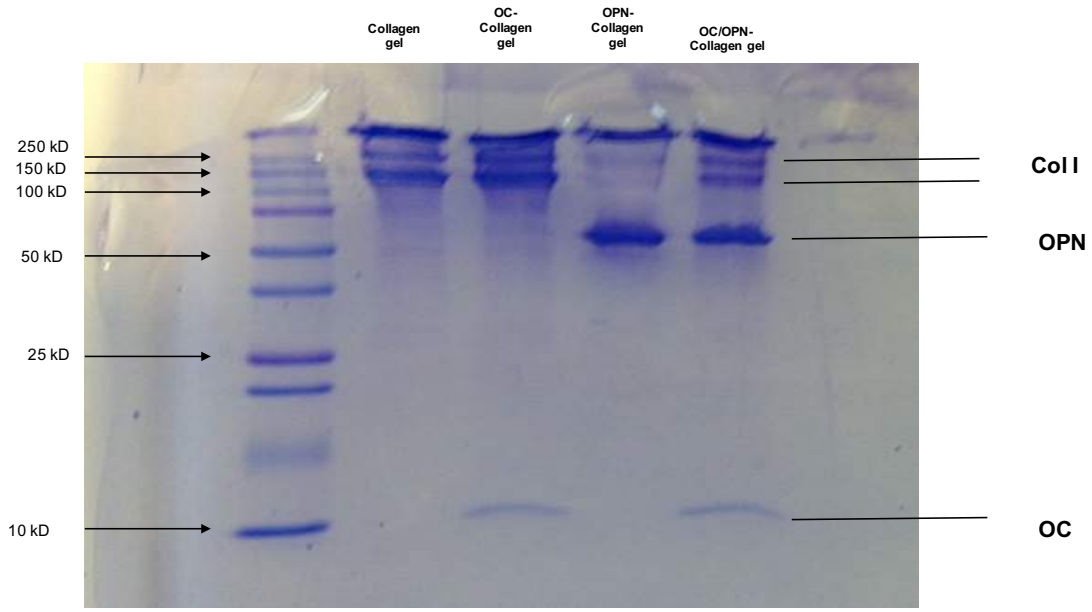

Figure IV.2. SDS-PAGE protein gel of collagen gel, OC-collagen gel, OPN-collagen gel and OC/OPN-collagen gel confirms the presence of OC/OPN in the matrices.

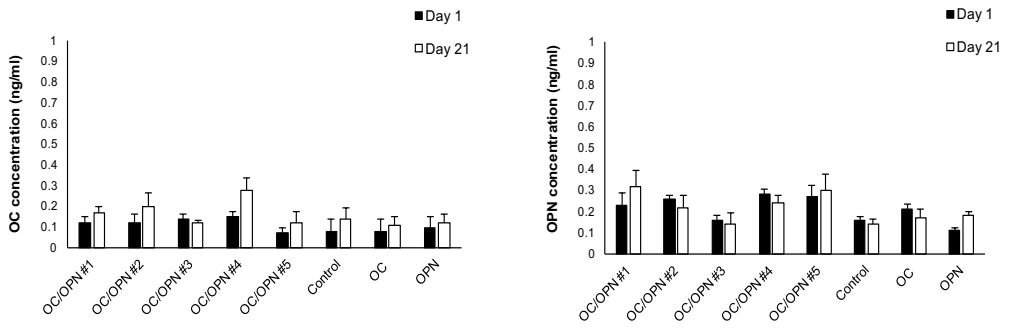

Figure IV.3. *In vitro* OC and OPN release from OC/OPN-enhanced collagen gels. OC and OPN levels in PBS were determined by ELISA measurements after 24h and 21 days. Results demonstrated that the biomimetic gels did not release OC and OPN proteins, being able to maintain the proteins on the gel.

The number of cells after 15 days was higher when cells were cultured with DMEM+10%FBS compared with osteogenic medium ($4.54\pm0.36x10^4$ cells *vs* $3.10\pm0.11x10^4$ cells in OC/OPN#1 condition). The proliferation rate of BM MSC cultured onto OC/OPN-enhanced collagen gels was higher compared to control collagen gels when both media were used, demonstrating a consistent effect of the integration of OC and OPN proteins into type I collagen matrices. Indeed, after 15 days in culture under DMEM+10%FBS, the cell number on OC/OPN#1-enhanced collagen gels was 97% higher than the number of cells on control collagen gels ($4.54\pm 0.36x10^4$ cells *vs* $2.30\pm 0.08x10^4$ cells). When osteogenic differentiation medium was used, after 15 days, BM MSC presented a cell number increase of 57% when cells were cultured on OC/OPN#1-enhanced collagen gels compared to control collagen gels ($3.10\pm 0.11x10^4$ cells *vs* $1.97\pm0.14x10^4$ cells).

Interestingly, when collagen gels were supplemented with only one of the proteins (OC-enhanced collagen gel or OPN-enhanced collagen gel), more cells were observed compared to control collagen gels, after 15 days of culture, although this increase in cell proliferation was not considered statistically significant, suggesting that OC and OPN have a synergistic effect on cell proliferation.

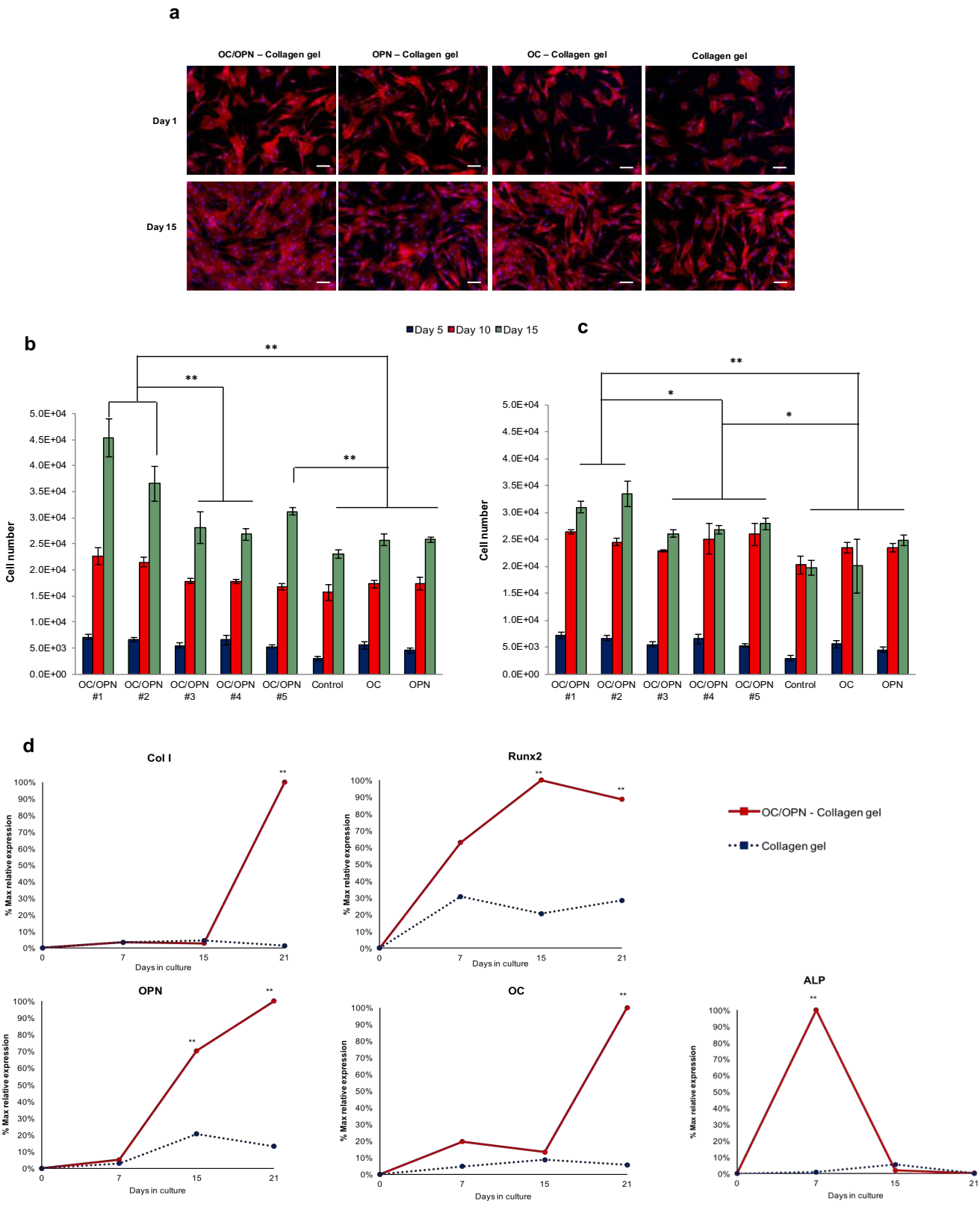

Figure IV.4. Effects of OC/OPN-enhanced collagen gels on cell proliferation and osteogenic differentiation of BM MSC. **a)** Fluorescence microscopy images of DAPI (blue) and Phalloidin (red) of BM MSC seeded on top of different substrates 24h and 15 days after cell seeding (OC/OPN #1) under DMEM+10%FBS. Scale bar, 100 µm. **b,c)** Proliferation of BM MSC cultured on OC/OPN-enhanced collagen gels for 15 days under **(b)** DMEM+10%FBS and **(c)** osteogenic differentiation medium. **d)** Percentage of maximum gene expression (collagen I [ColI], runt-related transcription factor 2 [Runx2], osteopontin [OPN], osteocalcin [OC] and alkaline phosphatase [ALP]) by BM MSC upon culture for 7, 15 and 21 days on control collagen gels and OC/OPN-enhanced collagen gels. Data are expressed as mean ± SD, **p<0.01; *p<0.05.

IV.3.2. Effects of OC/OPN-enhanced collagen gels on osteogenic differentiation

Experiments, conducted in triplicate, showed that the expression levels of key osteogenic genes (Col I, Runx2, OPN and OC) at day 21 were significantly higher in the OC/OPN-enhanced collagen gels than in the control collagen gels, indicating that the incorporation of OC and OPN onto the collagen gels enhanced the osteogenic differentiation of BM MSC (Figure IV.4d and Figure IV.5). More importantly, OC/OPN-enhanced collagen matrices promoted more osteogenic activity by sustaining the higher expression of osteogenic genes during the 21 days of culture and accelerating the osteogenic differentiation of BM MSC. In particular, when cells were cultured on OC/OPN-enhanced collagen gels, the highest level of ALP gene expression occurred 7 days earlier compared with cells cultured on control collagen matrices, indicating that osteogenic differentiation was accelerated when OC and OPN were incorporated into type I collagen gels.

OC/OPN-enhanced collagen gels also increased the expression levels of Runx2 gene after 7 days of osteogenic differentiation, reaching its maximum relative expression at day 15 and sustaining the higher expression until day 21 of culture. Control collagen gels also increased the expression of Runx2 gene on BM MSC after 7 days of osteogenic differentiation, however, the level of expression was only 30% compared with the maximum expression obtained with OC/OPN-enhanced collagen gels. Furthermore, the level of expression remained low at 20-30% compared with the maximum relative level of expression in OC/OPN-enhanced collagen gels. In contrast to collagen gel, the levels of OPN and OC genes increased throughout osteogenic differentiation, reaching higher expression levels when OC/OPN-enhanced collagen gels were used as a platform. Interestingly, after 21 days of osteogenic differentiation, OPN-enhanced collagen gels demonstrated also significantly higher expression levels of OPN and Col I gene compared with the control and even with the OC-enhanced collagen gels. On the other hand, OC-enhanced collagen gels presented significantly higher expression levels of Runx2 and OC osteogenic genes compared with the control and OPN-enhanced collagen gels. However, Only OC/OPN-enhanced collagen gels demonstrated significant expression levels that were consistent for osteogenic genes including Col I, Runx2, OC and OPN (Figure IV.5) compared with the control collagen gels. In addition, OC/OPN-enhanced collagen gels presented a statistically significant higher expression of Col I, OPN and OC genes compared with the OC-enhanced collagen gels and also Runx2 and OC osteogenic genes when compared with the OPN-enhanced collagen gels (Figure IV.5).

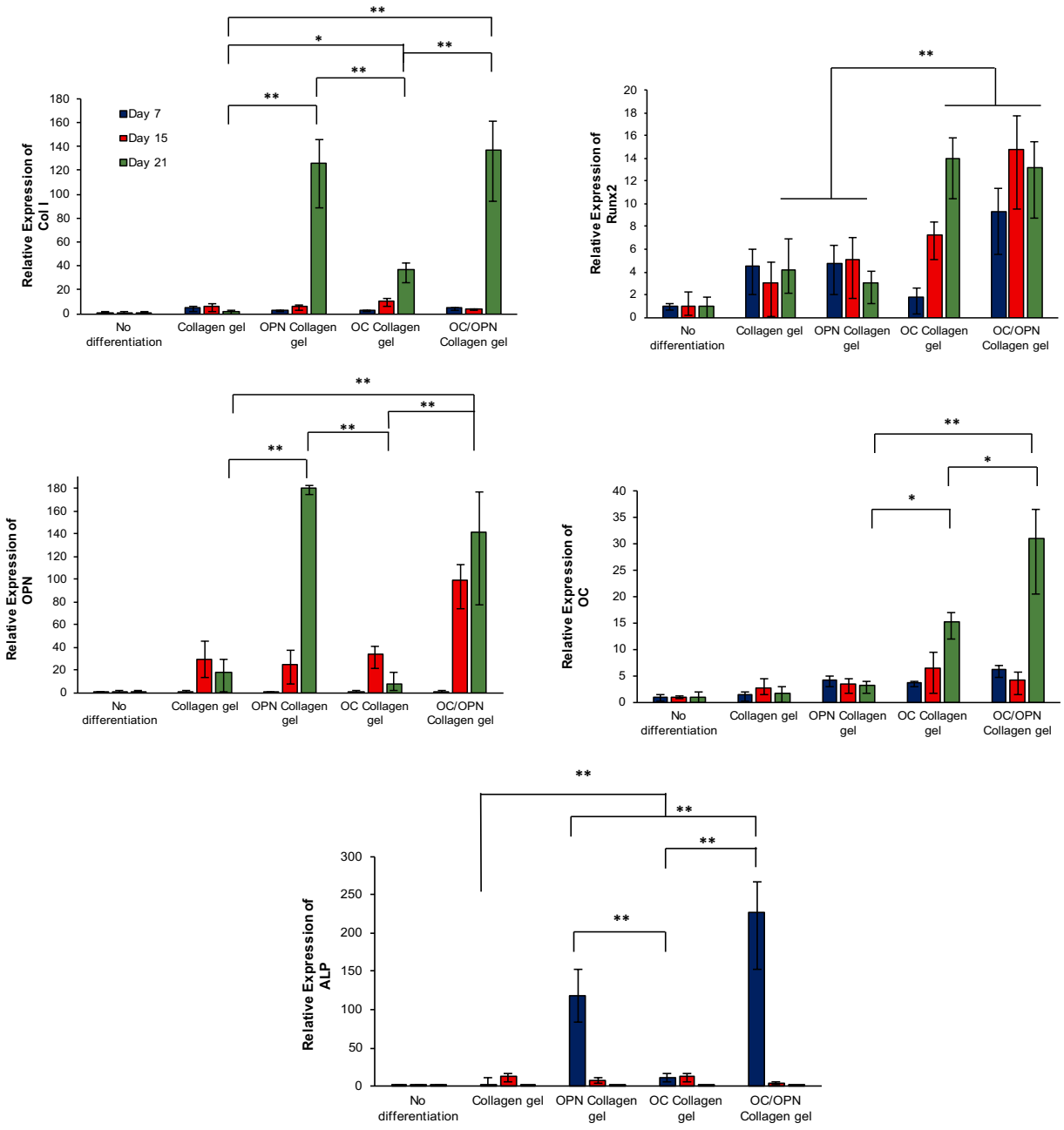

Figure IV.5. Relative gene expression (collagen I [Col I], runt-related transcription factor 2 [Runx2], osteopontin [OPN], osteocalcin [OC] and alkaline phosphatase [ALP]) by BM MSC upon culture for 7, 15 and 21 days on control collagen gels, OPN-enhanced collagen gels, OC-enhanced collagen gels and OC/OPN-enhanced collagen gels. Data are expressed as mean ± SD, **p<0.01; *p<0.05, relative to day 21 (Col I, Runx2, OPN, OC) and day 7 (ALP).

IV.3.3. Effects of OC/OPN-enhanced collagen gels on angiogenic properties

To evaluate whether OC/OPN-enhanced collagen gels could positively enhance the release of soluble factors that stimulate chemotaxis and angiogenesis, an *in vitro* cell migration assay using scratch wound healing and an endothelial tube formation assay were performed. Figure IV.6a shows that cell migration was observed after 8 hours in all groups. Under culture conditions employed in this study, HUVEC treated with conditioned medium from BM MSC cultured on OC/OPN-enhanced collagen gels migrated faster than HUVEC treated with conditioned medium from BM MSC cultured on control collagen gels, suggesting that OC/OPN-enhanced collagen gels enhance migration, reaching a remarkable increase of 45% in cell migration distance after 8 hours.

Conditioned medium from OPN-enhanced collagen gels also presented a significant increase of HUVEC migration when compared with the migration distance achieved by HUVEC treated with conditioned medium from control collagen gels. After 24 hours, the initial scratch was almost completely closed when HUVEC were treated with conditioned medium from OC/OPN-enhanced collagen gels, reaching almost the same migration rate of HUVEC treated with endothelial growth medium (EGM-2), the positive control.

The endothelial cell tube formation assay showed a similar pattern to the one observed with the cell migration assay. Figure IV.6d shows that the addition of conditioned medium from BM MSC cultured on OC/OPN-enhanced collagen gels increased the tube formation of endothelial cells compared to conditioned medium from BM MSC cultured on control collagen gels. Quantitative analysis revealed that the number of total capillary tubes and branch points formed were significantly increased by the conditioned medium from BM MSC cultured on OC/OPN-enhanced collagen gels, indicating the favored angiogenic potential of these new biomimetic matrices (Figure IV.6e,f). The results also showed that OC-collagen gels and OPN-collagen gels enhanced tube formation of endothelial cells, by the significant increase in the total number of tubes and branches points formed. Although all the three groups (OC/OPN, OC and OPN) demonstrated enhanced angiogenesis compared with the control, a more robust network of capillary-like structure was observed when conditioned medium from cells cultured on OC/OPN-enhanced collagen gels was used (Figure IV.6d). We observed that the length of the tubes was slightly higher, compared with OPN and OC groups, leading to a better interconnected structure, therefore, the quantification of number of tubes and branches per field was lower with the OC/OPN group. Furthermore, the relative level of VEGF gene expression was significantly increased when BM MSC were cultured on OC/OPN-enhanced collagen gels (Figure IV.6c).

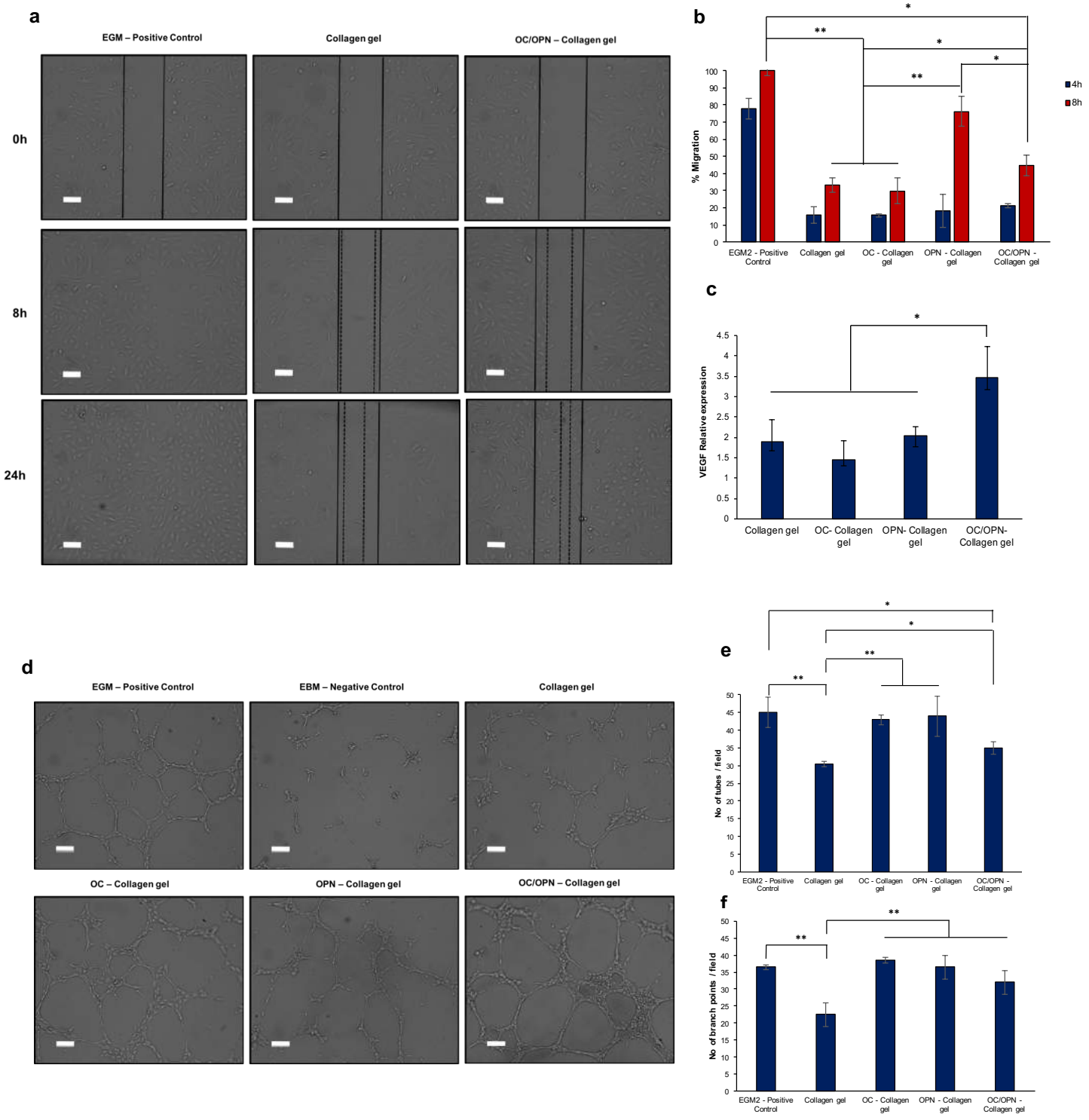

Figure IV.6. Effects of OC/OPN-enhanced collagen gels on BM MSC *in vitro* angiogenic properties assessed by multiple assays. **a)** Cell migration assay. Scratch at t=0h, t=8h and t=24h when HUVEC were treated with EGM-2 (positive control), conditioned medium from BM MSC cultured on control collagen gels and conditioned medium from BM MSC cultured on OC/OPN-enhanced collagen gels. Borders of the scratch at t=0 are indicated with solid lines, borders after migration at t=8 and t=24 hours with dashed lines. **b)** Percentage of migration distance quantification of HUVEC treated with conditioned medium from BM MSC cultured on control collagen gels, OC-collagen gels, OPN-collagen gels and OC/OPN-collagen gels. **c)** VEGF relative expression of BM MSC cultured on OC/OPN-enhanced collagen gels, OC-enhanced collagen gels, OPN-enhanced collagen gels and control collagen gels after 21 days of culture under osteogenic differentiation, normalized to VEGF relative expression of undifferentiated BM MSC. **d-f)** Endothelial cell tube formation assay: **(d)** Tube formation of HUVEC on a Matrigel substrate incubated with EGM-2 (positive control), EBM-2 (negative control) and conditioned medium from BM MSC cultured on collagen gels, OC-collagen gels, OPN-collagen gels and OC/OPN-collagen gels. **e-f)** Number of tubes/field **(e)** and number of branch points/field **(f).** Scale bars, 100μm. Data are expressed as mean ± SD, **p<0.01; *p<0.05.

IV.3.4. Effects of OC/OPN-enhanced collagen gels on mineralization and mineral quality

Here we sought to determine whether enhanced and accelerated osteogenic differentiation of MSC on OC/OPN-enhanced collagen gel results in deposition of mineral similar to the one produced by bone tissue, *in vivo* – a key aspect of high quality functional bone tissue and a gold standard of clinical practice (determined using periodical X-rays). Figure IV.7 shows cell morphology of BM MSC cultured on OC/OPN-enhanced collagen gels and control collagen gels before and after osteogenic differentiation. We can note that BM MSC seem to produce more mineral deposits when cultured on OC/OPN-enhanced collagen gels (darker regions).

We found that after 21 days of osteogenic differentiation, BM MSC demonstrated higher calcium deposition when cells were seeded onto OC/OPN-enhanced collagen gels (Figure IV.8a) compared to control, OC-collagen gels and OPN-collagen gels. Moreover, statistically significance was observed when cells were cultured on OC/OPN#1, OC/OPN#2 and OC/OPN#3-enhanced collagen gels. Figure IV.8a shows that when BM MSC were cultured and differentiated onto OC/OPN supplemented with 3 µg/ml OC and 0.6 µg/ml OPN (OC/OPN #1), a significant increase of calcium deposition of 48% was observed compared with the control collagen gels (1.42±0.11 $\mu g/10^4$ cells *vs* 0.96±0.04 $\mu g/10^4$ cells).

Mineralized nodules of human MSC were visualized after 21 days of culturing in osteogenic differentiation medium. The nodules were visualized by Xylenol orange staining in OC/OPN-enhanced collagen gels and in control collagen gels without OC and OPN incorporation (Figure IV.8b). Scanning electron microscopy (SEM) micrograph of mineral deposition of BM MSC cultured on OC/OPN-enhanced collagen gels is shown in Figure IV.8c-e. After 21 days, OC/OPN-enhanced collagen gels presented pores filled with globular mineralized nodules, indicating osteoblastic differentiation.

Next, we conducted spectroscopic analysis using SEM coupled with energy dispersive spectroscopy (EDS) and found that the mineral deposition of MSC cultured on OC/OPN-enhanced collagen gels consisted of calcium and phosphate. The Ca/P ratio of minerals formed within the OC/OPN-enhanced collagen gels was ~1.75, which is comparable to apatite in bone matrix (i.e., Ca/P ~1.66) (Cairns and Price 1994), in contrast with the control collagen gels that demonstrated a Ca/P ratio of 1.35. (Figure IV.8f).

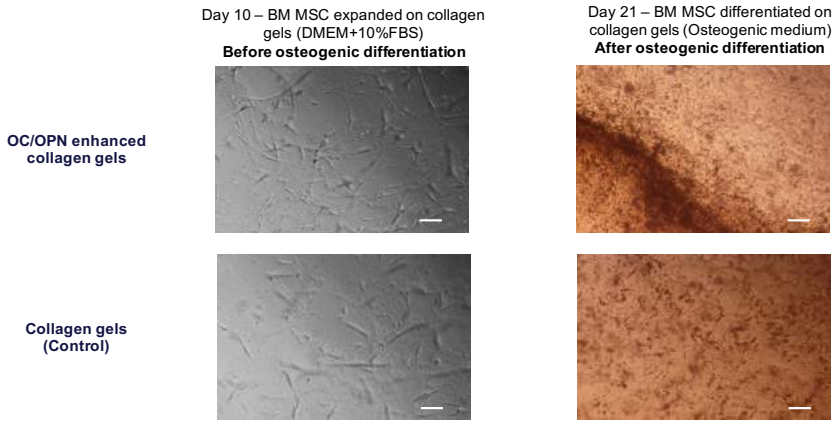

Figure IV.7. Micrographs of BM MSC before and after osteogenic differentiation on OC/OPN-enhanced collagen gels (OC/OPN #1) and control collagen gels. Scale bars, 100 µm.

ALP activity is another key osteoblast differentiation marker. ALP activity quantitative analysis showed that OC/OPN-enhanced collagen gels (OC/OPN#1, OC/OPN#3) presented significantly higher ALP activity compared with the control collagen gels, OC-collagen gels and OPN-collagen gels at day 15 (Figure IV.8g). Moreover, in OC/OPN#1-enhanced collagen gel, ALP activity was two times higher than the control at day 15 of osteogenic differentiation (0.70±0.12 (μmol/(L.min))/10^4 cells *vs* 0.35 ±0.07(μmol/(L.min))/10^4cells).

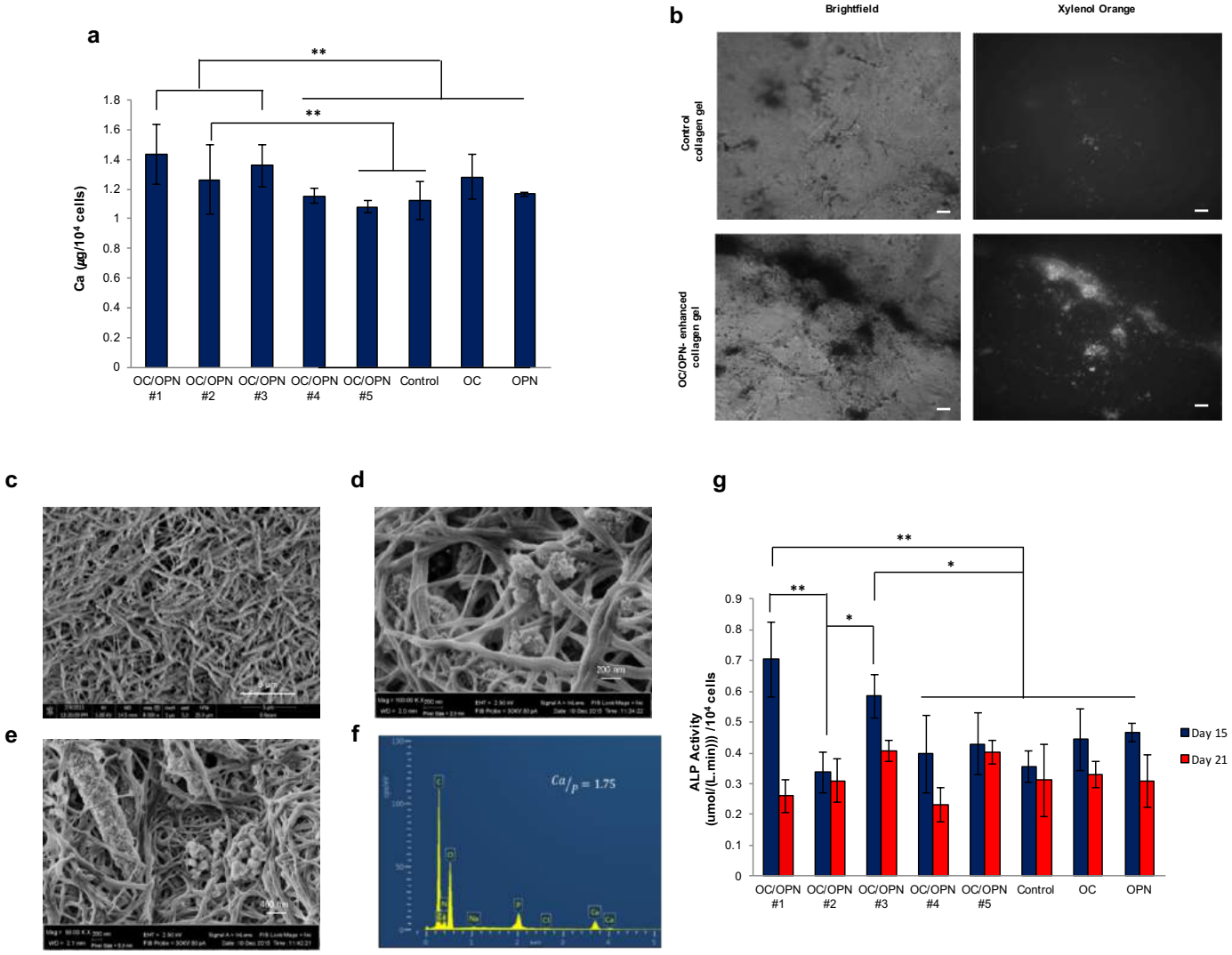

Figure IV.8. Effects of OC/OPN-enhanced collagen gels on BM MSC mineralization and ALP activity. **a)** Calcium content quantification of BM MSC on OC/OPN-enhanced collagen gels cultured for 21 days. **b)** Mineralized nodules of MSC after 21 days of culturing in osteogenic differentiation medium on OC/OPN-enhanced collagen gels and control collagen gels without OC/OPN incorporation. The nodules were visualized by Xylenol orange staining. Scale bars, 100 μm. **c-e)** SEM images of BM MSC cultured on OC/OPN-enhanced collagen gels. **c)** OC/OPN-enhanced collagen gels before cell culture, **d,e)** BM MSC mineralization of OC/OPN-enhanced collagen gels after 21 days of osteogenic differentiation. **f)** EDS spectrum of mineral deposition of BM MSC cultured on OC/OPN-enhanced collagen gels. **g)** ALP activity of BM MSC cultured on OC/OPN-enhanced collagen gels for 15 days and 21 days of differentiation. Data are expressed as mean ± SD, **p<0.01; *p<0.05.

IV.3.5. Effects of OC/OPN-enhanced mineralized collagen scaffolds on bone regeneration in a critical sized-defect rabbit long-bone model

Here we sought to determine the local inflammatory response of the OC/OPN-enhanced mineralized collagen scaffolds. Thus, we evaluated if the presence of OC/OPN-collagen scaffolds *in vivo* would promote any infection or foreign body reaction while new bone was being formed.

Therefore, we developed OC/OPN-enhanced mineralized collagen scaffolds, according with the protocol in Figure IV.1b. Scaffolds were characterized using μ-CT (Figure IV.9). We observed that most of the mineral was incorporated in the surface area of the collagen sheets.

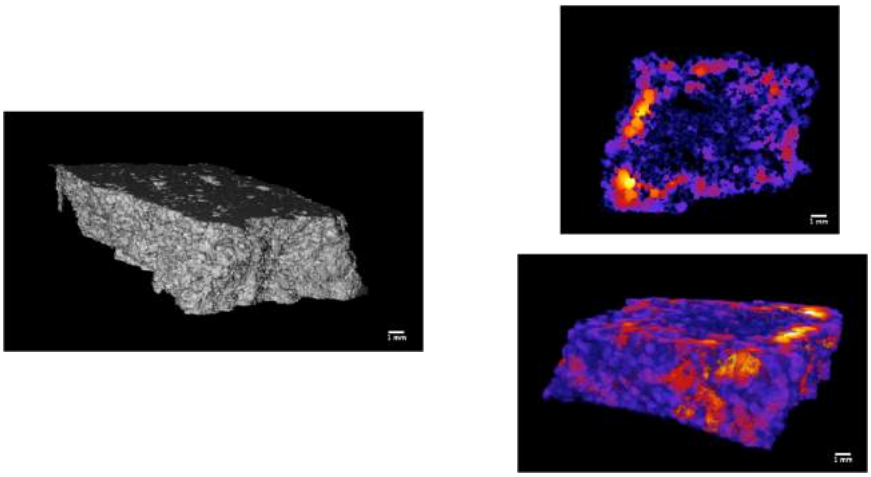

Figure IV.9. Microcomputed tomography images of OC/OPN-enhanced mineralized collagen scaffolds. Scale bars, 1 mm. Reddish areas demonstrate the mineral distribution throughout the scaffold.

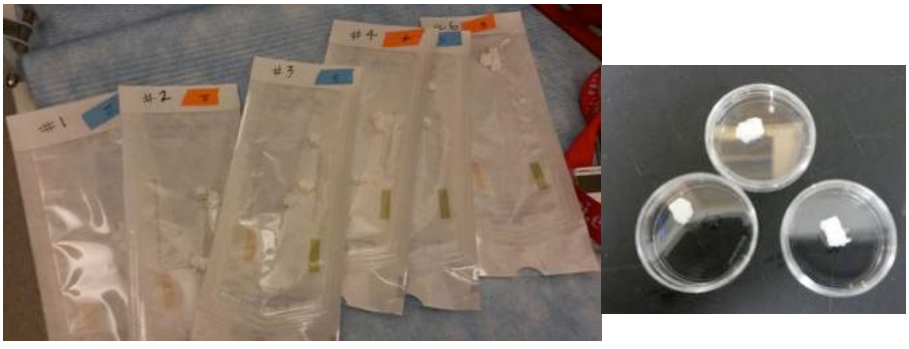

Figure IV.10. OC/OPN-enhanced mineralized collagen scaffolds before being implanted into a rabbit model.

To this end a critical sized-defect was induced in a rabbit model followed by femoral/tibial implantation of the scaffolds. In bone, a critical sized-defect does not heal without intervention over the natural lifetime.

Bone regeneration of a critical-sized defect was observed when OC/OPN-enhanced mineralized collagen scaffolds were implanted into a femoral/tibial defect after 6 weeks postimplantation (Figure IV.11). The surgical incision site was observed for wound healing and signs of infection daily for at least ten days following surgery. No signs of inflammation, discharge or wound dehiscence and abscess were observed. No specimen revealed any evidence of infection or foreign body reaction, and all wounds showed a good healing response.

Histological images showed new bone formation surrounding the implant area (Figure IV.11). Connective tissue was found between the new bone formed area and the implant. Osteoblasts were observed between the new mineralized bone and evidence of angiogenesis, in the form the new vessel formation, was seen. Green and purple areas observed using Goldner's Trichrome (GT) and Toluidine Blue (TB) stains, respectively, confirmed that new bone was formed after 6 weeks post-implantation. Osteoclasts were found in the implanted scaffold via Tartrate-resistant acid phosphatase (TRAP) staining, indicating a possible initial stage of bone remodeling. However, further studies are required to confirm that bone remodeling is occurring. In addition, further studies are needed to evaluate the mechanism of action, determining if the new bone formation observed herein is due to the presence of OC/OPN or due to the collagen scaffold.

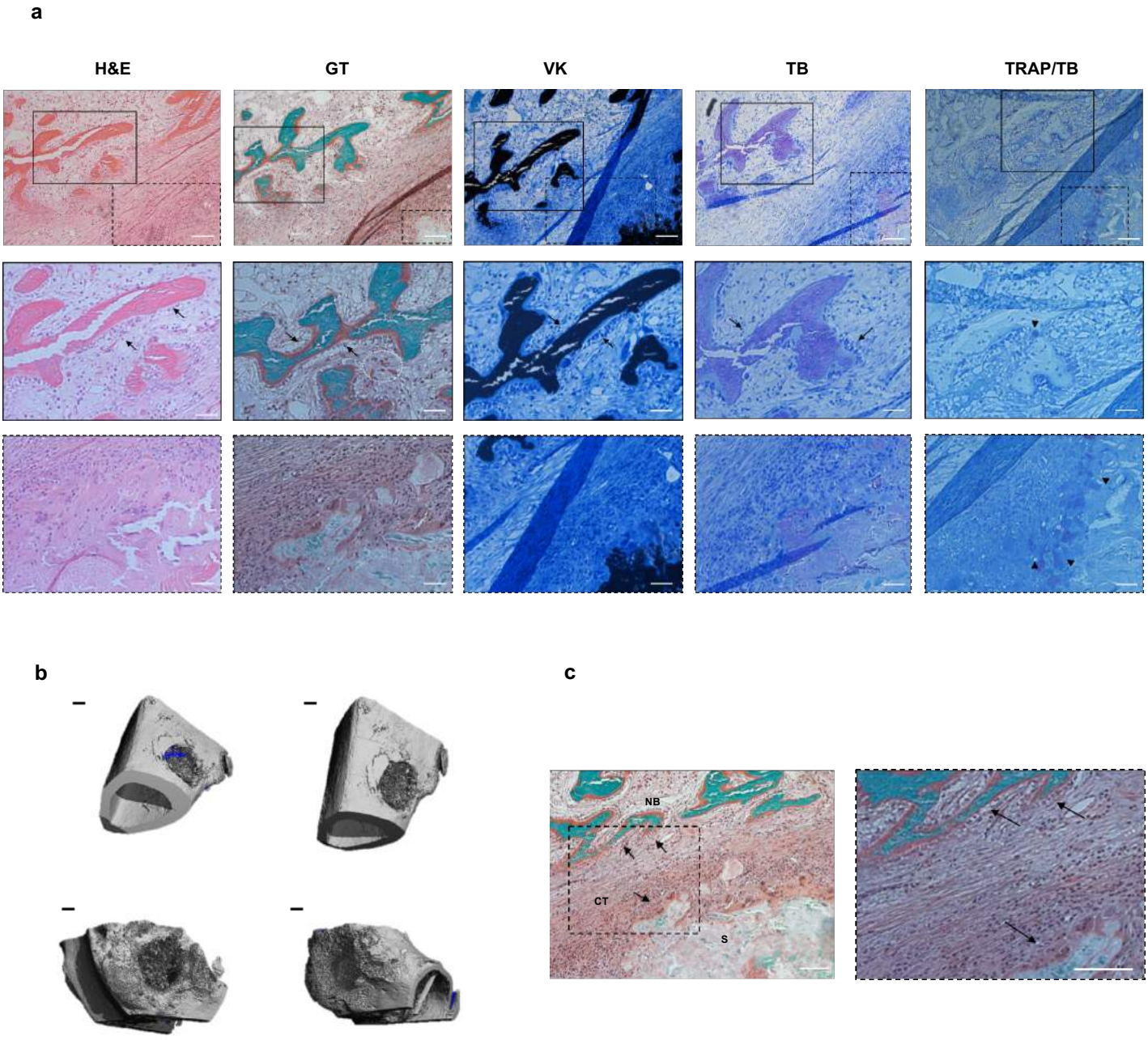

Figure IV.11. Bone regeneration in a critical sized-defect rabbit long-bone model using OC/OPN-enhanced mineralized collagen scaffolds**. a)** Representative histological images of the rabbit critical sized-defect at 6 weeks postimplantation. Hematoxylin and Eosin (H&E), Goldner's Trichrome (GT), Von Kossa (VK), Toluidine Blue (TB) and Tartrate-resistant acid phosphatase (TRAP) stainings. Panels on the first row are at 100x magnification. Black squares represent the area of new bone formed. Dashed squares represent the area of the implanted scaffold. Scale bars, 100 μm. Panels on the second row are at 200x magnification and represent the area of new bone formation (black squares). Scale bars, 50 μm. Panels on the third row are at 200x magnification and represent the area nearby the implanted scaffold (dashed squares). Black arrows outline the osteoblasts covering the new bone formed. Black arrowheads represent the osteoclasts by TRAP staining, indicating a possible remodeling of bone. White circle represents new vessels formed. Scale bars, 50 μm. **b)** Representative microcomputed tomography images of bone regeneration in the rabbit model at 6 weeks postimplantation. Top row represents a tibial defect, bottom row represents a femoral defect. Scale bars, 1 mm. **c)** Goldner's trichrome staining – detailed investigation. Detailed description of new bone formation within the OC/OPN-enhanced mineralized collagen scaffolds. NB – new bone; CT – connective tissue; S – scaffold. Scale bars, 100 μm.

IV.3.6. Effects of OC/OPN-enhanced collagen gels on human MSC from different tissue sources

In order to evaluate the synergistic effect of OC/OPN with MSC from multiple sources beyond bone marrow-derived MSC, we investigated responses of MSC isolated from different human tissue sources on OC/OPN-enhanced collagen gels.

MSC from umbilical cord matrix (UCM) and adipose tissue (AT) were seeded onto the biomimetic matrices. Proliferation assay showed more cells on most of the OC/OPN-enhanced collagen gels compared with the control collagen gels for all the different tissue sources (UCM, BM and AT) (Figure IV.12a).

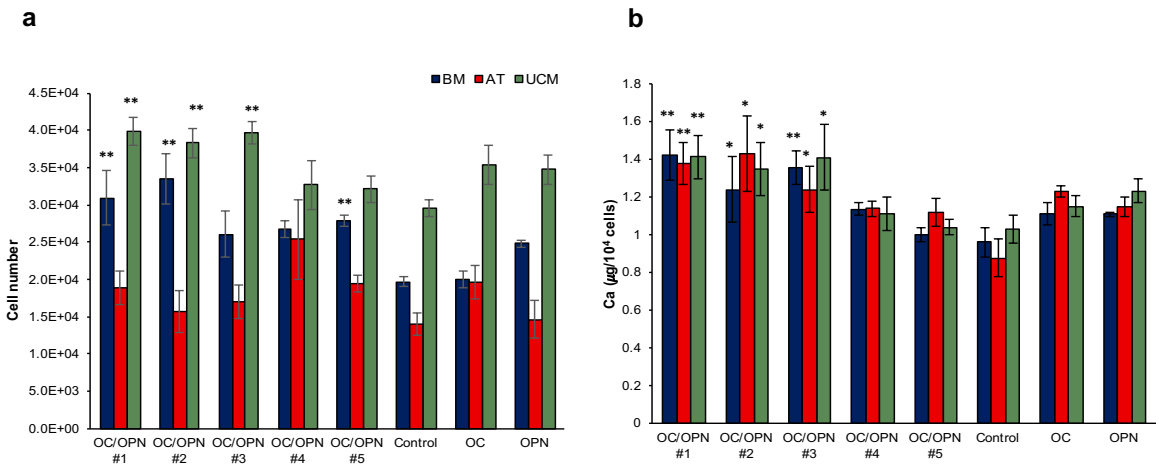

c

	Cell number			Calcium quantification		
	BM	AT	UCM	BM	AT	UCM
OC/OPN #1	** ## +	n.s.	**	** ## ++	** ## ++	** ## ++
OC/OPN #2	** ## ++	n.s.	*	*	** +	* # +
OC/OPN #3	n.s.	n.s.	**	** # +	*	* # +
OC/OPN #4	n.s.	* #	n.s.	n.s.	n.s.	n.s.
OC/OPN #5	** ##	n.s.	n.s.	n.s.	n.s.	n.s.

Figure IV.12. Proliferation and mineralization of human MSC from different tissue sources cultured on OC/OPN-enhanced collagen gels. **a)** Proliferation of MSC from BM, AT and UCM on OC/OPN-collagen gels after 15 days of culture. **p<0.01; *p<0.05 relative to the control group for each cell source **b)** Calcium quantification of MSC from BM, AT and UCM cultured on OC/OPN-enhanced collagen gels after 21 days of osteogenic differentiation. Data are expressed as mean ± SD, **p<0.01; *p<0.05 relative to the control group for each cell source **c)** Summary of statistically significant differences between each different composition of OC/OPN and control collagen gels, OC-collagen gels and OPN-collagen gels for each cell source (BM, AT, UCM), regarding cell number and calcium quantification after 15 days of culture. **p<0.01, *p<0.05 relative to control collagen gel; ++p<0.01, +p<0.05 relative to OC- collagen gel; ##p<0.01, #p<0.05 relative to OPN- collagen gel; n.s. – not significant.

Compared to the BM MSC, AT MSC reached lower number of cells after 15 days of culture. Moreover, when OC and OPN were incorporated individually into the gel, a slight increase of number of AT MSC was seen compared with the control collagen gels. We observed that UCM MSC cultured on OC-collagen gels and OPN-collagen gels presented more number of cells after 15 days compared with some OC/OPN compositions, such as OC/OPN #4 and OC/OPN #5, however, these values are not statistically significant

compared with the control and with the other OC/OPN compositions. Calcium quantification did not demonstrate any significant difference between cells from all the different tissue sources, however, consistent with results presented above, cells cultured on OC/OPN-enhanced collagen gels presented higher amount of calcium levels (Figure IV.12b). The synergistic effect of the incorporation of OC/OPN was observed in terms of proliferation and mineralization for all the different tissue sources, showing that the effects of OC/OPN are independent of cell source.

IV.4. Discussion

The biological process of bone healing is complex and is influenced by multiple factors such as the patient's health and nutritional conditions, and the degree and stability of the fracture experienced (Giannotti *et al.* 2013). Overall, 5-10% of fractures demonstrate delayed or impaired healing, affecting the patient's quality of life and leading to socioeconomic consequences and repeated surgeries (Giannotti *et al.* 2013). Non-union fractures represent the most dramatic case in which bone healing fails in the absence of treatment. In this case, autografts or allografts can be used to treat non-union fractures, however bone grafts must consider the characteristics, localization and healing potential of the non-unions fractures, ensuring graft stability, osteogenesis and osteoinduction (Yaszemski *et al.* 1996, Giannotti *et al.* 2013). Depending on the type of non-union fractures, bone substitutes from different materials can be used to fix and repair non-union fractures. Moreover, some molecular signals have been incorporated into these materials, such as bone morphogenetic proteins (BMP) that play the leading role in the field of bone tissue engineering. However, BMP have some drawbacks, such as the high costs of production and the high doses required, raising questions about their cost effectiveness (Yaszemski *et al.* 1996). With increasing clinical use of BMP, side effects have also been reported, including postoperative inflammation, ectopic bone formation, osteoclast-mediated bone resorption and inappropriate adipogenesis (James *et al.* 2016).

Therefore, there is an urgent need for development of new techniques that accelerate fracture healing process, enhance bone regeneration and remodeling and result in new bone tissue that is similar to human bone in structure and function. Such changes will ultimately improve patient's quality of life and decrease the high health-care costs associated with delayed bone healing, repeated surgeries and longer rehabilitation. Biomimetic construction of engineered bone tissue using selected proteins represents a promising alternative to the use of poor quality bone grafts and BMP in order to address the increasing worldwide demand of fracture repair and bone regeneration in an aging and osteoporotic population with limited bone regeneration potential.

The present study identified a new biomimetic strategy to accelerate osteogenic differentiation and sustained bone formation response from MSC obtained from multiple tissue sources. In particular, it demonstrates, for the first time, the synergistic effect of different concentrations of bone matrix non-collagenous proteins, OC and OPN, incorporated onto type I collagen gels, showing enhancement of proliferation and acceleration of osteogenic differentiation of human MSC and angiogenesis, eventually resulting in increased mineralization and bone regeneration *in vitro*.

To mimic the *in vivo* 3D ECM of connective tissue, a 3-D type I collagen matrix is often used as scaffold, since type I collagen is a predominant ECM molecule (Ramshaw *et al.* 1996). However, different tissues have

a different composition of the ECM, and the composition provides specific information and clues to cells. Consequently, ECM composition of native tissue, in particular the role of key matrix proteins, should be carefully considered for the development of novel biomaterials based on collagen scaffolds (Ramshaw *et al.* 1996). Regarding bone ECM, we incorporated OC and OPN as non-collagenous extracellular bone matrix components in scaffold design as an attempt to achieve a better osteogenic potential of the gels while selectively mimicking the bone environment. Few studies have used components of the organic bone matrix other than collagen to create bone substitutes (Rammelt *et al.* 2005, He *et al.* 2012). Here we used OC and OPN for the first time as together they provide structural integrity to bone matrix and both are lost with tissue aging leading to altered mineralization and bone formation (Sroga *et al.* 2011, Rodriguez *et al.* 2014, Poundari *et al.* 2012, Boskey 1989). Furthermore, autografts as well as allografts, typically obtained from older donors or patients that were subjected to total hip arthroplasty procedures (Passias and Bono 2006), are likely to contain bone tissue that has reduced concentrations of OC and OPN (Sroga *et al.* 2011) and, therefore, is structurally compromised (Poundarik *et al.* 2012) and not fully functional to promote mineralization.

During fracture healing, the new bone formation includes three coordinated biological events: osteogenic cell recruitment and proliferation; osteogenic cell differentiation and mineralization; and vascularization of the repair site. Disruption of any one of these can lead to delayed or impaired healing (Phillips *et al.* 2005).

As confirmed here, biomimetic OC/OPN-enhanced collagen matrices enhanced cell proliferation, promoted early osteogenic differentiation and angiogenesis, and produced a sustained bone formation response resulting in mineralized tissue, similar to bone.

OPN is commonly found surrounding mineralized tissues (McKee and Nanci 1996) and has been considered to play an important role in cell attachment and in the recruitment of osteoblasts during the early stage of bone formation (Boskey *et al.* 2002, Shapses *et al.* 2003). OPN can bind to $\alpha_v\beta_3$ integrins through their RGD domain (Denhardt *et al.* 1993). Additionally, OPN can also present an RGD-independent mechanism, in which OPN may engage CD44 (Weber *et al.* 1996), a cell surface adhesion molecule, involved in cell-cell and cell-matrix interactions. Shin and co-workers demonstrated that OPN enhanced MSC adhesion and proliferation on biomimetic hydrogels modified with an OPN-derived peptide (Somerman *et al.* 1989, Shin *et al.* 2004). On the other hand, OC has not been reported to induce MSC proliferation, however recent studies have shown that exogenous OC is sufficient to induce myoblast (Liu *et al.* 2017) and β-cell (Meredith *et al.* 2016) proliferation. In contrast to above, our results show that both OPN and OC are required for increased MSC proliferation on collagen gels, since OPN-enhanced collagen gels and OC-enhanced collagen gels did not demonstrate a statistically significant increase on cell proliferation (Figure IV.4b). Therefore, the synergistic effect of these two proteins is required.

On the other hand, OC has affinity for calcium through the gama-carboxyglutamic acids (Hauschka *et al.* 1975) and by binding hydroxyapatite, it can accelerate its nucleation, playing an active role in the early stage of bone healing (Rammelt *et al.* 2005). Nucleation and growth of hydroxyapatite crystals within the collagenous matrix are two fundamental steps for bone mineralization. Therefore, OC might favor mineralization and osteogenic differentiation of MSC on OC/OPN-enhanced collagen gels. Consistent with this notion, we found that OC and OPN enhanced the osteogenic differentiation of human BM MSC cultured on the OC/OPN-enhanced collagen gels. During the immediate post-proliferative period, the extracellular matrix undergoes a series of modifications in composition and organization that makes it competent for

mineralization. Therefore, after 21 days of osteogenic differentiation, OC/OPN-enhanced collagen gels presented significantly higher calcium deposition and expression of osteogenic genes (Col I, Runx2, OPN and OC) compared with the control collagen gels without OC and OPN incorporation (Figure IV.4,5,8). Interestingly, OC-enhanced collagen gels also upregulated the expression of Runx2 and OC gene levels, demonstrating also better osteogenic differentiation (Figure IV.5), suggesting that osteocalcin is favoring this phenomenon.

During this post-proliferative phase, the cells also express ALP that reaches its peak of expression and declines as the cultures progress into the mineralization stage (Stein *et al.* 1990). Interestingly, when BM MSC were cultured on OC/OPN-enhanced collagen gels, the ALP gene expression was highest at day 7 of osteogenic differentiation and then progressively declined at 15 and 21 days of osteogenic differentiation. On the other hand, when BM MSC were cultured on control collagen gels, the overall ALP gene expression was lower than OC/OPN-enhanced collagen gels reaching the highest value at day 15 of osteogenic differentiation (Figure IV.4d) followed by a progressive decline. This result confirmed that BM MSC cultured on OC/OPN-enhanced collagen gels presented not only a higher extent of ALP expression but also the earlier temporal ALP gene expression after 7 days of osteogenic differentiation, indicating an acceleration in the osteogenic differentiation based on the early ALP gene expression.

OC/OPN-enhanced collagen gels also enhanced the expression levels of Runx2 gene after only 7 days of osteogenic differentiation, reaching its maximum relative expression at day 15 and sustaining the high level thereafter.

Regarding the mineralization process, several genes were induced to maximal levels, paralleling to accumulation of mineral in bone regeneration. OPN and OC are bone proteins known to be associated with the mineralized matrix *in vivo* and achieve their peak levels of expression during mineralization of the extracellular matrix (Stein *et al.* 1990). As shown in our results, after 21 days of osteogenic differentiation, OC/OPN-enhanced collagen gels presented higher levels of OPN and OC gene expression, indicating the formation of a more mature extracellular matrix compared with control collagen gels without OC and OPN incorporation.

Notably, OC-enhanced collagen gels and OPN-enhanced collagen gels were able to upregulate some osteogenic genes. OPN-enhanced collagen gels demonstrated upregulation of Col I and OPN genes, however Runx2 and OC did not show any statistically significant increase. On the other hand, OC-enhanced collagen gels demonstrated enhancement of Col I, Runx2 and OC genes but did not show improvement of OPN gene levels. Moreover, OC and OPN genes were only both upregulated when MSC were cultured on OC/OPN-enhanced collagen gels (Figure IV.5).

These results of higher and sustained osteogenic gene expression of OC/OPN-enhanced matrices were associated with more accumulation of mineral, and the mineralized nodules contained a Ca/P ratio comparable to native bone matrix (Figure IV.8). Close correspondence of Ca/P ratio between the regenerated and natural bone tissue provides supporting evidence on the quality of new formed bone. For example, in osteogenesis imperfecta patient biopsies, a condition derived from mutation in type I collagen, the Ca/P ratio was shown to be lower than normal bone, leading to imperfect bone formation, demonstrating a compromised bone quality and bone fragility (Casella *et al.* 1995). To our knowledge, very few studies have reported similar information on newly regenerated bone.

Furthermore, in contrast to OC or OPN-enhanced matrices, optimal levels of mineralization were obtained when MSC were seeded on collagen gels incorporated with both OC and OPN, suggesting that these proteins act in a synergistic manner. Therefore, we hypothesize that the enhancement of osteogenic differentiation of BM MSC on OC/OPN-enhanced collagen gels observed herein might be due to the presence of both OC/OPN in the matrix. In fact, the mechanisms responsible for bone formation and remodeling likely involve the association of bone matrix proteins into specific complexes that helps the organization of the matrix (Ritter *et al.* 1992).

Previous studies have shown that these two proteins have the ability to interact (Ritter *et al.* 1992). In fact, Ritter and colleagues have investigated the association of OPN with OC using three different ligand binding techniques, indicating that OPN specifically associates with OC (Ritter *et al.* 1992), forming stable complexes, however their metabolic role was not investigated. OC has been shown to bind strongly to the bone mineral hydroxyapatite and it complexes with and links to collagen through OPN (Ritter *et al.* 1992). In this study, results shown by ELISA measurements demonstrated that OC/OPN-enhanced collagen matrices released a negligible amount of OC and OPN, indirectly proving the association between these proteins and collagen (Figure IV.3).

Both OC and OPN have sequence motifs that could allow each protein to interact with other molecules. Through its γ-carboxyglutamate residues, OC forms a calcium binding pocket (Otowara *et al.* 1981). It has been suggested that via this pocket, OC can bind to other calcium binding proteins. Moreover, the COOH terminus of OC can also participate in protein binding, since it adopts a β-sheet conformation that is exposed even when the molecule is bound to hydroxyapatite. OPN also comprises motifs that would allow it to interact with other proteins. It has an integrin binding RGD sequence that functions in cell attachment (Oldberg *et al.* 1986). Therefore, this RGD sequence present in OPN might be the trigger to the enhancement of cell proliferation. Also, OPN is a substrate for transglutaminase activity (Prince 1981), a reaction that can produce complexes between proteins *in vivo*. In this study, we did not evaluate the interaction of both proteins, however we were able to observe better biological responses from BM MSC when these cells were seeded on OC/OPN-collagen gels, compared with only OC-collagen gels and OPN-collagen gels. Our data suggests that the presence of both proteins in the matrix enhanced cellular responses, such as proliferation and osteogenesis and supported the evidences reported by Ritter and colleagues regarding the metabolic effects of the presence of OC/OPN.

Previous work from our group found that fracture in bone initiates as dilatational bands that form as a result of OC-OPN interaction. In the absence of either protein, the complex is disrupted, resulting in a loss of the structural integrity of bone matrix (Poundarik *et al.* 2012). However, further studies need to be done to understand better how these two proteins interact within the collagen matrix.

After implantation of biomimetic scaffolds in a defect, cell migration is a critical step for bone regeneration. In the present study, experiments demonstrated that conditioned medium from BM MSC seeded on biomimetic OC/OPN-enhanced collagen gels stimulated a faster migration of HUVEC. Notably, conditioned medium from OPN-collagen gels also demonstrated a faster migration of HUVEC, even when compared with the results obtained with conditioned medium from cells cultured on OC/OPN-enhanced gels. In fact, OPN alone has been reported to improve cell migration and wound healing response (Wang *et al.* 2016), a phenomenon that is linked with the migration potential of cells. However, it is not yet clear which soluble

factors and mechanisms are responsible for stimulating the migration of cells. Indeed, MSC have been described as inducers of wound healing and angiogenesis where they secrete paracrine factors to indirectly initiate repair following injury (Yew *et al.* 2011). Bone is a highly-vascularized tissue and for bone regeneration an adequate blood flow is required to provide sufficient supply of nutrients and oxygen to the cells (Kanczler *et al.* 2008, Hoeben *et al.* 2004). In response to angiogenic signals found in conditioned media obtained from BM MSC cultures, endothelial cells may form capillary like structures (Pankajakshan & Agrawal 2014). In our study, conditioned medium from BM MSC seeded onto OC/OPN-enhanced collagen gels increased the tube formation of endothelial cells, when compared with the control, by increasing the number of total capillary tubes and branch points formed. We believe that two different mechanisms may be responsible for the improvement of angiogenic properties demonstrated by OC/OPN. Indirectly, the increase in cell number present in the OC/OPN-enhanced collagen gels might be responsible for a higher concentration of angiogenic soluble factors released from cells. On the other hand, the significant increase of mRNA levels of VEGF by BM MSC cultured on OC/OPN-enhanced collagen gels demonstrated that the enhancement of expression levels of VEGF might be, directly, acting on the improvement of the angiogenic properties. These results confirm the effect of OC/OPN on angiogenesis by stimulating the release of angiogenic factors and enhancing the VEGF gene expression. OC-enhanced collagen gels and OPN-enhanced collagen gels did not promote an increase in the expression of VEGF mRNA levels by BM MSC, demonstrating the synergistic effect of both proteins in angiogenesis. However, further studies need to be done to quantify and identify the angiogenic factors secreted by these cells that were exposed with OC/OPN.

Consistent with our above proposal, previous studies show that the presence of OPN induces HUVEC proliferation, survival and migration resulting in tube formation and VEGF expression (Dai *et al.* 2009, Chakraborty *et al.* 2008, Egusa *et al.* 2009, Hamada *et al.* 2007, Hamada *et al.* 2003). Regarding the effect of OC on angiogenesis, Cantatore and colleagues show that OC alone, exogenously applied to chick embryo chorioallantoic membrane, stimulates angiogenesis (Cantatore *et al.* 2005). Although our results demonstrated that OC-collagen gels and OPN-collagen gels also enhanced tube formation and migration of endothelial cells, we demonstrated that by applying the synergistic strategy of both proteins onto the collagen gels, both osteogenesis and angiogenesis processes were enhanced. Of note, our study evaluates for the first time the effect of both non-collagenous proteins, used in combination in a biomimetic collagen gel, on the angiogenic capacity of human MSC.

We also evaluated and compared the influence of OC/OPN-enhanced collagen gels on MSC derived from different sources: UCM, BM and AT. MSC derived from all three tissues showed enhanced proliferation and mineralization results when OC/OPN were incorporated into the biomimetic collagen gels (Figure IV.12). UCM MSC have been shown to exhibit superior proliferative capacity (Simões *et al.* 2013). Our work confirmed that these cells reached higher number of cells than BM MSC in all the biomimetic collagen gels. Although some differences in proliferation were observed between MSC from different tissues, here we demonstrate that the effect of OC/OPN on the *ex-vivo* proliferation and osteogenic potential of MSC is not tissue source dependent, indicating a great potential to translate these findings to a clinical context (Figure IV.12).

In vivo data using a critical sized-defect rabbit long-bone model revealed that OC/OPN-enhanced mineralized collagen scaffolds did not promote any adverse reaction, while new bone was being formed after

6 weeks of implantation in a femoral/tibial defect. Moreover, osteoblasts and blood vessels were found surrounding the new bone formed (Figure IV.11).

OC/OPN-enhanced collagen matrices, developed here, can be applied in other systems in which the production of OC and OPN might be compromised, due to medical conditions or to the age of the patient. In fact, variation of non-collagenous bone protein concentrations in diseased human bones have already been reported (Grynpas *et al.* 1994). Findings to date are that OC and OPN levels are reduced in osteoporotic bone (Boskey 2013) and in older bone tissue (Sroga *et al.* 2011). Moreover, it was reported that older people may have a 10-fold increased 10-year fracture risk compared with younger people with the same bone mineral density (Kanis *et al.* 2002). Therefore, with aging there is an increased susceptibility to fractures due to the increase in skeletal fragility. We believe that, since these proteins are important for fracture resistance (Sroga *et al.* 2012), OC/OPN-enhanced collagen matrices might help to sustain bone formation when patients are not or less able to produce naturally these proteins, producing high quality functional bone to improve bone regeneration.

Taken together, our results demonstrate, for the first time, the significant synergistic impact of OC and OPN on proliferation, osteogenic differentiation and angiogenic capacity of MSC engineered within a combined type I collagen matrix. Further studies need to be done to evaluate the efficacy of these matrices in bone tissue engineering and regenerative medicine settings to be applied as biomimetic scaffolds that accelerate bone healing.

IV.5. References

Bailey S., Karsenty G., Gundberg C., Vashishth D., Osteocalcin and osteopontin influence bone morphology and mechanical properties. *Ann. N.Y. Acad. Sci.,* 1-6 (2017).

Boskey A.L., Bone composition:relationship to bone fragility and antiosteoporotic drug effects. *Bonekey Reports* **2**, 447 (2013).

Boskey A.L., Coleman R., Aging and bone. *J. Dent. Res.* **89**, 1333-1348 (2010).

Boskey A.L., Noncollagenous matrix proteins and their role in mineralization. *Bone and Mineral* **6,** 111–123 (1989).

Boskey A.L., Spevak L., Paschalis E., Doty S.B., McKee M.D., Osteopontin deficiency increases mineral content and mineral crystallinity in mouse bone. *Calcif. Tissue Int*. **71,** 145-154 (2002).

Bruder S.P., Jaiswal N., Haynesworth S.E. Growth kinetics, self-renewal, and the osteogenic potential of purified human mesenchymal stem cells during extensive subcultivation and following cryopreservation. *J. Cell. Biochem.* **64,** 278–294 (1997).

Cairns J.R., Price P.A., Direct demonstration that the vitamin K-dependent bone gla protein is incompletely γ – carboxylated in humans. *J. Bone Miner. Res.* **9,** 1989-1997 (1994).

Cantatore F.P., Osteocalcin is angiogenic in vivo. *Cell Biol. Int.* **29,** 583–585 (2005).

Caplan A., Mesenchymal stem cells. *J. Orthopaedic Res.* **9,** 641–650 (1991).

Casella J.P., Garrington N., Stamp T.C.B., Ali S.H., An electron probe X-ray microanalytical study of bone mineral in osteogenesis imperfecta. *Calcif. Tissue Int.* **56**, 118-122 (1995).

Chakraborty G., Jain S., Kundu G.C., Osteopontin promotes vascular endothelial growth factor-dependent breast tumor growth and angiogenesis via autocrine and paracrine mechanisms. *Cancer Research* **68,** 152–161 (2008).

Dai J., Peng L., Fan K., Wang H., Wei R., Ji G., Cai J., Lu B., Li B., Zhang D., Kang Y., Tan M., Qian W., Guo Y., Osteopontin induces angiogenesis through activation of PI3K/AKT and ERK1/2 in endothelial cells. *Oncogene* **28,** 3412–3422 (2009).

DeFranco D.J., Glowacki J., Lian J.B., Normal bone particles are preferentially resorbed in the presence of osteocalcin-deficient bone particles in vivo. *Calcif. Tissue Int.* **49,** 43-50 (1991).

Denhardt D.T., Guo X., Osteopontin: a protein with diverse functions. *FASEB J*. **7,** 1475–1482 (1993).

Dominici M., Le Blanc K., Mueller I., Slaper-Cortenbach I., Marini F., Krause D., Deans R., Keating A., Prockop D.J., Hoewitz E. Minimal criteria for defining multipotent mesenchymal stromal cells. The International Society for Cellular Therapy position statement. *Cytotherapy* **8,** 315–317 (2006).

dos Santos F., Andrade P.Z., Boura J.S., Abecasis M.M., da Silva C.L., Cabral J.M. Ex vivo expansion of human mesenchymal stem cells: a more effective cell proliferation kinetics and metabolism under hypoxia. *J. Cell. Physiol.* **223,** 27–35 (2010).

Ducy P., Desbois C., Boyce B., Pinero G., Story B., Dunstan C., Smith E., Bonadio J., Goldstein S., Gundberg C., Bradley A., Karsenty G., Increased bone formation in osteocalcin-deficient mice. *Nature* **382,** 448-452 *(1996)*.

Egusa H., Kaneda Y., Akashi Y., Hamada Y., Matsumoto T., Saeki M., Thakor D.K., Tabata Y., Matsuura N., Yatani H., Enhanced bone regeneration via multimodal actions of synthetic peptide SVVYGLR on osteoprogenitors and osteoclasts. *Biomaterials* **30,** 4676–4686 (2009).

Fialkov J.A., Holy C.E., Shoichet M.S., Davies J.E., In vivo bone engineering in a rabbit femur. *J. Craniofac. Surg.* **14,** 324-332 (2003).

Giannotti, S., Bottai V., Dell'Osso G., Pini E., De Paola G., Bigelli G., Guido G. Current medical treatment strategies concerning fracture healing. *Clin. Cases Miner. Bone Metab.,* **10**, 116-120 (2013).

Gimble J.M., Katz A.J., Bunnel B.A., Adipose-derived stem cells for regenerative medicine. *Circ. Res.***100,** 1249–1260 (2007).

Grynpas M.D., Tupy J.H., Sodek J., The distribution of soluble, mineral-bound, and matrix-bound proteins in osteoporotic and normal bones. *Bone* **15**, 505-513 (1994).

Gundberg C.M., Matrix proteins. *Osteoporos. Int.* **Supp.5**, 37-42 (2003).

H. Shin, S. Jo, A.G. Mikos, Modulation of marrow stromal osteoblast adhesion on biomimetic oligo[poly(ethylene glycol) fumarate] hydrogels modified with Arg-Gly-Asp peptides and a poly(ethyleneglycol) spacer. *J. Biomed. Mater Res. A* **61**, 169-179 (2002).

Hamada Y., Egusa H., Kaneda Y., Hirata I., Kawaguchi N., Hirao T., Matsumoto T., Yao M., Daito K., Suzuki M., Yatani H., Daito M., Okazaki M., Matsuura N., Synthetic Osteopontin-derived Peptide SVVYGLR can Induce Neovascularization in Artificial Bone Marrow Scaffold Biomaterials. *Dent. Mater. J.* **26,** 487–492 (2007).

Hamada Y., Nokihara K., Okazaki M., Gujitani W., Matsumoto T., Matsuo M., Umakoshi Y., Takahashi J., Matsuura N., Angiogenic activity of osteopontin-derived peptide SVVYGLR. *Biochem. Biophys. Res. Commun.* **310,** 153–157 (2003).

Hauschka P.V., Lian J.B., Gallop P.M., Direct identification of the calcium binding amino acid, 7-carboxyglutamate, in mineralized tissue. *Proc. Natl. Acad. Sci. USA* **72,** 3925-3929 (1975).
He X., Yang X., Jabbari E. Combined effect of osteopontin and BMP-2 derived peptides grafted to an adhesive hydrogel on osteogenic and vasculogenic differentiation of marrow stromal cells. *Langmuir* **28,** 5387–5397 (2012).

Hesse E., Hefferan T.E., Tarara J.E., Haasper C., Meller R., Krettek C., Lu L., Yaszemski M.J., Collagen type I hydrogel allows migration, proliferation and osteogenic differentiation of rat bone marrow stromal cells. *J. Biomed. Mater. Res. A* , **94,** 442–449 (2010).

Hoeben A., Landuyt B., Highley M.S., Wildiers H., Van Oosterom A.T.,,De Bruijn E.A., Vascular endothelial growth factor and angiogenesis. *Pharmacolo. Rev.* **56,** 549–580 (2004).

Ingram R.T., Park Y.K., Clarke B.L.,. Fitzpatrick L.A, Age- and gender- related changes in the distribution of osteocalcin in the extracellular matrix of normal male and female bone. Possible involvement of osteocalcin in bone remodeling. *J. Clin. Invest.* **93**, 989-997 (1994).

James A.W., LaChaud G., Shen J., Asatrian G., Nguyen V., Zhang X., Ting K., Soo C. A review of the clinical side effects of bone morphogenetic protein-2. *Tissue Eng. Part B* **22**, 284-297 (2016)

Kanczler J.M., Osteogenesis and Angiogenesis : the potential for engineering. *Eur. Cell Mater.* **15,** 100–114 (2008).
Kanis J.A., Diagnosis of osteoporosis and assessment of fracture risk. *Lancet* **359**, 1929-1936 (2002).

Komaki H., Tanaka T., Chazono M., Kikuchi T., Repair of segmental bone defects in rabbit tibiae using a complex of β-tricalcium phosphate, type I collagen, and fibroblast growth factor-2. *Biomaterials* **27**, 5118-5126 (2006).

Lindley E.M., Guerra F.A., Krauser J.T., Matos S.M., Burger E.L., Patel V.V., Small peptide (P-15) bone substitute efficacy in a rabbit cancellous bone model. *J. Biomed. Mater. Res. B Appl. Biomater.* **94**, 463-468 (2010).
Liu S., Gao F., Wen L., Ouyang M., Wang Y., Wang Q., Luo L., Jian Z., Osteocalcin induces proliferation via positive activation of the PI3K/Akt, P38 MAPK pathways and promotes differentiation through activation of the GPRC6A-ERK1/2 pathway in C2C12 myoblast cells. *Cell. Physiol. Biochem.* **43**, 1100-1112 (2017).

Lutolf, M.P., Weber F.E., Scmoekel H.G., Schense J.C., Kohler T., Müller R., Hubbell J.A. Repair of bone defects using synthetic mimetics of collagenous extracellular matrices. *Nat. Biotechnol*. **21,** 513-518 (2003).

McKee M.D., Nanci A., Osteopontin at mineralized tissue interfaces in bone, teeth, and osseointegrated implants: ultrastructural distribution and implications for mineralized tissue formation, turnover, and repair. *Microsc Res Tech.* **33,** 141-164 (1996).

Meredith L.Z., Clemens T.L., Riddle R.C., New insights into the biology of osteocalcin. *Bone* **82**, 42-49 (2016).
Morgan S., Poundarik A.A., Vashishth D., Do non-collagenous proteins affect skeletal mechanical properties? *Calcif. Tissue Int.* **97**, 281-291 (2015).
Nikel O., Laurencin D., McCallum S.A., Gundberg C.M., Vashishth D., NMR investigation of the role of osteocalcin and osteopontin at the organic-inorganic interface in bone. *Langmuir* **29**, 13873-13882 (2013).

Pankajakshan D., Agrawal D.K.Mesenchymal Stem Cell Paracrine Factors in Vascular Repair and Regeneration, *J. Biomed. Mater Res. A* **1**, 1-9 (2014).

Passias P.G., Bono J.V, Total hip arthroplasty in the older population. *Geriatrics and Aging* **9**, 535-543 (2006)

Passias P.G., Bono J.V, Total hip arthroplasty in the older population. *Geriatrics and Aging,* **9**, 535-543 (2006)

Phillips A.M., Overview of the fracture healing cascade. *Injury* **36,** S5–S7 (2005).

Plantalech L., Guillaumont M., Vergnaud P., Leclercq M., Delmas P.D., Impairment of gamma carboxylation of circulating osteocalcin (bone gla protein) in elderly women. *J. Bone Miner. Res.***6,** 1211-1216 (1991).

Poundarik A.A., Diab T., Sroga G.E., Ural A., Boskey A.L., Gundberg C.M., Vashishth D., Dilatational band formation in bone. *Proc. Natl. Acad. Sci. USA* **109,** 19178–19183 (2012).

Rammelt S., Neumann M., Hanisch U., Reinstorf A., Pompe W., Zwipp H., Biewener A. Osteocalcin enhances bone remodeling around hydroxyapatite/collagen composites. *J. Biomed. Mater. Res. A* **73,** 284–294 (2005).

Ramshaw J.A., Werkmeister J.A., Glattauer V., Collagen-based biomaterials. *Biotechnol. Genet. Eng. Rev.* **13,** 335-382 (1996).

Rodriguez D.E., Thula-Mata T., Toro E.J., Yeh Y.W., Holt C.,. Holliday L.S, Gower L.B., Multifunctional role of osteopontin in directing intrafibrillar mineralization of collagen and activation of osteoclasts. *Acta Biomater.* **10,** 494-507 (2014).
Shin H., Zygourakis K., Farach-Carson M.C., Yaszemski M.J., Mikos A.G. Attachment, proliferation, and migration of marrow stromal osteoblasts cultured on biomimetic hydrogels modified with an osteopontin-derived peptide. *Biomaterials* **25,** 895-906 (2004).

Simões I.N., Boura J.S., dos Santos F., Andrade P.Z., Cardoso C.M, Gimble J.M., da Silva C.L., Cabral J.M. Human mesenchymal stem cells from the umbilical cord matrix: successful isolation and ex vivo expansion using serum-/xeno-free culture media. *Biotechnol. J.* **8,** 448–458 (2013).

Somerman M.J., Prince C.W., Butler W.T., Foster R.A., Moehring J.M., Sauk J.J., Cell attachment activity of the 44 kilodalton bone phosphoprotein is not restricted to bone cells. *Matrix* **9,** 49-54 (1989).

Sroga G.E., Karim L., Colón W., Vashishth D., Biochemical characterization of major bone-matrix proteins using nanoscale-size bone samples and proteomics methodology. *Mol. Cell. Proteomics* **10,** M110.006718-M110.006718 (2011).

Sroga G.E., Vashishth D., Effects of bone matrix proteins on fracture and fragility in osteoporosis. *Curr. Osteopor. Rep.* **10**, 141-150 (2012).

Stein G.S., Lian J.B., Owen T.A., Relationship of cell growth to the regulation of tissue-specific gene expression during osteoblast differentiation. *FASEB J.* **4**, 3111–3123 (1990).

Stock, U.A. & Vacanti J.P. Tissue Engineering : Current State and Prospects. *Annu.Rev.Med.,* **52,** 443 (2001).

Sun Y., Jiang Y., Liu Q., Gao T., Feng J.Q., Dechow P., D'Souza R.N., Qin C., Liu X., Biomimetic engineering of nanofibrous gelatin scaffolds with noncollagenous proteins for enhanced bone regeneration, *Tissue Eng. Part A* **19,** 1754–1763 (2013).

Vashishth D., The role of the collagen matrix in skeletal fragility. *Curr. Osteoporos. Rep.* **5,** 62–66 (2007).

Wang W. *et al.* Osteopontin activates mesenchymal stem cells to repair skin wound. *PLoS ONE* **12**:e0185346 (2016).

Weber, G.F., Ashkar S., Glimcher M.J., Cantor H.*,* Receptor-ligand interaction between CD44 and osteopontin (Eta-1). *Science* **271,** 509–512 (1996).

Yaszemski, M.J., Payne R.G., Hayes W.C., Langer R., Mikos A.G. Evolution of bone transplantation: Molecular, cellular and tissue strategies to engineer human bone. *Biomaterials,* **17,** 175–185 (1996).

Yew T.L., Hung Y.T., Li H.Y., Chen H.W., Chen L.L., Tsai K.S., Chiou S.H., Chao K.C., Huang T.F., Chen H.L., Hung S.C., Enhancement of wound healing by human multipotent stromal cell conditioned medium: The paracrine factors and p38 MAPK activation. *Cell Transplant.* **20,** 693–706 (2011).

CHAPTER V – Cultured cell-derived extracellular matrices to enhance osteogenic differentiation and angiogenic properties of human mesenchymal stem/stromal cells

Outline

Cell-derived extracellular matrix (ECM) consists of a complex assembly of fibrillary proteins, matrix macromolecules and associated growth factors that mimics the composition and organization of native ECM microenvironment. Therefore, cultured cell-derived ECM has been used as a scaffold for tissue engineering settings to create a biomimetic microenvironment, providing physical, chemical and mechanical cues to cells and supporting cell adhesion, proliferation, migration and differentiation. Here, we present a new strategy to produce different combinations of decellularized cultured cell-derived ECM (dECM) obtained from different cultured cell types, namely mesenchymal stem/stromal cells (MSC) and human umbilical vein endothelial cells (HUVEC), as well as the co-culture of MSC:HUVEC. We investigated the effects of various compositions of dECM on cell proliferation, osteogenic differentiation and angiogenic properties of human bone marrow-derived MSC, vital features for adult bone tissue regeneration and repair. Our findings demonstrate that all dECM supported cell proliferation, presenting higher cell numbers compared with tissue culture polystyrene (TCP). More importantly, we show that MSC:HUVEC ECM enhanced the osteogenic and angiogenic potential of MSC, as assessed by *in vitro* assays. Interestingly, MSC:HUVEC (1:3) ECM demonstrated the best angiogenic response of MSC in the conditions tested. To the best of our knowledge, this is the first study that demonstrates that dECM derived from a co-culture of MSC:HUVEC impacts the osteogenic and angiogenic capabilities of MSC, suggesting the potential use of MSC:HUVEC ECM as a therapeutic product to improve clinical outcomes in bone regeneration.

V.1. Introduction

Every year, millions of people develop bone defects due to trauma or disease. In fact, over two million bone grafting procedures are performed annually worldwide (Campana *et al.* 2014). Several strategies have been developed to improve the current clinical practices for repairing large bone defects by designing functional scaffolds to integrate and regenerate the defect site. An ideal functional scaffold for bone tissue should be osteoinductive, osteoconductive, biodegradable and bioactive, not only supporting cell attachment, but also stimulating osteogenic differentiation of progenitor cells and bone formation (Bose *et al.* 2012). Currently, biomaterials composed of hydroxyapatite and tricalcium phosphate have been used commercially to enhance bone regeneration. However, the ability of these scaffolds to promote osteogenesis is still not satisfactory. Selected osteogenic factors, such as transforming growth factor beta-1 (TGF-β1) (Zhang *et al.* 2003), collagen type I (Roehlecke *et al*. 2001) and bone morphogenetic proteins (BMP) (Yang *et al*. 2000) have been incorporated into these scaffolds to enhance their osteoinductive capabilities. However, challenges remain to recreate the native tissue in a more reliable and effective way, since isolated components do not mimic the molecular complexity and hierarchically organized structure of the native bone tissue.

The extracellular matrix (ECM) is the non-cellular component within all tissues and organs, consisting of water and a fibrillary basement network of proteins and polysaccharides secreted by cells, and comprising structural and functional molecules such as collagen, fibronectin, laminin, glycosaminoglycans and proteoglycans (Badylak *et al.* 2009). ECM provides an appropriate microenvironment to support cell adhesion and direct other cell behaviors, such as cell migration, proliferation, differentiation, immune response and wound healing (Kleinman *et al.* 1987, Reilly *et al.* 2010, Giancotti *et al.* 1999), resulting in structural and physical stability to the tissue. Each tissue source has an ECM with unique composition and topography (George *et al.* 2005), which provides anchorage for cytokines and growth factors that can be presented to cells playing a major role in regulating cellular activity and functions (Hynes *et al.* 2009). The association between ECM proteins and receptors like integrins can directly activate intracellular signaling pathways (Giancotti *et al.* 1999, Hynes *et al.* 2002). Furthermore, cellular functions can also be regulated by the transduction of mechanical signals, since cells present different responses according to the elasticity of the substrate (Engler *et al.* 2006).

Ideal scaffolds and substrates for cell culture and tissue engineering settings should provide a microenvironment similar to the native ECM *in vivo.* Previous studies have used ECM proteins such as collagen, laminin, fibronectin and vitronectin to coat the surface of different materials (Mistry *et al.* 2005, Khademhosseini *et al.* 2009, Kundu *et al.* 2006, Ku *et al.* 2005). Although ECM proteins can enhance cell attachment and differentiation, the use of strict protein-coating only insufficiently reproduce the desired composition, function, microstructure and architecture of native ECM. Moreover, extraction procedures and other practical limitations have precluded determination of the exact composition of ECM proteins, present in different tissues *in vivo*.

Creating a native ECM on a synthetic scaffold may facilitate cellular activities by combining biological cues with a proper 3-D mechanical support (Hoshiba *et al.* 2010). Decellularized ECM derived from human or animal tissues, such as bladder, heart valves or small intestine (Crapo *et al.* 2011, Badylak *et al.* 1999) have been used to produce engineered constructs mimicking the native microenvironment of the tissue. However,

there are some limitations of using tissue-derived ECM such as the lack of availability, especially in the context of an autologous application, and the potential pathogen transmission (Crapo *et al.* 2011, Badylak *et al.* 2009).

Cultured cell-derived ECM has been used as an alternative to tissue-derived ECM. In fact, ECM proteins can be secreted by cells cultured *in vitro* and then decellularized to create the cell-derived ECM (Hoshiba *et al*. 2006). Cell-derived ECM has several advantages over tissue-derived ECM, since it is easy to eliminate pathogen content and it can be derived from autologous cells (Lu *et al.* 2011, Noh *et al*. 2016). In fact, cell-derived ECM can be created *in vitro* using patient-specific cells. Some studies have already shown promising results on the application of cultured cell-derived ECM to enhance the bioactivity and osteogenic capabilities of scaffolds for tissue engineering applications (Cheng *et al*. 2009, Choi *et al.* 2010, Liao *et al.* 2010, Wolchok *et al.* 2010). Mikos and colleagues showed that titanium fiber meshes containing ECM derived from rat marrow stromal cells increased bone matrix deposition *in vitro* compared to titanium fiber mesh without ECM (Pham *et al*. 2008, Datta *et al*. 2005, Datta *et al. 2006)*. Chen and colleagues demonstrated that cell-derived ECM from bone marrow cultured cells, in the absence of osteogenic growth factors, facilitated the expansion of mesenchymal colony-forming units *in vitro* while maintaining stem cell properties (Chen *et al.* 2007). In another study, Kang and colleagues showed that porous scaffolds containing human umbilical vein endothelial cells (HUVEC)-derived ECM could promote osteogenic differentiation of human mesenchymal stem/stromal cells (MSC) (Kang *et al.* 2012) compared to porous scaffolds without ECM. These results suggest that cell-derived ECM holds the potential to create a biomimetic microenvironment that enhances osteogenic differentiation. As previously mentioned, cells derived from different tissues typically produce matrices that will recreate the composition of the natural tissue matrix. In this context, we anticipate that ECM elements such as proteins and growth factors, derived from key cellular sources including stem and endothelial cells, can provide a better microenvironment for cell adhesion, proliferation and differentiation and that the ECM components derived from such cellular sources can slowly release bioactive factors into the microenvironment that can accelerate tissue regeneration. In fact, the co-culture of MSC with other bone marrow (BM) cell populations, including endothelial cells (EC), hematopoietic stem cells (HSC) and osteoblasts, has been investigated in what concerns its effect on the osteogenic differentiation of MSC (Sun *et al*. 2007, Ball *et al.* 2004). Co-culture systems of MSC and EC have demonstrated extensive cellular crosstalk through a variety of mechanisms, such as paracrine and juxtacrine (contact-dependent signaling) interaction or vesicle trafficking between MSC and EC, enhancing the angiogenic response of cells (Aguirre *et al.* 2010, Nassiri *et al.* 2014), as well as the osteogenic capabilities (Zhao *et al*. 2012).

The aim of this study was to evaluate the effect of different compositions of decellularized cultured cell-derived ECM produced from MSC, HUVEC and co-culture of MSC:HUVEC (MSC:HUVEC 1:1, 1:3, 3:1) on cell proliferation, osteogenic differentiation and angiogenic properties of human bone marrow MSC, since both cell types reside in the bone niche and secrete important factors known to enhance osteogenic differentiation of MSC (Zhao *et al.* 2012, Lee *et al.* 2017). Therefore, we hypothesize that a MSC:HUVEC ECM could stimulate both osteogenesis and angiogenesis and consequently represent a new strategy for enhanced bone healing and accelerated vascularization of the defect site.

V.2. Materials & Methods

V.2.1. Cell culture

Human bone marrow (BM) MSC used are part of the cell bank available at the Stem Cell Engineering Research Group (SCERG), Institute for Bioengineering and Biosciences (iBB) at Instituto Superior Técnico (IST). MSC were previously isolated/expanded according to protocols previously established at iBB-IST. Bone marrow samples were obtained from Instituto Português de Oncologia Francisco Gentil, Lisboa, under collaboration agreements with iBB-IST. All human samples were obtained from healthy donors after written informed consent according to the Directive 2004/23/EC of the European Parliament and of the Council of 31 March 2004 on setting standards of quality and safety for the donation, procurement, testing, processing, preservation, storage and distribution of human tissues and cells (Portuguese Law 22/2007, June 29), with the approval of the Ethics Committee of the respective clinical institution. Isolated cells were kept frozen in liquid/vapour nitrogen tanks until further use.

BM MSC were thawed and plated on T-75 flasks using low-glucose Dulbecco's Modified Eagle's Medium (DMEM: Gibco, Grand Island, NY) supplemented with 10% fetal bovine serum (FBS MSC qualified: Gibco) and 1% antibiotic-antimycotic (Gibco) and kept at 37ºC, 5% CO_2 and 21% O_2 in a humidified atmosphere. Medium renewal was performed every 3-4 days. Cells between passages 3 and 6 were used. Three independent donors were used in all experiments. Cells were tested for the expression of cell surface markers used to attest MSC identity according to standardized criteria (Dominici *et al.* 2006) (i.e., $CD73^+$, $CD90^+$, $CD105^+$, HLA-DR^-, $CD34^-$, $CD45^-$), and their ability to differentiate into osteoblasts, adipocytes, and chondrocytes. HUVEC were purchased from Lonza (Basel, Switzerland) and maintained in commercial Endothelial Growth Medium-2 (EGM-2: Lonza).

V.2.2. Decellularized cultured cell-derived ECM preparation

MSC and HUVEC cultures as well as the co-culture of three different ratios of MSC:HUVEC (1:1, 1:3, 3:1) were initiated with a seeding density of 5000 cells/cm^2 using tissue-culture polystyrene (TCP) wells. MSC culture was maintained with DMEM+10% FBS, HUVEC culture with EGM-2 growth medium and the co-culture of MSC:HUVEC was kept with a mixture between DMEM+10%FBS and EGM-2 (1:1). Cells were expanded in the same conditions described above and medium was renewed every 3-4 days. After reaching confluency, between day 7 and 10, medium was discarded and cells were washed with phosphate buffer saline (PBS: Gibco). Monolayers of cells were then stripped of from the wells using a solution of 0.5% Triton X-100 (Sigma-Aldrich, St. Louis, MO) containing 20 mM NH_4OH (Sigma-Aldrich) in PBS for 5 min, according to previously reported methods (Yang *et al.* 2018, Gong *et al.* 2017, Kusuma *et al.* 2017, Kang *et al.* 2012), expecting to leave structurally-intact ECM exposed and uniformly attached on the surface of the wells. Finally, for all conditions, cultured cell-derived ECM were gently washed five times using PBS and air-dried under the laminar flow hood.

V.2.3. Immunofluorescent staining of cultured cell-derived ECM

To investigate the protein components and distribution pattern of the different decellularized cultured cell-derived ECM, immunofluorescent staining was performed. Five ECM proteins, collagen I, collagen IV, fibronectin, laminin and osteocalcin were immunofluorescently stained. After decellularization, dECM were washed with PBS and fixed with 4% paraformaldehyde (PFA; Santa Cruz Biotechnology, Dallas, TX) for 20 min at room temperature. Then, cell-derived ECM were washed three times with 1% bovine serum albumin (BSA) in PBS for 5 min. Samples were blocked with a solution of 0.3%Triton X-100, 1% BSA and 10% donkey serum in PBS at room temperature for 45 min. Primary antibodies including mouse anti-human collagen I, collagen IV, laminin, fibronectin and osteocalcin (10 µg/ml in 0.3%Trinton X-100, 1% BSA, 10% donkey serum) (R&D systems, Minneapolis, MN) were added into the samples followed by incubation overnight at 4ºC. After washing with 1% BSA in PBS, a NorthernLights^{TM} 557-conjugated anti-mouse IgG secondary antibody (dilution 1:200 in 1% BSA PBS) (R&D systems) was added into the samples and incubated in the dark for 1 h at room temperature. Finally, the cell nuclei were counterstained with DAPI (Invitrogen, Carlsbad, CA) (1.5 µg/ml) for 5 min and then washed with PBS. The fluorescent staining was imaged by fluorescence microscope (Olympus IX51 Inverted Microscope: Olympus America Inc., Melville, NY) and recorded by an attached digital camera, at a magnification of 10x.

V.2.4. Cell proliferation and osteogenic differentiation assays

BM MSC were seeded on dECM at a density of 3000 cells/cm^2 using expansion medium (DMEM+10% FBS). Medium renewal was performed every 3-4 days. The metabolic activity of MSC was evaluated using AlamarBlue® cell viability reagent (Molecular Probes, Eugene, OR), on days 1, 4 and 7. AlamarBlue® cell viability reagent was added to the cells and incubated at 37ºC in 5% CO_2 chamber for 2.5h. Fluorescence was quantified (560nm – 590nm) and compared to a calibration curve to access the equivalent number of viable cells under each condition. Cell proliferation was measured in triplicates in all groups.

After reaching confluency, osteogenic medium composed by low glucose DMEM supplemented with 10% FBS, 10 mM β-glycerophosphate (Sigma-Aldrich), 10 nM dexamethasone (Sigma-Aldrich) and 50 µg/ml ascorbic acid (Sigma-Aldrich) was added to the culture. Medium renewal was performed every 3-4 days. After 21 days of osteogenic differentiation, total calcium content and Alkaline phosphatase (ALP) activity assays were performed. For determination of total calcium content, samples (n=3) were washed twice with PBS and extracted off using a 0.5 M HCl solution (Sigma-Aldrich, St Louis, MO). Accumulated calcium was removed from the cellular component by shaking overnight at 4ºC. The supernatant was used for calcium determination according to the manufacturer's instructions contained in the calcium colorimetric assay kit (Stanbio Laboratory, Boerne, TX). Absorbance at 550 nm was measured for each condition and normalized to the total number of cells after 21 days and determined by AlamarBlue® cell viability assay. Total calcium was calculated from calcium standard solution prepared in parallel.

ALP activity was detected using a colorimetric ALP kit (BioAssays Systems, Hayward, CA) according to the manufacturer's protocol. Samples (n=3) were washed with PBS and were incubated in the lysis buffer (0.1% Triton X-100 in PBS) by shaking for 30 min at room temperature. The lysate was added to p-nitrophenyl

phosphate solution (10 mM) provided with the ALP kit. The absorbance was measured at 405 nm and normalized to the total number of cells in each sample, after 21 days, determined by AlamarBlue® cell viability assay.

After 21 days of osteogenic differentiation, samples were stained with ALP staining and Von Kossa staining. Cells that were not cultured with osteogenic medium and maintained in expansion medium for 21 days were also stained and used as negative controls. Culture medium was removed and cells were washed with PBS. Cells were fixed with 4% PFA for 20 min. Then, cells were rinsed in miliQ water during 15 min and then incubated with a Fast Violet solution (Sigma-Aldrich) and Naphthol AS-MX Phosphate Alkaline solution (Sigma-Aldrich) in a final concentration of 4% for 45 min, at room temperature in the dark. Cells were then washed three times with miliQ water and once with PBS. Von Kossa staining was performed by incubating the cells with a 2.5% silver nitrate solution (Sigma-Aldrich) during 30 min at room temperature in the dark. Cells were washed three times with miliQ water and visualized using an inverted microscope (Olympus IX51 Inverted Microscope: Olympus America Inc., Melville, NY) at a magnification of 10x, and recorded by an attached digital camera.

V.2.5. Cell morphology assay

BM MSC were seeded on dECM at a density of 3000 cells/cm^2 and cell morphology was assessed. After 7 days of culture under expansion conditions, cells were washed twice with PBS, fixed with 4% PFA for 20 min and then permeabilized with 0.1% Triton X-100 for 10 min. After permeabilization, cells were incubated with phalloidin-TRITC (Invitrogen) (dilution 1:250, 2 µg/ml) for 45 min in the dark. Then, cells were washed twice with PBS and counterstained with DAPI (Invitrogen) (1.5 µg/ml) for 5 min and then washed with PBS. The fluorescent staining was imaged by fluorescence microscope (Olympus IX51 Inverted Microscope: Olympus America Inc., Melville, NY) and recorded by an attached digital camera, at a magnification of 10x. DAPI/phalloidin staining was performed also after 21 days of culture of BM MSC under osteogenic differentiation conditions upon seeding on different dECM.

V.2.6. qRT-PCR analysis

Total RNA was extracted with a RNeasy Mini Kit (QIAGEN, Hilden, Germany). cDNA was synthesized from the purified RNA using iScript™ Reverse Transcription Supermix (Bio-Rad, Hercules, CA). Reaction mixtures (20 µl) were incubated in a thermal cycler (Veriti 96-well thermal cycler: Applied Biosystems, Foster City, CA) for 5 min at 25ºC, 30 min at 42ºC and 5 min at 85ºC and then were maintained at 4ºC. The sequences of the specific primer sets used are given in Table V.1.

The quantitative reverse transcription-polymerase chain reaction (qRT-PCR) was performed using SYBR® Green PCR Master Mix (Applied Biosystems) and StepOnePlus real-time PCR system (Applied Biosystems). All reactions were carried out at 95ºC for 10 min, followed by 40 cycles of 95ºC for 15 sec and 60ºC for 1 min; all were performed in triplicate. Glyceraldehyde 3-phosphate dehydrogenase was used as internal control to normalize differences in total RNA levels in each sample. A threshold cycle (Ct) was observed in the exponential phase of amplification, and quantification of relative expression levels was performed with the use

of standard curves for target genes and endogenous control. Geometric means were used to calculate the $\Delta\Delta$Ct values and are expressed as $2^{-\Delta\Delta Ct}$. The mean values from triplicate analysis were compared. The values obtained for TCP group were set as 1 and were used to calculate the fold difference in the target gene.

Table V.1. Sequences of primers used for qRT-PCR analysis

Genes	Sequences
GAPDH	For: 5' AAC AGC GAC ACC CAC TCC TC Rev: 5' CAT ACC AGG AAA TGA GCT TGA CAA
Col I	For: 5' CAT CTC CCC TTC GTT TTT GA Rev: 5' CCA AAT CCG ATG TTT CTG CT
Runx2	For: 5' AGA TGA TGA CAC TGC CAC CTC TG Rev: 5' GGG ATG AAA TGC TTG GGA ACT
ALP	For: 5' ACC ATT CCC ACG TCT TCA CAT TT Rev: 5' AGA CAT TCT CTC GTT CAC CGC C
OPN	For: 5' ATG AGA TTG GCA GTG ATT Rev: 5' TTC AAT CAG AAA CCT GGA A
OC	For: 5' TGT GAG CTC AAT CCG GCA TGT Rev: 5' CCG ATA GGC CTC CTG AAG C

V.2.7. *In vitro* endothelial cell tube formation assay

In order to study the effect of dECM on angiogenesis, a three-dimensional capillary *in vitro* tube formation assay was performed. Conditioned medium from BM MSC cultured for 72 h on all the different substrates (dECM and TCP) (without FBS) were collected. HUVEC ($2x10^4$ cells) were cultured on a Matrigel substrate (50 μl/well) (Corning, Corning, NY) in a 96-well plate with the different conditioned media collected as mentioned above. After incubation for 8h at 37ºC, cells were labeled by adding calcein AM (Corning) (8 μg/ml) and incubated for 30 min at 37ºC. Three photomicrographs per well were taken under fluorescence microscope and the number of tubular-like structures formed were counted with the use of ImageJ (NIH) software. Endothelial growth medium supplemented with angiogenic growth factors (EGM-2) and endothelial basal medium, without growth factors, were served as positive and negative controls, respectively

V.2.8. Scanning electron microscope evaluation

The surface morphology of the different dECM obtained was examined using scanning electron microscopy (SEM) (FEI Versa 3D Dual Beam). dECM were rinsed with PBS and then fixed with 4% PFA for 20 min, after which these were dehydrated in a graded series of ethanol (20%, 40%, 60%, 80%, 100%), and dried. The dECM were sputter-coated with a thin layer of 60% gold-40% palladium before imaging. Samples were imaged at different magnifications with an operating voltage between 2-3 kV.

V.2.9. Statistical analysis

Each experiment was conducted in triplicate. Shapiro-Wilk test was performed to test for the normality of data. Statistical analysis of the data was performed using Student's t-test, comparing each condition with the control condition (TCP) at the same timepoint, using GraphPad Prism version 7. The statistical significance of results is reported at 95% confidence intervals ($P<0.05$). Throughout this chapter, results are presented as mean ± standard deviation (SD).

V.3. Results

V.3.1. Characterization of decellularized extracellular matrix produced from MSC, HUVEC and co-culture of MSC:HUVEC

Decellularized cultured cell-derived extracellular matrices (dECM) were obtained from different cell types: BM MSC, HUVEC and three different ratios of MSC:HUVEC co-culture (1:1, 1:3, 3:1), in order to produce substrates (in this case TCP) coated with the respective ECM (Figure V.1).

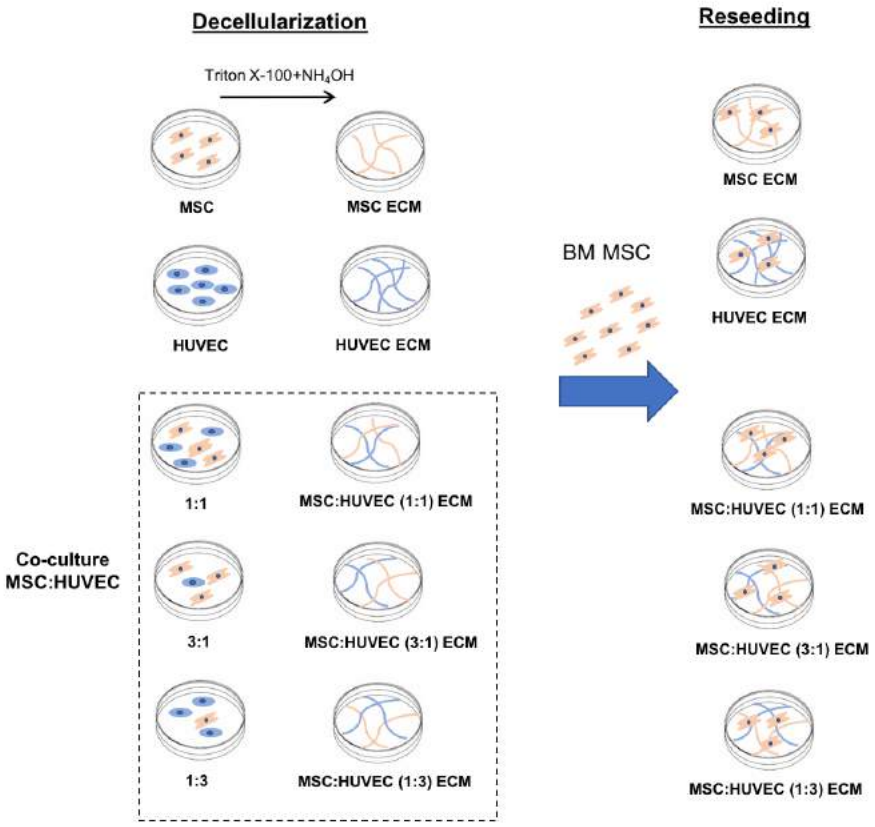

Figure V.1. Schematics of decellularization of cultured cell-derived ECM (dECM) derived from BM MSC and HUVEC cultures and co-cultures of BM MSC:HUVEC at different ratios (1:1; 3:1; 1:3). After decellularization, BM MSC were reseeded onto the various dECM and cell proliferation, osteogenic differentiation and angiogenic properties were evaluated.

Confluent cultures of MSC, HUVEC, MSC:HUVEC (1:1), MSC:HUVEC (1:3) and MSC:HUVEC (3:1) were decellularized according to previously published procedures (Yang *et al.* 2018, Gong *et al.* 2017, Kusuma *et al.* 2017, Kang *et al.2012*). Figure V.2 reveals that cell cultures were completely confluent before decellularization and fluorescent micrographs of DAPI/phalloidin stained cultures showed well-defined cell nuclei before decellularization. After treatment with a solution of 0.5% Triton X-100 containing 20mM NH_4OH in PBS, the ECM produced by cells remained and DAPI staining demonstrated a residual amount of cellular nuclei, indicating that most of the cellular nuclei were disrupted after the decellularization process (Figure V.2 and V.3).

Red fluorescent protein (RFP)-expressing HUVEC were used to evaluate HUVEC distribution during co-culture with BM MSC at three different ratios Interestingly, HUVEC presented a different organization when co-cultured with MSC at a ratio of MSC:HUVEC 1:3, creating a more interconnected network. HUVEC alone did not create such an interconnected network, instead a confluent cell monolayer was observed (Figure V.4), indicating that MSC are important to support the formation of this capillary structure.

In order to verify that the remaining material on the culture substrates was composed by ECM elements, following decellularization, different substrates were stained for common ECM proteins such as collagen type I, collagen type IV, laminin and fibronectin. The results demonstrated that, after the decellularization procedure, the substrates were coated with a biological network of extracellular matrix. Figure V.3 shows that there were some differences among the components of the different dECM. All dECM stained positive for collagen type I. Interestingly, collagen IV, laminin and fibronectin produced by BM MSC and HUVEC showed different relative abundance throughout the different dECM obtained. HUVEC-derived ECM expressed relatively low level of collagen IV, laminin and fibronectin in the form of a sparse dot-like morphology (Figure V.3). Notably, osteocalcin, a non-collagenous protein found in bone ECM, showed higher relative abundance throughout the dECM produced by the co-culture of MSC:HUVEC (all ratios). Immunostaining of osteocalcin showed that its expression was strongly detected in the ECM obtained from MSC:HUVEC co-culture, regardless the cell ratio, but not well detected in the others dECM. Therefore, consistent with our proposed strategy, the composition of the dECM could be modulated with various combinations of cultured cell types.

Scanning electron microscopy (SEM) revealed differences in the architecture of dECM derived from different cell types after the decellularization protocol (Figure V.5). SEM images confirmed that BM MSC-derived ECM presented a fibrillar architecture. Notably, HUVEC-derived ECM and ECM obtained from MSC:HUVEC co-cultures (1:1 and 1:3) ECM demonstrated a globular structure, presenting a similar pattern between these. Moreover, ECM derived from BM MSC:HUVEC co-cultures at a 3:1 ratio showed a more fibrillar structure, like BM MSC ECM, possibly due to the higher ratio of this cell type in this particular condition.

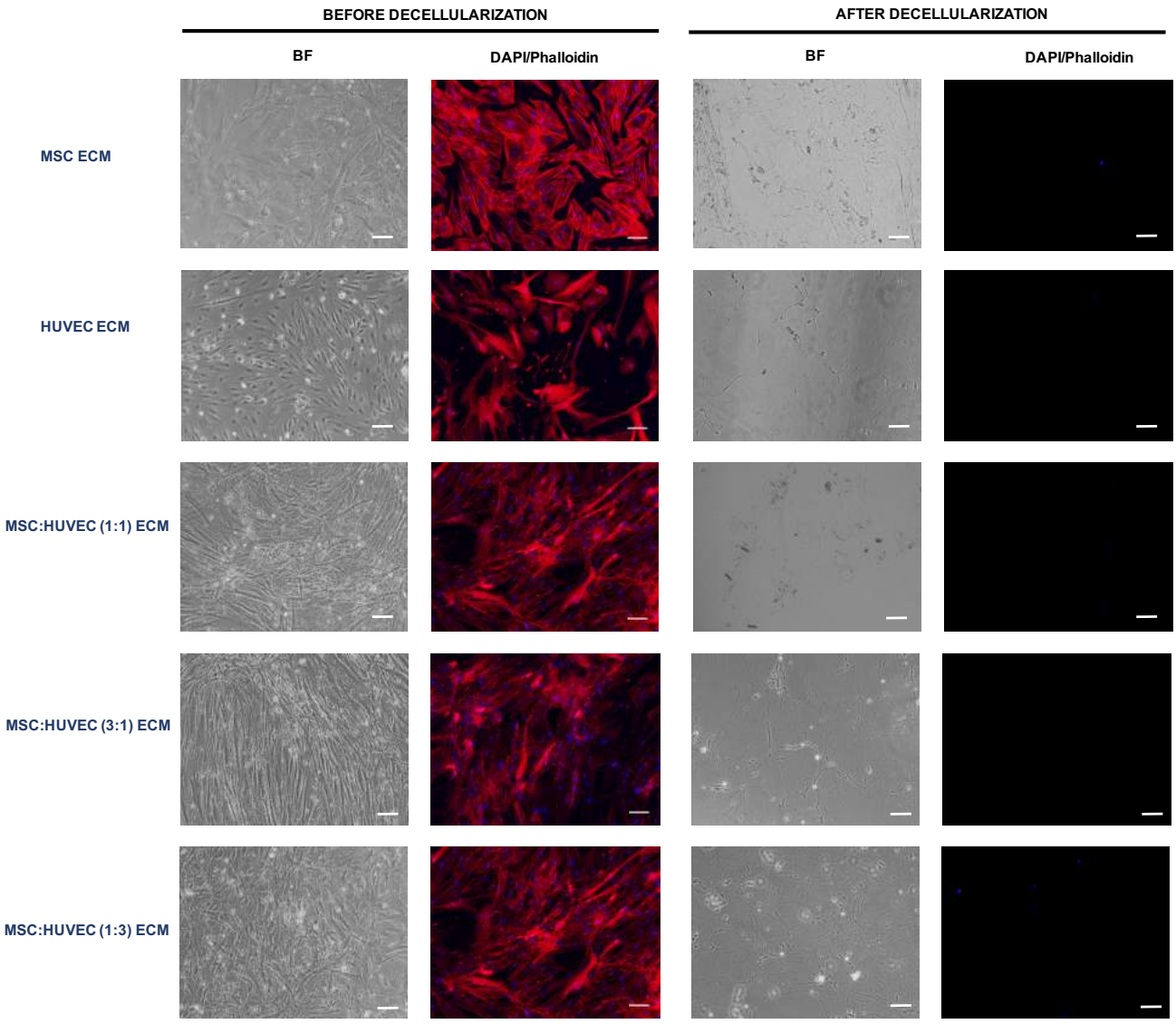

Figure V.2. Characterization of dECM derived from BM MSC and HUVEC cultures and co-cultures of BM MSC:HUVEC at different ratios (1:1; 3:1; 1:3). Phase contrast microscopy images and DAPI/phalloidin stainings taken before and after decellularization with 20 mM NH_4OH + 0.5% Triton solution confirmed the decellularization process. Red: Alexa Fluor® 594 phalloidin; Blue: DAPI. Scale bars, 100 µm.

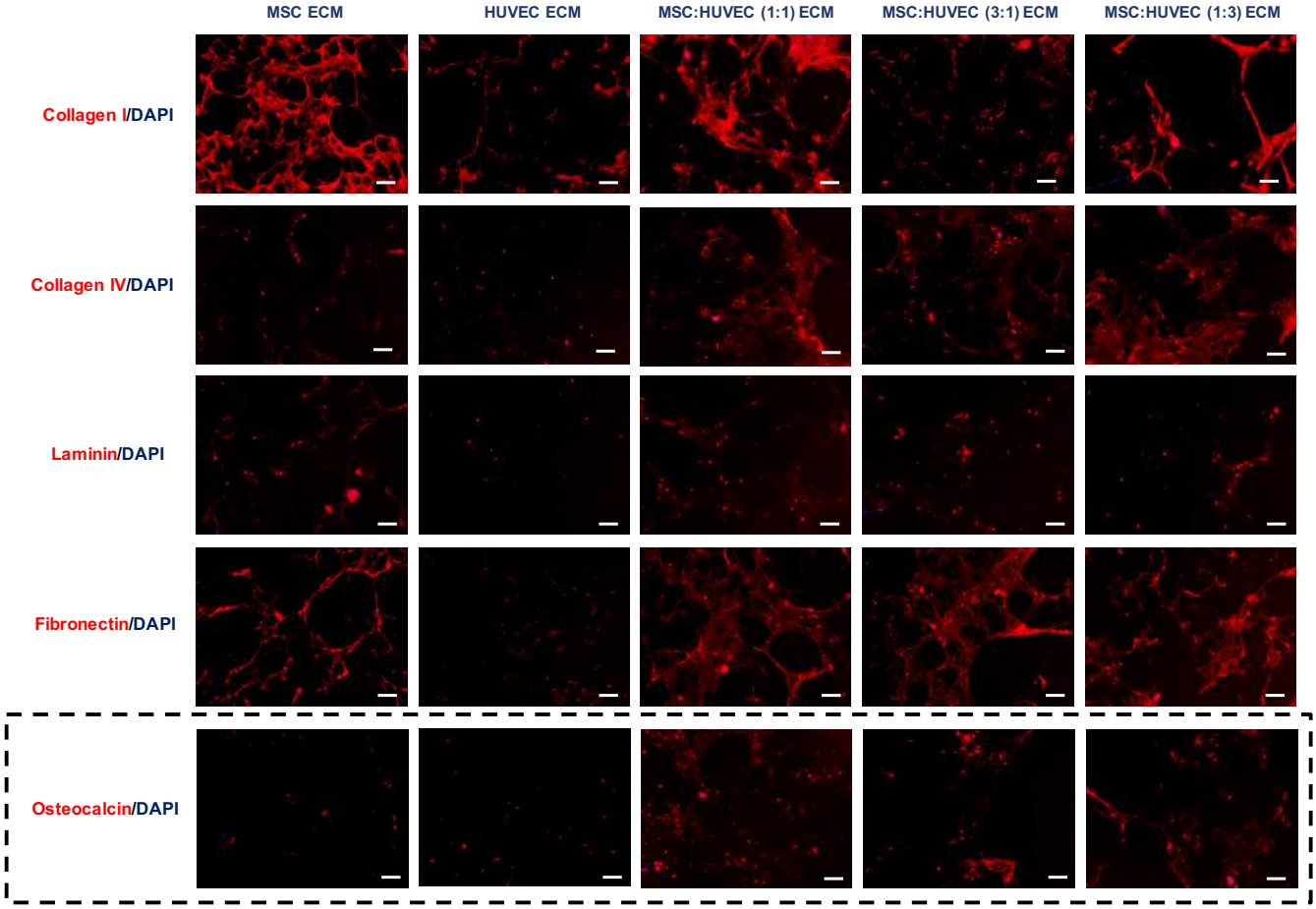

Figure V.3. Comparison of dECM derived from MSC, HUVEC, MSC:HUVEC 1:1, MSC:HUVEC 3:1 and MSC:HUVEC 1:3. Immunofluorescent staining images of collagen I, collagen IV, laminin, fibronectin and osteocalcin showed different distribution of the ECM proteins after the decellularization protocol. Red: NothernLights™ 557 donkey anti-mouse antibody; Blue: DAPI. Scale bars, 100 μm.

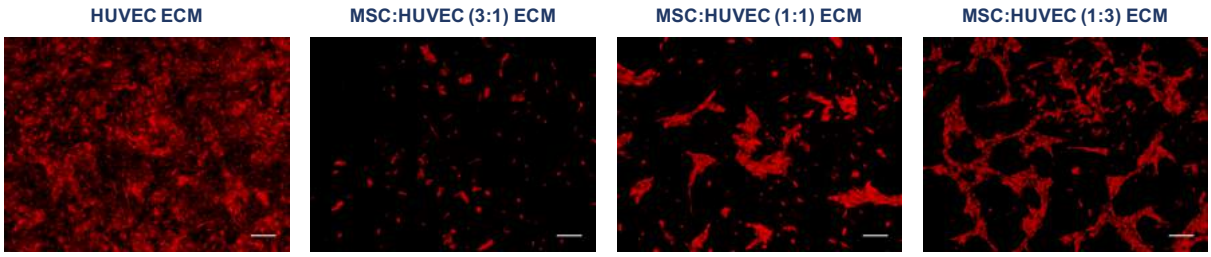

Figure V.4. Morphology and cell distribution of HUVEC when co-cultured with BM MSC at different ratios, before the decellularization protocol. When HUVEC were co-cultured with MSC at ratio 1:3 (MSC:HUVEC 1:3), HUVEC rearranged as a capillary-like structure. Scale bars, 200 μm.

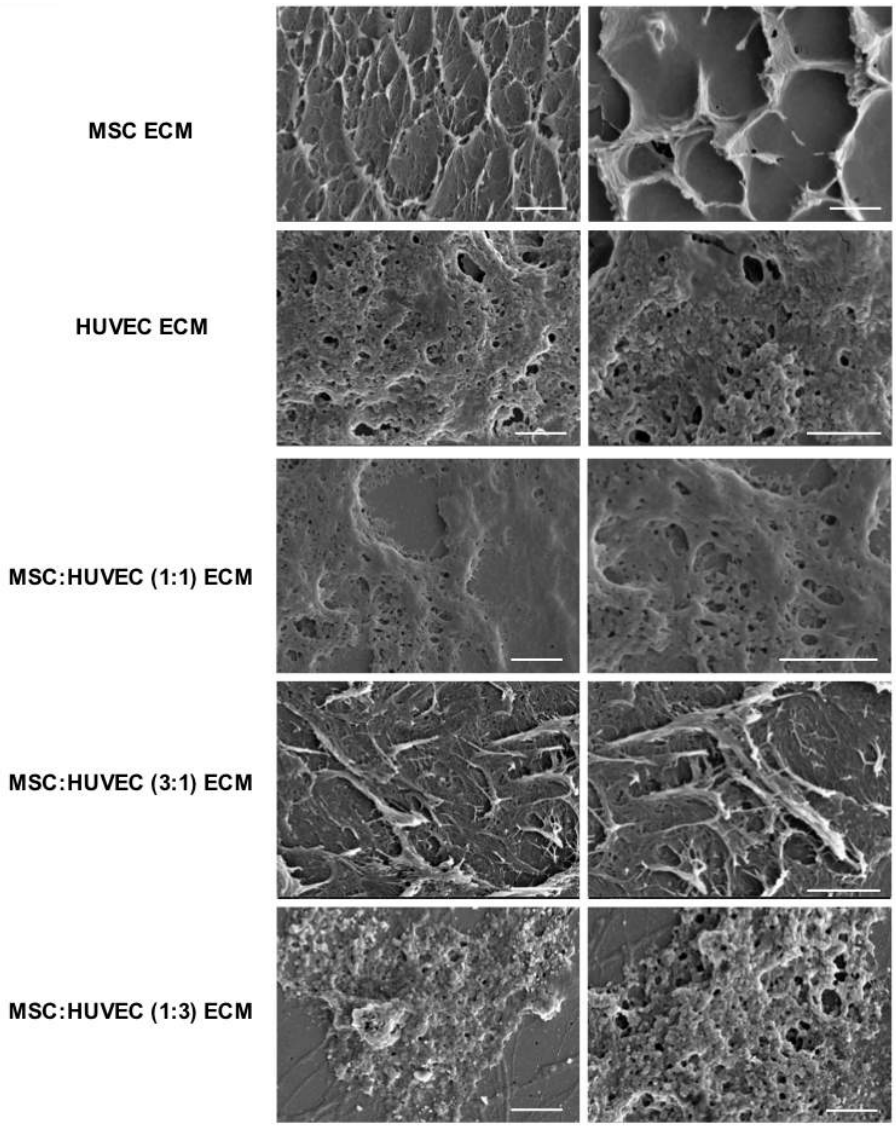

Figure V.5. Scanning electron microscopy (SEM) images of dECM derived from BM MSC and HUVEC cultures and co-cultures of BM MSC:HUVEC at different ratios (1:1; 3:1; 1:3) after the decellularization protocol. Scale bars, 1 μm.

V.3.2. Decellularized cultured cell-derived extracellular matrix promotes the proliferation of BM MSC *in vitro*

To determine whether dECM derived from BM MSC, HUVEC and MSC:HUVEC cultures promoted the proliferation of MSC *in vitro*, cellular metabolic activity of BM MSC cultured on different dECM was measured by Alamar blue assay after 1, 4 and 7 days of culture. Comparison of cell proliferation between BM MSC cultured on different dECM and on tissue culture polystyrene (TCP – no ECM) is shown in Figure V.6. After 4 days, BM MSC cultured on ECM coatings obtained from BM MSC, HUVEC and MSC:HUVEC (1:1) cultures showed a statistically significant increase in cell numbers compared with cells cultured on TCP without an ECM substrate (control). Interestingly, after 7 days of cell culture, results showed that cells seeded on all dECM proliferated faster than those on TCP, reaching higher cell number. In particular, BM MSC cultured on MSC:HUVEC (1:1)-derived ECM reached a cell number of 7.22 x 10^4 compared to 5.19 x 10^4 cells obtained when BM MSC were cultured on TCP (no ECM, control). These results indicate that ECM derived from both cell types, BM MSC and HUVEC, can enhance the proliferation of BM MSC *in vitro*. Furthermore, BM MSC seeded onto all different substrates showed the same cell morphology, after 7 days of cell culture (Figure V.6b).

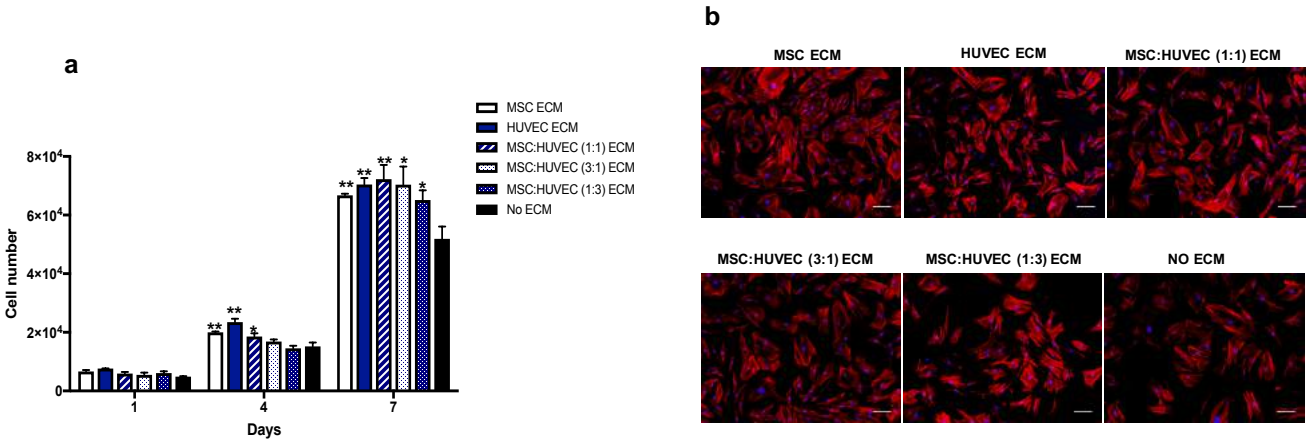

Figure V.6. *In vitro* proliferation and morphology of BM MSC cultured on different substrates produced by cell-derived ECM. **a)** Numbers of BM MSC cultured on dECM obtained from different cell types and on TCP (No ECM-control). **b)** Representative photomicrographs showing the morphology of BM MSC seeded on dECM and on TCP on day 7. Red: phalloidin; blue: DAPI. Scale bars, 100 µm. Data are expressed as mean ± SD, **p<0.01; *p<0.05 (n=3).

V.3.3. Decellularized cultured cell-derived extracellular matrix promotes the osteogenic differentiation of BM MSC *in vitro*

To investigate the effect of the different dECM obtained on the osteogenic differentiation of BM MSC, we evaluated ALP activity, calcium deposition, as well as osteogenic gene expression of MSC after 21 days of cultivation under osteogenic culture conditions.

ALP activity of BM MSC was quantified after 21 days of osteogenic differentiation on all different substrates, as well as observed by histochemical stainings. The ALP activity of BM MSC seeded on HUVEC-derived ECM, and ECM derived from BM MSC:HUVEC co-cultures (1:1 and 1:3 ratios) demonstrated a statistically significant increase compared with BM MSC seeded on TCP (control). Interestingly, ALP activity of

BM MSC differentiated on BM MSC-derived ECM did not show any improvement compared with the TCP substrate. Histochemical staining confirmed the quantitative results obtained herein (Figure V.7a,b).

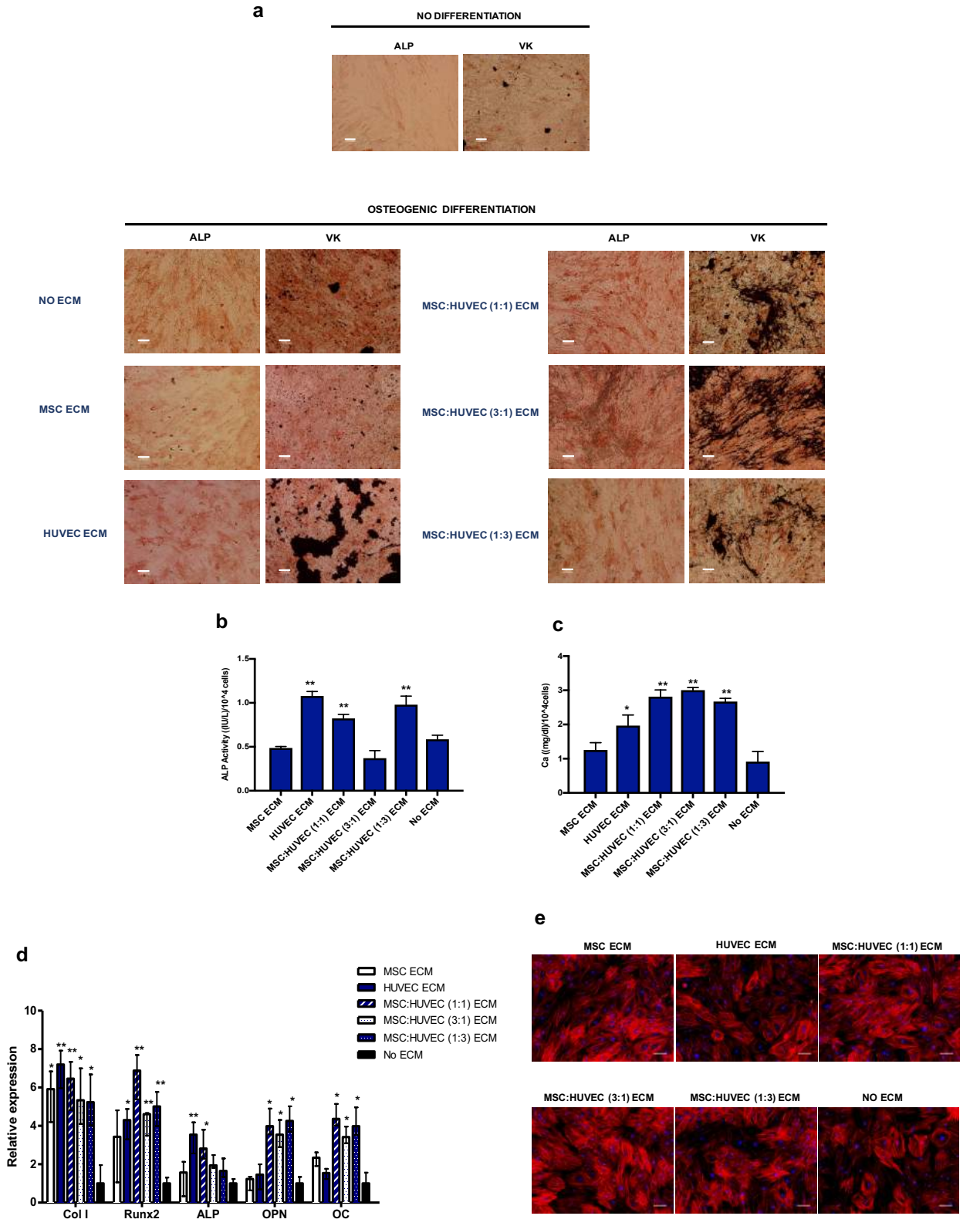

Figure V.7. Osteogenic differentiation of BM MSC on the different dECM substrates obtained. **a)** Representative images of BM MSC stained with alkaline phosphatase (ALP) and Von Kossa (VK) dyes after 21 days of osteogenic induction. **b)** ALP activity of BM MSC differentiated on dECM and TCP (No ECM) after 21 days of osteogenic differentiation. **c)** Calcium quantification of BM MSC differentiated after 21 days on dECM and TCP. **d)** qRT-PCR analysis for determination of the expression of osteogenic genes after 21 days of culture under osteogenic conditions. **e)** Cell morphology of BM MSC differentiated under osteogenic culture medium on different dECM and TCP after 21 days of differentiation. Red: phalloidin; blue: DAPI. Scale bars, 100 μm. Data are expressed as mean ± SD, **p<0.01; *p<0.05 (n=3).

After 21 days of osteogenic induction, Von Kossa staining revealed mineralized deposits on all groups, which shows that BM MSC cultured on all surfaces (ECM coatings and TCP-control) maintained their osteogenic differentiation potential. However, enhanced mineralization, demonstrated by the darker regions stained with Von Kossa, was observed when BM MSC were differentiated on ECM derived from BM MSC:HUVEC co-cultures (all ratios) (Figure V.7a). Calcium quantification was also assessed with a colorimetric assay after 21 days of differentiation. A slight increase on calcium deposition was observed when BM MSC were cultured on HUVEC-derived ECM, however, a statistically significant improvement on calcium deposition occurred when cells were differentiated on MSC:HUVEC-derived ECM. Interestingly, the mineralization enhancement was observed for all the MSC:HUVEC-derived ECM produced with the three different cell ratios. On the other hand, when BM MSC were differentiated on MSC-derived ECM, no statistically significant increase on calcium levels quantification was observed, compared to TCP (control) (Figure V.7c).

The expression levels of *Col I*, *ALP*, *Runx2*, *OC* and *OPN* genes were measured by real-time PCR analysis after BM MSC were cultured under osteogenic differentiating conditions on all different dECM and TCP (no ECM, control) for 21 days (Figure V.7d). BM MSC cultured on all ratios of MSC:HUVEC-derived ECM exhibited the greatest degree of osteogenic differentiation, especially in what concerns mRNA expression levels of late osteogenic markers (OPN and OC). Col I and ALP are osteogenic markers associated with early osteogenic differentiation, while OPN and OC are osteogenic-specific ECM proteins. Therefore, the expression levels of OPN and OC were evaluated as indicators of late osteoblastic differentiation.

All dECM substrates resulted in an increase of the expression levels of osteogenic genes by BM MSC. ECM derived from MSC:HUVEC co-culture (1:1) presented significantly higher levels of osteogenic gene expression compared with TCP (no ECM coating). We found that MSC cultured on MSC:HUVEC-derived ECM (all ratios) upregulated the expression of late osteogenic genes, such as OPN and OC.

These data illustrate that ECM derived from BM MSC and HUVEC cultures can improve the osteogenic differentiation capacity of BM MSC, compared to cells differentiated on TCP, since cells grown on dECM were able to maintain a better osteogenic phenotype as indicated by the higher mRNA expression levels of *Col I*, *Runx2*, *ALP*, *OPN* and *OC* (Figure V.7d).

V.3.4. Decellularized cultured cell-derived extracellular matrix enhances angiogenic properties

The angiogenic promoting effects of the different dECM obtained were investigated by evaluating HUVEC response to conditioned medium from BM MSC cultured on the different substrates. To this end, an *in vitro* functional tube formation assay was performed where HUVEC were cultured on Matrigel using the conditioned media collected from cultures of BM MSC cultivated for 72 hours on the different substrates (dECM and TCP), according to the previously described in Materials & Methods section. Endothelial cell growth medium, with or without VEGF, served as positive and negative controls, respectively. The results obtained are presented in Figure V.8.

After 8h post seeding, tubular-like structures were found on Matrigel seeded with HUVEC using the conditioned medium retrieved from cultures of BM MSC on all substrates (Figure V.8a). Our data indicate that conditioned medium collected from MSC cultured in all groups for 72 hours can promote endothelial cell tube formation. However, complex web-like structures were only detected when HUVEC were cultured with conditioned medium from MSC:HUVEC (1:3) ECM culture, indicating that MSC:HUVEC (1:3) ECM enhanced the pro-angiogenic capacity of BM MSC. Quantitative analysis showed significantly higher number of tubes formed by HUVEC cultured with conditioned medium obtained from MSC:HUVEC (1:3) ECM culture compared with conditioned medium from cells cultured on TCP (Figure V.8b). We believe that there is a difference in amount and composition of angiogenic factors that are secreted from MSC cultured on different dECM and TCP. Moreover, we hypothesize that some ECM proteins and growth factors responsible for angiogenesis may be retained in the dECM, allowing a slow release of these factors to the medium, enhancing the angiogenic potential of these cells.

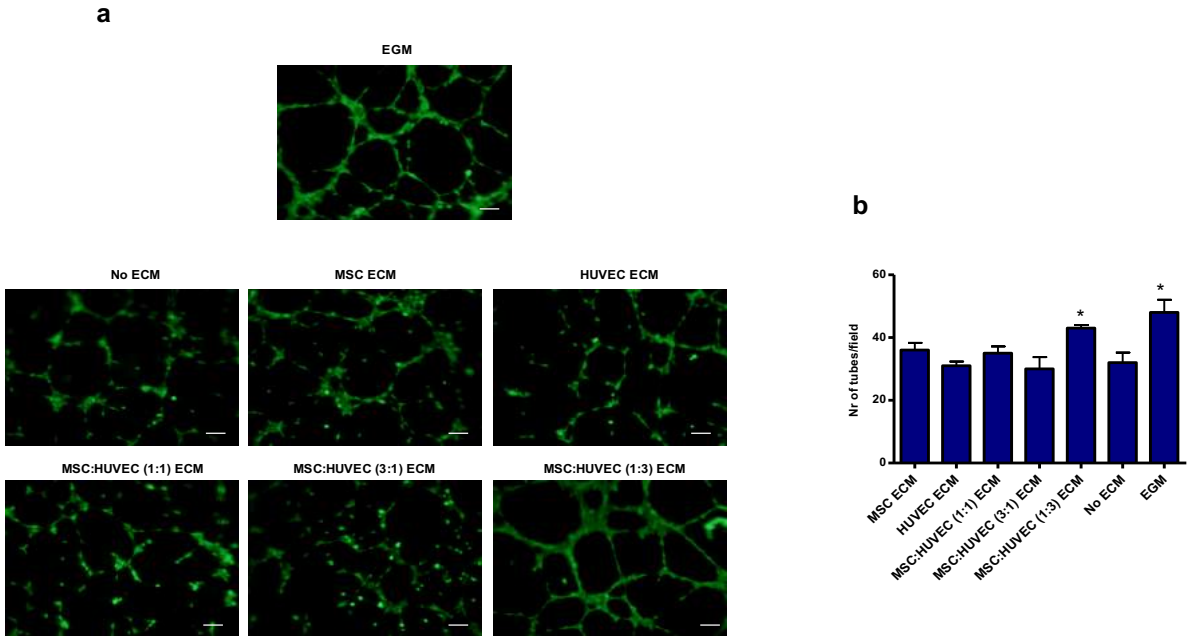

Figure V.8. The angiogenic promoting effects of the different dECM were investigated by evaluating HUVEC response to conditioned medium from BM MSC cultured on the different substrates: MSC ECM, HUVEC ECM, MSC:HUVEC (1:1) ECM, MSC:HUVEC (3:1) ECM, MSC:HUVEC (1:3) ECM. **a)** Tube formation assay of HUVEC cultured on Matrigel with conditioned medium produced from BM MSC seeded on different dECM and TCP (No ECM, control) after 8h. HUVEC were cultured with VEGF-supplemented EGM on Matrigel as a positive control. **b)** Quantification of number of tubes formed by HUVEC on Matrigel cultured with conditioned medium derived from BM MSC cultured on different dECM and TCP after 8h. Scale bars, 100 μm. Data are expressed as mean ± SD, *$p<0.05$ compared to no ECM group.

V.4.Discussion

ECM in bone is composed by a complex network of proteins, glycoproteins, proteoglycans and polysaccharides. It influences cell behavior through interactions with the cell surface receptors and with other proteins. In fact, ECM can interact and/or store several growth factors and cytokines, modulating the cellular functions (Hynes 2009), providing signals for cell growth and influencing cell adhesion, migration and differentiation, as well as the regulation of gene expression (Lai *et al.* 2010, Sun *et al.* 2011). Therefore, biomimetics of the native ECM could provide an effective strategy for biomaterials, used for tissue engineering applications, to provide the necessary biological and physical cues to the cells, recapitulating the different ECM functions (Fitzpatrick *et al*. 2015). Consequently, different approaches have been used to culture cells in the presence of ECM proteins to stimulate the interactions between cells and ECM, mimicking the natural microenvironment. For example, ECM proteins have been used as coatings in tissue culture to modify cell behavior (Ragetly *et al.* 2010, Vleggeert-Lankamp *et al*. 2004). However, this approach has some limitations, because the surface coating process is difficult to control and adsorption may lead to denaturation of the proteins resulting in reduced functionality. Furthermore, instead of the complex assembly of proteins present in the native ECM, coating approaches, utilize only few selected proteins and, therefore, offer limited functionality. In fact, synthetic materials formed from isolated biological materials, such as collagen, fibronectin or hyaluronan, fail to achieve the molecular complexity and organization of native tissue matrices (Ravindran *et al.* 2012). Therefore, there is a high demand for developing surfaces for *in vitro* cell growth and differentiation that represents, more accurately, the biological microenvironment.

To address the above limitations, decellularized ECM has emerged as a new strategy to create a natural bioactive material that could be used for tissue engineering applications (Zhang *et al.* 2016). Based on the ECM source, different approaches to produce dECM have been described, including the tissue-derived ECM or cell-derived ECM. Tissue-derived matrices, harvested from cadaveric sources, suffer from inherent heterogeneity and have limited ability for customization (Fitzpatrick *et al.* 2015). These matrices have demonstrated several disadvantages, such as potential pathogen transfer and inflammatory or anti-host immune responses (Badylak *et al*. 2009, Skora *et al.* 2012, Liao *et al.* 2010, Cheng *et al.* 2009). In contrast, cell-derived ECM are considered to be a safer alternative ECM source, since they offer the possibility to use autologous cells, thereby minimizing any potential risk of immune responses and pathogen transmission (Yang *et al.* 2018). Furthermore, cell source is a determinant for the resulting cell-derived ECM composition. Indeed, cells derived from different tissues typically yield matrices that mimic the relative composition of the natural tissue matrix (Fitzpatrick *et al.* 2015).

MSC are a common source of cell-derived ECM due to their ability to deposit ECM that mimics various tissues depending on culture conditions, such as bone, cartilage, adipose. MSC-derived ECM has been shown to have good biocompatibility and bioactivity and has been used as a culture substrate to rejuvenate aged mouse stem cells and enhance their lineage differentiation ability (Li *et al.* 2014). It has been shown that dECM from human MSC cultures could drastically promote MSC proliferation compared with TCP (Lai *et al.* 2010). In fact, previous studies demonstrated that coating of an urea-extracted fraction of human MSC ECM improves MSC proliferation compared to coating consisting of single proteins, such as collagen type I, suggesting an important role for the synergistic effect of multiple proteins in the ECM (Lin *et al*. 2012). Moreover, Yang and colleagues have shown that MSC ECM from human BM also functions as a robust

substrate for chondrocyte proliferation and maintenance of chondrocytic phenotype (Yang *et al.* 2018). A different study from Lu and co-workers showed that MSC ECM incorporated into scaffolds supported cell adhesion and proliferation, promoting the production of ECM and demonstrating a stronger stimulatory effect on the chondrogenesis of MSC (Lu *et al.* 2011). Mikos and colleagues have already reported that ECM derived from rat marrow stromal cells increases bone matrix deposition, enhancing osteogenic properties (Pham *et al.* 2008, Datta *et al.* 2005, Datta *et al.* 2006).

The properties of HUVEC ECM have also been investigated. Enhanced osteogenic differentiation of human BM MSC was observed in a beta-tricalcium phosphate scaffold incorporated with HUVEC ECM (Kang *et al.* 2012). Another study from Gong and co-workers demonstrated that HUVEC ECM enhanced adhesion, proliferation and endothelial differentiation of stem cells from exfoliated deciduous teeth (Gong *et al.* 2017*)*.

In this study we evaluated the effect of different compositions of decellularized cultured cell-derived ECM produced from MSC, HUVEC and co-culture of MSC:HUVEC (MSC:HUVEC 1:1, 1:3, 3:1) on cell proliferation, osteogenic differentiation and angiogenic properties of human BM MSC and we hypothesized that a MSC:HUVEC ECM could stimulate both osteogenesis and angiogenic properties and, consequently, represent a new strategy for enhanced bone healing and accelerated vascularization of the defect site.

Here we demonstrate that the decellularized ECM deposited by co-culture of BM MSC and HUVEC (MSC:HUVEC ECM) is able to mimic the native bone niche and this new strategy achieves synergistic effects on promoting the angiogenic features and osteogenic differentiation of BM MSC. Our results are consistent with recent suggestions that co-culture systems of MSC and EC can, indeed, incite a cellular crosstalk through the paracrine and juxtacrine cellular interaction or vesicle trafficking between MSC and EC, leading to the modulation of the angiogenic response (Aguirre *et al.* 2010, Nassiri *et al.* 2014). Furthermore, it has been demonstrated that co-culture of MSC and HUVEC can form a vascular tissue-like network *in vitro* through the induction of VEGF production (Greillier *et al.* 2009). Conceptually, our findings are consistent with the observation that, during osteogenic differentiation, osteoblasts secrete VEGF, which can be used by EC, while EC secrete BMP, which in turn can be used by osteoblasts (Zhao *et al.* 2012). Moreover, HUVEC are also known to enhance the osteogenic differentiation of BM MSC (Lee *et al.* 2017). Therefore, the co-culture of both cell types hold the promise of activating multiple signaling pathways to enhance the biological effects of MSC, namely in the context of bone regeneration. We hypothesized that decellularized ECM deposited by co-culture of MSC and HUVEC (MSC:HUVEC ECM) would mimic, in a more reliable way, the native bone niche and this strategy would achieve synergistic effects on angiogenesis and tissue regeneration by osteogenic differentiation of MSC.

The optimal cell ratio in co-cultures of human MSC and EC is still under investigation, although for some of the co-cultures (e.g. BM MSC/HUVEC) a 1:1 ratio was reported to be optimal for both osteogenesis and angiogenesis (Ma *et al.* 2011). Therefore, we decided to investigate if ECM produced by a co-culture of BM MSC with HUVEC at different ratios would influence the biological response of MSC. The MSC:HUVEC ratios 1:1, 1:3 and 3:1 were used to produce the respective cell-derived ECM. The results presented here show that decellularized cultured cell-derived ECM, as a culture substrate, promoted cell proliferation, osteogenic differentiation and enhanced the angiogenic properties of BM MSC, compared to TCP.

The comparison of BM MSC growing on different cultured cell-derived ECM substrates demonstrated that cells reached similar cell numbers for all dECM, although higher number of cells was obtained on dECM

substrates compared with TCP (no ECM, negative control) (Figure V.6). All groups of dECM substrates supported the *in vitro* proliferation of BM MSC. The underlying mechanism responsible for the proliferation supportive activity of the ECM derived from stem cells is not known. However, we consider that ECM can provide anchorage to growth factors and cytokines, which can be presented to cells in a physiological way, stimulating cell proliferation. Moreover, ECM elements derived from key cellular sources can slowly release bioactive factors into the microenvironment. We, therefore, hypothesize that cultured cell-derived ECM proteins retained after a decellularization process, as well as sequestered growth factors, will contribute to the enhancement of the proliferation of BM MSC, although the exact underlying mechanism requires further study.

Moreover, for all conditions tested, the obtained dECM enhanced the osteogenic differentiation of BM MSC, characterized by the increase of alkaline phosphatase activity and calcium levels in comparison with cells cultured on TCP. In particular, MSC:HUVEC-derived ECM improved the osteogenic potential of BM MSC, suggested by the enhancement of mineralization and ALP activity levels. BM MSC cultured on dECM significantly increased the expression of osteogenic genes, such as *Col I, Runx2* and *ALP* (Figure V.7d). Interestingly, MSC cultured on all MSC:HUVEC ECM upregulated expression of late osteogenic genes, such as OPN and OC, suggesting that, regardless of the cell ratio, cells differentiated on MSC:HUVEC-derived ECM were producing a more mature matrix and, likely, accelerating the mechanism of differentiation. These results were also confirmed by histochemical staining: Von Kossa staining was enhanced with BM MSC differentiated on MSC:HUVEC-derived ECM (all ratios) compared with other ECM substrates (Figure V.7a). Furthermore, calcium levels were also higher for MSC:HUVEC-derived ECM (Figure V.7c). These results suggest that MSC:HUVEC ECM enhanced mineralization when used as a substrate for BM MSC adhesion and spreading. In terms of osteogenesis, no clear differences were observed between ECM obtained from co-cultures of MSC:HUVEC at different ratios.

In this study, the dECM obtained were characterized by immunostaining and SEM. Immunostaining of ECM proteins revealed the fibrillar organization and web-like structure of some ECM proteins, such as collagen I, collagen IV, fibronectin and laminin (Figure V.3). Interestingly, immunostaining of osteocalcin was more abundant in cultures where MSC:HUVEC-derived ECM (all ratios) compared with the other dECM. We thus hypothesized that some possible osteocalcin, a late marker of osteogenesis (Zoch *et al.* 2016), present in the MSC:HUVEC ECM facilitated the enhancement of osteogenic differentiation of BM MSC observed when cells were cultured on MSC:HUVEC-derived ECM substrates, inducing the production of a more mature mineralized matrix. However, further quantitative studies are needed to determine the amount of osteocalcin present in those dECM. SEM images revealed that dECM from different cell types present a different structure (Figure V.5). BM MSC-derived ECM presented a more fibrillar structure compared with HUVEC-derived ECM where a globular pattern was observed. Notably, only MSC:HUVEC (3:1)-derived ECM demonstrated a fibrillar architecture, similar to MSC-derived ECM. We believe that the higher amount of BM MSC available in the condition MSC:HUVEC (3:1) contributed to the fibrillar structure of this dECM. On the other hand, MSC:HUVEC (1:1) and MSC:HUVEC (1:3)-derived ECM presented a more globular morphology with only few fibrillar structures observed.

Angiogenesis is the process of formation of new blood vessels from pre-existing vasculature and plays an important in bone healing (Mongiat *et al.* 2016). BM MSC secrete angiogenic factors that improve the

formation of a capillary-like structure from HUVEC (Wang *et al.* 2012). Our results demonstrate that conditioned medium obtained from cultures where a MSC:HUVEC (1:3)-derived ECM is used allowed the formation of a robust network of HUVEC, compared with conditioned medium from cells cultured on all the others dECM and on substrates without ECM coating (TCP, control) (Figure V.8a). These results indicate that MSC:HUVEC (1:3)-derived ECM is able to enhance the pro-angiogenic capacity of BM MSC. Different studies have shown that the deposition of fibronectin in a 3D cell-derived ECM appears to be imperative for matrix assembly and vascular morphogenesis (Mongiat *et al.* 2016). Consistent with the study by Mongiat and collaborators, immunostaining for fibronectin in our study confirmed and this protein was strongly detected in the MSC:HUVEC-derived ECM (all ratios), compared with the other dECM (Figure V.3). MSC:HUVEC (1:3)-derived ECM promoted better formation of tubular-like structures by HUVEC than TCP, likely due to some pro-angiogenic molecules embedded with the dECM, such as VEGF (Martino *et al.* 2015). Further studies should analyze the differences in what concerns ECM proteins, growth factors and glycosaminoglycans composition for the different proportions of proteins in dECM.

Overall, our findings demonstrate that MSC:HUVEC-derived ECM enhances the osteogenic and angiogenic potential of BM MSC suggesting the use of MSC:HUVEC ECM as a new strategy to improve clinical outcomes of bone regeneration by improving the biological activity of tissue engineered constructs. Moreover, the ECM obtained from co-cultures at a ratio MSC:HUVEC (1:3) resulted in the best angiogenic response. To the best of our knowledge, this is the first study that demonstrates that dECM derived form a co-culture of MSC:HUVEC influenced the osteogenic and angiogenic capabilities of BM MSC. Herein, we showed that all the dECM enhanced cell proliferation, however mineralization and angiogenic potential were only enhanced when cells were cultured on MSC:HUVEC ECM.

Cultured cell-derived ECM appears to be a successful technology to enhance osteogenesis and angiogenesis, however some limitations remain. In order to prepare the cell-derived ECM, cells have to be isolated and cultured *ex-vivo* with additional costs. Moreover, the exact mechanism by which cultured cell-derived ECM enhances the proliferation and osteogenic differentiation of BM MSC is not fully understood. Although this work did not quantify the relative amounts of ECM proteins, it demonstrates the impact of the cell type used on matrix composition. Future research should focus on identifying and quantifying the key extracellular proteins present in the different cell-derived ECM through proteomics approaches, as well as analyzing the activation of intracellular signaling pathways. However, despite these limitations, our findings, together with other results in the literature, strongly suggest that BM MSC are highly responsive to their ECM environment, which may be manipulated for their optimal application in bone repair and regeneration. Additionally, in contrast to TCP, dECM is able to more closely mimic the bone niche where MSC reside *in vivo*, reproducing, in a more robust way, the architecture of native ECM and providing a more beneficial microenvironment for osteogenic differentiation.

In summary, our data demonstrate that an ECM derived from a co-culture of MSC:HUVEC produces an osteogenic and angiogenic response from BM MSC, suggesting the potential use of this matrix as a therapeutic product to be used for bone regeneration applications and as a new strategy to enhance bone healing while accelerating the vascularization of the defect site. In this context, *in vivo* studies are needed to further validate the translational application of these findings.

V.5. References

Aguirre A., Planell J.A., Engel E. Dynamics of bone marrow-derived endothelial progenitor cell/mesenchymal stem cell interaction in co-culture and its implications in angiogenesis. *Biochem. Biophys. Res. Commun.*, **400**, 284–291 (2010).

Badylak S., Liang A., Record R., Tullius R., Hodde J. Endothelial cell adherence to small intestinal submucosa: an acellular bioscaffold. *Biomaterials*, **20**, 2257-2263 (1999).

Badylak S.F., Freytes D.O., Gilbert T.W. Extracellular matrix as a biological scaffold material: structure and function. *Acta Biomater.,* **5**, 1-13 (2009).

Ball S.G., Schuttleworth A.C., Kielty C.M. Direct cell contact influences bone marrow mesenchymal stem cell fate. *Int. J. Biochem. Cell Biol.*, **36**, 714-727 (2004).

Bose S., Roy M., Bandyopadhyay A. Recent advances in bone tissue engineering scaffolds. *Trends Biotechnol.*, **30**, 546-554 (2012).

Campana V., Milano G., Pagano E., Barba M., Cicione C., Salonna G., Lattanzi W. Logroscino G. Bone substitutes in orthopaedic surgery: from basic science to clinical practice. *J. Mater. Sci. Mater. Med.*, **25**, 2445-2461 (2014).

Chen X.D., Dusevich V., Feng J.Q., Manolagas S.C., Jilka R.L. Extracellular matrix made by bone marrow cells facilitates expansion of marrow-derived mesenchymal progenitor cells and prevents their differentiation into osteoblasts. *J. Bone Miner. Res.*, **22**, 1943-1956 (2007).

Cheng H.W., Tsui Y.K., Cheung K.M., Chan D., Chan B.P. Decellularization of chondrocytec-encapsulated collagen microspheres: a three-dimensional model to study the effects of acellular matrix on stem cell fate. *Tissue Eng. Part C Methods*, **15**, 697-706 (2009).

Cheng N.C., Estes B.T., Awad H.A., Guilak, F. Chondrogenic differentiation of adipose-derived adult stem cells by a porous scaffold derived from native articular cartilage extracellular matrix. *Tissue Eng Part A*, **15**, 231-241 (2009b).

Choi K.H., Choi B.H., Park S.R., Kim B.J., Min B.H. The chondrogenic differentiation of mesenchymal stem cells on an extracellular matrix scaffold derived from porcine chondrocytes. *Biomaterials*, **31**, 5355-5365 (2010).

Crapo P.M., Gilbert T.W., Badylak S.F. An overview of tissue and whole organ decellularization processes. *Biomaterials*, **32**, 3233-3243 (2011).

Datta N., Holtorf H.L., Sikavitsas V.I., Jansen J.A., Mikos A.G. Effect of bone extracellular matrix synthesized in vitro on the osteoblastic differentiation of marrow stromal cells. *Biomaterials*, **26**, 971-977 (2005).

Datta N., Pham Q.P., Sharma U., Sikavitsas V.I., Jansen J.A., Mikos A.G. In vitro generated extracellular matrix and fluid shear stress synergistically enhance 3D osteoblastic differentiation. *Proc. Natl. Acad. Sci. U.S.A*, **103**, 2488-2493 (2006).

Engler A.J., Sen S., Sweeney H.L., Discher D.E. Matrix elasticity directs stem cell lineage specification. *Cell*, **126**, 677-689 (2006).

Fitzpatrick L. E., McDevitt T.C. Cell-derived matrices for tissue engineering and regenerative medicine application. *Biomater. Sci.*, **3**, 12-24 (2015).

Giancotti F.G., Ruoslahti E. Integrin signaling. *Science,* **285**, 1028-1032 (1999).

Gong T., Heng B.C., Xu J., Zhu S., Yuan C., Lo E.C., Zhang C. Decellularized extracellular matrix of human umbilical vein endothelial cells promotes endothelial differentiation of stem cells from exfoliated deciduous teeth. *J. Biomed. Mater. Res. A.*, **105**, 1083-1093 (2017).

Grellier M., Ferreira-Tojais N., Bourget C., Bareille R., Guillemot F., Amédée J. Role of vascular endothelial growth factor in the communication between human osteoprogenitors and endothelial cells. *J. Cell. Biochem.*, **106**, 390–398 (2009).

Hoshiba T., Cho C.S., Murakawa A., Okahata Y., Akaike T. The effect of natural extracellular matrix deposited on synthetic polymers on cultured primary hepatocytes. *Biomaterials*, **27**, 4519-4528 (2006).

Hoshiba T., Lu H., Kawazoe N., Chen G. Decellularized matrices for tissue engineering. Expert Opin. Biol. Ther., **10**, 1717-1728 (2010).

Hynes R.O. Extracellular matrix: not just pretty fibrils. *Science*, **326**, 1216-1219 (2009).

Hynes R.O. Integrins: bidirectional, allosteric signaling machines. *Cell*, **20**, 673-687 (2002).

Kang Y., Kim S., Bishop J., Khademhosseini A., Yang Y. The osteogenic differentiation of human bone marrow MSCs on HUVEC-derived ECM and β-TCP scaffold. *Biomaterials*, **33**, 6998-7007 (2012).

Khademhosseini A., Vacanti J.P., Langer R. Progress in tissue engineering. *Sci. Am.*, **300**, 64-71 (2009).

Kleinman H.K., Luckenbill-Edds L., Cannon F.W., Sephel G.C. Use of extracellular matrix components for cell culture. *Anal. Biochem.*, **166**, 1-13 (1987).

Ku Y., Chung C.P., Jang J.H. The effect of the surface modification of titanium using a recombinant fragment of fibronectin and vitronectin on cell behavior. *Biomaterials*, **26**, 5153-5157 (2005).

Kundu A.K., Putnam A.J. Vitronectin and collagen I differentially regulate osteogenesis in mesenchymal stem cells. *Biochem. Biophys. Res. Commun.*, **347**, 347-357 (2006).

Kusuma G.D., Brennecke S.P., O'Connor A.J., Kalionis B., Heath D.E., Decellularized extracellular matrices produced from immortal cell lines derived from different parts of the placenta support primary mesenchymal stem cell expansion. PLoS One, **12**, e0171488 (2017).

Lai Y., Sun Y., Skinner C.M., Son E.L., Lu Z., Tuan R.S., Jilka R.L., Ling J. and Chen X.D. Reconstitution of marrow-derived extracellular matrix ex vivo: a robust culture system for expanding large-scale highly functional human mesenchymal stem cells. *Stem Cells Dev.,* **19**, 1095-1107 (2010).

Lee M.K., Lin S.P., HuangFu W.C., Yang D.S., Liu I.H. Endothelial-derived extracellular matrix ameliorate the stemness deprivation during *ex vivo* expansion of mouse bone marrow-derived mesenchymal stem cells. PLoS One, **12**, e0184111 (2017).

Li J., Hansen K.C., Zhang Y., Dong C., Dinu C.Z., Dzieciatkowska M., Pei M., Rejuvenation of chondrogenic potential in a young stem cell microenvironment. *Biomaterials,* **35**, 642-653 (2014).

Liao J., Guo X., Grande-Allen K.J., Kasper F.K., Mikos A.G. Bioactive polymer/extracellular matrix scaffolds fabricated with a flow perfusion bioreactor for cartilage tissue engineering. *Biomaterials,* **31**, 8911-8920 (2010).

Lin H., Yang G., Tan J., Tuan R.S., Influence of decellularized matrix derived from human mesenchymal stem cells on their proliferation, migration and multi-lineage differentiation potential. *Biomaterials,* **33**, 4480–4489 (2012).

Lu H., Hoshiba T., Kawazoe N., Kod I., Song M., Chena G. Cultured cell-derived extracellular matrix scaffolds for tissue engineering. Biomaterials, **32**, 9658-9666 (2011).

Ma J., van den Beucken J.J., Yang F., Both S.K., Cui F.Z., Pan J., Jansen J.A. Coculture of osteoblasts and endothelial cells: optimization of culture medium and cell ratio. *Tissue Eng. Part C: Methods*, **17**, 349-357 (2011).

Mistry A.S., Mikos A.G. Tissue engineering strategies for bone regeneration. *Adv. Biochem. Eng. Biotechnol.*, **94**, 1-22 (2005).

Mongiat M., Andreuzzi E., Tarticchio G., Paulitti A., Extracellular matrix, a hard player in angiogenesis. *Int. J. Mol. Sci.,* **17**, e1822 (2016).

Nassiri S.M., Rahbarghazi R. Interactions of mesenchymal stem cells with endothelial cells, *Stem Cells Dev.*, **23**, 319-332 (2014).

Noh Y.K., Du P., Kim I.G., Ko J., Kim S.W., Park K. Polymer mesh scaffold combined with cell-derived ECM for osteogenesis of human mesenchymal stem cells. *Biomater. Res.*, **20**, 1-7 (2016).

Pham Q.P., Kasper F.K., Scott Baggett L., Raphael R.M., Jansen J.A., Mikos A.G. The influence of an in vitro generated bone-like extracellular matrix on osteoblastic gene expression of marrow stromal cells. *Biomaterials*, **29**, 2729-2739 (2008).

Ragetly G., Griffon D.J., Chung Y.S. The effect of type II collagen coating of chitosan fibrous scaffolds on mesenchymal stem cell adhesion and chondrogenesis. *Acta Biomater.*, **6**, 3988-3997 (2010).

Ravindran S., Gao Q., Kotecha M., Magin R.L., Karol S., Bedran-Russo A., George, A. Biomimetic extracellular matrix-incorporated scaffold induces osteogenic gene expression in human marrow stromal cells. *Tissue Eng. Part A*, **18**, 295-309 (2012).

Reilly G.C., Engler A.J. Intrinsic extracellular matrix properties regulate stem cell differentiation. *J. Biomech.*, **43**, 55-62 (2010).

Roehlecke C., Witt M., Kasper M., Schulze E., Wolf C., Hofer A., Funk R.W. Synergistic effect of titanium alloy and collagen type I on cell adhesion, proliferation and differentiation of osteoblast-like cells. *Cells Tissues Organs*, **168**, 178–87 (2001).

Skora J., Pupka A., Dorobisz A., Barc P., Korta K., Dawiskiba, T. Evaluation of the humoral and cellular immune responses after implantation of a PTFE vascular prosthesis. *Postepy. Hig. Med. Dosw. (Online)*, **66,** 469-474 (2012).

Sun H., Qu Z., Guo Y., Zang G., Yang B. In vitro and in vivo effects of rat kidney vascular endothelial cells on osteogenesis of rat bone marrow mesenchymal stem cells growing on polylactide-glycoli acid (PLGA) scaffolds. *Biomed. Eng. Online*, **6**, 41 (2007).

Sun Y., Li W., Lu Z., Chen R., Ling J., Ran Q., Jilka R.L., Chen X.D. Rescuing replication and osteogenesis of aged mesenchymal stem cells by exposure to a young extracellular matrix. *FASEB J.*, **25**, 1474-1485 (2011).

Vleggeert-Lankamp C.L., Pêgo A.P., Lakke E.A., Deenen M., Marani E., Thomeer R.T. Adhesion and proliferation of human Schwann cells on adhesive coatings. *Biomaterials*, **25**, 2741-2751 (2004).

Wolchok J.C., Tresco P.A. The isolation of cell derived extracellular matrix constructs using sacrificial open-cell foams. *Biomaterials*, **31**, 9595-9603 (2010).

Yang S., Wei D., Wang D., Phimphilai M., Krebsbach P.H., Franceschi R.T. In vitro and in vivo synergistic interactions between the Runx2/Cbfa1 transcription factor and bone morphogenetic protein-2 in stimulating osteoblast differentiation. *J. Bone Miner. Res.* **18**, 705-715 (2003).

Yang Y., Lin H., Shen H., Wang B., Lei G., Tuan R.S. Mesenchymal stem cell-derived extracellular matrix enhances chondrogenic phenotype of and cartilage formation by encapsulated chondrocytes in vitro and in vivo. *Acta Biomater.* ,**15**, 71-82 (2018).

Zhang H., Ahmad M., Gronowicz G. Effects of transforming growth factor-beta 1 (TGF-beta1) on in vitro mineralization of human osteoblasts on implant materials. *Biomaterials*, **24**, 2013-2020 (2003).

Zhang W., Zhu Y., Li J. Guo Q., Peng J., Liu S., Yang J., Wang Y. Cell-derived extracellular matrix: basic characteristics and current applications in orthopedic tissue engineering. *Tissue Eng. Part B. Rev.,* **22**, 193-207 (2016).

Zhao X., Liu L., Wang F.K., Zhao D.P., Dai X.M., Han X.S. Coculture of vascular endothelial cells and adipose-derived stem cells as a source for bone engineering. *Ann. Plast. Surg.*, **69**, 91-98 (2012).

CHAPTER VI – Cell-derived extracellular matrix electrospun fibers for bone tissue engineering applications

Outline

Extracellular matrix (ECM) is composed by a complex and highly organized assembly of fibrillar proteins, matrix macromolecules and associated growth factors. Cell-derived ECM has been employed as scaffold for tissue engineering, creating a biomimetic microenvironment that provides physical, chemical and mechanical cues for cells and supports cell adhesion, proliferation, migration and differentiation by mimicking its *in vivo* microenvironment.

Despite the enhanced bioactivity of cell-derived ECM, its application as a scaffold to regenerate hard tissues such as bone is still hampered by its insufficient mechanical properties. The combination of cell-derived ECM with synthetic biomaterials might result in an effective strategy to enhance scaffold mechanical properties and structural support.

Electrospinning has been used in bone tissue engineering to fabricate fibrous and porous scaffolds, mimicking the hierarchical organized fibrillar structure and architecture found in the bone ECM. However, although the structure of the scaffold might be similar to the ECM architecture, most of these electrospun scaffolds failed to achieve functionality due to the lack of bioactivity and osteoinductive factors.

In this study, we fabricate cell-derived ECM electrospun poly(ε-caprolactone) (PCL) scaffolds produced from ECM derived from mesenchymal stem/stromal cells (MSC), human umbilical vein endothelial cells (HUVEC) and their co-culture (MSC:HUVEC). We hypothesize that the cell-derived ECM incorporated into the PCL fibers will enhance biofunctionality of the scaffold. Therefore, the aims of this study were to fabricate and characterize cell-derived ECM electrospun PCL scaffolds and assess their ability to enhance osteogenic differentiation of MSC, envisaging bone tissue engineering applications. In particular, we investigate different compositions of ECM produced from different cell sources and evaluate their biological effect. Our findings demonstrate that all cell-derived ECM electrospun scaffolds promoted significant cell proliferation compared to PCL alone, while presenting similar physical/mechanical properties. Additionally, MSC:HUVEC ECM electrospun scaffolds significantly enhanced osteogenic differentiation of MSC as verified by increased ALP activity and osteogenic gene expression levels. To our knowledge, these results describe the first study suggesting that MSC:HUVEC ECM might be developed as a biomimetic electrospun scaffold for bone tissue engineering applications.

VI.1. Introduction

The extracellular matrix (ECM) is composed of a complex and highly organized assembly of molecules, such as fibrillar proteins (e.g. collagens, fibronectin, laminin), glycosaminoglycans (e.g. heparin sulfate, chondroitin sulfate, hyaluronan), proteoglycans (e.g. decorin, versican, aggrecan) and matricellular proteins (e.g. osteopontin, thrombospondin) (Badylak *et al.* 2009, Kleinman *et al.* 1987). Although being composed mainly by the above-mentioned components, ECM composition and distribution of the matrix molecules vary considerably with the type of tissue and can be altered during the stages of tissue development and due to some pathological conditions (Badylak *et al.* 2009).

Currently, tissue engineering and regenerative medicine is focused on developing biomaterials that can mimic the native ECM by incorporating features that recapitulate its architecture, structure, composition and functionality, recreating the *in vivo* microenvironment. In fact, some isolated ECM proteins, such as collagen, fibronectin, vitronectin (Mistry *et al.* 2005, Khademhosseini *et al.* 2009, Kundu *et al.* 2006, Ku *et al.* 2005), have been used in the design of new biomaterials. However, these materials fail to achieve the molecular complexity of the native ECM. Moreover, most of the secreted factors and ECM molecules are still unknown or have an unknown biological concentration thus hindering the development of optimized cell culture media.

Therefore, cell-derived ECM appears a promising alternative approach to better mimic the *in vivo* microenvironment of cells. Cell-derived ECM serves as a reservoir of multiple cytokines and growth factors, such as factors involved in inflammation (*i.e.* MCP-1, M-CSF, IL-8), angiogenesis (*i.e.* VEGF-alpha) and remodeling (*i.e.* MMP-13, OPG) (Bourgine *et al.* 2014, Hynes *et al.* 2009).

Cell type is essential to determine the resulting composition of the ECM, since cells derived from different tissues typically yield matrices that mimic the composition of its natural tissue matrix (Fitzpatrick *et al.* 2015). In fact, mesenchymal stem/stromal cells (MSC) are a common material to obtain cell-derived ECM due to their ability to deposit ECM that can mimic different tissues depending on culture conditions, such as bone, cartilage and adipose tissue. Moreover, MSC-derived ECM has been shown to rejuvenate aged mouse stem cells and enhance their lineage differentiation ability (Li *et al.* 2014). Decellularized ECM from human MSC cultures have been shown to promote MSC proliferation (Lai *et al.* 2010). Human umbilical vein endothelial cells (HUVEC) have also been investigated to enhance osteogenic differentiation of MSC. Kang and colleagues have fabricated a β-TCP scaffold incorporated with HUVEC ECM, improving the osteogenic capacity of these scaffolds (Kang *et al.* 2012). Moreover, recent research has focused on the use of co-culture systems and co-cultured MSC and HUVEC were shown to enhance osteogenic differentiation of MSC. For instance, endothelial cells secrete factors, such as bone morphogenetic proteins (BMP) (Zhao *et al.* 2012) that are beneficial for osteogenic differentiation of MSC. To cope with this and with the advantage of affording a more reliable bone marrow niche *in vivo,* we produced ECM derived from co-cultured MSC and HUVEC, expecting to enhance the proliferation and osteogenic differentiation of MSC. In fact, our previous results showed that MSC:HUVEC ECM could stimulate osteogenic response of MSC, being an ideal material to be used for bone regeneration applications.

Although cell-derived ECM have shown improvements on biological activity, their mechanical properties are still insufficient to support and regenerate hard tissues such as bone (Hong *et al.* 2011, Bracaglia *et al.* 2015). Therefore, cell-derived ECM can be combined with synthetic biomaterials to improve the mechanical properties and enhance cell-material interactions. In particular, electrospinning has been often used to fabricate fibrous

and porous scaffolds from a variety of natural and synthetic materials for a broad range of tissue engineering applications (Li *et al.* 2002, Sill *et al.* 2008, Yoshimoto *et al.* 2003). Moreover, the high surface area, porosity and interconnectivity of the electrospun fibers are favorable for cell attachment and proliferation and also enable nutrient and waste exchange (Li *et al.* 2002, Bhardwaj *et al.* 2010). Electrospun fibers are highly relevant for bone tissue engineering due to the fact that their architecture mimics the hierarchical organized micro/nano scale fibrous structure found in the native bone ECM (Reznikov *et al.* 2014).

Poly (ε-caprolactone) (PCL) is a FDA-approved, biodegradable and biocompatible synthetic material that has been extensively used in biomedical applications (Cipitria *et al.* 2011). Due to its semi-crystalline and hydrophobic nature, PCL has a slow degradation rate and mechanical properties suitable for different tissue engineering settings, with special relevance in repairing defects in hard and slow regenerating tissue like bone (Engelberg & Kohn 1991, Middleton & Tripton 2000, Nair & Laurencin 2007). Accordingly, PCL electrospun fibrous scaffolds were previously used in bone repair either in their pristine form or in different coupled strategies to improve scaffold osteoinductive capacity. Such coupled strategies include fiber surface modification with bioactive coatings or immobilized biomolecules, or blending with other copolymers (Yoshimoto *et al.* 2003, Mattanavee *et al.* 2009, Kim *et al.* 2014, Yao *et al.* 2017).

Cell-derived ECM has been used in combination with electrospinning techniques to develop scaffolds that mimic not only the architecture and structure of ECM, but also its composition (Shtrichman *et al.* 2014, Jeon *et al.* 2016, Fu *et al.* 2018, Thakkar *et al.* 2013). Most of the studies reported in the literature developed strategies to decorate electrospun nanofibers with ECM by seeding cells onto the fibers, allowing them to grow followed by decellularization to obtain the ECM-decorated electrospun fibers. A different approach has also emerged in which the cell-derived ECM is produced in regular *in vitro* cell culture dishes, collected and lyophilized to generate ECM powder that can be added to the polymer solution and electrospun to generate fibers with incorporated cell-derived ECM particles (Thakkar *et al.* 2013). Accordingly, we expected that by directly incorporating cell-derived ECM into PCL electrospun fibers, we could develop hybrid bioactive scaffolds with the appropriate structural and mechanical support using a synthetic material and ECM-mediated signaling to target different cellular processes, such as proliferation, osteogenic differentiation and angiogenesis.

The aim of this study was to develop cell-derived ECM PCL electrospun scaffolds derived from different cell sources: MSC, HUVEC and co-culture of MSC:HUVEC and test their potential in bone regeneration. The scaffolds were characterized in terms of their structural, thermal and mechanical properties. Their ability to support MSC osteogenic differentiation was evaluated by assessing cell proliferation, biochemical activity and gene expression. To our knowledge, this is the first study in which ECM derived from a co-culture of MSC and HUVEC was incorporated into PCL electrospun fibers to develop a bioactive scaffold targeting bone repair applications.

VI.2. Materials & Methods

VI.2.1. Cell culture

Human bone marrow MSC were obtained from Lonza (Basel, Switzerland). Human bone marrow MSC were thawed and plated on T-75 cm^2 flasks using low-glucose Dulbecco's Modified Eagle Medium (DMEM:Gibco, Grand Island, NY) supplemented with 10% fetal bovine serum (FBS, Gibco) and 1% penicillin-streptomycin (Pen-Strep, Gibco) and kept at 37ºC, 5% CO_2 and 21% O_2 in a humidified atmosphere. HUVEC were purchased from Lonza and maintained in commercial endothelial growth medium-2 (EGM-2, Lonza) and kept at 37ºC, 5% CO_2 and 21% O_2 in a humidified atmosphere. Medium renewal was performed every 3-4 days. All the experiments were performed using cells between passages 3 and 5.

VI.2.2. Decellularized cell-derived ECM preparation

MSC, HUVEC and co-culture of MSC:HUVEC (1:1) were seeded at 5000 cells/cm^2. MSC were incubated with DMEM+10% FBS, HUVEC with EGM-2 growth medium and co-culture of MSC:HUVEC was cultured in a combination of DMEM+10% FBS and EGM-2 (1:1). Cells were expanded for 7-10 days and medium was changed every 3-4 days. After reaching confluency, medium was discarded and cells were washed in Phosphate buffered saline (PBS, Gibco). ECM isolation was performed by decellularization techniques using a 20 mM ammonium hydroxide (NH_4OH) + 0.5% Triton X-100 (Sigma-Aldrich, St.Louis, MO) solution, based on previously reported methods (Kang *et al.* 2012, Gibson *et al.* 2014). The solution was added to the culture and incubated for 5 min at room temperature. After microscopic confirmation of complete cell lysis and presence of intact ECM on the surface of the wells, ECM was gently washed 3 times with distilled water. After that, ECM layer was detached from the well using a cell scrapper and collected in falcon tubes. The different cell-derived ECM powders to be further used in electrospinning procedure were obtained after freeze-drying.

VI.2.3. Fabrication of cell-derived ECM electrospun PCL fibers

Poly (ε-caprolactone) (PCL, Mn=80000 Da, Sigma-Aldrich) was dissolved at 11% wt/v in 1,1,1,3,3,3-hexafluoro-2-propanol (HFIP, Sigma-Aldrich) under agitation overnight at room temperature. Lyophilized cell-derived ECM was incorporated into the PCL solution (0.25 mg/ml) followed by agitation overnight producing a final homogeneous solutions of PCL 11% wt/v-0.025%wt/v ECM (in HFIP). The fibrous scaffolds were fabricated by electrospinning. Therefore, 5 ml of PCL-ECM solution was loaded into a syringe placed in a pump and connected to a PTFE tube, which was attached on the other end to a 21G metallic needle (0.8 mm diameter). A controlled flow rate of 3 ml/h and an applied voltage of 20 kV were used, creating a potential difference between the needle and a grounded aluminum foil collector placed at a distance of 21 cm from the needle tip. The different PCL-ECM electrospun fiber mats were produced under the same process parameters and ambient conditions (temperature and relative humidity varied between 19-21°C and 20-25%, respectively) for

approximately 60 min to ensure scaffold thickness. An overview of the procedure to fabricate cell-derived ECM microfibrous scaffolds is presented in Figure VI. 1.

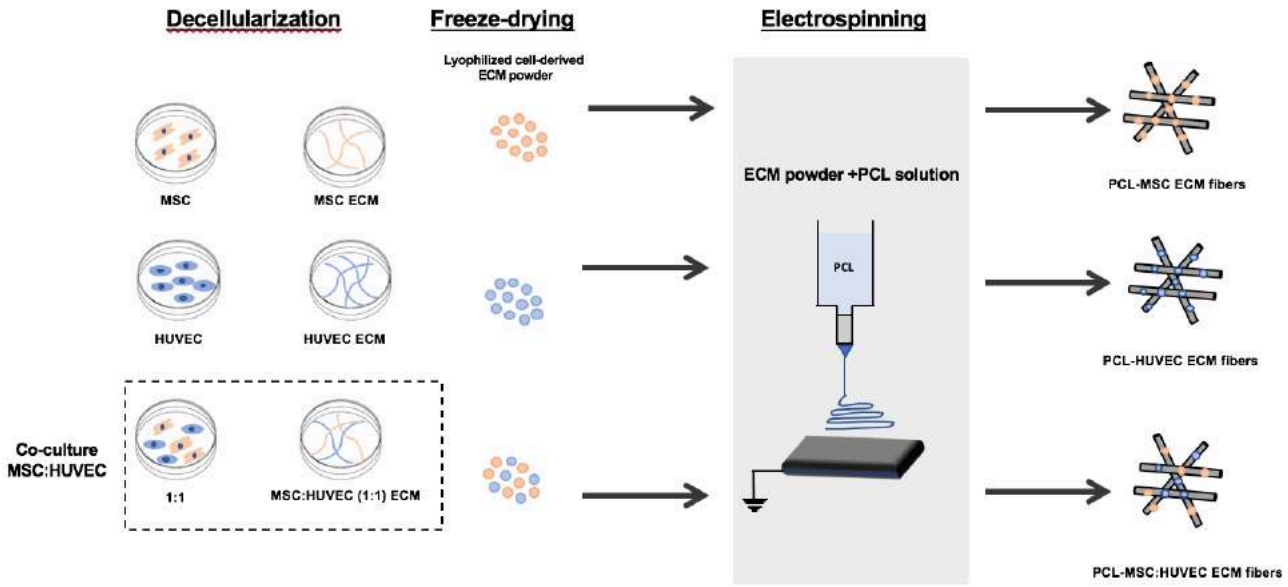

Figure VI.1. The schemata of the experimental procedure for the fabrication of cell-derived ECM microfibrous scaffolds.

VI.2.4. Characterization of cell-derived ECM electrospun scaffolds

VI.2.4.1. Scanning electron microscopy analysis

The morphological and structural characterization of the PCL-ECM electrospun fibers was performed using a field emission scanning electron microscope (FE-SEM, FEI-Versa 3D Dual Beam, Hillsboro). Prior to imaging, samples were mounted on a holder and sputter-coated with a thin layer of 60% gold-40% palladium (Au-Pd). Samples were imaged at several magnifications using an accelerating voltage of 2-3 kV. The average fiber diameters and subsequent distributions of PCL-ECM electrospun scaffolds were determined by measuring 100 individual fibers per condition from at least five different SEM images using ImageJ software (NIH).

VI.2.4.2. Picro-sirius red staining

Picro-sirius red stain kit (Abcam, Cambridge, MA) was used to identify collagen components on the PCL-ECM electrospun scaffolds, following the manufacturer's guidelines. Briefly, scaffolds were washed with PBS and incubated with Picro-sirius red solution for 60 min. The samples were rinsed twice with acetic acid solution, once with absolute ethanol and washed three times with PBS. Scaffolds were imaged using a bright field microscope (Olympus IX51 Inverted Microscope, NY USA).

VI.2.4.3. FTIR analysis

Fourier transform infrared (FTIR) (Perkin Elmer Spectrum One FT-IR Spectrometer, USA) was used to identify the functional groups of the different lyophilized cell-derived ECM powder and fibrous scaffolds. Powder cell-derived ECM samples were mixed with potassium bromide (KBr) in pellets before the analysis in transmission mode in the spectral region of 4000-450 cm^{-1} and a resolution of 4 cm^{-1}. Attenuated total reflectance (ATR-FTIR) mode was used to obtain the spectra of the different cell-derived ECM electrospun scaffolds. All spectra were collected between 4000-650 cm^{-1} with a resolution of 4 cm^{-1}.

VI.2.4.4. Differential scanning calorimetry analysis

Pre-weighed samples were hermetically sealed in aluminium pans and subjected to a heating and cooling cycles between -50°C and 100 °C at a constant heating rate of 5 °C/min using a TA Instruments DSC-Q100 apparatus (New Castle, Delaware, USA). Universal Analysis software V4.7A (TA Instruments) was used for data analysis to determine melting and crystallization temperatures.

VI.2.4.5. Mechanical tensile testing

Mechanical properties of cell-derived ECM electrospun scaffolds were tested under uniaxial tensile testing using a mechanical tester (Instron® Model 5843) with a 10 N load cell and a constant displacement rate of 10 mm/min. Five different test specimens (n=5) for each condition were prepared in a rectangular shape with a length of 15 mm, width of 10 mm and a thickness of 0.1 mm. Experimental data was collected and processed using the Bluehill® 2 software. The Young's modulus was determined from the slope of the initial linear strain region (0-15%) of the stress-strain curve. Ultimate tensile strength (UTS) and ultimate elongation were also obtained from the stress-strain curves.

VI.2.5. Cell culture on cell-derived ECM electrospun scaffolds

Prior to cell culture, cell-derived ECM electrospun scaffolds were sterilized by UV exposure for 4 h, placed in ultra-low cell attachment 24-well plates and washed three times with PBS+1% Pen-Strep solution. Then, scaffolds were soaked in culture medium and incubated at 37ºC for 1 h.

Human bone marrow MSC were seeded on cell-derived ECM electrospun PCL scaffolds at a density of 50000 cells per scaffold and incubated for 2 h at 37ºC, 5% CO_2 and 21% O_2 to allow cell attachment. Osteogenic medium composed by DMEM supplemented with 10% FBS, 10 mM β-glycerophosphate (Sigma-Aldrich), 10 nM dexamethasone (Sigma-Aldrich), 50 µg/mL ascorbic acid (Sigma-Aldrich) and 1% penicillin-streptomycin was added to the scaffolds. The metabolic activity of MSC was evaluated using AlamarBlue® cell viability reagent (ThermoFischer Scientific, USA) on days 3, 7, 14 and 21 following the manufacturer's guidelines. Briefly, a 10% AlamarBlue® solution in culture medium was added to the scaffolds and incubated at 37ºC in 5% CO_2 chamber for 3 h. Fluorescence intensity was measured in a microplate reader (SpectraMax M5, Molecular Devices, USA) at an excitation/emission wavelength of 560/590 nm and compared to a calibration curve to

access the number of cells in each scaffold. Four scaffolds were used for each condition and fluorescence was measured in triplicates.

To assess cell morphology, cells were washed twice with PBS, fixed with 4% paraformaldehyde (PFA: Santa Cruz Biotechnology, Dallas, TX, USA) for 20 min and then permeabilized with 0.1% Triton X-100 for 10 min. After permeabilization, cells were incubated with phalloidin-TRITC (Sigma-Aldrich) (dilution 1:250, 2 µg/mL) for 45 min in the dark. Then, cells were washed twice with PBS and counterstained with DAPI (Invitrogen) (1.5 µg/mL) for 5 min and washed with PBS. The fluorescent staining was imaged using a fluorescence confocal microscope (Leica STED TCS SP8 3x, Wetzlar, Germany). Cell morphology along the culture (days 7,14 and 21) was also analyzed by SEM (see Section VI.2.4.1). Fixed cells were stained with 1% (v/v) osmium tetroxide (Sigma-Aldrich) solution for 30 min and washed twice with PBS. After, samples were dehydrated using ethanol gradient solutions (20%, 40%, 60%, 80%, 95% and 100% (v/v)) and finally dried in a critical point dryer (supercritical Automegasamdri 915B, Tousimis, USA) in 100% isopropanol.

VI.2.6. Assessment of MSC osteogenic differentiation on cell-derived ECM electrospun scaffolds

VI.2.6.1. ALP activity assay

After 14 and 21 days of osteogenic differentiation, alkaline phosphate (ALP) activity was detected using a colorimetric ALP kit (BioAssays Systems, Hayward, CA) according to the manufacturer's protocol. Samples were washed with PBS and were incubated in the lysis buffer (0.1% Triton X-100 in PBS) overnight at room temperature. The lysate was added to *p*-nitrophenyl phosphate solution (10mM) provided with the ALP kit. The absorbance was measured on a plate reader (SpectraMax M5, Molecular Devices, USA) at 405 nm and normalized to the total number of cells in each scaffold. Three different scaffolds were used for each condition and absorbance was measured in triplicates.

VI.2.6.2. Calcium assay

Calcium content quantification was determined after 14 and 21 days of MSC osteogenic differentiation on cell-derived ECM electrospun scaffolds. Samples were washed with PBS and incubated with a 0.5 M HCl solution (Sigma-Aldrich) with agitation overnight at 4ºC. The supernatant was used for calcium determination according to the manufacturer's instructions in the calcium colorimetric assay kit (Sigma-Aldrich). Total calcium was calculated from calcium standard solution prepared in parallel. Absorbance at 575 nm was measured for each condition on a plate reader (SpectraMax M5, Molecular Devices, USA) and normalized to the total number of cells. Three scaffolds were used for each condition and absorbance values were measured in triplicates.

VI.2.6.3. Osteogenic staining

After 21 days of osteogenic differentiation, samples were assessed using ALP and Von Kossa stainings and Alizarin Red staining. Cell culture medium was removed and samples were washed once with PBS, and fixed with 4% PFA for 20 min. Afterwards, samples were rinsed in miliQ water during 5 min and incubated with

Fast Violet solution (Sigma-Aldrich) and Naphthol AS-MX Phosphate Alkaline solution (Sigma-Aldrich) in a final concentration of 4% (v/v) for 45 min at room temperature in the dark. In the case of Von Kossa staining, the scaffolds were washed twice with miliQ water and incubated with 2.5% silver nitrate solution (Sigma-Aldrich) for 30 min at room temperature protected from light. Finally, samples were washed three times with miliQ water and imaged using an inverted microscope (Olympus IX51 Inverted Microscope, NY USA). Different scaffold samples were stained with a 2% Alizarin red solution (Sigma-Aldrich) by incubation for 1h at room temperature. After, the scaffolds were washed three times with miliQ water and imaged (Olympus IX51 Inverted Microscope, NY USA). To further confirm the presence of mineral deposits formed after MSC osteogenic differentiation on cell-derived ECM electrospun scaffolds, a 20 mM Xylenol orange solution (Sigma-Aldrich) was added to previously fixed samples and incubated for 1 h at room temperature in the dark. After that, scaffolds were washed with miliQ water, counterstained with DAPI (Invitrogen) (1.5 µg/ml) for 5 min and washed with PBS. The fluorescent staining of the produced minerals was observed by fluorescence microscopy (Olympus IX51 Inverted Microscope, NY USA).

VI.2.6.4. Energy dispersive X-ray (EDX) analysis

Carl Zeiss Supra field emission scanning electron microscope (FESEM, Hillsboro, USA) was used to conduct energy dispersive x-ray spectroscopic (EDX) analysis on the scaffolds after 21 days of MSC osteogenic differentiation. Analysis was performed with an accelerating voltage of 10 kV and a spot size of 120 µm. The presence of mineral elements on the EDX spectra of each sample was analyzed using INCA Microanalysis Suite software.

VI.2.6.5. Quantitative real-time PCR analysis

Total RNA was extracted using the RNeasy Mini Kit (QIAGEN, Hilden, Germany). Briefly, the scaffolds were first incubated in lysis buffer with 200 rpm agitation for 1h at 4ºC. Afterwards, total RNA was isolated according to the manufacturer's protocol and quantified using a Nanodrop (ND-1000 Spectrophotometer, Nanodrop Technologies). cDNA was synthesized from the purified RNA using iScript™ Reverse Transcription Supermix (Bio-Rad, Hercules, CA USA) according to manufacturer's guidelines. Reaction mixtures (20 µl) were incubated in a thermal cycler (Veriti Thermal Cycler, Applied Biosystems, CA USA) for 5 min at 25ºC, 20 min at 46ºC and 1 min at 95ºC and then were maintained at 4ºC. The sequences of the specific primers used are given in table VI.1.

The quantitative reverse transcription-polymerase chain reaction (qRT-PCR) was performed using PowerUp SYBR® Green Master Mix (Applied Biosystems) and StepOnePlus real-time PCR system (Applied Biosystems). All reactions were carried out at 95ºC for 10 min, followed by 40 cycles of 95ºC for 15 sec and 60ºC for 1min. All samples were analyzed in triplicate. Results were analyzed using the $2^{-\Delta\Delta Ct}$ method to determine relative changes in target osteogenic marker gene expression as compared to untreated controls. Target gene expression was primarily normalized to the housekeeping gene glyceraldehyde 3-phosphate dehydrogenase (GAPDH) and then determined as a fold change relative to the baseline expression of that

target gene measured in MSC at day 0 (prior to scaffold seeding). Primer sequences used in the qRT-PCR analysis are presented in Table VI.1.

Table VI.1. Sequences of primers used for qRT-PCR analysis.

Genes	Sequences
GAPDH	For: 5' AAC AGC GAC ACC CAC TCC TC Rev: 5' CAT ACC AGG AAA TGA GCT TGA CAA
Runx2	For: 5' AGA TGA TGA CAC TGC CAC CTC TG Rev: 5' GGG ATG AAA TGC TTG GGA ACT
ALP	For: 5' ACC ATT CCC ACG TCT TCA CAT TT Rev: 5' AGA CAT TCT CTC GTT CAC CGC C
OPN	For: 5' TGT GAG GTG ATG TCC TCG TCT GTA G Rev: 5' ACA CAT ATG ATG GCC GAG GTG A
VEGF	For: 5' TGC CTC AGA AGA GCT GAA AAC Rev: 5' CAC AGA CTC CCT GCT TTT GCT

VI.2.7. Statistical analysis

Each experiment was conducted in triplicate. Statistical analysis of the data was performed using Student's t-test, comparing each condition with the control condition (PCL scaffold) at the same timepoint, using GraphPad Prism version 7. The statistical significance of results is reported at 95% confidence intervals ($P<0.05$).

VI.3. Results

VI.3.1. Lyophilized cell-derived ECM structural characterization

Different cell types (MSC, HUVEC and co-culture of MSC and HUVEC) were cultured to obtain cell-derived ECM. After decellularization treatment, ECM was collected from the flasks and freeze-dried. Microstructural features were observed under SEM microscopy from lyophilized cell-derived ECM powders of different cell types including MSC, HUVEC and co-culture of MSC and HUVEC (Figure VI.2). All the lyophilized ECM produced from different cell types demonstrated similar patterns with a rugged surface. FTIR spectra of lyophilized ECM derived from different cell types, such as MSC, HUVEC and MSC:HUVEC showed different infrared peaks (Figure VI.2). Notably, FTIR spectra of lyophilized MSC:HUVEC ECM demonstrated infrared peaks corresponding to peaks present only in MSC ECM and HUVEC ECM spectra exclusively, indicating the presence of components from both types of ECM.

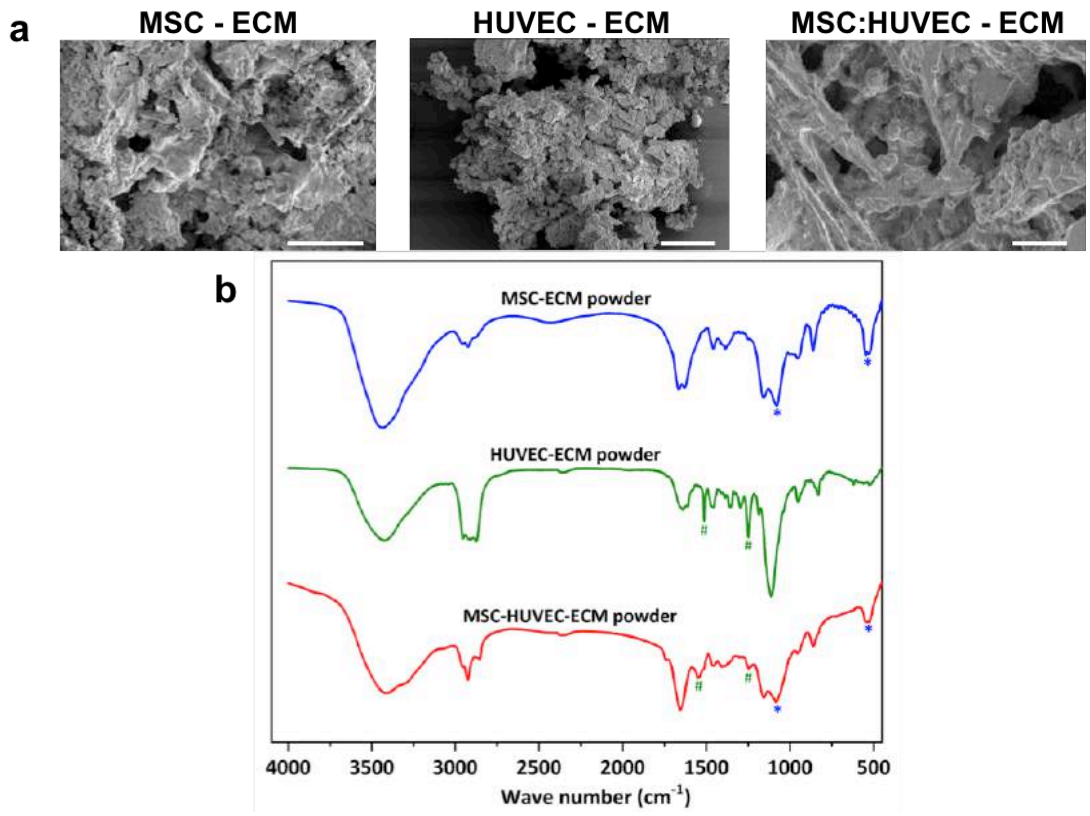

Figure VI.2. SEM images **(a)** and FTIR spectra **(b)** of the different cell-derived ECM powders. Asterisks and pound symbols are used to indicate the unique peaks in the MSC and HUVEC spectra respectively. All four of these unique peaks can also be seen in the IR spectrum of MSC-HUVEC ECM mixture. Scale bars, 10 μm.

VI.3.2. Cell-derived ECM electrospun scaffold characterization

Lyophilized ECM derived from different cell types were incorporated in PCL solution and electrospun to form a fibrous mesh. MSC ECM, HUVEC ECM and MSC:HUVEC ECM PCL electrospun fibers were fabricated and PCL scaffold without ECM was used as a control. SEM micrographs of MSC ECM, HUVEC ECM and MSC:HUVEC ECM PCL electrospun fibers and PCL scaffold without ECM (used as a control) showed that all the scaffolds were highly porous with high interconnectivity and micro/nanoscale structural features. Interestingly, ECM particles were clearly detectable in all the cell-derived ECM electrospun fibers as verified under SEM microscopy analysis (Figure VI.3a). Furthermore, all the fabricated scaffolds were composed mainly of microfibers. The average fiber diameter of electrospun PCL without ECM was 1.86 ± 0.19 μm whereas MSC ECM, HUVEC ECM, MSC:HUVEC ECM PCL electrospun scaffolds demonstrated an average fiber diameter of 1.80 ± 0.29 μm, 1.59 ± 0.27 μm and 1.56 ± 0.42 μm, respectively. Therefore, all the electrospun fibers presented similar diameters at the microscale, indicating that the incorporation of cell-derived ECM into the PCL casting solution did not affect considerably the electrospinning process and the average fiber diameter of scaffolds (Figure VI.3b). Further, to validate the presence of ECM in the electrospun fibers, we stained the fibers with picro-sirius red. Cell-derived ECM scaffolds stained positive with picro-sirius red, validating the presence of collagen. On the other hand, no collagen was observed in the PCL scaffolds without ECM incorporated (Figure VI.3c).

Analysis of mechanical properties of cell-derived ECM PCL scaffolds demonstrated that the incorporation of ECM into the PCL solution did not considerably affect the mechanical properties of the PCL scaffolds, as it shown by the representative stress-strain curves (Figure VI.4a) and by the elastic modulus, UTS and elongation values (Figure VI.4b,c,d and Table VI.2). PCL alone, MSC ECM, HUVEC ECM and MSC:HUVEC ECM PCL electrospun fibers presented values for elastic modulus of 11.99 ± 1.26 MPa, 8.65 ± 1.49 MPa, 11.50 ± 1.15 MPa and 11.98 ± 0.92 MPa, respectively. Average values for UTS and elongation are also summarized in the Table VI.2

ATR-FTIR spectrum of PCL electrospun scaffold showed all the major characteristic IR peaks of PCL at approximately 1724 and 1160 cm^{-1} that correspond to ester carbonyl bond stretching and carbon-oxygen bond stretching, respectively. The IR spectra of the cell-derived ECM PCL electrospun scaffolds appeared to have an identical pattern to PCL but did not show any major peaks that correspond to ECM (Figure VI.5). This is probably due to the low amount of ECM present in the PCL-ECM scaffolds compared to the large amount of PCL.

Thermal analysis of cell-derived ECM electrospun scaffolds was performed using differential scanning calorimetry (DSC). DSC thermograms of cell-derived ECM electrospun scaffolds are shown in Figure VI.6. PCL fibers showed characteristic endothermic (melting) and exothermic (crystallization) transformation points at around 57.7°C (Figure VI.6a) and 36.2°C (Figure VI.6.b), respectively. Thermograms of all the other samples containing the different cell-derived ECM are similar to the neat PCL fibers. The presence of ECM has no significant effect on the average phase transition temperatures of the composite fibers. There are slight decrements in the melting and crystallization points that can be accounted to experimental and instrumental variability.

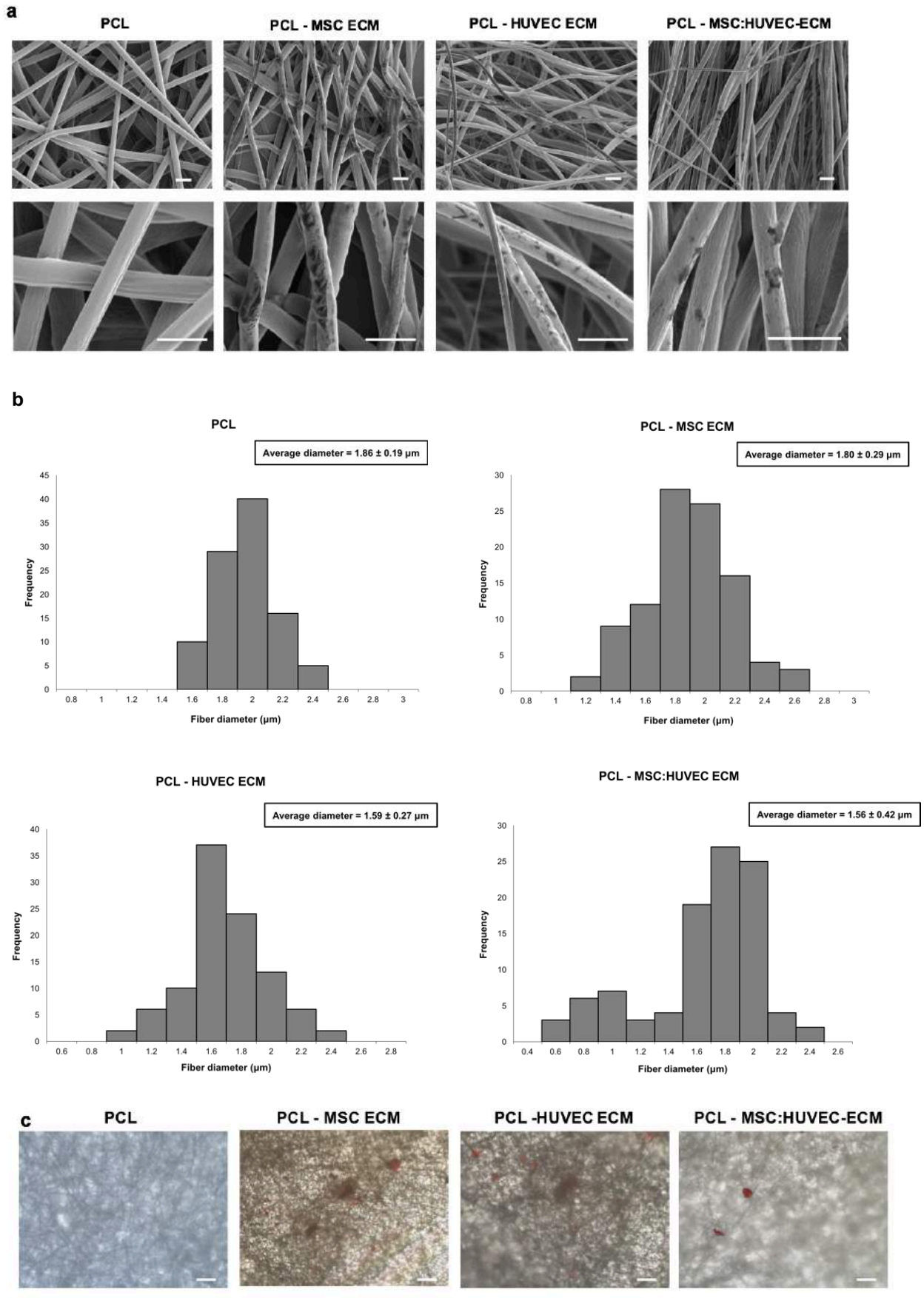

Figure VI.3. Characterization of cell-derived ECM PCL electrospun scaffolds. **a)** SEM images show the presence of ECM on PCL scaffolds. Scale bars, 5 µm. **b)** Fiber diameter distribution of cell-derived ECM PCL electrospun scaffolds. **c)** Picrosirius red staining confirms the presence of collagens in the cell-derived ECM PCL scaffolds, validating the presence of ECM. Scale bars, 50 µm.

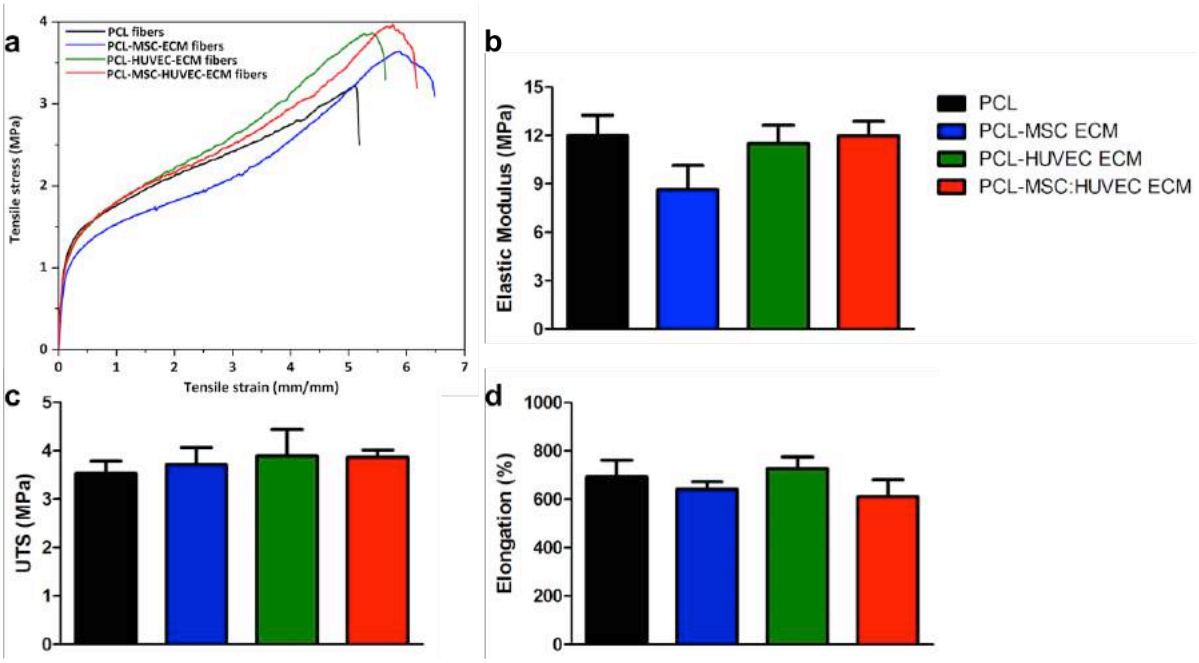

Figure VI.4. Mechanical properties of cell-derived ECM PCL scaffolds, obtained after tensile testing. **a)** Representative stress-strain curves. **b)** Elastic modulus (MPa). **c)** Ultimate tensile strength (UTS) (MPa). **d)** Elongation. Five different samples (n=5) were used in the analysis. Values are mean ± SD.

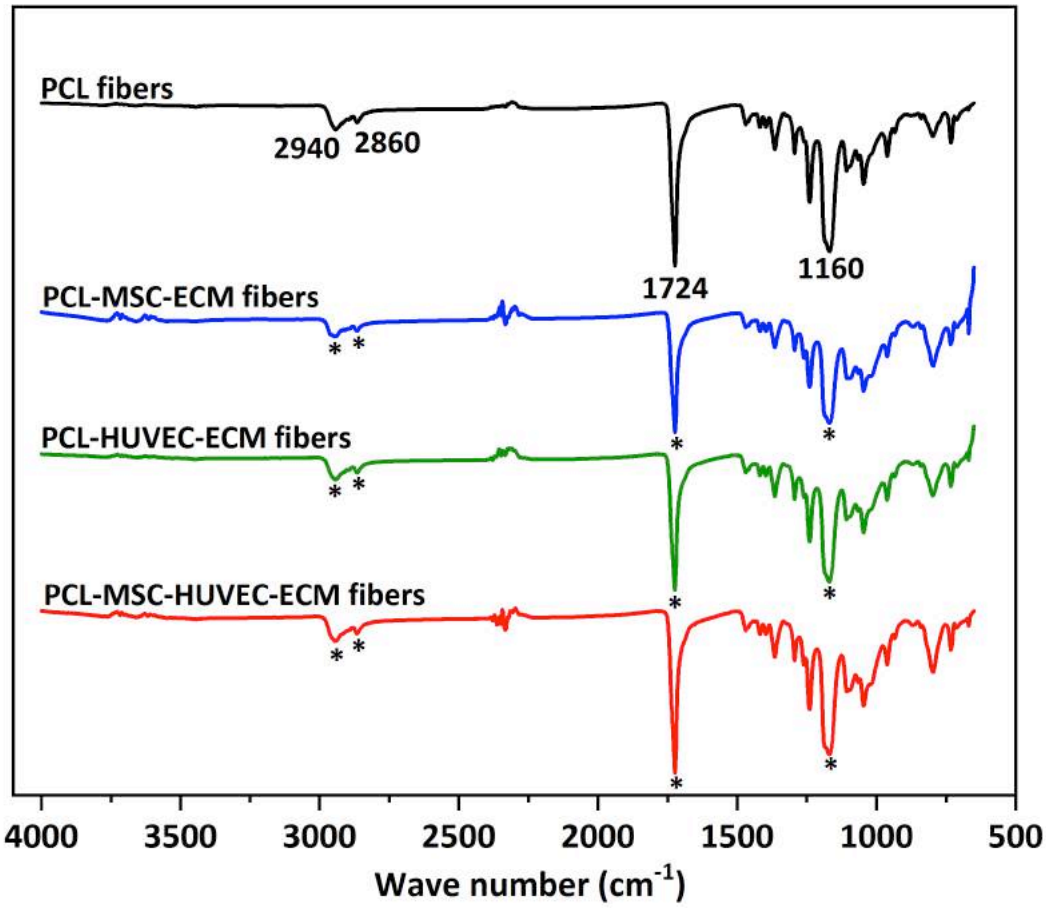

Figure VI.5. FTIR spectra of the different cell-derived ECM PCL electrospun scaffolds and PCL control scaffolds.

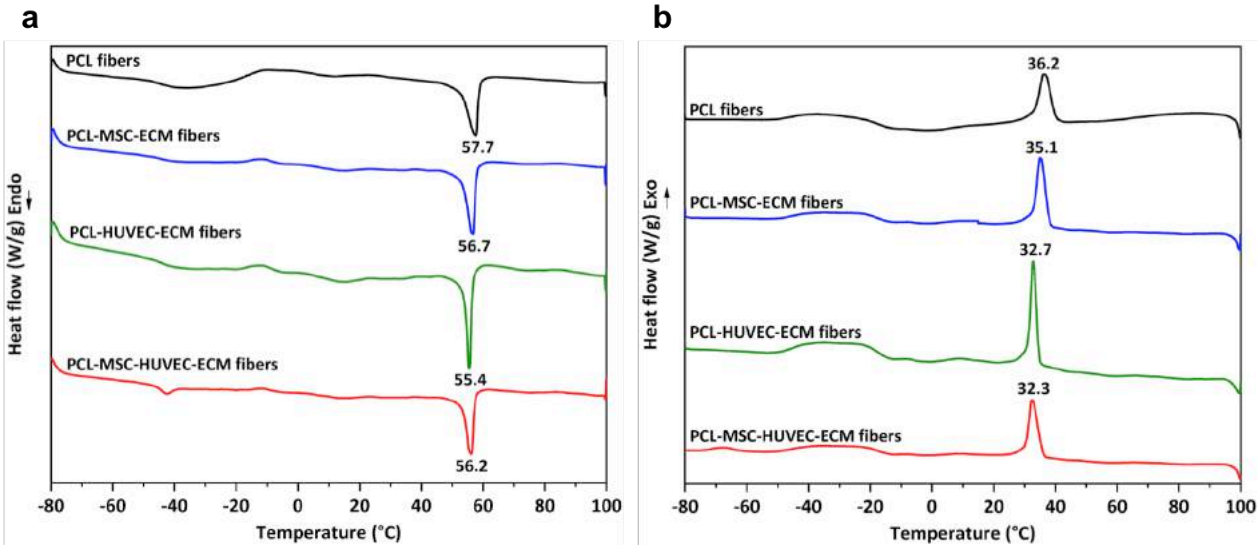

Figure VI.6. DSC thermograms respective to the heating cycle **(a)** and cooling cycle **(b)** of the different cell derived-ECM electrospun scaffolds. Obtained melting **(a)** and crystallization temperatures **(b)** for the different cell derived-ECM electrospun scaffolds are indicated in the respective thermograms.

Table VI.2. Summary of elastic modulus, ultimate tensile strength and ultimate elongation values obtained for the different cell-derived ECM electrospun scaffolds after mechanical tensile testing. Values are expressed as mean ± SD of five independent samples analyzed.

	Elastic Modulus (MPa)	UTS (MPa)	Elongation (%)
PCL	11.99 ± 1.26	3.53 ± 0.26	693 ± 69
PCL-MSC ECM	8.65 ± 1.49	3.72 ± 0.35	642 ± 31
PCL-HUVEC ECM	11.50 ± 1.15	3.89 ± 0.55	727 ± 48
PCL-MSC:HUVEC ECM	11.98 ± 0.92	3.87 ± 0.15	611 ± 70

VI.3.3. Effects of cell-derived ECM electrospun PCL fibers on cell proliferation

Metabolic activity of MSC was measured by AlamarBlue® assay on days 3, 7, 14 and 21 to assess the effect of the different cell-derived ECM electropsun scaffolds on cell proliferation (Figure VI.7a). Notably, after 7 days, a significant increase in cell number was found on all cell-derived ECM scaffolds compared to PCL scaffolds alone, which was also observed in the subsequent time points of the culture (days 14 and 21) (Figure VI.7a). The cell number increase suggests a beneficial MSC response to the presence of ECM in the microfibers. Although all cell-derived ECM scaffolds significantly enhanced cell proliferation when compared to PCL scaffold, no significant differences were observed between the ECM derived scaffolds generated from different cell sources. The morphology of cells cultured in the different cell-derived ECM PCL electrospun scaffolds was assessed at the end of the culture by DAPI-Phalloidin staining (Figure VI.7b). Figure VI.7b shows MSC morphology, distribution and organization throughout the electrospun scaffolds after 21 days of osteogenic differentiation. Cells seeded on all the scaffolds (with and without ECM) presented similar morphology, however a higher cell spreading and scaffold population in cell-derived ECM electrospun scaffolds is suggested by the observation of Figure VI.7b. SEM analysis throughout the culture at days 7,14 and 21 (Figure VI.8) is consistent with the results from cell proliferation assay. Cell-derived ECM PCL microfibrous scaffolds were already highly populated with MSC at day 7, which was not observed for the PCL only scaffold.

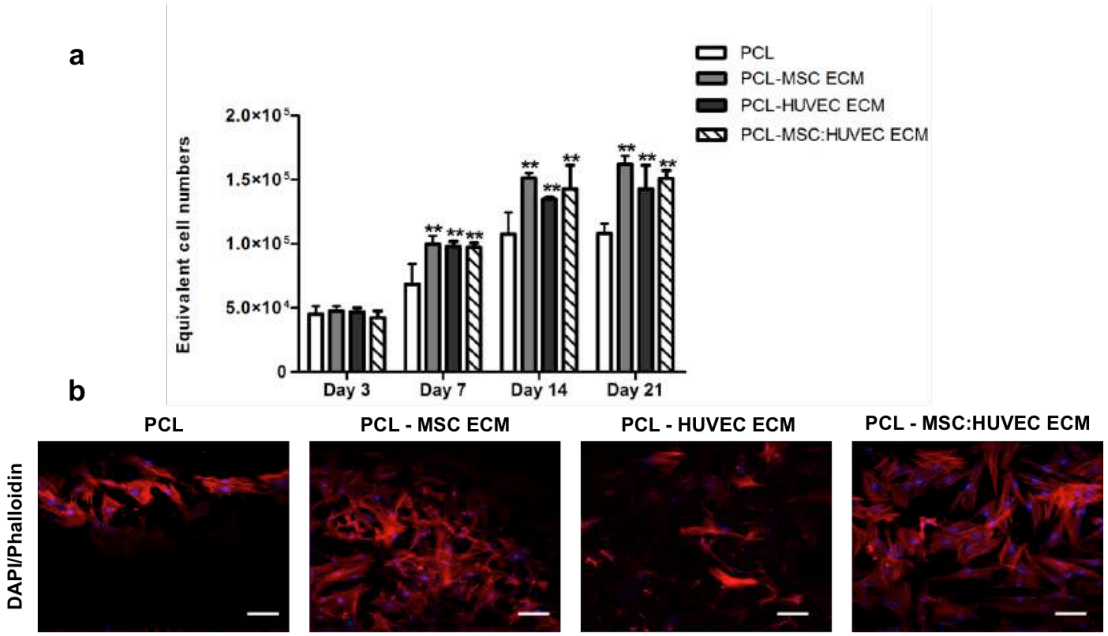

Figure VI.7. Effects of cell-derived ECM PCL scaffolds on MSC proliferation. Cell proliferation assay **(a)** and cell morphology assessment by DAPI/Phalloidin staining at day 21 **(b)**. Values are expressed as mean ± SD; **p<0.01. Scale bars, 100 μm.

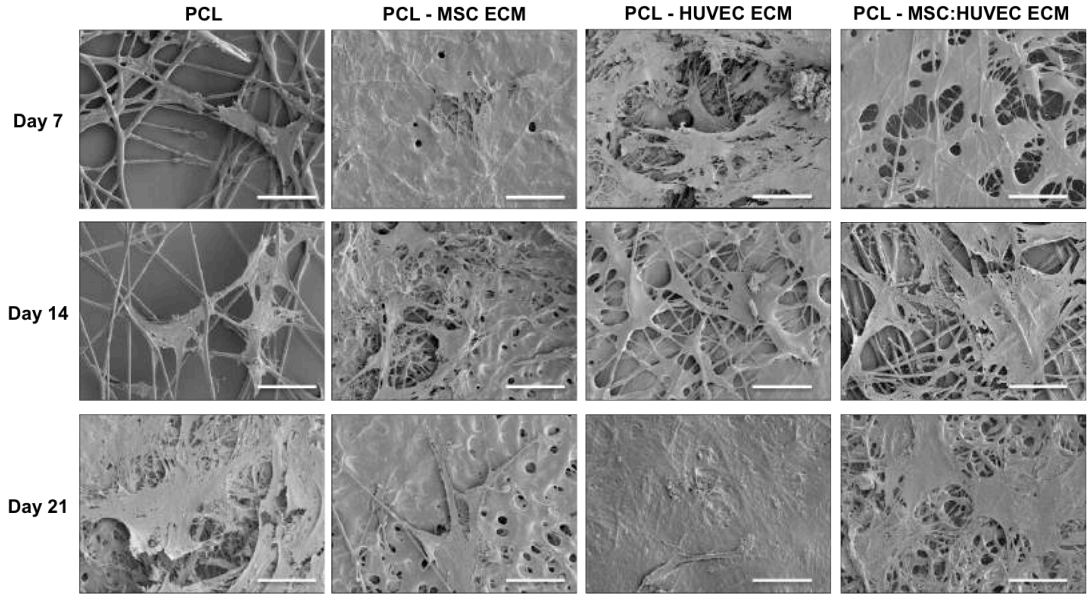

Figure VI.8. SEM morphological analysis of MSC cultured under osteogenic differentiation induction in the different cell-derived ECM electrospun scaffolds at days 7, 14 and 21. Scale bars, 50 μm.

VI.3.4. Influence of cell-derived ECM electrospun PCL fibers on osteogenic differentiation

Osteogenic differentiation was assessed by culturing MSC on electrospun ECM scaffolds under osteogenic differentiation medium for 21 days. At day 14 and 21 of osteogenic differentiation, ALP activity, as well as calcium levels were measured.

MSC cultured on cell-derived ECM scaffolds presented a significantly higher ALP activity after 14 days of differentiation, compared to PCL scaffolds. After 21 days, the ALP activity of MSC cultured on all electrospun scaffolds decreased, presenting similar results to the ones verified for PCL alone (Figure VI.9a).

Regarding mineralization, no drastic differences were observed between the scaffolds. After 21 days of osteogenic differentiation, the presence of ECM in the electrospun scaffolds only demonstrated a statistically significant enhancement in calcium accumulation when MSC were seeded on PCL-HUVEC ECM scaffold. All the remaining scaffolds demonstrated values of calcium deposition similar to PCL scaffold alone (Figure VI.9b).

The most common methods to visualize *in vitro* mineralization are the von Kossa, the Alizarin red and the Xylenol orange staining. Alizarin red staining confirmed the presence of calcium deposits in all scaffolds after 21 days of osteogenic differentiation, validating the results obtained with calcium deposition quantification. Moreover, ALP and Von Kossa stainings also confirmed ALP activity in all scaffolds (reddish areas), as well as, indirectly, the presence of calcium deposits by Von Kossa staining (darker regions) (Figure VI.9c), demonstrating the successful differentiation of MSC into osteoblasts in all PCL scaffolds. Xylenol orange fluorescent staining further confirmed the presence of calcium deposits on MSC cultured on all cell-derived ECM PCL electrospun scaffolds and PCL fibers after 21 days of osteogenic differentiation (Figure VI.10).

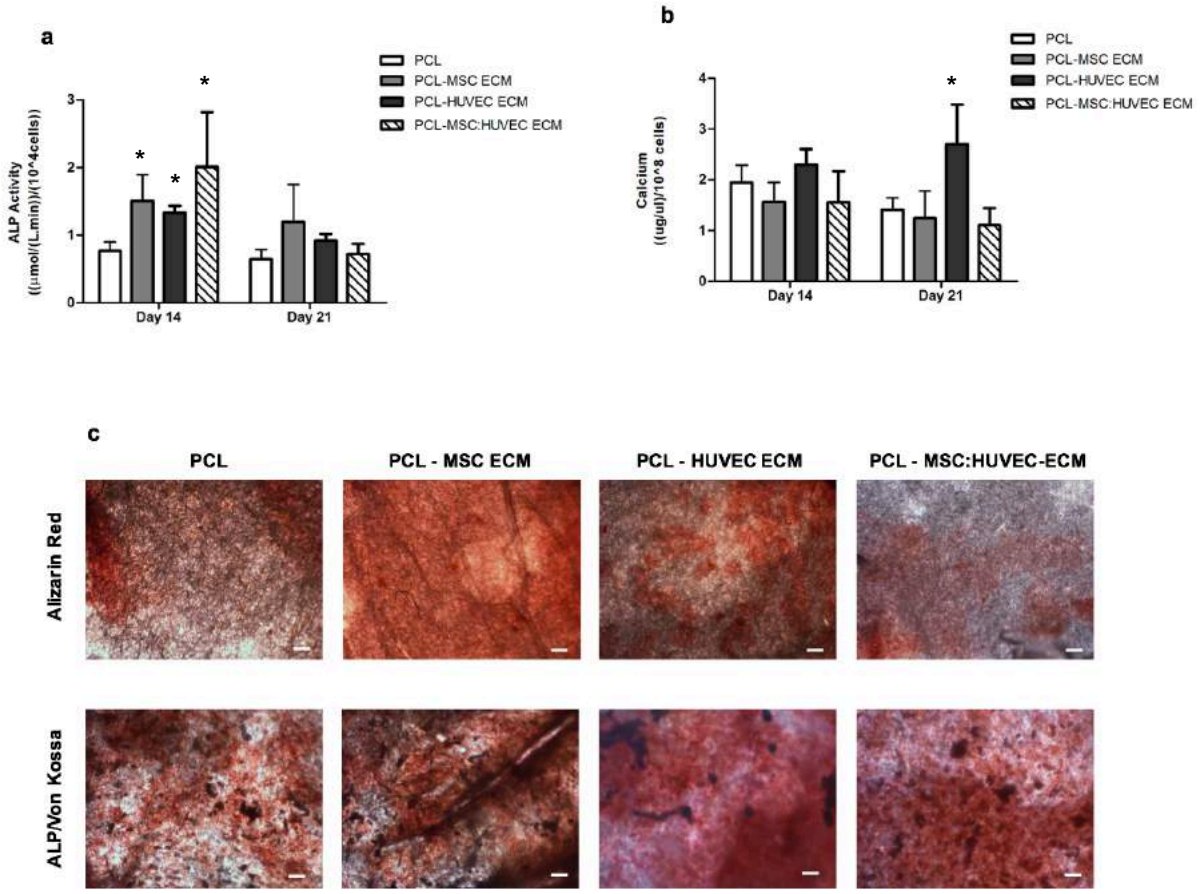

Figure VI.9. Osteogenic differentiation of MSC cultured on cell-derived ECM electrospun fibers. **a)** ALP activity of MSC cultured on cell-derived ECM PCL scaffolds after 14 and 21 days of osteogenic differentiation. **b)** Calcium deposition quantification of MSC seeded on cell-derived ECM PCL scaffolds after 14 and 21 days of osteogenic differentiation. **c)** Alizarin red, ALP and Von Kossa stainings of MSC differentiated on cell-derived ECM scaffolds after 21 days. Alizarin red and Von Kossa confirmed the presence of calcium deposits (reddish and darker areas, respectively). ALP staining demonstrated ALP activity of MSC cultured on all PCL scaffolds. Scale bars, 200 µm. Values are expressed as mean ± SD, **p<0.01; *p<0.05.

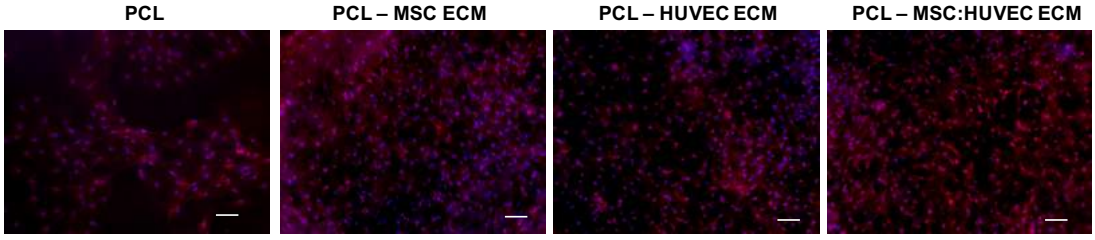

Figure VI.10. Xylenol orange staining demonstrated calcium deposits after 21 days of osteogenic differentiation. Xylenol orange (red) and DAPI (blue). Scale bars, 100 µm.

SEM micrographs showed MSC attached to the fibers and detected some ECM produced and deposited by cells surrounding the fibers (Figure VI.11a). Additionally, elemental analysis of MSC differentiated for 21 days on cell-derived ECM scaffolds further confirmed the presence of calcium and phosphorous (Figure VI.11b).

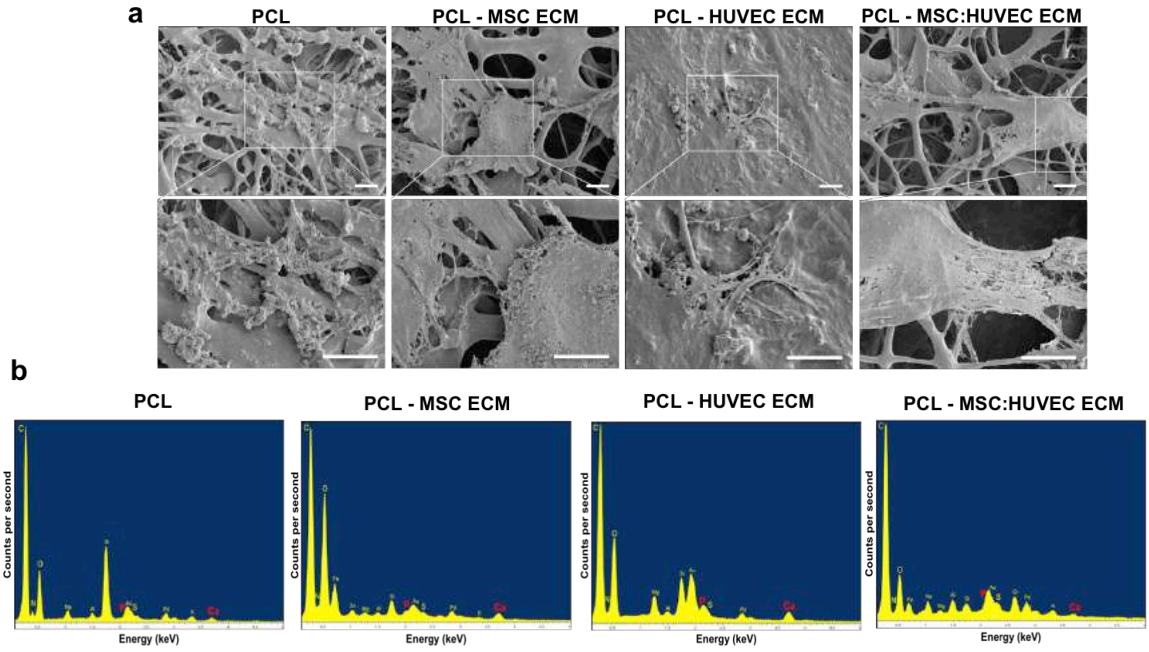

Figure VI.11. Morphology and elemental composition analysis of MSC cultured on cell-derived ECM PCL electrospun fibers and PCL electrospun fibers after 21 days of osteogenic differentiation. **a)** SEM images and respective magnification (blank square). **b)** EDS spectrogram for the different cell-derived ECM electrospun scaffolds. Scale bars, 10 µm.

VI.3.5. Gene expression analysis

qRT PCR was performed after 21 days of osteogenic differentiation on MSC cultured on PCL scaffolds and cell-derived ECM PCL electrospun scaffolds. Different osteogenic markers were analyzed (Runx2, ALP and OPN, a late osteogenic marker), as well as the angiogenic marker gene VEGF. Interestingly, all the scaffolds (with and without ECM) upregulated the expression of Runx2 and OPN compared to the control (cells at day 0). Regarding Runx2, OPN and ALP gene expression, only cells cultured on PCL-MSC:HUVEC ECM demonstrated a statistically significant increase compared to PCL scaffold, presenting the highest osteogenic gene expression levels. In contrast, VEGF gene expression levels were only significantly enhanced when cells were cultured on PCL-HUVEC ECM (Figure VI.12). Although a slight increase in VEGF expression was also observed in PCL-MSC ECM and PCL-MSC:HUVEC ECM group, this was not considered statistically significant.

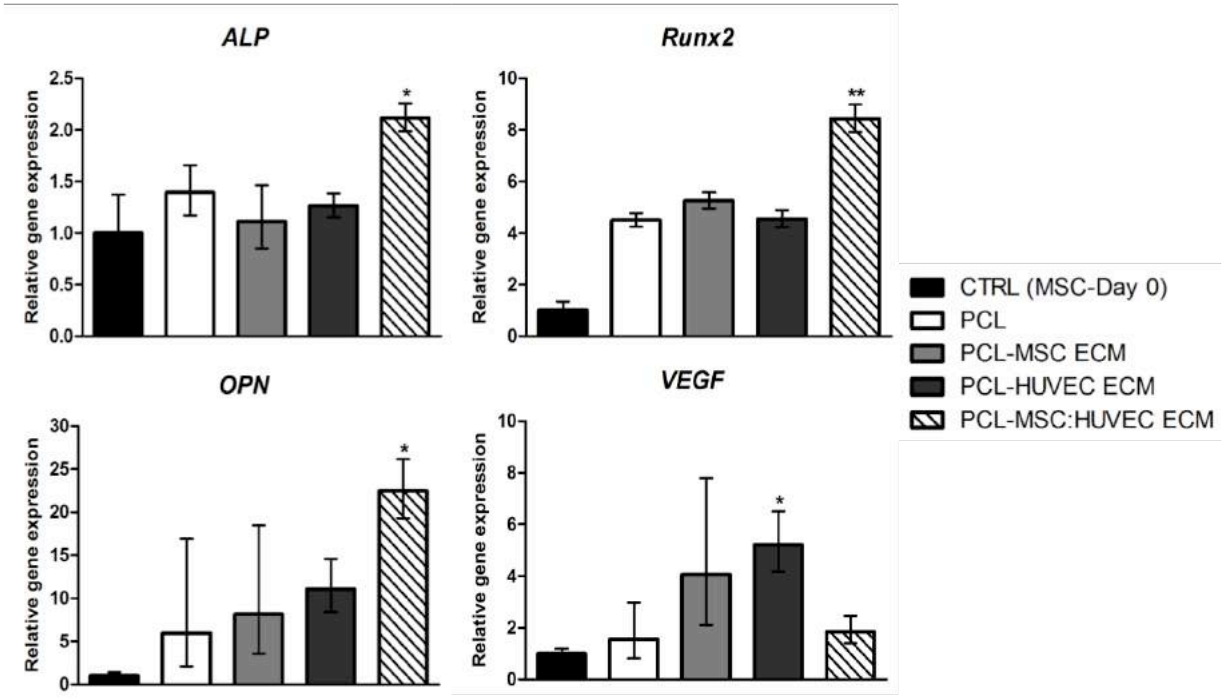

Figure VI.12. Effects of cell-derived ECM-PCL microfibrous scaffolds on the gene expression of ALP, Runx2, OPN and VEGF of MSC. *p<0.05, **p<0.01 relative to PCL scaffold expression.

VI.4. Discussion

ECM is a highly complex system of organized assembly of macromolecules and signaling factors, such as collagens, fibronectin and proteoglycans (Badylak *et al.* 2009). Moreover, ECM not only provides structural and mechanical support for tissue but also regulates cellular functions, such as cell adhesion, migration, survival, proliferation and differentiation. Therefore, ECM has been widely exploited as a biological scaffold material to be used in a broad range of tissue engineering applications.

Some synthetic materials have been developed by using isolated ECM components, such as collagen elastin, laminin and fibronectin (Mistry *et al.* 2005, Khademhosseini *et al.* 2009, Kundu *et al.* 2006, Ku *et al.* 2005), aiming to enhance the bioactivity and functionality of the scaffold. However, these scaffolds do not really mimic the *in vivo* ECM, which is composed by a highly complex mixture of proteins almost impossible to reproduce it *in vitro*, due to its high production cost. Moreover, optimized doses for each component should be investigated first, as well as identification of all the molecules present in the ECM.

Cell-derived ECM can be used as an alternative approach to obtain more complex systems to enhance scaffold bioactivity. For this, cells were cultured *in vitro* until confluence and allowed to secrete ECM. Afterwards, a decellularization treatment is used to remove the cellular components, while retaining the ECM structure. Different studies have already been reported the effects of cell-derived ECM on cellular activities by combining it into scaffolds (Gibson *et al.* 2014, Jeon *et al.* 2016). In particular, for bone tissue engineering applications, Gibson and colleagues fabricated a PCL electrospun scaffold incorporated with decellularized ECM

nanoparticles from bone, demonstrating upregulation of osteogenic gene expression markers (Gibson *et al.* 2014). Moreover, Jeon and colleagues have cultured pre-osteoblasts on electrospun PCL scaffolds and decellularize it to obtain decellularized cell-derived ECM scaffolds, improving cell proliferation and osteogenic differentiation (Jeon *et al.* 2016). However, most of these studies use cell-derived ECM as a strategy to decorate the scaffold. Thus, cells are cultured and allowed to grow on top of the scaffolds and upon application of the decellularization treatment, the ECM components remain attached to the scaffold, conferring bioactivity to the scaffold. Notably, in this study, we used a different approach to fabricate cell-derived ECM PCL scaffolds. Here, cell-derived ECM, produced from different cell types relevant for bone homeostasis, was obtained after culturing them *in vitro* and collecting the secreted ECM upon application of a previously reported decellularization method (Kang *et al.* 2012). Afterwards the obtained ECM was collected and lyophilized. The lyophilized ECM was then directly mixed into the PCL solution and electrospinning technique was used to produce cell-derived ECM PCL microfibrous scaffolds. Indeed, it has been previously reported that ECM lyophilization leads to water removal and drying of the biologically active component contained in it, making the ECM proteins more stable (Sheridan *et al.* 2013). Therefore, we added the lyophilized ECM to the PCL solution and electrospun the mixture to produce cell-derived ECM PCL fibers.

Cell source is known to be determining factor for the composition of the cell-derived ECM. Indeed, cells derived from different tissues typically produce matrices that will recreate the composition of the natural tissue matrix (Fitzpatrick *et al.* 2015). Therefore, in this study we fabricated cell-derived ECM PCL scaffolds, composed with ECM derived from MSC, HUVEC and a co-culture of MSC:HUVEC (ratio 1:1). In fact, co-culture of MSC and endothelial cells has demonstrated extensive cellular crosstalk, enhancing the angiogenic response of MSC (Aguirre *et al.* 2010, Nassiri *et al*. 2014), as well as the osteogenic capabilities (Zhao *et al.* 2012).

Cell-derived ECM from different cell types may present differences in protein composition. Although it is known that the basic molecules that constitute the ECM may be similar in all organisms, their distribution and organization varies with tissue type, age of the host and species (Mouw *et al.* 2014). Therefore, cell-derived ECM generated from different cell types may present differences in their composition and these structural differences may induce different cellular responses when used as scaffolds for tissue engineering. However, we did not evaluate the exact composition of each cell-derived ECM, evaluating only their biological activity. Therefore, future studies should focus on identifying the composition of each ECM-type using proteomics/glycomics analysis.

Lyophilized ECM powders derived from different cell types and their co-culture were characterized by SEM and FTIR (Figure VI.2). Results showed that morphology of the different cell-derived ECM was similar between the different cell types and co-culture and consistent with other lyophilized ECM powders previously reported (Figure VI.2a) (Thakkar *et al.* 2013, Chang *et al.* 2014). FTIR spectra of each lyophilized ECM demonstrated slight differences, presenting different infrared peaks. FTIR spectra of MSC and HUVEC ECM powder samples revealed peaks that are unique to each other. Additionally, all four of these unique peaks can also be seen in the IR spectrum of MSC-HUVEC ECM mixture, suggesting that a combination of cell types in the selected proportion successfully combines components from both types of cell-derived ECM that are known to produce a functional bone matrix. IR peaks correspondent to carbon-hydrogen alkyl bond stretching are also present in all the IR spectra collected (νC-H-, 2940 - 2860 cm^{-1}) (Figure VI.2b).

We used electrospinning to fabricate cell-derived 3-D microfibrous scaffolds with high porosity structure and interconnectivity, mimicking the architecture and composition of the natural ECM. Figure VI.3a shows SEM images of cell-derived ECM electrospun fibers revealing the presence of micro/nano-scale cell-derived ECM fragments attached to the fiber surface. SEM analysis of control PCL scaffolds did not present fragments of ECM attached to the fibers. The presence of ECM fragments was further validated using picro-sirius red staining, a collagen histological staining (Figure VI.3c). Collagen is the major component of the ECM, therefore we confirmed the presence of collagens in the electrospun scaffolds with incorporated ECM. However, immunohistochemistry of specific collagens or other ECM biomolecules should be performed to identify and distinguish more specifically the ECM produced from different cells.

Mechanical tensile testing of cell-derived ECM scaffolds demonstrated that the presence of the ECM into the PCL scaffolds did not affect the mechanical properties of PCL (Figure VI.4), which are reported as promising for bone regeneration applications (Yoshimoto *et al.* 2003), since MSC can sense the mechanical characteristics of the surface of the scaffolds, which promote some cellular activities, such as proliferation and mineralization (Hu *et al.* 2018, Chen *et al.* 2015).

MSC are a common material to obtain cell-derived ECM due to their ability to deposit ECM that can mimic different tissues depending on culture conditions, such as bone, cartilage and adipose tissue. Moreover, MSC-derived ECM has been shown to rejuvenate aged mouse stem cells and enhance their lineage differentiation ability (Li et al. 2014). Decellularized ECM from human MSC cultures have been shown to promote MSC proliferation (Lai et al. 2010) and can act as a substrate for chondrocyte proliferation and maintenance of chondrocytic phenotype (Yang *et al.* 2018, Lu *et al.* 2011). In addition, HUVEC-derived ECM was used with success to enhance the biocompatibility of pure titanium surfaces (Xue *et al.* 2010), whereas Kang and colleagues have fabricated a β-TCP scaffold containing HUVEC-ECM and demonstrated the improved osteogenic capacity of such scaffolds (Kang *et al.* 2012). Co-culture of HUVEC and MSC have been shown to enhance osteogenic differentiation of MSC, due to the BMP secreted by endothelial cells (Zhao *et al.* 2012). Therefore, it is expected that ECM produced by MSC:HUVEC co-culture will enhance proliferation and osteogenic differentiation of MSC, mimicking more accurately the *in vivo* bone marrow niche.

In this study, a significant enhancement in proliferation of MSC seeded on cell-derived scaffolds was observed after 7 days of culture and was maintained after 21 days (Figure VI.7a). All the cell-derived ECM microfibrous scaffolds presented a statistically significant higher cell number when compared to PCL scaffolds alone at days 7,14 and 21. However, no dramatic differences between the cell-derived scaffolds (MSC-ECM, HUVEC-ECM and MSC:HUVEC-ECM) were observed. We hypothesized that ECM present in these scaffolds may have triggered a faster proliferation due to the signaling molecules and growth factors that were embedded in the ECM. In fact, our results are in accordance with previous findings that showed that the presence of ECM in synthetic scaffolds increased proliferation of MSC and induced their osteogenic differentiation (Kang *et al.* 2012, Thakkar *et al.* 2013, Gibson *et al.* 2014, Shtrichman *et al.* 2014, Jeon *et al.* 2016, Fu *et al.* 2018).

Regarding osteogenic differentiation, all the PCL electrospun scaffolds (with and without ECM) promoted osteogenic differentiation of MSC. In fact, FDA-approved PCL has been used as electrospun fibers or in other scaffold configurations in bone tissue engineering applications for many years, mainly due to its biochemical/mechanical properties and biocompatibility. Recently, Xue and colleagues showed that PCL electrospun nanofibers were able to enhance osteogenic differentiation potential of MSC derived from different

tissues (Xue *et al.* 2017). Here we found a significant increase of calcium levels for MSC cultured on PCL-HUVEC ECM scaffolds, after 21 days of differentiation (Figure VI.9b). However, Alizarin red, Von Kossa and Xylenol Orange stainings suggested that all the scaffolds enabled the osteogenic differentiation of MSC after 21 days. SEM images also suggest the formation of mineralized nodules after 21 days of osteogenic differentiation (Figure VI.9, Figure VI.10). This observation is in accordance with work of Fu and colleagues in which they observed the formation of mineralized nodules after 14 days of osteogenic differentiation of mouse bone marrow MSC in PLLA electrospun scaffolds decorated with ECM generated by mouse osteoblastic (MC3T3-E1) cells (Fu *et al.* 2018). Moreover, elemental analysis indicated the presence of calcium and phosphorous after 21 days of culture in the electrospun scaffolds, suggesting a successful differentiation of MSC into osteoblasts (Figure VI.11b).

MSC cultured on cell-derived ECM scaffolds presented a significantly higher ALP activity after 14 days of differentiation, compared to PCL scaffolds. After 21 days, the ALP activity of MSC cultured on all electrospun scaffolds decreased, presenting similar results to the ones verified for PCL alone. In fact, during osteogenic differentiation of MSC, transcription and protein expression of ALP is enhanced as an early marker of osteogenesis (Aubin *et al.* 2001). After this initial peak of ALP, its level starts to decline, as we also observed when cells were cultured on PCL scaffolds.

Real time quantitative PCR analysis was performed to evaluate the expression of osteogenic marker genes and angiogenic marker VEGF in the different scaffolds studied. We decided to evaluate both osteogenic and angiogenic markers together due to the known major role of angiogenesis and vascularization in successful bone regeneration (Stegen *et al.* 2015, Curry *et al.* 2016). Our results showed increased ALP, Runx2 and OPN expression in all the scaffolds after 21 days of osteogenic differentiation (Figure VI.12). However, a statistically significant increase (relative to the PCL alone scaffold) in ALP, Runx2 and OPN gene expression was only observed when MSC were cultured on PCL-MSC:HUVEC-ECM electrospun scaffolds. In fact, our results are in accordance with previously reported literature in which increased expression of osteogenic markers ALP, Runx2 and OPN were seen when MSC were cultured either in MSC-derived (Chen *et al.* 2007) or HUVEC- derived ECM (Kang *et al.* 2012). Moreover, to evaluate angiogenic properties of MSC exposed to cell-derived ECM scaffolds, VEGF gene expression levels were evaluated. Interestingly, only cells cultured on PCL-HUVEC-ECM electrospun fibers demonstrated a statistically significant increase in VEGF expression levels. Therefore, we hypothesize that, although enhanced osteogenic expression levels are being achieved by PCL-MSC:HUVEC-ECM electrospun fibers, in order to also enhance angiogenic properties, a different composition of MSC:HUVEC ECM should be assessed by generating ECM derived from a different co-culture ratio of MSC:HUVEC, instead of the ratio 1:1 that was used in this study. Comparing with the results obtained in the previous chapter, only the ratio 1:3 (MSC:HUVEC) was able to enhance the capillary-tube formation by HUVEC. Therefore, we confirmed in this chapter that a different composition of MSC:HUVEC ECM should be assessed to be able to stimulate angiogenesis and osteogenesis, simultaneously.

The results of the current study demonstrated that cell-derived ECM PCL electrospun scaffolds promote MSC proliferation and their osteogenic differentiation *in vitro* by mimicking the *in vivo* ECM composition and structure produced using MSC and HUVEC. However, further studies including the optimization of ECM amounts loaded in the scaffold and of the cell ratios in the co-culture to generate ECM are still required to obtain constructs with ideal osteogenic performance. *In vivo* testing of such scaffolds should also be considered.

VI.5. References

Aguirre A., Planell J.A., Engel E. Dynamics of bone marrow-derived endothelial progenitor cell/mesenchymal stem cell interaction in co-culture and its implications in angiogenesis. *Biochem. Biophys. Res. Commun.*, **400**, 284–291 (2010).

Aubin J. E. Regulation of osteoblast formation and function. *Rev. Endocr. Metab. Disord.*, **2**, 81-94 (2001).

Badylak S.F., Freytes D.O., Gilbert T.W. Extracellular matrix as a biological scaffold material: structure and function. *Acta Biomater.,* **5**, 1-13 (2009).

Bhardwaj N., Kundu S.C. Electrospinning: a fascinating fiber fabrication technique. *Biotechnol. Adv.,* **28**, 325-347 (2010).

Bracaglia L. G., Fisher J. P. Extracellular matrix-based biohybrid materials for engineering compliant, matrix-dense tissues. *Adv. Healthc. Mater.*, **4**, 2475-2487 (2015).

Bourgine P.E., Scotti C., Pigeot S., Tchang L.A., Todorov A., Martin I. Osteoinductivity of engineered cartilaginous templates devitalized by inducible apoptosis. *Proc. Natl. Acad. Sci. U.S.A.*, **111**, 17426-17431 (2014).

Chang C. H., Chen C. C., Liao C. H., Lin F. H., Hsu Y. M., Fang H. W. Human acellular cartilage matrix powders as a biological scaffold for cartilage tissue engineering with synovium-derived mesenchymal stem cells. *J. Biomed. Mater. Res. A*, **102**, 2248-2257 (2014).

Chen X.D., Dusevich V., Feng J.Q., Manolagas S.C., Jilka R.L. Extracellular matrix made by bone marrow cells facilitates expansion of marrow-derived mesenchymal progenitor cells and prevents their differentiation into osteoblasts. *J. Bone Miner. Res.*, **22**, 1943-1956 (2007).

Chen G., Dong C., Yang L., Lv Y. 3D scaffolds with different stiffness but the same microstructure for bone tissue engineering. *ACS Appl. Mater. Interfaces*, **7**, 15790-15802 (2015).

Cipitria A., Skelton A., Dargaville T.R., Dalton P.D., Hutmacher D.W. Design, fabrication and characterization of PCL electrospun scaffolds – a review. *J. Mater. Chem.,* **21**, 9419-9453 (2011).

Curry A. S., Pensa N. W., Barlow A. M., Bellis S. L. Taking cues from the extracellular matrix to design bone-mimetic regenerative scaffolds. *Matrix Biology*, **52**, 397-412 (2016).

Engelberg I., Kohn J. Physico-mechanical properties of degradable polymers used in medical applications: a comparative study. *Biomaterials*, **12**, 292-304 (1991).

Fitzpatrick L. E., McDevitt T.C. Cell-derived matrices for tissue engineering and regenerative medicine application. *Biomater. Sci.*, **3**, 12-24 (2015).

Fu Y., Liu L., Cheng R., Cui W. ECM decorated electrospun nanofiber for improving bone tissue regeneration. *Polymers*, **10**, 272 (2018).

Gibson M., Beachley V., Coburn J., Bandinelli P.A., Mao H.Q., Elisseeff J. Tissue extracellular matrix nanoparticle presentation in electrospun nanofibers. *Biomed. Res. Int.* **2014**, 469120 (2014).

Gong T., Heng B.C., Xu J., Zhu S., Yuan C., Lo E.C., Zhang C. Decellularized extracellular matrix of human umbilical vein endothelial cells promotes endothelial differentiation of stem cells from exfoliated deciduous teeth. *J. Biomed. Mater. Res. A*., **105**, 1083-1093 (2017).

Hong Y., Huber A., Takanari K., Amoroso N. J., Hashizume R., Badylak S.F., Wagner W. R. Mechanical properties and in vivo behavior of a biodegradable synthetic polymer microfiber–extracellular matrix hydrogel biohybrid scaffold. *Biomaterials,* **32**, 3387-3394 (2011).

Hoshiba T., Lu H., Kawazoe N., Chen G. Decellularized matrices for tissue engineering. Expert Opin. Biol. Ther., **10**, 1717-1728 (2010).

Hu Q., Liu M., Chen G., Xu Z., Lv Y. Demineralized bone scaffolds with tunable matrix stiffness for efficient bone integration. *ACS Appl. Mater. Interfaces* (2018).

Hynes R.O. Extracellular matrix: not just pretty fibrils. *Science*, **326**, 1216-1219 (2009).

Jeon H., Lee J.Y., Lee H., Kim G.H. Nanostructured surface of electrospun-PCL/dECM fibres treated with oxygen plasma for tissue engineering. *RSC Adv.*, **6**, 32887-32896 (2016).

Kang Y., Kim S., Bishop J., Khademhosseini A., Yang Y. The osteogenic differentiation of human bone marrow MSCs on HUVEC-derived ECM and β-TCP scaffold. *Biomaterials*, **33**, 6998-7007 (2012).

Kim S. E., Yun Y.P., Han Y.K., Lee D.W., Ohe J.Y., Lee B.S., Song H.R., Park K., Choi B.J., Osteogenesis induction of periodontal ligament cells onto bone morphogenic protein-2 immobilized PCL fibers. *Carbohydr. Polym.*, **99**, 700-709 (2014).

Khademhosseini A., Vacanti J.P., Langer R. Progress in tissue engineering. *Sci. Am.*, **300**, 64-71 (2009).

Kleinman H.K., Luckenbill-Edds L., Cannon F.W., Sephel G.C. Use of extracellular matrix components for cell culture. *Anal. Biochem.*, **166**, 1-13 (1987).

Ku Y., Chung C.P., Jang J.H. The effect of the surface modification of titanium using a recombinant fragment of fibronectin and vitronectin on cell behavior. *Biomaterials*, **26**, 5153-5157 (2005).

Kundu A.K., Putnam A.J. Vitronectin and collagen I differentially regulate osteogenesis in mesenchymal stem cells. *Biochem. Biophys. Res. Commun.*, **347**, 347-357 (2006).

Lai Y., Sun Y., Skinner C.M., Son E.L., Lu Z., Tuan R.S., Jilka R.L., Ling J. and Chen X.D. Reconstitution of marrow-derived extracellular matrix ex vivo: a robust culture system for expanding large-scale highly functional human mesenchymal stem cells. *Stem Cells Dev.,* **19**, 1095-1107 (2010).

Lee M.K., Lin S.P., HuangFu W.C., Yang D.S., Liu I.H. Endothelial-derived extracellular matrix ameliorate the stemness deprivation during *ex vivo* expansion of mouse bone marrow-derived mesenchymal stem cells. PLoS One, **12**, e0184111 (2017).

Li J., Hansen K.C., Zhang Y., Dong C., Dinu C.Z., Dzieciatkowska M., Pei M. Rejuvenation of chondrogenic potential in a young stem cell microenvironment. *Biomaterials,* **35**, 642-653 (2014).

Li W.J., Laurencin C.T., Caterson E.J., Tuan R.S., Ko F.K. Electrospun nanofibrous structure: a novel scaffold for tissue engineering. *J. Biomed. Mater. Res.,* **60**, 613-621 (2002).

Lin H., Yang G., Tan J., Tuan R.S., Influence of decellularized matrix derived from human mesenchymal stem cells on their proliferation, migration and multi-lineage differentiation potential. *Biomaterials,* **33**, 4480–4489 (2012).

Lu H., Hoshiba T., Kawazoe N., Kod I., Song M., Chena G. Cultured cell-derived extracellular matrix scaffolds for tissue engineering. Biomaterials, **32**, 9658-9666 (2011).

Mattanavee W., Suwantong O., Puthong S., Bunaprasert T., Hoven V. P., Supaphol P., Immobilization of biomolecules on the surface of electrospun polycaprolactone fibrous scaffolds for tissue engineering. *ACS Appl. Mater. Interfaces,* **1**, 1076-1085 (2009).

Middleton J.C., Tripton A.J. Synthetic biodegradable polymers as orthopedic devices. *Biomaterials*, **23**, 2335-2346 (2000).

Mistry A.S., Mikos A.G. Tissue engineering strategies for bone regeneration. *Adv. Biochem. Eng. Biotechnol.*, **94**, 1-22 (2005).

Mouw J.K., Ou G., Weaver V.M. Extracellular matrix assembly: a multiscale deconstruction. *Nat. Rev. Mol. Cell Biol.,* **15**, 771-785 (2014).

Nassiri S.M., Rahbarghazi R. Interactions of mesenchymal stem cells with endothelial cells, *Stem Cells Dev.*, **23**, 319-332 (2014).

Nair L.S., Laurencin C.T. Biodegradable polymers as biomaterials. *Prog. Poly. Sci.,* **32**, 762-798 (2007).

Pham Q.P., Kasper F.K., Scott Baggett L., Raphael R.M., Jansen J.A., Mikos A.G. The influence of an in vitro generated bone-like extracellular matrix on osteoblastic gene expression of marrow stromal cells. *Biomaterials*, **29**, 2729-2739 (2008).

Reznikov, N., Shahar, R., Weiner, S. Bone hierarchical structure in three dimensions. *Acta Biomater.,* **10**, 3815-3826 (2014).

Sheridan W.S., Duffy G.P., Murphy B.P. Optimum parameters for freeze-drying decellularized arterial scaffolds. *Tissue Eng. Part C Methods*, **19**, 981-990 (2013).

Shtrichman R., Zeevi-Levin N., Zaid R., Barak E., Fishman B., Ziskind A., Shulman R., Novak A., Avrahami R., Livne E., Lowenstein L., Zussman E., Itskovitz-Eldor J. The generation of hybrid electrospun nanofiber layer with extracellular matrix derived from human pluripotent stem cells, for regenerative medicine applications. *Tissue Eng. Part A.,* **20**, 2756-2767 (2014).

Sill T.J., von Recum H.A. Electrospinning: applications in drug delivery and tissue engineering. *Biomaterials*, **29**, 1989-2006 (2008).

Stegen S., van Gastel N., Carmeliet G. Bringing new life to damaged bone: the importance of angiogenesis in bone repair and regeneration. *Bone*, **70**, 19-27 (2015).

Thakkar S., Ghebes C.A., Ahmed M., Kelder C., van Blitterswijk C.A., Saris D., Fernandes H.A., Moroni L. Mesenchymal stromal cell-derived extracellular matrix influences gene expression of chondrocytes. *Biofabrication*, **5**, 025003 (2013).

Xue X., Wang J., Zhu Y., Tu Q., Huang N. Biocompatibility of pure titanium modified by human endothelial cell-derived extracellular matrix. *Appl. Surf. Sci.*, **256**, 3866-3873 (2010).

Xue R., Qian Y., Li L., Yao G., Yang L., Sun Y. Polycaprolactone nanofiber scaffold enhances the osteogenic differentiation potency of various human tissue-derived mesenchymal stem cells. *Stem Cell Res. Ther.,* **8**, 148 (2017).

Yang Y., Lin H., Shen H., Wang B., Lei G., Tuan R.S. Mesenchymal stem cell-derived extracellular matrix enhances chondrogenic phenotype of and cartilage formation by encapsulated chondrocytes in vitro and in vivo. *Acta Biomater.*, **15**, 71-82 (2018).

Yao Q., Cosme J. G., Xu T., Miszuk J. M., Picciani P. H., Fong H., Sun H. Three dimensional wlectrospun PCL/PLA blend nanofibrous scaffolds with significantly improved stem cells osteogenic differentiation and cranial bone formation. *Biomaterials***, 115**, 115-127 (2017).

Yoshimoto H., Shin Y.M., Terai H., Vacanti J.P. A biodegradable nanofiber scaffold by electrospinning and its potential for bone tissue engineering. *Biomaterials*, **12**, 2077-2082 (2003).

Zhang W., Zhu Y., Li J. Guo Q., Peng J., Liu S., Yang J., Wang Y. Cell-derived extracellular matrix: basic characteristics and current applications in orthopedic tissue engineering. *Tissue Eng. Part B. Rev.,* **22**, 193-207 (2016).

Zhao X., Liu L., Wang F.K., Zhao D.P., Dai X.M., Han X.S. Coculture of vascular endothelial cells and adipose-derived stem cells as a source for bone engineering. *Ann. Plast. Surg.*, **69**, 91-98 (2012).

VII. FINAL REMARKS AND FUTURE DIRECTIONS

Although a lot of research and developments have been made in the bone tissue engineering field, the translation of these discoveries into clinical applications on a large scale has still not been done. Besides that, there is a gap between the large number of scaffolds and materials developed in the laboratory and the resulting number of commercialized products. In fact, in order to be clinically translated, the developed scaffolds must meet some requirements to guarantee their functionality and bioactivity, triggering cellular activities, such as cell migration, proliferation and osteogenic differentiation.

Isolated ECM components have already been incorporated into biomaterials using different approaches and techniques (Ragetly *et al.* 2010, Vleggeert-Lankamp *et al*. 2004). However, most of these scaffolds fail to mimic the native ECM complex architecture and composition, highlighting the urgent need to develop more relevant approaches (Ravindran *et al.* 2012). Currently, most of the bone defects are still treated with autografts and allografts, leading to several side effects to the patient, such as morbidity, pain and infection.

Herein, we sought to recapitulate the native ECM composition and structure, suggesting two different approaches: the use of non-collagenous bone extracellular matrix proteins and the use of decellularized cell-derived extracellular matrix to enhance bone formation.

Of the non-collagenous proteins present in the bone matrix, osteopontin (OPN) and osteocalcin (OC) are two of the most abundant, representing 10-20% of the non-collagenous proteins (Sroga *et al.* 2011). Aiming to understand the role of these proteins at the cellular level, we isolated MSC from murine bone marrow of double knockout *OC/OPN* mice ($OC^{-/-}$ $OPN^{-/-}$) and evaluated, at the cellular level, the effect of the lack of these two proteins in cell proliferation, differentiation and mineralization. Previous studies conducted by our group and others have demonstrated the role of OPN and/or OC as structural molecules in bone matrix (Sroga *et al.* 2011, Nikel *et al.* 2013, Morgan *et al.* 2015, Bailey *et al.* 2017), linking the organic and inorganic matrices by forming a tether between collagen fibrils and mineral crystals (Poundarik *et al.* 2012). Moreover, loss and modification of OC and/or OPN from bone matrix, known to occur with tissue age (Sroga *et al.* 2011) and with aging in humans (Boskey & Coleman 2010, Plantalech *et al.* 1991, Ingram *et al.* 1994, Grynpas *et al.* 1994), lead to loss of structural integrity (Poundarik *et al.* 2012) and altered mineralization (Boskey *et al.* 1989, Rodriguez *et al.* 2014). However, the actual synergistic role of these two proteins at the cellular level was never studied. Therefore, we characterized for the first time $OC^{-/-}$ $OPN^{-/-}$ MSC derived from bone marrow and showed that their proliferative capacity is impaired. Interestingly, osteogenic differentiation was dramatically reduced by the lack of OC/OPN, however adipogenesis and chondrogenesis were not affected. Moreover, by using spectroscopic analysis, we showed that mineralization was being delayed and the mineral produced by $OC^{-/-}$ $OPN^{-/-}$ after 21 days of osteogenic differentiation did not present the same similarities to bone tissue *in vivo*.

Furthermore, we showed that non-collagenous proteins, more specifically OC and OPN, can be used in combination to promote a synergistic effect on MSC proliferation, osteogenic differentiation and angiogenic properties. In addition, the synergistic effect between both proteins can be further used in bone tissue engineering applications.

In this thesis, we also developed a different approach to mimic native ECM. Therefore, we explored the characteristics and composition of ECM derived from different cell types, since cell sources can determine the

composition of their natural matrix secreted. Although research published about decellularized cell-derived ECM has been increasing during last years, very few studies compare the biological effect of ECM derived from different cell types. Here, we assessed the effect of ECM derived from MSC, HUVEC and co-culture of MSC:HUVEC on cell proliferation, osteogenic differentiation and angiogenic properties. Our findings demonstrated that all cell-derived ECM supported cell proliferation, however only MSC:HUVEC ECM was able to enhance the osteogenic and angiogenic potential of MSC, *in vitro*, suggesting the use of MSC:HUVEC ECM as a new strategy to improve clinical outcomes of bone regeneration. To further investigate its possible application in the bone tissue engineering field, we fabricated cell-derived ECM electrospun PCL scaffolds. We demonstrated that cell-derived ECM electrospun scaffolds were able to mimic the composition and structure of native ECM, enhancing osteogenic capability of MSC seeded on these scaffolds. In particular, MSC:HUVEC ECM scaffolds demonstrated the best results, enhancing the mRNA levels of osteogenic genes and confirming the results previously obtained. Therefore, we demonstrated here that functionality of scaffolds can be enhanced by playing with the natural characteristics and properties of ECM, such as by incorporating non-collagenous proteins into the scaffolds, in particular OC and OPN, or by fabricating cultured cell-derived ECM scaffolds that already have incorporated the required factors and signals, present in the ECM, to trigger cellular activity *in vivo*. This approach might be easier to translate into a clinical context, especially as an acellular product, fabricating the scaffold only with decellularized cell-derived ECM.

Study limitations/ future directions:

During the timeline of this research, several questions were raised and study limitations could be foreseen as an opportunity to develop future work. Therefore, we summarize some of the limitations and questions that remain to be addressed:

- We showed that the absence of both OC and OPN genes impairs stem cell proliferation, osteogenic differentiation and delays mineralization. Although we evaluated the contribution of each protein individually by supplementing the culture medium with each protein and evaluating how $OC^{-/-}$ $OPN^{-/-}$ MSC respond to this extracellular supplementation, we believe that MSC from single knockout mice ($OC^{-/-}$ mice and $OPN^{-/-}$ mice) should also be isolated to evaluate how each protein, individually, affects the cellular processes.

- Another future direction for this work could be the incorporation of these proteins in a specific matrix, such as collagen, and evaluate how $OC^{-/-}$ $OPN^{-/-}$ MSC respond to it. In our studies, we only evaluated how $OC^{-/-}$ $OPN^{-/-}$ MSC behave when the proteins were extracellularly supplemented to the medium. We believe that it would be more relevant to assess how $OC^{-/-}$ $OPN^{-/-}$ MSC respond to scaffolds that have these proteins incorporated, in a 3-D configuration. Currently, the composition and quality of the organic part of bone matrix has been well established as having an extremely important role in bone fragility. In particular, non-collagenous proteins present in the bone extracellular matrix have been

reported to be responsible for bone mineralization, despite their low amount compared to type I collagen. Thus, these OC/OPN-enhanced matrices could be further designed and developed to be applied as an approach to enhance bone healing response to specific diseases in which the amount of these two proteins is compromised.

- Another question raised in this study was how to assess the quality of bone mineral produced by cells. Indeed, most of the studies still rely on chemical analysis and histological stainings, such as calcium quantification and Von Kossa and Alizarin red staining. Although we have evaluated the mineral produced by $OC^{-/-}OPN^{-/-}$ MSC using spectroscopic analysis, such as FTIR, Raman spectroscopy and energy dispersive X-ray spectroscopy (EDX), we believe that a better characterization should be done using other techniques, such as, X-ray diffraction (XRD) and small-angle X-ray scattering (SAXS). Moreover, the mineral yield in cell cultures is often small, being necessary to pool material from multiple cultures. Thus, we understand that a better protocol to extract minerals produced by cells should be optimized and developed, aiming to obtain higher amount of mineral to be able to use these samples in the above mentioned techniques. We believe that new tests for quality control of bone tissue engineered constructs should be developed, in order to evaluate the quality of the mineral produced by cells seeded on these scaffolds *in vitro*, mimicking what potentially could happen *in vivo*.

- Angiogenesis is closely related with osteogenesis. In fact, we have explored this interaction during this thesis. Despite having used different functional assays to evaluate cellular angiogenic properties, such as tube formation assay, “scratch” wound healing assay and VEGF mRNA expression level quantification, we acknowledge that evaluation of the secreted factors by cells should have been done, for example performing enzyme-linked immunosorbent assays (ELISA). Therefore, a detailed investigation of the pro-angiogenic factors that were secreted by cells, as well as their relative amounts would give us more relevant information, contributing to clarify in particular how MSC respond to non-collagenous bone proteins or to different cell-derived ECM, regarding angiogenesis.

- In this study, we developed OC/OPN-enhanced collagen gels to evaluate the synergistic effect of OC/OPN. Although we were focused on studying the effects of the proteins in a matrix that would mimic bone matrix, instead of developing an optimized biomaterial, we believe that new scaffolds can be designed and developed so that they will incorporate these proteins, by different techniques, and can be further used for bone tissue engineering applications.

- Another limitation of our study was that we did not incorporate a collagen scaffold without OC/OPN proteins in our *in vivo* study, since we were focused on evaluating the effect of OC/OPN on local inflammatory response, while new bone was being formed. We believe that our study would be more relevant if we had included also a collagen control (without proteins), so that we could get more information data from these *in vivo* studies.

- Regarding cell-derived ECM studies, we believe that our main limitation was that we did not perform proteomics analysis to understand the compositional differences of ECM produced by different cell types. In this study, we were able to observe different biological responses of MSC seeded in different cell-derived ECM substrates and we characterized the ECM produced by MSC, HUVEC and MSC:HUVEC (different ratios) using SEM and immunocytochemistry with specific antibodies (Col I, Col IV, laminin, fibronectin and osteocalcin). Although we observed different structure and architecture of these ECM (SEM analysis) and different ECM composition and distribution (immunocytochemistry assays), we just selected the most common ECM proteins to perform immunostainings, having not quantified the ECM molecules present. Since native ECM is composed by an organized and highly complex assemble of macromolecules, we recognize that we could have missed important information about other ECM molecules that could be varying from different cell sources.

- Aiming to develop scaffolds that can incorporate cell-derived ECM, we developed cell-derived ECM electrospun PCL fibers. One of the most interesting features about electrospinning technique is its ability to tailor the diameter of the produced fibers, mimicking the specific architecture of the native tissue. Therefore, for bone tissue engineering applications, nanotopography has been shown to enhance osteogenic properties. In this study, the mean diameter of the electrospun fibers was between 1500-1800 nm. Although, we have demonstrated increased osteogenic response when using these fibers, we believe that optimization of the fibers diameter can be done, trying to decrease their size to nanoscale. However, it is important to note that a compromise between the decrease of the diameter of the fibers and the possibility to spin ECM has to be done. Since in this work cell-derived ECM was added to the polymer solution and then the solution was electrospun, we opted to use a syringe needle with a diameter that would allow the spinning of the particles of ECM. Thus, we had to compromise the diameter of the fibers, since we could not use a syringe needle with a lower diameter.

- Another interesting pathway that can be further study is the development of cell-derived ECM 3-D scaffolds to enhance osteogenesis. Moreover, we believe that, in particular, incorporation of MSC:HUVEC ECM in 3-D scaffolds could be used as an approach to target osteogenesis and angiogenesis, simultaneously. To the best of our knowledge, research has not been focusing on using ECM produced by co-culture of MSC and HUVEC, and, according to our results, MSC:HUVEC ECM will be able to mimic better the bone microenvironment, enhancing bone regeneration and repair and angiogenesis. Moreover, tissue engineering has been focusing on 3-D printing applications. We believe that further studies can be done to develop bioinks composed with cell-derived ECM. Therefore, cell-derived ECM 3-D printing scaffolds can be fabricated in a more fashion way, mimicking the composition and microenvironment of bone tissue.

In conclusion, the main findings of this study are summarized in the following points:

(1) OC and OPN are important regulators of mineralization and angiogenesis at the cellular level. The lack of both proteins impairs proliferative capacity of MSC, as well as osteogenic differentiation ability, delaying mineralization of the matrix and producing minerals not sufficiently mature.

(2) OPN is fundamental for normal angiogenesis, an important process also in bone repair.

(3) OC and OPN act in a synergistic manner, enhancing osteogenesis and cellular angiogenic potential.

(4) OC and OPN exert their regulatory role in MSC differentiation mainly in an extracellular manner, since $OC^{-/-}$ $OPN^{-/-}$ MSC were able to recover their proliferative and osteogenic capabilities when these proteins were added extracellularly to the stem cell culture.

(5) OC/OPN-enhanced collagen matrices can be developed to enhance cell proliferation and to promote and accelerate osteogenesis.

(6) Cultured cell-derived ECM can be explored as new biomaterial to enhance osteogenic differentiation of MSC.

(7) Different cell types can produce ECM that will trigger different cellular responses. In particular, osteogenic differentiation of MSC is enhanced when cells are cultured on ECM derived from a co-culture of MSC and HUVEC (MSC:HUVEC ECM).

(8) Cell-derived ECM PCL electrospun fibers can be fabricated to be applied in bone tissue engineering applications. Therefore, these fibers will mimic architecture of collagen fibers in bone tissue and the cell-derived ECM incorporated into the fibers provides important factors and signals that will trigger specific cellular responses, such as migration, proliferation, osteogenesis and angiogenesis.

VII. References

Bailey S. Karsenty G., Gundberg C., Vashishth D. Osteocalcin and osteopontin influence bone morphology and mechanical properties. *Ann. N.Y. Acad. Sci.,***1409**, 74-84 (2017).

Boskey A., Maresca M., Appel J. The effects of noncollagenous matrix proteins on hydroxyapatite formation and proliferation in a collagen gel system. *Connect. Tissue Res.*, **21**, 171-176 (1989).

Boskey A.L.,Coleman R. Aging and bone. *J. Dent. Res.* **89**, 1333-1348 (2010).

Grynpas M.D, Tupy J.H., Sodek J. The distribution of soluble, mineral-bound, and matrix-bound proteins in osteoporotic and normal bones. *Bone,* **15**, 505-513 (1994).

Ingram R.T. Park Y.K., Clarke B.L., Fitzpatrick L.A. Age- and gender- related changes in the distribution of osteocalcin in the extracellular matrix of normal male and female bone. Possible involvement of osteocalcin in bone remodeling. *J. Clin. Invest.,* **93**, 989-997 (1994).

Morgan S. Poundarik A.A., Vashishth D. Do non-collagenous proteins affect skeletal mechanical properties? *Calcif. Tissue Int.,* **97**, 281-291 (2015).

Nikel O. Laurencin D., McCallum S.A., Gundberg C.M., Vashishth D. NMR investigation of the role of osteocalcin and osteopontin at the organic-inorganic interface in bone. *Langmuir,* **29**, 13873-13882 (2013).

Plantalech L. Guillaumont M., Vergnaud P., Leclercq M., Delmas P.D. Impairment of gamma carboxylation of circulating osteocalcin (bone gla protein) in elderly women. *J. Bone Miner. Res.,***6,** 1211-1216 (1991).

Poundarik A.A., Diab T., Sroga G.E., Ural A., Boskey A.L., Gundberg C.M., Vashishth D. Dilatational band formation in bone. *Proc. Natl. Acad. Sci. U.S.A.,* **109,** 19178–19183 (2012).

Ragetly G., Griffon D.J., Chung Y.S. The effect of type II collagen coating of chitosan fibrous scaffolds on mesenchymal stem cell adhesion and chondrogenesis. *Acta Biomater.*, **6**, 3988-3997 (2010).

Ravindran S., Gao Q., Kotecha M., Magin R.L., Karol S., Bedran-Russo A., George, A. Biomimetic extracellular matrix-incorporated scaffold induces osteogenic gene expression in human marrow stromal cells. *Tissue Eng. Part A*, **18**, 295-309 (2012).

Rodriguez D.E., Thula-Mata T., Toro E.J., Yeh Y.W., Holt C., Holliday L.S. Gower L.B. Multifunctional role of osteopontin in directing intrafibrillar mineralization of collagen and activation of osteoclasts. *Acta Biomater.,* **10,** 494-507 (2014).

Sroga G.E., Karim L., Colón W., Vashishth D. Biochemical characterization of major bone-matrix proteins using nanoscale-size bone samples and proteomics methodology. *Mol. Cell. Proteomics* **10,** M110.006718 (2011).

Vleggeert-Lankamp C.L., Pêgo A.P., Lakke E.A., Deenen M., Marani E., Thomeer R.T. Adhesion and proliferation of human Schwann cells on adhesive coatings. *Biomaterials*, **25**, 2741-2751 (2004).

LIST OF PUBLICATIONS

Oral Communications

Pre-College Teachers Training Program in Stem Cell Biology & Bioengineering: "Biophysical regulation of stem cells: directing stem cell fate by mechanical cues", funded by New York State Stem Cell Initiative (NYSTEM) C30161GG, Rensselaer Polytechnic Institute, Troy, NY, USA, June 2017.

Poster communications

TERMIS EU 2016, European Chapter Meeting of the Tissue Engineering and Regenerative Medicine International Society 2016, Uppsala, Sweden, 28th June – 1st July, **M. Carvalho**, A. Poundarik, J.M.S. Cabral, C.L. da Silva, D. Vashishth, "Biomimetic collagen type I gels for enhanced stem cell mediated osteogenesis".

American Chapter Meeting of the Tissue Engineering and Regenerative Medicine International Society 2017 (TERMIS 2017), Charlotte, NC, USA, 3rd December – 6th December 2017, **M.S. Carvalho**, A. Poundarik, J.M.S. Cabral, C.L. da Silva, D. Vashishth, "Biomimetic matrices for enhanced stem cell-mediated osteogenesis".

European Orthopaedic Research Society 2018 (EORS 2018), Galway, Ireland, 25th September – 28th Spetember 2018, J.C. Silva, **M. S. Carvalho,** W.M.R.N. Udangawa, J.M.S. Cabral, C.L. da Silva, F.C. Ferreira, D. Vashishth, R.J. Linhardt, "Extracellular matrix decorated porous polycaprolactone scaffolds for bone tissue engineering".

American Society of Bone and Mineral Research 2018 (ASBMR 2018), Montréal, Canada, 28th September – 1st October 2018, **M.S. Carvalho**, J.M.S. Cabral, C.L. da Silva, D. Vashishth, "Osteocalcin and osteopontin mediate osteogenic differentiation of mesenchymal stem/stromal cells by controlling the maturation level of mineral species".

List of publications

Patent: Biomimetic nano-composite scaffold for enhanced bone healing and fracture repair", Patent N. WO2016179089 (10 Nov 2016) A.Poundarik, **M. Carvalho**, D. Vashishth.

M.S. Carvalho, A.A. Poundarik, J.M.S. Cabral, C.L. da Silva, D. Vashishth, "Biomimetic matrices for rapidly forming mineralized bone tissue based on stem cell-mediated osteogenesis", *Scientific Reports*, 8(1):14388, 2018 (doi: 10.1038/s41598-018-32794-4).

M.S. Carvalho, J.M.S. Cabral, C.L. da Silva, D. Vashishth, "Synergistic effect of extracellularly supplemented osteopontin and osteocalcin on stem cell proliferation, osteogenic differentiation and angiogenic properties", *Journal of Cellular Biochemistry*, accepted on 2 October 2018 (doi:10.1002/jcb.27948).

M.S. Carvalho, J.C. Silva, J.M.S. Cabral, C.L. da Silva, D. Vashishth, "Cultured cell-derived extracelular matrices to enhance the osteogenic differentiation and angiogenic properties of human mesenchymal stem/stromal cells", 2018 (under revision in *Journal of Tissue Engineering and Regenerative Medicine).*

M.S. Carvalho, J.C. Silva, W.M.R.N. Udangawa, J.M.S. Cabral, F.C. Ferreira, C.L. da Silva, R.J. Linhardt, D. Vashishth, “Cell-derived extracelular matrix electrospun microfibrous scaffolds for bone tissue engineering”, 2018 (under revision in *Materials Science and Engineering:C*).

J.C. Silva, **M.S. Carvalho**, X. Han, K. Xia, P.E. Mikael, J.M.S. Cabral, F.C. Ferreira, R.J. Linhardt, “Compositional and structural analysis of glycosaminoglycans in cell-derived extracellular matrices”, 2018 (under revision in *Glycoconjugate Journal*).

M.S. Carvalho, J.C. Silva, C. Hoff, J.M.S. Cabral, R.J. Linhardt, C.L. da Silva, D. Vashishth, “Osteocalcin and osteopontin mediate osteogenic differentiation of mesenchymal stem/stromal cells by controlling the maturation level of mineral species”, 2018 (under submission).

Awards

Student Scientist Award for TERMIS-AM 2017 Conference (December 2017).